ANNALS OF THE NEW YORK ACADEMY OF SCIENCES

Volume 79, Art. 11 Pages 761–1098

Editor in Chief
Otto v. St. Whitelock

Managing Editor
Franklin N. Furness

Associate Editors
Marguerite Selzer Peter A. Sturgeon

MOLTEN SALTS

LIST OF AUTHORS

Benson R. Sundheim (*Conference Chairman*), P. A. Agron, E. Aukrust, J. Berkowitz, B. Björge, M. Blander, G. E. Blomgren, J. O'M. Bockris, C. R. Boston, A. L. Bowman, J. Braunstein, M. A. Bredig, R. I. Bretz, W. T. Carnall, B. Chu, W. A. Chupka, D. Cubicciotti, M. D. Danford, F. R. Duke, J. J. Egan, S. N. Flengas, H. Flood, T. Førland, L. M. Foster, H. Garfinkel, D. M. Gruen, G. Harrington, A. E. Harvey, G. J. Hills, D. Inman, G. J. Janz, J. Kooi, R. W. Laity, H. A. Levy, N. L. Lofgren, E. B. Luchsinger, A. Lundén, K. J. Macleod, R. L. McBeth, J. D. E. McIntyre, G. W. Mellors, R. A. Osteryoung, R. Piontelli, T. A. Rodgers, S. Senderoff, G. P. Smith, K. H. Stern, C. J. Wassink, F. E. W. Wetmore, E. Wolf, S. J. Yosim, and L. Young

Consulting Editor
Benson R. Sundheim

NEW YORK
PUBLISHED BY THE ACADEMY
January 30, 1960

THE NEW YORK ACADEMY OF SCIENCES

(Founded in 1817)

BOARD OF TRUSTEES

BORIS PREGEL, *Chairman of the Board*

Class of 1960
GORDON Y. BILLARD
HENRY C. BRECK

Class of 1960–1961
HARDEN F. TAYLOR

Class of 1960–1962
W. STUART THOMPSON

Class of 1960–1963
DEAN RUSK
LOWELL C. WADMOND

M. J. KOPAC, *President of the Academy*

HILARY KOPROWSKI, *Past President*
BORIS PREGEL, *Past President*

EUNICE THOMAS MINER, *Executive Director*

COUNCIL, 1960

President, M. J. KOPAC

President-Elect, FREDERICK Y. WISELOGLE

EMERSON DAY *Vice-President*
THEODORE SHEDLOVSKY, *Vice-President*

Recording Secretary
KARL MARAMOROSCH

Corresponding Secretary
CHARLES W. MUSHETT

Elected Councilors

1958–1960
DAVID A. KARNOFSKY
WAYNE W. UMBREIT
GUSTAV J. MARTIN
JOHN E. VANCE

1959–1961
JOHN E. DEITRICK
ROBERT S. MORISON
CHARLES W. MUSHETT
E. L. TATUM

1960–1962
JOHN JOSEPH LYNCH, S.J.
MORRIS SCHAEFFER

Executive Director, EUNICE THOMAS MINER

SECTION OF BIOLOGICAL AND MEDICAL SCIENCES
ROBERT L. KROC, *Chairman*
CHARLES NOBACK, *Vice-Chairman*

DIVISION OF ANTHROPOLOGY
DOROTHY L. KEUR, *Chairman*
ETHEL BOISSEVAIN LESSER, *Vice-Chairman*

DIVISION OF INSTRUMENTATION
ANDRES FERRARI, *Chairman*
WALTER E. TOLLES, *Vice-Chairman*

DIVISION OF MYCOLOGY
KARL MARAMOROSCH, *Chairman*
EMANUEL GRUNBERG, *Vice-Chairman*

DIVISION OF PSYCHOLOGY
GREGORY RAZRAN, *Chairman*
LOUIS W. MAX, *Vice-Chairman*

DIVISION OF CHEMICAL SCIENCES
FREDERICK R. EIRICH, *Chairman*
EVERETT S. WALLIS, *Vice-Chairman*

DIVISION OF BIOCHEMISTRY
JAMES B. ALLISON, *Chairman*
RAYMOND L. GARNER, *Vice-Chairman*

SECTION OF GEOLOGICAL SCIENCES
R. W. FAIRBRIDGE, *Chairman*

DIVISION OF OCEANOGRAPHY AND METEOROLOGY
CHARLES KNUDSEN, *Chairman*
JAMES K. McGUIRE, *Vice-Chairman*

DIVISION OF ENGINEERING
JACOB FELD, *Chairman*
JOSEPH F. SKELLY, *Vice-Chairman*

Past Presidents
HILARY KOPROWSKI
BORIS PREGEL

The Sections and the Divisions hold meetings regularly, one evening each month, during the academic year, October to May, inclusive. All meetings are held at the building of The New York Academy of Sciences, 2 East Sixty-third Street, New York 21, New York.

Conferences are also held at irregular intervals at times announced by special programs.

ANNALS OF THE NEW YORK ACADEMY OF SCIENCES

VOL. 79, ART. 11 PAGES 759–1098

January 30, 1960

Editor in Chief

OTTO V. ST. WHITELOCK

Managing Editor

FRANKLIN N. FURNESS

Associate Editors

MARGUERITE SELZER
PETER A. STURGEON

MOLTEN SALTS*

Consulting Editor and Conference Chairman

BENSON R. SUNDHEIM

CONTENTS

Introductory Remarks. *By* BENSON R. SUNDHEIM 761

X-ray and Neutron Diffraction Studies of Molten Alkali Halides. *By* H. A. LEVY, P. A. AGRON, M. A. BREDIG, M. D. DANFORD 762

Partition Functions for Normal Liquids and Molten Salts. *By* G. E. BLOMGREN 781

Structure of Molten Mercuric Halides. *By* GEORGE J. JANZ AND JAMES D. E. MCINTYRE 790

Some Thermodynamic Aspects of Molten Salts: Halides of Uranium, Zirconium, Thorium, and Cerium in Alkali Halide Eutectics. *By* D. INMAN, G. J. HILLS, L. YOUNG, J. O'M. BOCKRIS 803

Activities in Molten Salt Mixtures of Potassium-Lithium-Halide Mixtures: A Preliminary Report. *By* E. AUKRUST, B. BJÖRGE, H. FLOOD, T. FØRLAND 830

A Quasi-Lattice Model of Molten Reciprocal Salt Systems. *By* MILTON BLANDER AND JERRY BRAUNSTEIN 838

Solubilities of Titanium Tetrachloride in Mixtures of Potassium Chloride and Sodium Chloride, and the Electrode Potentials of the Titanium Chlorides in 1/1 (Mole) KCl-NaCl Solutions. *By* S. N. FLENGAS 853

Freezing Points of Binary Nitrate Melts. *By* K. J. MACLEOD AND F. E. W. WETMORE 873

* This series of papers is the result of a conference on *Molten Salts* held and supported by The New York Academy of Sciences on April 13, 14, and 15, 1959.

Thermodynamic Properties of Solutions of Cerium Chloride in Molten Alkali Halides. *By* S. Senderoff, G. W. Mellors, R. I. Bretz 878

Measurement of the Uranium-Uranium (III)Potential in LiCl-KCl Eutectic. *By* Dieter M. Gruen and Robert A. Osteryoung 897

Thermodynamics of Molten Binary Chloride Mixtures Calculated from the Phase Diagrams. *By* Benjamin Chu and James J. Egan 908

The Cryolite Situation. *By* L. M. Foster 919

Absorption Spectra of Fused-Salt Solutions. *By* G. Pedro Smith and Charles R. Boston 930

Oxidation States of the Elements and Their Potentials in Fused-Salt Solutions: the Actinide Elements. *By* Dieter M. Gruen, R. L. McBeth, J. Kooi, W. T. Carnall 941

Absorption Spectra in Molten Salts. *By* George Harrington and Benson R. Sundheim 950

Isothermal and Isopiestic Decomposition of Potassium Perchlorate and Potassium Chlorate. *By* Aubrey E. Harvey, Carl J. Wassink, Tommy A. Rodgers, Kurt H. Stern 971

Isotope Enrichment by Electromigration in a Mixture of Molten $RbNO_3$ and $LiNO_3$. *By* Arnold Lundén 988

Interionic Friction Coefficients in Molten Salts. *By* Richard W. Laity 997

Ion Mobilities in Pure Fused Silver Chloride. *By* F. R. Duke, A. L. Bowman, E. Wolf, H. Garfinkel 1023

Reference Electrodes and Overvoltage Measurements in Molten Salts. *By* R. Piontelli 1025

Composition of Vapors in Equilibrium with Salts at High Temperatures. *By* Joseph Berkowitz and William A. Chupka 1073

Solubilities of Salts in Metals. *By* S. J. Yosim and E. B. Luchsinger 1079

Electrolysis of Liquid Bismuth-Bismuth Chloride Mixtures. *By* Daniel Cubicciotti and Norman L. Lofgren 1088

Copyright, 1960, by The New York Academy of Sciences

INTRODUCTORY REMARKS

Benson R. Sundheim
New York University, Washington Square College, New York, N.Y.

In the last few years, research activity on molten salts has increased so rapidly that we can now recognize a rather well-defined field. There is a nucleus of generally recognized problems; there are also some broad conceptual frameworks in terms of which experiments are interpreted and a number of specialized techniques. Moreover, many distinguished scientists devote a large part of their time to molten-salt experimentation, as the list of contributors to this monograph shows.

Scientific interest in molten salts stems from several sources. As methods for working at high temperatures evolve, the possibility of progressively extending previous studies into new temperature ranges presents itself. Thus there is a certain challenge to carrying out viscosity, X-ray diffraction, and other measurements on very hot systems. Molten salts offer an opportunity to study concentrated electrolytes without the annoying interference by small amounts of dipolar materials such as water. There is a whole new chemistry in molten-salt systems, one characterized by different sequences of the oxidation potentials, solubilities, and stability constants. A number of special situations occur in molten salts, making possible experiments that cannot be done in other systems. The study of molten salts leads to the discovery of difficulties in such concepts as transference numbers, complex ions, and quantities of transport. The unique systems composed of metals dissolved in molten salts, in addition to their intrinsic interest, provide unusual testing grounds for theories of liquid metals, solubility parameters, metallic bonding, and molecular structure. Probably the most powerful motive that leads scientists to work in this field is the exotic nature of molten salts.

The papers presented in this monograph are products of the results of recent research exclusively. Limitations of time precluded the inclusion of review articles or of material dealing with technological applications. Some of the papers deal with methods of studying the structure of molten salts by such techniques as X-ray diffraction, mass spectrometry of the vapor, and optical absorption spectrometry. Considerable attention is devoted to activities in simple molten-salt mixtures, from both experimental and theoretical points of view. There are papers on transport properties, electrode potentials and kinetics, and the properties of metal-molten salt systems.

Taken as a whole, the contributions to this monograph give a good picture of the current degree of sophistication in this field and of the directions in which research is being pressed. It is to be hoped that this report will raise at least as many questions as it settles.

X-RAY AND NEUTRON DIFFRACTION STUDIES OF MOLTEN ALKALI HALIDES

H. A. Levy, P. A. Agron, M. A. Bredig, M. D. Danford
Chemistry Division, Oak Ridge National Laboratory, Oak Ridge, Tenn.*

INTRODUCTION

The study of structure in molten alkali halides by X-ray and neutron diffraction has been undertaken as part of a general investigation of the properties of molten salts. A previous X-ray study by Lark-Horovitz and Miller[1,2] yielded information concerning molten LiCl and KCl, and recent papers by Zarzycki[3-6] have presented results for LiCl, KCl, NaCl, LiF, NaF, and KF, as well as for $BaCl_2$, CaF_2, and vitreous SiO_2 and GeO_2. Two alkali nitrates, KNO_3 and $NaNO_3$, have been investigated by Danilov and Krasnitskii.[7]

The complex nature of liquids precludes the possibility of deriving unambiguous, detailed descriptions of their structures from diffraction data, in the sense that is well known in the cases of gases and crystalline solids. In the latter cases, the complexity of the system is limited: in gases by the wide separation of discrete molecules and, in crystals, by the periodicity of structure; the number of independent data yielded by diffraction methods is sufficient by and large to establish the parameters needed for description of their structures. On the other hand, the task of describing the atomic structure of a liquid is in itself not unambiguously defined, since the number of atoms or molecules whose relations must be specified is limited in principle only by the size of the sample studied, and no observational method is capable of supplying data sufficient for this task.

Nevertheless on a more modest level, diffraction studies can furnish useful information about the atomic structure of liquids. This information is usually provided in the form of a pair radial distribution function (RDF), giving the probability that pairs of atoms are to be found separated by a given distance. From the form of the RDF, more detailed descriptions sometimes may be inferred. It is this sort of description that the present study has developed for certain molten salts.

A novel feature of the present study is the simultaneous use of neutron and X-ray diffraction data. Because the scattering processes of atoms for neutrons are usually quite different from those for X rays, this combination of observational methods offers the possibility of resolving some of the ambiguity inherent in each method alone.

* Operated by the Union Carbide Corporation, New York, N.Y., for the United States Atomic Energy Commission, Washington, D.C.

EXPERIMENTAL

X-ray Data

Apparatus. All X-ray diffraction patterns were measured by counting methods with a spectrometer[8] specially designed for liquid studies. This instrument, which will be reported separately, employs the Bragg-Brentano para-focusing arrangement with a stationary, horizontal sample surface. The X-ray source and detector assembly rotate in opposite sense about an axis lying in the sample surface. Radiation accepted by the receiving slit is monochromatized by reflection from the (200) planes of a bent and ground crystal of NaCl, and counted by a Na(Tl)I crystal scintillation counter. A single-channel pulse analyzer rejects pulses corresponding to half wave length or shorter radiation. The source is a Norelco Mo target tube operating at 50 kv. and 20 mAmp., both voltage and current being automatically stabilized.

An evacuated furnace and sample carrier equipped with beryllium foil windows for passage of the X-ray beam was placed within the circle of travel of the X-ray source and receiving slits, coaxial with the spectrometer. The sample was usually in the form of a shallow pool of liquid, about 2.5 cm. square, and was contained in a tray of polished MgO or Pt. The space immediately surrounding the sample was enclosed by a thin shell of Be and filled with He at a pressure of several centimeters. In an alternate technique, the sample was held in a half-filled vitreous silica cylinder with integral uniformly ground window 0.010 in. thick to provide for passage of X rays. This procedure, because the sample was highly stable against creep and evaporation, proved especially valuable for obtaining diffraction data at high temperatures at large scattering angles. A cylindrically wound resistance heater surrounded the sample container. Radiation shields of Mo foil, with slots for passage of the X-ray beams, were placed between the heater and the vacuum jacket. Full details of the arrangement will be reported in another paper.

Measurement procedure. At small incidence angles, θ less than 12°, the scattered intensity was measured by means of a recording ratemeter, while the incidence angle was advanced continuously at a rate of 1° every 32 min. (time). At larger angles, measurements were made at stationary settings, at intervals in θ of $\frac{1}{2}$° or 1°, until a preset number of counts of scattered X rays had been accumulated; this number (up to 50,000) was chosen so that the error due to counting statistics in the reduced, sharpened intensity function was held roughly constant throughout its principal region. The primary beam was limited by divergence slits ($\frac{1}{6}$°, $\frac{1}{2}$°, 1°, 2°, or 4°) in the usual manner, depending on the incident angle.

The intensity at selected scattering angles was remeasured from time to time during the collection of data from a given sample in order to detect and correct any instability, such as creep or evaporation of the sample, in the arrangement. The background, always very small, was measured with the sample in place and with a shutter over the receiving slit.

A measurement of Compton scattering at a large scattering angle was made, filtering first the primary beam and then the scattered beam through 0.004 in. of Zr foil, taking the difference in scattered intensity, and normalizing to the unfiltered level. The Compton scattering at other angles was computed by a semiempirical procedure that takes into account the shape of the exciting spectrum, the resolution function of the monochromator, and the theoretical Compton function for the sample under study. Details will be given in another article.

Reduction of data. The various measured counting rates were corrected for background and normalized to a consistent slit size and, sometimes to a standard intensity level; replicate measurements were averaged. The usual polarization correction for monochromatic radiation was then applied, and the intensity of Compton scattering was subtracted.

The absolute scale of intensity was established in the usual way by normalizing the high-angle portion to the theoretical independent atomic-scattering function for the sample. Dispersion-corrected functions were used when appropriate.[9]

The several steps in the treatment of the X-ray data are illustrated in FIGURE 1 for the case of molten LiCl. In the main, upper part of the figure are plotted (*open circles*) the observed scattered intensity after subtraction of background, normalization to standard slit size, and correction for Compton scattering and polarization. Below this the Compton intensity is plotted. The dashed line represents the theoretical independent atomic-scattering function derived, in this case, from Hartree-Fock values for Li^+ and Cl^-. At the bottom of the figure is the reduced, sharpened intensity curve. The inset shows the pair RDF given by EQUATION 6.

FIGURES 2 and 3 show the X-ray intensity curves for the other molten salts studied.

Neutron Data

Apparatus and measurements. All neutron measurements were made with a neutron spectrometer and furnace already described.[12] The samples were precast in vitreous silica tubes and transferred in a dry atmosphere to thin-walled (0.010-in.) vanadium cylinders that were welded shut and mounted in the furnace. The scattered intensity was measured by means of a recording ratemeter, with scattering angle 2θ advancing at 2° per hour. Since normal lithium is highly opaque to neutrons (because of capture in Li^6), lithium chloride containing 99.9 atom per cent Li^7 was employed.

Reduction of data. Scattering due to the furnace and empty vanadium cylinders was directly measured, corrected for absorption in the sample,

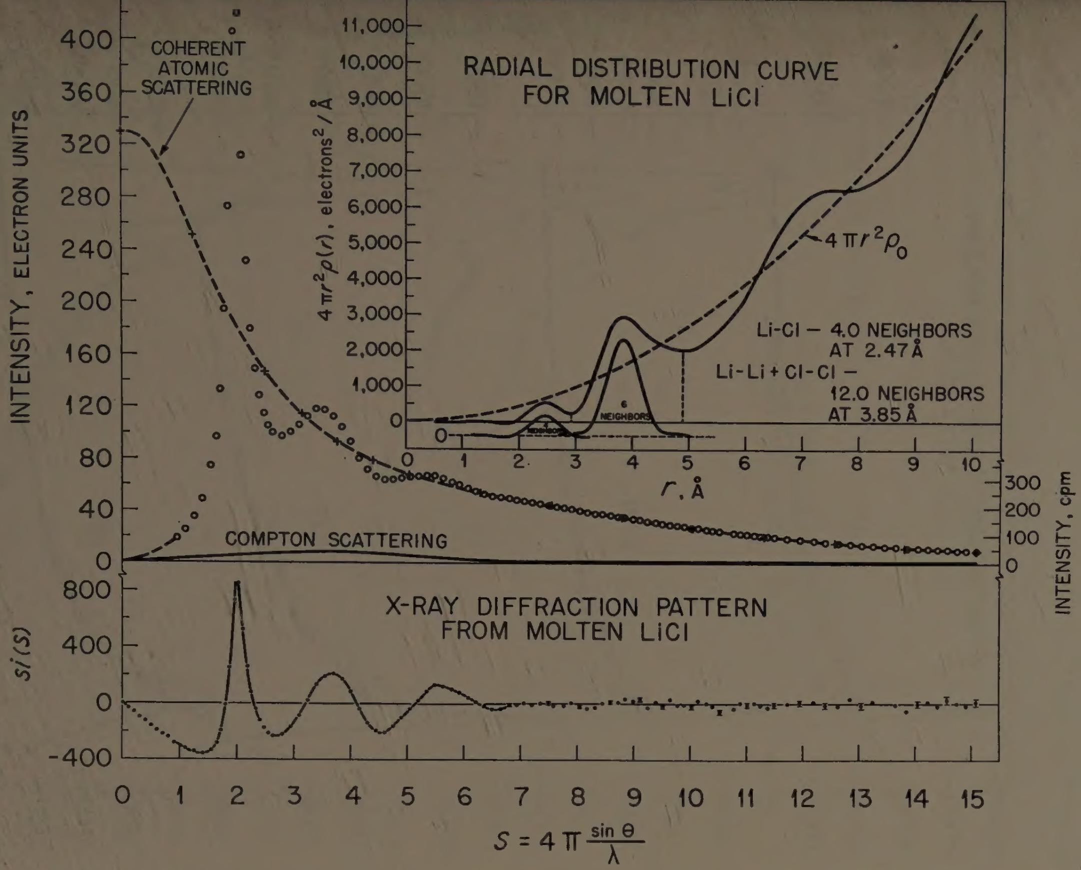

FIGURE 1. Observed-intensity and Compton scattering curve, reduced-intensity curve with indicated statistical errors, and RDF for molten LiCl by X-ray diffraction.

and subtracted from the scattered intensity. The remaining intensity was assumed to consist of two components: the desired coherent single scattering, and an isotropic contribution from nuclear diffuse processes and multiple collisions. The level of the former at a high scattering angle was estimated in the following way.

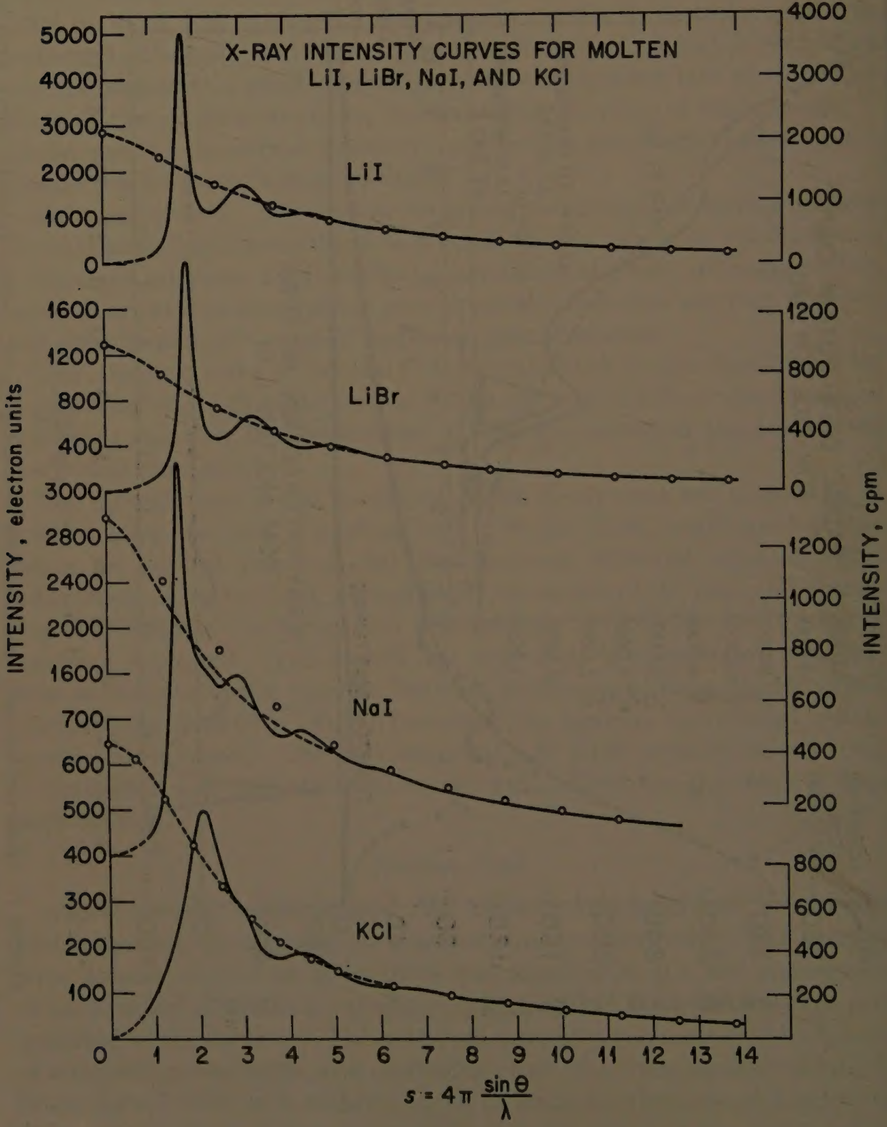

FIGURE 2. Observed-intensity curves for LiI, LiBr, NaI, and KCl by X-ray diffraction. Theoretical independent scattering curves are indicated by circles; for LiBr, LiI, and NaI, empirical values derived by the method of Krogh-Moe[10] and Norman[11] are shown by dashed lines.

The total scattered intensity I_T is proportional to the total scattering cross section, σ_s, of the sample reduced by a factor, $A(\sigma_c)$, representing capture of neutrons in the sample:

$$I_T = k\sigma_s A(\sigma_c) \tag{1}$$

The coherent part is proportional to the coherent part of the scattering cross section, σ_{coh}, reduced by all processes, capture or scattering, that remove neutrons from the beam:

$$I_{\text{coh}} = k\sigma_{\text{coh}} A(\sigma_c + \sigma_s) \tag{2}$$

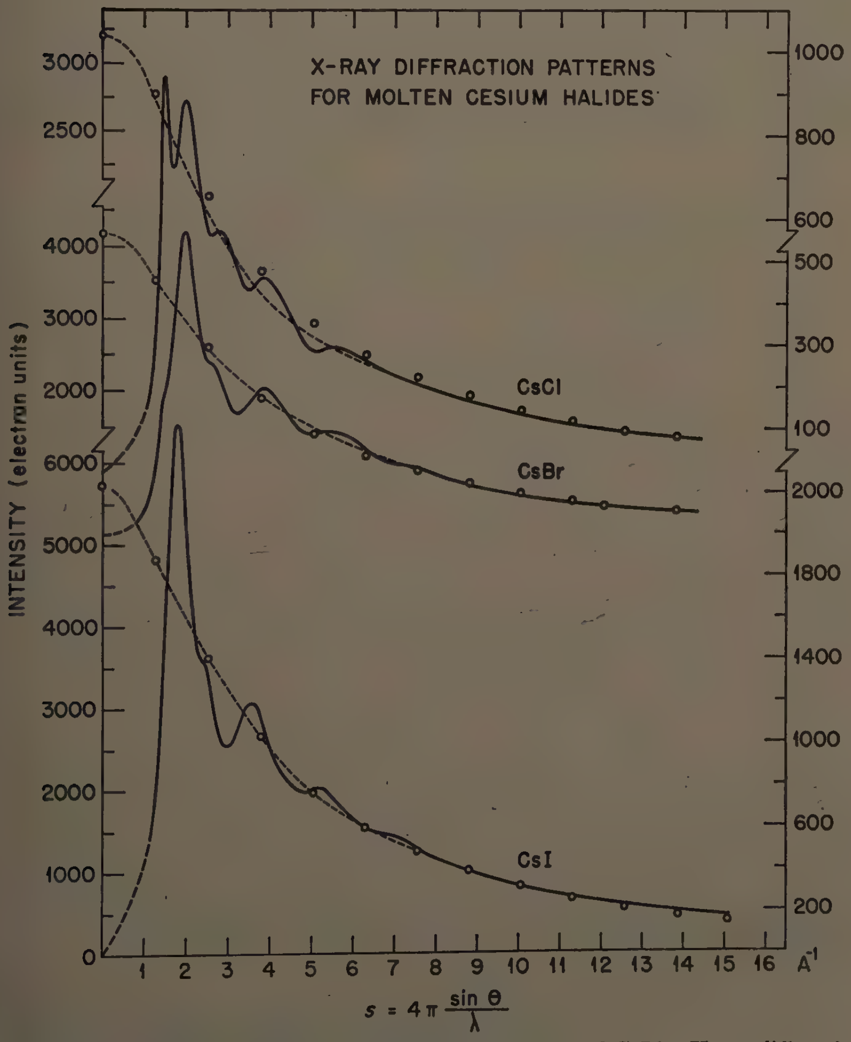

FIGURE 3. Intensity curves for molten CsCl, CsBr, and CsI by X-ray diffraction.

The ratio

$$I_{\text{coh}}/I_T = (\sigma_{\text{coh}}/\sigma_s)\,[A(\sigma_c + \sigma_s)/A(\sigma_c)], \tag{3}$$

given by quantities that can be determined, indicates how the high-angle intensity should be divided between coherent and assumed isotropic components, and subtraction of the latter leaves an estimate of the desired coherent part. Atomic cross sections[13] employed in these studies are listed in TABLE 1.

In each case, the attenuation of a narrow beam of neutrons through the sample was measured and agreed with the attenuation computed from the cross sections. The coherent intensity was expressed on an absolute scale by nomalizing to the theoretical independent atomic scattering in the usual manner. Observed intensity curves for Li^7Cl, CsBr, and KCl are shown in FIGURE 4. The static approximation[14-16] (neglecting the change in energy of the neutron on scattering) was employed throughout.

TABLE 1

NUCLEAR CROSS SECTIONS[13] FOR NEUTRON DIFFRACTION STUDIES

Atom	σ_{coh}	σ_s	σ_{cap}	f
Li^7	0.8	1.4	0	−0.25
Cl	12.1	16	18.6	0.98
K	1.5	1.5	1.16	0.35
Cs	3.0	6	17	0.49
Br	5.7	6	3.9	0.67

ANALYSIS OF DATA

Complete details of the treatment of the coherent-intensity function will be given in a separate publication. The interatomic part of the coherent intensity (already normalized for a chosen stoichiometric unit) is obtained by subtraction of the independent atomic scattering, $\sum_i f_i^2(s)$, which, for the neutron case, is a constant. A reduced-intensity function, illustrated in FIGURE 1 (*bottom*), is obtained from

$$si(s) = s[I(s) - \textstyle\sum_i f_i^2(s)]M(s) \tag{4}$$

where the summation is over the atoms in the stoichiometric unit, $I(s)$ is the normalized observed intensity, and $s = (4\pi/\lambda)\sin\theta$.

The "modification function" $M(s)$ is included to sharpen the distribution function to be obtained by Fourier inversion,[17] in effect removing some of the breadth arising in the X-ray case from the characteristic electron distribution of the atoms. In the present X-ray work, the function

$$M(s) = [\textstyle\sum_i f_i(0)/\sum_i f_i(s)]^2 \tag{5}$$

was used, with the summation being over the stoichiometric unit of composition and $f_i(0)$ the value of the form factor for atom i at $s = 0$. For the present neutron work, $M(s) = 1$ was found satisfactory.

The RDF associated with the Fourier transform of $si(s)$ is

$$D(r) = 4\pi r^2 \rho_0 + (2r/\pi) \int_0^{s_{\max}} si(s)M(s) \sin sr \, ds \qquad (6)$$

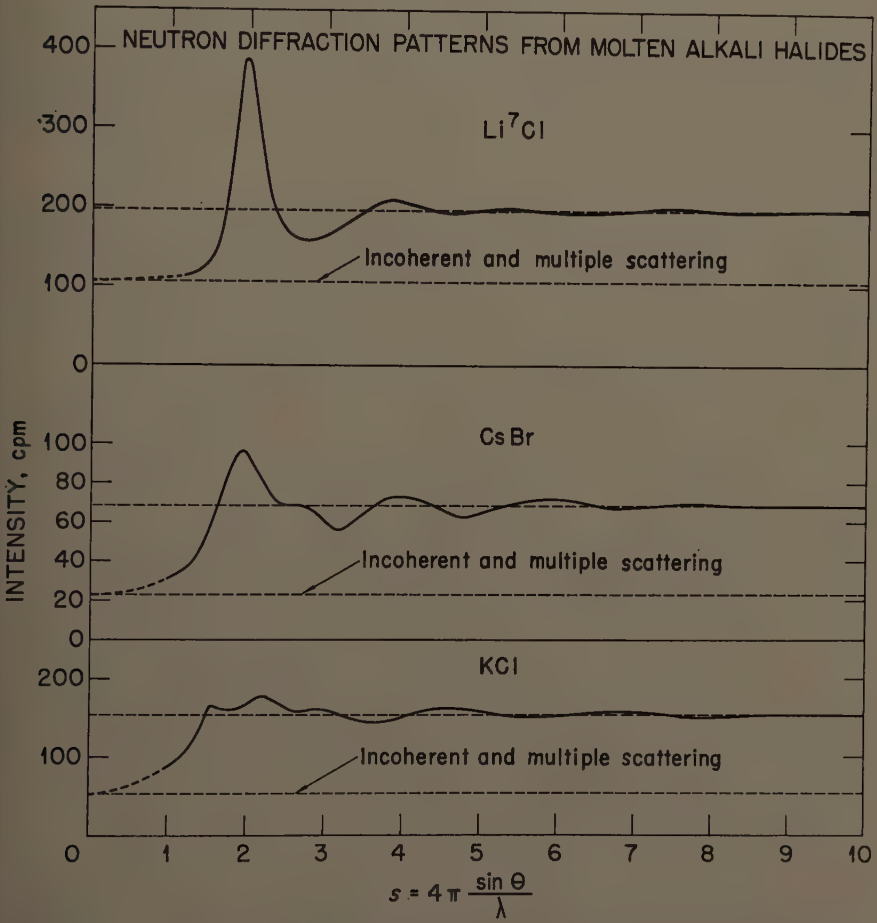

FIGURE 4. Neutron diffraction intensity curves for Molten Li^7Cl, CsBr, and KCl. Positions of the theoretical independent atomic scattering (*upper line*) and multiple and incoherent scattering are indicated by dashed lines.

where ρ_0 is the average scattering density of the sample in electron units (given by the square of the number of electrons per unit volume). The function $D(r)$ represents a superposition of modified atomic pair distribution functions for the various kinds of atom pairs. The modification inherent in EQUATION 6 of a given pair distribution function ρ_{jk} is expressed by[17]

$$D_{jk}(r) = 4\pi r \int_{-\infty}^{\infty} \mu \rho_{jk}(\mu) T_{jk}(\mu - r)\, d\mu \tag{7}$$

with

$$T_{jk}(r) = (1/\pi) \int_{0}^{s_{\max}} f_j(s) f_k(s) M(s) \cos sr\, ds \tag{8}$$

f_j and f_k being the form factors for atoms of kind j and k. The function $T_{jk}(r)$ can be visualized as a shape function into which a sharp pair distribution is transformed by the combined effects of the inherent electron distribution and treatment of the data.

The Interpretation of Radial Distributions for Binary Systems

The distribution functions presented in FIGURES 1, 5, 6, and 7 may be described as superpositions of averaged, sharpened, and weighted distributions of interactions of three kinds: M^+X^-, M^+M^+, X^-X^-. Here M^+ and X^- refer to the cations and anions making up the sample. The weighting refers to the differences in X-ray or neutron scattering power of different atoms, and its presence is implicit in the data. Thus, a peak in an X-ray distribution function representing one pair of atoms at a given distance will have an area proportional to the product of the numbers of electrons contained in these two atoms. Similar considerations apply to distributions derived from neutron data. It follows that, in order to derive a number of interactions from a peak appearing in an RDF, the nature of the interaction must be assumed first (from considerations apart from the diffraction experiment). In the case of the molten salts, the reasonable assumption has been made that the interactions at shortest distance represent atom pairs of unlike charge, and that those following at longer distance represent atoms of like charge. This presumption has been confirmed directly by neutron data in the case of $\mathrm{Li^7Cl}$, as will be shown in the following section.

The term "sharpened" refers to the feature of the X-ray data reduction process that is concerned with the breadth of the electron shells of the atoms making up the sample substance. Because it is the electrons that scatter X rays, a simple interpretation would yield a RDF for electrons. Since the electron distribution of individual ions is relatively well-known, an analysis into atom pairs could, in principle, be carried out. A simpler procedure, however, is to incorporate a partial analysis into the data reduction process; the measured scattering function is converted into that which would be given by atoms sharpened in a known way. This modification can be represented graphically by a computed peak shape corresponding to a given pair distribution, and this can be compared to the experimental function. This procedure has been followed throughout this paper.

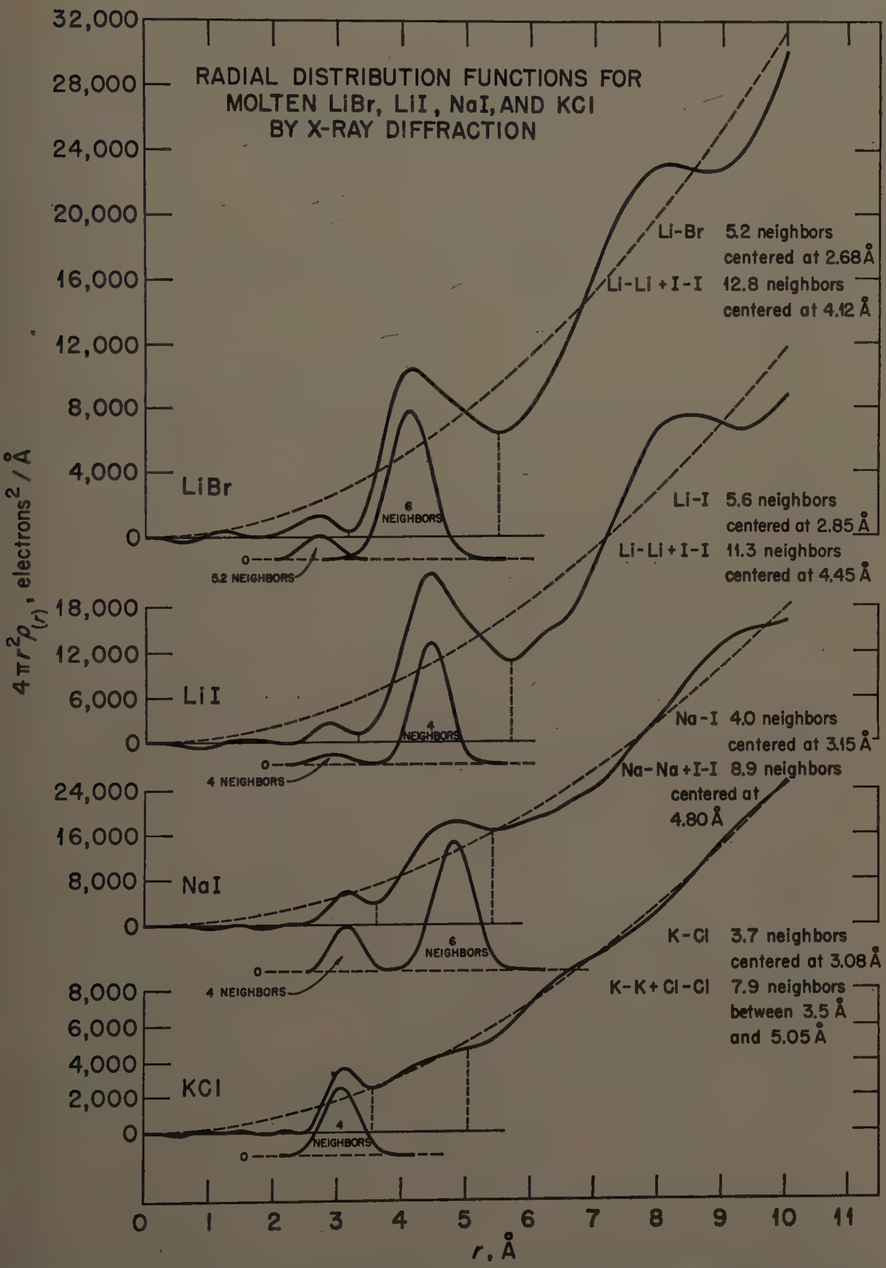

FIGURE 5. RDFs for LiBr, LiI, NaI, and KCl by X-ray diffraction, showing standard synthetic peaks and boundaries by which co-ordination numbers were obtained.

One other feature of the RDF must be borne in mind: in general, unlike the case of a simple crystal, all atoms of a given "kind" are not structurally equivalent in an instantaneous configuration. It follows that the RDF must be regarded as the *average* (over a volume that is large compared to atomic dimensions) of the actual instantaneous distribution. Thus, for example, the appearance of a first peak with area corresponding to four neighbors does not imply that all, or even necessarily any, atoms in the sample have exactly four neighbors at the given distance.

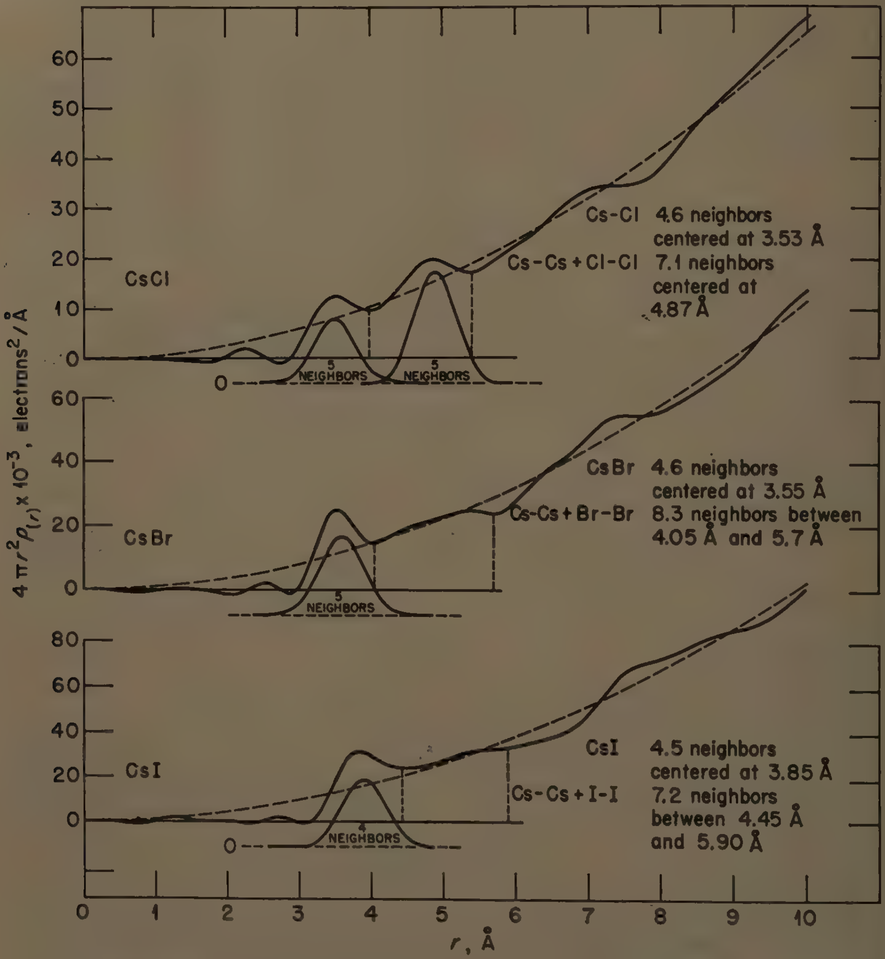

Figure 6. RDFs for CsCl, CsBr, and CsI by X-ray diffraction.

Discussion of the Radial Distribution Functions

The RDFs for the molten salts studied will be examined in the light of the foregoing general discussion. In each case, the curve is nearly flat at zero value for short distances, followed by one or more broad, incompletely resolved peaks at distances comparable with atomic diameters. At longer distances, peaks become less prominent, and the curves approach the parabola, $4\pi r^2\rho_0$, corresponding to the distribution of a uniform fluid with the average scattering density of the sample.

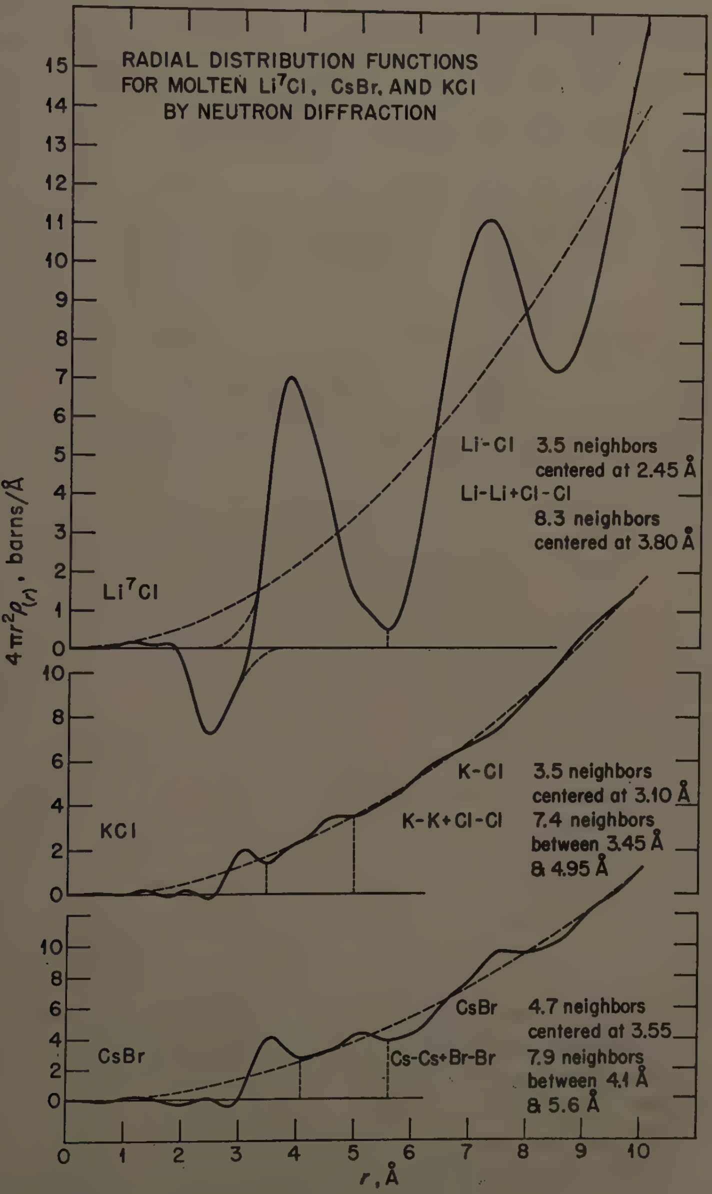

Figure 7. RDFs for molten Li⁷Cl, CsBr, and KCl from neutron diffraction data.

Resolution of the curves into discrete pair distributions is seen to offer difficulty. We have adopted the arbitrary practice of bounding the peaks with vertical lines drawn at the minima of the total function. No great change in the derived peak areas would result if resolution into error-type components were attempted.

It is noteworthy that the kernels of all the Fourier integrals, including the sharpening functions, were quite well converged at the limit of the experimental data. Therefore little error should be introduced because of the finite range of measurements. By the same token, the considerable breadth of the features of the radial distribution function can be ascribed to the physical nature of the sample and not to the limited resolution of the measurements.

The synthetic peaks shown with the RDF curves correspond to Gaussian distributions of atomic pairs. They were computed from

$$P_{jk}(r) = (N/\pi) \int_0^{s_{\max}} f_j(s) f_k(s) e^{-as^2} M(s) \cos rs\, ds \qquad (9)$$

The parameter a was chosen to correspond to full widths at half height of the underlying Gaussian distribution between 0.56 and 0.76 Å, as required to yield well-converged integrals. The constant N corresponds to the number of neighbors indicated in the figures.

The Closest Approach

Each curve shows a well-defined first peak following a nearly flat section, representing the minimal distance of approach of atoms in the sample. That this approach is between anions and cations is confirmed by comparison of the results of X-ray and neutron studies for LiCl. Since the scattering factor of Li^7 for neutrons is negative, while that for Cl is positive, the "peak" representing the Li^7-Cl interaction for neutrons should be negative; the first peak of FIGURE 7 is indeed negative, while that in FIGURE 1 for X rays is positive at about the same distance.

TABLE 2 summarizes the observations on the short-distance interactions for the 8 salts studied, in each case interpreted as an M^+X^- approach. It must be emphasized once more that, in view of the great breadth of the peaks (~0.5 Å full breadth at half height), the significance of the distance at the peak maximum is that of the most frequent one only; however, intercomparision of these peak distances and correlation with those in the crystals is none the less of interest. It will be seen that this "most frequent" distance is up to 0.28 Å shorter than the corresponding distance in the solid at the melting point and, in fact, is somewhat shorter than that in the solids at room temperature.

The breadth of the first peak shows that ion pairs are to be found significantly closer (and also more widely separated) than the most frequent separation. The "shortest distances" are comparable to those found in the monomeric vapor molecules. In TABLE 3, these gas distances[19-21] are compared with the distances read from the leading edge of the first RDF peaks at one quarter maximum height.

The numbers of neighbors, as derived from the peak areas, are also subject to considerable uncertainty because of the impossibility of establishing a unique resolution from longer interactions. It is striking, however, that these "coordination numbers" are relatively low, ranging from about 3.5 to 5.6 as compared with 6 or 8 in crystals.

TABLE 2

CATION-ANION DISTANCES AND COORDINATION IN MOLTEN AND CRYSTALLINE SALTS

	Liquid			Solid*		
	Distance (Å)	No.	Method†	m.p. Distance (Å)	No.	Room temp. Distance (Å)
LiCl	2.47	4.0	*X*	2.66	6	2.57
	2.45	3.5	*N*			
LiBr	2.68	5.2	*X*	2.85	6	2.75
LiI	2.85	5.6	*X*	3.12	6	3.00
NaI	3.15	4.0	*X*	3.35	6	3.23
KCl	3.10	3.7	*X*	3.26	6	3.14
	3.10	3.5	*N*			
CsCl	3.53	4.6	*X*	3.57	6	(3.47)
				(3.70)	8	3.57
CsBr	3.55	4.6	*X*	(3.72)	(6)	(3.62)
	3.55	4.7	*N*	3.86	8	3.71
CsI	3.85	4.5	*X*	(3.94)	(6)	(3.83)
				4.08	8	3.95

* Values for metastable forms (parentheses) were calculated from molar volumes estimated by Johnson *et al.*[18]

† *X* represents X-ray diffraction; *N*, neutron diffraction.

TABLE 3

COMPARISON OF SHORT CATION-ANION DISTANCES IN MOLTEN SALTS, WITH CORRESPONDING DISTANCES IN GASES

Distance	Liquid (Å)*	Gas (Å)†
Li-I	2.48	2.39
Na-I	2.70	2.71
K-Cl	2.69	2.67
Cs-Cl	3.03	2.91
Cs-Br	3.14	3.07
Cs-I	3.35	3.32

* Obtained arbitrarily from the value of r at one quarter peak maximum.

† Obtained from microwave results.[19-21]

The Second Interaction

The second interaction peak is usually less well defined than the first. It is most prominent in LiI, most obscure in CsI; this variation is, at least partly, a consequence of the relative magnitudes of the scattering factors. TABLE 4 lists the most frequent distances for this interaction, and the coordination numbers based on areas interpreted as composite M^+-M^+ and X^--X^- interactions. It will be seen that these distances are comparable to and usually somewhat greater than the corresponding distances in the solid at the melting point. Again the great breadth, particularly to the long-distance side, shows that a great variety of individual configurations occurs. The estimated numbers of neighbors vary from 7 to 12; however, it should be remembered that these occur over a band nearly 2 Å wide and that, for this reason, great caution is required in their interpretation.

TABLE 4

ANION-ANION OR CATION-CATION DISTANCES AND COORDINATION IN MOLTEN AND CRYSTALLINE SALTS

	Liquid			Solid* (m.p.)	
	Distance (Å)	No.	Method†	Distance (Å)	No.
LiCl	3.85	12.0	*X*	3.76	12
	3.80	8.3	*N*		
LiBr	4.12	12.8	*X*	4.03	12
LiI	4.45	11.3	*X*	4.41	12
NaI	4.80	8.9	*X*	4.74	12
KCl	—	<12	*X*	4.61	12
	~4.7	7.4	*N*		
CsCl	4.87	7.1	*X*	5.05	12
				(4.27)	(6)
CsBr	~5.4	8.3	*X*	(5.26)	(12)
	~5.2	7.9	*N*	4.46	6
CsI	~5.5	7.2	*X*	(5.57)	(12)
				4.72	6

* Values for metastable forms (parentheses) are those estimated by Johnson *et al.*[18]

† *X* represents X-ray diffraction; *N*, neutron diffraction.

Longer Interactions

All the radial distribution curves show continued fluctuations at distances beyond the second peak. Since these are most prominent in the lithium salts, where the greatest distinction in scattering factors exists, some degree of charge-ordering extending to 10 Å and beyond is suggested. The RDF for Li^{7}Cl, based on neutron diffraction, also shows these long-range fluctuations in a striking manner. However, since errors in the Fourier analysis may be expected to become important at longer distances, no detailed consideration of these fluctuations is attempted.

COMPARISON OF X-RAY AND NEUTRON RESULTS

Although the interpretation of the neutron data involves uncertainties inherent in the static approximation, it seems likely that the main features of the neutron RDFs are valid. It has already been pointed out that the first peak of Li^7Cl confirms that this is an interaction of type M^+X^- and implies the validity of this interpretation in the other systems. The agreement between neutron and X-ray methods as to distances and neighbor numbers is also considered to be satisfactory. Although, in principle, it may be possible to combine the two results to obtain a more detailed resolution of the various interactions in LiCl, in view of the uncertainties no such attempt has been made.

Neutron measurements are also presented for CsBr. In this case it happens that the ratio

$$f_{Cs}f_{Br}/(f_{Cs}^2 + f_{Br}^2)$$

has very nearly the same value for neutrons and X rays, so that for CsBr no distinction between M^+-X^- and composite M^+-M^+, X^--X^- interactions can be made by comparing the two measurements. The striking similarity shown in FIGURES 6 and 7 of the X-ray and neutron RDF curves for CsBr arises from the equality of these ratios and, incidentally, lends credence to the neutron results. By use of the neutron X-ray comparison, however, it is possible to distinguish Cs^+-Cs^+ from Br^--Br^- interactions, since Br^- is the stronger scatterer for neutrons and Cs^+ the stronger for X rays. Thus, a Cs^+-Cs^+ peak should be enlarged in the X-ray curve as compared with the neutron curve, while the reverse should occur for a Br^--Br^- peak. Examination of the details of the second peaks from this point of view suggests that the Cs^+-Cs^+ interaction may tend to occur at a shorter separation (∼4.7 Å) than does the Br^--Br^- interaction (∼5 Å); however, the effect is quite small.

Comparison of neutron and X-ray distributions for molten KCl also shows good agreement between the two methods. In this case, the Cl^--Cl^- interaction for neutrons is more important than K^+-K^+. However, little new information appears to be available.

COMPARISON WITH PREVIOUS RESULTS

X-ray studies of two of the salts studied by us, LiCl and KCl, have been reported by other investigators, Lark-Horovitz and Miller[1] and Zarzycki.[5] Both former studies are based on photographically recorded intensity data.

The RDF resulting from the Lark-Horovitz and Miller study of LiCl is so badly perturbed by false detail (peaks in the RDF at distances less than 2 Å) as to obscure the observation of a Li-Cl interaction. The second peak corresponding to Cl-Cl (and Li-Li) interactions, however, is in good general agreement with that of the present study, both as to number and distance. The curve resulting from the Zarzycki study is in good agreement with ours over both interaction peaks.

In the case of KCl, comparison with the earlier studies discloses some nonconcordance. Here the only well-defined feature of the RDF is that corresponding to the K-Cl interaction. The previous studies yielded a number of first-coordination neighbors of 5.8 and 5.2, respectively, contrasting with our result of 3.7. In the Zarzycki study, a part of the discrepancy appears to arise from a numerical error in evaluating the average distribution curve, $4\pi\rho_0 r^2$, which forms an additive component of the complete RDF. Re-evaluation of Zarzycki's data with this error corrected yields 4.5 for this number. In addition, our study yields a smaller value for the most frequent K-Cl interaction distance: 3.10 Å as compared with 3.14 Å (3.20 Å in our re-evaluation of Zarzycki's data). The reason for these remaining discrepancies remains obscure; we feel, however, that they are well beyond the experimental error associated with the present study.

THE STRUCTURE OF THE MOLTEN ALKALI HALIDES

A question often raised in connection with the structure of liquids is the extent to which a liquid, on the scale of a few atomic diameters, is like that of the solid material. Some aspects of this question to which the present study may contribute information are the interatomic distances and their distribution, and the average coordination. We shall discuss these aspects separately.

Interatomic Distances

The interatomic distances most frequently occurring in the structure, as indicated by the RDF, are by and large similar to those found in the corresponding solids. Close comparison indicates, however, that the most frequent interatomic M^+X^- approach is always somewhat shorter than that found in the solid at the melting temperature and, in fact, is close to the sum of commonly tabulated ionic radii. The most frequent M^+-M^+ and X^--X^- approach, on the other hand, is nearly always larger than that found in the solid. These observations indicate that a representative configuration in the molten salts involves, in comparison with the solid, a collapsed array of anions about cations (or vice versa), but an expanded array of anions about anions.

Distribution of Distances

The appearance of broad peaks in the RDF curves indicates that interatomic distances in the liquid are distributed correspondingly. The distribution of distances in the first peaks has been shown to extend downward to values comparable to those in the gas molecules, some 0.5 Å shorter than the most frequent distances. On the long-distance side, the distribution must extend over a similar range. In the second peaks, even broader distributions of distances are indicated. In contrast, in a crystal, an interatomic-distance spectrum covering even a few tenths of an Angstrom unit implies very large amplitudes of thermal vibration, or even disorder.

It is clear, therefore, that with respect to homogeneity of interatomic distance crystals and melts are quite unlike.

Average Coordination

Without exception, the first peak areas indicate that the average *M*-*X* coordination is significantly less than 6, the coordination occurring in the typical solid structure. The average second coordination is much less well estimated because of limited resolution of the second peaks, but generous assignment of areas results in values roughly between 7 and 12, as compared with 12 in the typical solid. In this connection it seems significant that in the lithium halides, in which the best resolution of the second peak occurs, the values are the largest.

The foregoing discussion of the interatomic distances and average coordination does not suggest a pseudocrystalline model for molten salts. In contrast, the evidence indicates a considerable degree of inhomogeneity to be the most significant characteristic of these systems. That is to say, there appears to be no simple equivalent of a characteristic coordination polyhedron that can describe the microstructure of the melt. Rather, it appears that a broad spectrum of ion clusters occurs, in which ions tend to approach to a "contact" distance, and which does not have a fixed value as in a crystalline structure. An engaging idea is the supposition that the less frequently occurring distances occur in clusters of only a few ions, the small values describing short distances within the small cluster and the large ones the distances from one such cluster to other ions in its neighborhood.

Within this inhomogeneity, suggested as the most characteristic feature of molten salt structures, it is possible to point to certain regularities. Thus, in the lithium halides, where the cation-to-anion size ratio is smallest, the greatest homogeneity in *X*-*X* distance spectrum and the most pronounced suggestion of longer range order appear. In these systems also, and especially in LiI, the largest *M*-*X* coordination numbers are suggested. On the other hand, in systems in which the cation-anion size ratio is larger, specifically KCl, CsBr, and CsI, there is the least suggestion of long-range structure, the *X*-*X* distance spectrum is least well defined, and the *M*-*X* coordination number is smallest. These features are consistent with a tendency toward regularity of packing of large anions within which small cations such as Li^+ may fit; when larger cations are introduced, this regularity of packing is destroyed.

The data of TABLE 2 suggest that the first coordination tends to be high for the cesium salts as well as the lithium salts. This behavior, although not to be considered firmly established, is reminiscent of the solids, in which the cesium salts assume the CsI-type structure with coordination number 8 and simple cubic arrangement of anions, as compared with the usual 6, with face-centered anions.

There can be no doubt also, as emphasized by Zarzycki,[5] that the structures are to be described as decidedly open in nature, signifying that there is considerable unoccupied volume surrounded by ions in near contact. We do not feel it appropriate at this time, however, to describe the "openness" in terms of holes, fissures, or interstices between compact islands, for these concepts imply a degree of homogeneity in the microstructure that we believe not to be present.

SUMMARY

Eight molten alkali halide salts have been studied by X-ray diffraction, and 3 of them also by neutron diffraction. Radial distribution functions clearly show the first 2 coordination shells, although not completely resolved. The first shell is a band of about 0.5 Å half-width, with the most frequent interatomic distance being smaller than that in the solid at room temperature. It corresponds to an average coordination of about 4 to 5 neighboring ions. Neutron patterns confirm that the first coordination shell involves unlike ions. The second shell, which corresponds to 7 or more ion neighbors, is less well defined. This information, together with the density decrease on melting, indicates that the melts have quite open structures with a wide variety of individual ion coordinations.

ACKNOWLEDGMENT

The work described in this paper owes much to P. C. Sharrah, who helped with the design of the X-ray spectrometer and the neutron furnace, and with some of the early collection of data. His assistance is gratefully acknowledged.

REFERENCES

1. LARK-HOROVITZ, K. & E. P. MILLER. 1937. Phys. Rev. **51:** 61.
2. MILLER, E. P. 1936. X-Ray Scattering from Liquids. Dissertation. Purdue Univ. Layfayette, Ind.
3. ZARZYCKI, J. 1957. Compt. rend. **244:** 758.
4. ZARZYCKI, J. 1957. J. phys. radium (Suppl. Phys. Appl.). **18:** 65A.
5. ZARZYCKI, J. 1958. J. phys. radium (Suppl. Phys. Appl.). **19:** 13A.
6. ZARZYCKI, J. 1957. Verres et réfractaires. **11:** 3.
7. DANILOV, V. I. & S. I. KRASNITSKII. 1955. Akad. Nauk SSSR, Doklady. **101:** 661.
8. AGRON, P. A., M. D. DANFORD, M. A. BREDIG, H. A. LEVY & P. C. SHARRAH. 1957. Acta Cryst. **10:** 739.
9. DAUBEN, C. H. & D. H. TEMPLETON. 1955. Acta Cryst. **8:** 841.
10. KROGH-MOE, J. 1956. Acta Cryst. **9:** 951.
11. NORMAN, N. 1957. Acta Cryst. **10:** 370.
12. SHARRAH, P. C. & G. P. SMITH. 1953. J. Chem. Phys. **21:** 228.
13. HUGHES, D. J. & J. A. HARVEY. 1955. Neutron Cross Sections. Brookhaven Natl. Lab. (BNL-325).
14. PLACZEK, G. 1952. Phys. Rev. **86:** 377.
15. WICK, G. C. 1954. Phys. Rev. **94:** 1228.
16. VINEYARD, G. H. 1958. Phys. Rev. **110:** 999.
17. WASER, J. & V. SCHOMAKER. 1953. Rev. Mod. Phys. **25:** 671.
18. JOHNSON, J. W., P. A. AGRON & M. A. BREDIG. 1955. J. Am. Chem. Soc. **77:** 2734.
19. HONIG, A., M. L. STITCH & M. MANDEL. 1953. Phys. Rev. **92:** 901.
20. LEE, C. A., B. P. FABRICAND, R. O. CARLSON & I. I. RABI. 1953. Phys. Rev. **91:** 1395.
21. HONIG, A., M. MANDEL, M. L. STITCH & C. H. TOWNES. 1954. Phys. Rev. **96:** 629.

PARTITION FUNCTIONS FOR NORMAL LIQUIDS AND MOLTEN SALTS

G. E. Blomgren
Research Laboratories, National Carbon Company Division of Union Carbide Corporation, Cleveland, Ohio

Introduction

The problem of describing a liquid system by means of statistical mechanics is a formidable one to which there have been many approaches, involving various degrees of abstraction. Among these may be mentioned the distribution function calculations by Born and Green[1] and of Kirkwood[2] and his collaborators, the cell theory of Lennard-Jones and Devonshire,[3] the hole theory,[4] and the theory of significant structures of Eyring and his collaborators.[5]

If the distribution function (the probability of finding a molecule at a distance r from any given molecule, as a function of r) for a liquid system could be calculated exactly, a basis would exist for calculating all thermodynamic as well as physical properties of the system. In principle, this can be done if the physical requirement of additivity of intermolecular forces is fulfilled. In practice, however, the calculation cannot be made without using extreme mathematical approximations and, even then, computation is very difficult and tedious. An advantage in this method is the fact that the approximations are mathematical rather than physical and may be evaluated mathematically rather than intuitively, but this in itself is very difficult and has not been done. The agreement with experiments is not good, but the fact that no adjustable parameters are used and a purely statistical approach is made recommend this theory.

The cell theory of liquids uses a physical model of a molecule confined within a spherical cell, the boundaries of which are formed by neighboring molecules that take all possible orientations on the sphere. Thus, by considering nearest-neighbor interactions only and averaging over orientations, the average potential energy of the molecule in the cell may be calculated as a function of the distance from the center of the cell. This in turn allows calculation of the classic phase integral and, thus, the partition function of the liquid. The phase integral is evaluated numerically. Here the approximations are physical, but they have been related[6] to the statistical model of Kirkwood and have been assessed. Agreement with experiment is good for certain quantities and poor for others, but general agreement indicates that the physical model is certainly nearly correct.

The hole theory has been shown to be a first approximation to the cell theory.[7] Here each molecule is presumed trapped in a spherical potential well having a flat bottom. Vacancies are also presumed to be present in this array of trapped molecules, but these are not taken into account specifically in the partition function. The vacancies, however, play a central role in the absolute-rate theory treatment of transport processes.[8]

The theory of significant structures considers the liquid phase at equilibrium to be made up of molecules that can undergo at least two different sorts of motion. One type of motion, called solidlike, is that of a bound oscillator. The other sort, called gaslike, is that of a particle in a constant potential free to move in the excess volume gained on melting: that is, in the vacancy space. The *ad hoc* assumption is made that the number of solidlike particles N_s is given by the expression

$$N_s = N\frac{V_s}{V}$$

where N is Avogadro's number, V_s is the volume of the solid at the melting point, and V is the equilibrium volume of the liquid at the temperature considered. The number of gaslike particles N_g is then given by the condition $N = N_s + N_g$ or

$$N_g = N\left(\frac{V - V_s}{V}\right)$$

Also, the assumption is made that the solidlike particles adjacent to vacancies can take additional equilibrium positions. This requires a weighting factor g_s for the solidlike particles, which is given the empirical form

$$g_s = \left(1 + n\frac{V - V_s}{V_s}\exp\frac{-aE_sV_s}{(V - V_s)RT}\right)$$

where E_s is the potential energy of the solid at the melting point and n and a are adjustable parameters. One further assumption is that the potential energy of the liquid is given by the expression

$$E_l = E_s\frac{V_s}{V}$$

The partition function is then written

$$f = \left[\frac{1 + n\dfrac{V - V_s}{V_s}\exp\dfrac{-aE_sV_s}{(V - V_s)RT}}{(1 - e^{-\theta/T})^3}\right]^{NV_s/V} \times \left[\left(\frac{2\pi mkT}{h^2}\right)^{3/2}\frac{eV}{N}\right]^{N(V-V_s)/V}\exp\frac{NE_sV_s}{VRT}$$

where θ is the characteristic temperature of an Einstein solid at the melting point and the other symbols have their usual meanings. The parameters are chosen to give agreement with two properties of the liquid at the melting point, and the rest of the properties follow from the partition function and give excellent agreement with results of experiments. Unfortunately, it is not possible to test the assumptions made, especially with regard to the theories discussed earlier; therefore, this expression must be regarded as largely empirical. However, it is an expression that should be useful in application to the absolute-rate theory of transport properties, and one that should also be susceptible of extension to the case of molten salts. These applications are made below.

Application of the Partition Function to Transport Properties

The absolute-rate theory has been applied to the problem of viscosity[8] and gives the result that the viscosity, η, is

$$\eta = \frac{hN}{6V}\frac{f}{f^{\pm}}\, e^{E_0/RT}$$

where f is the partition function of a molecule at equilibrium, $f^{\pm}$ is the partition function of the "activated complex" or a molecule at the top of the barrier to viscous flow, and E_0 is the height of the barrier with respect to the potential energy of a molecule at equilibrium. The factor 6 is a modification made by Li and Chang[9] of the original expression of Eyring, and is necessary to take into account relative motion of the layers of liquid. The quantity $f^{\pm}$, through the formulation of absolute-rate theory, has lost one degree of translational freedom: that along the "reaction coordinate."

If we wish to use the partition function from the theory of significant structures, it is necessary to decide what the partition function of the activated complex should be. A natural assumption would be that a solidlike molecule would lose a degree of oscillation to the reaction coordinate, and that a gaslike molecule would lose a degree of translation. An average molecule, then, described by the partition function for N molecules to the $1/N$ power, may be presumed to lose a fraction of an oscillation equal to the fraction of solidlike particles and a fraction of a translation equal to the fraction of gaslike particles. We could then write the partition function for the activated complex as

$$f^{\pm} = \left[\frac{1 + n\dfrac{V - V_s}{V_s}\exp\dfrac{-aE_sV_s}{(V - V_s)RT}}{(1 - e^{-\theta/T})^3}\right]^{2V_s/3V} \cdot \left[\left(\frac{2\pi mkT}{h^2}\right)^{3/2}\frac{eV}{N}\right]^{2(V-V_s)/3V}$$

where we now omit the potential energy term, as it is to be included in the activation energy for flow. The expression for the viscosity is then given fairly simply by

$$\eta = \frac{hN}{6V}\left[\frac{1 + n\dfrac{V - V_s}{V_s}\exp\dfrac{-aE_sV_s}{(V - V_s)RT}}{(1 - e^{-\theta/T})^3}\right]^{V_s/3V} \times \left[\left(\frac{2\pi mkT}{h^2}\right)^{3/2}\frac{eV}{N}\right]^{V-V_s/3V} e^{E_0/RT}$$

where E_0 is the activation energy for flow. Since the potential energy for the liquid has been assumed to vary inversely with the volume, the activation energy will be assumed to have a similar nature; that is,

$$E_0 = E\frac{V_s}{V}$$

where E is a parameter to be determined by experiment.

Eyring (private communication) has determined the parameters n and a at equilibrium for liquid argon, and the viscosity is known[10] from the melting point almost to the critical point. Eyring has also determined n and a for liquid methane and nitrogen and the viscosity is again known for almost the entire liquid range.[11,12] The parameters used for calculating the viscosities of these three liquids are summarized in TABLE 1. In the case of nitrogen and methane, the internal vibrational degrees and the presumed rotational degrees are considered to be unaffected by flow and so do not contribute to the expression. The activation energy E was determined from one point on the experimental η versus T curve near the melting point. The results for argon, methane, and nitrogen are shown in FIGURES 1, 2, and 3. As can be seen, the calculation for argon agrees very well with experiment. For methane and nitrogen the calculated results are somewhat lower than the experimental values at high temperatures. This may be due to an inadequate description of the rotation in the solidlike positions (which would be reflected in the parameters θ, n, and a), to a change in the factor 6 introduced by Li and Chang, or to a contribution of rotation to the viscosity at high temperatures. In conclusion, the generally gratifying agreement of the theory with experiment validates the absolute-rate theory mechanism for viscosity, and a method is now provided for accurate prediction of viscosity as a function of temperature from the properties of the equilibrium state.

TABLE 1
PARAMETERS FOR CALCULATION OF VISCOSITY OF LIQUID ARGON, METHANE, AND NITROGEN

	Argon	Methane	Nitrogen
Potential energy, E_s (cal.)	1888.6[5]	2200*	1529.9*
Solid volume, V_s (cc.)	24.98[5]	30.96[15]	29.31[18]
Einstein characteristic temperature	60.0[5]	75.33[16]	55.94*
a	0.00534*	0.00296*	0.0034*
n	10.8*	13.3*	12.9*
Liquid volume, V (cc.)	†	—[17]	—[17]
Activation energy, E (cal.)	690.1	737.8	562.9
Viscosity (experimental)	—[10]	—[11]	[11,12]

* Private communication from H. Eyring.
† International critical tables.

Extension of the Partition Function to Molten Salts

It is more difficult to describe a molten salt than a normal liquid, and only recently has an attempt been made to calculate the distribution function of such a system (private communication from J. G. Kirkwood). Numerical results have not, as yet, been obtained.

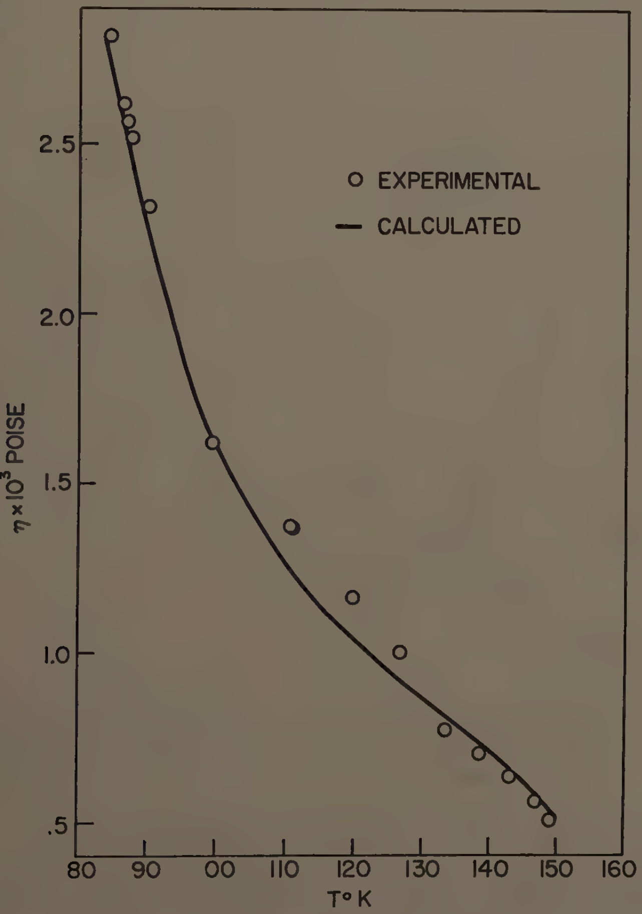

FIGURE 1. Viscosity (poise) as a function of temperature (°K) for liquid argon.

The most important point to be settled when a physical model is to be used, as with the cell model or the theory of significant structures, is the effect on the partition function of the coulomb forces. This problem has been solved for the case of the solid lattice by Born and his co-workers,[13] but it remains a difficult problem for a disordered liquid. In the theory of significant structures, it is presumed that the effect of the coulomb forces is shown explicitly only in the potential energy, as in the solid case, and that the rest of the partition function is the same as that for a normal liquid, account being taken of the different kinds of particles. The potential energy is then taken to be in two parts, a coulomb part and a noncoulomb part. The noncoulomb part will be expected to vary with the volume in the same way that a rare gas does; that is, as V_s/V. The coulomb part will be assumed to vary with volume in the same way as the solid; that is, as $(V_s/V)^{1/3}$. The potential energy can then be written as

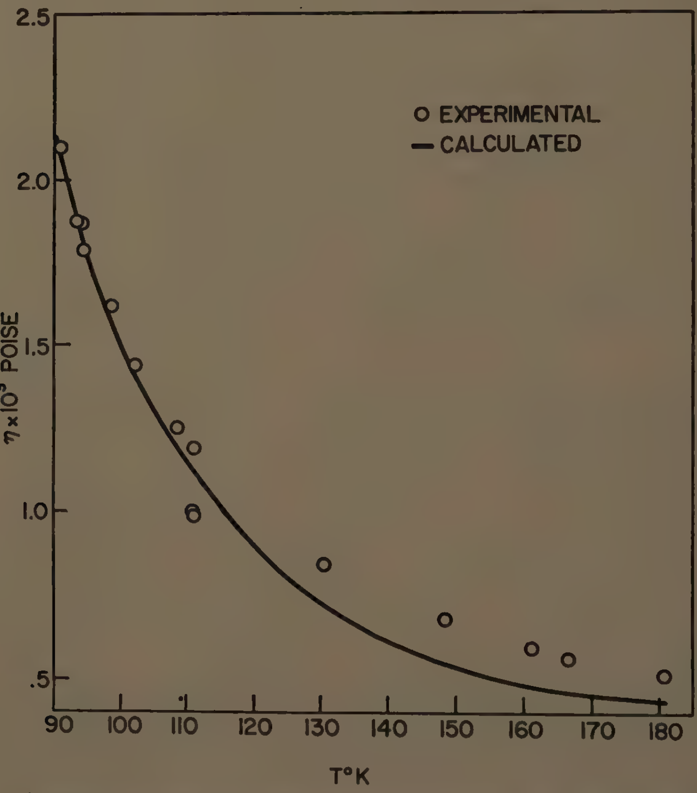

FIGURE 2. Viscosity (poise) as a function of temperature (°K) for liquid methane.

$$E_l = E_1\left(\frac{V_s}{V}\right)^{1/3} + E_2\left(\frac{V_s}{V}\right)$$

The term E_2, in the case of KCl, can be taken to be the same as E_s for liquid argon, or about 2000 cal./mole. The term E_1, however, cannot be taken simply as the coulomb part for the potential energy of the solid, because the long-range order is destroyed and also because the coordination number of the liquid is reduced for the first coordination number from 6 to 4. If the ratio of the first coordination numbers (4/6) for liquid to solid is arbitrarily taken to be a sort of average effect on the Madelung constant of the solid resulting from fusion, the coulomb part E_1 can be obtained from the coulomb part of the solid lattice energy at the melting point $E_{s,\text{coulomb}}$ by

$$E_1 = \frac{2}{3} E_{s,\text{coulomb}}$$

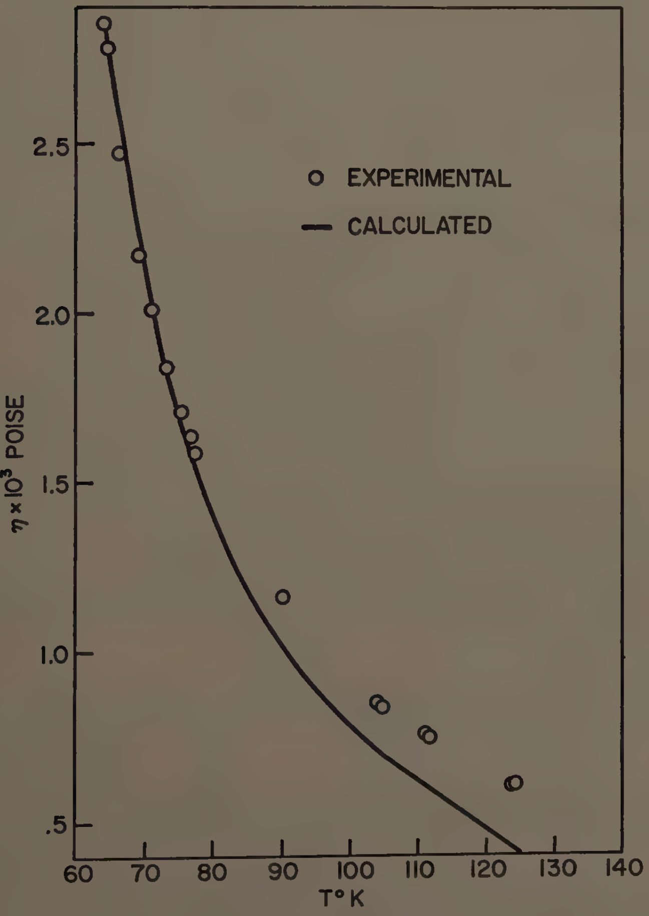

FIGURE 3. Viscosity (poise) as a function of temperature (°K) for liquid nitrogen.

The partition function can now be written as

$$f = \left[\frac{1 + n \dfrac{V - V_s}{V_s} \exp \dfrac{-a(E_1 + E_2)V_s}{(V - V_s)RT}}{(1 - e^{-\theta/T})^3} \right]^{2NV_s/V} \left\{ \left[\left(\frac{2\pi m_1 kT}{h^2} \right)^{3/2} \frac{eV}{N} \right] \cdot \left[\left(\frac{2\pi m_2 kT}{h^2} \right)^{3/2} \frac{eV}{N} \right] \right\}^{N(V-V_s)/V} \exp N \left[E_1 \left(\frac{V_s}{V} \right)^{1/3} + E_2 \left(\frac{V_s}{V} \right) \right]$$

Here, the energy in the exponential part of the weighting factor is taken as $E_1 + E_2$, but the presence of the adjustable parameter a allows this choice to be made arbitrarily. The masses of the two different ions are m_1 and m_2.

TABLE 2
PARAMETERS FOR CALCULATION OF MOLAR VOLUME OF MOLTEN KCl

Einstein characteristic temperature	172.5[7]
Solid volume (cc.)	40.43[19]
Liquid volume[14]	
Entropy of fusion (eu)	5.8*
Calculated values E_1 (cal.)	105,000
E_2 (cal.)	2,000
n	4.9
a	0.005

* Circular 500 (1952) of the National Bureau of Standards, Washington, D.C.

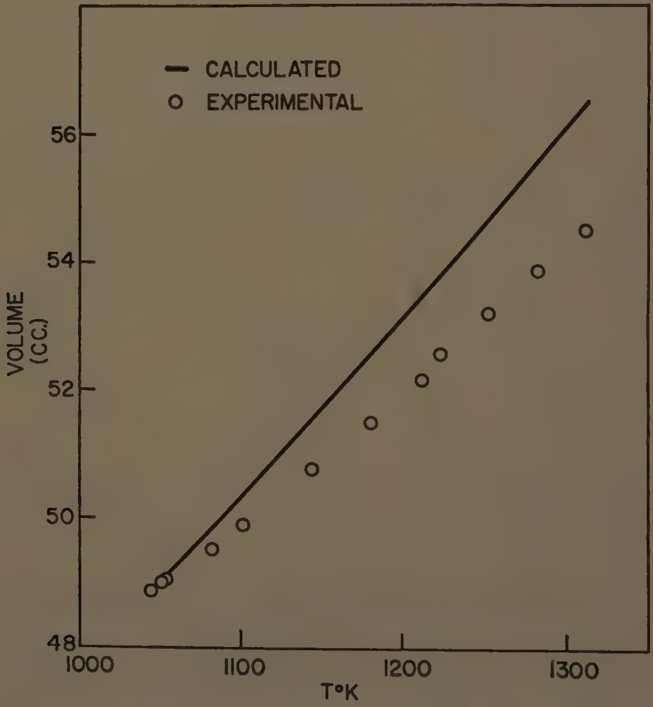

FIGURE 4. Molar volume (cubic centimeters per mole) as a function of temperature for molten KCl.

A trial calculation has been made on the molar volume as a function of temperature for KCl. The parameters n and a were chosen to give the entropy of melting and the volume of the liquid at the melting point. The volume was found from the minimum in a plot of the Helmholtz free energy versus the volume. The necessary data for the calculation are summarized in TABLE 2. The results are shown in FIGURE 4 together with experimental values.[15] As may be seen, the results deviate from the experimental values, but by only about 4 per cent in the high-temperature region. It would be expected that the thermodynamic properties would agree somewhat better.

It is felt that a promising approach has been made toward deriving a semiempirical partition function for molten salts. It is hoped that this partition function will prove applicable to a wide variety of salts and to many basic properties of salts. It is also anticipated that the theory of transport properties in the section *Application of the Partition Function to Transport Properties* will also be capable of being extended to molten salts.

Conclusions

The partition function for liquids, developed by Eyring *et al.*,[5] has been applied to the absolute-rate theory expression for viscosity[8] for liquid argon, methane, and nitrogen with very satisfactory results. It is held that the agreement obtained lends support to the validity of the mechanism for viscosity. The partition function has also been extended to the case of molten salts, and reasonable agreement with experiment is obtained for the molar volume of molten KCl.

Acknowledgments

I acknowledge stimulating discussions with H. Eyring of the University of Utah, Salt Lake City, Utah, and J. G. Kirkwood of Yale University, New Haven, Conn., and also the aid and encouragement of E. R. Van Artsdalen of the National Carbon Company research laboratories.

References

1. Born, M. & H. A. Green. 1946. Proc. Roy. Soc. London. **A188:** 10.
2. Kirkwood, J. G. 1955. J. Chem. Phys. **3:** 300.
3a. Lennard-Jones, J. E. & A. F. Devonshire. 1937. Proc. Roy. Soc. London. **A163:** 53.
3b. Lennard-Jones, J. E. 1938. *Ibid.* **165:** 1.
4. Eyring, H. & J. O. Hirschfelder. 1937. J. Phys. Chem. **41:** 249.
5. Eyring, H., T. Ree & N. Hirai. 1958. Proc. Natl. Acad. Sci. U. S. **44:** 683.
6. Kirkwood, J. G. 1950. J. Chem. Phys. **18:** 380.
7. Fowler, R. & E. A. Guggenheim. 1952. Statistical Thermodynamics. Cambridge Univ. Press. London, England.
8. Glasstone, S., K. J. Laidler & H. Eyring. 1941. The Theory of Rate Processes. McGraw-Hill. New York, N.Y.
9. Li, J. C. M. & P. Chang. 1955. J. Chem. Phys. **23:** 518.
10. Zhdanova, N. F. 1957. J. Exptl. Theoret. Phys. (USSR). **4:** 749.
11. Gerf, A. F. & G. I. Galkov. 1940. J. Tech. Phys. (USSR). **10:** 725; 1941. *Ibid.* **11:** 801.
12. Rudenko, N. S. 1939. J. Exptl. Theoret. Phys. (USSR). **9:** 1078.
13. Born, M. 1923. Atom theorie des festen Zustandes. Teubner. Leipzig, Germany.
14. Van Artsdalen, E. R. & I. S. Yaffe. 1955. J. Phys. Chem. **59:** 118.
15. Sackmann, H. & F. Sauerwald. 1950. Z. Physik. Chem. **195:** 295.
16. Storch, H. H. 1931. J. Am. Chem. Soc. **53:** 1266.
17. Landolt-Bornstein. Physikalische Chemische Tabellen. 5th ed.
18. Simon, F., M. Rubemann & W. Edwards. 1930. Z. Physik. Chem. **B6:** 331.
19. Landon, G. J. & A. R. Ubbelohde. 1956. Trans. Faraday Soc. **52:** 647.

STRUCTURE OF MOLTEN MERCURIC HALIDES

George J. Janz and James D. E. McIntyre
Department of Chemistry, Rensselaer Polytechnic Institute, Troy, N.Y.

Introduction

Knowledge of the nature of the structural units in molten salts and of the intensity of the force fields and energy barriers between them is fundamental to an understanding of the physical properties and behavior of these systems. Melts of salts having a strong covalent component of bonding are particularly suited for the study of the conditions necessary to form associated groups (complex ions, molecules). In contrast to salt systems predominantly ionic in character, these have received relatively little attention. Compounds such as the mercuric and cadmium halides fall in this class, their melts being characterized by values of electric conductivity intermediate between those of highly ionic melts ($\Lambda \sim 100$) and those of nonconducting liquids.

The constitution of the melt does not depend solely upon the crystal lattice structure of the solid salt. Low conductivity generally implies a high degree of covalency in the melt (with structural units either finite molecules or polymeric molecular species), but does not necessarily imply the existence of molecules in the crystal. The process of fusion may cause fundamental changes in bonding. Although the lattice types of the salts may be alike, the bonds between the individual atoms are able to exhibit appreciable differences with respect to their polarity and polarizability.[1] At the disintegration of the lattice during fusion, these differences come into effect. Whether ions or molecules predominate in the melt depends upon whether the decrease in free energy of the system is greater on solvation of molecules or on solvation of ions. Only in the extreme case, where the bonds in the molecules are slightly polar and slightly polarizable, is the molecule preserved in interaction with its like, whether in the lattice, in solution, or in the melt. Such is known to be the case for the mercuric halides, HgX_2($X{=}Cl$, Br, I) in the solid and gaseous states. This paper reports the results of investigations in progress on the structure and constitution of the mercuric halides in the molten state. Considered are the physical properties and the conditions necessary to form associated groups (complex ions, molecules), with particular reference to mercuric bromide.

Experimental

Electric conductance. Precise measurement of the conductivity of mercuric halide melts requires the use of conductance cells of low cell constant. The cells used for the conductivity measurements were constructed of Pyrex glass and were sealed off after introduction of the salts. Circular grey platinum disks of 1-cm. diameter served as electrodes. The cells were calibrated at 25° C. with a standard aqueous KCl solution, about 0.01 demal. Temperature corrections are of the order of 1 per cent at 250° C., but have not been applied.

The salts used were of reagent quality. They were initially dried with a stream of dry argon or nitrogen for 10 hours and were then further purified by vacuum sublimation from the melt.

Conductivities were measured at a series of temperatures between the melting and boiling points of the salts. The melts were brought to constant temperature in an electric resistance furnace before making resistance measurements. By adjustment of shunt resistors in parallel with the furnace windings the temperature gradient of the melt was reduced to 0.2° C. Melt temperatures were measured with a platinum-platinum-10 per cent rhodium thermocouple. Conductivities were measured with increasing and decreasing temperature in order to detect possible decomposition at higher temperatures. The measurements were made with a conductance bridge* designed in this laboratory and employing an impedance comparator† as a variable frequency source and null detector.

TABLE 1
ELECTRIC CONDUCTIVITY, VISCOSITY, AND DENSITY OF MOLTEN MERCURIC BROMIDE

T (°C.)	T (°K)	d (gm.·cm.$^{-3}$)	κ (ohm^{-1}·cm.$^{-1}$)	μ (ohm^{-1}·cm.^{2}·mole^{-1})	η (cp.)	$\mathfrak{k}$ (ohm^{-1}·cm.^{2}·cp.·mole^{-1})
240	513.2	5.116	1.42×10^{-4}	1.00×10^{-2}	(2.52)	2.52×10^{-2}
250	523.2	5.082	1.59×10^{-4}	1.13×10^{-2}	2.29	2.59×10^{-2}
260	533.2	5.048	1.76×10^{-4}	1.23×10^{-2}	2.09	2.57×10^{-2}
270	543.2	5.015	1.94×10^{-4}	1.40×10^{-2}	1.92	2.69×10^{-2}
280	553.2	4.981	2.12×10^{-4}	1.54×10^{-2}	1.76	2.71×10^{-2}
290	563.2	4.947	2.30×10^{-4}	1.69×10^{-2}	(1.63)	2.75×10^{-2}
300	573.2	4.913	2.49×10^{-4}	1.88×10^{-2}	(1.50)	2.82×10^{-2}
310	583.2	4.880	2.69×10^{-4}	1.98×10^{-2}	(1.39)	2.75×10^{-2}
320	593.2	4.846	3.17×10^{-4}	2.12×10^{-2}	(1.29)	2.73×10^{-2}

The specific conductivities, κ (mho·cm.$^{-1}$), of mercuric bromide melts at a series of temperatures between the freezing and the boiling points of the salt are shown in TABLE 1. The molar conductivities, μ, were calculated using the density data of Prideaux.[2] The reduced conductivities, $\mathfrak{k} = \mu\eta$, were calculated with the aid of viscosity values extrapolated from the data of Jander and Brodersen.[3a] The data are in excellent agreement with the values given by Jander and Brodersen[3b] at 242° C., but depart considerably from those of Belyaev and Mironov,[4] particularly at higher temperatures. This is probably an indication of a higher degree of purity of the salt used in the present work. The energies of activation for the process of electric conductance and viscous flow, calculated in the conventional manner from graphs of these data against $1/T(°K)$, are thus found to be 6.2 and 5.1 kcal./mole, respectively, in the region of the melting point. In FIGURE 1 it may be seen that ΔE_μ is a monotonic decreasing function of temperature. Measurements are in progress for the chloride and iodide.

---

* Described in an unpublished work by G. J. Janz and J. D. E. McIntyre.
† General Radio Co., Ridgefield, N.J., Type 1605-AS5.

Heat and entropy of fusion. The heat of fusion for pure mercuric bromide has been determined calorimetrically with an accuracy of ±2 per cent in this laboratory. This work will be described in detail in another

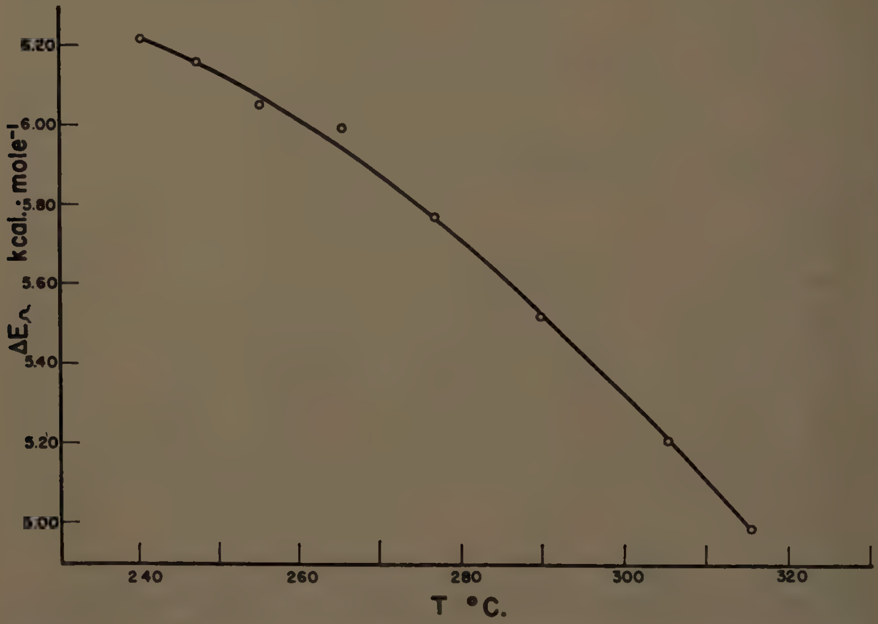

FIGURE 1. Activation energy for electric conductance in molten mercuric bromide.

work.* The values for the heat and entropy of fusion thus are 4.28 kcal./mole and 8.4 eu, respectively.

Discussion

Some of the physical properties and structural data for the mercuric halides are summarized in TABLES 2 and 3. Consideration of the information on the solid and gaseous states is of interest with reference to the physical structure and constitution of the molten salts.

Solid state. Mercuric fluoride has a distinct ionic structure and will not be considered in this discussion. The chloride, bromide, and iodide form molecular lattices, with the layer-type structure readily distinguished

---

* By G. J. Janz and J. Goodkin, *The Journal of Physical Chemistry.* In press.

TABLE 2

PHYSICAL PROPERTIES OF MERCURIC HALIDES

Solid state

Salt	T_f (°C.)	Lattice energy (kcal.·mole^{-1})	ΔH_f (cal.·mole^{-1})	ΔS_f (eu)	Density at 25° C. (gm.·cm.$^{-3}$)	Color
$HgCl_2$	277	608	4150	7.5	5.44	white
$HgBr_2$	238	604	4280	8.4	6.11	white
HgI_2	259	599	4500	8.6	6.27	red, yellow

Liquid state

Salt	T_b (°C.)	Viscosity (T_f°) cp.	ΔH_v (cal.·mole^{-1})	ΔS_v (eu)	Density (T_f°) (gm.·cm.$^{-3}$)	Color	Molar conductivity (ohm^{-1}·cm.^{2}) at T_f°	at T_b°
$HgCl_2$	304		13,900	24.1	4.41	colorless	0.0025	0.0069
$HgBr_2$	319	(2.52)	14,200	23.8	5.12	yellow	0.0098	0.0212
HgI_2	354	(0.64)	14,700	23.5	5.23	red	2.02	1.54

Gas state

Molecular species	Dissociation to Hg and X_2 (per cent) at 1000° C.
monomeric	3
monomeric	14
monomeric	—

TABLE 3

STRUCTURE OF MERCURIC HALIDES

Solid state

Salt	Structure type	Coordination	Internuclear distance Hg—X (A°)
HgF_2	fluorite	8	2.40(8)
$HgCl_2$	octahedral, distorted	6	2.25(2); 3.34(2); 3.63(2)
$HgBr_2$	octahedral, distorted	6	2.48(2); 3.23(4)
HgI_2 (red)	tetrahedral	4	2.78(4)
(yellow)	octahedral, distorted	6	2.78(2); 4.11(4)

Gas state

			(X—Hg—X) Bond properties Ionic character (per cent)	d (A°)	Force constant ($10^5 \cdot d$/cm.)
$HgCl_2$	linear	2	22	2.29	2.67
$HgBr_2$	linear	2	17	2.41	2.32
HgI_2	linear	2	11	2.59	1.81

for the latter two. The low melting points (TABLE 2) are to be associated with the crystal structures rather than directly with the nature of the Hg—X bond. Disintegration of the lattice at fusion results from the rupture of the weak cohesive bonds between the highly polymeric (HgX_2) layers and the secondary bonds among molecules arising from polarization of the halogen atoms. In addition to the two halogen atoms with which a mercury atom is covalently bonded to form a HgX_2 molecule, it is also secondarily bonded by its coulombic interaction with the free outer electrons of the four remaining halogen atoms in its coordination polyhedron.[1] As a result of these coulombic attractions from several directions, the outer electronic configuration of the halogen atoms tends partially to assume the spherical symmetry of the halide ion. This deformation of the primary Hg—X bond imparts a partial ionic character to the lattice structures. The degree of polarization is reflected by the melting points of the three halides. Thus, while the Hg—I bond is the most covalent in the gaseous state, the iodine atom is more polarizable than that of bromine and, as a result, mercuric iodide has a more ionic lattice and a higher melting point than mercuric bromide. Although the chlorine atom is the least polarizable, mercuric chloride has the highest melting point. This is probably due to the somewhat different packing of the atoms in the mercuric chloride lattice.

The structural data (TABLE 3) show clearly that in the lattices of the chloride, the bromide, and the yellow (high-temperature) form of the iodide, 2 of the 6 nearest neighbor halide atoms are closer than the other 4. The result in each case is a distorted octahedral arrangement in which individual HgX_2 molecules may be recognized in the lattice. The mercury and halogen atoms lie in layers in the sequence XHgXXHgX. The structure types and the stereochemical arrangement of the entities in these compounds are illustrated schematically in FIGURE 2 for the bromide and iodide, which have the same packing (*a*,*c*), and for the chloride (*b*,*d*). X-ray analyses of the chloride and bromide have shown[5,6] that the "molecules" have a linear configuration in the solid state.

Gas state. Vapor density measurements[7] have established the fact that the only species of importance below 1000° C. are the monomeric molecules, HgX_2 (TABLE 2). The configurations, internuclear distances, and force constants (TABLE 3) have been determined by spectroscopic studies.[7-12] The infrared studies[11,12] have shown clearly that the bond-bond interaction force constants in these molecules are small. From the force constants, it is readily estimated (as a first approximation) that the ratio of the bond dissociation energies $D(XHg—X)/D(Hg—X)$ is 0.8 for the chloride and 1.0 for the bromide and for the iodide. The ionic character for the Hg—X bond (TABLE 3) was estimated from electronegativities and the empirical equation of Hannay and Smyth.[13]

Liquid state. The relatively low melting and boiling points and related properties such as electric conductivities are understood if it is assumed that a high degree of covalency is retained in the molten state on fusion of the mercuric halides. The colors of the bromide and iodide melts are in accord with anion polarization[14] effects in such systems. An insight into the polar nature of the bonding in the liquid state can be gained from the spectroscopic frequency shifts between the gaseous and liquid states. With the mercuric halides, the differences in the Raman frequencies accompanying the change in state have been observed as quite marked[15] (for example, for $HgCl_2$ it is 11.6 per cent) in comparison with the hydrogen halides (for example, 3 per cent for HCl). The decrease in frequency in the molten state may be attributed in part either to coupling between molecules (an increase of the vibrating masses) or a diminution of the bonding forces as a result of the interaction of neighboring molecules (a perturbed covalency bonding). Both effects would increase with increasing intermolecular forces; the frequency shift would be greater the more pronounced the polar nature of the bonding in the system. Quantitative calculations await more precise spectroscopic data (Raman and infrared) for these molten-salt systems, but the results qualitatively confirm the predictions based

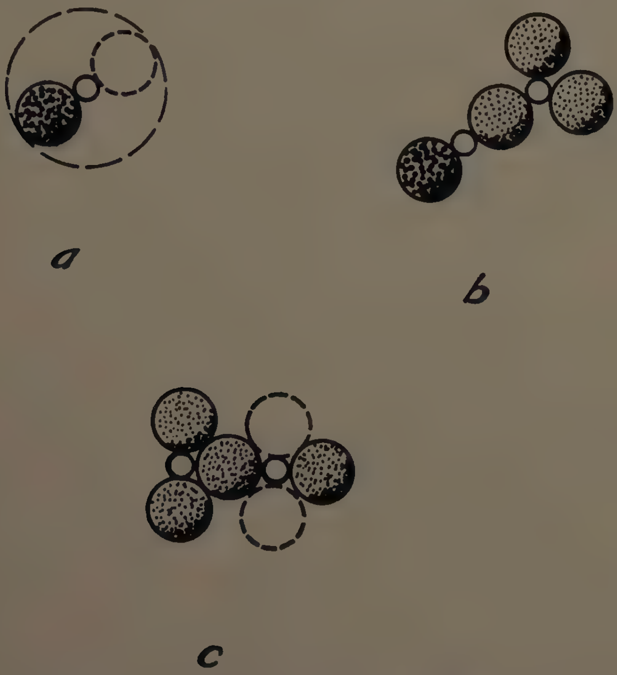

FIGURE 2. Structure type and stereochemical arrangements for the mercuric halides in the solid state. Mercuric bromide and iodide have the stereochemical arrangement illustrated in *a*, with packing as shown in *c*. Mercuric chloride has the somewhat different stereochemical arrangement and packing shown in *b* and *d*, respectively. The large circles are the halide atoms.

on the estimates of the ionic nature of the Hg—X bond (TABLE 3). The shielding efficiency and the anion affinities of the mercuric ion, Hg^{+2}, are noteworthy. Extremely inefficient shielding by the internal electron shells is related to a pronounced tendency to form molecular complexes—that is, absence of structurally ionic character. The shielding efficiencies of the mercuric ion and the alkali metal cations are 0.67 and 1.0, respectively. The anion affinity has been defined[16a,b] as a measure of the attractive force for anions of free cationic species. The anion affinity of the mercuric ion is found to be 1.70 times greater than that of the cationic species, which normally form ionic compounds. Thus, while the mercuric halides are 2:1 type salts in the conventional sense and may conceivably dissociate with the ultimate formation of the Hg^{+2} species, the existence of the latter would seem highly improbable in the molten salts. It follows that the species $HgBr_2$, $HgBr^+$, and $HgBr_3^-$ may be predicted as the most probable entities in the molten state in accord with the ionization processes

$$\text{Ionization: } Hg\,X_2 \rightleftharpoons Hg\,X^+ + X^- \qquad (1)$$

$$\text{Solvation: } X^- + Hg\,X_2 \rightleftharpoons Hg\,X_3^- \qquad (2)$$

$$\text{and} \quad 2Hg\,X_2 \rightleftharpoons Hg\,X^+ + Hg\,X_3^- \qquad (3)$$

where the over-all process (Reaction 3) corresponds to the primary dissociation (Reaction 1) and solvation (Reaction 2) in the melt. Should the ionization equilibrium (Reaction 3) lie far to the right, the molten salts would correspond to ionic melts in which the autocomplexes, the predominant species, still retain a high degree of covalency in view of their polyatomic natures. By contrast, if the ionization equilibrium lies far to the left, the properties of the melts should be interpreted as those of essentially molecular-type liquids, with formation of the species $HgBr^+$ and $HgBr_3^-$ on incipient ionization. Knowledge of the degree of ionization is essential to the resolution of this problem.

Complete ionization. Interpretation of the physical properties for molten mercuric bromide in the light of the completely ionized model for the melt is of interest. Electric conductance in molten salts is generally assumed to be due largely to the smaller ionic species, whereas the viscous flow rate is limited by the lower mobility of the larger ions (usually anions).[17,18] Approximate equality of the activation energies in ionic melts has been interpreted as an indication that the structural units involved in conduction are larger than the simple ion and, indeed, more nearly comparable in size to the units for viscous flow; ionic association in such systems is thus postulated. For mercuric bromide, the only halide for which reliable values are available at present, the energies of activation for electric conductance and viscous flow are 6.2 and 5.1 kcal./mole, respectively. The concept that the predominant species in the melt are $HgBr^+$ and $HgBr_3^-$ if the molten salt is assumed to be ionic is in accord with this approach.

For ionic melts an empirical rule for the entropy of fusion, namely that ΔS_f is about 3 eu/gram ion for systems with simple ionic species as the structural entities, has been noted.[19] In accord with the ionic model for mercuric bromide, the entropy of fusion should be interpreted as for a 1:1 electrolyte (Reaction 1) rather than a 2:1 electrolyte. The entropy of fusion per gram ion, 4.2 eu is somewhat larger than that noted for KBr and KCl, 2.5 and 3.1 eu, respectively. Because of the polyatomic nature of the $HgBr^+$ and $HgBr_3^-$ species, a higher value than that for the alkali halides would be predicted to account for the vibrational-rotational contributions in these melts, but insufficient data prevent quantitative estimates. Certainly the entropy of fusion is much larger than that for SiO_2 (0.93 eu), the melt of which is conceived as a highly polymerized or cross-linked type of liquid.[20] The percentage volume increase at fusion for mercuric bromide is estimated as 19.7 (compare KCl and KBr, 17.0 and 16.2, respectively[19]). Only qualitative significance should be attributed to this, since the densities of the solid mercuric halides near the melting point are not available for the precise calculation of this factor.

The very low values of the molar conductivities, and the solid- and gaseous-state structural data are difficult to understand in the light of this model. The order of increasing conductivity in ionic melts—that is, iodide < bromide < chloride—is the reverse of that for the mercuric halides (TABLE 2*b*). For salts only partially ionized in the molten state, both ionic mobilities and ionic concentrations contribute to the molar conductivities. When the degree of ionization varies markedly from one halide to the next for a given metal, the molar conductivities may well be determined primarily by the relative concentrations of the free ions.

Partial ionization. There is little doubt that the finite conductivity of the molten mercuric halides may be attributed to the autocomplex ionic species. There have been attempts to account quantitatively for the character of the changes in electric conductivity of molten salts with respect to the periodic classification of elements. These attempts have been made in terms of shielding of ions by gegen-ion species,[21] or in terms of disparities in moments of the ion and its gegen-ion species,[22] and have achieved a measure of success qualitatively, although they do not lend themselves well to quantitative analyses. The concept of the reduced conductivity, $\mathfrak{k}$, proposed by Martin[23] seems most promising for calculation of the extent to which "kinetically free" ions are formed in such systems.

From the fundamental definition of α, the degree of ionization

$$\alpha = \frac{1000\kappa}{CNeF(u_+ + u_-)} \tag{4}$$

where the symbols have their conventional significance, it can be readily shown that for a 1:1 type salt

$$\alpha = \frac{\mu\eta}{2\,\bar{\lambda}_0} \tag{5}$$

where $\bar{\lambda}_0$ is the average mobility for the cationic and anionic species reduced to unit viscosity (1 cp.), and the molten salt obeys Walden's rule. Reference to tables of ionic mobilities indicates that all mobilities fall within a factor of 10 of each other, and that in a medium of unit viscosity (1 cp.), the value $\bar{\lambda}_0 = 50$ ohm^{-1}·cm.^{2}·gram ion^{-1} represents all ionic mobilities within a factor of 2 (with the exception of the hydronium and hydroxyl ions). Thus it follows that the degree of dissociation is expressed simply by

$$\alpha = \mu\eta/100 = \mathfrak{f} \tag{6}$$

or that $\mathfrak{f}$, defined as the reduced conductivity, is equal to 100α. It should be recognized that for molten salts in which ΔE_μ and ΔE_η differ markedly, but for which the general relation $\mu^m\eta$ = constant holds, the reduction of the conductivities to the standard state of unit viscosity should be by $\eta^{1/m}$ rather than by η itself, as in the preceding equations. The degrees of dissociation thus obtained for some inorganic halides are summarized in TABLE 4 together with the value for mercuric bromide. In view of the approximations involved, the values for the simple salts, for example KBr, may be taken as confirmation that they are completely ionized. It follows from this that the degree of dissociation for $HgBr_2$ is approximately 2×10^{-4} in the region of the melting point. Inspection of the values for $\mathfrak{f}$ in TABLE 1 (*last column*) shows that the degree of dissociation is essentially constant in this melt over the entire temperature range for which the liquid state is stable.

TABLE 4
MOLTEN INORGANIC HALIDES AT THEIR MELTING POINTS

Compound	m.p. (°C.)	ΔE_μ	ΔE_η	m	$\mathfrak{f}$ (ohm^{-1}·cm.^{2}·cp.·mole^{-1})	$\mu^m\eta$
		(kcal.·mole^{-1})				
KBr	728	3.4	7.9	2.3	141	109
AgI	552	0.9	5.8	6.4	361	121
$HgBr_2$	238	6.3	5.1	0.79	0.0251	0.0208

Using an entirely different approach based on emf measurements on concentration cells with molten mercuric bromide, the value of the ion product for $HgBr_2$ at 250° C. has been reported[4c] as:

$$(HgBr^+)(Br^-) = 2 \times 10^{-8}$$

This corresponds to a value for α equal to 1×10^{-5}. The agreement, all that could be expected in view of the approximations, is in support of an essentially molecular-type liquid for mercuric bromide. The equality of ΔE_μ and ΔE_η and the magnitude of the entropy of fusion also may be understood in the light of an essentially molecular model for these melts.

In covalent melts, only incipiently dissociated, viscosity is determined primarily by undissociated molecules rather than by ionic species. The molecules may be considered as constituting a solvent medium in which the ions are dissolved and with which they are in dynamic equilibrium with respect to the process of dissociation. Although Walden's rule, as originally proposed, was empirical, it can be shown to be a direct consequence of the application of Stokes' law to the motion of ions. For an electrolyte dissociating into *p* kinds of ions, it can thus be shown that for infinite dilution

$$\Lambda^0\eta_0 = 8.19 \times 10^{-9} \sum_{i=1}^{p} \frac{|Z_i|}{r_i} = \text{constant} \tag{7}$$

While the condition of infinite dilution cannot be realized in a pure molten salt, for melts such as mercuric bromide, where ionization is only incipient, the above is probably valid as a good approximation. A direct consequence of this is, then, that the energies of activation for electric transport and viscous flow should be equal in melts with a high degree of covalency. The close correspondence of the values found for mercuric bromide is thus understood in the light of this model. It may be predicted that Walden's rule will be obeyed more closely in the vicinity of the boiling point of a melt than near the freezing point, since an increasingly close-packed arrangement of molecules may well result with increasing temperatures.

The decrease in ΔE_μ with increasing temperature for molten mercuric bromide may be attributed to the increase in free volume of the liquid. The predominant cohesive forces in molecular-type liquids are dipole-dipole and ion-dipole, and the coulombic ion-ion interactions are long-range secondary effects. This is in contrast to the alkali-halide melts, which may be regarded as completely dissociated.[23] As a result, covalent melts, as compared with ionic melts, are characterized by higher thermal-expansion coefficients and free volumes or higher hole production rates, or all three. The slight downward curvature of the curve of ΔE_μ in FIGURE 2, if significant, may indicate some retention of solid-state structure just above the melting point. The relatively high value of ΔE_μ (5–6 kcal.) is thus readily understood as due to the large size of the conducting species. The problem is schematically illustrated in FIGURE 3, with the conduction visualized as a concerted rotation of ions and neighboring molecules. Thus, in FIGURE 3*a*, *b*, and *c* are shown the relatively large sphere evolved by $HgBr^+$ rotation, the ($HgBr^+$) ($HgBr_3^-$) ion pair, and the stereochemical limitations to entirely free rotation of the molecular species in the liquid state.

A summary of the entropy of fusion calculations for the 3 mercuric halides is given in TABLE 5. It has been assumed that the transition of the librational motion of the molecules in the crystal lattice to free rotation in the liquid state occurs during the process of fusion.[24] Similarly, the communal entropy has been assumed to appear entirely at the melting point. Librational frequencies of 50, 37, and 30 cm.$^{-1}$ were assumed for the chloride, bromide, and iodide, respectively, in accord with values ob-

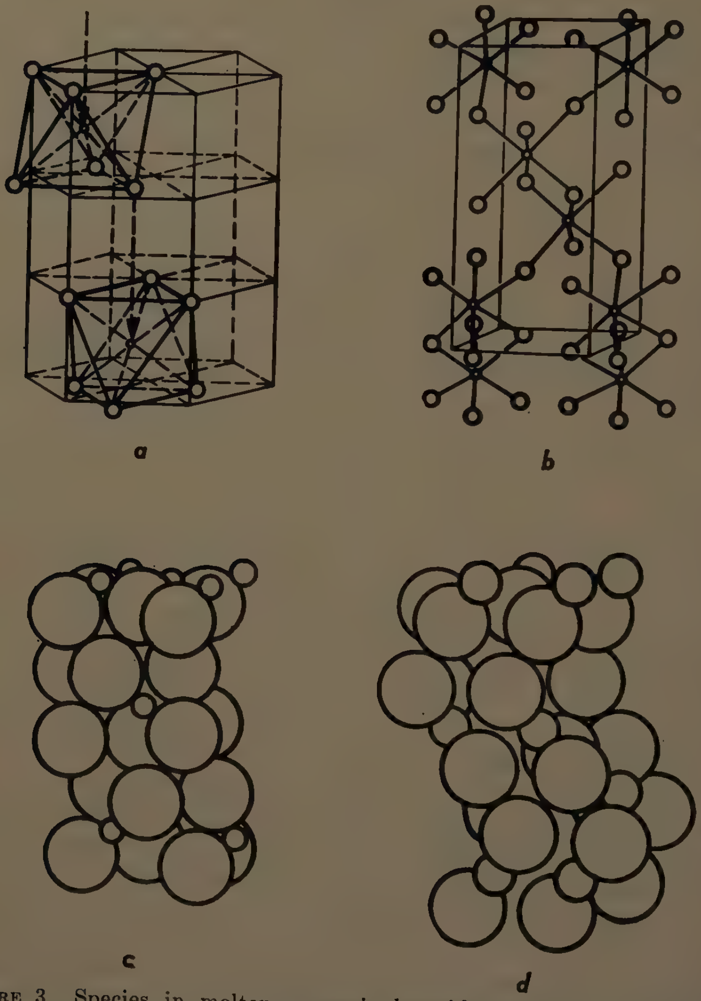

FIGURE 3. Species in molten mercuric bromide. (*a*) $HgBr^+$ (rotation), (*b*) $HgBr^+ \cdot HgBr_3^-$, and (*c*, *d*) stereochemical aspects of molecule-molecule rotation in the melt.

served for other polyatomic molecules in the crystalline state.[25-27] Exact correspondence with the experimentally observed entropies of fusion is found if $S_{rot.}$ is decreased by 1 eu to allow for possible hindered rotation in the liquid state (see FIGURE 3*c*). No account has been taken of the entropy increase due to the change in volume on fusion, since this amounts to only a few tenths of an eu. Refinement of these calculations may be made if the librational frequencies of these compounds in the solid state can be determined experimentally.

The problem of mercuric iodide presents the interesting feature that ΔE_μ cannot be calculated directly from conductivity data. Preliminary results show that the conductivity of mercuric iodide has a negative temperature coefficient. An explanation for the much higher conductivity, relative to the bromide and chloride (TABLE 2), is seen in the light of viscosity data recently published.[28] The value of ΔE_η for mercuric iodide thus found, that is, 1.75 kcal.·mole^{-1}, is much less than that for mercuric bromide. If the "true" value of ΔE_μ is taken equal to ΔE_η in mercuric iodide in the light of the preceding discussions on covalent melts, the conductivity of mercuric iodide would be predicted to be approximately 25 times greater than that of the bromide at 270° C. In part, the large difference between conductivities of the iodide and those of the chloride and bromide is thus understood. A possible explanation for this is that the highly polarizable iodide ion effectively reduces the potential barrier for ionic migration in the iodide melt. A more detailed discussion awaits further experimental data.

TABLE 5
ENTROPIES OF FUSION (MOLECULAR LIQUIDS)

Salt	S (eu)				
	$S_{\text{rot.}}$	$S_{\text{vib.}}$	$S_{\text{comm.}}$	$S_{\text{fus.}}$ calculated	$S_{\text{fus.}}$ observed
$HgCl_2$	18.6	12.1	2.0	8.5	7.5
$HgBr_2$	20.3	12.9	2.0	9.4	8.4
HgI_2	21.5	13.9	2.0	9.6	8.6

References

1. Hückel, W. 1951. Structural Chemistry of Inorganic Compounds. Elsevier. Houston, Texas.
2. Prideaux, E. B. R. 1910. J. Chem. Soc. **97:** 2032.
3a. Jander, G. & K. Brodersen. 1951. Z. anorg. Chem. **264:** 57.
3b. *Ibid.* 1950. **261:** 261.
3c. *Ibid.* 1951. **264:** 92.
4. Belyaev, I. N. & K. E. Mironov. 1952. Zhur. Obshcheĭ Khim. **22:** 1734.
5. Scholten, W. & J. M. Bijvoet. 1941. Z. Krist. **103:** 415.
6. Braekken, H. & W. Scholten. 1934. Z. Krist. **89:** 448.
7. Braune, H. & S. Knoke. 1931. Z. physik. Chem. (Leipzig). **A152:** 409.
8. Gregg, A. H., G. C. Hampson, G. I. Jenkins, P. F. L. Jones & L. E. Sutton. 1937. Trans. Faraday Soc. **33:** 852.
9. Akishin, P. A. & V. P. Spiridonov. 1957. Kristallografiya. **2:** 475.
10. Sponer, H. & E. Teller. 1941. Rev. Mod. Phys. **13:** 75.
11. Klemperer, W. & L. Lindeman. 1956. J. Chem. Phys. **25:** 397.
12. Klemperer, W. 1956. J. Chem. Phys. **25:** 1066.
13. Hannay, N. B. & C. P. Smyth. 1946. J. Am. Chem. Soc. **68:** 71.
14. Pitzer, K. S. & J. H. Hildebrand. 1941. J. Am. Chem. Soc. **63:** 2472.
15. Braune, H. & G. Engelbrecht. 1932. Z. physik. Chem. **B19:** 303.

16a. Ahrens, L. H. 1955. Nature. **174:** 644.
16b. *Ibid.* 1953. Geochim. Cosmochim. Acta. **3:** 1.
17. Frenkel, J. 1937. Bull. acad. sci. U. R. S. S., Sér. phys. **3:** 319.
18. Frenkel, J. 1946. Kinetic Theory of Liquids. : 439. Clarendon Press. Oxford, England.
19. Ubbelohde, A. R. 1950. Quart. Revs. (London). **4:** 365.
20. Førland, T. 1957. Norg. Tek. Høgskole Avhandl. **4:** 1.
21. Camescasse, P. 1957. J. chim. phys. **54:** 795.
22. Antipin, L. N. 1956. Uspekhi Khim. **30:** 632.
23. Greenwood, N. N. & R. L. Martin. 1953. J. Chem. Soc. **1953:** 1427.
24. Hirschfelder, J., D. Stevenson & H. Eyring. 1937. J. Chem. Phys. **5:** 896.
25. Pauling, L. 1930. Phys. Rev. **36:** 430.
26. Hexter, R. M. & H. Cheung. 1956. J. Chem. Phys. **24:** 1186.
27. Sidorova, A. I. 1937. Acta Physicochim. U. R. S. S. **7:** 193.
28. Polyakov, V. D. 1955. Izvest. Sektora Fiz.-Khim. Anal., Inst. Obshcheĭ Neorg. Khim., Akad. Nauk S. S. S. R. **26:** 191.

SOME THERMODYNAMIC ASPECTS OF MOLTEN SALTS: HALIDES OF URANIUM, ZIRCONIUM, THORIUM, AND CERIUM IN ALKALI HALIDE EUTECTICS*

D. Inman, G. J. Hills, L. Young,† J. O'M. Bockris
Chemistry Department, Imperial College, London, England, and John Harrison Laboratory of Chemistry, University of Pennsylvania, Philadelphia, Pa.

INTRODUCTION

The transition elements are of interest because of the variety of electrode reactions to which the presence of their compounds in an alkali halide eutectic may give rise: for example, their stepwise reduction and the possible reduction of their anionic complex halides. Information concerning the nature and concentration of such complexes may be obtained from such reactions; also from electrode mechanism studies. In addition, the behavior of transition metal compounds in molten salts has technical importance.

Fundamental studies of the mechanism of electrode reactions in fused salts are, as yet, sparse,[1-6] although studies involving electrode reactions in fused salts in which determination of the mechanism of the reaction has not been the aim are more numerous.[7-26]

The experimental part of the studies reported in this paper was terminated in 1956.

URANIUM

Experimental

Cell and adding device. For systems in LiCl-KCl, Pyrex glass cells (FIGURE 1*a*) were used. They contained parallel ground-glass joints with which the electrodes could be raised, lowered, and rotated. The vacuum lock used for adding material to the melt is shown in FIGURE 1*b*. Its use avoided contamination of the system by the atmosphere.

Furnaces. Furnaces were the simple-resistance type and used Nichrome exponential windings; the tube was of Vitreosil.

Vacuum apparatus. It is possible to outgas melts at low temperature by pumping for several days to remove permanent gases and water vapor. The last traces of water and hydrolytic products can be removed more rapidly by pre-electrolysis,[27] which is also carried out *in vacuo*. For both the initial outgassing and pre-electrolysis, a rotary pump was used to back a glass 3-stage mercury diffusion pump; the pressure in the system was $<10^{-4}$ mm. Hg.

---

* The work reported in this paper was supported in part by grants from the United Kingdom Atomic Energy Establishment, Harwell, England, and the United States Atomic Energy Commission, Washington, D.C.

† British Columbia Research Council, University of British Columbia, Vancouver, B.C., Canada.

Gas purification. When the system investigated was not under vacuum, it was kept filled with Ar obtained from 99.95 per cent Ar that had been passed through SiO_2 gel and P_2O_5, preliminarily gettered with Cu at 600° C. and then with U turnings at 600° C.

HCl was produced by dripping concentrated H_2SO_4 onto concentrated HCl. It was carried into the melt in an Ar stream through a CO_2-acetone trap.

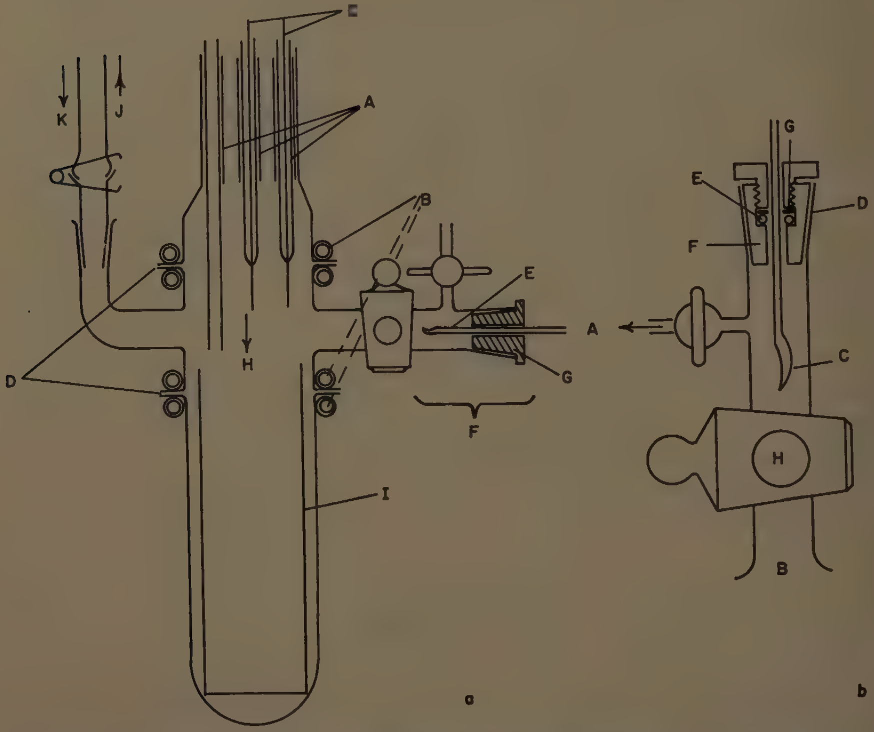

FIGURE 1. (*a*) Pyrex cell: *A*, parallel ground glass joints; *B*, cooling coils; *C*, tungsten electrode leads; *D*, flanges; *E*, spoon for addition of UCl_3; *F*, addition device (vacuum lock); *G*, modified Wilson O-ring seal; *H*, to electrodes; *I*, melt container; *J*, to vacuum line; *K*, argon in. (*b*) UCl_3 addition device in detail. *A*, to vacuum line; *B*, cell; *C*, spoon; *D*, modified Wilson O-ring seal; *E*, O-ring; *F*, brass; *G*, brass washer; *H*, ~1-cm. bore.

Purification of solvent. An LiCl-KCl eutectic normally evolves HCl on heating as a result of its hydrolysis by previously absorbed water. This hydrolysis must be prevented or reversed before the melt can be used. Methods to achieve this have employed prolonged outgassing,[28] evacuation and treatment with HCl,[29,30] and pre-electrolysis.[31]

Evacuation and HCl treatment were not considered sufficient in the present work because it has been shown that (1) 0.5 per cent by weight of

H_2O or its hydrolysis products remained in an LiCl-KCl mixture after heating at 400° C. for 24 hours at a pressure of 10^{-4} mm. Hg,[32] and (2) from current-potential determinations, traces of HCl were not removed by evacuation for 12 hours at 10^{-4} mm. Hg at about 450° C. Therefore, an alternative procedure was adopted.

The LiCl (pure grade) and KCl analytical reagent (A. R.) were mixed rapidly, melted in a glass tube, and filtered through glass wool into a Pyrex beaker. This eutectic was transferred to the main electrolytic cell where it was remelted and pumped out until the pressure in the system fell to $\sim 10^{-4}$ mm. Hg. Anhydrous HCl was then bubbled through the molten eutectic in a stream of purified Ar. The final traces of impurities, including dissolved HCl, were removed by pre-electrolyzing the melt *in vacuo* with W or Mo cathodes and C anodes, at a potential below the decomposition potential of the melt.

The progress of the purification was followed by either the steadily falling residual current at constant potential or the steadily rising voltage at constant current. During the pre-electrolysis, a vacuum was maintained so that gases evolved at the electrodes were removed immediately from the cell and prevented from dissolving and recombining (FIGURE 2). The current density (c.d.) corresponding to the final residual current after pre-electrolysis for several (up to 12) hours was about 0.1 mAmp.-cm.$^{-2}$ This corresponds to a residual impurity content of $< 5.10^{-8}$ moles-cc.$^{-1}$

Preparation of solute. UCl_3 was available only in a powdered form, which was neither sufficiently pure nor suitable for introduction into the melt without further contamination (with water vapor). It was prepared freshly for each run by one of two processes, the lead chloride process[33] or anodic dissolution. The former exploited the fact that, for many metals, the equilibrium

$$M + xPbCl_2 \rightleftharpoons MCl_{2x} + xPb \qquad (1)$$

is displaced almost completely to the right; as molten metallic lead can be separated easily from the rest of the system, this is a convenient method of preparing heavy metal chlorides in the anhydrous state.

Reaction 1 was performed in the cell illustrated in FIGURE 3. Twenty-five gm. of KCl and 93 gm. of $PbCl_2$ were heated slowly (450 to 460° C.) in an alumina crucible under vacuum (to remove adsorbed water vapor). As soon as the mixture melted, Ar was immediately admitted to the apparatus to reduce the volatilization of $PbCl_2$. A rod of U was then lowered into the melt and the temperature raised to 650° C. The rod was kept above the pool of molten Pb that slowly formed in the bottom of the crucible. The mixture was cooled and the metallic and salt layers separated after about 2 hours, which was the average reaction time. The small residual concentration of $PbCl_2$ in the salt melt was removed by means of pre-electrolysis.

In anodic dissolution, a more convenient method and one that introduces fewer impurities into the system, a U electrode is anodized, at a low current density of $\ngtr 50$ mAmp.·cm.$^{-2}$

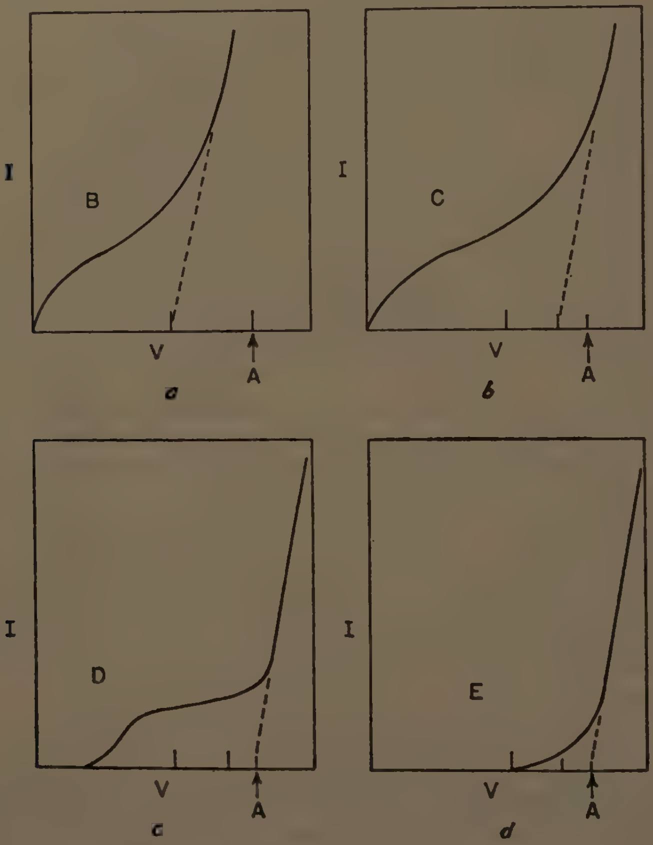

FIGURE 2. Current-potential relations during purification of solvent melt. (*a*) After molten filtration. (*b*) After molten evacuation. (*c*) After passage of dry HCl through melt. (*d*) After pre-electrolysis *in vacuo*. *A*, decomposition voltage for the pure substance in the absence of impurities; *B*, high residual current due to impurities; *C*, reduced residual current; *D*, hump due to dissolved HCl; *E*, residual current removed.

In spite of the fact that the cells contained no diaphragms, the steady-state concentration of U in the system increased continually because of the loss of alkali metal by such means as evaporation and reaction with electrodes and containers.

Electrodes. The three basic types of electrodes used were: (1) quarter-inch-diameter graphite rods used for anodes, cleaned and polished with emery cloth, and heated to redness in flame before use; (2) quarter-inch-diameter W and Mo rods used for cathodes, cleaned with emery cloth; and (3) quarter-inch-diameter U rods used as anodes and cathodes.

Electrode mounting. Ground-glass syringes sealed to the roof of the glass envelope (FIGURE 1*a*) allowed a vertical movement of about 2½ in. and free circular motion even during evacuation of the cell. Connection to the electrodes was made via W rods of 2-mm. diameter sealed into C7 glass that was, in turn, sealed to the bottom end of the glass plunger.

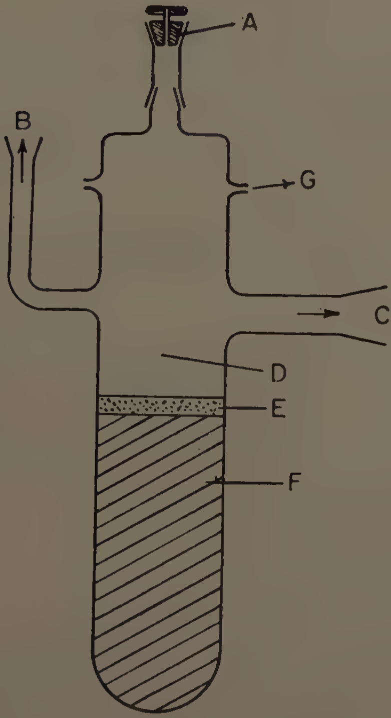

FIGURE 3. Apparatus for preparation of UCl_3 by lead chloride process: *A*, modified Wilson O-ring seal; *B*, to vacuum line and argon purification train; *C*, to adding device; *D*, Pyrex glass; *E*, W1 glass; *F*, mullite ($Al_2O_3 \cdot SiO_2$ mineral); *G*, glass flanges.

Temperature control and measurement. The temperature was controlled by means of a Pt resistance thermometer used as one arm of a Wheatstone bridge. The Pt wire (~11 Ω) was either wound on the furnace tube or inserted, coiled, inside a twin-bore alumina tube, between the furnace tube and the cell. The bridge was balanced for the desired temperature. Any out-of-balance current through the connecting arm of the bridge was amplified and used to actuate an electronic relay connected in series with the furnace for rough control or, for fine control, in series with a 10-ohm resistance in the furnace circuit. The temperature of the furnace was brought near the desired temperature first by means of the adjustment provided by a Variac autotransformer. Control was better than ±1° C. The temperature was measured with a chromel-alumel thermocouple enclosed in a Pyrex sheath.

Reference electrode. Two types of reference electrodes were used in the course of the present work. The first was similar to that described by Senderoff and Brenner,[31] that is, Ag in pure molten AgCl in a SiO_2 capillary tube, the junction between this liquid and the melt being formed at an asbestos plug. The main disadvantages of this electrode were its instability and the high liquid junction potential associated with its use.* The second electrode consisted of an Ag wire in contact with a solution of AgCl in an LiCl-KCl eutectic; this was held in a Pyrex tube, the bottom of which was closed by a thin diaphragm. This electrode has been described in Bockris *et al.*[34]

General procedure. A sample of filtered salt was transferred rapidly from a desiccator to the cell, which was then immediately pumped out. The temperature of the system was raised to above the m.p. of the salt, and the evacuation continued until the vacuum had decreased to a satisfactorily low value (10^{-4} mm. Hg). In some cases, HCl was bubbled through the melt at this stage and then pumped off. The pre-electrolysis electrodes were then lowered into the melt, which was electrolyzed until removal of impurities was complete, as judged by the current-voltage curve criteria (*see above*). The reference and working electrodes were then lowered into the melt and such measurements as potential difference, current, and temperature were made.

TABLE 1

ANALYSIS OF URANIUM PRODUCED ELECTROLYTICALLY FROM FUSED SALTS*

Uranium	98.7	Potassium	0.02	Magnesium	0.01
Silicon	0.5	Lithium	0.01	Calcium	0.01
Chloride	0.1	Aluminum	0.01	Manganese	<1
Fluoride	0.1	Copper	0.01	Silver	<1
Iron	0.02			Sodium	0.01

* All figures are percentages except those for manganese and silver, which are given in parts per million.

Results

Current efficiency and metal purity. The criterion was adopted that the proper standards of purity would be evidenced by the quality of metal produced by a simple electrolysis of the system.[35]

A typical electrolysis product was a dendritic material, the analysis of which is shown in TABLE 1. About 0.5 per cent remained unidentified in most samples, and doubtless represents oxide picked up during leaching and storage of the deposits, which were ball-milled before analysis. The absence of silver in the product reflects the impermeability of the liquid junction diaphragm.

---

* A rough calculation of this potential, by means of the Henderson equation in the form $e_{LJP} = (RT/F) \ln (\Lambda_1/\Lambda_2)$ suggests that $e_{LJP} \sim 70$ mv.

At current densities of <100 mAmp.$\cdot$cm.$^{-2}$, the anodic and cathodic current efficiencies (based on the *total*, that is, adherent and nonadherent, deposit) were 100 per cent on the basis of the single electrode reaction

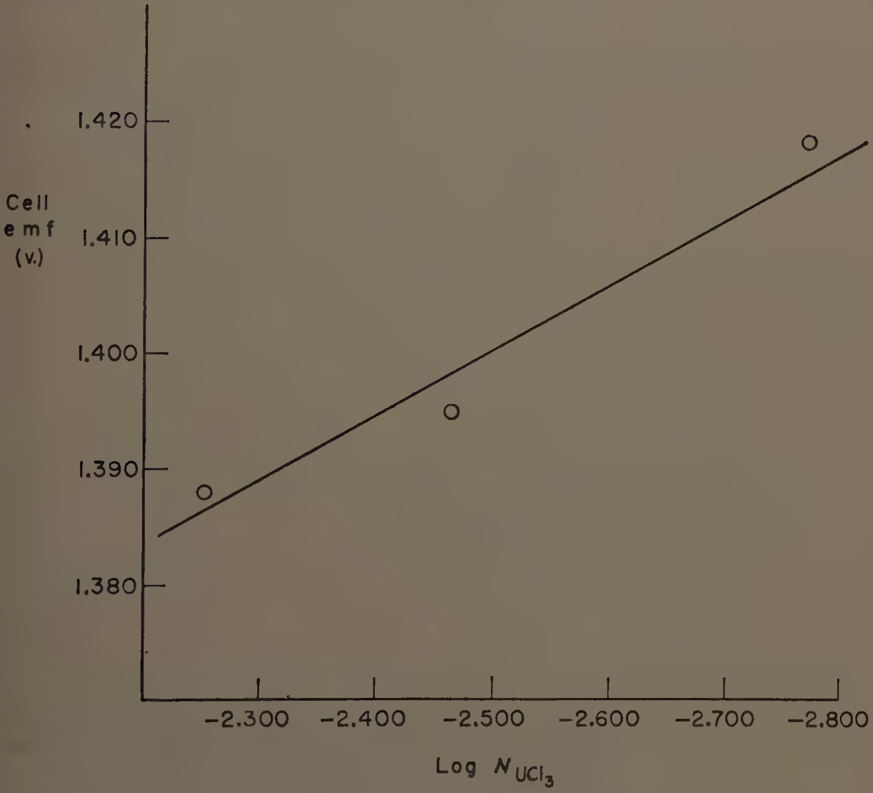

FIGURE 4. Reversible cell emf in relation to mole fraction UCl_3 in LiCl-KCl (463° C.). Theoretical slope ($n = 3$) = 49.2 mv.; experimental slope = 57.0 mv.

$U \rightleftarrows U^{3+} + 3e_o$. Thus, at these temperatures and in the absence of oxygen, the U^{3+} state is the most probable potential-determining component, in the absence of current flow.

Mechanism of $U^{3+} \rightarrow U$ reaction. FIGURES 4 and 5 show for the reversible electrode reaction the dependence of the reversible emf of the cell *A* on concentration of UCl_3 and temperature. This type of data for the cell under reversible conditions allows an evaluation of thermodynamic aspects of the over-all cell reaction:

$$Ag^+ \mid AgCl, LiCl\text{-}KCl \,\vdots\, LiCl\text{-}KCl, UCl_3 \mid U^- \qquad (A)$$

Typical examples of the electrode reaction under current flow (with current-potential relation at constant time) for cell reaction *A* are shown in FIGURES 6, 7, and 8. The first current-potential relation always differed from the succeeding ones. FIGURES 7 and 8 indicate that the variations of potential are principally a function of the cathode process.

With respect to potential-time relation at constant current, typical behavior for cathode and anode, including the effect of stirring, is shown in FIGURE 9.

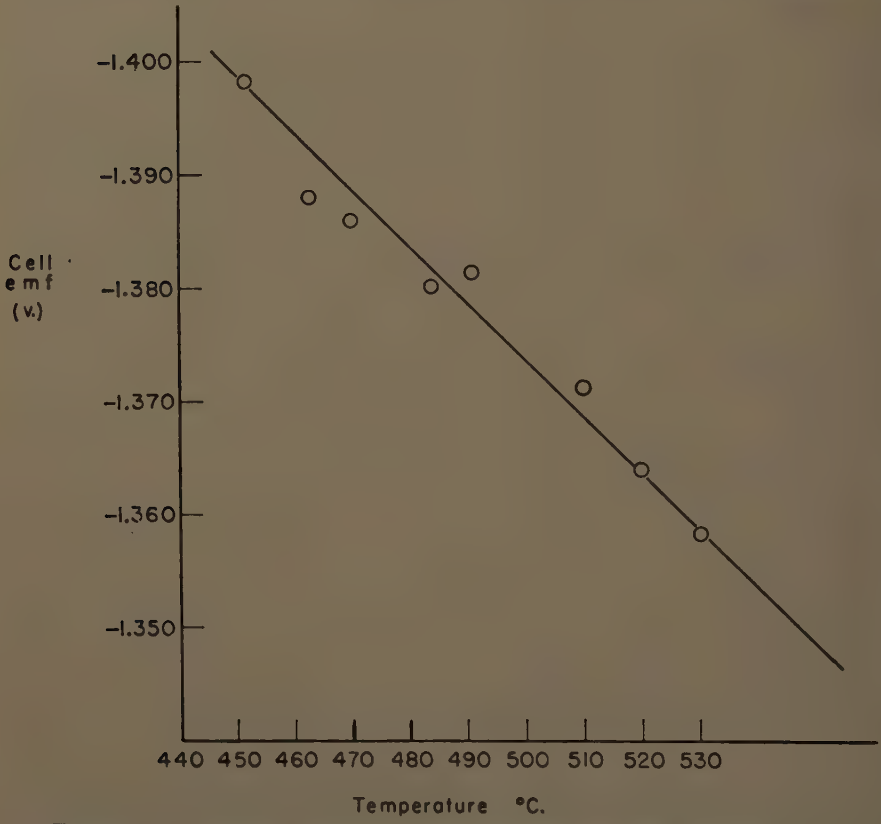

FIGURE 5. Reversible cell emf in relation to temperature ($N_{UCl_3} \cdot 5.6 \cdot 10^{-3}$).

Discussion

Nature of over-all reaction. The variation of the emf of cell *A* with UCl_3 concentration is in accord with the Nernst relation and with three-electron transfer as the potential-determining reaction. The reversibility of the system is manifested by the rapid attainment of a steady, reproducible emf after the addition of fresh UCl_3; the identity of the electrode potentials exhibited by several electrodes immersed in the same solution;

and the fact that a U electrode rapidly returns to its original value after being polarized. The values of the anodic and cathodic current efficiencies at low current densities are in agreement with the reaction $U^{3+} + 3e_o \rightleftharpoons U$.

Thermodynamics of the cell reaction. This reaction is:

$$U + 3AgCl \rightarrow 3Ag + UCl_3 \tag{2}$$

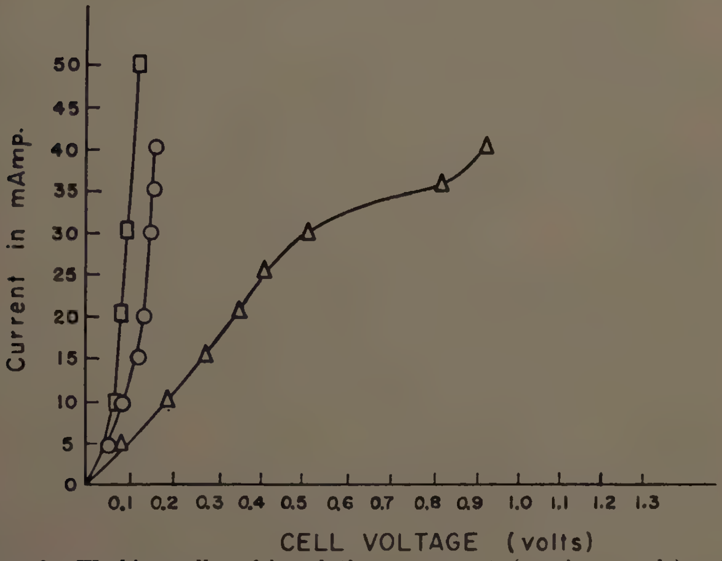

FIGURE 6. Working cell emf in relation to current (uranium anode). △, first run; ○, second run, □, third run.

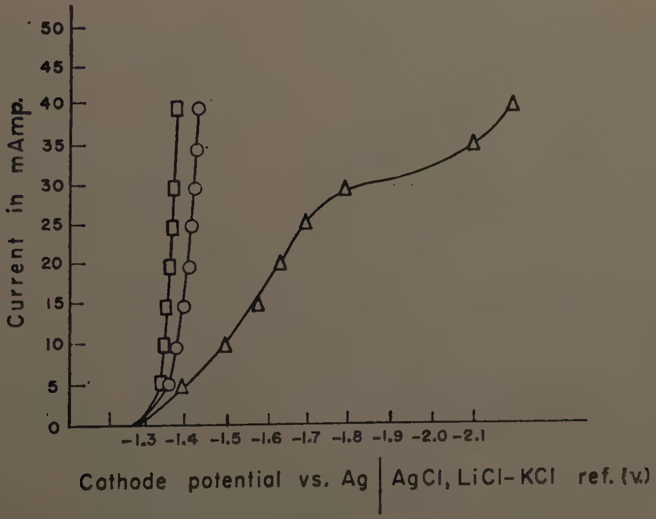

FIGURE 7. Cathode potential in relation to current: △, first run; ○, second run; □, third run.

Hence, at equilibrium,

$$E = E_\circ^{UCl_3} - E_\circ^{AgCl} - \frac{RT}{3F}\ln a_{UCl_3} + \frac{RT}{F}\ln a_{AgCl} \tag{3}$$

where $E_\circ^{UCl_3}$ is the emf corresponding to the free energy of formation of

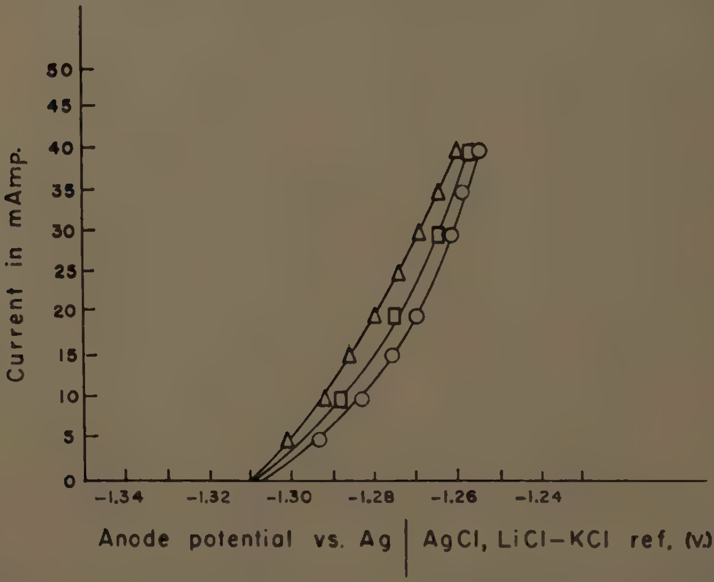

Figure 8. Anode potential in relation to current: △, first run; ○, second run; □, third run.

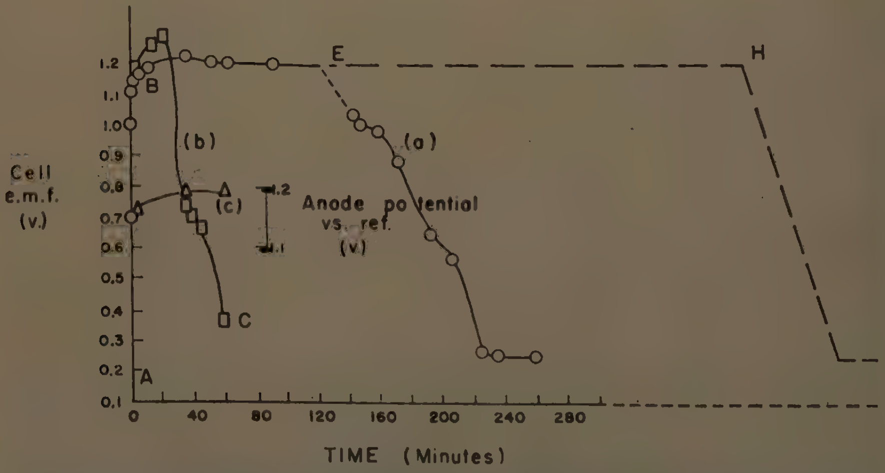

Figure 9. Working cell emf and anode potential in relation to time (at constant current): (*a*) cell emf with no stirring; (*b*), cell emf with stirring; (*c*), anode potential; *H*, a transition that takes place at times ≫280 min.

pure UCl_3 from the elements, at $T°$ K and 1 atm. pressure. $E_\circ^{AgCl}$ is the analogous quantity for AgCl, and a_{UCl_3} and a_{AgCl} are the activities of UCl_3 and AgCl. Activity coefficients are defined with the compositions expressed as mole fractions.

The activity coefficient of AgCl may be taken as unity,[36-38] so that:

$$E = E_\circ^{UCl_3} - E_\circ^{AgCl} - \frac{RT}{3F} \ln \frac{N_{UCl_3}}{N_{AgCl}^3} - \frac{RT}{3F} \ln f_{UCl_3} \tag{4}$$

where N_i is the molar fraction of i, and f_{UCl_3} is the rational activity coefficient of UCl_3.

Some emf-temperature data for the composition $N_{UCl_3} = 5.59 \times 10^{-3}$, $N_{AgCl} = 2.2 \times 10^{-3}$ are given in TABLE 2. From this data (FIGURE 5), $(dE/dT)_P = 0.48$ mv.·°C.$^{-1}$

TABLE 2
EMF-TEMPERATURE DATA FOR CELL A

Temp. (°C.)	emf (v.)	Temp. (°C.)	emf (v.)
452	−1.398	530	−1.358
491	−1.381	484	−1.380
510	−1.371	470	−1.386
520	−1.364		

From

$$\Delta H_P = -nF \left[E - T \left(\frac{dE}{dT} \right)_P \right] \tag{5}$$

the observed heat change in the cell reaction at the concentration $N_{UCl_3} = 5.59 \times 10^{-3}$ is −69.4 kcal.·mole^{-1}. This ΔH includes the heat due to the formation of complexes between the UCl_3 and the components of the eutectic.

Thermodynamics of complex formation. By using measured values of E, N_{UCl_3}, and N_{AgCl} and values of $E_\circ$ from Hamer *et al.*,[39] one obtains f_{UCl_3} from EQUATION 4 (TABLE 3).

The value of the activity coefficient suggests that significant complexing occurs between UCl_3 and the molten salt. From cryoscopic and emf studies,[36-38] it is known that the activity coefficient for AgCl in LiCl-KCl, where no complexing occurs, is unity and does not change over a wide range of concentrations. Hence it is reasonable to assume that the activity coefficients of all the individual types of ions (including U^{3+}) in the system UCl_3-LiCl-KCl are unity (that is, after the complexing effect has been taken into account).

According to Katz and Rabinowitch,[40] UCl_3 may form (in the solidus) the compound K_2UCl_5 with KCl. Assuming UCl_5^{--} to represent the complex concerned:[*]

$$\begin{array}{ccccc} UCl_3 & + & 2Cl^- & \rightleftharpoons & UCl_5^{--} \\ (1-\alpha)N_o & & N_{Cl^-} & & \alpha N_o \end{array} \tag{6}$$

where α is the degree of complex formation, N_o the nominal mole fraction of UCl_3, and N_{Cl^-} the anionic fraction of halide ions in the melt.

TABLE 3

ACTIVITY COEFFICIENTS OF UCl_3 IN UCl_3-KCl-LiCl AT 463° C.

UCl_3 (mole fraction)	f_{UCl_3}
1.7×10^{-3}	5×10^{-2}
3.4×10^{-3}	8×10^{-2}
5.6×10^{-3}	7×10^{-2}

TABLE 4

COMPLEXING CONSTANT AND STANDARD FREE ENERGY (T = 463° C.) OF COMPLEX FORMATION BETWEEN UCl_3 AND Cl^- IN THE MOLTEN STATE

K	$\Delta F°$ (kcal.·mole^{-1})	Mole fraction UCl_3
17.2	−4.2	1.7×10^{-3}
10.9	−3.5	3.4×10^{-3}
12.7	−3.7	5.6×10^{-3}

Hence,

$$(1-\alpha)N_o = \frac{1}{1+K}\cdot N_o = [UCl_3] \text{ uncomplexed} = [U^{3+}] \tag{7}$$

and

$$K = \frac{\alpha}{1-\alpha} \tag{8}$$

as $N_{Cl^-} = 1$ ($N^{2-}_{UCl_5} \ll N_{Cl^-}$).

From EQUATION 7:

$$f_{UCl_3} = \frac{1}{1+K} \tag{9}$$

that is, K may be calculated from the value of f_{UCl_3} obtained from EQUATION 4 (TABLE 3).

Values of K in relation to composition are given in TABLE 4 for a temperature of 463° C.

---

[*] In view of the existence of Cl^- as common both to the solvent and the solute, the same results would be obtained for any complex ion subject to an equilibrium of this type.

In TABLE 5 the results are given for the complexing constant at various temperatures and at a concentration of $N_{UCl_3} = 5.6 \cdot 10^{-3}$.

Mechanism of cathodic deposition. The singular behavior of the potential-time relations (FIGURE 9) may be interpreted as follows.

Considering the portion AB, the depositing ions must consist of either Li^+ or U^{3+}. However, the potential corresponding to the plateau BE is -2.4 with respect to the Ag-AgCl reference (at $N_{AgCl} = 2.2 \cdot 10^{-3}$).

For the cell B:

$$\mathrm{Li} \left| \begin{matrix} \mathrm{LiCl} \\ \mathrm{KCl} \end{matrix} \right\vdots \begin{matrix} \mathrm{AgCl} \\ \mathrm{LiCl} \\ \mathrm{KCl} \end{matrix} \Big| \mathrm{Ag} \qquad (B)$$

$$E = \left(-\frac{\Delta F_\circ^{\mathrm{LiCl}}}{F} + \frac{\Delta F_\circ^{\mathrm{AgCl}}}{F} \right) - \frac{RT}{F} \ln \frac{a_{\mathrm{LiCl}}}{a_{\mathrm{Li}}} + \frac{RT}{F} \ln a_{\mathrm{AgCl}} \qquad (10)$$

TABLE 5

THE VARIATION OF THE COMPLEXING CONSTANT FOR THE UCl_3-Cl COMPLEX WITH TEMPERATURE: THERMODYNAMICS OF COMPLEX FORMATION

K	Temp. (°C.)	$\Delta F°$ (kcal.·mole⁻¹)	$\Delta H°$ (kcal.·mole⁻¹)	$\Delta S°$ (cal.·°C.⁻¹·mole⁻¹)
14.1	450	−3.8	+11.9	+21.7
23.7	500	−4.9		+21.7
38.8	555	−5.6		+21.1

where $\Delta F_\circ^{\mathrm{LiCl}}$ and $\Delta F_\circ^{\mathrm{AgCl}}$ are the standard free energies of formation of LiCl and AgCl at 450° C. If $a_{\mathrm{Li}} = 1$ for the liquid Li phase formed at the cathode, then E should be -2.42 v. As the observed value is -2.4, it is evident that, in the time region corresponding to BE, Li is the depositing entity.

Conversely, the deposition potential of U^{3+} in the concentration used in the melt (at 450° C.) may be calculated to be -1.35 v. on the scale referred to above. Hence, U should be deposited before Li, unless the limiting current for U deposition is exceeded. It follows that the concentration of uncomplexed U^{3+} ions in the UCl_3-LiCl-KCl at 450° C. (TABLE 4) will have an order of magnitude of 10^{-5} moles·cc.$^{-1}$ Also, $D_{U^{3+}}$ may be taken as about 6.10^{-5},[41] $z = 3$, $F = 9.6 \cdot 10^4$, and δ may be assumed to have the order of magnitude of 10^{-2} cm. Hence, as

$$i_L \approx \frac{D_z F}{\delta} \cdot a_{M^{z+}} \qquad (11)$$

then,

$$(i_L)_{U^{3+}} \simeq 6.10^{-3} \text{ amp.}\cdot\text{cm.}^{-2} \qquad (12)$$

The apparent electrode area was of the order of 8 sq.cm.; hence, the limiting current for U^{3+} deposition would be expected to be 48 mAmp. However, the currents passed during the recording of the potential-time curves (FIGURE 9) were in excess of i_L for uncomplexed U^{3+} (but not for the nominal concentration of U^{3+} without complexing), thus allowing Li to be deposited in accordance with the agreement noted between the observed potential and that calculated for the $Li^+ + e_o^- \rightarrow Li$ reaction.

Thus, when the current is first turned on at the value corresponding to that of the potential-time curve of FIGURE 7, (that is, 50 mAmp.) it is expected that U deposits first. However, the transition time for the concentration of U^{3+} ions of the order of 10^{-5} mole·cc.$^{-1}$ is of the order of 1 sec.; hence, the first observed readings (taken after an interval of about 30 sec.) would not indicate this primary U^{3+} deposition, because Li deposition would have commenced about 1 sec. after turning on the current. Thus, about 5 min. after turning on the current, the cathode potential reaches a value of about -1.7 v. with respect to the Ag-AgCl reference electrode, and this value would correspond to an a_{Li} value having (from EQUATION 10) an order of magnitude of 10^{-5}.

During the course of the electrolysis, the concentration of U^{3+} in the solution increases because of its production from the dissolving anode. Examination of the *p*H of the melt at the end of a run suggests that there is free Li present in the melt, and this fact is consistent with the assumption that, for considerable periods, not all the UCl_3 produced at the anode (where there is no limiting current for U dissolution) is removed at the cathode. At the same time, the growth of crystals on the cathode causes a large increase in available surface area and, therefore, increases the limiting current for U^{3+} deposition. At *E*, these factors evidently have reached such a value that the over-all current density in the cell does not exceed that for U^{3+} deposition. This, therefore, now becomes the predominant reaction and, consequently, the potential of the cathode falls to a value corresponding to the (almost reversible) deposition potential of U^{3+}.

When the U^{3+} concentration is zero at the beginning of the electrolysis there is a much longer plateau *BH* (FIGURE 9) during which Li and U are codeposited (U being deposited largely by the secondary mechanism). At *H*, however, the area of the U cathode has grown to such an extent that the limiting current of U^{3+} deposition is no longer exceeded, and sufficient current can be carried by U^{3+} deposition.

Furthermore, when the melt was stirred (*B*, FIGURE 9), the limiting current density for the deposition of U^{3+} was again increased to a value greater than the total current density, and the potential immediately fell to *C*. Removal of the agitation causes return of the potential to that for Li deposition.

Thus, during the electrolysis of UCl_3-LiCl-KCl, it appears that the conditions of concentration, current density, and agitation of the melt determine whether primary deposition of Li^+ or U^{3+} will occur.

Mechanism of formation of powdery and dendritic deposits. When, during the course of a potential-time relation, the electrode potential remained at a value corresponding to that of $Li^+ + e_o \rightarrow Li$, the U obtained was largely a nonadherent powder. Conversely, when the current had flowed for sufficient time for the potential to be reduced to that corresponding to $U^{3+} + 3e_o \rightarrow U$, the deposits obtained were relatively compact powders overlaid with dendritic growths.

Furthermore, when the potential of the cathode was maintained in the region corresponding to that of $U^{3+} + 3e_o \rightleftharpoons U$, then the dendrites were obtained in greater profusion the *lower* the current density.

These results strongly suggest that the mechanisms of the formation of finely powdered or large crystal deposits of U are respectively the secondary deposition of U, caused by a homogeneous liquid-phase reduction of UCl_3 by dissolved Li, and the primary deposition from U^{3+}.

ZIRCONIUM

Experimental

The methods used for Zr were analogous to those used for U. In melts not sufficiently purified from oxygen or water, $ZrOCl_2$ and ZrO_2 were formed. The cell examined was:

$$Ag^+ \mid AgCl, LiCl\text{-}KCl \;\vdots\; LiCl\text{-}KCl, ZrCl_4 \mid Zr^- \qquad (C)$$

Results

Current efficiency and metal purity. Only a small fraction of the cathodic product was essentially 100 per cent Zr metal. The majority of the cathodic product of the electrolysis of $ZrCl_4$ (1 to 5 per cent by weight) in the LiCl-KCl eutectic is, at temperatures in the range 400 to 500° C., a black powder, which was shown by analysis and current efficiency measurements to be $ZrCl_2$.[42]

Mechanism of electrode reactions. In reversible electrode reactions the over-all process occurring at the cathode can be represented, on the basis of the current efficiency measurements, by:

$$Zr^{4+} + 4e_o^- \rightarrow Zr$$

$$Zr^{4+} + 2e_o^- \rightarrow Zr^{2+}$$

$$Zr^{2+} + 2Cl^- \rightarrow ZrCl_2 \downarrow$$

The anodic current efficiency was approximately constant, with time at 100 per cent for $Zr \rightarrow Zr^{4+}$.

Satisfactory measurements of the reversible electrode potential were not possible, because the rate of volatilization of $ZrCl_4$, at the concentration levels used, caused concentration changes that gave rise to significant changes of cell emf with time.

For electrode reactions under current flow (with *current-potential relation at constant time*) typical examples of the cell potential-current density relation (taken at intervals of a few minutes) are shown in FIGURE 10. The qualitative differences must be noted between results obtained shortly after commencing polarization and those obtained after successive current-potential curves had been measured during a period of about one hour.

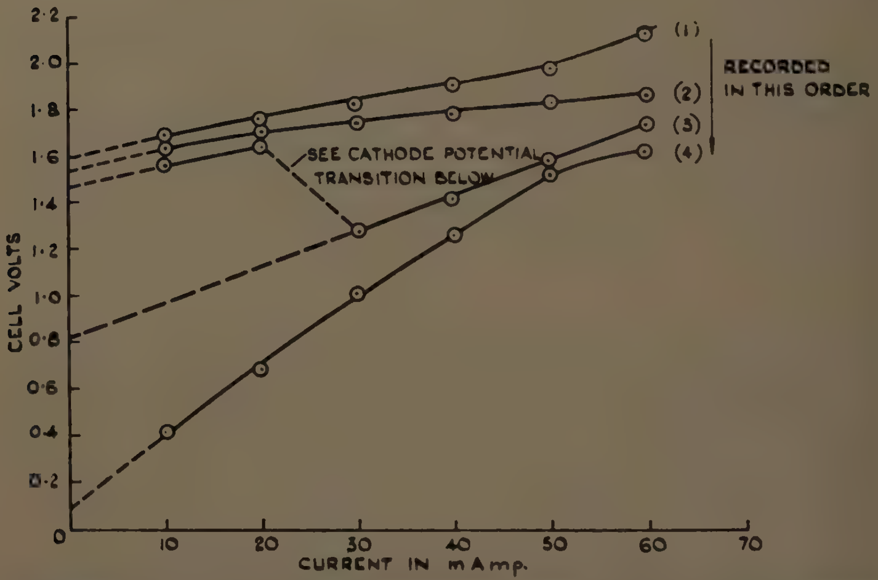

FIGURE 10. Cell volts in relation to current in a $Zr/ZrCl_4$, LiCl-KCl system; Zr anode.

Similar results for individual cathodic and anodic current-potential relations are shown in FIGURE 11.

The behavior for cathode and anode, in the case of potential-time relation at constant current, and including the effect of stirring, is shown in FIGURE 12*a* and *b*.

Discussion

The main features of the behavior of the Zr deposition resemble those of U. Thus, the relations of current to cell and electrode potentials are consistent with formations of alkali metal at short times after turning on the current. The cathode potential-current and cell potential-time relations are also consistent with this mechanism. At later times, after sufficient Zr has built up by means of the secondary electrode process, the effective area of the cathode has increased sufficiently so that the actual limiting current *density* for Zr comes within the range of the actual current through the cell, whereupon the deposition of Zr becomes primary and the electrode potential drops to the appropriate corresponding value. Consequently, the effect of stirring also can bring about a change from secondary to primary Zr deposition, in agreement with the results of FIGURES 12*a* and *b*.

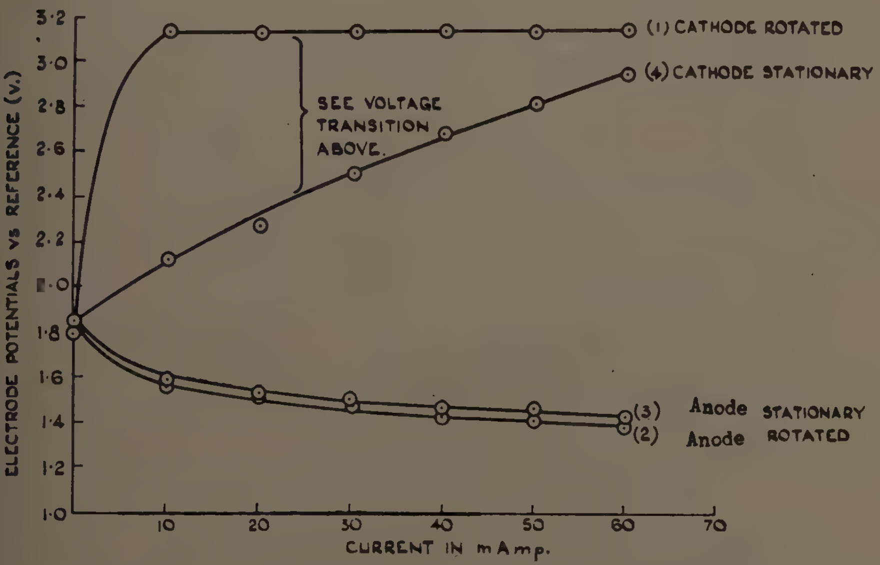

FIGURE 11. Electrode potentials in relation to current in a Zr/$ZrCl_4$, LiCl-KC system; Zr anode.

THORIUM

Experimental

The experimental methods used with Th were substantially the same as those for U and Zr. The cell examined was:

$$Ag^+ \mid AgCl, LiCl\text{-}KCl \;\vdots\; KCl\text{-}LiCl, ThCl_4 \mid Th^- \qquad (D)$$

Results

Current efficiency and metal purity. The cathodic current efficiency was about 74 per cent, and the cathodic metal gave the same analysis as that of the metal used (in anodic dissolution) to prepare the solution of $ThCl_4$ in LiCl-KCl.

The anodic current efficiency was 100 per cent for $Th \rightarrow Th^{4+} + 4e_o^-$.

Mechanism of electrode process. For the reversible electrode reaction, the dependence of the reversible emf of cell *D*, according to concentration of $ThCl_4$ and temperature is given in FIGURES 13 and 14. FIGURE 15 shows electrode reaction under current flow with current-potential relation at constant time.

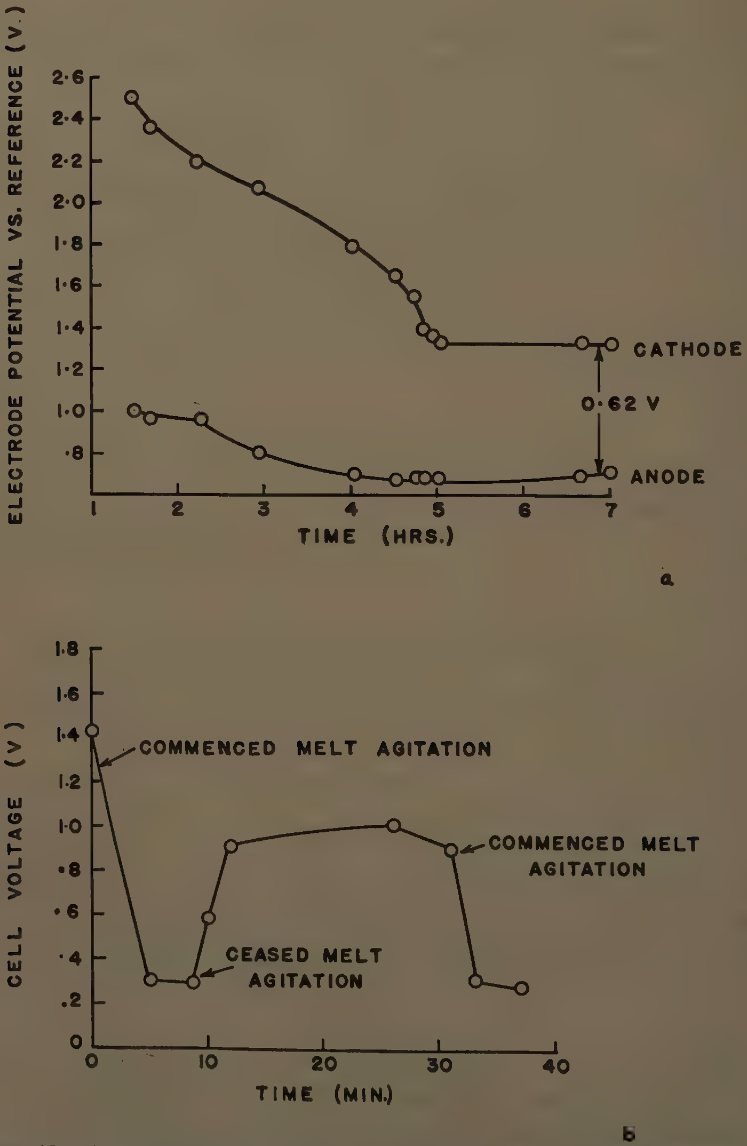

FIGURE 12. (*a*) Electrode potentials in relation to time at constant current (30 mAmp.); $Zr/ZrCl_4$, LiCl-KCl. Zr anode and cathode; agitated by Ar bubbling. (*b*) Cell voltage in relation to time at constant current (30 mAmp.); $Zr/ZrCl_4$, LiCl-KCl. Recorded near end of electrolysis; Zr anode.

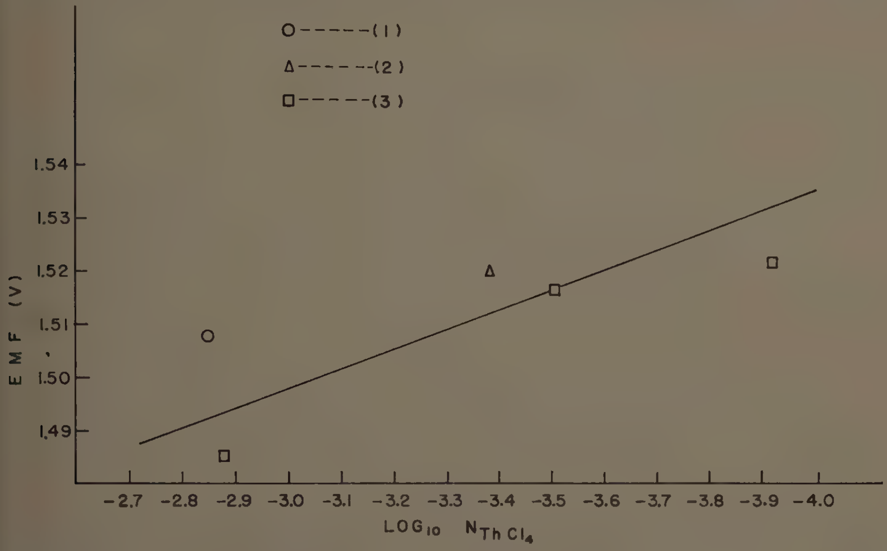

FIGURE 13. *E* in relation to $\log_{10} N_{ThCl_4}$ (420° C.) for the cell Th/ThCl$_4$, LiCl-KCl glass LiCl-KCl, AgCl/Ag.

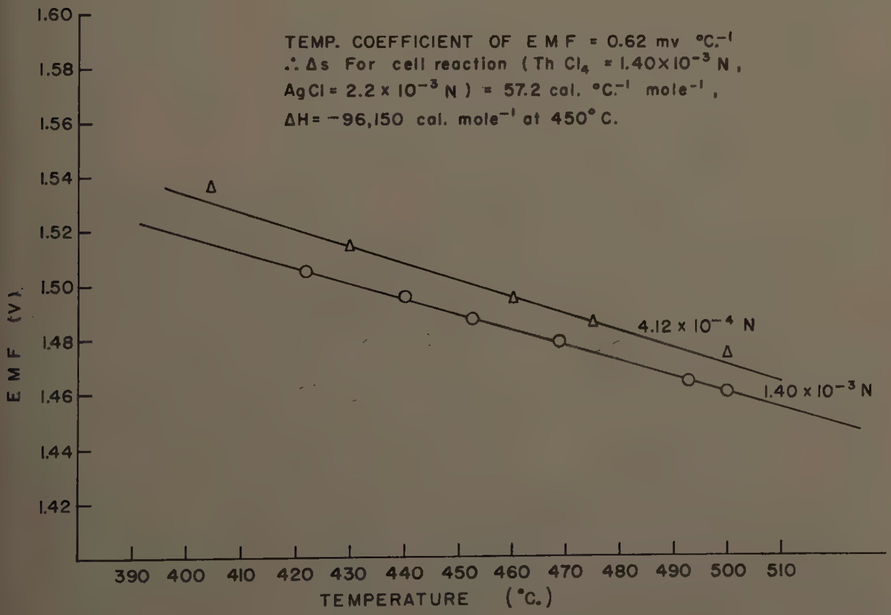

FIGURE 14. The emf in relation to temperature for the cell Th/ThCl$_4$, LiCl-KCl glass LiCl-KCl, AgCl/Ag.

Discussion

Nature of the over-all reaction. The Nernst equation is essentially applicable, although the scattering of points is considerable. The *e*-log N_{ThCl_4} plot is consistent with a value of n between 3.7 and 4.5 and therefore consistent with the value of 4 corresponding to

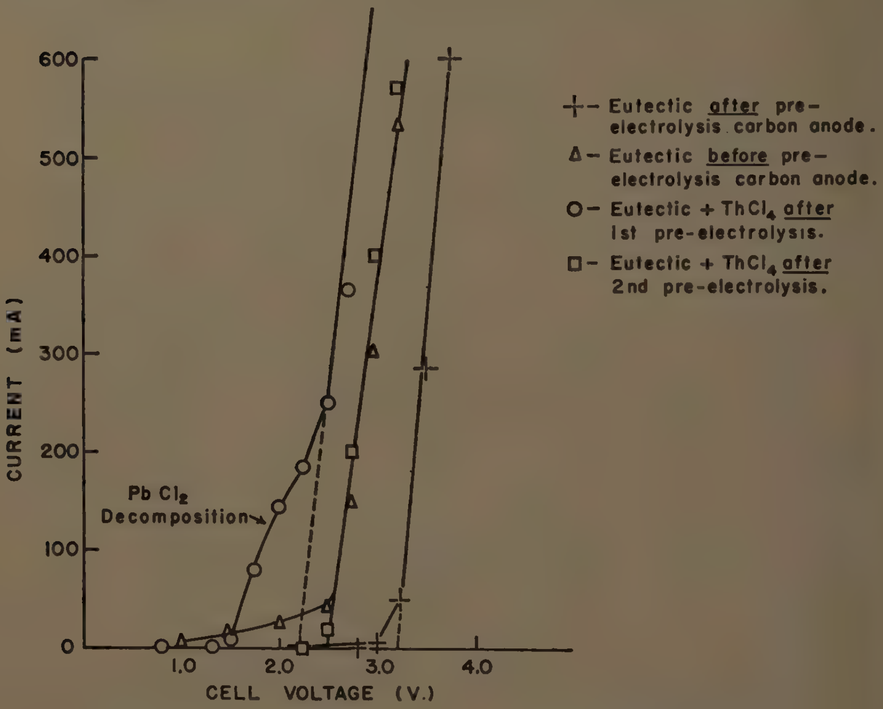

FIGURE 15. Cell volts in relation to current; Th/$ThCl_4$, LiCl-KCl.

TABLE 6

ACTIVITY COEFFICIENTS OF $ThCl_4$ IN $ThCl_4$-KCl-LiCl AT 420° C.

$ThCl_4$ (mole fraction)	f_{ThCl_4}
1.4×10^{-3}	1.1×10^{-5}
4.12×10^{-4}	1.2×10^{-5}
1.19×10^{-3}	4.8×10^{-5}
3.17×10^{-4}	2.5×10^{-5}
1.31×10^{-4}	5.0×10^{-5}

$$Th^{4+} + 4e_o^- \rightleftharpoons Th$$

This reaction is doubtless the predominant potential-determining reaction at zero current flow. The current-efficiency information suggests the introduction of a second electrode reaction at passage of a net current. The reaction probably is:

$$Th^{4+} + 2e_o^- \rightarrow Th^{2+}$$

identified as occurring in a recent polarographic examination of Smirnov and Yushina.[43]

Thermodynamics of the cell reaction. The cell reaction is:

$$Th + 4AgCl \rightleftharpoons 4Ag + ThCl_4$$

Hence, at equilibrium:

$$E = E_\circ^{ThCl_4} - E_\circ^{AgCl} - \frac{RT}{4F} \ln a_{ThCl_4} + \frac{RT}{F} \ln a_{AgCl}$$

where E^{ThCl^4} is the emf corresponding to the free energy of formation of pure $ThCl_4$ from the elements, at T °K and 1 atm. pressure; other terms are analogous to those defined in the section URANIUM.

TABLE 7

COMPLEXING CONSTANT AND STANDARD FREE ENERGY (T = 420° C.) OF COMPLEX FORMATION BETWEEN $ThCl_4$ AND Cl^- IN THE MOLTEN STATE

K	$\Delta F°$ (kcal.·mole^{-1})	Mole fraction $ThCl_4$
9.1×10^4	−15.8	1.4×10^{-3}
8.3×10^4	−15.7	4.12×10^{-4}
2.1×10^4	−13.8	1.19×10^{-3}
4.1×10^4	−14.7	3.17×10^{-4}
2.0×10^4	−13.7	1.31×10^{-4}

Hence, with the same assumptions as those made in the case of U, analogous thermodynamic calculations can be made. The results of these are given in FIGURE 14 and TABLES 6 to 8.

The thermodynamic data for the complex Th-containing anion indicates a much greater degree of complex formation than do the values with UCl_3, in agreement with the qualitative conclusion of Smirnov and Yushina,[43] and consistent with the increased polarizing power of Th^{4+} as compared with that of U^{3+}.

Mechanism of cathodic deposition. The higher degree of complexing of Th^{4+} as compared with that of U^{3+} suggests that a secondary mechanism should predominate, and that the current-potential curve should show only alkali metal deposition, or a very low limiting current, succeeded by a large increase in current corresponding to alkali metal deposition (the latter case is exactly that observed, for example, with UCl_3).

In fact, however, for the $ThCl_4$ system, no limiting current is observed. Furthermore, the value of the potential at which steady deposition occurs is nearly equal to the potential exhibited by the reversible Th electrode at the same concentration (compare FIGURES 15 and 13).

In this case, therefore, it seems as though a primary deposition of Th is occurring, but at a value exceeding the current density that would be obtained from Th^{4+} ions at the concentration indicated by the complexity constants. These facts suggest that the dissociation of the complex anion occurs to yield the equilibrium number of Th^{4+} ions at a rate equal to that at which they are removed by electrolysis.[44]

Cerium

Experimental

The technique used with Ce is similar to that used for the previous metals. Care was necessary in the preparation of $CeCl_3$ by means of the reaction of Ce with $PbCl_2$ because of the explosive nature of the reaction.

Table 8

The Variation of the Complexing Constant for the $TlCl_4$-Cl^- Complex with Temperature: Thermodynamics of Complex Formation

K	Temp. (°C.)	$\Delta F°$	$\Delta H°$	$\Delta S°$ (cal.·°C.$^{-1}$·mole^{-1})
		(kcal.·mole^{-1})		
10.7×10^4	400	−15.6	−6.8	+13.1
6.8×10^4	450	−16.1		+12.9
5.53×10^4	500	−16.9		+13.1

The cell examined was:

$$Ag^+ \mid AgCl, LiCl\text{-}KCl \;\vdots\; LiCl\text{-}KCl, CeCl_3 \mid Ce^- \tag{E}$$

Results

The anodic current efficiency was about 108 per cent. The high value is significant and probably depended upon the existence of the reaction:[45,46]

$$Ce + 3LiCl \rightarrow 3Li + CeCl_3$$

The cathodic current efficiency was determined by removal of Ce from the melt, and detected by observation of the number of coulombs needed to cause the current-voltage (I-V) curve to return to the value obtained in the absence of Ce. The efficiency was 100 per cent.

The current efficiency figures indicate that the metal deposit had a purity of 100 ± 1 per cent. The pyrophoric nature of the freshly prepared material prohibited direct analysis of the metal.

The metal always was obtained in a finely divided form mixed with alkali metal (indicated by the results of reaction with water). The metal was soft and, when cut with a knife, exhibited a faint straw color (probably due to formation of the yellow $CeO_2 \cdot H_2O$).

Mechanism of the $Ce^{3+} + 3e_o^- \rightarrow Ce$ *reaction.* Electrode reaction under current flow (with current-potential relation at constant time) shows that the current-potential curve for Ce is very close to that of the alkali metal (FIGURE 16).

With respect to reversible electrode potential, TABLE 9 shows the dependence of the potential of Ce upon the amount of added $CeCl_3$. There is a negligible dependence upon concentration; the dependence on temperature is shown in FIGURE 17.

Discussion

The constancy of the reversible potential with addition of $CeCl_3$ doubtless has an explanation similar to that given for the cell[47]

$$\text{Ti} \mid \text{TiCl}_3\text{-TiCl}_2\ \text{LiCl-KCl} \;\vdots\; \text{AgCl, LiCl-KCl} \mid \text{Ag}$$

Thus the reaction of Ce with LiCl gives rise to an equilibrium quantity of $CeCl_3$ and the addition of further amounts of $CeCl_3$ only forces the equilibrium to the Ce metal side and makes little change in the net concentration of $CeCl_3$ in the solution.

The initial electrode process corresponds to a mixed primary and secondary reduction of Ce, as was evidenced by the large amount of alkali metal in the deposit. After considerable periods of electrolysis, the potential of the working cathode was reduced, corresponding to an increased component of current due to the primary deposition of Ce, which was brought about by the increase in surface area effect discussed above.

SUMMARY

(1) The technique of thermodynamic studies of molten salts by means of experiments on galvanic cells and the processes occurring at working electrodes is described.

(2) Measurements of the dependence of the reversible, or stationary, electrode potential upon concentration, temperature, current density, and time are described for the systems U/UCl_3; $Zr/ZrCl_4$; $Th/ThCl_4$, and $Ce/CeCl_3$.

(3) U deposits with 100 per cent current efficiency according to $U^{3+} + 3e_o^- \rightarrow U$. It is complexed mainly in an alkali chloride eutectic to a complex anion. The thermodynamic parameters of this complex are given. In the deposition, alkali metal at first deposits and gives rise to secondarily produced U, indicated by an electrode potential that corresponds to Li deposition. Conditions can be achieved such that the potential at which the U is produced becomes much less negative; that is, primary deposition of U is occurring. In the former state, the U is powdery; in the latter, dendritic.

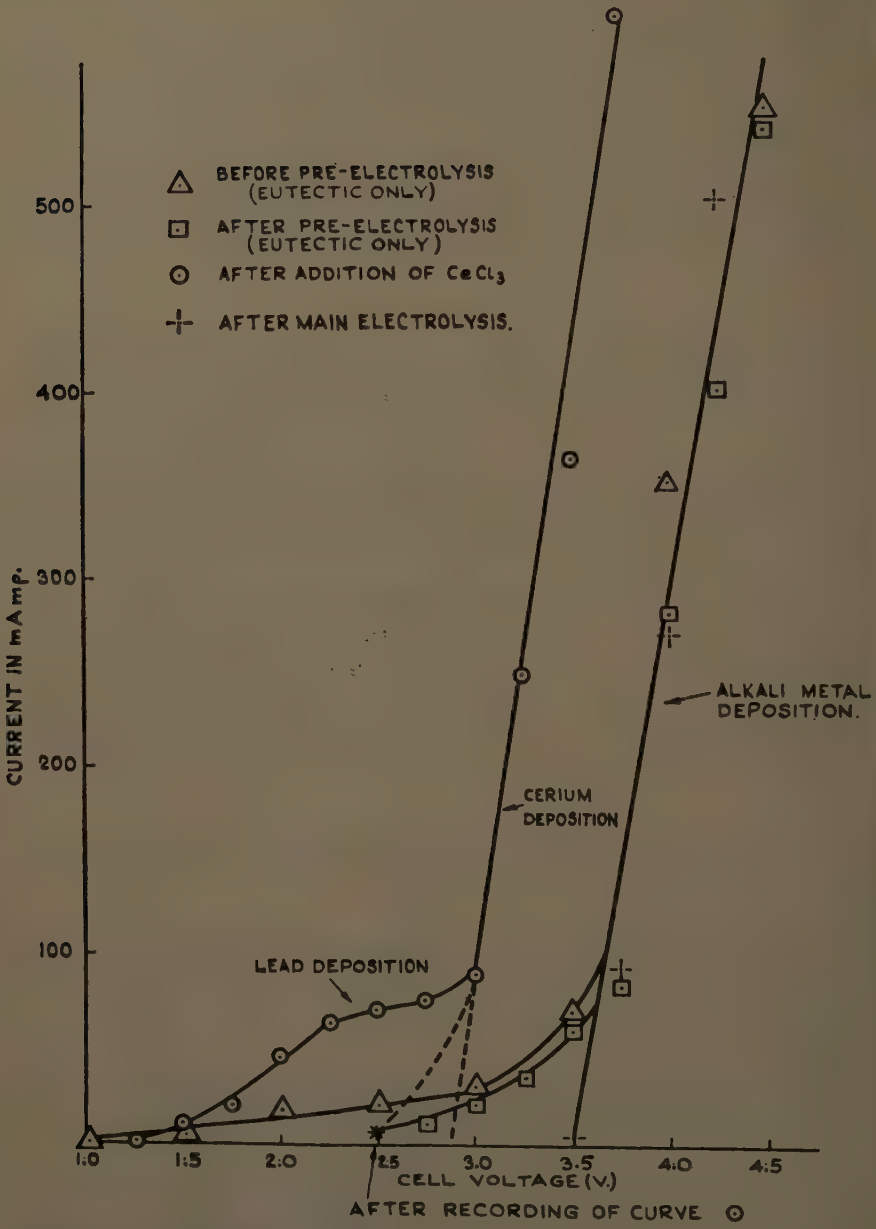

FIGURE 16. Cell voltage in relation to current (steel cathode and carbon anode); $CeCl_3$, LiCl-KCl system.

(4) For Zr, satisfactory reversible potentials could not be recorded. The deposition mechanism is analogous to that for U.

(5) The potential of the reversible Th electrode is controlled by the reaction $Th^{4+} + 4e_o^- \rightarrow Th$. In the cathodic deposition, the reaction $Th^{4+} + 2e_o^- \rightarrow Th^{2+}$ also occurs. Complexing with Cl^- takes place much more completely for Th than for U. The thermodynamics of such com-

TABLE 9

POTENTIALS OF THE CELL *E*

Weight of $CeCl_3$/KCl added (gm.)	emf (v.)	Temp. (°C.)
0.04	−2.069	435
	−2.069	415
	−2.064	415
0.25	−2.067	415
	−2.074	415
0.50	−2.058	420
	−2.058	418

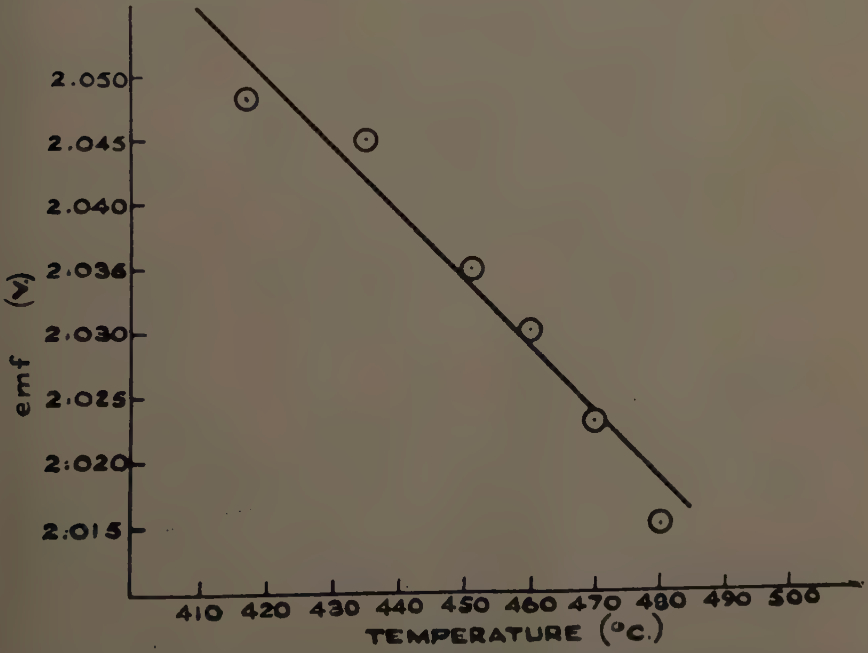

FIGURE 17. The emf in relation to temperature ($N = 4.57 \times 10^{-3}$); for the cell $Ce/CeCl_3$, LiCl-KCl glass LiCl-KCl, AgCl/Ag. Temperature coefficient of emf = 0.52 mv.·°C.$^{-1}$ Therefore ΔS for cell reaction ($CeCl_3 = 4.57 \times 10^{-3}$ *N*, AgCl = 2.2×10^{-3} *N*) = 36.1 cal.·°C.$^{-1}$·mole^{-1}, and $\Delta H = -115{,}000$ cal.·mole^{-1} at 450° C. This concentration of $CeCl_3$ was added externally.

plexes are calculated. For the deposition reaction the results are consistent with the hypothesis that dissociation of the complex halide allows direct deposition of Th at current densities greater than those corresponding to the concentration of Th^{4+} as indicated by the thermodynamic measurements.

(6) The Ce electrode undergoes reaction with the solvent to form $CeCl_3$, and this buffers the electrode, which becomes insensitive to the $CeCl_3$ concentration. In the deposition, a mixed primary deposition of alkali metal and Ce occurs at first, and is followed by increasingly primary deposition of Ce.

References

1. Antipin, L. N. 1954. Doklady Akad. Nauk S.S.S.R. **99:** 1019.
2. Smirnov, M. V. & L. D. Yushina. 1956. Isvest. Akad. Nauk S.S.S.R., Otdel. Khim. Nauk. **11:** 1285.
3. Smirnov, M. V. & N. Y. Chukreev. 1958. Zhur. Fiz. Khim. **32:** 2165.
4. Smirnov, M. V. & L. D. Yushina. 1957. Doklady Akad. Nauk S.S.S.R. **115:** 949.
5. Smirnov, M. V. & S. F. Pal'guev. 1953. Zhur. Priklad. Khim. **26:** 1166.
6. Bockris, J. O'M., G. J. Hills, I. A. Menzies & L. Young. 1956. Nature. **178:** 654.
7. Laitinen, H. A. & H. C. Gaur. 1958. Analytica Chim. Acta. **18:** 1.
8. Laitinen, H. A. & W. S. Ferguson. 1957. Anal. Chem. **29:** 4.
9. Laitinen, H. A., C. H. Liu & W. S. Ferguson. 1958. *Ibid.* **30:** 1266.
10. Lyalikov, Yu. S. 1953. Zhur. Anal. Khim. **8:** 38.
11. Steinberg, M. A. & N. H. Nachtrieb. 1950. J. Am. Chem. Soc. **72:** 3558.
12. Flengas, S. N. 1956. J. Am. Chem. Soc. **109:** 534.
13. Black, E. D. & T. DeVries. 1955. Anal. Chem. **27:** 906.
14. Panchenko, I. D. 1956. Ukrain. Khim. Zhur. **22:** 153.
15. Chovnyk, N. G. 1956. Zhur. Fiz. Khim. **30:** 277.
16. Chovnyk, N. G. & V. V. Vashchenko. 1956. Zhur. Neorg. Khim. **1:** 710.
17. Delimarskii, Yu. K. 1954. Uspekhi Khim. **23:** 766.
18. Rempel, S. I. 1950. Doklady. Akad. Nauk. **24:** 331.
19. Drossbach, P. & P. Petrick. 1954. Z. Elektrochem. **58:** 95.
20. Randles, J. E. B. & W. White. 1955. *Ibid.* **59:** 666.
21. Laitinen, H. A. & R. A. Osteryoung. 1955. J. Electrochem. Soc. **102:** 598.
22. Laitinen, H. A. & H. C. Gaur. 1957. *Ibid.*, **104:** 730.
23. Hill, D. L., G. J. Hills, L. Young & J. O'M. Bockris. 1959. In preparation.

24a. Drossbach, P. 1954. Z. Elektrochem. **58:** 686.
24b. *Idem.* 1955. *Ibid.* **59:** 512.
24c. *Idem.* 1956. *Ibid.* **60:** 387.

25. Drossbach, P. & E. Rossberger. 1956. *Ibid.* **60:** 470.
26. Drossbach, P. & P. Petrick. 1957. *Ibid.* **61:** 410.
27. Azzam, A. M., J. O'M. Bockris, B. E. Conway & H. Rosenberg. 1950. Trans. Faraday Soc. **46:** 918.
28. Gardner, H. J., C. T. Brown & G. J. Janz. 1956. J. Phys. Chem. **60:** 1458.
29. Laitinen, H. A., W. S. Ferguson & R. A. Osteryoung. 1957. J. Electrochem. Soc. **104:** 516.
30. Solomons, C., J. Goodkin, H. J. Gardner & G. J. Janz. 1958. J. Phys. Chem. **62:** 248.
31. Senderoff, S. & A. Brenner. 1954. J. Electrochem. Soc. **101:** 31.
32. Bockris, J. O'M., G. J. Hills, I. A. Menzies & L. Young. Unpublished work. Quoted in J. O'M. Bockris and N. E. Richards. 1957. Proc. Roy. Soc. London. **A241:** 44.
33. Gibson, A. R. —— M/M 44 (A.E.R.E. Report).
34. Bockris, J. O'M., G. J. Hills, D. Inman & L. Young. 1956. J. Sci. Instr. **33:** 438.
35. Inman, D. 1957. Thesis. London, England.

36. Salstrom, E. J. 1934. J. Am. Chem. Soc. **56:** 1272.
37. Salstrom, E. J. *et al.* 1936. J. Am. Chem. Soc. **58:** 1848.
38. Kordes, E., W. Bergmann & W. Vogel. 1951. Z. Elektrochem. **55:** 600.
39. Hamer, W. J., M. S. Malmberg & B. Rubin. 1956. J. Electrochem. Soc. **103:** 8.
40. Katz, J. J. & E. Rabinowitch. 1951. The Chemistry of Uranium. National Nuclear Energy Series. McGraw-Hill. New York, N.Y.
41. Borucka, A. Z., J. O'M. Bockris & J. A. Kitchener. 1957. Proc. Roy. Soc. **A241:** 554.
42. Kroll, W. J., W. R. Carmody & A. W. Schlechten. 1952. U.S. Bureau Mines Rept. Inves. No. 4915.
43. Smirnov, M. V. & L. D. Yushina. 1956. Isvest. Akad. Nauk S.S.S.R., Otdel. Khim. Nauk. **11:** 1285.
44. Delahay, P. 1954. Discussion Faraday Soc. **17:** 205.
45. Bareis, D. W., R. H. Wiswall & W. E. Winsche. 1954. Nucleonics.
46. Eastman, E. D., *et al.* 1955. TID-5212, 14–24 (A.E.C. Report).
47. Menzies, I. A., G. J. Hills, L. Young & J. O'M. Bockris. 1959. In press.

ACTIVITIES IN MOLTEN SALT MIXTURES OF POTASSIUM-LITHIUM-HALIDE MIXTURES: A PRELIMINARY REPORT

E. Aukrust, B. Björge, H. Flood,* T. Førland
Institute of Silicate Science, Norwegian Institute of Technology, Trondheim, Norway

General Experimental

The chemistry of molten salt mixtures still is to be considered as a recent field of research, and very much of the basic empirical information still is missing. This missing information seems necessary to obtain a clear picture of even the most general rules.

If, for example, the simplest systems, binary mixtures of salts with one common ion, are considered, fundamental questions such as the following are still far from being answered satisfactorily.

How do the deviations from ideal mixtures depend on the charge, radius, polarizability, or electronic shell type of the three participating ions?

In the investigations reviewed below we present a contribution to one aspect of the question: How do the deviations from ideality depend on the size of the common ion?

We elucidate this question by examining the following systems: (K-Li)F, (K-Li)Cl, and (K-Li)Br, using experimental data from phase diagrams combined with calorimetrically determined heats of mixing. The K-Li combination was chosen in order to avoid systems with solid solubility.

From the phase-diagram values of the activity of a component, independence of composition is available. The liquidus curve, however, gives the free energy of the component by a simultaneous variation of both temperature and composition, which generally will make it difficult to separate the free energy into an entropy term and a heat-content term.

Furthermore, it is desirable for the phase-diagram calculations to have an independent determination of the heat of fusion of the component, as the calculation of a heat of fusion from the phase diagram generally will require some knowledge of the species of the liquid mixture.

Finally, it is desirable to know the difference in specific heat of the components in the fused and solid states. This difference enters as a correction term in the equation for the activity from the liquidus curve

$$-RT \ln a_A = \Delta H_f\left(1 - \frac{T}{T_f}\right) - \Delta C_p\left[T_f - T\left(1 + \ln\frac{T_f}{T}\right)\right]$$

for a binary mixture A-B with no solid solution; ΔC_p is the difference in specific heat for liquid† and solid A.

---

* Visiting Professor, Department of Engineering, University of California at Los Angeles, Los Angeles, Calif.

† More exactly, the partial molar specific heat in the mixture.

Calorimetric measurements thus are a most valuable supplement to phase-diagram investigations. In addition, by combining phase-diagram data with calorimetrically determined heats of mixing, information regarding the entropy of mixing can be obtained.

We shall not go into details regarding the experimental methods that followed those described in detail in earlier papers.[1a,b] Earlier investigations on the Li-K-halide phase diagrams[2a-e] were not of sufficient accuracy for our purpose; it was necessary, therefore, to reinvestigate the systems. The liquidus curves of the phase diagrams were determined by thermal analysis, by high-temperature filtration, and also partly by a visual method of observing the temperature at which the first formation of crystals was visible. These crystals were formed directly on the thermo element dipping in the melt. The high-temperature filtrations in the system KBr-LiBr were combined with an examination of the possibility of formation of solid solutions, using small additions of a radioactive cation (Co^{60}) that was unable to enter the KBr and LiBr lattices.[1b] Within the limits of experimental error no formation of solid solutions was detectable. The resulting phase diagrams are shown in FIGURES 1 to 3.

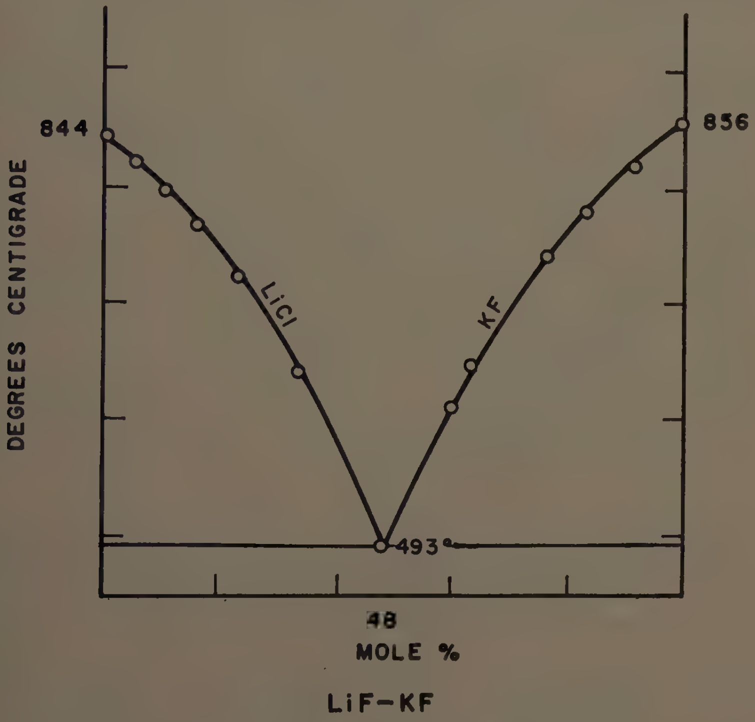

FIGURE 1. Phase diagram for the system LiF-KF.

The heat content of the alkali halides and their mixtures were obtained with a calorimeter similar to that first used by Oelsen and his co-workers,[3] and later modified by Tashiro.[4] As the calorimeter still is undergoing improvements, the results obtained should be considered as preliminary only. A more rigorous treatment of calorimetric and phase-diagram data awaits more accurate measurements, which we hope to complete in the near future. The values obtained for the heat of fusion of the pure components are shown in TABLE 1. The limits of error for these measurements are of the order of magnitude ±0.2 kcal. (TABLE 1).

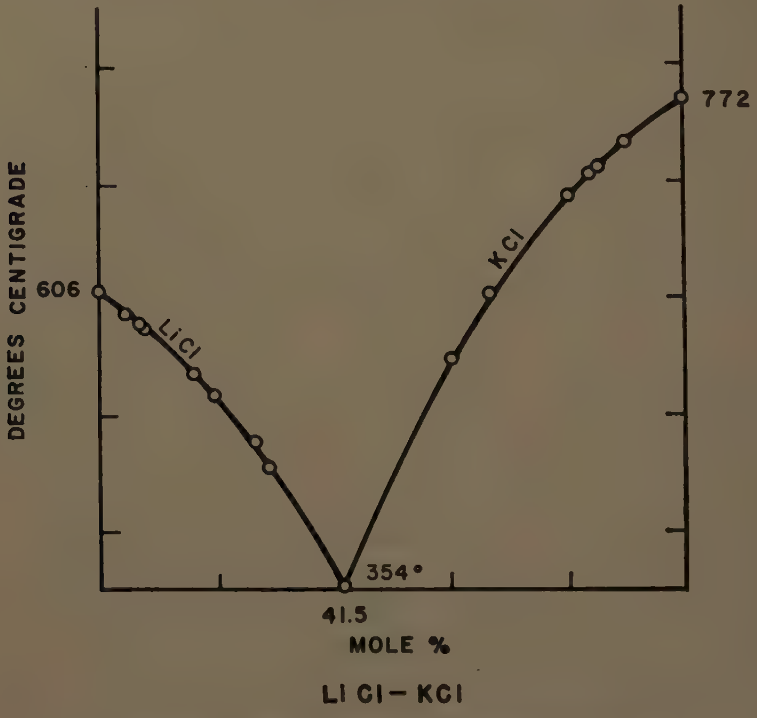

FIGURE 2. Phase diagram for the system LiCl-KCl.

For LiF and KF there is satisfying agreement between data calculated from our phase diagrams and previously published calorimetric values.

Regarding KCl, the calorimetric value of Lyashenko[6] is 0.4 kcal. lower than our phase-diagram value. Our preliminary calorimetric value is in agreement with the value from the phase diagram.

Regarding LiCl, LiBr, and KBr, our phase-diagram values are definitely higher than those given earlier in Kelley's compilation.[5] Our preliminary calorimetric values support the phase-diagram values.

The heat of fusion of the eutectic mixture of LiCl-KCl recently was reported by Solomons *et al.*[8] to be 3.20 ± 0.06 kcal. This is in agreement with our preliminary value, 3.3 kcal. with limits of error of about ±0.2 kcal.

From the calorimetrically determined heat content-temperature curves one can estimate also the correction term due to specific heats in the equa-

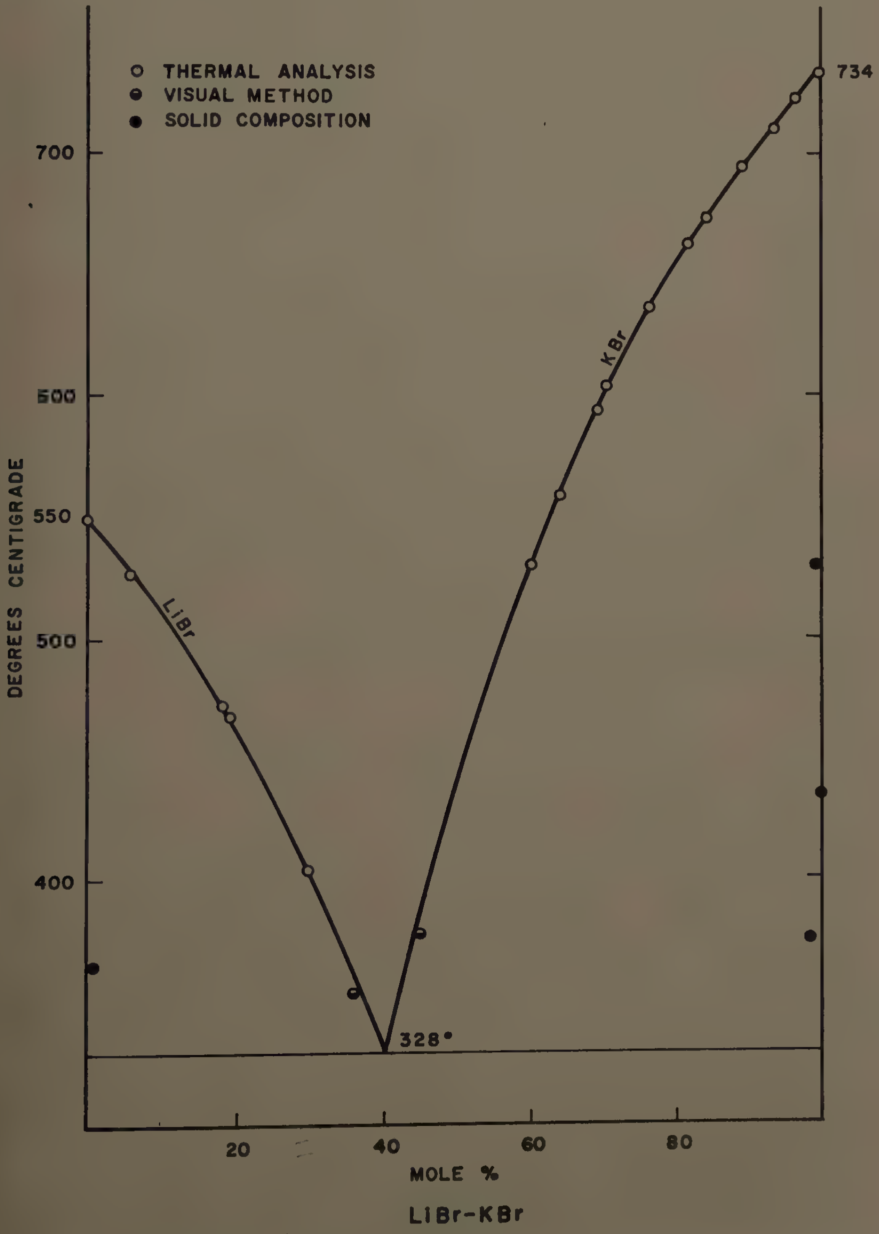

Figure 3. Phase diagram for the system LiBr-KBr.

tion for the liquidus curve of the phase diagram. For temperature ranges not very far from the melting point of the compounds this correction is insignificant. At about 100° C. from the melting point the correction is of the order of 50 cal. However, for temperature ranges of about 400° C. from the melting point, as occurs in the region of the eutectic composition, the correction term increases to an order of magnitude of 200 cal. The correction is of such a magnitude that it will tend to straighten out the curves for the activity coefficients of one component as compared to the square of the fraction of the second component. This means that the deviations from regular solution in this area of compositions are definitely smaller than that appearing from the calculations based on phase-diagram data alone.

TABLE 1
HEAT OF FUSION (KCAL./MOLE)

	From phase diagrams	From calorimetric measurements	Previously published values
LiF	6.5		6.41[7]
KF	6.7		6.75[6]
KCl	6.5	6.4	6.41[5]; 6.1[6]
LiCl	4.3	4.6	3.2[5]
LiBr	4.1	4.5	ca. 3.0[5]
KBr	6.2	6.7	ca. 5.0[5]

Discussion

The activities calculated from the phase diagram according to the formula

$$\ln a_{MX} = -\frac{\Delta H_f}{R}\left(\frac{1}{T} - \frac{1}{T_f}\right)$$

demonstrate that in all three systems there are considerable negative deviations from ideality.

Next, we are interested in which direction the deviations from ideality change with the size of the anion in the three halide systems. As the phase diagrams give data at temperature ranges, it is convenient to compare $RT \ln \gamma = \bar{F}_A - \bar{F}_{A(\text{ideal})}$ which, in regular mixtures, should be the same as the partial molar heat of mixing $\bar{H}$. In FIGURE 4, $RT \ln \gamma_1$ is plotted against N_2^2.

It seems evident that the activity-coefficient curves are asymmetrical and, furthermore, that there are no definite systematic trends in the deviations from ideal behavior when comparing the Li-K mixtures in F, Cl, and Br milieu. For the Li components the deviations are greatest in the fluoride system; the potassium components show greatest deviations in the fluoride and chloride systems (about the same in both). This some-

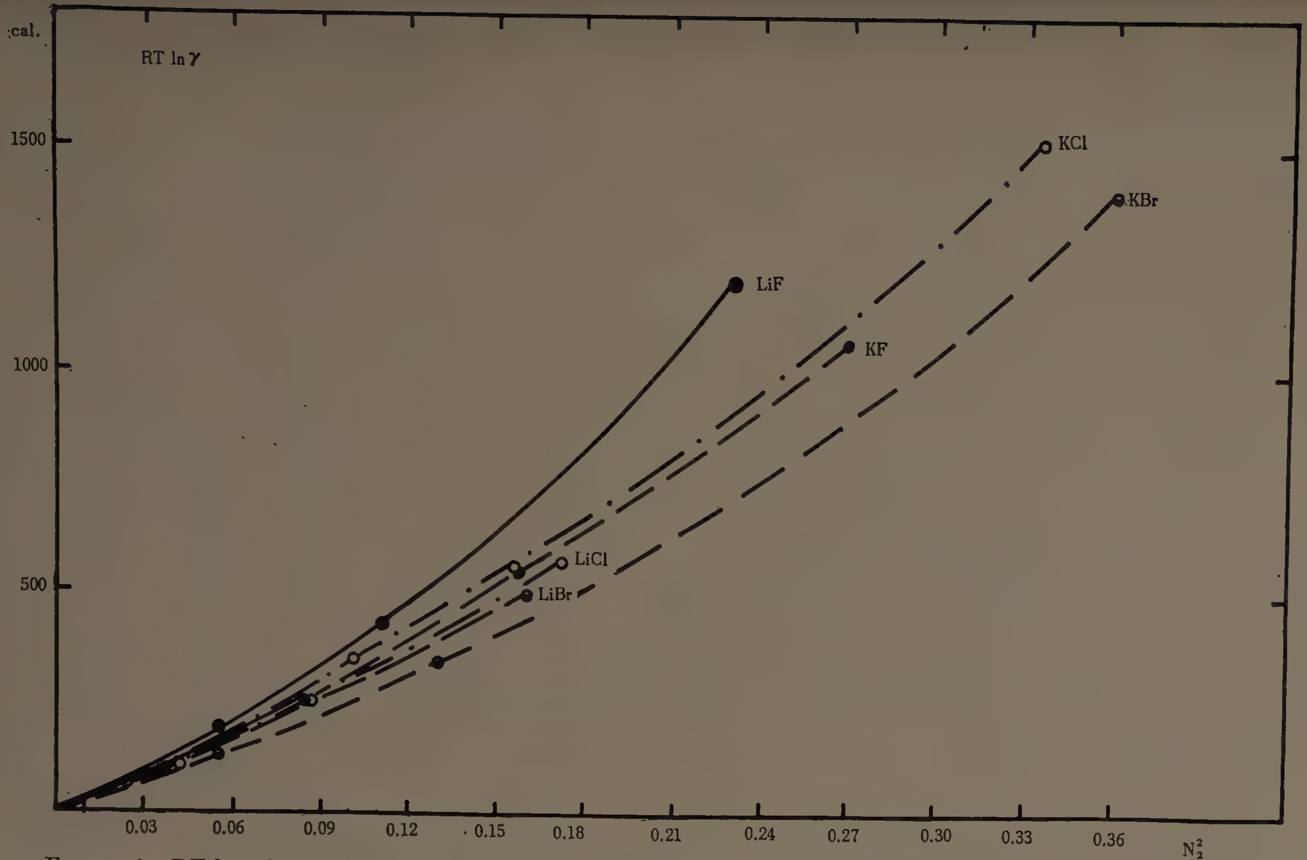

FIGURE 4. RT ln γ for a salt component plotted versus the square of the mole fraction of the second component.

what unexpected sequence may be due partly to the use of the approximate formula of log a. This, however, cannot change the important statement that the effect of an anion exchange from F to Br evidently cannot be very large. Both the nonlinear slope and the differences in the γ_1 and γ_2 functions indicate that our systems do not fit too well simple symmetrical activity expressions of the type

$$RT \ln \gamma_1 = bN_2^2$$

Assuming, however, an ideal entropy of mixing, it follows from the values of FIGURE 4 that the maximum integral heat of mixing should be of a numerical order of magnitude $\leqslant 0.8$ kcal. (Br), 0.9 to 1.0 kcal. (Cl), and 1.2 kcal. (F).

For the system (Li-K)Cl there are three different calorimetric values of the integral heat of mixing and for the system (Li-K)Br, one. These values are shown in TABLE 2.

TABLE 2

	System		$\Delta H_{\text{kcal.}}$	$\Sigma N RT \ln \gamma$
	Li	K	775° C.	
Cl	40	60	−0.6	−1.0
	58.5	41.5	−0.9 ± 0.2	
	70	30	−0.9	
			650° C.	
Br	40	60	−0.65	−0.8

Remembering that the phase-diagram values are expected to be numerically too high (as calculated from the approximate formula), our present results seem to indicate that at least a larger part of the difference $\bar{F} - \bar{F}_{\text{ideal}}$ arises from ΔH_{mixing}, and only a minor, if any at all, from deviations from ideal entropy. Compared with the values of RT 2.1 kcal. (775° C.) and 1.8 kcal. (650° C.), this result seems reasonable. At the eutectic temperatures (~350° C., RT = 1.2), however, deviations from random distribution might be of more importance.

References

1a. FLOOD, H., T. FØRLAND & A. NESLAND. 1951. Acta Chem. Scand. **5:** 1193.
1b. SELTVEIT A. & H. FLOOD. 1958. Acta Chem. Scand. **12:** 1030.
2a. BERGMAN, A. G. & E. P. DERGUNOV. 1941. Compt. rend. acad. sci. USSR. **31:** 753.
2b. ZEMCZUZNYI, S. & F. ROMBACH. 1910. Z. Anorg. Chem. **65:** 403.
2c. SCHAFER, H. N. 1913. Jahrb. Min. **43:** 932.
2d. ELCHARUS, E. & P. LAFITTE. 1932. Bull. soc. chim. France. **51:** 1572.
2e. KELLNER, G. Z. 1917. Angreg. Chem. **99:** 144.
3. OELSEN, W., K. H. RIESKAMP & O. OELSEN. 1955. Arch. Eisenhüttenwesen. **26:** 253.

4. Tashiro, M. 1956. The Glass Industry. **37:** NR10.
5. Kelley, K. K. 1936. Heat of fusion of inorganic substances. Bur. Mines Bull. **392.**
6. Lyashenko, V. S. 1950. Quoted from K. K. Kelley. Bur. Mines Bull. **477.**
7. Douglas, T. R. & J. L. Devas. 1953. Tech. Rept. Natl. Bur. Standards. 53–201.
8. Solomons, C., J. Goodkin, H. J. Gardner & G. J. Janz. 1958. J. Phys. Chem. **62:** 248.

A QUASI-LATTICE MODEL OF MOLTEN RECIPROCAL SALT SYSTEMS

Milton Blander
Oak Ridge National Laboratory, Oak Ridge, Tenn.*

Jerry Braunstein†
Department of Chemistry, University of Maine, Orono, Maine

Abstract

The activity coefficients γ_{AD} of the component AD have been calculated theoretically, using two different approximations based on the lattice model for the molten reciprocal salt system A^+, B^+, C^-, D^-. The first is the asymmetric approximation in which the groupings $AC_n^{+(1-n)}$ are included where $n \leq Z$. This leads to the relation

$$\gamma_{AD} = \frac{(1 - X)^Z \left[1 + \frac{X}{\beta(1 - X)}\right]^{Z-1}}{N_{D^-}} \tag{1}$$

where Z is the lattice coordination number, $\beta = e^{-\Delta E/RT}$, and ΔE is the relative energy of interaction of a mole of A^+-C^- pairs; X, the fraction of positions adjacent to an A^+ ion that are occupied by C^- ions, can be calculated from the distribution function for the asymmetric approximation in terms of Z, ΔE, and the concentrations of all the ions in solution. The second or symmetric approximation includes the groupings $A_mC_n^{+(m-n)}$ where m and n are any integers. This method leads to the relation

$$\gamma_{AD} = \left(\frac{1 - Y}{1 - N_{C^-}}\right)^Z \tag{2}$$

where Y can be calculated from the distribution function for the symmetric approximation in terms of Z, ΔE, and the concentrations of the ions in solution.

The activity coefficients of $AgNO_3$ in the two molten solvents KNO_3 and $NaNO_3$ dilute in Ag^+ and Cl^- ions were measured in an electromotive-force (emf) cell. The activity coefficients of $AgNO_3$, γ_{AgNO_3}, are much lower in the KNO_3 solvent than in the $NaNO_3$ solvent at the same temperature and at the same concentrations of Ag^+ and Cl^- ions. The concentration dependence of γ_{AgNO_3} in the KNO_3 solvent corresponds more closely to the concentration dependence of γ_{AD} as calculated from the

---

* Operated for the United States Atomic Energy Commission, Washington, D.C., by the Union Carbide Corporation, New York, N.Y.

† Summer participant with the Chemistry Division of the Oak Ridge National Laboratory, Oak Ridge, Tenn.

asymmetric approximation (for $Z = 6$, $\Delta E = -5.6_5$) than to the concentration dependence calculated from the symmetric approximation. In the $NaNO_3$ solvent, the concentration dependence of γ_{AgNO_3} corresponds more closely to the calculation based on the symmetric approximation (for $Z = 6$, $\Delta E = -4.5_5$).

The differences between the behavior in the two solvents can be correlated with the relative sizes of the K^+ and Na^+ ions and with the relative effects of the fields of these two solvent cations on the energy of interaction of an Ag^+-Cl^- pair.

Introduction

The concept of complex ions has been used so freely and in so many different senses in describing molten salt solution behavior that its meaning has become unclear. Even simple physical theories may help to separate the different physical factors that cause nonideal solution behavior and may lead to better-defined and more general descriptions of molten salt behavior. In this paper a quasi-lattice model for molten reciprocal salt systems is described, and calculations based on this model are compared to experimental measurements of the activity of $AgNO_3$ in the KNO_3-$AgNO_3$-KCl system and in the $NaNO_3$-$AgNO_3$-$NaCl$ system. The theory demonstrates one fallacy in the description of molten salt behavior in terms of complex ions.

Reciprocal molten salt mixtures are those containing at least two cations and two anions. The equations for the solution behavior of an ideal reciprocal salt solution are given by Temkin.[1] The first physical theory of a nonideal reciprocal salt solution was the quasi-thermodynamic theory of Flood *et al.*,[2] which, although incorrect, was valuable in the derivation of the theory given here. The method of calculation from the quasi-lattice model described here is similar to that used in the quasi-chemical theory.[3]

The Quasi-Lattice Model

The quasi-lattice model has been described previously.[4] While it is certain that molten salts are not perfectly ordered arrays of ions, a lattice model can be justified since free-energy differences are calculated between two liquid states, each of which is approximated by a lattice, and most of the errors stemming from the use of a lattice model are eliminated.

The simplest reciprocal salt system is that containing two cations, A^+ and B^+, and two anions, C^- and D^-. The lattice model is an assembly of these ions in a vacuum and consists of two interlocking sublattices, one a lattice of cations A^+ and B^+ and the other a lattice of anions C^- and D^-. The nearest neighbors of the cations are anions and of the anions, cations. All of the ions have the same coordination number, Z. The model is restricted to the case in which cations and anions, respectively, have the same size and charge. This eliminates any difference in the coulombic interactions between A^+ or B^+ ions or C^- or D^- ions and the solution, and limits the model to short-range extracoulombic interactions. Further, a nearest-neighbor relative interaction between A^+ and C^- ions is postulated such that the energy of interaction of an A^+-C^- ion pair that are nearest neighbors is not zero. FIGURE 1 is a two-dimensional representation of the lattice. The interchange of the circled D^- ion that is adjacent to one A^+ and $(Z - 1)B^+$ ions with the C^- ion that is adjacent to ZB^+ ions gives rise to an energy change $\Delta\epsilon = (\Delta E/\mathcal{N})$, where $\mathcal{N}$ is Avogadro's number. Defining the pair interaction energy of A^+-D^- as ϵ_1, B^+-C^- as ϵ_2, A^+-C^- as ϵ_3, and B^+-D^- as ϵ_4, then

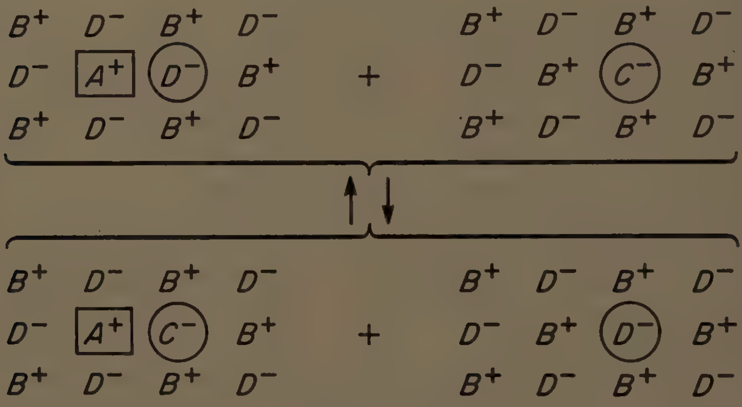

FIGURE 1.

$$\Delta\epsilon = \epsilon_4 + \epsilon_3 - \epsilon_2 - \epsilon_1 = \frac{\Delta E}{\mathcal{N}} \qquad (1)$$

The Asymmetric Approximation

The asymmetric approximation has been described previously in more detail[4] and only the salient features will be discussed here. In this approximation the interaction of an A^+ ion with as many as ZC^- ions is included with each A^+-C^- pair interaction having an energy $\Delta\epsilon$. A C^- ion can interact, in this approximation, with only one A^+ ion. This approximation thus includes the groupings $AC_n^{+(1-n)}$, where $n \leq Z$.

The positions in the anionic lattice are divided into two types, a and b. Type a positions are those adjacent to one A^+ ion and $(Z - 1)B^+$ ions; type b positions are those adjacent to ZB^+ ions. In solutions dilute in A^+ ions and for the case in which a C^- ion will interact strongly with only one A^+ ion, those C^- ions adjacent to more than one A^+ ion may be neglected.

The C^- and D^- ions are distributed between positions of type a and b. The relative energy of a C^- ion in an a position is $\Delta\epsilon$.

The most probable distribution of C^- and D^- ions was calculated by maximizing Ω', the total number of ways of distributing C^- and D^- ions in regions a and b, under the restrictions of constant total energy and at a constant number of C^- ions. The most probable distribution function is:

$$\left(\frac{X}{1-X}\right) = \left(\frac{N_{C^-} - ZXN_{A^+}}{1 - Z(1-X)N_{A^+} - N_{C^-}}\right)\beta \tag{2}$$

where $N_{A^+} \equiv [(n_{A^+})/(n_{A^+} + n_{B^+})]$ and is the cationic fraction of A^+ ions, where $N_{C^-} \equiv [(n_{C^-})/(n_{C^-} + n_{D^-})]$ and is the anionic fraction of C^- ions, and where $n_{i\pm}$ is the number of moles of the i'th ion, $\beta = e^{-(\Delta E/RT)} = e^{-(\Delta\epsilon/kT)}$, and X is the fraction of positions adjacent to an A^+ ion that are occupied by C^- ions. Since the dilution of the solution to infinite dilution of A^+ and C^- ions will separate all the A^+-C^- pairs, the total heat of dilution is given by the negative of the total energy of interaction of all the A^+-C^- pairs:

$$-\Delta H_{\text{dil.}} = Zn_{A^+}X\Delta E \tag{3}$$

The total entropy of solution is given by

$$\Delta S = k \ln \Omega_T \tag{4}$$

where

$$\Omega_T = \Omega\,\frac{[(n_{A^+} + n_{B^+})\mathcal{N}]!}{[n_{A^+}\mathcal{N}]!\,[n_{B^+}\mathcal{N}]!} \tag{5}$$

and where

$$\Omega = \frac{[Zn_{A^+}\mathcal{N}]!\,[(n_{C^-} + n_{D^-} - Zn_{A^+})\mathcal{N}]!}{[Zn_{A^+}\mathcal{N}(1-X)]!\,[Zn_{A^+}\mathcal{N}X]!\,[(n_{D^-} - Zn_{A^+}(1-X))\mathcal{N}]!\,[(n_{C^-} - Zn_{A^+}X)\mathcal{N}]!} \tag{6}$$

The approximation given by EQUATION 5 implies that there is no correlation between the positions occupied by A^+ ions. By combining EQUATIONS 2, 3, 4, and 5 to obtain the total free energy of dilution, and differentiating with respect to n_{AD}; the equation

$$\bar{F}_{AD} - \bar{F}^*_{AD} = RT \ln N_{A^+}(1-X)^Z \left(1 + \frac{X}{\beta(1-X)}\right)^{(Z-1)} \tag{7}$$

is obtained,* where the asterisk as superscript denotes a standard state chosen such that the activity coefficient is unity at infinite dilution. If the activity coefficient γ_{AD} is defined by the equation

---

* EQUATIONS 2, 3, 5, and 6 can be given in terms of n_{A^+}, n_{B^+} and n_{C^-}. The choice of three components AD, BC, and BD leads to the substitution of $n_{AD} = n_{A^+}$, $n_{BC} = n_{C^-}$, and $n_{BD} + n_{BC} = n_{B^+}$. It is easy to show that differentiating with respect to n_{AD} in the substituted expressions is the same as differentiating the original expression with respect to n_{A^+}.

$$\bar{F}_{AD} - \bar{F}^*_{AD} \equiv RT \ln N_{A^+} N_{D^-} \gamma_{AD} \tag{8}$$

then*

$$\gamma_{AD} = \frac{(1 - X)^Z}{N_{D^-}} \left(1 + \frac{X}{\beta(1 - X)}\right)^{(Z-1)} \tag{9}$$

The Symmetric Approximation

In the symmetric approximation, the method of Guggenheim[3] is applied to the calculation. The assumption is made that the relative energy of interaction of any given pair of ions that are nearest neighbors is the same, independent of the local environment. This is equivalent to the assumption of the noninterference of pairs. The energy of interaction of the pair A^+-C^-, $\Delta\epsilon$, is given by EQUATION 1 as in the asymmetric approximation. In the symmetric approximation a given C^- ion may interact with as many as ZA^+ ions, and an A^+ ion with as many as ZC^- ions, the relative energy of each interaction being $\Delta\epsilon$. This approximation includes all groupings of A^+ and C^- ions $A_mC_n^{+(m-n)}$, where m and n can be any integer. In dilute solutions of A^+ and C^- the major groupings will be for small m and n.

The four types of pairs are A^+-D^-, B^+-C^-, A^+-C^-, and B^+-D^-, and the total number of all these pairs is $Z(n_{A^+} + n_{B^+})\mathcal{N}$. If Y' is defined as the fraction of positions adjacent to the A^+ ions that are occupied by C^- ions, then the number of pairs of each kind and the total energy of such pairs are as given in TABLE 1. $R_a' = Zn_{A^+}\mathcal{N}$ and is the number of positions adjacent to all the A^+ ions; $R_b' = Zn_{B^+}\mathcal{N}$ and is the number of positions adjacent to all the B^+ ions; S_a' is the number of positions adjacent to the A^+ ions occupied by C^- ions; and S_b' is the number of positions adjacent to the B^+ ions occupied by C^- ions.

---

* An alternate derivation of EQUATION 9 can be made by evaluating the integral

$$\frac{\Delta F^E}{T} = -\int_{(1/T')=0}^{(1/T')=(1/T)} \Delta H_{\text{dil.}}\, d\left(\frac{1}{T'}\right) = \int_{(1/T')=0}^{(1/T')=(1/T)} Zn_{A^+} X \Delta E\, d\left(\frac{1}{T'}\right) \tag{i}$$

to obtain ΔF^E, the total excess free energy of dilution. The lower limit of integration is fixed, since $(\Delta F^E/T') \rightarrow 0$ as $(1/T') \rightarrow 0$. Differentiating $\Delta F^E(T)$ with respect to n_{AD} leads to EQUATION 8. This method of calculation has been discussed by Guggenheim.[3]

It is interesting to note that the need for the lattice model may be eliminated by use of EQUATION i if two regions for possible occupation by C^- ions are postulated. One region is the coordination sphere adjacent to A^+ ions with relative energy $\Delta\epsilon$: and volume v_a, and the other region is of volume v_b and zero energy. If X is defined as the fraction of v_a occupied by C^- ions, Z as the maximum number of C^- ions that can fit into the coordination sphere of one A^+ ion, and v_b is set equal to $n_{C^-} + n_{D^-} - Zn_{A^+}$, then it is easy to derive EQUATION 2 without the lattice model. Substituting for X in EQUATION 3, $\Delta H_{\text{dil.}}$ is obtained; from it ΔF^E and EQUATION 9 may be derived by use of EQUATION i. The lattice model is thus merely a method of choosing v_a, v_b, and reasonable values of Z.

The number of ways of distributing these pairs, ω_s', is:

$$\omega_s' = \frac{(R_a' + R_b')!}{(R_a' - S_a')!S_a'!(R_b' - S_b')!S_b'!} \tag{10}$$

ω_s', when summed over all possible values of Y', leads to an incorrect value for the total number of configurations. A normalization factor that will correct for this can be calculated.[5] With the normalizing factor the combinatory formula becomes

$$\Omega_s' = \frac{S_a^\dagger!(R_a^\dagger - S_a^\dagger)!S_b^\dagger!(R_b^\dagger - S_b^\dagger)![(n_{A^+} + n_{B^+})\mathcal{N}]![(n_{C^-} + n_{D^-})\mathcal{N}]!}{S_a'!(R_a' - S_a')!S_b'!(R_b' - S_b')!(n_{A^+}\mathcal{N})![n_{B^+}\mathcal{N}]!(n_{C^-}\mathcal{N})!(n_{D^-}\mathcal{N})!} \tag{11}$$

TABLE 1

Type of pair	Total number	Total energy
A^+-D^-	$Zn_{A^+}(1 - Y')\mathcal{N} = R_a' - S_a'$	0
B^+-C^-	$Z(n_{C^-} - n_A Y')\mathcal{N} = S_B'$	0
A^+-C^-	$Zn_{A^+}Y'\mathcal{N} = S_a'$	$Zn_{A^+}Y'\Delta\epsilon$
B^+-D^-	$Z(n_{B^+} - n_{C^-} + n_A Y')\mathcal{N} = R_B' - S_B'$	0

where the superscript dagger on a symbol means that the value of the quantity represented by that symbol is for a random distribution of the ions (that is, $Y' = N_{C^-}$). If one maximizes Ω_s' under the condition of constant total energy and constant number of the ions involved, the most probable distribution of ions is obtained:

$$\left(\frac{Y}{1 - Y}\right) = \left(\frac{N_{C^-} - N_{A^+}Y}{N_{B^+} - N_{C^-} + N_{A^+}Y}\right)\beta \tag{12}$$

where the absence of a prime on Y (or Ω_s) denotes the values of Y' (or Ω_s') for the most probable distribution. The total heat of dilution is*

$$-\Delta H_{\text{dil.}} = Zn_{A^+}Y\Delta E \tag{13}$$

and the total entropy of solution is

$$\Delta S = k \ln \Omega_s \tag{14}$$

By combining EQUATIONS 13 and 14 to obtain the total free energy of dilution, substituting for Ω_s and Y from EQUATIONS 11 and 12, and differentiating this quantity with respect to n_{AD}, the following equations are obtained:

$$\bar{F}_{AD} - \bar{F}_{AD}^* = RT \ln N_{A^+}N_{C^-}\left(\frac{1 - Y}{1 - N_{C^-}}\right)^Z \tag{15}$$

---

* The equations to be derived can be obtained by the integration of EQUATION *i* in the preceding footnote. The introduction of the normalizing factor is equivalent to setting $(\Delta F^E/T') = 0$ at $(1/T') = 0$.

and

$$\gamma_{AD} = \left(\frac{1 - Y}{1 - N_{C^-}}\right)^Z \tag{16}$$

Critique of the Approximations

The approximations used in the calculations place limitations upon the derived equations that are independent of any limitations imposed by the use of a lattice model for liquids. Since the model has been restricted to nearest-neighbor interactions the theory should, strictly speaking, not be applicable to systems in which either the cations or the anions have a different size and charge. The form of the derived equations is, however, probably good in many cases for dilute solutions of A^+ and C^- ions in such systems.

Another restriction is the one imposed by assuming that the energy of interaction of each nearest-neighbor pair is the same. For example, in the equation

$$AC_{(n-1)}^{+(2-n)} + C^- \rightleftharpoons AC_n^{+(1-n)} \qquad \Delta\epsilon_n \qquad 1 \leq n \leq Z$$

which represents all the interactions accounted for in the asymmetric approximation, the assumption has been made that the values of $\Delta\epsilon_n$ are equal for all the n. If there were a saturation effect on A^+-C^- pair interactions such that $|\Delta\epsilon_1| > |\Delta\epsilon_2|$, then the calculated activity coefficients γ_{AD} for negative values of $\Delta\epsilon_n$ would be too low for values of X large enough for the existence of an appreciable fraction of the AC_2^- groupings. In the asymmetric approximation, interactions

$$AC_n^{+(1-n)} + A^+ \rightleftharpoons A_2C_n^{+(2-n)} \qquad \Delta\epsilon_a$$

are completely neglected. If groupings $A_2C_n^{+(2-n)}$ exist then at such high concentrations of A^+ ions that there is an appreciable number of these groupings present, the values of γ_{AD} calculated from the asymmetric approximation will be too high. In the symmetric approximation $\Delta\epsilon_a = \Delta\epsilon_1$. If there is a saturation effect on A^+-C^- interactions such that $|\Delta\epsilon_a| < |\Delta\epsilon_1|$, then the activity coefficients calculated from the symmetric approximation for negative values of $\Delta\epsilon$ at concentrations of A^+ sufficiently high to have an appreciable number of $A_2C^{+(2-n)}$ will be too low, since the number of members of the species $A_2C_n^{+(2-n)}$ included in the calculation is too high. The extent of deviation of measurements from theory will depend on the extent of the saturation of bonds (or the effect of the interference of pairs). It should be noted that, as expected, the asymmetric and the symmetric approximations are equal at $N_{A^+} = 0$.

An interesting observation can be made from EQUATIONS 9 and 15. In EQUATION 9, X is the fraction of positions adjacent to an A^+ ion occupied by C^- ions in the asymmetric approximation. The quantity $(1 - X)$ is the fraction of positions adjacent to an A^+ ion that are not occupied by C^- ions. $(1 - X)^Z$ and similarly $(1 - Y)^Z$ are then the fractions of the total number of A^+ ions that have no C^- ions in any of the Z positions adjacent to them. This might be termed the fraction of free A^+ ions. In the complex ion terminology it is usually implied that the fraction of free A^+ ions, with suitable small correction factors for use with other concentration scales, should be equal to the activity coefficient.[6,7] EQUATIONS 9 and 16 demonstrate that this usage in the complex ion terminology is not consistent with the lattice model and that correction terms or activity coefficients for the free A^+ ions are necessary for solutions not very dilute in C^- ions.

Experimental

Values of the activities of $AgNO_3$ in the KNO_3-$AgNO_3$-KCl system have been obtained from emf measurements of the concentration cell A at 370°, 385°, 402°, 423°, and 436° C.[8,9]

$$\text{Ag}\;\left|\begin{matrix}\text{KNO}_3\\ \text{AgNO}_3\end{matrix}\right\|\begin{matrix}\text{KNO}_3\\ \text{AgNO}_3\\ \text{KCl}\end{matrix}\left|\;\text{Ag}\right. \qquad (A)$$

for dilute solutions of $AgNO_3$ and KCl in molten KNO_3. In FIGURE 2 are plotted the derived values of $-\log \gamma_{AgNO_3}$ at 402° C. as a function of the mole ratios of KCl, R_{KCl} at several values of the mole ratio of $AgNO_3$, R_{AgNO_3}, where $R_{KCl} = (n_{KCl}/n_{KNO_3})$ and $R_{AgNO_3} = (n_{AgNO_3}/n_{KNO_3})$. The mole ratios R_{KCl} and R_{AgNO_3} are larger than the ion fractions N_{Cl^-} and N_{Ag^+}, respectively, by the factor $1 + R_{KCl} + R_{AgNO_3}$, which is not very different from unity in dilute solutions.

Measurements were also made of the activity of $AgNO_3$ in the $NaNO_3$-$AgNO_3$-NaCl system at 402° C. from emf measurements in cell B

$$\text{Ag}\;\left|\begin{matrix}\text{NaNO}_3\\ \text{AgNO}_3\end{matrix}\right\|\begin{matrix}\text{NaNO}_3\\ \text{AgNO}_3\\ \text{NaCl}\end{matrix}\left|\;\text{Ag}\right. \qquad (B)$$

Derived values of $-\log \gamma_{AgNO_3}$ as a function of R_{NaCl} at several values of R_{AgNO_3} are shown in FIGURE 3.

Comparison to Theory

The correspondence of the KNO_3-$AgNO_3$-KCl and the $NaNO_3$-$AgNO_3$-NaCl systems to the theoretical systems, A^+, B^+, C^-, D^-, can be made if $A^+ \equiv Ag^+$, $B^+ \equiv K^+$ or Na^+, $C^- \equiv Cl^-$ and $D^- \equiv NO_3^-$. The sizes of the Ag^+ and Na^+ ions in the melt are probably similar, whereas the K^+ ion is probably larger than the Ag^+ ion. The size and shape of the spherically symmetric Cl^- ion are different from those of the flat NO_3^- ion. In dilute solutions these deviations in the size and shape of the ions from the conditions imposed by the lattice model probably do not affect the form of the equations derived from the model. FIGURE 4 is a plot of $-\log \gamma_{AD}$ versus N_{C^-} at several values of N_{A^+} for $Z = 6$ and for $\beta = 67$ as calculated using the asymmetric approximation, from EQUATIONS 2 and 9. This corresponds to the measurements on the KNO_3-$AgNO_3$-KCl system at 402° C. Qualitatively, there is a striking similarity between the experimental results on $-\log \gamma_{AgNO_3}$ and the calculated values of $-\log \gamma_{AD}$. The values calculated from the theory were relatively insensitive to the variation of Z at constant values of $Z\beta$. At $R_{AgNO_3} = 0.279 \times 10^{-3}$ the curvature of $-\log \gamma_{AgNO_3}$ is greater than the theoretical results, the values of $\log \gamma_{AD}$ being more negative at the higher values of N_{C^-} (and X) than the measured values. As already discussed, this can be explained by a saturation effect

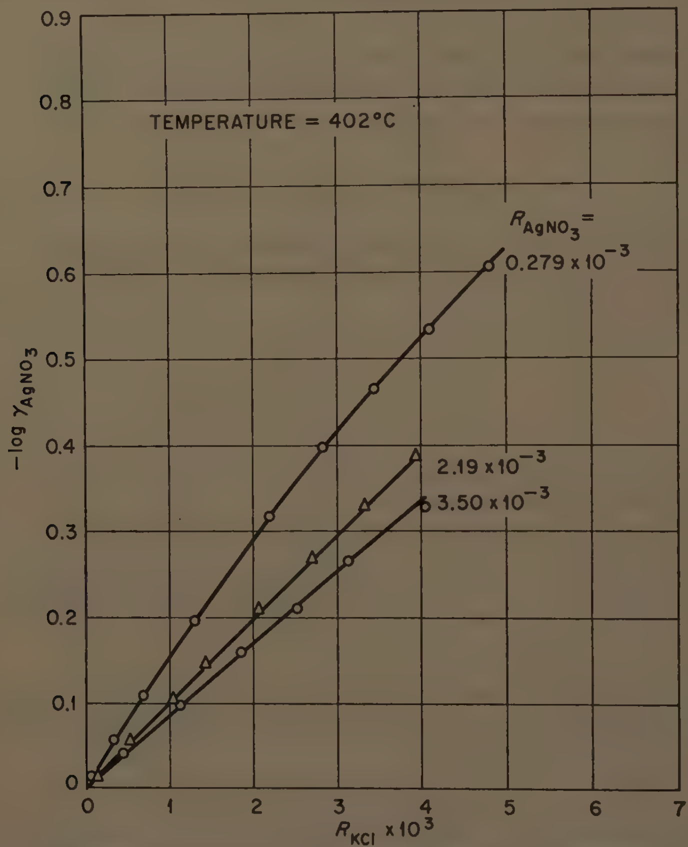

FIGURE 2. Measured values of $-\log \gamma_{AgNO_3}$ in KNO_3 as a function of R_{KCl} and R_{AgNO_3} at 402° C.

on A^+-C^- bonds such that $|\Delta\epsilon_2| < |\Delta\epsilon_1|$. The variation of $-\log \gamma_{AD}$ with N_{A^+} at a fixed value of N_{C^-} is greater than the variation of $-\log \gamma_{\mathrm{AgNO_3}}$ with $R_{\mathrm{AgNO_3}}$ at fixed values of R_{KCl}.

FIGURE 5 is a plot of $-\log \gamma_{AD}$ versus N_{C^-} at several values of N_{A^+} for $Z = 6$ and $\beta = 62$ as calculated from the symmetric approximation. The values of $\log \gamma_{AD}$ were fitted to the measured values of $\log \gamma_{\mathrm{AgNO_3}}$ in the dilute solutions of Ag^+ and Cl^- ions. The variation of $\log \gamma_{AD}$ with N_{A^+} at a fixed value of N_{C^-} is much smaller than for the asymmetric approximation or than the experimental measurements of $\log \gamma_{\mathrm{AgNO_3}}$. The experimental measurements lie between the calculated values for the symmetric and the asymmetric approximation, being much closer to the asymmetric approximation. This may be a consequence of the saturation effect such that $0 < |\Delta\epsilon_a| \ll |\Delta\epsilon_1|$.

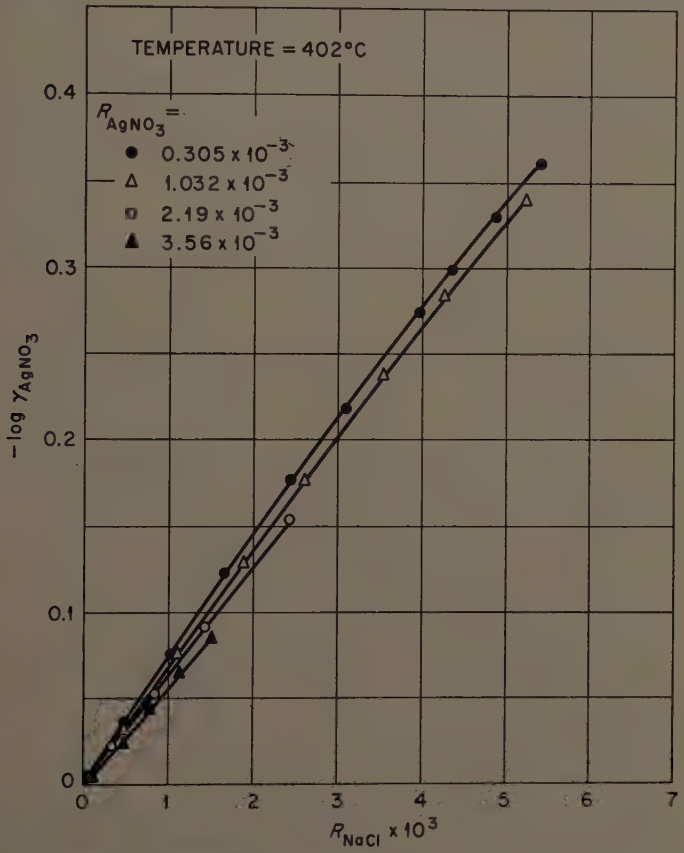

FIGURE 3. Measured values of $-\log \gamma_{\mathrm{AgNO_3}}$ in $NaNO_3$ as a function of R_{NaCl} and $R_{\mathrm{AgNO_3}}$ at 402° C.

In a similar manner, the measurements on the KNO_3-$AgNO_3$-KCl system at 370°, 385°, 423°, and 436° C. were fitted to the asymmetric theory at low concentrations of Ag^+ and Cl^- (for values of $X < 0.15$ and $N_{A^+} = 0.00028$) where the theory is most valid.[4,8,9] For a coordination number of 6 values of the energy of formation of a mole of ion pairs, of -5.65 ± 0.03 kcal./mole were obtained at all temperatures. The constancy of ΔE for all the temperatures studied lends credence to the proposed lattice model.[9] The dependence on N_{Ag^+} and N_{Cl^-} predicted by the asymmetric theory is much closer than the dependence predicted by the symmetric theory to the experimentally determined concentration dependence of log γ_{AgNO_3} in the KNO_3 solvent.

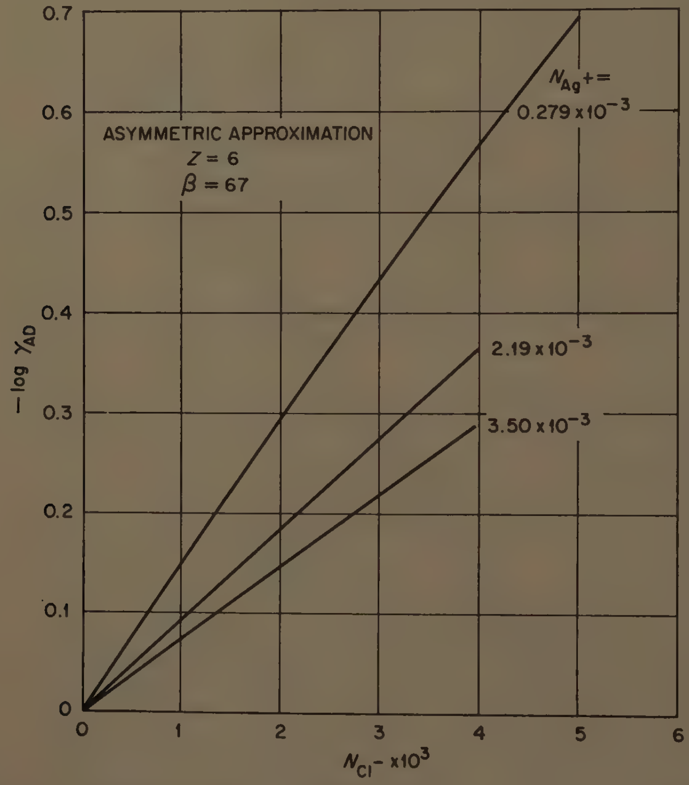

FIGURE 4. Calculated values of $-\log \gamma_{AD}$ for $Z = 6$, $\beta = 67$; the asymmetric approximation.

The values of $-\log \gamma_{AgNO_3}$ in FIGURE 3 indicate less negative deviations from ideality in the $NaNO_3$-$AgNO_3$-NaCl system than in the KNO_3-$AgNO_3$-KCl system, and hence a smaller value of β and $-\Delta E$. FIGURES 6 and 7 are plots of $-\log \gamma_{AD}$ as a function of N_{C^-} at several values of N_{A^+}, for $Z = 6$ and $\beta = 30$ ($\Delta E = -4.55$ kcal./mole) for the asymmetric and the symmetric approximations, respectively. These calculations correspond to the experimental measurements of $-\log \gamma_{AgNO_3}$ in the $NaNO_3$-$AgNO_3$-$NaCl$ system at 402° C. The experimental measurements lie between the two approximations, but in this case are closer to the symmetric approximation than to the asymmetric approximation, and they indicate a relatively smaller difference between $\Delta\epsilon_a$ and $\Delta\epsilon_1$ in the $NaNO_3$ solvent than in the KNO_3 solvent.

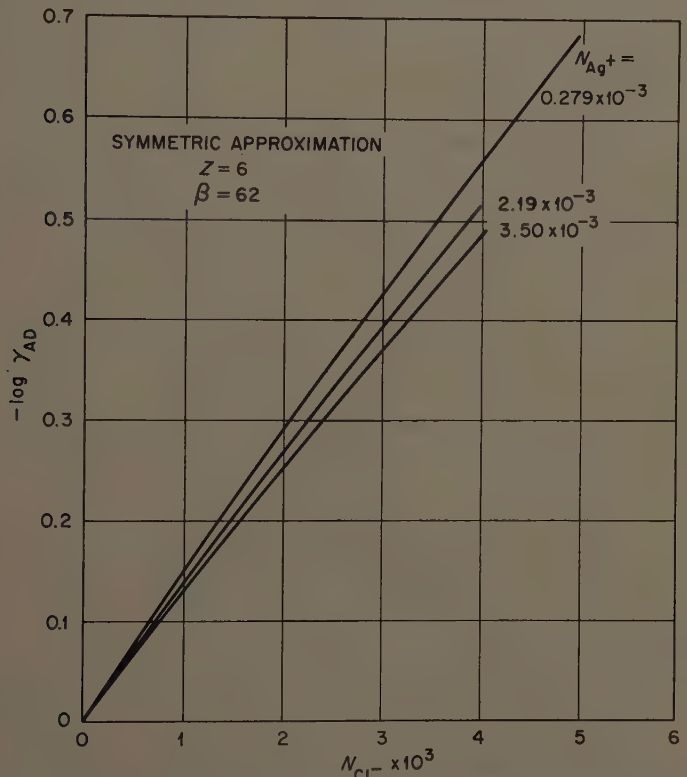

FIGURE 5. Calculated values of $-\log \gamma_{AD}$ for $Z = 6$, $\beta = 62$; the symmetric approximation.

The differences between the two systems might be related to the field effect of the solvent cation. The K^+ ion is larger than the Na^+ ion and, as nearest neighbor to a Cl^- ion that is part of an Ag^+-Cl^- pair "bond," it will polarize the electrons in the "bond" less than Na^+ due to its weaker field. If the "bond" strength (that is, relative energy of interaction $\Delta\epsilon_1$) is related to the electron density in the bond between the two ions, it is easy to see that the energy of ion-pair formation is more negative in the

KNO_3 solvent than in the $NaNO_3$ solvent.* This explanation is consistent with the relative order of the deviations from ideality in the binary systems MCl-AgCl in which M^+ are alkali metal ions.

If, judging by the relative molar volumes of the molten or solid AgCl, NaCl, or KCl, the relative size of the three cations is $Ag^+ < Na^+ < K^+$, the relative differences between $\Delta\epsilon_a$ and $\Delta\epsilon_l$ in the two systems can be related to the relative field effect of the Ag^+ ion as compared to the K^+ or Na^+ ions. In the KNO_3 solvent, for example, the nearest-neighbor field on the Cl^- of the first Ag^+-Cl^- "bond" formed to that Cl^- ion is the relatively

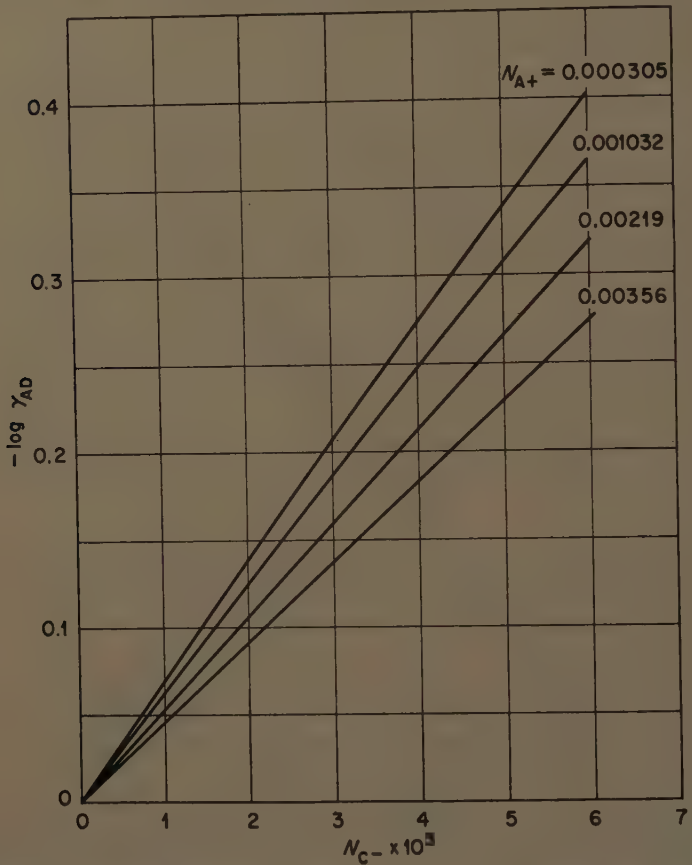

FIGURE 6. Calculated values of $-\log \gamma_{AD}$ for $Z = 6$, $\beta = 30$; the asymmetric approximation.

---

* The energy of interaction sometimes is related to the penetration of ligand electrons through the outer electron shell of the central ion,[10] leading to a higher effective ionic charge. The penetration would be less the stronger the positive field of the solvent cation, and hence the smaller would be the energy of interaction of an Ag^+-Cl^- pair.

weak one of the K^+, whereas the field on the Cl^- ion for the formation of Ag_2Cl^+ from Ag^+-Cl^- in solution is stronger, since it includes the field of the relatively smaller ion Ag^+. This leads to relatively large differences between $\Delta\epsilon_a$ and $\Delta\epsilon_1$. Since Ag^+ and Na^+ are more nearly the same size than are Ag^+ and K^+, the relative differences between $\Delta\epsilon_a$ and $\Delta\epsilon_1$ are probably smaller in the $NaNO_3$ solvent than in the KNO_3 solvent. This would lead to a relatively closer correspondence to the symmetric approximation in the $NaNO_3$ solvent. Of course, one cannot rule out the possibility that this may be, in part, a coulombic effect.

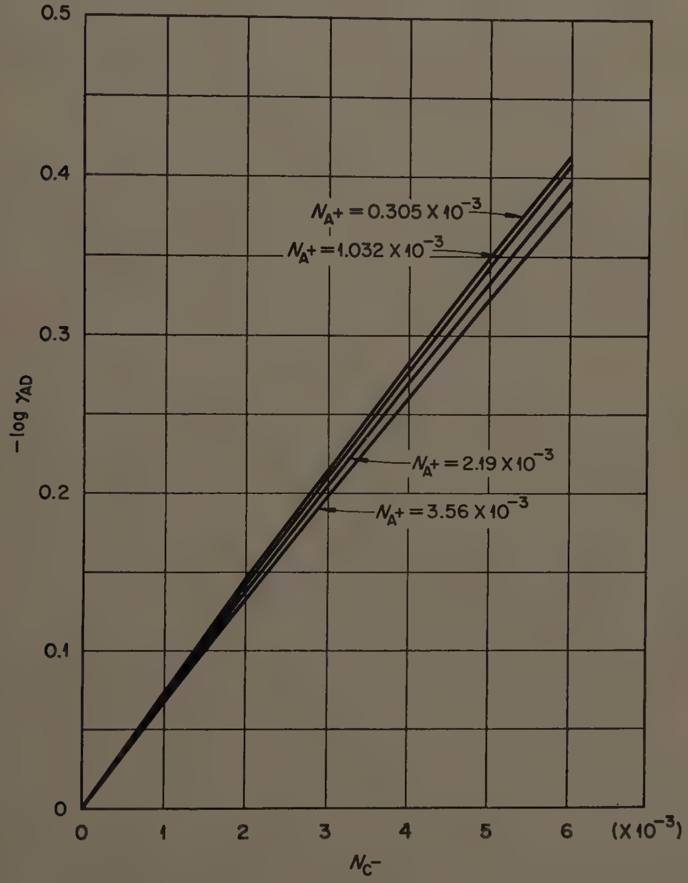

FIGURE 7. Calculated values of $-\log \gamma_{AD}$ for $Z = 6$, $\beta = 30$; the symmetric approximation.

Conclusions

The correspondence of the calculations based on the lattice model to experiment lends confidence in the lattice model of fused reciprocal salt solutions. Modifications of the lattice model will be attempted so as to include a saturation effect on bonds. This would put the qualitative discussion of relative bond strengths on a more quantitative basis.

This work demonstrates the applicability of even a simple physical theory to molten salt solutions and demonstrates a fallacy in the methods of the chemical or "complex ion" modes of description in solutions that are not very dilute. It must be emphasized that the reasonable correlation of the theory with the experimental data cannot be considered as proof that the lattice model accurately describes the interactions in solution.

Acknowledgments

We express appreciation to F. F. Blankenship and R. F. Newton of this laboratory and to G. Scatchard for many fruitful discussions and particularly for suggesting the symmetric approximation; to Richard Mashburn for the numerical calculations; and to W. R. Grimes for encouragement in this work.

References

1. Temkin, M. 1945. Acta Physicochim. U.R.S.S. **20**: 411.
2. Flood, H., T. Førland & K. Grjotheim. 1954. Z. anorg. u. allgem. Chem. **276**: 289.
3. Guggenheim, E. A. 1952. Mixtures. Oxford Univ. Press. Oxford, England.
4. Blander, M. 1959. J. Phys. Chem. In press.
5. Guggenheim, E. A. 1952. Mixtures. : 43. Oxford Univ. Press. Oxford, England.
6. Duke, F. R. 1958. J. Phys. Chem. **62**: 417.
7. Van Artsdalen, E. R. 1956. J. Phys. Chem. **60**: 172.
8. Blander, M., F. F. Blankenship & R. F. Newton. 1959. J. Phys. Chem. **63**: 1259.
9. Braunstein, J. & M. Blander. 1959. J. Phys. Chem. In press.
10. Basolo, F. & R. G. Pearson. 1958. Mechanisms of Inorganic Reactions. : 72. Wiley. New York, N.Y.

SOLUBILITIES OF TITANIUM TETRACHLORIDE IN MIXTURES OF POTASSIUM CHLORIDE AND SODIUM CHLORIDE, AND THE ELECTRODE POTENTIALS OF THE TITANIUM CHLORIDES IN 1/1 (MOLE) KCl-NaCl SOLUTIONS

S. N. Flengas

Scientific Officer, Extractive Metallurgy Division, Mines Branch, Department of Mines and Technical Surveys, Ottawa, Canada

INTRODUCTION

In previous publications[1-5] from the Mines Branch laboratories, the standard electrode potentials for several metal-metal chloride systems in dilute solutions in fused salts were reported. To make these measurements, an equimolar mixture of potassium and sodium chlorides was used as the solvent for the metal chloride, and a silver-silver chloride electrode, developed earlier in this work,[1] was used as the reference electrode in determining the electrode potentials.

The behavior of the silver-silver chloride electrode also was investigated,[6] using a chlorine electrode, and the results indicated that the solutions of silver chloride in the molten-salt solvent were ideal.

In the present investigation, the technique has been applied to the determination of the potentials of the titanium chlorides in solution in an equimolar mixture of potassium chloride and sodium chloride.

During the course of the preliminary experiments, it became apparent that the determination of the potential of the tetravalent titanium depended on the preparation of stable solutions of titanium tetrachloride in the molten salt. For this reason the solubilities of titanium tetrachloride in this medium were studied first.

Both of these problems, namely, the solubilities of titanium tetrachloride and the electrode potentials of the titanium chlorides, are closely associated with the electrolytic preparation of titanium metal from fused salts. Many of the electrolytic processes use titanium tetrachloride as the source of titanium for the cell and an equimolar mixture of potassium chloride and sodium chloride as the fused salt solvent. However, despite industrial developments, the mechanism of the electrolytic process is still open to various interpretations because of the scarcity of information concerning the electrode potentials of the system and the extent of solubility of titanium tetrachloride in the fused salt.

SOLUBILITIES OF TITANIUM TETRACHLORIDE IN MIXTURES OF POTASSIUM CHLORIDE AND SODIUM CHLORIDE

Very little is known about the solubility of titanium tetrachloride in fused chlorides. In fact, it has been stated that titanium tetrachloride is insoluble in chlorides of the alkali and alkaline earth metals.[7]

Kreye *et al.*,[8] in a recent investigation using a sampling and quenching technique, concluded that titanium tetrachloride is soluble to the extent of only 0.27 mole per cent in the equimolar mixture of potassium chloride and sodium chloride at 690° C. However, the authors stated that the methods used for this study were subject to serious errors, since dissolved titanium tetrachloride apparently was released from the melt during quenching.

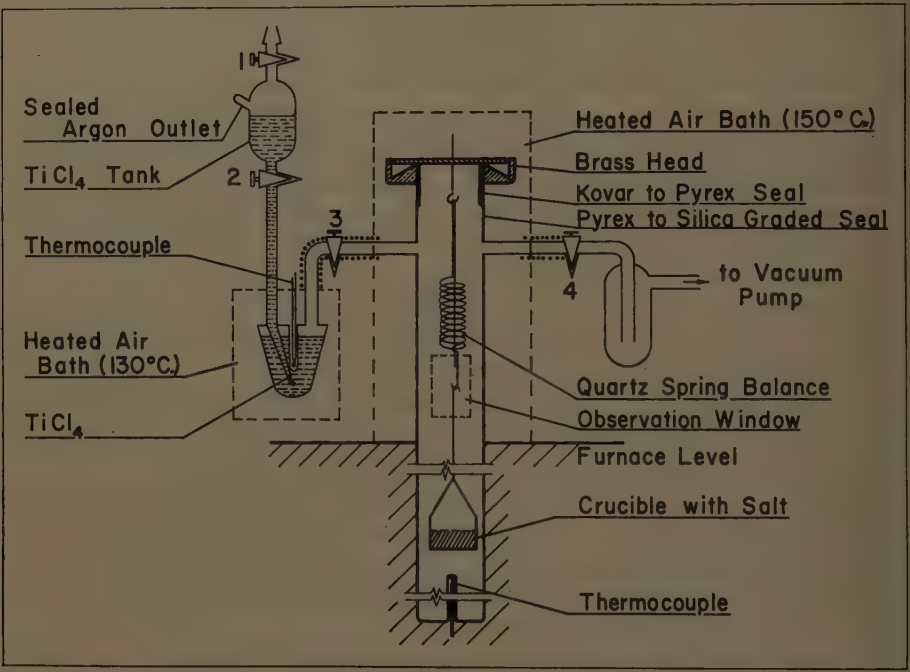

FIGURE 1. Apparatus for measurements of the solubilities of titanium tetrachloride in potassium chloride-sodium chloride mixtures.

Experimental

In the present investigation, the solubilities of titanium tetrachloride in the potassium and sodium chloride mixture were measured, using a quartz spring balance. The method involved direct observation of the increase of weight of the salt solution in contact with titanium tetrachloride vapor. It was free of the errors introduced by sampling and quenching techniques.

The apparatus used for these experiments is shown in FIGURE 1. It consists of three individually heated and temperature-controlled parts: the quartz spring balance suspended inside a silica tube, 2 in. diameter and 35 in. long; the quartz crucible containing the salt; and the titanium tetrachloride bath. Details of the apparatus are as follows:

The quartz spring had a maximum capacity of 10 gm., which corresponded to an elongation of 20 cm. The elongation of the spring was measured, using a traveling microscope that could be read to 0.001 mm. The spring was suspended from a hook in the center of a brass plate at the top of the cell. The plate was lead-soldered to the metal top of the cell, which also was made from brass. A Kovar-to-Pyrex joining and a Pyrex-to-silica graded seal were used to connect the top of the cell to the silica tube. The high-vacuum valves in the apparatus were of an all-metal type and were operated through a metal bellows. These valves had stainless steel seated needles and were connected to the Pyrex tubing by metal-to-glass joints.

The lower part of the cell, which contained the crucible with the salts, was heated in a tubular furnace 20 in. long. The temperature was controlled by a Honeywell Pyrovane electronic controller. Using the double wiring circuit previously described,[1] a temperature control of ±0.5° C. to a temperature of 850° C. was obtained.

The part of the cell projecting outside the furnace was enclosed in an asbestos box maintained at a temperature of 150° C. by a Sunvic thermoregulator. This temperature was above the dew point of titanium tetrachloride.

During the experiments, the temperature of the titanium tetrachloride in the bath was kept at 130 ± 0.5° C., using a small electrically heated furnace that was regulated by a Fisher pyrometer and a thermocouple. The vapor pressure of titanium tetrachloride at this temperature is 660 mm. of mercury.[9] Finally, all other exposed parts of the apparatus were heated with Nichrome wire and insulated with asbestos tape.

Commercially pure titanium tetrachloride was purified further by distillation in the presence of copper filings under a stream of argon gas. The first part of the distillate was rejected and the remainder was collected under argon in the storage tank shown in FIGURE 1. The product was colorless.

When the distillation was complete, the argon outlet at the side tube of the storage tank was sealed with a gas flame and all valves were closed. Titanium tetrachloride was then introduced under vacuum into the apparatus reservoir.

Prior to each run the cell was evacuated to a pressure of about 5 μ, the temperature of the various parts was set as required, and the valve leading to the vacuum system was closed. Next, the valve leading to the titanium bath was opened and measurements of the elongation of the spring were begun.

Results

During the first run, it became apparent that the solubility of titanium tetrachloride in the 1/1 mole potassium chloride and sodium chloride melt at 690° C. was much higher than that reported previously.[8] The weight increase shown by the spring balance was continuous over a period of 30 hours, and solutions containing up to 14 per cent of titanium tetrachloride were obtained without any indication that the system had reached equilibrium. The extent of solubility was confirmed by chemical analysis of the contents of the crucible.

In all experiments, to ensure that the compound did not decompose, the salt solution was cooled in the cell under titanium tetrachloride pressure. When the temperature of the cell had reached 150° C., the top of the cell was opened by melting the solder and the crucible was withdrawn.

In the next group of experiments an equimolar mixture of powdered potassium chloride and sodium chloride was treated with $TiCl_4$ vapor at temperatures below the melting point (660° C.). It was found that the reaction rate was appreciably faster than with the molten mixture, and varied with the temperature of the salt. Using 1/1 mole potassium chloride-sodium chloride powder of a particle size of less than 325 mesh, the reaction was very fast. At 485° C. the equilibrium was attained in about 3 hours, and the saturation concentration of titanium tetrachloride in the mixture was 0.65 gm./gm. of potassium chloride-sodium chloride mixture.

Experiments at temperatures between 280° and 480° C. indicated that the reaction rate at the lower temperatures was slower, but the same saturation concentration ultimately was reached in each experiment.

Subsequent X-ray examination of the samples showed that the potassium chloride had almost completely disappeared from the mixture and was replaced by a compound having a diffraction pattern not previously reported in the literature.

To investigate the mechanism of the reaction, separate experiments were done using potassium chloride and sodium chloride powders of particle size less than 325 mesh.

With sodium chloride, at temperatures up to 750° C. there was no evidence of reaction over a period of 24 hours. At 800° C. a slow increase of weight was observed, but this was offset by evaporation of salt from the crucible. After 30 hours' exposure to the titanium tetrachloride vapor, a chemical analysis of the solidified mixture indicated a titanium tetrachloride content of only 4 per cent.

With potassium chloride at 350° C., a reaction was immediately evident. The weight of the crucible increased rapidly; at equilibrium the saturation concentration of titanium tetrachloride was 1.27 gm. per gram of potassium chloride. This amount corresponds exactly to a stoichiometric proportion $KCl/TiCl_4 = 2$. These results also explain the magnitude of the saturation concentration of titanium tetrachloride in the potassium chloride-sodium chloride mixture reported above. The observed value of 0.65 gm. of titanium tetrachloride per gram of 1/1 mole potassium chloride-sodium chloride mixture corresponds approximately to the formation of K_2TiCl_6 from the amount of potassium chloride present in the mixture. It was concluded that the titanium tetrachloride reacted chemically with solid potassium chloride to give a complex of molecular formula K_2TiCl_6, according to the reaction:

$$TiCl_4 + 2\ KCl = K_2TiCl_6 \tag{1}$$

These conclusions were confirmed by subsequent chemical analysis of the product. The results of analysis are given in TABLE 1.

Table 1

Chemical Analyses of K_2TiCl_6

	Found in sample (per cent)	Calculated as K_2TiCl_6 (per cent)
Total titanium	14.2	14.16
Total chlorine	62.5	62.78
Total potassium	23.3	23.06

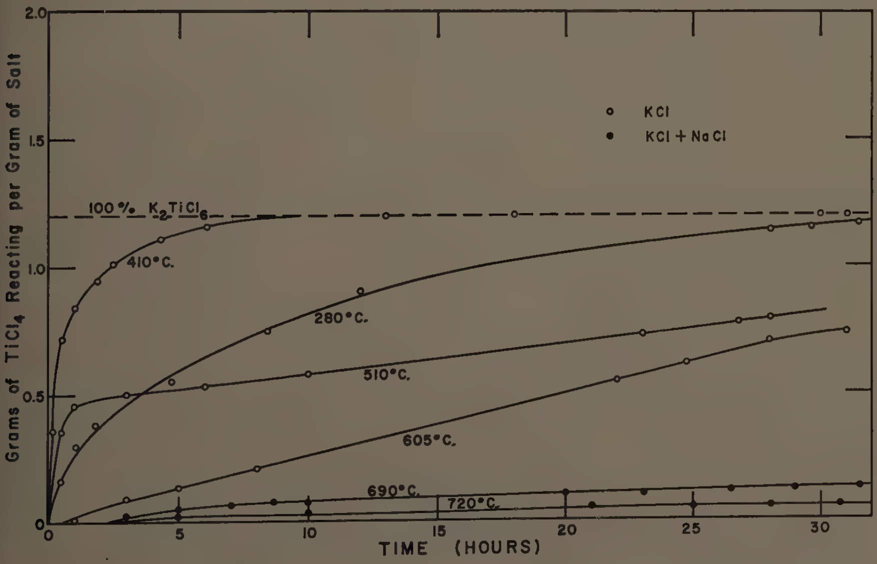

Figure 2. Reaction rates between gaseous $TiCl_4$, or 1/1 mole KCl + NaCl, at various temperatures.

The formation of K_2TiCl_6 by a wet method at room temperature already has been reported in the literature,[10] where it is stated that attempts to prepare it at 300° C. in a sealed bomb were unsuccessful.

The effect of potassium chloride temperature on the rate of formation of K_2TiCl_6 also was investigated. The results are given in FIGURE 2. Included in this figure, also, are the results obtained with the fused equimolar mixture of potassium chloride and sodium chloride.

It is evident from the curves in FIGURE 2 that the reaction rate increases rapidly with temperature and, at 410° C., the formation of 100 per cent K_2TiCl_6 takes place in about 6 hours. However, at higher temperatures the reaction behaves abnormally and the rate decreases. At 510° C. a sudden decrease of the rate occurs. Examination of the crucible after the run at 510° C. showed that fusion had taken place. It seems reasonable to assume that the slower reaction rate can be explained by the formation of a eutectic mixture between potassium chloride and the complex potassium chlorotitanate. The gradual formation of the molten phase of the eutectic would indeed reduce the reacting surface of the potassium chloride powder in the mixture. However, the possibility that the rate of the reverse process, that is, the thermal decomposition of potassium chlorotitanate, contributes to the decrease of the rate of formation should not be excluded. The data available at present are insufficient to explain the kinetic mechanism of the reaction.

The results of the experiments with fused equimolar mixtures of potassium chloride and sodium chloride at 690° and 720° C. indicate that in the molten phase the reaction rate is very slow. At 720° C., after 30 hours exposure to titanium tetrachloride vapor, the amount of titanium tetrachloride found in the mixture was only 5 per cent; at 690° C., the amount was 14 per cent. Neither result represents the attainment of equilibrium. It may be concluded that, by allowing sufficient time for reaction, the saturation concentration of titanium tetrachloride in the potassium chloride-sodium chloride melt would be reached eventually, and that potassium chlorotitanate would be formed in proportion to the amount of potassium chloride present in the mixture.

Potassium chlorotitanate has a bright yellow color and decomposes on heating under vacuum. It is stable in the presence of titanium tetrachloride vapor at 1 atm. pressure.

The X-ray diffraction pattern of pure potassium chlorotitanate indicated that the compound has a cubic cell of side 9.7 Å and is isomorphous with K_2PtCl_6. The powder pattern has exactly the same series of lines[11] as has K_2PtCl_6, but different intensities.

The density of K_2TiCl_6 was measured by the displacement method in carbon tetrachloride and was found to be 2.40 ± 0.15 gm./cm.^{3} at 27° C. This value may be compared with 2.45 gm./cm.^{3} calculated from the X-ray data on the basis of 4 formula units of K_2TiCl_6 per unit cell.

The melting point of K_2TiCl_6 also was determined in a sealed silica capillary and found to be 695 ± 5° C.

Potassium chlorotitanate is soluble in water. The resulting solutions were slightly opaque and strongly acidic. Hydrated TiO_2 was not precipitated even after these solutions were boiled.

Conclusions

The foregoing results indicate that titanium tetrachloride vapor reacts with potassium chloride to form a complex having the molecular formula

K_2TiCl_6. The optimum temperature for the formation of this compound under a vapor pressure of titanium tetrachloride of 1 atm. is between 350° and 400° C.

At temperatures above 800° C. a reaction between titanium tetrachloride vapor and sodium chloride is evident, and the formation of the complex Na_2TiCl_6 may be postulated.

ELECTRODE POTENTIALS OF THE TITANIUM CHLORIDES IN SOLUTION IN 1/1 MOLE POTASSIUM CHLORIDE-SODIUM CHLORIDE MELTS

The potentials associated with titanium and its multivalent ions in the chloride system are as follows:

(1) The metal electrode potentials expressing the equilibria between the metallic electrode and its ionic species in solution, that is, the potentials

$$(E_2)\ \mathrm{Ti/Ti^{2+}_{(TiCl_2\ in\ KCl+NaCl)}}$$

$$(E_3)\ \mathrm{Ti/Ti^{3+}_{(TiCl_3\ in\ KCl+NaCl)}}$$

$$(E_4)\ \mathrm{Ti/Ti^{4+}_{(K_2TiCl_6\ in\ KCl+NaCl)}}$$

(2) The redox potentials due to the equilibria between two successive oxidation states of the ions, that is, the potentials

$$(E_{2,3})\ \mathrm{Ti^{2+}/Ti^{3+}_{(TiCl_2\ and\ TiCl_3\ in\ KCl+NaCl)}},$$

$$(E_{3,4})\ \mathrm{Ti^{3+}/Ti^{4+}_{(TiCl_3\ and\ K_2TiCl_6\ in\ KCl+NaCl)}}$$

The relationship between these potentials is given by the following cyclic process

$$\begin{tikzcd}
\mathrm{Ti} \arrow[r, "\Delta G = -2E_2\mathfrak{F}"] \arrow[dr, "\Delta G = -3E_3\mathfrak{F}"'] & \mathrm{Ti}^{2+} \arrow[d, "\Delta G = -E_{2,3}\mathfrak{F}"] \\
\mathrm{Ti}^{4+} \arrow[u, "\Delta G = +4E_4\mathfrak{F}"] & \mathrm{Ti}^{3+} \arrow[l, "\Delta G = -E_{3,4}\mathfrak{F}"]
\end{tikzcd}$$

For a complete cycle, the equation relating the various potentials of the system is

$$\sum(\Delta G) = 0 \tag{2}$$

When any three of the four potentials are known, that is, one metal electrode potential and the two redox potentials, the unknown metal electrode potential can be calculated.

This method was applied to obtain the metal electrode potentials of the systems Ti/Ti^{3+} and Ti/Ti^{4+}, neither of which could be measured directly because of the reactivity of the metal with the corresponding metal chlorides in solution.

Experimental

In the course of the experimental work, two different types of cells were used for determining the electrode potentials: (1) for measuring metal electrode potentials, and (2) for measuring redox potentials.

(1) *A cell for measurements of metal electrode potentials of the system* $\mathrm{Ti/Ti^{2+}_{(TiCl_2\ in\ KCl+NaCl)}}$. This was of the type

$$\begin{array}{c|c||c||c|c} \mathrm{Ti} & \mathrm{TiCl_2}\ (x_2) & & \mathrm{AgCl}\ (x_1) & \mathrm{Ag} \\ (-) & \mathrm{KCl} + \mathrm{NaCl} & \text{asbestos fiber} & \mathrm{KCl} + \mathrm{NaCl} & (+) \\ & (1/1 \text{ mole}) & & (1/1\text{mole}) & \end{array}$$

The chemical reaction in the cell is:

$$\mathrm{Ti}_{(s)} + 2\mathrm{Ag}^{+}_{(\mathrm{AgCl\ in\ KCl+NaCl})} = \mathrm{Ti}^{2+}_{(\mathrm{TiCl_2\ in\ KCl+NaCl})} + 2\mathrm{Ag}_{(s)}$$

The relationship between the electromotive force and the concentrations of the reacting species in the cell is given by the Nernst equation in the form

$$E_2 = (E^\circ_{\mathrm{TiCl_2}} - E^\circ_{\mathrm{AgCl}}) - (2.303RT/2\mathfrak{F}) \log (x_2/x_1^2) - (2.303RT)\ 2\mathfrak{F} \log (\gamma_2/\gamma_1^2) \qquad (3)$$

where $E^\circ_{\mathrm{TiCl_2}}$ and E°_{AgCl} are the formation potentials of, respectively, titanium dichloride and silver chloride in their standard states. For the purpose of this paper, the standard state will be defined as the state of the pure metal chlorides at the temperature of the experiments. In so doing, all activity coefficients are referred to the state of the pure metal chlorides. The γ and x terms are, respectively, the mean activity coefficients and the mole fractions of the metal chlorides in the solutions in the two half-cells. Mole fractions are defined in the usual way, that is,

$$x_i = n_i/\sum n$$

where n_i is the number of moles of any one constituent.

From EQUATION 3, assuming that the activity coefficients for dilute solutions are constants, it is possible to calculate a cell potential that will be apparently independent of concentration. This is done simply by subtracting the log (x_2/x_1^2) term from the experimentally obtained potential, E_2. The potential thus derived is constant over the range of concentrations for which the activity coefficients are constant and is given by the equation

$$E^\circ_{\mathrm{cell}} = E_2 + (2.303RT/2\mathfrak{F}) \log (x_2/x_1^2) = (E^\circ_{\mathrm{TiCl_2}} - E^\circ_{\mathrm{AgCl}}) - (2.303RT/2\mathfrak{F}) \log (\gamma^2/\gamma_1^2) \qquad (4)$$

It follows from EQUATION 4 that, when log $(x_2/x_1^2) = 0$, then $E^\circ_{\mathrm{cell}} = E_2$. It will be observed that log (x_2/x_1^2) is zero for all mole fractions for which the relationship $x_2/x_1^2 = 1$, including the special case when both mole fractions x_1 and x_2 are unity. It is, therefore, permissible to call the potential $E^{\circ}_{\mathrm{cell}}$ the apparent standard cell potential of the system.

Since the potentials of the standard state are known by calculation from thermal data[12] and the activity coefficients of silver chloride in solution in 1/1 mole potassium chloride and sodium chloride were found to be unity,[6] EQUATION 4 can be used to calculate the activity coefficients of titanium dichloride solutions in fused salts.

(2) *Cells for measurements of redox potentials of the systems* $\mathrm{TiCl_2/TiCl_{3(KCl+NaCl)}}$ *and* $\mathrm{TiCl_3, TiCl_{4(KCl+NaCl)}}$. These were of the type

$$\begin{array}{c|c||c||c|c} \mathrm{Pt} & \mathrm{TiCl_2}\ (x_2) & & \mathrm{AgCl}\ (x_1) & \mathrm{Ag} \\ (-) & \mathrm{TiCl_3}\ (x_3) & \text{asbestos fiber} & \mathrm{KCl + NaCl} & (+) \\ & \mathrm{KCl + NaCl} & & (1/1\ \text{mole}) & \\ & (1/1\ \text{mole}) & & & \end{array}$$

and

$$\begin{array}{c|c||c||c|c} \mathrm{Ag} & \mathrm{AgCl}\ (x_1) & & \mathrm{TiCl_3}\ (x_3) & \mathrm{Pt} \\ (-) & \mathrm{KCl + NaCl} & \text{asbestos fiber} & \mathrm{K_2TiCl_6}\ (x_4) & (+) \\ & (1/1\ \text{mole}) & & \mathrm{KCl + NaCl} & \\ & & & (1/1\ \text{mole}) & \end{array}$$

The cell reactions are, respectively,

$$\mathrm{Ag}^{+}_{\substack{(\mathrm{AgCl\ in}\\ \mathrm{KCl+NaCl})}} + \mathrm{Ti}^{2+}_{\substack{(\mathrm{TiCl_2\ in}\\ \mathrm{KCl+NaCl})}} = \mathrm{Ti}^{3+}_{\substack{(\mathrm{TiCl_3\ in}\\ \mathrm{KCl+NaCl})}} + \mathrm{Ag}_{(s)} \tag{5}$$

and

$$\mathrm{Ag}_{(s)} + \mathrm{Ti}^{4+}_{\substack{(\mathrm{K_2TiCl_6\ in}\\ \mathrm{KCl+NaCl})}} = \mathrm{Ti}^{3+}_{\substack{(\mathrm{TiCl_3\ in}\\ \mathrm{KCl+NaCl})}} + \mathrm{Ag}^{+}_{\substack{(\mathrm{AgCl\ in}\\ \mathrm{KCl+NaCl})}} \tag{6}$$

The corresponding forms of the Nernst equation applied to each of the above redox systems are, respectively,

$$\begin{aligned} E_{2.3} = (E^{\circ}_{\mathrm{TiCl_2/TiCl_3}} - E^{\circ}_{\mathrm{AgCl}}) - (2.303RT/\mathfrak{F}) \log (x_3/x_1x_2) \\ - (2.303RT/\mathfrak{F}) \log (\gamma_3/\gamma_1\gamma_2) \end{aligned} \tag{7}$$

$$\begin{aligned} E_{3.4} = (E^{\circ}_{\mathrm{AgCl}} - E^{\circ}_{\mathrm{TiCl_3/K_2TiCl_6}}) - (2.303RT/\mathfrak{F}) \log (x_1x_3/x_4) \\ - (2.303RT/\mathfrak{F}) \log (\gamma_1\gamma_3/\gamma_4) \end{aligned} \tag{8}$$

where the $E^{\circ}_{\mathrm{TiCl_2/TiCl_3}}$ and $E^{\circ}_{\mathrm{TiCl_3/K_2TiCl_6}}$ are the redox potentials of the standard states. These potentials can be calculated readily from EQUATION 2 using the formation potential of the standard states.

Every x and γ is, respectively, the mole fraction and the mean activity coefficient of a metal chloride in solution.

Assuming constancy of the activity coefficients in dilute solutions, EQUATIONS 7 and 8 can be used to calculate an experimental apparent standard redox potential that will be apparently independent of concentrations, as in EQUATION 4.

Preparation of Materials and Apparatus

The experimental technique and the apparatus used to study the potentials of the titanium chlorides were both similar to those described in the previous investigations.[1-6] The cell, however, was modified to contain the highly hygroscopic titanium dichloride and the pyrophoric titanium trichloride. The design of the silica cell is given in FIGURE 3.

To prevent contamination by air during operation, the cell was provided with a sulfuric acid bubbler and air trap, and the cell was flushed continuously with a slow stream of purified argon. Effective separation between the two half-cell solutions was achieved by an asbestos fiber sealed into the end of the silica tubing of the reference electrode. The fiber had the property of preventing diffusion and, at the same time of establishing electric contact between the two solutions. For dilute solutions the presence of a large excess of the same ionic solvent on both sides of the junction effectively eliminated junction potentials.

Titanium trichloride (99 per cent pure) was available from previous investigations.[13]

Titanium dichloride was prepared by the thermal disproportionation of titanium trichloride in a process involving two stages. In the first stage, the disproportionation reaction

$$2\,TiCl_3 = TiCl_4 + TiCl_2 \qquad (9)$$

was done under vacuum in an inverted U tube sealed on both sides. The arm containing the titanium trichloride was heated at 500° C. for 12 hours, during which the other arm was immersed in liquid air. At the end of this period the amount of titanium dichloride produced by disproportionation was calculated from the weight of titanium tetrachloride that had condensed in the tube. The proportion of $TiCl_2/TiCl_3$ in the mixture was close to 1/1. As a by-product of disproportionation, 0.5 per cent of finely divided titanium metal also was produced. The titanium dichloride and trichloride mixture prepared in this manner was used in the subsequent experiments to obtain the redox potentials of the system.

In the second stage of the preparation, titanium dichloride was sublimed under hydrogen at 650° C. over a period of 24 hours. The sublimed product had a Ti:Cl ratio of 2.02:1. This titanium dichloride was used in the experimental work on divalent titanium.

Pure potassium chlorititanate (99.5 per cent) was prepared from potassium chloride and titanium tetrachloride by a modification of the method established in the first part of this study. A Pyrex tube was bent at a right angle and was sealed at one end; purified titanium tetrachloride was introduced into the closed vertical arm and was frozen with liquid air. A silica boat containing potassium chloride powder of particle size less than 325 mesh was placed in the horizontal arm, and the tube was evacuated and sealed. By heating titanium tetrachloride to 130° to 134° C. and the potassium chloride to 350° to 400° C. for about 12 hours, potassium chlorititanate was formed quantitatively.

The titanium chlorides were pelletized in a dry box under an inert argon atmosphere, placed in the piston-type feeding apparatus shown in FIGURE 3, and transferred into the cell. The dry box also was used for handling these salts during preparation.

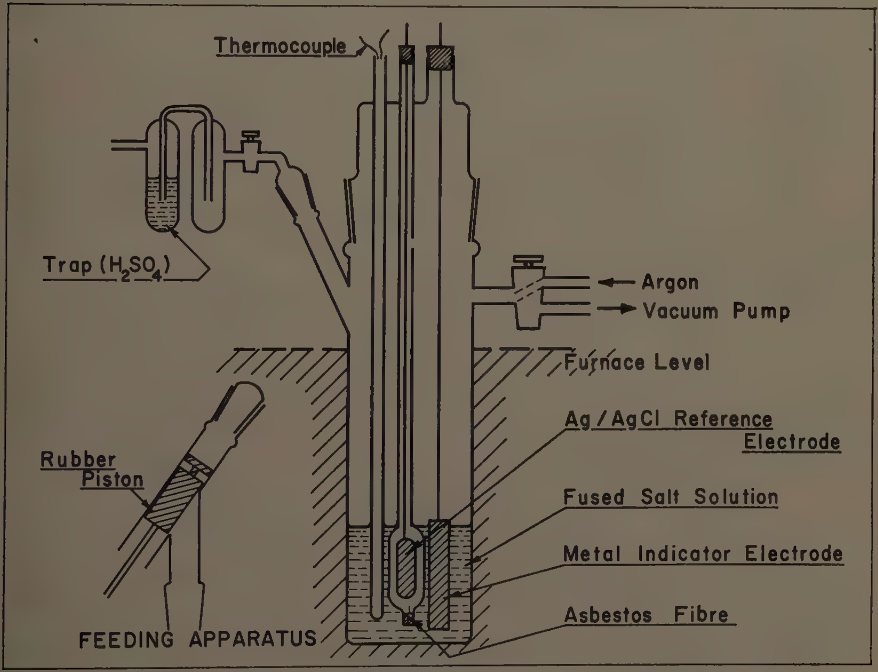

FIGURE 3. Cell for electrode potential measurements in fused cells.

The titanium electrode used in this study was a strip of pure iodide titanium connected to a titanium wire of the same purity. The silver electrode was a rod of pure silver (99.99 per cent) connected to a silver wire. The platinum electrode for the measurements of redox potentials was a platinum cylinder of ½-in. diameter and 3-in. length, connected to a platinum wire.

Thermoelectric potentials due to the bimetallic systems of the electrodes were measured separately, and the appropriate corrections were applied to the potential measurements.

Results

The electromotive forces of the titanium-titanium dichloride system were measured as functions of both temperature and concentration.

The variations of the cell potentials with temperature at various concentrations of titanium dichloride are given in FIGURE 4. It is seen that the curves are linear for the range of mole fractions investigated, namely rom 2.6×10^{-3} to 1×10^{-2}.

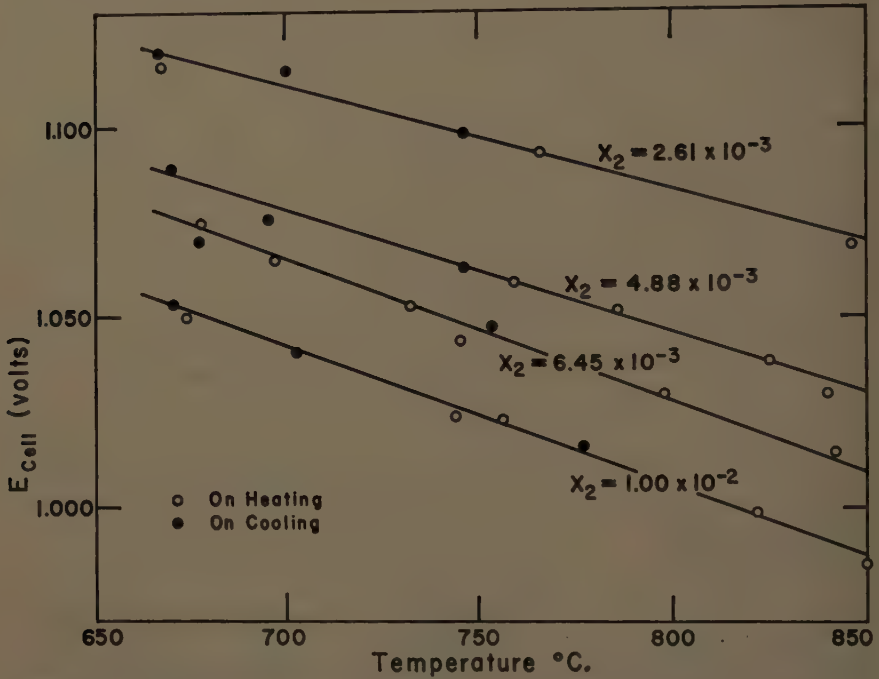

FIGURE 4. The effect of temperature on the potential of the cell at various mole fractions of titanium dichloride.

Ti (−)	$TiCl_2$ (x_2) KCl + NaCl (1/1 mole)	AgCl (x_1) KCl + NaCl (1/1 mole)	Ag (+)

The potentials of these cells over a period of 48 hours were constant to within 0.5 mv. It was observed that titanium metal dissolved in the fused salt to the extent of about 0.5 per cent. However, the slow dissolution of titanium metal in the fused salt during the experiments did not interfere with the cell potential.

When the electromotive forces shown in FIGURE 4 were plotted against the logarithm of mole fraction, the results were well represented by straight lines. This is shown in FIGURE 5. The slopes of the straight lines are in agreement with the theoretical slopes for a two-electron electrode process, as calculated from the Nernst equation. The results of these calculations are given in the summary of results in TABLE 2.

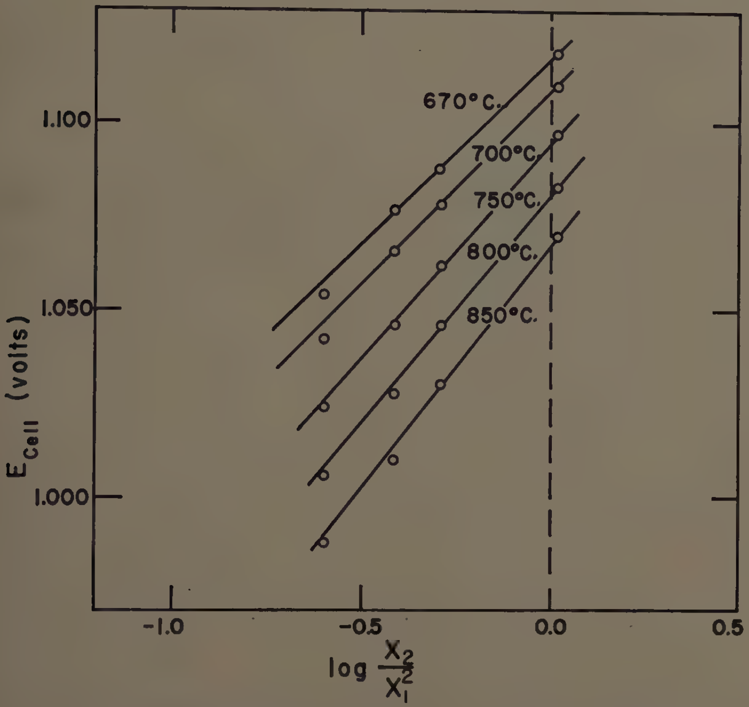

FIGURE 5. Electromotive forces of the cell as a function of log (x_2/x_1^2), at various temperatures..

Ti | $TiCl_2$ || AgCl (x_1) | Ag
(−) | KCl + NaCl (1/1 mole) || KCl + NaCl (1/1 mole) | (+)

TABLE 2
SUMMARY OF RESULTS

Indicator electrode	Cell reaction in molten KCl + NaCl	Cell potential at 670° C. (volts)		Slope of the Nernst equation at 670° C.	
		E°_{cell} experimental*	$E^{\circ\prime}_{cell}$ calculated†	Experimental	Calculated
Ti, Ti^{2+}	$Ti + 2Ag^+ = Ti^{2+} + 2Ag$	−1.115	−0.985	0.099	0.094
Ti, Ti^3	$Ti + 3Ag^+ = Ti^3 + 3Ag$	−1.046	−0.895	—	—
Ti^{2+}, Ti^{3+}	$Ti^{2+} + Ag^+ = Ti^{3+} + Ag$	−0.910	−0.715	0.196	0.188
Ti, Ti^{4+}	$Ti + 4Ag^+ = Ti^{4+} + 4Ag$	−0.697	—	—	—
Ag, Ag^+		0.0	0.0	—	—
Ti^{3+}, Ti^{4+}	$Ti^{4+} + Ag = Ti^{3+} + Ag^+$	0.350	—	0.190	0.188
Cl^-, Cl	$Ag + \frac{1}{2}Cl_2 = AgCl$	0.852‡	−0.854	—	—

* It will be noted that the sign of the experimentally obtained apparent standard potentials shown in this table has been changed to conform with the recommendations of the IUPAC Stockholm convention, as reported by Light and deBéthune.[14]

† Potentials calculated from existing thermodynamic data on the pure metal chlorides.[12]

‡ The potential of the chlorine electrode against the silver-silver chloride electrode has been determined in a previous investigation,[6] and the value is given here for comparison.

The linearity of the curves in FIGURE 5 indicates that the activity coefficient of titanium dichloride in solution in the potassium chloride-sodium chloride molten solvent is constant for the range of concentrations studied. Thus the assumption for the derivation of EQUATION 4 is justified by the experimental results.

In FIGURE 5 the apparent standard cell potential for titanium dichloride at different temperatures can be obtained readily by interpolation at the zero $\log(x_2/x_1^2)$ term. The variation of the apparent standard cell potential with temperature, corrected for the thermoelectric effects, is given in FIGURE 6. The curve is linear between 760° and 850° C.; the relationship can be represented by the equation

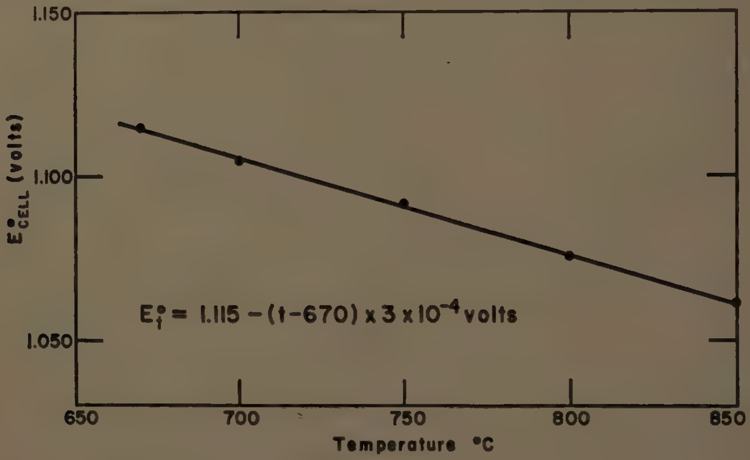

$$E^\circ_{CELL} = \left[E^\circ_{TiCl_2} - E^\circ_{AgCl}\right] - \frac{RT}{\mathcal{F}} \ln \frac{\gamma_2}{\gamma_1^2}$$

FIGURE 6. Variation of the standard cell potential of the titanium dichloride system with temperature.

$$E^\circ_t = 1.115 - (t - 670) \times 3.0 \times 10^{-4} \qquad (10)$$

where 1.115 is the apparent standard cell potential at 670° C.

The electromotive forces of the redox systems Ti^{2+}, $Ti^{3+}_{(TiCl_2\text{, }TiCl_3\text{ NaCl})}$, and Ti^{3+}, $Ti^{4+}_{(TiCl_3\text{, }K_2TiCl_6\text{ in }KCl+NaCl)}$ were measured as a function of the metal ion concentration at the indicator electrode. The results of these measurements at 670° C. are given in TABLES 3 and 4. The corresponding curves of the logarithmic plots are given in FIGURES 7 and 8.

The curve for the Ti^{2+}, Ti^{3+} redox system given in FIGURE 7 is linear over the range of concentrations investigated, which indicates that the activity coefficient of titanium trichloride in solution in the equimolar mixture of potassium chloride and sodium chloride is constant. The slope of the straight line shown in FIGURE 7 is in agreement with the calculated slope for a one-electron electrode process (0.196 instead of the calculated 0.188).

TABLE 3

ELECTROMOTIVE FORCES OF THE REDOX CELL AS A FUNCTION OF THE METAL ION CONCENTRATION AT THE INDICATOR ELECTRODE AT 670° C.

Pt (−)	$TiCl_2$ (x_2) $TiCl_3$ (x_3) KCl + NaCl (1/1 mole)	AgCl (x_1) KCl + NaCl (1/1 mole)	Ag (+)

Run	Mole fraction of AgCl (x_1)	Mole fraction of $TiCl_2$ (x_2)	Mole fraction of $TiCl_3$ (x_3)	E_{cell} (v.)
1	4.9×10^{-2}	1.44×10^{-4}	1.54×10^{-3}	0.439
	4.9×10^{-2}	1.43×10^{-4}	2.69×10^{-3}	0.381
	4.9×10^{-2}	1.43×10^{-4}	4.36×10^{-3}	0.354
	4.9×10^{-2}	1.43×10^{-4}	6.31×10^{-3}	0.324
	4.9×10^{-2}	1.43×10^{-4}	8.53×10^{-3}	0.284
2	4.9×10^{-2}	2.47×10^{-3}	8.47×10^{-3}	0.560
	4.9×10^{-2}	2.47×10^{-3}	1.05×10^{-2}	0.545
	4.9×10^{-2}	2.47×10^{-3}	1.40×10^{-2}	0.486

TABLE 4

ELECTROMOTIVE FORCES OF THE REDOX CELL AS A FUNCTION OF THE METAL ION CONCENTRATION AT THE INDICATOR ELECTRODE AT 670° C.

Ag (−)	AgCl (x_1) KCl + NaCl (1/1 mole)	$TiCl_3$ (x_3) K_2TiCl_6 (x_4) KCl + NaCl (1/1 mole)	Pt (+)

Run	Mole fraction of AgCl (x_1)	Mole fraction of $TiCl_3$ (x_3)	Mole fraction of K_2TiCl_6 (x_4)	E_{cell} (v.)
1	5.0×10^{-2}	2.27×10^{-3}	7.00×10^{-4}	0.498
	5.0×10^{-2}	2.24×10^{-3}	1.08×10^{-3}	0.551
	5.0×10^{-2}	2.22×10^{-3}	1.43×10^{-3}	0.561
	5.0×10^{-2}	2.18×10^{-3}	2.28×10^{-3}	0.584
	5.0×10^{-2}	5.83×10^{-3}	2.27×10^{-3}	0.520
	5.0×10^{-2}	6.79×10^{-3}	2.26×10^{-3}	0.500
2	5.0×10^{-2}	2.35×10^{-3}	8.02×10^{-4}	0.532
	5.0×10^{-2}	2.33×10^{-3}	1.78×10^{-3}	0.579
	5.0×10^{-2}	3.66×10^{-3}	1.77×10^{-3}	0.513
	5.0×10^{-2}	4.57×10^{-3}	1.75×10^{-3}	0.488
3	6.23×10^{-2}	5.33×10^{-3}	3.03×10^{-3}	0.541
	6.32×10^{-2}	5.52×10^{-3}	4.20×10^{-3}	0.570
	6.23×10^{-2}	5.50×10^{-3}	5.09×10^{-3}	0.580
	6.23×10^{-2}	7.70×10^{-3}	5.09×10^{-3}	0.553

The potentials of these cells were reproducible and remained stable over long periods of time.

The experimental data for the Ti^{3+}, Ti^{4+} system, as shown in FIGURE 8, are scattered as a result of the instability of the solutions. After the addition of the K_2TiCl_6 pellet to the melt, the concentration equilibrium was established in a few minutes. The potential of the cell remained constant for about 20 min. and then began to drift slowly. The drift of potential was associated with the observation of $TiCl_4$ evaporation from the salt solution. In FIGURE 8, only the steady values of the experimental potentials are shown. The points shown are considered to represent the steady state within the cell. The best straight line that can be drawn through the experimental points has a slope of 0.190, which agrees well with the calculated slope of 0.188 for a one-electron electrode process.

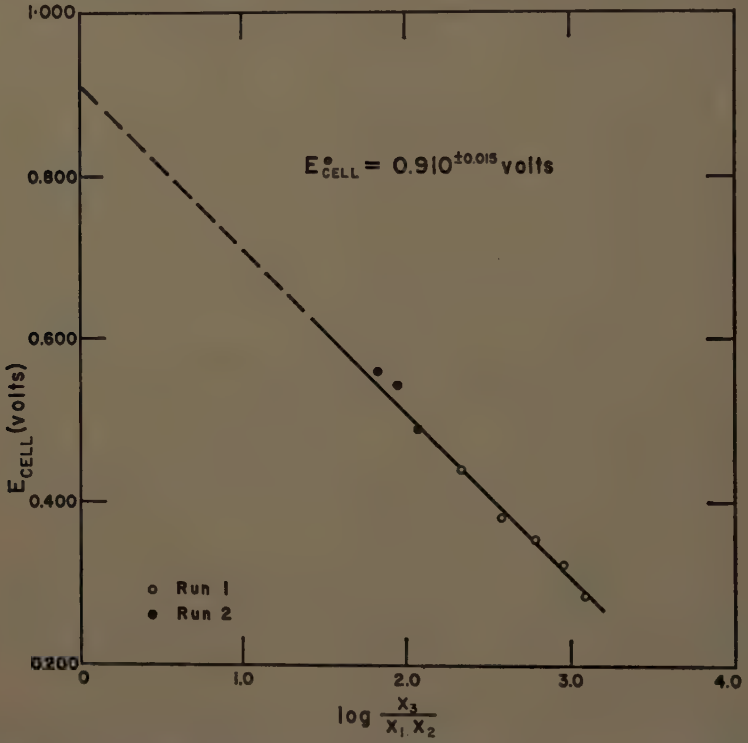

FIGURE 7. Redox potentials of the cell as a function of log $[(x_3)/(x_1 \cdot x_2)]$ at 670° C.

Pt (−)	$TiCl_2$ (x_2) $TiCl_3$ (x_3) KCl + NaCl (1/1 mole)	AgCl (x_1) KCl + NaCl (1/1 mole)	Ag (+)

The linearity of the curves indicates that the activity coefficient of the tetravalent titanium ion is constant over the range of mole fractions investigated, that is, from 7.0×10^{-4} to 5.0×10^{-3}.

Following the same procedure as used previously, apparent standard redox potentials of the systems were obtained by graphic extrapolation of the curves in FIGURES 7 and 8 to zero log terms. The potentials obtained by this method are given in TABLE 2. Standard cell potentials, calculated from the formation potentials of the metal chlorides given by Hamer *et al.*,[12] are also included in TABLE 2.

DISCUSSION

Having established the apparent standard cell potentials (E°_{cell}) of the system Ti, $TiCl_{2(KCl+NaCl)}$ and the apparent standard redox potentials of the systems $TiCl_2$, $TiCl_{3(KCl+NaCl)}$ and $TiCl_3$, $K_2TiCl_{6(KCl+NaCl)}$, EQUATION 2 was applied to calculate the apparent standard cell potentials of the systems Ti, $TiCl_{3(KCl+NaCl)}$, and Ti, $K_2TiCl_{6(KCl+NaCl)}$, which are unobtainable by direct measurements. The results of these calculations are given in the summary of results in TABLE 2. From the data in TABLE 2, it is possible to calculate the free energy and the equilibrium constants of the reactions between titanium metal and the various titanium ions in solution in the equimolar mixture of potassium and sodium chlorides. These equilibria are of interest because they are related to the chemical reactions that take place in a fused salt-electrolysis titanium cell. The results of these calculations are given in TABLE 5.

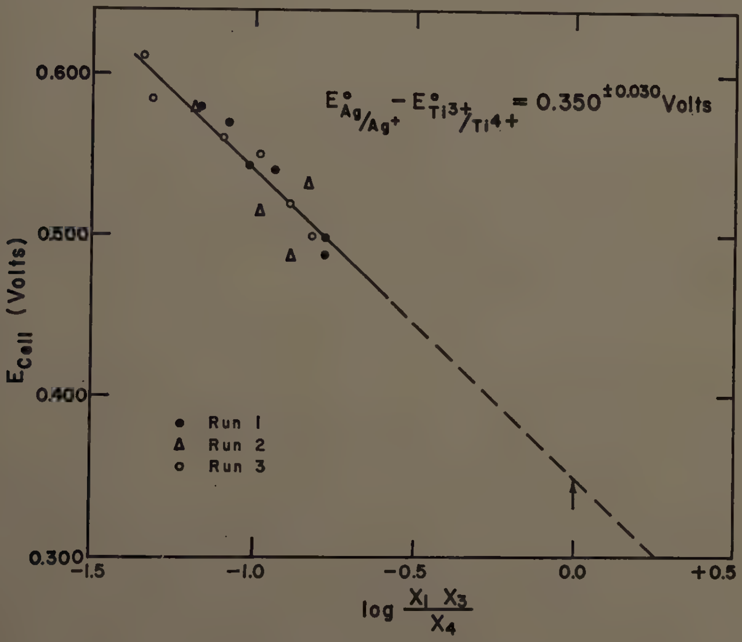

FIGURE 8. Redox potentials of the cell as a function of log [$(x_1 \cdot x_3)/(x_4)$] at 670° C.

Ag (−) | AgCl (x_1) KCl + NaCl (1/1 mole) || $TiCl_3$ (x_3) K_2TiCl_6 (x_4) KCl + NaCl (1/1 mole) | Pt (+)

The relationship between the various reduction processes is best shown by the cycle appearing on the next page. It may be seen readily that in an electrolysis cell using titanium tetrachloride as the feeding material, the final cell reaction is likely to proceed through the divalent ion.

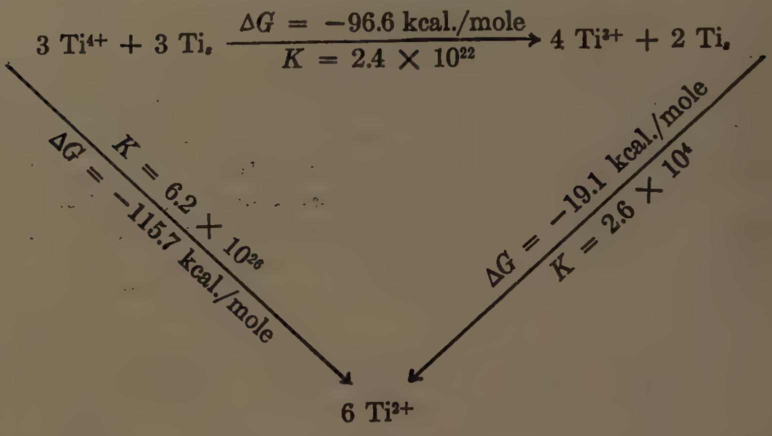

From these results, it is also possible to calculate that in a solution of titanium trichloride, in the presence of titanium metal, the composition of the solution at equilibrium should be a mixture of di- and trivalent titanium of a ratio about 9 to 1.

TABLE 5

Reaction in 1/1 mole KCl + NaCl at 670° C.	ΔG (kcal./mole)	$K_{\text{eqm.}}$
$Ti_2 + 2Ti^{3+} = 3Ti^{2+}$	−9.55	1.6×10^2
$Ti_2 + Ti^{4+} = 2Ti^{2+}$	−38.66	9.1×10^8
$Ti_s + 3Ti^{4+} = 4Ti^{3+}$	−96.57	2.4×10^{22}
$Ti^{2+} + Ti^{4+} = 2Ti^{3+}$	−29.00	5.2×10^6

By taking the state of the pure metal chlorides at the temperature of the experiments as the standard state, the activity coefficients and the other thermodynamic properties of the solutions of titanium chlorides in the fused salt can be calculated.

Thus, from EQUATION 4, by substituting

$$E^{\circ}_{\text{MCl}_n} - E^{\circ}_{\text{AgCl}} = E^{\circ\prime}_{\text{cell}}$$

and noting that since the activity coefficients of silver chloride in solution in 1/1 mole KCl + NaCl were found in a previous investigation[6] to be unity, the following relationship can be obtained:

$$\log \gamma_{(\text{MCl}_n)} = \frac{n\mathfrak{F}}{2.303RT}\left(E^{\circ\prime}_{\text{cell}} - E^{\circ}_{\text{cell}}\right) \qquad (13)$$

In this equation, $E^{\circ\prime}_{\text{cell}}$ is the calculated apparent standard cell potential with respect to the pure metal chlorides, and E°_{cell} the apparent standard cell potentials obtained experimentally in the present investigation.

Partial molal free energies of solution of titanium dichloride and trichloride and the partial entropy of mixing of titanium dichloride in the melt can be calculated from the well-known relationships

$$\Delta \bar{G}_A = -RT \ln \gamma_A = n\mathfrak{F}\,(E^{\circ\prime}_{\text{cell}} - E^{\circ}_{\text{cell}}) \qquad (14)$$

$$\left(\Delta \frac{\Delta \bar{G}_A}{\Delta T}\right)_p = -\Delta \bar{S}_A \qquad (15)$$

where $\Delta \bar{G}_A$ is the partial molal free energy of mixing and $\Delta \bar{S}_A$ is the partial molal entropy of mixing. The quantity defined by EQUATION 14 represents the difference between the free-energy change of the salt in its hypothetical standard state as a solute (that is, a solution containing a unit mole fraction of the salt but having, in all other respects, the thermodynamic properties of the state of infinite attenuation of the solute, as defined by Lewis and Randall[15]) and the free energy of the salt in its actual standard state as the pure salt.

TABLE 6

THERMODYNAMIC PROPERTIES OF DILUTE SOLUTIONS OF TITANIUM CHLORIDES IN 1/1 MOLE KCl + NaCl

System	Range of mole fractions investigated $x \times 10^3$	Partial molal free energy of mixing ($\Delta \bar{G}_A$) (kcal./mole)			Partial molal entropy of mixing $\Delta \bar{S}_A$ (eu)			Activity coefficients $\gamma \times 10^2$		
		670° C.	750° C.	800° C.	670° C.	750° C.	800° C.	670° C.	750° C.	800° C.
$TiCl_2$	2.60–10.0	−6.00	−6.36	−6.60	−5.0	−5.0	−5.0	4.1	4.3	4.5
$TiCl_3$	1.5–14.0	−10.45	—	—	—	—	—	0.38	—	—

The results of these calculations are given in TABLE 6. Data for potassium chlorotitanate are not included in this table because the standard state potentials of this complex are not available in the literature.

The magnitude of the activity coefficients given in TABLE 6 indicates that titanium dichloride and trichloride, in solution in the equimolar molten mixture of potassium chloride and sodium chloride, are present as complexes. In fact, only 4×10^{-2} and 4×10^{-3}, respectively, of the amount present are free to contribute to the electrode potential. The activity coefficients of titanium dichloride show the expected behavior, that is, they increase with increasing temperature. The constancy of the activity coefficient at constant temperatures over the mole fraction range 10^{-3} to 10^{-2} indicates that in these solutions the complex species remain unchanged.

The partial molal entropies of mixing, as shown in TABLE 6, also suggest the formation of a complex for this system.

SUMMARY

The solubilities of titanium tetrachloride in mixtures of potassium chloride and sodium chloride at various temperatures were investigated, using a quartz spring balance.

It was found that titanium tetrachloride vapor reacted with potassium chloride to form the compound K_2TiCl_6. Some of the physical properties of this compound, and the rates of its formation between 280° and 720° C., were investigated.

Using a silver-silver chloride reference electrode developed in a previous investigation, the apparent standard electrode potential of the system Ti, $TiCl_{2(KCl+NaCl)}$, and the apparent standard redox potentials of the systems $TiCl_2$, $TiCl_{3(KCl+NaCl)}$ and $TiCl_3$, $K_2TiCl_{6(KCl+NaCl)}$ were measured at 670° C., and found to be, respectively, 1.115, 0.910, and −0.350 volts.

From the data, the apparent standard electrode potentials of the systems Ti, $TiCl_{3(KCl+NaCl)}$, and Ti, $K_2TiCl_{6(KCl+NaCl)}$ were calculated and found to be 1.046 and 0.697 volts, respectively, at 670° C.

The activity coefficients and partial molal properties of titanium dichloride and titanium trichloride, in dilute solutions in the equimolar mixture of potassium chloride and sodium chloride, were calculated. It was found that for the range of mole fraction investigated, namely 10^{-4} to 10^{-2}, the solutions are nonideal and obey Henry's law.

ACKNOWLEDGMENTS

I thank T. R. Ingraham for many helpful discussions during the course of this work and J. A. Bland for the identification of K_2TiCl_6 by X-ray measurements. Thanks also are due to P. Hernandez, Mines Branch glassblower, for his assistance in constructing complex parts of the apparatus.

REFERENCES

1. FLENGAS, S. N. & T. R. INGRAHAM. 1957. Can. J. Chem. **35**: 1139.
2. FLENGAS, S. N. & T. R. INGRAHAM. 1957. Can. J. Chem. **35**: 1254.
3. FLENGAS, S. N. & T. R. INGRAHAM. 1958. Can. J. Chem. **36**: 780.
4. FLENGAS, S. N. & T. R. INGRAHAM. 1958. Can. J. Chem. **36**: 1103.
5. FLENGAS, S. N. & T. R. INGRAHAM. 1958. Can. J. Chem. **36**: 1062.
6. FLENGAS, S. N. & T. R. INGRAHAM. 1959. J. Electrochem. Soc. **106**(8): 714.
7. KROLL, W. J. 1955. Metallurgy. **9**(9/10): 360.
8. KREYE, W. C., C. J. B. PINCHAN, L. NANIS, M. JAWORSKY & H. H. KELLOG. 1956. Physical chemistry of NaCl-KCl melts containing dissolved titanium chlorides. O.N.R. Contract Nonr. 226 (24). School of Mines, Columbia Univ. New York, N. Y.
9. PERRY, J. H. 1950. Chemical Engineering Handbook. : 152. 3rd ed. McGraw-Hill. New York, N. Y.
10. EHRLICH, B. & E. FRAMM. 1954. Z. Naturforsch. **9b**: 326.
11. UNITED STATES NATIONAL BUREAU OF STANDARDS CIRCULAR. 1955. **539**: 49.
12. HAMER, W., M. MALMBERG & B. RUBIN. 1956. J. Electrochem. Soc. **103**: 8.
13. INGRAHAM, T. R., K. W. DOWNES & P. MARIER. 1957. Can. J. Chem. **35**: 850.
14. LIGHT, T. S. & A. J. DEBÉTHUNE. 1957. J. Chem. Educ. **34**: 443.
15. LEWIS, G. N. & M. RANDALL. 1923. Thermodynamics. Chap. XXII. McGraw-Hill. New York, N. Y.

FREEZING POINTS OF BINARY NITRATE MELTS

K. J. Macleod and F. E. W. Wetmore
Department of Chemistry, University of Toronto, Toronto, Canada

In an earlier study Murphy[5] determined the density and electric conductivity of the binary melts $AgNO_3$-$Ba(NO_3)_2$, $AgNO_3$-$Ca(NO_3)_2$, and $AgNO_3$-$Mg(NO_3)_2$. According to his results, the melts are far from ideal in terms of additivity of conductivity; a mechanism involving restricted jumps provides an explanation more consistent with the findings. The thermodynamic properties of these systems now have been studied through cryoscopy; determinations of heat quantities also are under way.

Experimental Methods

All salts used in the preparation of the melts were of reagent grade, treated as described earlier.[5,8] As only low temperatures of fusion were to be studied, the cryoscope was constructed of Pyrex vessels; thus the phase changes could be observed visually. The melts were placed in a tube suspended within an electrically heated cylinder, the whole arrangement being covered by an inverted, unsilvered Dewar flask. The system was stirred by an oscillating gas pressure in a tube immersed in the melt; a reciprocating pump created the fluctuations.

For measurement of temperature the output of a Chromel-Alumel thermocouple was balanced partially by a White potentiometer; the remainder was fed to an amplifier (Leeds and Northrup 9835-A) and thence to a recorder (L N Speedomax). The sensitivity was about 8 in. of chart run per degree.

Freezing points of the melts were determined by letting the temperature fall at an initial rate of approximately 0.5° C./min. Undercooling was generally less than 0.5° C., except with quite concentrated solutions, and the subsequent cooling curve could be extrapolated back with precision. Likewise, the upper melting point or thaw point was found by heating a mixture of liquid and crystals above the point of complete liquefaction, and extrapolating the segments of the heating curve. With dilute solutions, the freezing point and upper melting point were found to be the same within 0.01° C. With concentrated solutions the difference was greater and the upper melting point was found to be the more reproducible.

Results and Discussion

FIGURE 1 shows the freezing-point depression for all three binary melts up to 1 mole per cent. The curve is a straight line of slope $dT/dN_1 = 167$. The limiting slope calculated from the reported[7] heat of fusion of $AgNO_3$ and the melting point found here (209.7° C.) is 168. Kordes *et al.*[3] stated the cryoscopic constant to be 167, from a substantial series of determinations.

The eutectic point of the system $AgNO_3$-$Ba(NO_3)_2$ was found to be 208.0° C., 0.99 mole per cent. Palkin[6] reported 207° C., 1.8 mole per cent.

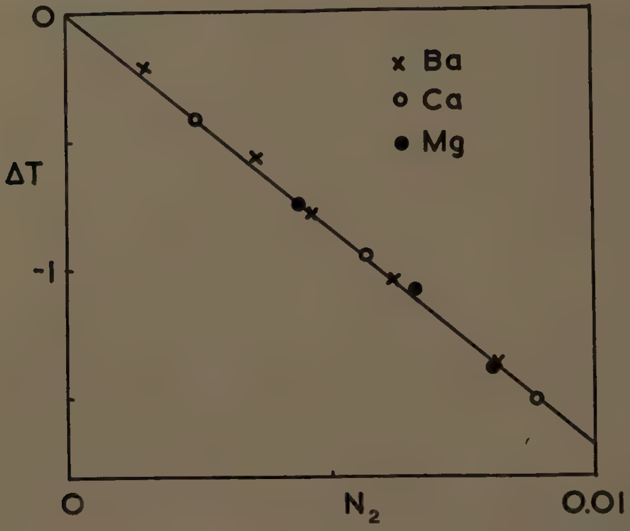

FIGURE 1. Depression of the freezing point of silver nitrate by divalent nitrates.

TABLE 1
SYSTEM: $AgNO_3$-$Ca(NO_3)_2$

Seq.	N_1	F.p. depression	a_1	γ_1
6	0.9799	3.16	0.9813	1.001
8	0.9713	4.71	0.9722	1.001
1	0.9646	5.86	0.9655	1.001
2	0.9568	7.06	0.9585	1.002
3	0.9348	10.5	0.9368	1.004
9	0.9225	12.5	0.9272	1.005
7	0.9202	12.7	0.9260	1.006
4	0.9174	13.3	0.9226	1.006
5	0.9000	15.8	0.9084	1.009

The eutectic point of the system $AgNO_3$-$Ca(NO_3)_2$ was found to be 193.7° C., 10.1 mole per cent. Palkin[6] reported 202° C., 10.7 mole per cent. The freezing-point curve, T versus N_2, is slightly concave upward as it approaches the eutectic point. The data are given in detail in TABLE 1 and FIGURE 2.

The eutectic point of the system $AgNO_3$-$Mg(NO_3)_2$ was estimated to be 159.5° C., 22.1 mole per cent. Exact determination was made difficult by the existence of a sluggish transition of solid silver nitrate at 159.4° C., so reported by Bridgman[1] and confirmed in this work. TABLE 2 and FIGURE 3 show the data in detail.

At present the differential heat of solution of solid silver nitrate in the saturated binary melts is not known; therefore, activity coefficients of the components cannot be calculated without assumption. The values for silver nitrate (TABLES 1 and 2) were computed with the aid of the expression given by Lewis and Randall[4] and acceptance of the datum:[7] $\Delta C = C_{\text{liq.}} - C_{\text{solid}} = 4.5$ cal. mole^{-1} deg.$^{-1}$. Data being gathered at present suggest that this value of ΔC may be high, but the effect of correction on the activity coefficients would be small.

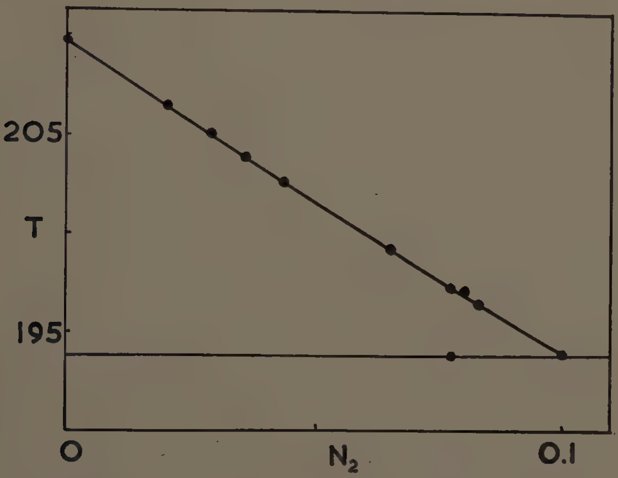

FIGURE 2. Freezing points of $AgNO_3$-$Ca(NO_3)_2$ melts.

TABLE 2
SYSTEM: $AgNO_3$-$Mg(NO_3)_2$

Seq.	N_1	F.p. depression	a_1	γ_1
1	0.9748	4.02	0.9762	1.001
9	0.9514	8.34	0.9510	1.000
2	0.9481	8.76	0.9486	1.001
3	0.9217	13.6	0.9205	0.999
7	0.9204	14.3	0.9169	0.996
10	0.9046	17.4	0.8995	0.994
4	0.9028	17.4	0.8995	0.996
5	0.8795	22.4	0.8717	0.991
6	0.8602	26.3	0.8504	0.989
13	0.8477	30.5	0.8278	0.977
11	0.8428	31.4	0.8231	0.977
14	0.8221	37.0	0.7936	0.965
12	0.7974	43.1	0.7621	0.956
15	0.7947	46.6	0.7446	0.937
8	0.7853	49	0.733	0.934
16	0.7792	49.2	0.7315	0.939

Estimates of the activities of the components in the melt can be begun from the expression for the free energy of the melt, $F = n_1\mu_1 + n_2\mu_2$, by comparing it with the free energy of the separate components and the free energy of their mixing, $F = n_1F^\circ_1 + n_2F^\circ_2 + \Delta F_{\text{mixing}}$.

Temkin[9] has proposed simple assumptions for calculation of ΔF of mixing: (1) that $\Delta H = 0$ and (2) that ΔS is calculable as an entropy of configuration, with related statistical weight W. Temkin's postulate applied to our melts would concern the number of ways of filling $(n_1 + n_2)$ cation sites by n_1-like silver ions and n_2-like divalent ions, and $(n_1 + 2n_2)$ anion sites by $(n_1 + 2n_2)$-like anions. Then $W_+ = (n_1 + n_2)!/n_1!n_2!$ and $W_- = 1$, from which $\Delta S = -R(n_1 \ln N_1 + n_2 \ln N_2)$ and $F = n_1(F^\circ_1 + RT \ln N_1) + n_2(F^\circ_2 + RT \ln N_2)$. According to Temkin's assumptions, $\mu_1 = F^\circ_1 + RT \ln N_1$ and $\gamma_1 = 1$ at all concentrations when the standard state of silver nitrate is chosen to be the pure liquid component.

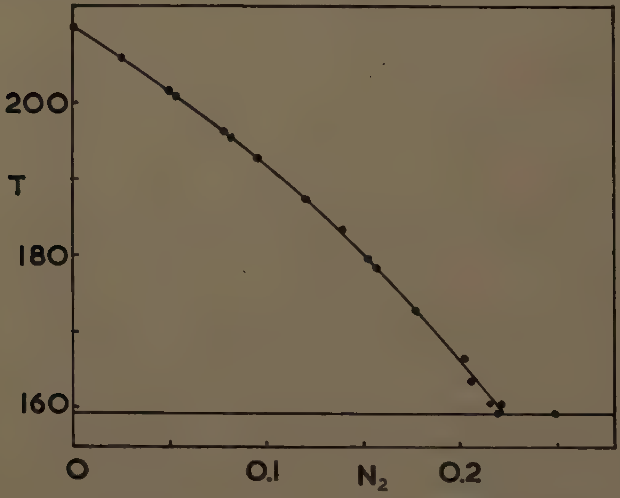

FIGURE 3. Freezing points of $AgNO_3$-$Mg(NO_3)_2$ melts.

The data of TABLES 1 and 2 are in accord with Temkin's theory up to $N_2 = 0.1$, but not for the more concentrated magnesium nitrate solutions. A rough test of assumption 1 was made by a readily devised experiment with an adiabatic calorimeter. Successive portions of magnesium nitrate were added to liquid silver nitrate at 232° C. The curve of ΔH versus N_2 was a straight line within 7 cal. mole^{-1}, up to $N_2 = 0.11$, beyond which dissolving was sluggish. A more definitive test then was made by adding liquid silver nitrate to a melt containing 21 mole per cent magnesium nitrate to yield a melt of 0.14 mole per cent. The reaction was exothermic by 2.8 cal. mole^{-1}. Thus $H_1 - H^\circ_1$ is roughly -3 cal. mole^{-1} and inclusion of this value in the ΔF of mixing would decrease $\ln \gamma_1$ by only $3/RT$, or 0.003. It is unlikely that, even at the highest concentrations met here, γ_1 would be lowered by more than 0.01 by inclusion of the heat of mixing term. The deviation of γ_1 from unity may be ascribed more properly to error in the calculation of the ΔS term.

Flood *et al.*[2] pointed out that cation vacancies may be created in the mixing of divalent with univalent salts. If, in the extreme case, there were one cation vacancy for each divalent cation added, $W_+ = (n_1 + 2n_2)!/n_1!n_2!n_2!$ and therefore $\mu_1 = F^\circ_1 + RT \ln N_1^*$, in which N_1^* is the equivalent fraction; $\gamma_1 = N_1^*/N_1$, substantially lower than shown in TABLE 2. The shrinkage of the equivalent volume found by Murphy on adding divalent nitrate to silver nitrate indicated that the creation of vacancies is probably much less than one per divalent ion; this view is in accord with the present results.

The smallness of the heat of mixing provides assurance that the variation of a_1 with temperature is negligible, since $(H^\circ_1 - H_1)/RT^2 = d \ln a_1/dT$ is of the order of 10^{-5}. Therefore the Gibbs-Duhem expression can be used to determine γ_2 from values of γ_1 found at various temperatures. The values of γ_2 for calcium nitrate at $N_2 = 0.05$, 0.075, and 0.1 are 0.98, 0.92, and 0.89, respectively; for magnesium nitrate at $N_2 = 0.1$, 0.15, and 0.2, they are, respectively, 1.00, 1.16, and 1.35. It should be noted that for a_2 the reference state is the infinitely dilute solution, whereas for a_1 it is pure liquid silver nitrate.

Acknowledgments

We are indebted to the National Research Council of Canada, Ottawa, Ont., and to the Advisory Committee on Scientific Research of the University of Toronto, Toronto, Ont., Canada for financial support of the research, and to Canadian Industries Limited, Montreal, P. Q., Canada for award of a scholarship to one of the authors (K. J. M.). We also acknowledge the help of V. C. Reinsborough in determining heat quantities.

References

1. BRIDGMAN, P. W. 1916. Proc. Am. Acad. Arts Sci. **51:** 581.
2. FLOOD, H., T. FØRLAND & K. GRJOTHEIM. 1953. The Physical Chemistry of Melts. : 46. Inst. of Mining and Metallurgy. London, England.
3. KORDES, E., W. BERGMANN & W. VOGEL. 1951. Z. Elektrochem. **55:** 600.
4. LEWIS, G. N. & M. RANDALL. 1923. Thermodynamics and Free Energy of Chemical Substances. : 282. McGraw-Hill. New York, N.Y.
5. MURPHY, J. W. & F. E. W. WETMORE. 1959. Can. J. Chem. **37:** 1397–1401.
6. PALKIN, A. P. 1929. Bull. univ. état Asie centrale. **18:** 77.
7. ROSSINI, F. D., D. D. WAGMAN, W. H. EVANS, S. LEVINE & I. JAFFE. 1952. Selected Values of Chemical Thermodynamic Properties. Natl. Bur. Standards (U.S.) Circ. **561.**
8. SHOMATE, C. H. & K. K. KELLEY. 1944. J. Am. Chem. Soc. **66:** 1490.
9. TEMKIN, M. 1945. Acta Physicochim. U.R.S.S. **20:** 411.

THERMODYNAMIC PROPERTIES OF SOLUTIONS OF CERIUM CHLORIDE IN MOLTEN ALKALI HALIDES

S. Senderoff, G. W. Mellors, R. I. Bretz
Research Laboratories, National Carbon Company, Division of Union Carbide Corporation, Cleveland, Ohio

Introduction

In recent years there has been increasing interest in molten salt systems in nuclear, metallurgic, and other applications; as a result, the need for information on the thermodynamic properties of molten salt solutions has become more evident. The usual methods for obtaining thermodynamic information in these high temperature systems include some of those used for many years in aqueous solutions: for example, cryoscopy,[1] determination of vapor pressure,[2-5] and determination of emf of cells with fused salt electrolytes.[6,7] The experimental difficulties involved in adapting these standard methods for use at elevated temperatures are frequently considerable and are often the determining factor in the choice of a method. It is for this reason that the emf method has been favored whenever suitable reversible and reproducible electrodes are available for the measurement. Unfortunately, these requirements for the electrodes are difficult to meet in many systems. While a satisfactory chlorine-graphite electrode may be prepared for use in molten chlorides up to a temperature of at least 900° C.,[8] the metal electrode is frequently dissolved or attacked by the metal chloride under study. Under these circumstances, only very dilute solutions of the metal chloride[6] may be studied at comparatively low temperature[9,10] if necessary, or, if it is desired to study the full composition range, a suitable dilute metal alloy electrode may be used.[11]

Cerium is soluble in cerium trichloride to the extent of almost 9 mole per cent[12] and thus cannot be used as an electrode. The melting point of cerium trichloride (812° C.) defines the lower limit of temperature for a study of the full composition range of cerium chloride dissolved in the alkali halides.

Electrodes

Since cerium metal could not be used as an electrode, a search of cerium-alloy phase diagrams indicated that the cerium-tin system might meet the requirements of a suitable alloy electrode. These requirements are:

(1) The diluent metal of the alloy should be very noble compared with cerium, so that the equilibrium concentration of the diluent metal ion in the electrolyte be negligible.

(2) In the temperature range in which it is to be used, the alloy should consist of two phases over a considerable range of composition. The ac-

tivity of the cerium in such a heterogeneous alloy would be constant so long as both phases are present; therefore, the composition of the alloy would not be critical in its use as an electrode.

(3) The activity of the cerium in the alloy should be sufficiently low so that it will not reduce the cerium trichloride or alkali metal ion in the electrolyte.

(4) The alloy must behave reversibly as a Ce^{3+}/Ce^{0} electrode.

The first requirement is satisfied, since the difference in potential between cerium and tin is about 1.0 to 1.4 v., depending on the reaction chosen.[13] This corresponds to an equilibrium constant of about 10^{-10} for the reduction of cerium ion by tin.

The phase diagram of the Ce-Sn system[14] shows how the second requirement is met. From 25 atom per cent cerium to almost pure tin, the solid compound, $CeSn_3$ (m.p. 1140° C.), exists in equilibrium with a tin-rich liquid above 220° C. Since the liquidus line is above 900° C. at 10 mole per cent cerium, any composition between 10 and 25 mole per cent cerium may be used in the 800 to 900° C. range in which we are interested. To confirm the constancy of the potential over a wide range of composition, a 5 mole per cent and a 15 mole per cent Ce alloy electrode were compared in electrolytes of the same composition with a chlorine electrode, and values of potentials were obtained that differed by less than 2 mv. The electrode used throughout this work was approximately 15 mole per cent cerium and was prepared in an induction furnace by melting cerium and tin in a Morganite ΔRR alumina crucible, holding at 1200° C. in an argon atmosphere for 30 min., and quenching.

With regard to the third requirement, it was found that the alloy electrode was noble with respect to a pure cerium electrode by about 0.5 v., and visual examination of the melts after a few days' contact with the alloy showed no evidence of the black reaction product of cerium with cerium trichloride.

The reversible behavior specified in the fourth requirement was demonstrated by the Nernstian concentration dependence of the potential in very dilute solutions as the concentration of cerium chloride was varied. This will be discussed below.

The other electrode was the chlorine-graphite electrode described previously[8] in which the chlorine gas is forced through a porous graphite cylinder into the melt.

Experimental

Materials. $CeCl_3$ was prepared by chlorination of Ce_2S_3 as described previously.[15] A slight modification was introduced which consisted of continuing the chlorination at 900° C. for 3 or 4 hours after all visible evidence of reaction had disappeared. In this manner the last traces of oxychloride were removed, and $CeCl_3$ was obtained in which the Cl:Ce atom ratio was 3.004 and the over-all purity was 99.9 per cent. The salt dissolved in water and in ethyl alcohol without any discernible turbidity.

The electrolyte for the cell was prepared by adding the pure $CeCl_3$ to dried NaCl or KCl in a graphite crucible. The mixture was slowly heated to 900° C. in a chlorine atmosphere with the chlorine bubbling through the liquid mixture for 2 to 3 hours. The mixture was quenched, transferred to a dry box, broken out of the crucible in large lumps, and charged into the cell without additional pulverization. A sample of the electrolyte was dissolved in water, and the batch was used only if no turbidity was observed. Samples of the electrolyte were analyzed before and after each cell run, and the results were discarded in the few instances in which a significant change in composition occurred.

Cell. The cell in which the emfs were measured is shown in FIGURE 1 and has been described in detail previously.[15] Two concentric Morganite ΔRR crucibles are so positioned that the alloy electrode forms a pool at the bottom of the outer crucible. This is covered with a layer of electrolyte in contact with the same electrolyte in the inner crucible through a small (1⁄32-inch) asbestos-filled hole in the bottom of the inner crucible. The graphite cylinder that constitutes the chlorine electrode is immersed in the inner crucible. A molybdenum collar is sealed into the bottom of the outer crucible to form the electric contact to the alloy electrode. The molybdenum is covered completely by the alloy electrode. A liquid seal of electrolyte separates the chlorine atmosphere of the inner crucible from the argon atmosphere of the outer one. A long iron tube is threaded onto the molybdenum rod that emerges from the bottom of the outer crucible. The iron tube supports the cell in the furnace and acts as the electric lead-in to the cell. Although there are many contacts between dissimilar metals in this arrangement, they are all within the high temperature zone. The only thermoelectric potential that need be considered is that between iron and graphite, since these are the ones that pass through the temperature gradient of about 800° C. The thermal emf for the iron-graphite couple for an 800° gradient is less than 0.1 mv.[16] and has been ignored in this work.

Furnace and temperature control. These also have been described previously.[15] A Marshall Products tensile-test furnace was used that, with an appropriate baffle, gave a temperature zone constant to within 1° C. at 900° C. over the length of the cell. The temperature was controlled with a thermocouple adjacent to the winding of the furnace by means of a Wheelco controller of the saturable-core reactor type. The temperature was measured with a thermocouple in a quartz thermowell, the end of which rested on the edge of the inner crucible and well below the top of the outer crucible. The thermocouple output was read on an L & N Azar recorder with 33-mv. suppressed and 10-mv. range on scale. Temperatures could be read to 1° C.

Operating procedure. Cerium-tin alloy was added to the outer crucible in an amount sufficient to cover the molybdenum collar. The electrolyte in large lumps (to reduce the effect of momentary exposure to the atmosphere) was added to the inner and outer crucibles in amounts to make a volume, when molten, of 15 and 20 cc., respectively. The cell was assembled as in FIGURE 1, inserted into the furnace, and flushed with argon. While heating to the desired temperature, argon was passed through both

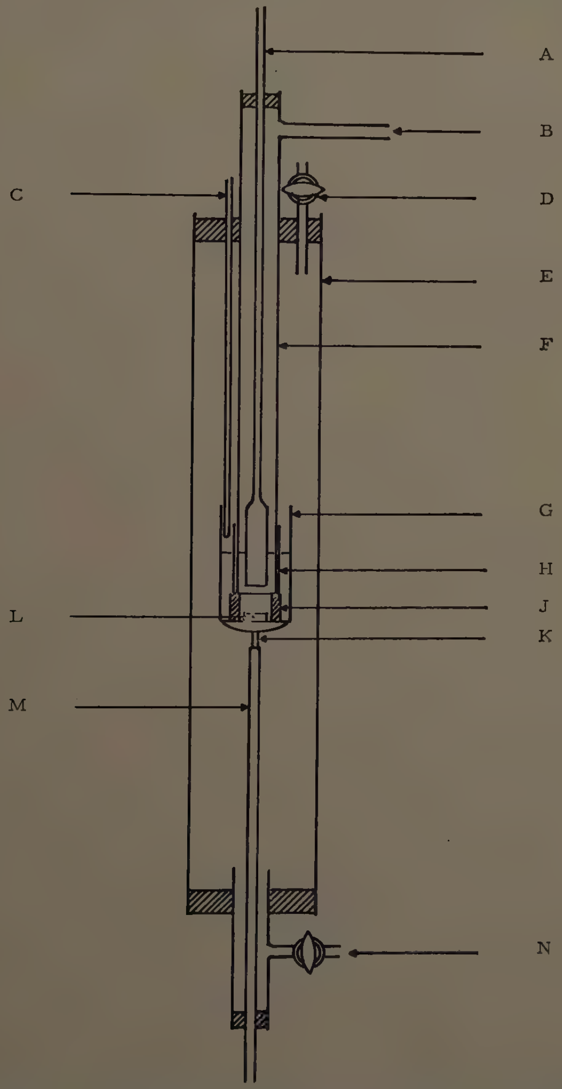

FIGURE 1. Cell for emf measurements. Key: A, chlorine electrode; B, chlorine exit; C, thermocouple sheath; D, argon exit; E, 51 mm. o.d. Vycor glass envelope; F, 25 mm. o.d. Vycor glass sheath; G, XN100 alumina crucible; H, XN20 alumina crucible; J, ΔRR alumina pedestal; K, molybdenum rod, threaded 6/32; L, molybdenum collar; M, iron pedestal and N, argon entry tube.

the inner and outer chambers. When the electrolyte melted, the graphite electrode was immersed in the liquid, and chlorine flow begun. Measurements of potential were made at 20° to 25° C. intervals between 800° and 925° C. The potential was measured only after the temperature had become constant. Two or three measurements in the course of 10 to 15 min. at a given temperature were made to ensure the constancy of the system. After equilibrium had been attained, the measurements made over 3 or 4 heating and cooling cycles had an average deviation from the mean of less than 1 mv. Equilibrium usually was attained within 3 or 4 hours, but occasionally standing at room temperature overnight was required. To test the stability of some cells, measurements were taken over a period of 2 or 3 days after equilibrium was established, with no significant change in potential.

The potentials were measured with a Rubicon Type B potentiometer. An Eveready Air Cell was used as a source of bucking potential, since voltages in excess of 2 v. were to be read. The potential of the Air Cell was measured before each cell measurement.

Results. The cell to be measured may be written:

$$\mathrm{Ce(1)}\mid \mathrm{CeCl_3}(N),\ \mathrm{MCl}(1-N)\mid \mathrm{Cl_2},\ \text{graphite} \qquad \text{Cell I}$$

where N = mole fraction and M = sodium or potassium. This could not be done directly because of the interaction between cerium and cerium chloride. However, when N is small the interaction is negligible and so the following cells may be measured:

$$\mathrm{Ce(1)}\mid \mathrm{CeCl_3}(N < 10^{-2}),\ \mathrm{MCl}\mid \mathrm{Cl_2},\ \text{graphite} \qquad \text{Cell II}$$

$$\mathrm{Ce\text{-}Sn(1)}\mid \mathrm{CeCl_3}(N),\ \mathrm{MCl}(1-N)\mid \mathrm{Cl_2},\ \text{graphite} \qquad \text{Cell III}$$

For $N_{\mathrm{Cell\ II}} = N_{\mathrm{Cell\ III}}$, the difference in emf between Cells II and III is the potential difference between the Ce-Sn(1) and Ce(1) electrodes in any electrolyte in which they behave reversibly. The emf of Cell I for any value of N is obtained by adding this potential difference between Ce and Ce-Sn alloy to the measured emf of Cell III at the corresponding value of N.

A direct measurement of $\mathrm{Ce}\mid \mathrm{CeCl_3},\ \mathrm{KCl}\mid \mathrm{Ce\text{-}Sn}$ could not be made satisfactorily because of slow continuous drift of the potential. It is believed that, even at the lowest concentration tried, a slow attack on the pure cerium electrode occurs and introduces a mixed potential involving a product of the interaction such as $\mathrm{Ce^{+1}}$. The stability of Cell II for $N < 10^{-2}$ may result from an extremely small leak of chlorine from the cathode compartment that scavenges the $\mathrm{Ce^{+1}}$ in the anolyte, but does not represent a sufficiently large corrosion current for the anode to be displaced significantly from its equilibrium potential.

TABLE 1 lists the results of measurements of the emf of Cells II and III with KCl as diluent for values of $N = 1.6 \times 10^{-2}$ and 1.5×10^{-3}. TABLE 2 lists ΔE, the change in emf of each of the cells for the approximately tenfold variation of the mole-fraction N, the concentration. Also shown in TABLE 2 is ΔE_{Nernst} calculated by $\Delta E = (RT/3f) \ln 10.666$. Comparison of the fourth and seventh columns of TABLE 1 shows that at low temperatures the agreement of $E_{\text{Ce, Ce-Sn}}$ obtained in the 2 electrolytes is good. The deviation at higher temperatures results from a large temperature coefficient in the more concentrated solution (0.80 compared to 0.57 mv./degree). It also may be seen that the large temperature coefficient arises from Cell II, since the temperature coefficients of Cell III are almost identical in the two concentrations. In TABLE 2 the increasing departure of Cell II from the ideal concentration dependence may be noted as the temperature is increased. It appears, therefore, that even at $N = 1.6 \times 10^{-2}$, interaction between the electrolyte and pure cerium is not negligible above 840° C. The concentration dependence of Cell III agrees fairly well with the theoretical value, especially at higher temperature. For this study the values of $E_{\text{Ce, Ce-Sn}}$ at 800° to 900° C. were taken to be those in the last column of TABLE 1.

TABLE 1
POTENTIAL OF CERIUM ALLOY ELECTRODE

Temp. (°C.)	1.6 mole per cent $CeCl_3$			0.15 mole per cent $CeCl_3$		
	Ce, Cl_2 (v.)	Ce-Sn, Cl_2 (v.)	Ce, Ce-Sn (v.)	Ce, Cl_2 (v.)	Ce-Sn, Cl_2 (v.)	Ce, Ce-Sn (v.)
800	2.927_5	2.363_0	0.565	3.007_0	2.444_0	0.563
820	2.906_0	2.357_5	0.549	2.990_0	2.438_5	0.552
840	2.884_5	2.352_0	0.533	2.972_5	2.432_5	0.540
860	2.863_0	2.346_5	0.517	2.955_0	2.427_0	0.528
880	2.841_5	2.341_0	0.501	2.938_0	2.420_5	0.518
900	2.820_0	2.335_5	0.485	2.920_5	2.414_5	0.506
dE/dT (mv./°C.)	1.07	0.27	0.80	0.87	0.29	0.57

TABLE 2
CONCENTRATION DEPENDENCE OF THE POTENTIAL

Temp. (°C.)	ΔE, Ce, Cl_2 (mv.)	ΔE, Ce-Sn, Cl_2 (mv.)	ΔE Nernst (mv.)
800	79.5	81	75
820	84	81	76
840	88	80	77
860	92	80	79
880	96	80	80
900	100	79	81

The results of the measurements of Cell III with KCl as diluent are shown in FIGURE 2 and with NaCl as diluent in FIGURE 3. The emfs are the sum of the observed emf and the potential difference between Ce-Sn alloy and pure cerium, that is, the emf of Cell I at corresponding composition and temperature. TABLES 3 and 4 list the emfs and associated thermodynamic data for the two systems at 800°, 850°, and 900° C. At each composition shown in FIGURE 3 the emf can be expressed as a linear function of temperature, $E = p + qT$ where $nfE = -\Delta F$, $nfp = -\Delta H$ and $nfq = \Delta S$ for that composition ($N = 3$, f = Faraday constant, q = observed dE/dT of the cell, T = absolute temperature). The values for the free energy, enthalpy, and entropy of formation refer to the reaction

TABLE 3

EMF VALUES AND THERMODYNAMIC PROPERTIES OF $CeCl_3$-KCl SYSTEM

N	emf (v.)	800° C. $-(\bar{F} - F^0)$ kcal.	γ	emf (v.)	850°C. $-(\bar{F} - F^0)$ kcal.	γ	emf (v.)	900° C. $-(\bar{F} - F^0)$ kcal.	γ	dE/dT (mv./°C.)	$-(\bar{H} - H^0)$ kcal.	$-(\bar{S} - S^0)$ cal./deg.
1.0000	2.607_0	—	1.0000	2.562_5	—	1.0000	2.520_0	—	1.0000	0.87	—	—
0.8246	2.611_0	0.277	1.0651	2.566_0	0.242	1.0386	2.522_0	0.139	1.1429	0.89	1.00	0.67
0.6796	2.623_5	1.142	0.8615	2.579_0	1.142	0.8423	2.536_0	1.108	0.9152	0.88	2.70	1.45
0.4993	2.646_0	2.700	0.6954	2.600_0	2.595	0.5980	2.555_0	2.423	0.7090	0.91	4.20	1.39
0.4797	2.661_5	3.772	0.3558	2.617_0	3.772	0.3675	2.575_0	3.807	0.4075	0.87	5.20	1.33
0.3305	2.717_0	7.614	0.08533	2.673_0	7.647	0.09401	2.630_5	7.648	0.1140	0.87	7.60	0.00
0.2660	2.739_0	9.136	0.06887	2.696_0	9.239	0.05726	2.655_0	9.344	0.06846	0.84	9.20	0.00
0.1578	2.814_0	14.327	0.007687	2.769_0	14.291	0.01053	2.725_0	14.188	0.01446	0.89	14.40	0.00
0.1111	2.840_5	16.161	0.004620	2.797_0	16.229	0.006276	2.754_0	16.230	0.008683	0.86	16.15	0.00
0.01567	2.926_0	22.078	0.002045	2.883_0	22.181	0.002955	2.841_5	22.251	0.004589	0.87	22.10	0.00
0.001518	3.007_0	27.684	0.001526	2.963_0	27.718	0.002555	2.920_5	27.719	0.004543	0.89	27.60	0.00

TABLE 4

EMF VALUES AND THERMODYNAMIC PROPERTIES OF $CeCl_3$-NaCl SYSTEM

N	emf (v.)	800° C. $-(F - F^0)$ kcal.	γ	emf (v.)	850° C. $-(F - F^0)$ kcal.	γ	emf (v.)	900° C. $-(F - F^0)$ kcal.	γ	dE/dT (mv./°C.)	$-(\bar{H} - H^0)$ kcal.	$-(\bar{S} - S^0)$ cal./deg.
1.0000	2.607_0	—	1.0000	2.562_5	—	1.0000	2.519_0	—	1.0000	0.870	—	—
0.6117	2.626_0	1.315	0.8826	2.581_0	1.280	0.9214	2.538_0	1.315	0.9302	0.880	2.05	0.684
0.6099	2.629_5	1.558	0.7903	2.584_0	1.458	0.8421	2.540_0	1.453	0.8793	0.895	2.40	0.888
0.5841	2.632_0	1.731	0.7613	2.583_0	1.418	0.9069	2.535_5	1.142	1.0406	0.985	2.60	0.903
0.4898	2.651_0	3.046	0.4899	2.606_5	3.045	0.5220	2.563_0	3.045	0.5532	0.880	4.60	1.438
0.4220	2.654_5	3.288	0.5075	2.609_0	3.218	0.5606	2.565_0	3.184	0.6052	0.885	5.00	1.595
0.3219	2.672_0	4.499	0.3771	2.626_5	4.429	0.4275	2.581_5	4.326	0.4862	0.905	6.90	2.237
0.2559	2.700_0	6.437	0.1913	2.652_5	6.229	0.2401	2.609_0	6.229	0.2707	0.910	9.40	2.760
0.1607	2.744_0	9.482	0.07312	2.699_0	9.447	0.09048	2.655_0	9.413	0.1100	0.890	11.95	2.299
0.09584	2.770_5	11.316	0.05189	2.724_5	11.212	0.06883	2.680_0	11.143	0.08780	0.905	13.20	1.755
0.01717	2.833_0	15.642	0.03813	2.787_5	15.572	0.05451	2.746_0	15.711	0.06913	0.870	15.65	0.007

$$Ce(1) + \frac{3}{2}\,Cl_2(g) = CeCl_3(N) \text{ in } MCl(1) \qquad (1)$$

Although the uncertainty in the values of emf is less than 2 parts per 1000, the uncertainty in dE/dT may be as much as 10 per cent. This will be discussed below. As a result, the values of ΔH and ΔS obtained from p and q show considerable scatter. The values of ΔH were plotted against the logarithm of the activity of $CeCl_3$ ($\log a_{CeCl_3}$), and a smooth curve was drawn through the points. The values of q and ΔS were calculated from

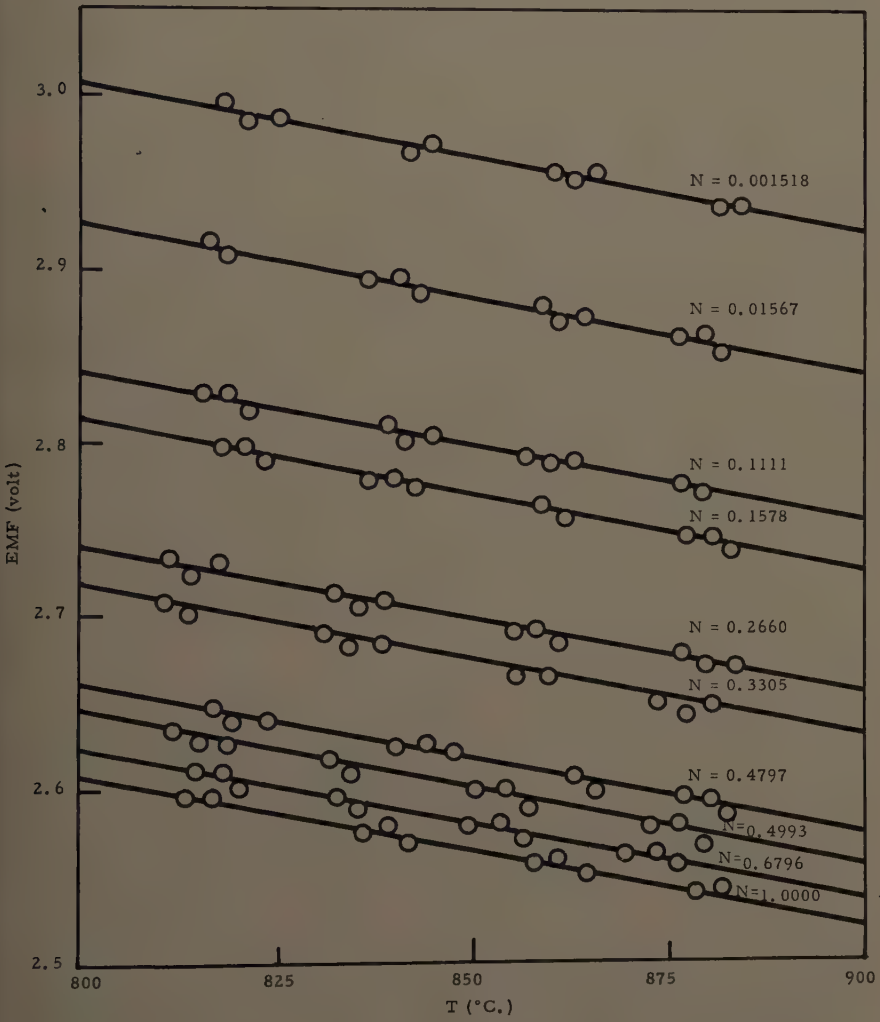

FIGURE 2. The emf as a function of temperature, KCl diluent.

$E = p + qT$, using the smoothed values of p. The values for pure $CeCl_3$ are listed in TABLE 5. The values for $\bar{H} - H^0$ and $\bar{S} - S^0$ listed in TABLES 3 and 4 are calculated from the smoothed values of p and q. Since

$$CeCl_3(1)(N = 1)$$

is taken as the standard state, the partial molar properties in TABLES 3 and

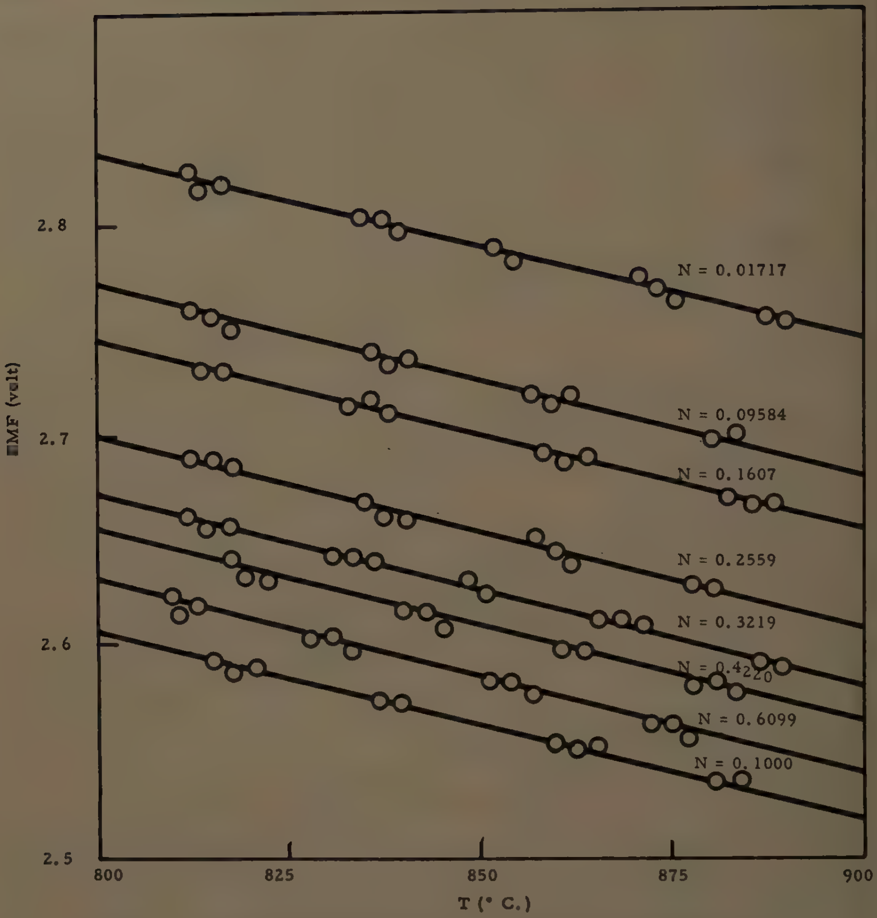

FIGURE 3. The emf as a function of temperature, NaCl diluent.

TABLE 5
THERMODYNAMIC PROPERTIES OF PURE LIQUID $CeCl_3$

Temp. (°C.)	emf (v.)	$-\Delta F^0$ (kcal.)	$-\Delta H^0$ (kcal.)	$-\Delta S^0$ (cal., deg.)
800*	2.607_0	180.4_5	245.0_0	60.2_0
825	2.585_0	178.8_5		
850	2.563_5	177.3_5		
875	2.542_0	175.9_0		
900	2.520_0	174.2_5		
925	2.498_0	172.8_5		

* Extrapolated from lowest temperature of measurement, 820° C.

4 correspond to the difference in each of the quantities between its value in pure $CeCl_3$ and that at the indicated composition.

The free-energy change for REACTION 1 in the system may be expressed as a function of temperature and activity, *a*, of $CeCl_3$ by

$$\Delta F(\text{kcal.}) = -245.0 + 6.02 \times 10^{-2}\, T + 4.58 \times 10^{-3}\, T \log a$$

with a standard deviation of 0.04 kcal. in the NaCl solvent and 0.07 kcal. in the KCl solvent.

The activity coefficient, γ, in TABLES 3 and 4 is obtained from the equation

$$\frac{3f}{RT}(E^\circ - E) - \ln N = \ln \gamma$$

Discussion

Thermodynamic properties of pure $CeCl_3$. In FIGURE 4 the emf at 850° C. of Cell I (KCl diluent) is plotted against the logarithm of the mole fraction of $CeCl_3$, and included are two straight lines drawn with the Nernst slope for $n = 3$. It will be noted that the theoretical Nernst slope is approached at both the concentrated and dilute ends of the composition range. The value of the emf of the cell with an electrolyte of pure $CeCl_3$ at 850° C. is 2.563 v. and corresponds to a free energy of formation of −177.3 kcal./mole. This compares with −192 kcal. (corresponding to an emf of 2.776 v.) estimated by Glassner[17] from aqueous heat of solution data.[18] It will be seen in FIGURE 4 that, by using the Nernst slope to extrapolate the emf values of the very dilute solutions to pure $CeCl_3$, the emf thus obtained is 2.754 (corresponding to −190.5 kcal.). Since the extremely dilute solutions of $CeCl_3$ in KCl almost certainly contain complex compounds involving $CeCl_3$ (as will be shown below), it is possible that the structure of the solid $CeCl_3$ and its aqueous solutions is more like that of the complexed form than that of the pure liquid $CeCl_3$.

Examination of the results of Walker and Danly[19] on $NiCl_2$ in KCl-LiCl solvent at 500° C. shows similar behavior. The extrapolation of their emf data in the dilute $NiCl_2$ solutions to $N_{NiCl_2} = 1$ gives a value of E° of 1.06 volts. This can be compared to 1.07 volts at 500° C. calculated by Hamer[20] from data apparently obtained near room temperature. The concentrated solutions of $NiCl_2$, however, indicated an E° of 0.94 v. compared with 0.976 v. calculated from Glassner's compilation.[17] The Glassner value was derived from heat-content measurements at high temperatures. Since complex formation by $NiCl_2$ and KCl in molten alkali nitrate solution has been demonstrated by absorption spectroscopy,[21,22] it may be inferred also in this case that the structure of solid $NiCl_2$ and its aqueous solution is more like that of the complexed form than the pure liquid.* It cannot be expected, however, that the very dilute molten system always will correspond to the room-temperature aqueous conditions. In the case of NaCl-$CeCl_3$ solutions (FIGURE 5) the same extrapolation as above gives a value of 2.651 v. about 0.1 v. (7 kcal.) lower than in the KCl system. It will be shown below that complex formation in the NaCl system is not as strong as in the KCl solution. Spedding and Miller[18] found ΔS_{298} to be −59.3 cal./degree mole, and Glassner estimates $\Delta S_{1123}°$ to be −43.3 cal./degree mole. The value of the entropy of formation is not obtained with as high precision as the free energy because the temperature coefficients of the emf are small. Thus, if the over-all uncertainty in the two cell measurements (Cells II and III) required is about 5 mv., then the uncertainty in ΔF is less than 2 parts per 1000. The uncertainty in dE/dT, however, may be in excess of 10 per cent.

---

* The entropy of formation of liquid $CeCl_3$ between 820° and 920° C. was found to be −60.2 cal./degree (corresponding to a dE/dT of 0.87 mv./degree).

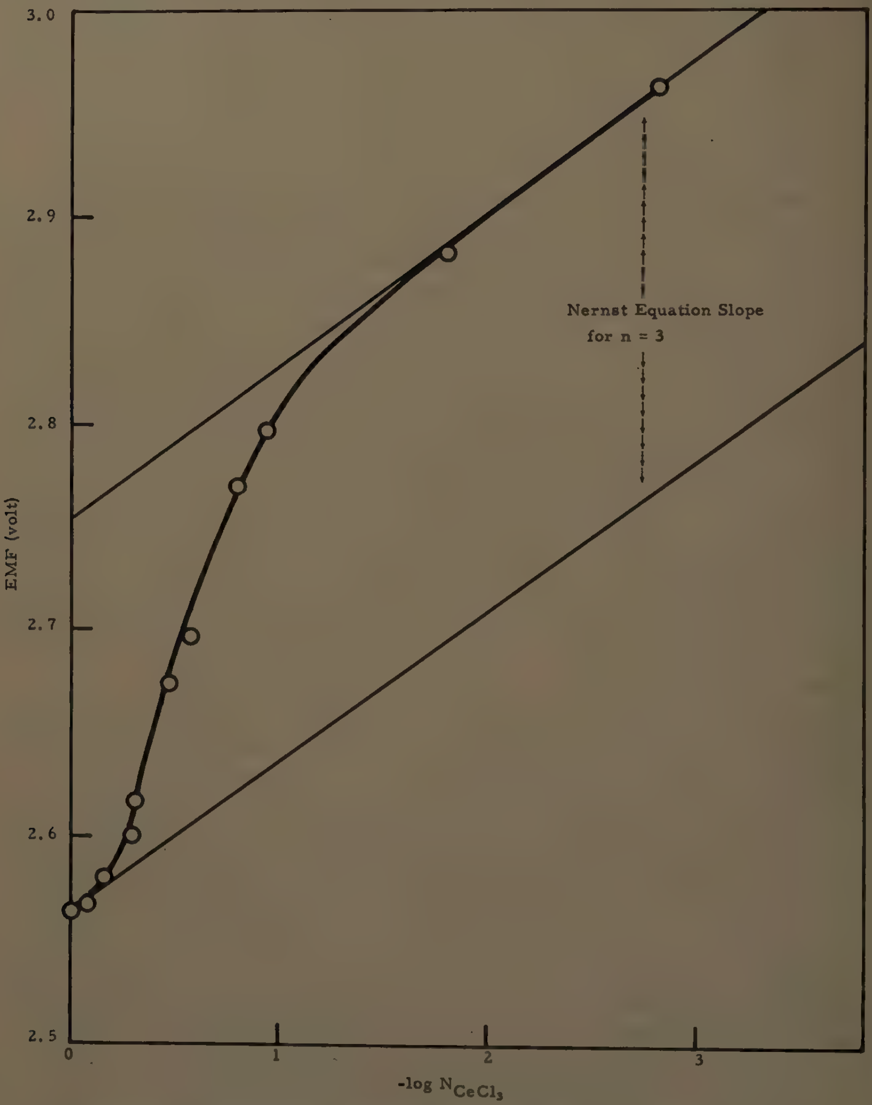

FIGURE 4. The emf as a function of composition (KCl system), 850° C.

Activity of $CeCl_3$. In FIGURES 4 and 5 the wide departure of the $CeCl_3$-KCl system and the $CeCl_3$-NaCl system from ideal behavior is noted. It also may be seen in TABLES 3 and 4 that the activity coefficients drop very sharply in the vicinity of $N = 0.5$ in the KCl solvent and somewhat less sharply in the same vicinity in the NaCl system. If it is assumed that this behavior is the result of formation of a 1:1 complex, that is, $CeCl_3 + KCl \rightleftarrows KCeCl_4$, or the equivalent expression $CeCl_3 + Cl^- \rightleftarrows [CeCl_4]^-$, and if one assumes further that the real components behave ideally, then the

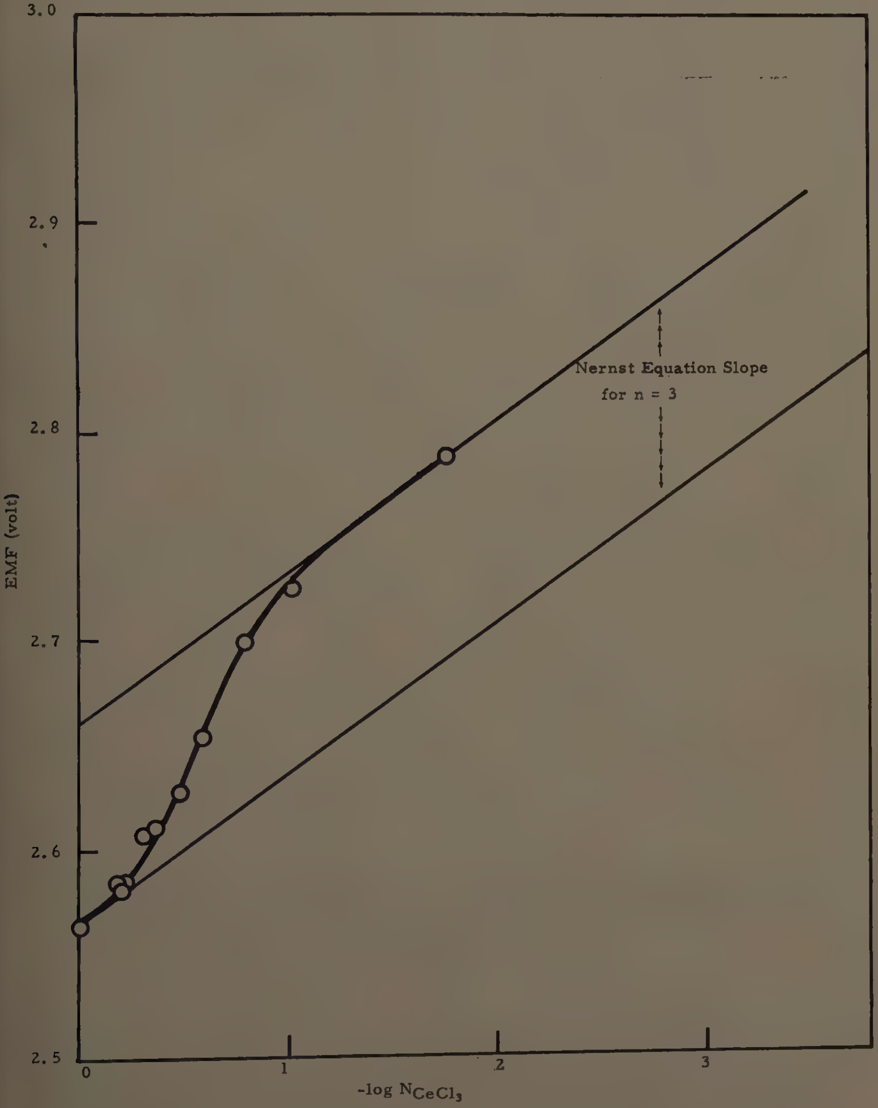

FIGURE 5. The emf as a function of composition (NaCl) system, 850° C.

variation of activity with mole fraction is given by[23]

$$a_1 = \frac{kN_1 - 2 + 2(1 - kN_1N_2)^{1/2}}{kN_1}$$

where a_1 = activity of $CeCl_3$, N_1 and N_2* = mole fraction of $CeCl_3$ and

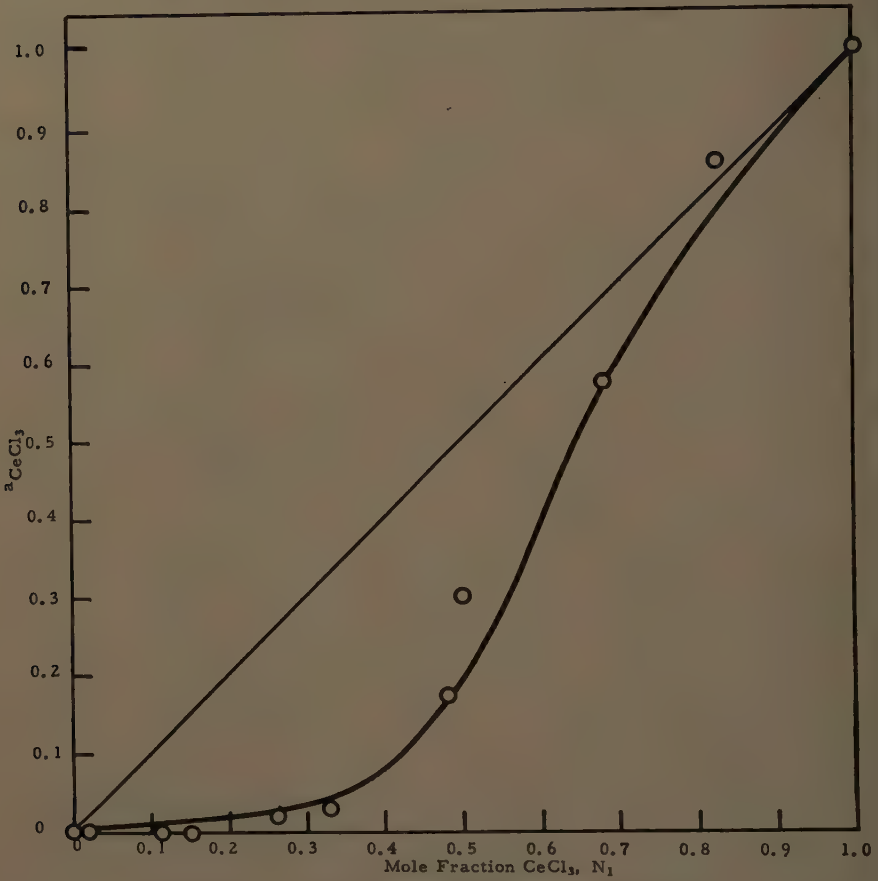

FIGURE 6. Activity of $CeCl_3$ (KCl system) at 850° C.

KCl (or NaCl), respectively, $k = 4K/(K + 1)$, and where

$$K† = ([CeCl_4]^-/[CeCl_3][Cl^-]),$$

that is, the equilibrium constant for the complex formation. Various values of the equilibrium constant may be assumed and the one that best fits the data may be determined. This has been done and is shown in FIGURES 6 and 7. The 45° straight line is that for ideal behavior. In FIGURE 6 the curve is the one obtained from the equation with K taken as 15 (dissociation constant $= 6.7 \times 10^{-2}$). Agreement is fair above 0.2-mole fraction, but considerable departure occurs at lower concentrations. In FIGURE 7 the value of K for the curve plotted is 4 (dissociation constant $= 2.5 \times 10^{-1}$); again, fair agreement above 0.2-mole fraction with considerable departure below this concentration is observed.

---

* N_1 and N_2 are the "apparent" mole fractions based on the weights of the components that were mixed to prepare the electrolyte.

† Inclusion of $[CeCl_3]$ in the equilibrium expression does not imply that it exists as a molecular species in the solution; rather, the assemblage of cerium and chloride ions of unknown structure corresponding to pure cerium chloride is taken, for simplicity, as a component in the mass action law. $[Cl^-]$ is the concentration of chloride ion that remains after deducting that in $[CeCl_4^-]$ and $[CeCl_3]$.

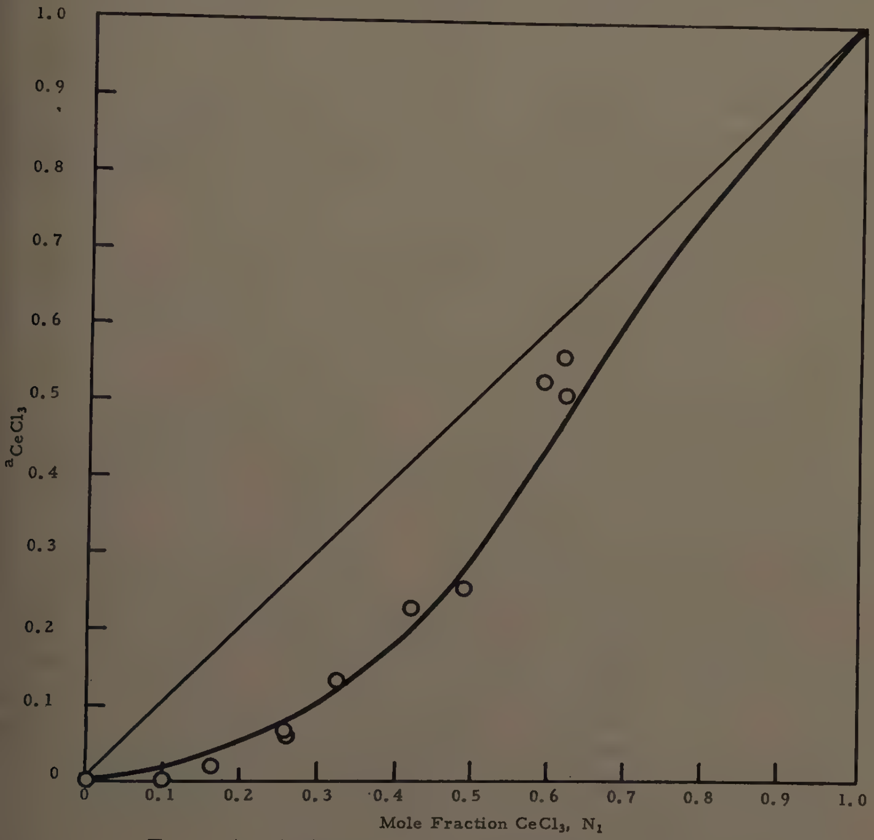

FIGURE 7. Activity of $CeCl_3$ (NaCl system) at 850° C.

It is clear that formation of a tetrachloro complex ion cannot account for the nonideal behavior except, possibly, in the region of 0.3 to 0.6 mole fraction. Comparison of FIGURES 6 and 7 indicates that in this concentration range the complex ion is more stable in the KCl solvent than in the NaCl solvent.

Another method is available to study the departure from ideality of the solutions extremely dilute in $CeCl_3$. Referring to FIGURES 4 and 5 it is noted that extrapolation of the emf values obtained in the dilute systems to unit mole fraction gives an emf $E_x°$, different from $E°$, the emf obtained with pure $CeCl_3$ electrolyte. If it is assumed that the difference between $E_x°$ and $E°$ results from some unspecified reaction, then $(-\Delta F°)$ for that reaction is $nf(E_x° - E°)$, and the equilibrium constant, K', for that unspecified reaction may be expressed as

$$\log K' = \frac{3f}{2.303\ RT}(E_x° - E°)$$

The values of K' and its reciprocal, $K_{\text{diss.}}$, obtained in this manner are listed in TABLE 6. From the data in TABLE 6 the enthalpy of the, thus far, unspecified reaction may be calculated. By plotting $\log K'$ against the reciprocal of the absolute temperature one obtains the values of $\Delta H = -20.7$ kcal. in the KCl solvent and $\Delta H = -3.7$ kcal. in the NaCl solvent.

TABLE 6

EQUILIBRIUM CONSTANTS CORRESPONDING TO $(E° - E_x°)$

Temp. (°C.)	KCl solvent		NaCl solvent	
	K'	$K_{\text{(diss.)}}$	K'	$K_{\text{(diss.)}}$
800	655.8	1.52×10^{-3}	25.61	3.91×10^{-2}
850	383.4	2.61×10^{-3}	17.84	5.60×10^{-2}
900	208.4	4.80×10^{-3}	14.44	6.93×10^{-2}

Let us now assume two of the many possible reactions that might have been responsible for $(E_x° - E°) \neq 0$, apply to them the equilibrium constants calculated above, and calculate the activity of $CeCl_3$ that would result. The two reactions assumed are:

$$CeCl_3 + Cl^- \rightleftarrows [CeCl_4]^- \qquad (2)$$

$$K_{\text{diss.}} = \frac{[CeCl_3][Cl^-]}{[CeCl_4^-]}$$

and

$$CeCl_3 + 3Cl^- \rightleftarrows [CeCl_6]^{-3}$$

$$K_{\text{diss.}} = \frac{[CeCl_3][Cl^-]^3}{[CeCl_6^{-3}]} \qquad (3)$$

In the last two columns of TABLE 7 are listed the activity of $CeCl_3$ in the dilute region at 850° C. obtained by use of these assumed reactions with the dissociation constants, 2.6×10^{-3} for the KCl system and 5.6×10^{-2} for the NaCl system. The second column shows the a_{CeCl_3} obtained directly from the measured $(E - E°)$.

It may be seen that in the most dilute range the calculated values of the activity do not distinguish between the reactions chosen because the chloride ion concentration approaches unity and the complex ion concentration is essentially N_{CeCl_3}. It may be added that rather unreasonable reactions might have been assumed and that these would have been eliminated by this method. At slightly higher concentration the a_{CeCl_3} obtained by the assumptions diverges and there is some slight indication that the $[\mathrm{CeCl}_6]^{-3}$ assumption may be the better one when compared to the activity obtained by direct measurement of the emf. A further indication of the existence of $[\mathrm{CeCl}_6]^{-3}$ may be seen in FIGURE 8, in which $\Delta\gamma/\Delta N$ is plotted against N. While only one peak (near $N = 0.5$) appears in the KCl solution, two peaks ($N = 0.53$ and 0.28) may be seen in the NaCl solution. An alternative explanation of the variation of the activity in this region would be merely a variation of the equilibrium constant of the tetrachloro complex with composition, that is, nonideal behavior of the real constituents.

TABLE 7

ACTIVITY OF CeCl_3 IN THE VERY DILUTE RANGE AT 850° C.

N_{CeCl_3}	Activity of CeCl_3 (NaCl diluent)		
	$E - E^0$ (calc.)	$[\mathrm{CeCl}_4]^-$ assumption	$[\mathrm{CeCl}_6]^{-3}$ assumption
0.01717	9.4×10^{-4}	9.8×10^{-4}	10×10^{-4}
0.09584	6.6×10^{-3}	5.9×10^{-3}	7.2×10^{-3}
0.1607	1.5×10^{-2}	1.1×10^{-2}	1.5×10^{-2}
	(KCl diluent)		
0.01567	4.6×10^{-5}	4.2×10^{-5}	4.3×10^{-5}
0.1111	7.0×10^{-4}	3.3×10^{-4}	4.1×10^{-4}
0.1578	1.7×10^{-3}	0.46×10^{-3}	0.70×10^{-3}

Partial molar entropy. The values for the partial molar entropy listed in TABLES 3 and 4 deviate widely from ideal behavior. In the ideal case $\bar{S}_1 - S^0 = -R \ln N$ and, for a tenfold dilution, should be 4.6 eu. It is recognized that, in a system in which extensive solvation occurs, the entropy of mixing will be less than the theoretical value, and the enthalpy of mixing will be negative.[23] This is true in both the NaCl and KCl solvents, and the large departure from ideality further confirms the formation of complex compounds in the liquid. It should be noted that $(\bar{S} - S^0) \leq 0$ in all cases, indicating that the negative entropy of complex formation was equal to or greater than the positive entropy of mixing.

More quantitative conclusions, however, cannot be drawn from this because of the lack of precision of the values for dE/dT, a fact that was discussed earlier. The estimated uncertainty of 10 per cent in the entropy values amounts, in these measurements, to about 6 eu, a major portion of the theoretical entropy of mixing even in the most dilute solutions studied. Further refinement in technique of emf measurements at elevated temperatures may permit fundamental conclusions to be drawn from the unique behavior of the partial molal entropy in these systems.

Effect of alkali metal cations. By every criterion thus far considered in this paper, the $CeCl_3$-NaCl solutions were more nearly ideal in behavior than the $CeCl_3$-KCl solutions. Although complex formation apparently

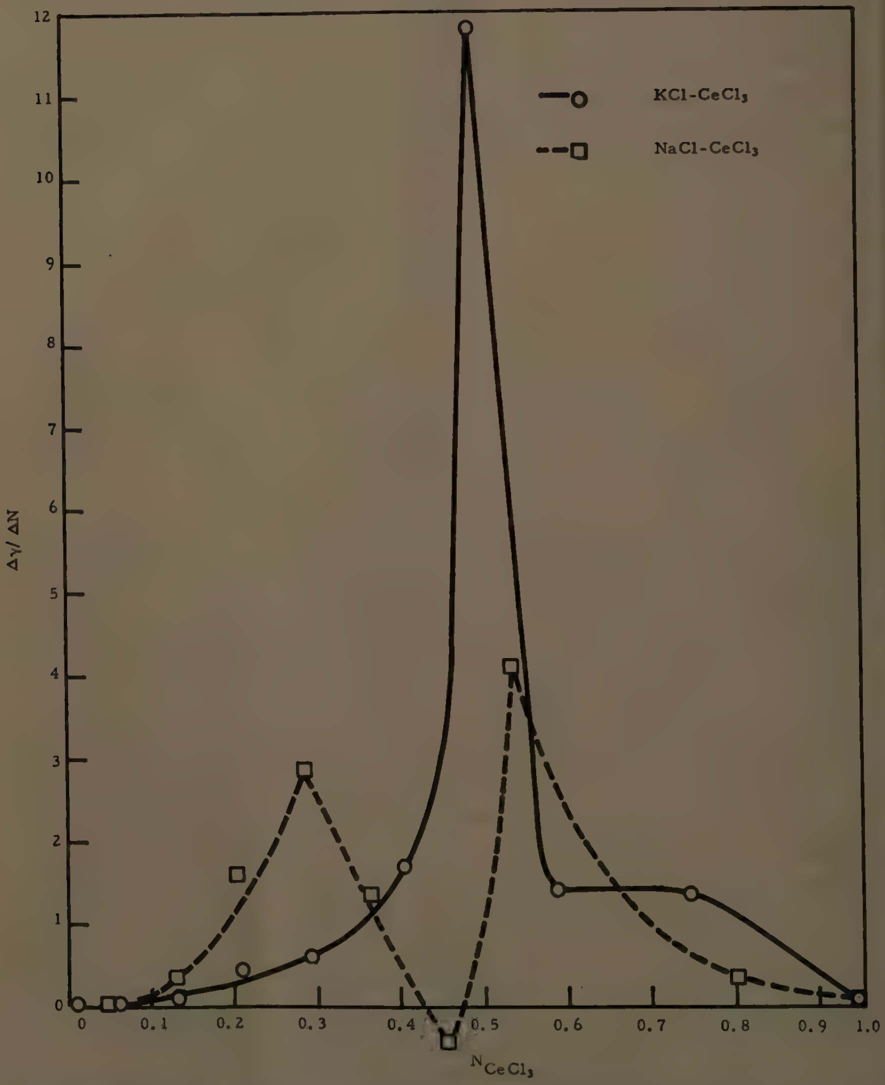

FIGURE 8. Variation of activity coefficient with composition in KCl and NaCl solutions at 850° C.

occurs in both, it can be seen in FIGURES 6 and 7 that the dissociation constant of the postulated complex is at least an order of magnitude greater in the NaCl solvent than in the KCl solvent. In the extremely dilute range, the emf of cells with the $CeCl_3$-NaCl solutions reach the Nernst concentration dependence in solutions at least an order of magnitude higher in concentration than is the case in the $CeCl_3$-KCl solution. The activity of $CeCl_3$ in the most dilute range and the calculated dissociation constants for postulated complexes are larger by an order of magnitude in the NaCl solutions, and the heat of formation of the postulated complex in the dilute region is smaller by an order of magnitude in the NaCl solution than in the KCl solution. All of these phenomena are consistent with the idea that there exists a competition for chloride ion between the Ce^{3+} and the alkali metal ion. The tetracoordinate or hexacoordinate Ce^{3+} complexes apparently formed in this system reduce the activity of the Ce^{3+}. If Na^+ is a stronger competitor than K^+ for the chloride ions in the cerium complexes, the chloro-cerium complexes could be expected to be more dissociated in the NaCl solutions than in the KCl solutions, and the activity of Ce^{3+} higher. This is what is observed. Since the charge on the Na^+ and K^+ ions is the same, it may be the smaller size or the higher charge density of the Na^+ that causes it to be a more effective halide ion acceptor than K^+. Work now in progress with $CaCl_2$ solutions will permit a distinction to be made between the relative effects of size alone or of charge density of the added cation, since the sizes of the Ca^{++} and the Na^+ ion are similar (0.99 and 0.95 Å, respectively).[24]

Summary

The thermodynamic properties of solutions of $CeCl_3$ in KCl and in NaCl have been determined over a concentration range extending from pure $CeCl_3$ to 10^{-3} mole fraction. In the extremely dilute range and in the nearly pure $CeCl_3$ solutions, the behavior is consistent with the Nernst equation for an $n = 3$ reaction. In the intermediate range, wide departures from ideality occur, which apparently are due to complex formation.

No simple assumption of one or a few complexes was found that can satisfactorily account quantitatively for the observed behavior. There is strong evidence, however, for the existence of a $[CeCl_4]^-$ complex ion in the region of 0.5 mole fraction, and further evidence that in the extremely dilute solutions a higher complex, probably $[CeCl_6]^{-3}$ may exist. The evidence for the latter is not conclusive, and the observed behavior at low concentration also may be explained by a decrease in the dissociation "constant" of $[CeCl_4]^-$ with increasing dilution.

The effects of NaCl and KCl as diluents are compared, and it is found that the $CeCl_3$-NaCl system is more nearly ideal in its behavior than the $CeCl_3$-KCl solution. This is attributed to the fact that Na^+ acts as a

better halide ion acceptor than K^+ and thus more effectively dissociates the chlorocerium complexes.

Experimentally determined thermodynamic values for $CeCl_3$ (1) between 800° and 900° C. are given. The values are about 8 per cent lower than the values estimated from aqueous calorimetric measurements near room temperature.

Acknowledgments

We gratefully acknowledge the enlightening and informative discussions with R. Didchenko and E. R. Van Artsdalen of our laboratory.

References

1. Janz, G. J., C. Solomons & H. J. Gardner. 1958. Chem. Rev. **58:** 461.
2. Sense, K. A. et al. 1954. J. Phys. Chem. **58:** 223, 995.
3. Sense, K. A. et al. 1957. J. Phys. Chem. **61:** 337.
4. Sense, K. A. et al. 1958. J. Phys. Chem. **62:** 453.
5. Cantor, S., R. F. Newton, W. R. Grimes & F. F. Blankenship. 1958. J. Phys. Chem. **62:** 96.
6. Flengas, S. N. & T. R. Ingraham. 1958. Can. J. Chem. **36:** 780, 1103.
7. Flengas, S. N. & T. R. Ingraham. 1957. Can. J. Chem. **35:** 1139, 1254.
8. Senderoff, S. & G. W. Mellors. 1958. Rev. Sci. Instr. **29:** 151.
9. Laitinen, H. A. & C. H. Liu. 1958. J. Am. Chem. Soc. **80:** 1015.
10. Senderoff, S. & A. Brenner. 1954. J. Electrochem. Soc. **101:** 31.
11. Smirnov, M. V. & L. E. Ivanovskii. 1957. Zhur. Fiz. Khim. **31:** 641.
12. Mellors, G. W. & S. Senderoff. 1959. J. Phys. Chem. **63:** 1110.
13. Hamer, W. J., M. S. Malmberg & B. Rubin. 1956. J. Electrochem. Soc. **103:** 8.
14. Hansen, M. 1958. Constitution of Binary Alloys. : 462. McGraw-Hill. New York, N.Y.
15. Senderoff, S. & G. W. Mellors. 1958. J. Electrochem. Soc. **105:** 224.
16. American Institute of Physics Handbook. 1957. Table 4a–5. McGraw-Hill. New York, N.Y.
17. Glassner, A. 1957. The Thermochemical Properties of the Oxides, Fluorides and Chlorides to 2500° K. ANL-5750. Argonne Natl. Lab. Lemont, Ill.
18. Spedding, F. H. & C. Miller. 1952. J. Am. Chem. Soc. **74:** 4195.
19. Walker, R. D., Jr. & D. E. Danly. 1958. Paper No. 150. Presented at Convention of Electrochemical Soc. New York, N.Y. (April).
20. Hamer, W. J., M. S. Malmberg & B. Rubin. 1956. J. Electrochem. Soc. **103:** 8.
21. Gruen, D. M. 1957. J. Inorganic Nuclear Chem. **4:** 74.
22. Gruen, D. M. 1957. Angew. Chem. **69:** 681.
23. Hildebrand, J. H. & R. L. Scott. 1950. Solubility of Non-Electrolytes. 3rd ed. : 47, 177. Reinhold. New York, N.Y.
24. Pauling, L. 1940. The Nature of the Chemical Bond. : 346. Cornell Univ. Press. Ithaca, N.Y.

MEASUREMENT OF THE URANIUM-URANIUM(III) POTENTIAL IN LiCl-KCl EUTECTIC*

Dieter M. Gruen
Argonne National Laboratory, Lemont, Illinois

Robert A. Osteryoung
Rensselaer Polytechnic Institute, Troy, N.Y.

This paper is a report on the measurement of the potential of the uranium-uranium(III) couple in fused KCl-LiCl eutectic melt, with respect to a silver-silver(I) chloride reference electrode. Recently several studies of potentiometric measurements in fused salt systems have been reported.[1,2] Because of the nature of the uranium-containing system, in particular its sensitivity to oxygen, a special cell capable of being operated under high vacuum at elevated temperatures was constructed for these measurements.

Apparatus and Materials

The cell used in this work is shown in FIGURE 1. The cell body and fritted inner compartments were constructed of fused silica. The "head" of the cell was a water-jacketed Pyrex top, fitting over the standard-taper male top of the cell body. The top of the head was fitted with three female standard-taper joints and a fused silica thermocouple well which, when the cell head was in place, reached to the bottom of the cell. The fused silica inner compartments had standard-taper male tops and medium-porosity sintered fused silica frits sealed to their bottom. When in position in the cell head, the inner compartments reached to within a few centimeters of the bottom of the cell. Silver, uranium, and platinum wires were sealed through glass caps that fitted the standard-taper male tops of the fritted compartments. The wires were sealed into the caps with Picein wax, effecting a vacuum-tight seal. The side arm of the cell was connected to a vacuum line.

A Nichrome heating element wound on a fused silica core that was wrapped in asbestos served as the furnace into which the cell was placed. Magnesia pipe lagging was placed about the entire furnace; a hole cut through the insulation permitted visual observation of the bottoms of the fritted compartments. Furnace power was supplied by means of a Variac transformer. The temperature of the salts in the cell was measured with a Chromel-Alumel thermocouple placed in the thermocouple well attached to the cell head. During the course of a run the temperature was steady to within ±2° C. of the initial value.

---

* The work reported in this paper was performed under the auspices of the United States Atomic Energy Commission, Washington, D.C.

A constant-current coulometric source was constructed; it consisted of a Heathkit regulated DC power supply, whose output was dropped through a 35,000-ohm resistor in series with the electrodes in the cell. The current through the cell was computed by measuring the voltage drop, with a potentiometer, across a 10-ohm precision resistor, also in series with the cell electrodes. A Standard electric timer was connected in such a manner that it was activated whenever the switch was thrown to the on position, which resulted in passage of current through the cell. In the off position, the current was diverted through a small resistor connected across the switch in parallel with the cell.

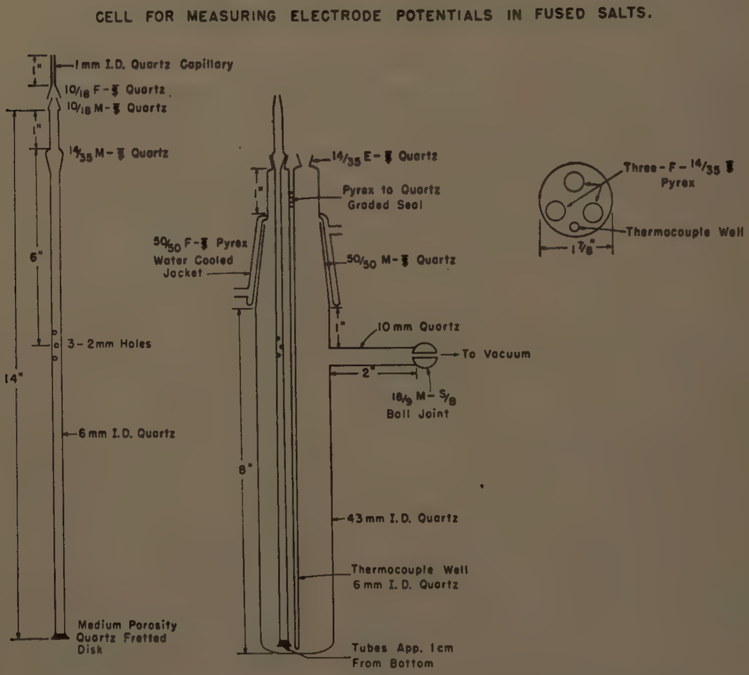
CELL FOR MEASURING ELECTRODE POTENTIALS IN FUSED SALTS.
1"
1 mm I.D. Quartz Capillary
10/18 F-₮ Quartz
10/18 M-₮ Quartz
1"
14/35 M-₮ Quartz
6"
3-2mm Holes
14"
6 mm I.D. Quartz
Medium Porosity Quartz Fretted Disk
14/35 E-₮ Quartz
1"
Pyrex to Quartz Graded Seal
50/50 F-₮ Pyrex Water Cooled Jacket
50/50 M-₮ Quartz
1"
10 mm Quartz
To Vacuum
2"
18/9 M-S/8 Ball Joint
8"
43 mm I.D. Quartz
Thermocouple Well 6 mm I.D. Quartz
Tubes App. 1 cm From Bottom
Three-F-14/35 ₮ Pyrex
Thermocouple Well
1 7/8"

Figure 1. High-vacuum cell for use at elevated temperatures.

The platinum and silver were commercial, high purity material; the uranium wire was obtained from the Metallurgy Division of the Argonne National Laboratory. Prior to use, the uranium wire was treated with HNO_3 to dissolve uranium oxide and was rinsed with water and then with acetone.

The potassium chloride-lithium chloride eutectic (40.5 mole per cent KCl) was prepared by passing hydrogen chloride gas through the molten eutectic in a heated three-necked flask until water was no longer evolved. Pellets of the eutectic were prepared by allowing the melt to flow dropwise through a capillary attached to the bottom of the flask and into a vessel filled with carbon tetrachloride. The pellets were then stored under carbon tetrachloride until used.[3]

Experimental Procedure

The cell head was placed on the cell and about 150 gm. of eutectic pellets poured into the cell. The cell was then capped, placed in the furnace, connected to the vacuum line, and evacuated, thus pumping off the carbon tetrachloride. The furnace temperature was raised slowly to the operating temperature. When the pellets had melted, nitrogen was admitted to the system, the caps on the three head openings were removed, and the fritted compartments, with the silver, uranium, and platinum wires in position, each in its own compartment, were inserted. This operation required about 1 min. The cell was evacuated once again, the melt slowly diffusing up through the quartz frits into the electrode compartments. When the level of the melt in the compartments reached the level of the melt in the cell proper, the compartments contained approximately 2 ml. of solvent. The silver, uranium, and platinum wires extended about 1½ inches into the melt in each fritted compartment.

When the compartments had filled, the leads from the constant-current source were connected, and the silver wire was anodized, using the platinum electrode as cathode. Silver (I) was formed in the silver compartment, while lithium metal deposited on the platinum cathode. The current was measured during the electrolysis, the anodization being conducted for sufficient time to bring the concentration of silver (I) to about 0.05 M. From the current-time product the number of equivalents of silver (I) generated could be computed.

After the reference electrode thus had been prepared, the uranium was anodized, again using the platinum as cathode. Several periods of anodization were carried out, the potential between the uranium and silver electrodes being measured after each period of anodization. When a steady potential had been achieved following an anodization, usually after about 5 to 10 min., the potential was recorded (polarization of the uranium wire on anodization also was measured with respect to the silver-silver(I) reference, and was of the order of 0.1 to 0.2 v. with respect to the equilibrium potential). In this manner, the potential between the uranium electrode and the silver reference could be measured at several different concentrations of uranium (III) in the uranium compartment.

At the conclusion of a series of measurements, nitrogen was admitted to the cell, the electrode wires and caps removed, and the fritted compartments quickly lifted out of the cell. The compartments were placed in a large glass tube through which a vigorous flow of helium was conducted. In this way the melt was cooled to room temperatures within a few minutes of its removal from the cell. The compartments were submitted for analysis, the sample weight being determined by weighing the compartment, leaching the salts in water, and reweighing the glass. The amount of salt in each compartment could be computed from an analysis for total chloride and from the weight of salts found in each compartment. The density of the eutectic was taken as 1.65 gm./cc. for all calculations in the temperature interval 440° to 452° C.[4] The amount of uranium (III) and silver (I) in the compartments could be computed from the coulombs passed in the anodization or, in the case of uranium, from the uranium analysis.

In one run the temperature was varied, and data on the emf-temperature behavior were obtained on heating and cooling the system.

Results and Discussion

The Nernst equation for the uranium-uranium(III) system, against an arbitrary reference electrode, is given by

$$E_U = E_U^{\circ} + RT/3F \ln C_{UCl_3} \qquad (1)$$

where R, T, and F have their usual significance, $E_U{}^{\circ}$ is the standard potential, in volts, of the U-U(III) system, and C_{UCl_3} represents the concentration of U(III) in the solvent. The concentration units may be in terms of molarity, molality, or mole fraction, resulting in three scales for E^0, which refers to unit concentration. These three scales may be designated $E^{\circ}_{M_U}$, $E^{\circ}_{m_U}$, or $E^{\circ}_{X_U}$, depending on whether unit molarity, molality, or mole fraction is chosen as the standard state.[1] As stated, the standard state for uranium (III) chloride and silver (I) chloride is unit concentration; for the metals involved the standard state is the solid metal under one atmosphere of pressure. In the mole fraction scale, the standard state of the uranium (III) chloride and silver (I) chloride would be the solids.

For the reversible cell utilized in these measurements, the emf will be given by

$$E_{\text{cell}} = E^{\circ}_{\text{Ag}} - E_U{}^{\circ} + RT/3F \ln C^3_{\text{Ag(I)}}/C_{\text{U(III)}} \qquad (2)$$

Precisely, of course, the activities of uranium (III) and silver (I) should appear in EQUATIONS 1 and 2. However, over the range of concentrations covered in this investigation [uranium (III) concentration was varied from about 10^{-3} to 10^{-1} M, or a mole fraction variation of 10^{-5} to 10^{-3}] EQUATION 1 as written was found to be valid. Similar behavior has been found for the silver-silver (I) couple in this eutectic for the concentration ranges herein involved.[1] Thus, EQUATION 2 is also valid and was used to calculate $E^{\circ}_{\text{Ag}} - E_U{}^{\circ}$. It would appear, therefore, that the activity coefficients of the species involved are invarient over the concentration ranges involved within the accuracy of the measurements.

In FIGURES 2 and 3 Nernst plots of millicoulombs of electricity passed through the uranium compartment versus E_{cell} are shown. Data for these plots are given in TABLE 1. Slopes of linear portions of these plots are in good agreement with the theoretical value of RT/nF for a three-electron process ($2.3RT/3F = 0.0478$ at 450° C.). The concentrations of uranium (III) and silver (I) shown in TABLE 1 were calculated from the weight of salt found in each compartment after the completion of the experiments and from the equivalents of electricity passed in the anodization process.

The solidified salts from the uranium compartments were submitted for analysis for soluble uranium. The results, given in TABLE 3, compare the amount of uranium coulometrically generated, assuming 100 per cent current efficiency, with the amount of uranium found by analysis. The amount of soluble uranium found is less than that calculated from the current-time product. Despite this, it seems unlikely that the current efficiency was less than 100 per cent. The experimental Nernst plot slopes are in good agreement with the theoretical. Furthermore, the polarization of the uranium electrode, as previously mentioned, was less than 0.2 v. on anodization; it is probable that the bulk of this was due to the build-up of

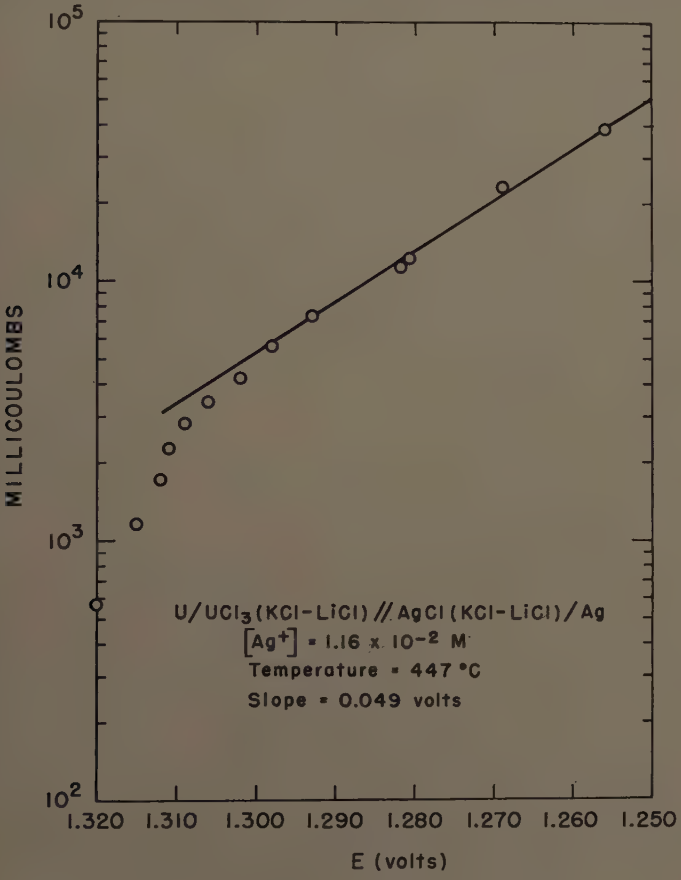

FIGURE 2. Log millicoulombs versus emf.

uranium (III) about the electrode during the electrolysis. Visual observation of the uranium electrode during the anodization indicated that a marked concentration gradient existed.

Recent work on an *in situ* analysis for uranium (III) in this eutectic system has indicated that the anodization takes place at 100 per cent current efficiency.[5]

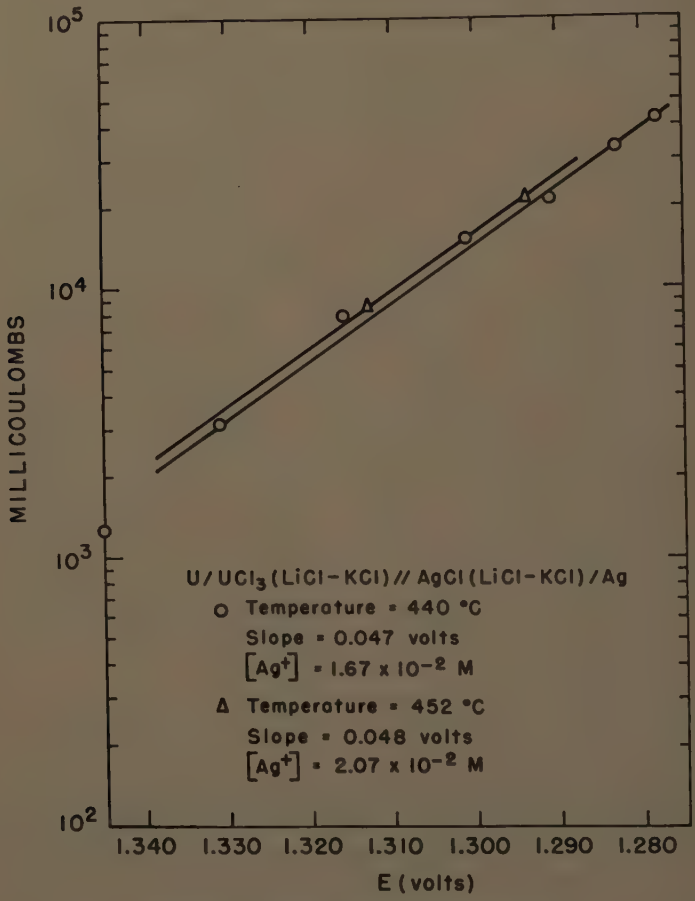

FIGURE 3. Log millicoulombs versus emf.

A possible explanation for the low uranium analytical results is that the uranium (III), which is extremely sensitive to oxidation, was partially converted to UO_2 during the period in which the compartments were removed from the cell and frozen. Although this procedure was performed as rapidly as possible, a certain amount of black, insoluble matter indicative of oxide formation was present when the salts from the uranium compartments were dissolved in water. Since the analysis determined only the water-soluble uranium, insoluble oxides would have escaped detection.

Calculations of a standard potential on the molarity scale, with respect to the unit molar silver-silver(I) reference, are given in TABLE 1. The calculations are made using the measured E_{cell} (column 5) and the concentrations given in columns 2 and 3, calculated as indicated above. The internal consistency of the calculated standard potentials is quite reasonable. However, it is worth noting that these $E°$ values are not very sensitive to changes in concentration of uranium (III); an error of ±10 per cent in the concentration of uranium (III) would amount to an error of only ±0.002 v. in the calculated standard potential. An $E^{\circ}_{M_{\text{U}}}$ value, with respect to the silver-silver(I) reference, of -1.475 ± 0.005 v. and 450° C. was obtained. This corresponds to a value of -1.616 ± 0.005 v. on the mole fraction scale.

TABLE 1

Millicoulombs generated (cumulative)	$[U^{+3}]$ (moles/ liter)	$[Ag^{+}]$ reference (moles/liter)	Temperature (°C.)	E Measured	E°_{M} (Ag/AgCl reference)
569	1.07×10^{-3}	1.16×10^{-2}	447	1.320	−1.454*
1,140	2.15×10^{-3}			1.315	−1.464*
1,710	3.23×10^{-3}			1.312	−1.469*
2,280	4.30×10^{-3}			1.3105	−1.474*
2,850	5.38×10^{-3}			1.309	−1.476*
3,420	6.43×10^{-3}			1.306	−1.477*
4,270	8.04×10^{-3}			1.302	−1.478
5,670	1.07×10^{-2}			1.298	−1.480
7,410	1.40×10^{-2}			1.293	−1.481
11,410	2.16×10^{-2}			1.282	−1.479
12,230	2.32×10^{-2}			1.281	−1.479
23,230	4.38×10^{-2}			1.269	−1.481
39,350	6.67×10^{-2}			1.256	−1.476
73,910	1.39×10^{-1}			1.242	−1.477
					Avg. −1.479 ± .001
1,286	2.44×10^{-3}	1.67×10^{-2}	440	1.345	−1.473*
3,180	6.02×10^{-3}			1.331	−1.478
7,935	1.50×10^{-2}			1.316	−1.482
15,240	2.89×10^{-2}			1.301	−1.480
21,630	4.11×10^{-2}			1.291	−1.477
33,540	6.37×10^{-2}			1.283	−1.477
42,740	8.11×10^{-2}			1.278	−1.477
					Avg. −1.479 ± .002
8,500	1.54×10^{-2}	2.07×10^{-2}	452	1.313	−1.469
21,290	3.84×10^{-2}			1.294	−1.469

* Not used in computing average.

TABLE 2 and FIGURE 4 give the temperature dependence of the emf for the cell indicated; TABLE 2 also gives $E^{\circ}_{X_{\text{Ag}}} - E^{\circ}_{X_{\text{U}}}$ calculated from the measured E_{cell} and the Nernst equation at each temperature. From

$$\text{Log } K = 3(E^{\circ}_{X_{\text{Ag}}} - E^{\circ}_{X_{\text{U}}})F/2.3RT \qquad (3)$$

values for the equilibrium constant for the cell reaction may be calculated and log K versus $1/T$ plotted (FIGURE 5). From the slope of this plot the enthalpy, ΔH was calculated according to the van't Hoff equation,

TABLE 2

TEMPERATURE EMF BEHAVIOR FOR CELL

$$\mathrm{U/UCl_3}\left\{\begin{matrix} X_{\mathrm{UCl_3}} = 1.29 \times 10^{-3} \\ M_{\mathrm{UCl_3}} = 3.84 \times 10^{-2} \end{matrix}\right\}\ \mathrm{KCl\text{-}LiCl} /\!\!/ \mathrm{KCl\text{-}LiCl, AgCl}\left\{\begin{matrix} X_{\mathrm{AgCl}} = 6.97 \times 10^{-4} \\ M_{\mathrm{AgCl}} = 2.07 \times 10^{-2} \end{matrix}\right\}\mathrm{/Ag}$$

Temperature (°C.)	E (volts)	$E^\circ_{X_{Ag}} - E^\circ_{X_U}$
452	*$\underline{1.2942}$, 1.295	$\underline{1.611}$, 1.612
457	1.2917	1.610
460	1.290	1.609
464	$\underline{1.2822}$	$\underline{1.603}$
470	1.2805	1.604
475	1.2733	1.599
486	$\underline{1.268}$	$\underline{1.599}$
490	1.2647	1.597
495	$\underline{1.260}$	$\underline{1.595}$
506	1.251	1.590
514	1.244	1.587
520	$\underline{1.2433}$, 1.239	$\underline{1.589}$, 1.585
525	1.237	1.584
532	1.2317	1.583
533	$\underline{1.231}$	$\underline{1.582}$
534	$\underline{1.229}$	$\underline{1.581}$

* Underlined data obtained from heating cycle; remainder on cooling.

TABLE 3

Expt. No.	Total coulombs generated	U theoretical (mg.)	U found (mg.)	U found (%)
1	73.91	60.8	48.1	79
2	42.74	34.9	31.1	89
3	21.29	17.5	9.9	56.5

yielding a value of $\Delta H = -130$ kcal. for the reaction

$$\mathrm{U} + 3\mathrm{AgCl}(s) = \mathrm{UCl_3}(s) + 3\mathrm{Ag} \qquad (4)$$

Comparison of the experimentally determined values with available data is of interest. From the tables of Hamer *et al.*[6] a difference in $E^\circ_{X_{Ag}} - E^\circ_{X_U}$ may be obtained. The difference thus obtained is -1.619 v. at 450° C., compared to the experimental value of -1.61 v. Comparison of the experimental ΔH with a calculated value also may be made.[7] Calculation yields a value of -124 kcal. for the reaction given in EQUATION 4 at 450° C., which compares with the experimental value of -130 kcal.

Comparison of the data herein obtained for U-U(III) with data recently obtained for Pu-Pu(III) couple also would be of interest.[8] It was found that the relation was valid for the reaction

$$\Delta F^0 = -221 + .0533T \text{ kcal.}$$

$$\text{Pu}(1) + \frac{3}{2}\,\text{Cl}_2(g) = \text{PuCl}_3(s)$$

in the range 958°–1014° K. Extrapolation of this data to 723° K and conversion to an $E_X°$ value with respect to the silver-silver chloride reference yields a calculated value of 1.73 v., compared to 1.62 v. for the U-U(III) system, a difference of 0.11 v. The tabulated differences in the free energies of formation of UCl_3 and $PuCl_3$ amount to about 15 kcal. per moles; this would represent an $E_X°$ difference of approximately 0.2 v.[7] According to Benz,[8] however, the tabulated value for the free energy of formation of $PuCl_3$ is slightly high; thus, the expected potential difference between the Pu-Pu(III) and U-U(III) would be somewhat less than 0.2 v.

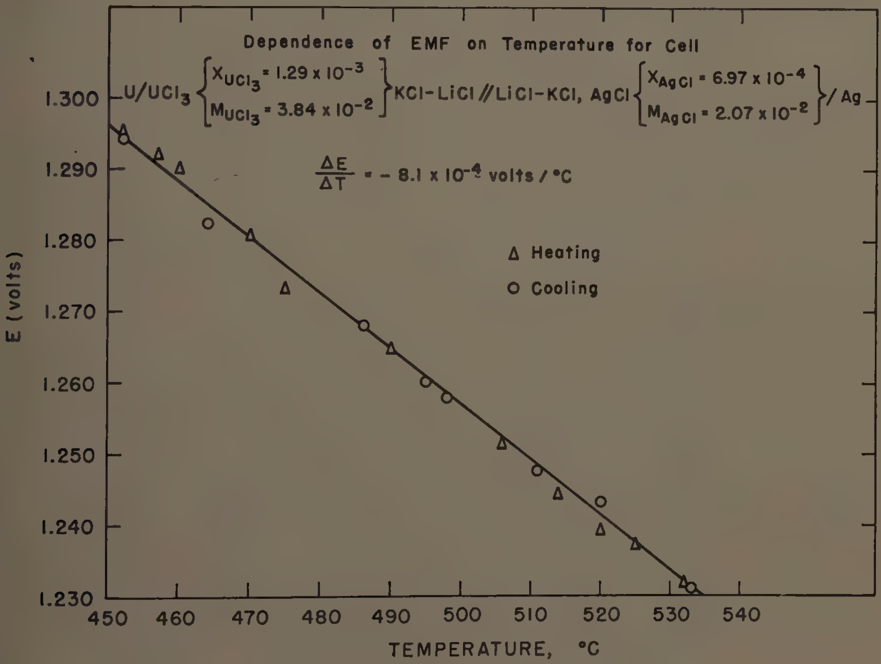

FIGURE 4. Temperature-emf behavior.

Further comment on FIGURE 2 may be of interest. It is to be noted that the plot of log coulombs versus emf deviates from linearity at low U(III) concentrations. This indicates that more U(III) was present in solution than could be accounted for coulometrically. This conclusion is supported by visual observation of a U wire immersed in the pure eutectic melt. There appeared to be a slow corrosive attack on the wire, as indicated by a very slow appearance of the red uranium (III) color in the melt in the immediate vicinity of the wire. An experiment was performed in which small pieces of uranium wire were placed, together with eutectic pellets, in two small crucibles, one of Pyrex, the other of sapphire. These crucibles were placed together in the bottom of the cell, which was capped, placed in the furnace, and attached to the vacuum line. The cell was evacuated, heated to 450° C., and maintained at that temperature under vacuum for about 18 hours. It was observed that the melt in the Pyrex crucible was red; that in the sapphire was clear. On cooling, it was found that the salt in the Pyrex vessel was dark red, while that in the sapphire vessel was white. On dissolution in water, the salt from the Pyrex vessel gave a slightly colored solution with black particles evident. The uranium

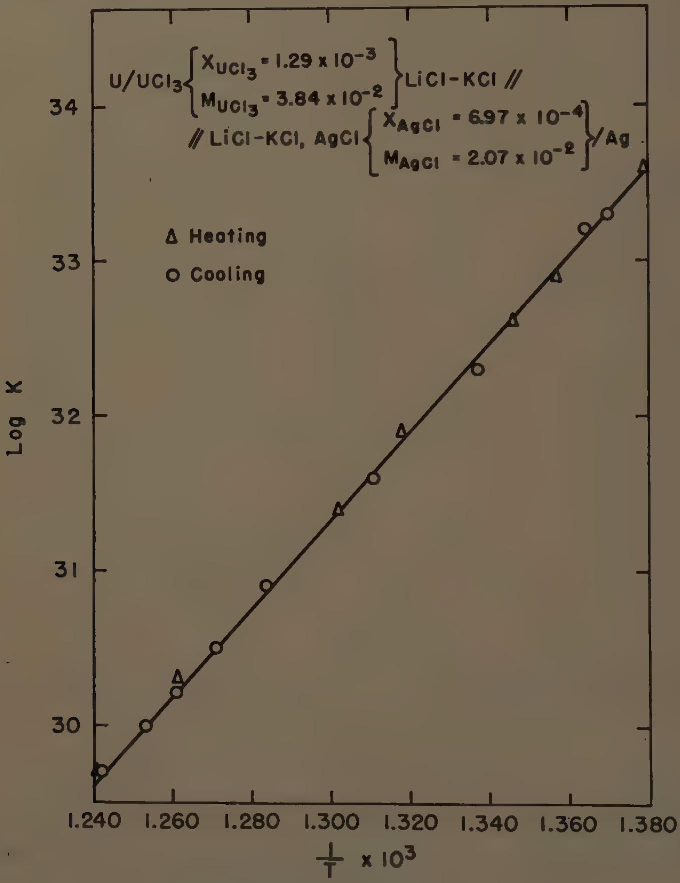

FIGURE 5. Log K versus $1/T$.

wire that had been in contact with the salt contained in the Pyrex vessel appeared to have an oxide coating. The salts from the sapphire vessel dissolved in water to give a clear solution, while the uranium wire appeared clean. These results indicate that there is a slight reaction between the melt and the fused silica or Pyrex vessel, resulting in the formation of a soluble silicon-containing species. This species could then react with the uranium metal to produce UCl_3 and Si. The reaction is slow and does not contribute appreciably to the uranium (III) concentration at long anodization times. At the high U(III) concentrations, therefore, the log plot becomes linear. An attempt to minimize this effect was made by carrying out the subsequent measurements as rapidly as possible.

Acknowledgments

The aid of Robert McBeth in carrying out certain aspects of this work is appreciated, as is the work of the Analytical Group at Argonne National Laboratory.

References

1. Laitinen, H. A. & C. H. Liu. 1958. J. Am. Chem. Soc. **80:** 1015.
2. Flengas, S. N. & T. R. Ingraham. 1957. Can. J. Chem. **35:** 1139, 1254. 1958. Can. J. Chem. **36:** 780, 1103, 1662.
3. Gruen, D. M., S. Fried, P. Graf and R. McBeth. 1958. The Chemistry of Fused Salts. The United Nations Conf. on Peaceful Uses of Atomic Energy. Geneva, Switzerland.
4. Van Artsdalen, E. R. & I. S. Yaffe. 1955. J. Phys. Chem. **59:** 118.
5. Hill, D. L. & R. A. Osteryoung. 1958. 1959. Report No. 6. Brookhaven Natl. Lab. 1958. 1959. Rensselaer Polytech. Inst. Troy, N.Y.
6. Hamer, W., M. S. Malmberg & B. Rubin. 1956. J. Electrochem. Soc. **103:** 8.
7. Glassner, A. 1957. The Thermochemical Properties of Oxides, Fluorides and Chlorides to 2500° K. United States Atomic Energy Commission Report ANL-5750.
8. Benz, R. 1958. Ph.D. Dissertation. Univ. New Mexico. Albuquerque, New Mexico.

THERMODYNAMICS OF MOLTEN BINARY CHLORIDE MIXTURES CALCULATED FROM THE PHASE DIAGRAMS*

Benjamin Chu† and James J. Egan
Brookhaven National Laboratory, Upton, N.Y.

Introduction

Phase diagrams have been used by several investigators to derive thermodynamic data for binary mixtures. For metal alloys Hauffe and Wagner,[1] Chipman,[2] Kleppa,[3] Schottky and Bever,[4] Sheil,[5] and others have used this method. For fused oxides Rey[6] and Richardson[7] report results on several systems; also, Haendler,[9] Flood,[8] and Buesman[10] report results on halide systems. An excellent review of the method is presented by Wagner.[11]

In the work reported here the technique is applied to binary chloride mixtures, with emphasis on systems that have stable intermediate phases or "double salts" in the equilibrium diagram, often an indication of large deviations from ideality in the liquid phase.[12]

In general, this type of calculation yields only approximate results, but is very useful in cases where conventional experiments are very difficult. In the systems $CaCl_2$-KCl, $CaCl_2$-RbCl, and $CaCl_2$-CsCl the vapor-pressure method would probably be difficult to employ owing to a variety of species in the vapor phase.[13,14] The emf method would be complicated by dissolution of metal electrodes[15] in the salt and side reactions at the electrodes due to a small difference in stability of the salts.

Basic Equations

The phase diagrams considered here are analyzed by considering 2 types of heterogeneous equilibria: first, that between a pure solid and a binary liquid mixture containing a common component; and, second, that between an intermediate solid phase and a liquid mixture of the same components as the intermediate phase.

In the first case the relative partial molar free energy of component 1 in the liquid mixture of mole fraction x_2 is given by the equation[11]

$$F_1^{M(l)}(T_e, x_2^{(l)}) = \frac{\Delta H_f}{T_{m_1}}(T_e - T_{m_1}) + T_e \int_{T_{m_1}}^{T_e} \frac{dT}{T^2} \int_{T_{m_1}}^{T} (C_{p_1}^{(l)} - C_{p_1}^{(s)})\, dT \qquad (1)$$

---

* The work reported in this paper was done under the auspices of the United States Atomic Energy Commission, Washington, D.C.

† Present address: Department of Chemistry, Cornell University, Ithaca, N.Y.

when the mixture is in equilibrium with the pure solid of component 1. Here T_e is the temperature of the liquidus at composition x_2, and ΔH_f, T_{m_1}, $C_{p_1}^{(l)}$, and $C_{p_1}^{(s)}$ are the heat of fusion, the melting temperature, and the molar heat capacities of pure component 1, respectively. Since pure liquid 1 is the standard state, this well-known equation is derived by merely calculating the free energy change on freezing pure supercooled liquid 1.

In the second case, by considering the equilibria between an intermediate solid phase of practically constant composition and a liquid mixture Hauffe and Wagner[1] have derived the following equations for a change in the relative partial molar free energy in terms of quantities obtainable from the phase diagram:

$$\Delta F_1^{M(l)} = F_1^{M(l)}(x_2) - F_1^{M(l)}(X_2) = \frac{\Delta H_f}{T_m}\left[-\frac{x_2^{(l)}}{x_2^{(l)} - X_2}(T_m - T_e) - X_2 \int_{x_2}^{x_2} \frac{T_m - T_e}{(x_2^{(l)} - X_2)^2}\, dx_2 \right] \tag{2a}$$

$$\Delta F_2^{M(l)} = F_2^{M(l)}(x_2) - F_2^{M(l)}(X_2) = \frac{\Delta H_f}{T_m}\left[\frac{1 - x_2}{x_2^{(l)} - X_2}(T_m - T_e) + (1 - X_2) \int_{X_2}^{x_2} \frac{T_m - T_e}{(x_2^{(l)} - X_2)^2}\, dx_2 \right] \tag{2b}$$

where T_m is the melting point of the intermediate phase at $x_2 = X_2$ and ΔH_f is the heat of fusion of the intermediate phase assumed independent of temperature. Again, these equations are derived by considering the freezing of a supercooled liquid, but are considerably complicated by the presence of 2 components in the solid phase.

It is sometimes advantageous to express the derived quantities in terms of the excess partial molar free energy:

$$F_1^{E(l)}(x_2) \equiv F_1^{M(l)}(x_2) - RT \ln (1 - x_2) \tag{3a}$$

$$F_2^{E(l)}(x_2) \equiv F_2^{M(l)}(x_2) - RT \ln x_2 \tag{3b}$$

If the solutions are regular in the sense that the entropy of mixing is ideal, the excess partial molar free energy is then temperature-independent. If the activity coefficients f_1 and f_2 are desired, they are readily obtainable from

$$F_1^{E(l)} = RT \ln f_1 \tag{4a}$$

$$F_2^{E(l)} = RT \ln f_2 \tag{4b}$$

With the use of EQUATIONS 1, 2, and 3 one obtains the free energy of at least one of the components at every composition of the binary mixture. An integrated form of the Gibbs-Duhem equation is used to obtain the excess free energy of the other component.

$$F_2^{E(l)}(x_2) - F_2^{E(l)}(x_2^*) = \int_{x_2^*}^{x_2} \frac{F_1^{E(l)}(x_2)}{(1-x_2)^2}\,dx_2 - \frac{x_2F_1^{E(l)}(x_2)}{1-x_2}\bigg|_{x_2^*}^{x_2} \qquad (5)$$

In this equation x_2^* is some composition where the excess free energy of both components is known.

Results

The phase diagram[16-18] for the LiCl-KCl system is shown in FIGURE 1. This mixture is commonly used as a solvent in fused salt work and is included here as an example of a simple eutectic system. By the use of EQUATIONS 1, 3, and 5 the excess free energies have been calculated and are shown in FIGURE 2. The thermochemical data used in EQUATION 1 are as follows:[19,20]

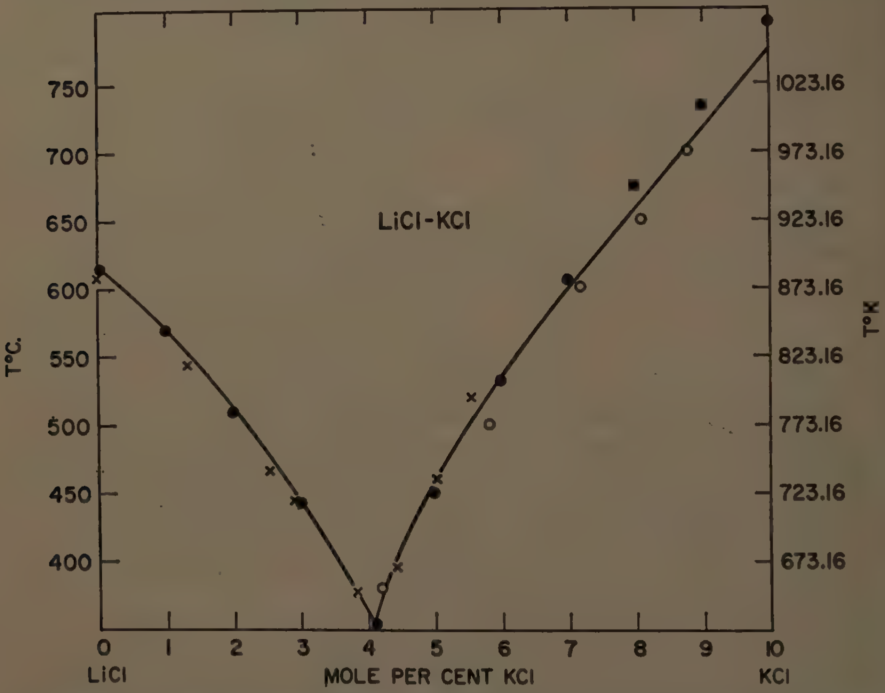

FIGURE 1. Phase diagram of the system LiCl-KCl. Symbols: cross, Elchardus and Lafitte;[16] open circle, Landolt-Bornstein;[17] solid circle, International Critical Tables.[18]

ΔH_f (KCl) = 6.1 kcal./mole

$C_p^{(l)}$ (KCl) = 16.00 cal./deg. mole

$C_p^{(s)}$ (KCl) = $9.89 + 5.20 \times 10^{-3}\,T + 0.77 \times 10^5\,T^{-2}$

ΔH_f (LiCl) = 3.2 kcal./mole

$C_p^{(l)}$ (LiCl) = 15.5 cal./deg. mole

$C_p^{(s)}$ (LiCl) = $11 + 3.4 \times 10^{-3}\,T$

Results are also presented in TABLE 1. Here F_i^M is calculated at the equi-

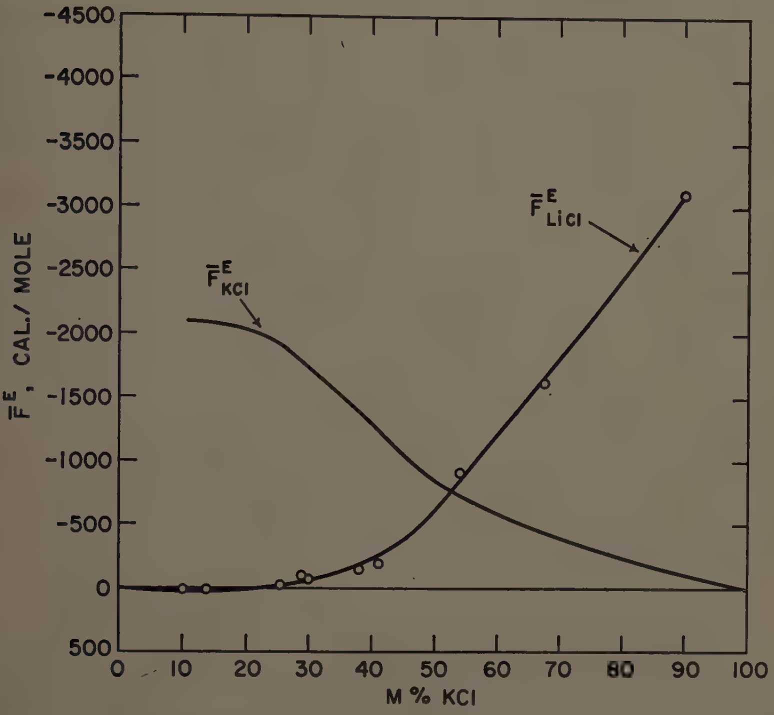

FIGURE 2. The excess partial molar free energy of LiCl-KCl versus composition.

TABLE 1

THERMODYNAMIC DATA ON THE SYSTEM LiCl-KCl

Mole % KCl	T_e (°K)	F^M_{LiCl}	F^M_{KCl}	F^E_{KCl}	F^E_{LiCl}	f_{KCl}	f_{LiCl}
0	883	0			0		1.00
11	838		−5775	−2099		3.83×10^{-1}	
13.4	816	−229			4.3		1.002
22	773		−4361	−2035		3.94×10^{-1}	
25	753		−4009	−1935		4.13×10^{-1}	
25.4	741	−453			−21.5		9.90×10^{-1}
28.8	717	−567			−81.1		9.64×10^{-1}
30	715	−578			−71.3		9.67×10^{-1}
33.7	688		−3040	−1553		4.91×10^{-1}	
37.7	655		−2684	−1414		5.24×10^{-1}	
38.2	651	−774			−151.5		9.33×10^{-1}
41	627	−853	−2358	−1247	−196	5.65×10^{-1}	9.14×10^{-1}
50	728		−1828	−825		6.86×10^{-1}	
54	763	−2090			−910		6.6×10^{-1}
60	804		−1410	−594		7.62×10^{-1}	
67.5	856	−3520			−1610		4.79×10^{-1}
70	872		−1000	−382		8.40×10^{-1}	
80	930		−690.7	−279		8.80×10^{-1}	
90	990	−7630	−340.9	−134	−3100	9.40×10^{-1}	
100	1048		0	0		1.00	2.42×10^{-1}

librium temperature T_e, and the activity coefficients are at 1100° K., assuming a regular solution.

The phases present in mixtures of $CaCl_2$ with KCl, RbCl, and CsCl are shown in FIGURE 3.[21] A series of double salts is formed at equimolar compositions of the pure components with relatively high melting points.

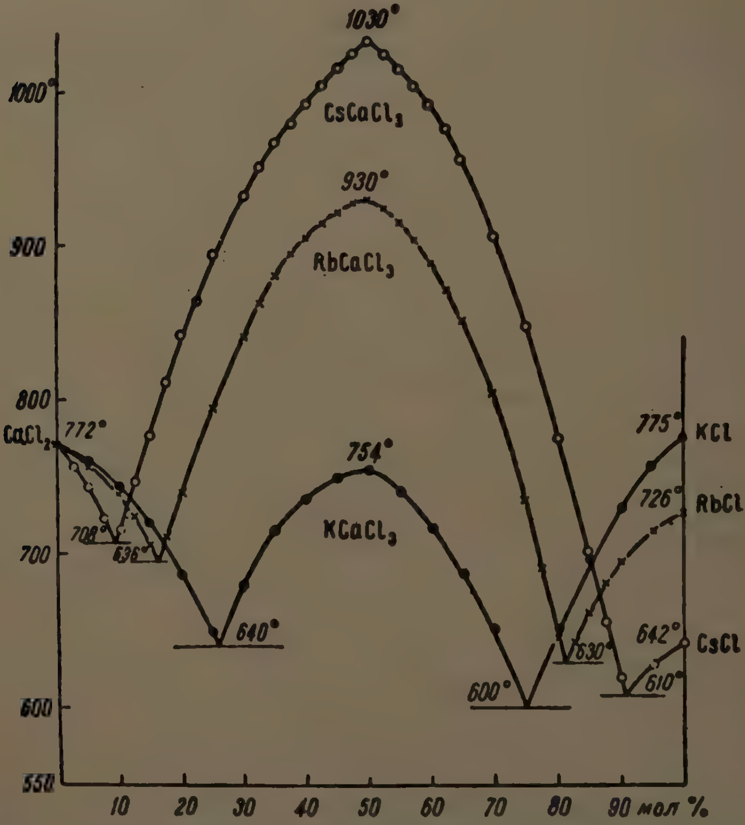

FIGURE 3. Phase diagrams for the systems $CaCl_2$-KCl, $CaCl_2$-RbCl, and $CaCl_2$-CsCl.

EQUATIONS 2a and 2b are therefore used along with EQUATIONS 1, 3, and 5. Results are presented in FIGURES 4, 5, and 6 and in TABLES 2, 3, and 4. The pertinent thermochemical data used are:[19,20]

$\Delta H_f\ (CaCl_2) = 6.8$ kcal./mole $\quad C_p^{(l)} = 24.7$ cal./deg. mole $\quad C_p^{(s)} = 17.2 + 3 \times 10^{-3}\, T$

$\Delta H_f\ (CsCl) = 3.6$ kcal./mole $\quad C_p^{(l)} =$ unknown

$\Delta H_f\ (RbCl) = 4.4$ kcal./mole $\quad C_p^{(l)} = 15.3$ cal./deg. mole $\quad C_p^{(s)} = 11.5 + 2.5 \times 10^{-3}\, T$

The heats of fusion for intermediate phases were approximated by assuming that their entropies of fusion were equal to the sum of the entropies of fusion of the pure components. Thus

$$\Delta H_f(\text{CaCl}_2\text{-KCl}) = 6.3 \text{ kcal./equiv.}$$

$$\Delta H_f(\text{CaCl}_2\text{-RbCl}) = 6.6 \text{ kcal./equiv.}$$

$$\Delta H_f(\text{CaCl}_2\text{-CsCl}) = 6.8 \text{ kcal./equiv.}$$

In all these systems the deviations from ideality are negative and large, with a definite inflection point at the composition of the double salt. The system KCl-$MgCl_2$ is shown[22] in FIGURE 7 and is studied here to check the calculations against experimental values obtained by emf studies. The results of the calculations are shown in FIGURE 8 and TABLE 5 and are compared with emf measurements of Markov[23] and Niel and Wiswall (in preparation). The thermochemical data used were

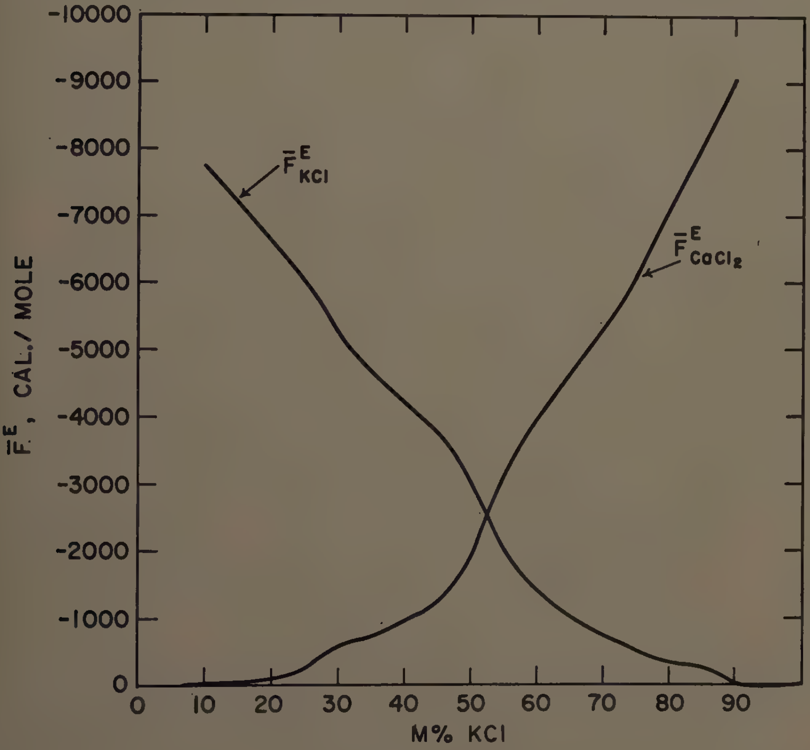

FIGURE 4. The excess partial molar free energy of $CaCl_2$ and KCl versus composition.

$$\Delta H_f(\text{MgCl}_2) = 10.3 \text{ kcal./mole}$$

$$C_p^{(l)}(\text{MgCl}_2) = 22.10 \text{ cal./deg. mole}$$

$$C_p^{(s)}(\text{MgCl}_2) = 18.90 \text{ cal./deg. mole}$$

The agreement between measured and calculated points leaves much to be desired but, since even the experimental values of separate investigators do not agree, the calculations should be usable as a first approximation in other systems where experiments are not available.

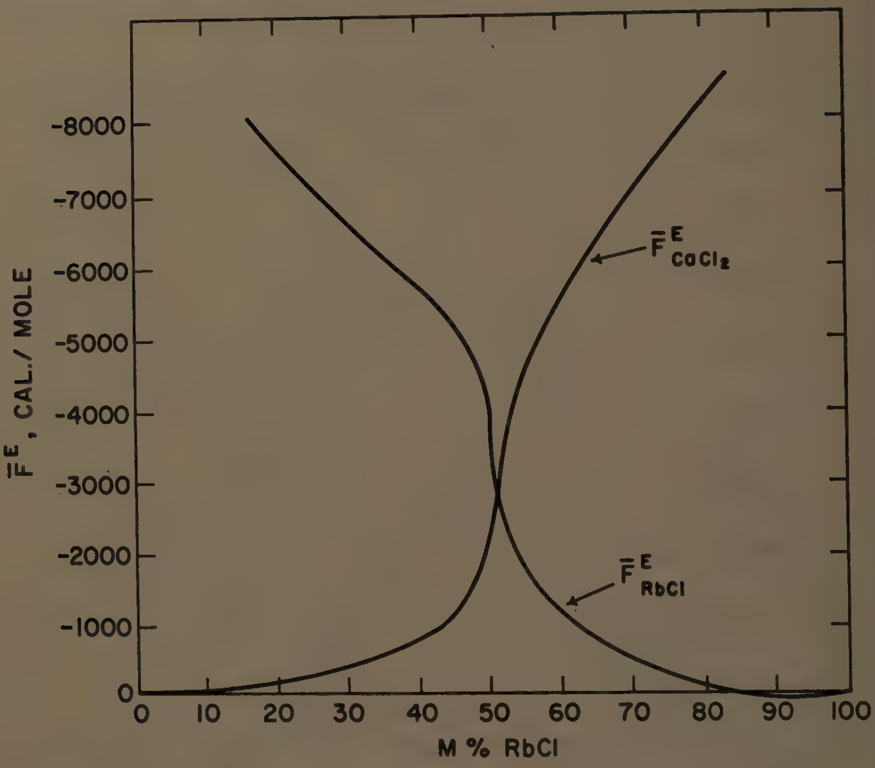

FIGURE 5. The excess molar free energy of $CaCl_2$ and RbCl versus composition.

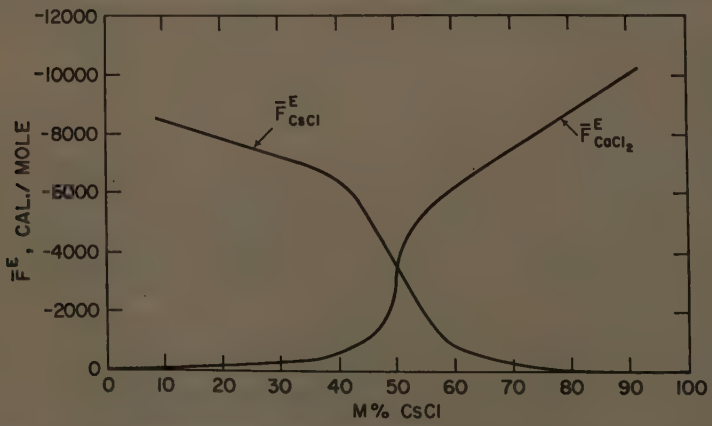

FIGURE 6. The excess partial molar free energy of $CaCl_2$ and CsCl versus composition.

Conclusions

Large deviations from ideality can exist in liquid chloride mixtures even when both components are predominantly ionic. This is especially true when cations of different valences are mixed, as shown by the above calculations. Whenever these systems are to be used in slagging or similar operations, the highly negative free energies of mixing will affect the final

TABLE 2

THERMODYNAMIC PROPERTIES OF THE SYSTEM KCl-$CaCl_2$

Mole % KCl	T_e (°K)	F^M_{KCl}	$F^M_{CaCl_2}$	F^E_{KCl}	$F^E_{CaCl_2}$	f_{KCl}	f_{CaCl_2}
0	1050		0		0		1
10	1015		−227	−7703	−14.5	2.95×10^{-2}	9.93×10^{-1}
15	994		−383		−62.0		9.72×10^{-1}
20	971		−532		−101		9.54×10^{-1}
22.2	958			−6391		5.38×10^{-2}	
25	937		−751		−215		9.06×10^{-1}
26.5	914	−8311	−899	−5899	−340	6.73×10^{-2}	8.56×10^{-1}
30	956	−7463	−1230	−5176	−562	9.38×10^{-2}	7.73×10^{-1}
35	987	−6724	−1587	−4665	−742	1.18×10^{-1}	7.12×10^{-1}
40	1009	−6047	−1994	−4210	−970	1.46×10^{-1}	6.42×10^{-1}
45	1022	−5434	−2447	−3812	−1233	1.75×10^{-1}	5.69×10^{-1}
50	1027	−4440	−3379	−3026	−1965	2.51×10^{-1}	4.07×10^{-1}
55	1018	−3094	−4836	−1885	−3220	4.22×10^{-1}	2.29×10^{-1}
60	998	−2388	−5788	−1375	−3975	5.33×10^{-1}	1.63×10^{-1}
65	966	−1813	−6757	−986	−4742	6.37×10^{-1}	1.14×10^{-1}
70	933	−1448	−7528	−787	−6296	6.98×10^{-1}	8.87×10^{-2}
75.5	873	−1007	−8708	−519	−6268	7.89×10^{-1}	5.69×10^{-2}
80	924	−714		−304		8.71×10^{-1}	5.72×10^{-2}
85	966	−575		−263		8.87×10^{-1}	
90	1007	−235		−241	−9024	8.96×10^{-1}	1.61×10^{-2}
95	1038	−60		+45.8		1.23	
100	1049	0		0		1	

TABLE 3

THERMODYNAMIC PROPERTIES OF THE SYSTEM $RbCl$-$CaCl_2$

Mole % RbCl	T (°K)	$\Delta F^{M(l)}_{RbCl}$	$\Delta F^{M(l)}_{CaCl_2}$	F^M_{RbCl}	$F^M_{CaCl_2}$	F^E_{RbCl}	$F^E_{CaCl_2}$
100	999			0		0	
96	989			−44		36	
90	963			−158		44	
85	931			−296		5	
82	903	5146	−8438	−416	−12337	−60	−9261
70	1080	4268	−5618	−1294	−9515	−529	−6939
60	1161	3220	−3681	−2342	−7580	−1164	−5466
55	1187	2403	−2578	−3159	−6477	−1749	−4593
50	1203	0	0	−5562	−3899	−3905	−2242
45	1196	−1470	1393	−7032	−2506	−5134	−1085
40	1177	−2266	1981	−7828	−1918	−5685	−723
30	1118	−3676	2738	−9238	−1161	−6564	−369
20	1018	−5304	3275	−10866	−624	−7610	−173
16	969	−5991	3423	−11553	−476	−8025	−140
12	995				−342		−89
6	1025				−128		−2
0	1045				0		0

equilibria appreciably. Results obtained here should be useful as a first approximation in calculating distribution coefficients.

Summary

The excess free energy of mixing of both components is calculated for the binary systems LiCl-KCl, $MgCl_2$-KCl, $CaCl_2$-KCl, $CaCl_2$-RbCl, and $CaCl_2$-

Table 4

Thermodynamic Properties of the System CsCl-$CaCl_2$

Mole % CsCl	T (°K)	$\Delta l^{M(l)}_{CsCl}$	$\Delta F^{M(l)}_{CaCl_2}$	F^{M}_{CsCl}	$F^{M}_{CaCl_2}$	F^{E}_{CsCl}	$F^{E}_{CaCl_2}$
100	915			0		0	
95	897			−70.9		20.5	
93	889			−102		26	
91	883	5193	−9577	−126	−14478	40	−10254
80	1049	4828	−7479	−491	−12380	−26	−9025
70	1182	4139	−5402	−1180	−10303	−342	−7476
60	1261	3173	−3612	−2146	−8513	−866	−6217
50	1303	0	0	−5319	−4901	−3525	−3107
40	1265	−3408	3011	−8727	−1890	−6423	−606
30	1205	−4781	3758	−10100	−1143	−7218	−289
20	1118	−6143	4212	−11462	−689	−7887	−193
9	981	−7860	4499	−13179	−402	−8486	−218
7	995				−323		−181
4	1019				−158		−75.0
0	1045				0		0

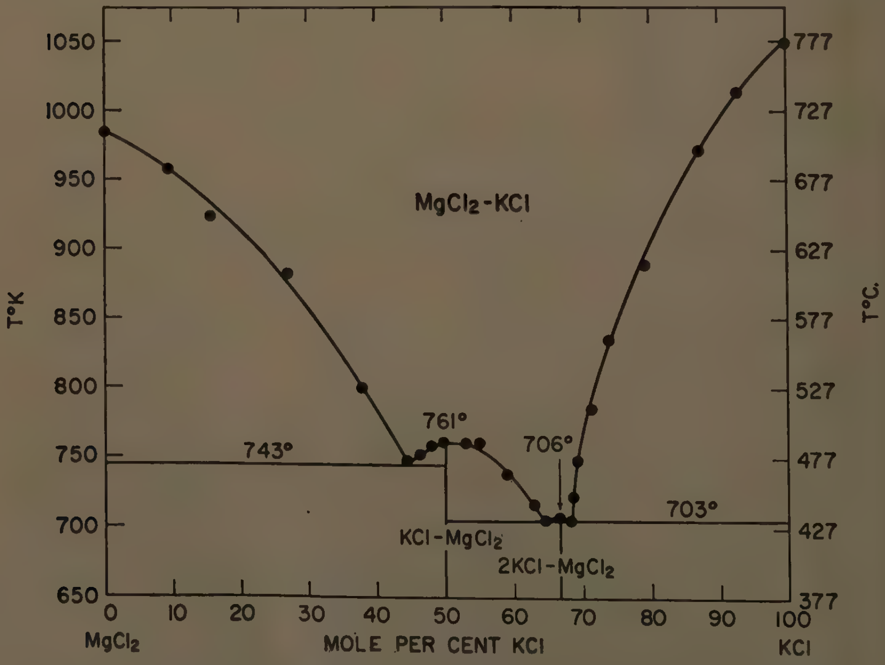

Figure 7. Phase diagram of the system $MgCl_2$-KCl. Data from Menge.[22]

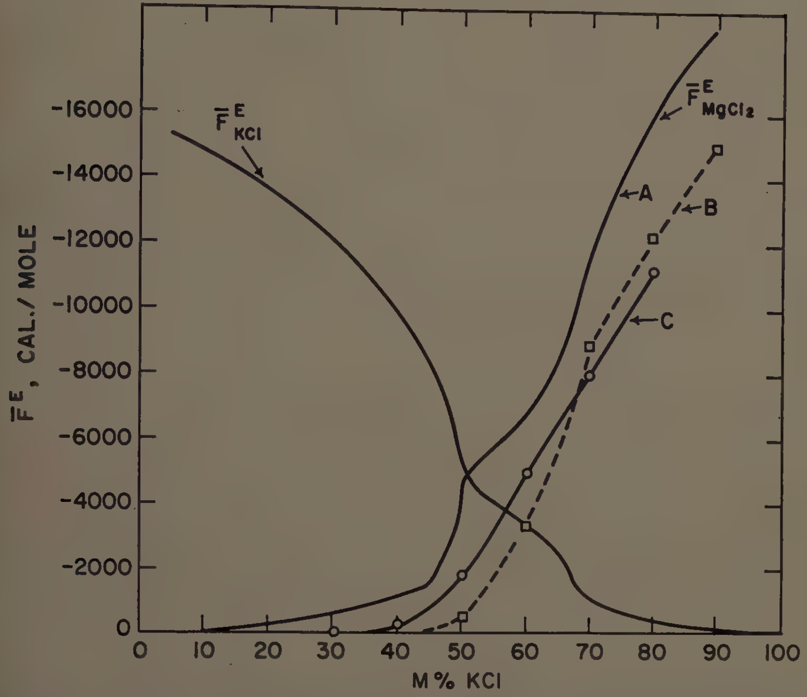

FIGURE 8. The excess partial molar free energy of $MgCl_2$ and KCl versus composition. Symbols: A, calculated from phase diagram; B, calculated from measurements at Brookhaven National Laboratory; C, calculated from emf measurements of Markov *et al.*[23]

TABLE 5

THERMODYNAMIC PROPERTIES OF THE SYSTEM KCl-$MgCl_2$

Mole % KCl	T_e (°K)	F^M_{KCl}	$F^M_{MgCl_2}$	F^E_{KCl}	$F^E_{MgCl_2}$	f_{KCl}	f_{MgCl_2}
0	984		0		0		1
10	956		−293	−16238	−92.4	5.94×10^{-4}	9.59×10^{-1}
20	913		−722		−317		8.65×10^{-1}
30	857		−1280	−12044	−673	4.05×10^{-3}	7.35×10^{-1}
40	785		−1987	−9961	−1190	1.05×10^{-2}	5.80×10^{-1}
45	743	−9417	−2390	−8238	−1507	2.31×10^{-2}	5.02×10^{-1}
47.5	756	−8073	−3734	−6955	−2766	4.15×10^{-2}	2.82×10^{-1}
49	760	−7156	−4667	−6079	−3650	6.20×10^{-2}	1.88×10^{-1}
50	761	−6204	−5156	−5156	−4555	9.46×10^{-2}	1.25×10^{-1}
52	760	−5545	−6278	−4558	−5170	1.24×10^{-1}	9.40×10^{-2}
53	759	−5389	−6451	−4432	−5312	1.32×10^{-1}	8.81×10^{-2}
55	755	−5009	−6898	−4112	−5700	1.53×10^{-1}	7.37×10^{-2}
60	735	−4078	−8163	−3332	−6825	2.18×10^{-1}	4.41×10^{-2}
64.5	703	−3269	−9505	−2656	−8058	2.97×10^{-1}	2.51×10^{-2}
65.5	705	−3044	−9912	−2451	−8422	3.26×10^{-1}	2.12×10^{-2}
67.5	705	−2216	−11606	−1665	−10032	4.67×10^{-1}	1.02×10^{-2}
68.3	703	−1934	−12178	−1401	−10573	5.27×10^{-1}	7.94×10^{-3}
70	763	−1615		−1075		5.33×10^{-1}	
75	848	−1149		−664	−13921	7.38×10^{-1}	1.72×10^{-3}
80	905	−829		−428		8.22×10^{-1}	
90	993	−325		−117	−19770	9.48×10^{-1}	1.07×10^{-4}
100	1049	0		0		1	

CsCl from existing phase diagrams. The method of Hauffe and Wagner[1] is employed for systems containing intermediate phases along with the conventional equations for freezing-point lowering and the Gibbs-Duhem equation. For the purposes of the calculations, approximations have been introduced concerning the heats of fusion of double salts present in these systems. Results of the calculations are checked with experimental data available in the case of $MgCl_2$-KCl, and the agreement is within the limits expected. Since the values obtained for the excess free energy of mixing show that large deviations from ideality are present, the importance of small errors inherent in this method is minimized.

References

1. Hauffe, K. & C. Wagner. 1940. Z. Electrochem. **46:** 160.
2. Chipman, J. 1948. Discussions Faraday Soc. **4:** 23.
3. Kleppa, O. J. 1952. J. Am. Chem. Soc. **74:** 6047.
4. Schottky, W. F. & M. B. Bever. 1958. Acta Metallurgica. **6.**
5. Sheil, E. 1943. Z. Electrochem. **49:** 242.
6. Rey, M. 1948. Discussions Faraday Soc. **4:** 257.
7. Richardson, F. D. 1953. The Physical Chemistry of Melts. Inst. Mining and Metallurgy. London, England.
8. Flood, H., O. Fykse & S. Urnes. 1955. Z. Electrochem. **59:** 364.
9. Haendler, H., P. Sennett & C. Wheeler. 1959. J. Electrochem. Soc. **106:** 264.
10. Buesman, C. 1957. Report No. ORNL-2323. Oak Ridge Natl. Lab. Oak Ridge, Tenn.
11. Wagner, C. 1952. Thermodynamics of Alloys. Addison-Wesley Press. Cambridge, Mass.
12. Wagner, C. 1958. Acta Metallurgica. **6.**
13. Miller, R. C. & P. Kusch. 1956. J. Chem. Phys. **25:** 860.
14. Friedman, L. 1955. J. Chem. Phys. **23:** 477.
15. Cubicciotti, D. 1947. AEC Report No. MDDC-1058. Technical Information Branch. Oak Ridge, Tenn.
16. Elchardus, E. & P. Lafitte. 1932. Bull. soc. chim. France. **51:** 1572.
17. Landolt-Bornstein. 1956. II Band. Physikalisch-chemische Tabellen. 3 Teil. : 237.
18. International Critical Tables. 1928. IV: 66.
19. Kelley, K. K. 1936. Bull. U. S. Bur. Mines. No. **393.**
20. Kelley, K. K. 1949. Bull. U. S. Bur. Mines. No. **476.**
21. Dergnnow, J. P. & A. G. Bergman. 1950. Ber. Akad. Wiss. USSR. **75:** 815.
22. Menge, O. 1911. Z. Anorg. Chem. **72:** 172.
23. Markov, B. F., I. K. Delimarskii & I. D. Panchenko. 1955. Zhur. Fiz. Khim. **29:** 51.

THE CRYOLITE SITUATION

L. M. Foster

Alcoa Research Laboratories, Aluminum Company of America, New Kensington, Pa.

One may wonder why there is still an unexplained situation with regard to cryolite in an industry that for seventy years has been producing aluminum from the electrolyte that is essentially unchanged in composition and manner of use from the time it was first melted by Charles Martin Hall. There is some justification for the paucity of fundamental information about this electrolyte, however. Cryolite is a molten fluoride and is one of the most corrosive materials known. It can be contained in platinum, but obviously platinum cannot be used if the experiment involves molten aluminum as well. It can be contained in graphite or boron nitride, but these materials have serious limitations.

Cryolite vaporizes with decomposition and changes its constitution and freezing point. It oxidizes in the air to produce soluble aluminum oxide, which greatly confuses thermodynamic data based on thermal arrests and phase-diagram studies in general. Finally, it hydrolyzes at high temperature to form aluminum oxide and hydrogen fluoride. It is not surprising, in view of these experimental handicaps, that most of the old information on cryolite was data obtained in plants during commercial operation and, considering the limitations, some of this information was reliable. However, the knowledge and understanding of cryolite that have been achieved in the last three years are probably greater than everything that had been gained in the previous sixty-seven. This paper will describe the present status of the cryolite problem, call attention to the inadequacies in current information, and point the direction in which future work probably will go.

Cryolite is a double fluoride of sodium and aluminum, $3NaF \cdot AlF_3$ or Na_3AlF_6. It occurs naturally in Greenland as a water-white crystal. The word cryolite means icelike. Cryolite can be produced synthetically from sodium aluminate and HF or by fusing together sodium and aluminum fluorides in the stoichiometric proportions.

The most recent phase diagram of the NaF-AlF_3 system is shown in FIGURE 1, based on the data of Grjotheim.[1] The principal point of interest here is the broad congruent melting at the cryolite composition. Such broadening of the liquidus boundary indicates partial decomposition of the solid compound on melting. Only the most naïve view would suggest that sodium fluoride and aluminum fluoride would be the most probable decomposition products. Nevertheless, this was the opinion for many years.

To keep events in chronological order, some transference work in molten cryolite-alumina reported by Frank and Foster[2] should be reviewed. The data shown in TABLE 1 were obtained in experiments carried out with porous membranes and by using radioactive aluminum, fluorine, and so-

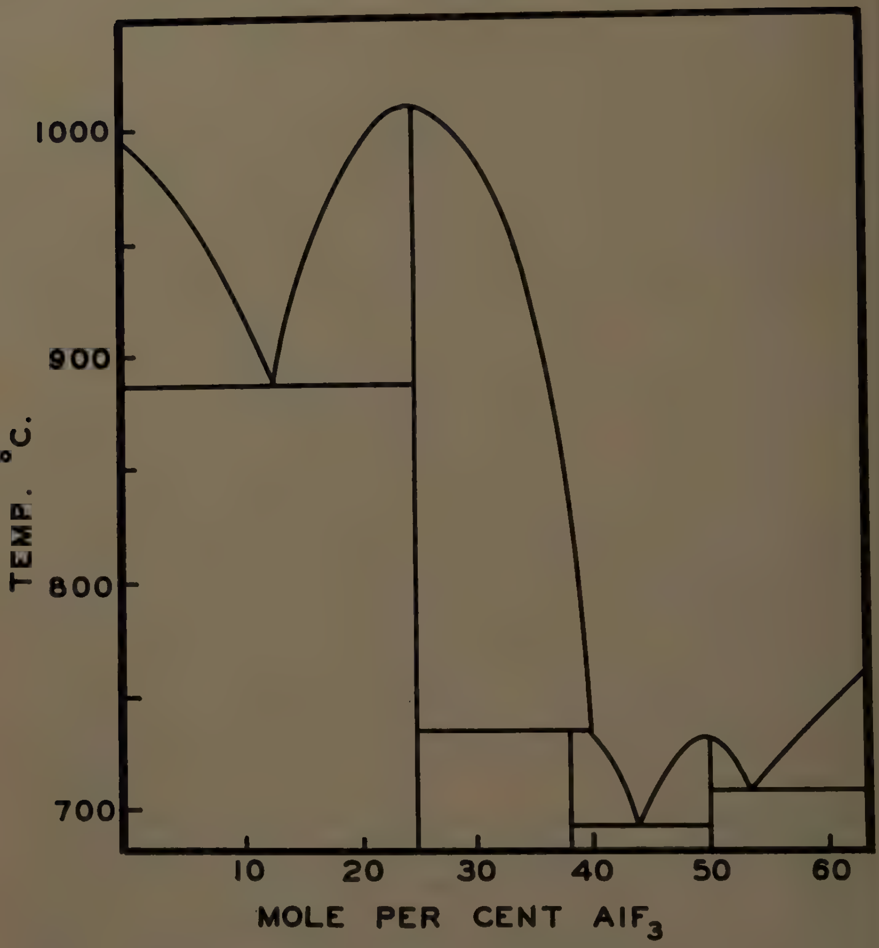

FIGURE 1. Phase diagram of NaF-AlF$_3$ system.

TABLE 1
TRANSPORT RESULTS

Element	Diaphragm	Transport, equivalent per faraday from	
		Anode to cathode	Cathode to anode
Sodium	Al_2O_3	1.01 ± 0.001*	
Sodium	Al_2O_3	1.07 ± 0.001	
Sodium	Al_2O_3	1.01 ± 0.001	
Sodium	BN		<0.003
Aluminum	BN		0.0357 ± 0.0007
Fluorine	BN		0.0205 ± 0.0008

* Precision limits refer to radioactive counting procedure only; total limits might be a few per cent of the absolute values.

dium. It is seen that, during the electrolysis of aluminum oxide dissolved in cryolite, almost all of the current is transported to the cathode by sodium ions. A very small percentage of the current is transported to the anode by sodium-free anions that contain aluminum and fluorine, either separately or combined (the transport of oxygen could not be followed since there is no satisfactory radioactive oxygen isotope). The transport data do not have an unequivocal interpretation since, within the precision of the experiment, it cannot be determined whether fluorine migrates with a single negative charge as a fluoride ion or whether it is combined with the aluminum as a complex anion of undetermined valence. Nevertheless, there are two striking features apparent: first, there is no migration of aluminum to the cathode; and, second, the migration of fluorine, whether singly or as a complex anion, does not contribute more than a small percentage to the total transfer of charge.

An explanation for the first effect is more obvious than for the second. The implication is that there are no free Al^{+++} ions in these melts, since such ions surely would carry a substantial part of the current.

The almost negligible conductivity by fluoride is more surprising when it is considered that there are one and one half times as many fluorine atoms as sodium and aluminum atoms combined. Clearly, any model for the structure of molten cryolite must provide for this rather anomalous transport behavior.

In the course of measuring the electric conductivity of NaF-AlF_3 melts, Edwards *et al.*[3] had determined the molten densities at several temperatures. A number of investigations had indicated that ideal additivity of volumes might be expected in many molten salt systems at high temperature. With this assumption, Frank and Foster[4] calculated the densities of NaF-AlF_3 melts at various temperatures over a considerable range of composition according to the following possible mechanisms for the dissociation of cryolite in the molten state:

$$Na_3AlF_6 \rightleftarrows 3NaF + AlF_3 \qquad \text{SCHEME 1}$$
$$3Na_3AlF_6 \rightleftarrows 4NaF + 5NaF \cdot 3AlF_3 \qquad \text{SCHEME 2}$$
$$Na_3AlF_6 \rightleftarrows 2NaF + NaAlF_4 \qquad \text{SCHEME 3}$$

In the calculations, no cognizance was taken of the degree of ionization of the various species, since the assumption of additive volumes did not require it. Scheme 1, therefore, could be considered to yield Na^+, Al^{+++}, and F^- ions, as well as AlF_6^{---} at equilibrium, but it does not preclude the possibility of un-ionized AlF_3 molecules. The second scheme was considered since chiolite ($5NaF \cdot 3AlF_3$) appears as a stable compound in the NaF-AlF_3 phase diagram, and was identified in vapors from the melt. The third scheme had some attractive features. The decrease in coordination of the aluminum at high temperatures was reasonable, and $NaAlF_4$ had been identified by Howard.[5]

By arbitrary but reasonable density assignment to the species present at equilibrium in each scheme and by adjustment of the dissociation constant, it was possible by means of successive approximations to obtain exact agreement with the experimental density curve at several temperatures according to the third dissociation scheme. It was not possible by any adjustment of parameters to get agreement with the first and second dissociation schemes.

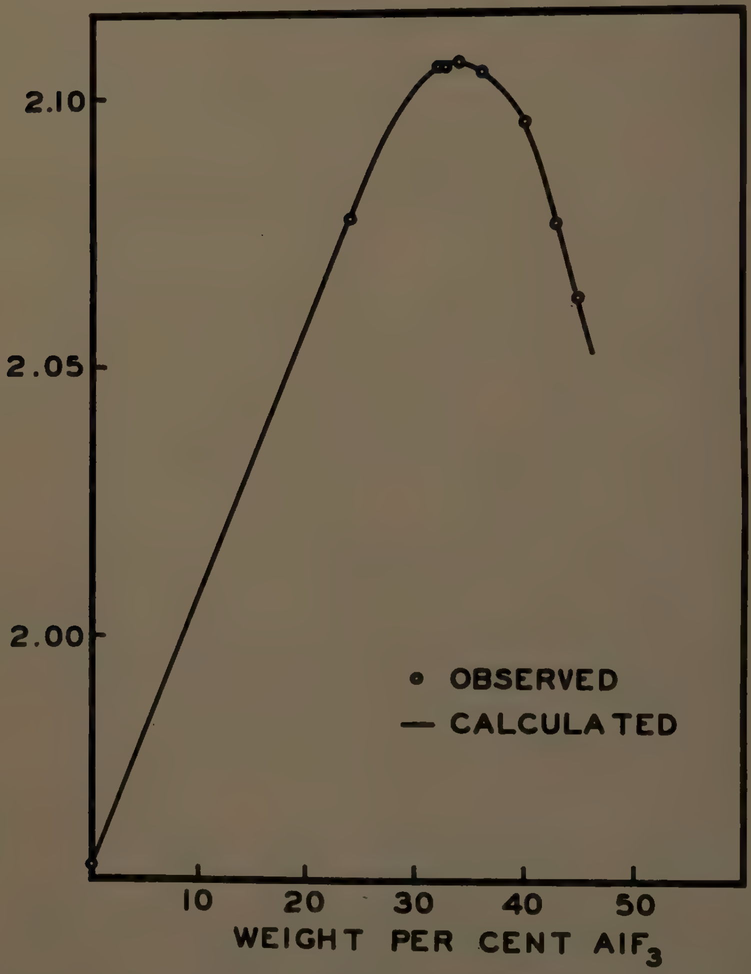

FIGURE 2. Densities of NaF-AlF$_3$ melts.

FIGURE 2 shows the experimental and calculated densities at 1000° C. according to Scheme 3, with a dissociation constant of 0.09. The equilibrium molecular composition of the melts at 1000° C. is shown in FIGURE 3. It is calculated that the melt at the cryolite composition consists of 65.2 per cent Na_3AlF_6, 13.9 per cent NaF, and 20.9 per cent $NaAlF_4$, by weight.

While these calculations were in progress, Grjotheim reported independent calculations on the constitution of cryolite. He attempted to reproduce a portion of the NaF-AlF$_3$ phase diagram by cryoscopic calcula-

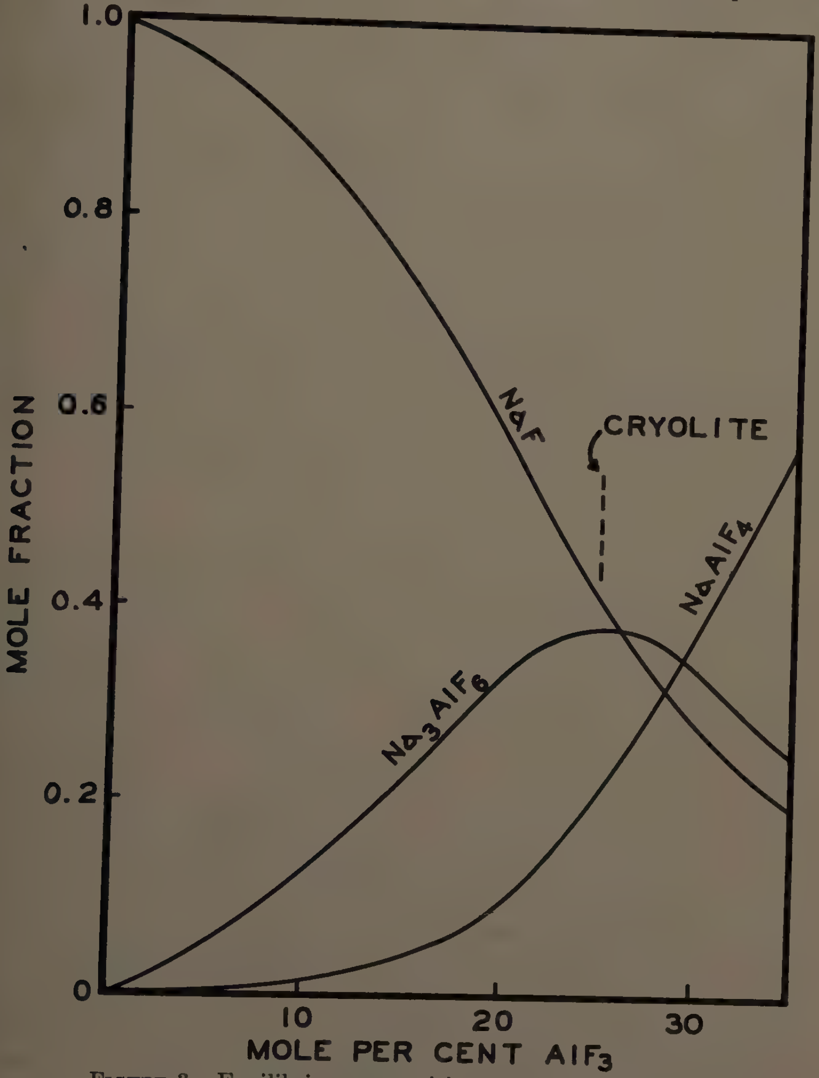

FIGURE 3. Equilibrium compositions of NaF-AlF$_3$ melts.

ions of the liquidus boundary according to several possible dissociation chemes. Grjotheim, too, arrived at the dissociation of cryolite to NaF nd NaAlF$_4$ as providing the best fit to the experimentally determined hase diagram. His dissociation constant was 0.06 at 1000° C., which ould give only slightly different compositions than those determined by rank and Foster. Several assumptions were made by both workers.

Both assumed unit activity coefficients. The assumption by Frank and Foster of completely additive volumes was, at best, an approximation. Grjotheim assumed a temperature-independent heat of fusion of cryolite and sodium fluoride, and a zero heat of dissociation of cryolite. Frank and Foster did not require the heat of fusion, and calculated the heat of dissociation of cryolite from the variation of the equilibrium constant with temperature as 22 kcal./mole.

There is other evidence for the existence of $NaAlF_4$ and the plausibility of the third dissociation scheme. At temperatures somewhat above the melting point these fluoride melts become quite volatile. It was known that the volatility was related to the AlF_3 content, but in no obvious manner. A natural assumption was that the volatile phase was principally aluminum fluoride; this appeared to be confirmed by X-ray patterns of the condensed vapor that always showed large proportions of AlF_3. X ray also showed chiolite, $5NaF \cdot 3AlF_3$, however, and its presence was not explained as readily. This anomaly was resolved by Howard who showed that, if the vapors were rapidly quenched, the product by X-ray and chemical analysis was $NaAlF_4$. Only on slow condensation or by reheating the quenched condensate would this material disproportionate, thus

$$5NaAlF_4 = 5NaF \cdot 3AlF_3 + 2AlF_3$$

Consequently, there was no evidence that AlF_3 was a component either of the vapor or the melt itself.

Ginsberg and Böhm[6] determined the "cold" composition of the volatile material from the above various melts in the NaF-AlF_3 system without, however, actually measuring vapor pressures. Their data are shown as the open circles in FIGURE 4. In work in progress, W. B. Frank (to be published) shows that by assigning relative vapor pressures of 5, 1, and 30 to the species Na_3AlF_6, NaF, and $NaAlF_4$, the solid line in FIGURE 4 is obtained by employing the melt compositions shown in FIGURE 3, thus substantiating the third cryolite dissociation scheme.

With this knowledge of the composition of molten NaF-AlF_3 melts, it is possible to obtain an insight into possible mechanisms of electric conductivity. The electric conductance of NaF-AlF_3 melts over a range of composition including cryolite was measured by Edwards *et al.*,[3] Yim and Feinleib,[7] and Winterhager and Werner.[8] These data are shown in FIGURE 5, with the best average shown by the solid line.

The transport experiments of Frank and Foster showed that conductivity in dilute solutions of alumina in cryolite was due very largely to sodium, with a small contribution from fluorine. Necessarily, of course, the small amount of aluminum that moved anodically would be tied up as a complex anion, possibly the aluminate, AlO_2^{-1}, and can be neglected in consideration of transport in pure cryolite.

From the equilibrium compositions of NaF-AlF_3 melts at various weighed-in mole ratios and the experimental specific conductivities, Frank and Foster[9] calculated the contribution of sodium and fluoride to the conductivity according to various conductance mechanisms, in all cases attributing all of the conductivity to the small Na^+ and F^- ions.

The basis of the calculations was the solution of equations relating the concentration of Na^+ and F^- to the measured specific conductivity of the melt, thus

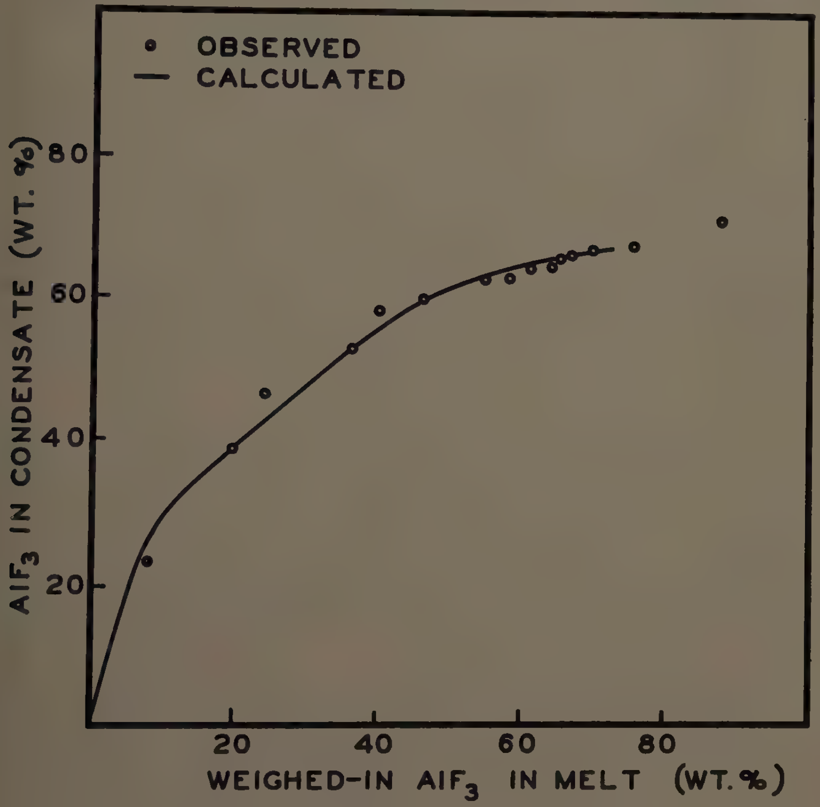

Figure 4. Vaporization of NaF-AlF_3 melts.

$$C_{Na^+}\Lambda_{Na^+} + C_{F^-}\Lambda_{F^-} = L$$

where C_{Na^+} and C_{F^-} are the concentrations of sodium and fluoride ions in proper units, L, the measured specific conductivity, and Λ_{Na^+} and Λ_{F^-}, the equivalent conductances of sodium and fluoride ion. Since the concentration of the ions could be calculated from the gross composition of the melt with various assumptions as to the degree and manner of ionization, pairs of these equations could be solved simultaneously for the equivalent conductances of the sodium and fluoride at any two compositions.

The simplest assumption as to the manner and degree of ionization, where all species are completely ionized, could not be correlated to the experimental data if the stipulation were made that sodium and fluorine should conduct in the inverse ratio of their ionic radii, as required by the Stokes-Einstein relation. However, very reasonable results, with Λ_{Na^+} and Λ_{F^-} in the proper ratio, were obtained according to either of two other mechanisms. In the first case, it was assumed that the conductance mechanism in a melt is the same as in the solid; that is, conductivity of cations by diffusion via cation vacancies and conductivity of anions by diffusion via anion vacancies. Carrying the analogy to the solid further, it was rea-

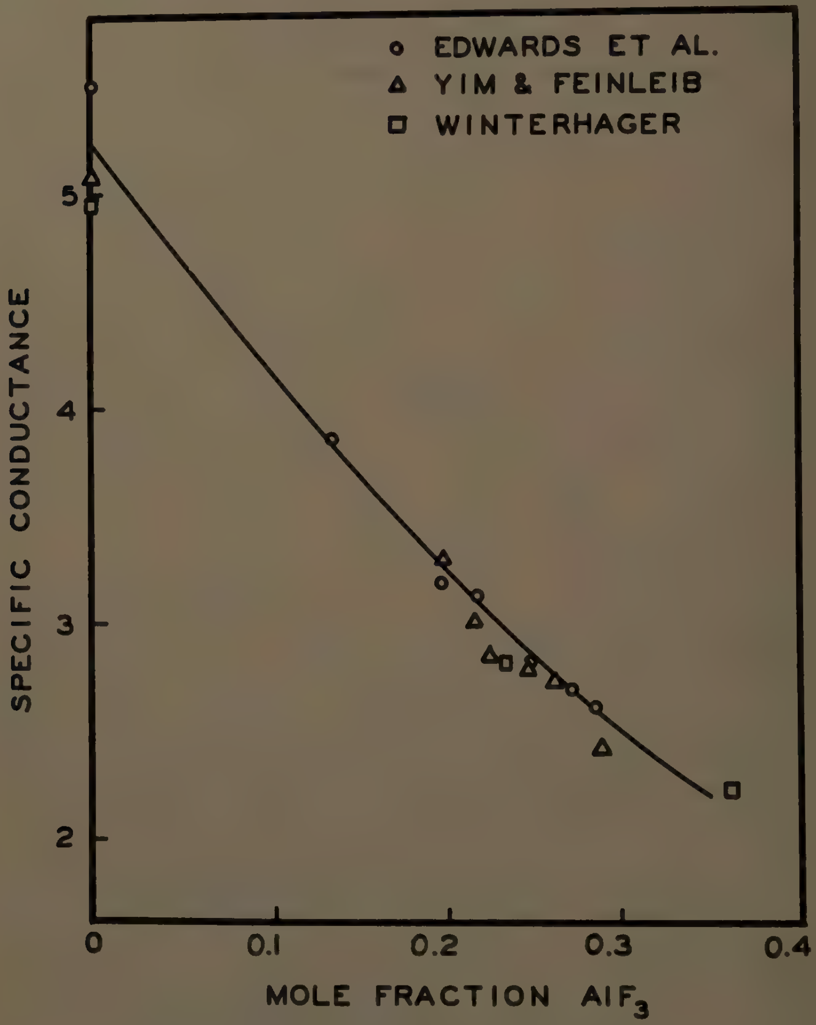

FIGURE 5. Electric conductivity of NaF-AlF$_3$ melts.

soned that there is a calculable probability that an anion and cation vacancy will occur together to form a paired vacancy, and if a sodium and a fluoride ion move into such a paired vacancy together, in opposition, if necessary, to the electric field gradient, it will constitute a gross diffusion of material that does not contribute to the electric conductivity, which results from single ion vacancy diffusion only. Borucka *et al.*[10] were able to show that the self-diffusion of sodium chloride could be explained in this way without violation of the Nernst-Einstein relation. It was shown in the present case that reasonable conductivities for sodium and fluoride were obtained ($\Lambda_{Na^+} = 96.4$, $\Lambda_{F^-} = 67.5$) in the ratio required by the Stokes-Einstein relation if, for 68 per cent of the time, Na^+ and F^- were diffusing via single ion vacancies and 32 per cent of the time by double ion vacancies. It also was shown that this situation would result from a vacancy of about 6 per cent of the total cation and anion sites.

It was not necessary to employ the "hole" theory of melts to explain the data in the cryolite system, however, and, in an alternative mechanism, it was shown that the conductivity could be explained if sodium fluoride were dimerized partially in the melt, thus

$$Na_2F_2 = 2NaF$$

with the dimers completely ionized to NaF_2^- and Na^+ and the monomers completely ionized to Na^+ and F^-. According to this scheme, correlation between melt compositions and conductivities was obtained with a degree of dissociation of the dimer of 0.69 at 1000° C. Equivalent conductances for sodium and fluoride of 83.8 and 58.7 were derived.

Having the equilibrium constants for the dissociation of cryolite to NaF and $NaAlF_4$ and for the dimerization of the NaF, the concentrations of Na^+ and F^- at the cryolite composition were calculated. From the equivalent conductance of Na^+ and F^- derived above, transference numbers of $t_{Na^+} = 0.88$, and $t_{F^-} = 0.12$ at the cryolite composition were obtained. This should be compared to approximately $t_{Na^+} = 0.95$ and $t_{F^-} = 0.05$ that were estimated from the transference experiments in alumina-cryolite melts after estimating the effect of the alumina on the behavior of pure cryolite.

It will be remembered that this agreement was obtained only by making the assumption in the calculations that sodium fluoride is dimerized partially. There is other substantiation for this. In Grjotheim's calculations of the $NaF-AlF_3$ phase diagram, the fit of the liquidus boundary on the sodium fluoride side of the eutectic was obtained by assuming a heat of fusion for sodium fluoride of 6.95 kcal./mole. Subsequently, however, calorimetric heat of fusion of 8.03 kcal./mole was reported.[11] At the time, this discrepancy was not resolved. It now appears that good agreement between the calculated and observed liquidus boundary on the sodium fluoride side of the eutectic can be obtained if the compositions determined by Frank and Foster or Grjotheim are modified to include a certain amount of sodium fluoride dimer in the melt. The difference between the calorimetric and the estimated heat of fusion of sodium fluoride is a heat of dissociation of the dimer to the monomer in the liquid. In the calculations of the various possible mechanisms of conductance in these melts, it was determined that good correlation could be obtained if pure sodium fluoride were 32 per cent dimerized at 1000° C. If the difference between the calorimetric and estimated heat of fusion of sodium fluoride (1.08 kcal./mole) represents the heat effect in dissociating 69 per cent of the dimers, the heat of dissociation per mole would be about 3.5 kcal.

In conclusion, it is seen that, in order to correlate various kinds of experimental data on cryolite and other compositions in the NaF-AlF_3 system, it is necessary to assume extensive dissociation into simpler compounds. Information on electric conductivity and transport, melt densities, cryoscopic lowering, and vapor pressures is best explained by dissociation of cryolite to NaF and $NaAlF_4$. A refinement of the general theory is required to get very good agreement of the cryoscopic lowering and electric conductivity, if it is assumed that the Stokes-Einstein relation must be obeyed in the latter. The suggested refinement is that sodium fluoride is substantially dimerized in the melt.

Summary

Information on electric conductivity, transport, melt densities, melt constitution, and vaporization processes in the NaF-AlF_3 system have been considered in an effort to obtain correlation. The simple picture of cryolite dissociating to sodium and aluminum fluorides and these ionizing to Na^+, Al^{+++}, and F^- ions is not acceptable. Dissociation to NaF and $NaAlF_4$ can be correlated to molten densities, cryoscopic lowering, and vaporization processes. Correlation with electric conductivity and transport data also is obtained if the sodium fluoride further is considered to be dimerized partially in the melt. The best information yields the following values: cryolite composition at 1000° C., 65.2 per cent Na_3AlF_6, 13.9 per cent NaF, 20.9 per cent $NaAlF_4$, by weight; vapor pressures of Na_3AlF_6, NaF and $NaAlF_4$ in the ratio 5:1:30; pure, molten NaF is 31 per cent dimerized at 1000° C.; equivalent conductances of Na^+ and F^- are 83.8 and 58.7, at the cryolite composition.

References

1. Grjotheim, K. 1956. Norske Videnskas Selskabs Skrifter. No. **5**.
2. Frank, W. B. & L. M. Foster. 1957. J. Phys. Chem. **61:** 1531–1536.
3. Edwards, J. D., C. S. Taylor, L. A. Cosgrove & A. S. Russell. 1953. J. Electrochem. Soc. **100:** 508.
4. Frank, W. B. & L. M. Foster. 1959. Constitution of Cryolite and NaF-ALF_3 Melts. Intern. Symposium on the Physical Chem. Process Metallurgy. Pittsburgh, Pa.
5. Howard, E. H. 1954. J. Am. Chem. Soc. **76:** 2041.

6. Ginsberg, H. & A. Böhm. 1957. Z. Electrochem. **61:** 315.
7. Yim, E. W. & M. Feinleib. 1957. J. Electrochem. Soc. **104:** 622–626.
8. Winterhager, H. & L. Werner. 1956. Forschungsber. Nr. 31 Wirtsch. u. Verkehrsmin. Nordrk-Westf.
9. Frank, W. B. & L. M. Foster. 1959. The Electrical Conductivity of Cryolite and NaF-AlF_3 Melts. Symposium on Molten Salts. 135th Meeting Am. Chem. Soc. Boston, Mass.
10. Borucka, A. Z., J. O'M. Bockris & J. A. Kitchener. 1957. Proc. Roy. Soc. London. **241:** 554–567.
11. Kelley, K. K. & C. J. O'Brien. 1957. J. Am. Chem. Soc. **79:** 5616–5618.

ABSORPTION SPECTRA OF FUSED-SALT SOLUTIONS

G. Pedro Smith and Charles R. Boston
Metallurgy Division, Oak Ridge National Laboratory, Oak Ridge, Tenn.*

Studies have been made of the ultraviolet absorption spectra of the oxy-anions nitrate, chromate, and nitrite in a variety of fused-salt mixtures. These oxy-anions are representative of an important class of inorganic anions in which covalent bonding is significant. Such ions have internal electronic transitions involving orbitals common to the entire ion. These transitions may have energies anywhere in the range from the visible to the vacuum ultraviolet and may have molar absorbancy indices of from less than 1 to greater than 10^4 liters/mole-cm.

The chromate, nitrate, and nitrite anions provide three distinctive symmetries ranging from the relatively high symmetry of the chromate ion to the low symmetry of the nitrite ion. These symmetries are tetrahedral (T_d) for chromate, planar-symmetrical (D_{3h}) for nitrate, and angular (C_{2v}) for nitrite. In crystals these structures have been confirmed by X-ray diffraction measurements and by some Raman and infrared spectra. For the nitrate ion, Raman spectral measurements on fused nitrates[1a-d] show that the D_{3h} symmetry is, at most, only slightly distorted in salt melts.

Spectral bands of the type considered here are sensitive to the medium in which the anion is dissolved; that is, for different solvent media the bands may shift in strength and in wave-length position. Such shifts arise from the perturbations of the anion orbitals by molecular neighbors. Substantial shifts may represent the formation of new molecular linkages such as the action of H^+ on NO_3^- to yield the HNO_3 molecule. When the perturbations are not excessive, it may be possible to correlate the measured spectral shifts with changes in neighbor-molecule configurations about a light-absorbing anion. It is very difficult to do this in a meaningful way for most solutions for which such shifts are observed—for example, for concentrated aqueous solutions—because the changes in configuration arise from complex solvation processes. However, fused salts with cations of rare-gas electronic configurations should provide uniquely simple liquid solutions with which to study the perturbations of light-absorbing anions by neighbor ions in which it may be possible to treat the perturbing effects of the cations as arising from their electrostatic fields. In order to apply such considerations to the spectra of nitrate, chromate, and nitrite ions in fused-salt media, it is necessary to show that the observed electronic bands are more or less mild perturbations of the familiar electronic transitions for these ions.

---

* Operated by the Union Carbide Corporation, New York, N.Y., for the United States Economic Energy Commission, Washington, D.C.

Previous Spectral Measurements

The low-energy end of the electronic absorption spectra of nitrate, chromate, and nitrite anions has been measured for a variety of nonfused-salt media. These studies show that, so long as strongly complexing cations are absent, the observed transitions persist in all solvent media and are perturbed only mildly from medium to medium. Although spectral measurements are available for fused-salt media that contain nitrate ions (but not chromate or nitrite ions), the results, taken as a whole, leave serious questions as to whether the characteristic electronic transitions persist in these media without profound modifications.

The observed electronic spectrum of the nitrate ion in nonfused-salt media consists of a weak lowest-energy band and a very strong second band. In dilute aqueous solutions these bands occur at 302 and 194 mμ with molar absorbancy indices of 6.4 and 12,000 liters/mole-cm., respectively.[2] Both bands also have been observed in crystalline KNO_3, where they occur at approximately 295 and 195 mμ, respectively.[3] The maximum of the second band seldom has been measured, but the first band has been the subject of numerous investigations, including many investigations of concentrated aqueous solutions,[4] of a large number of crystalline nitrates,[5,6] and of organic solutions of inorganic nitrates.[7] In all cases, the first band is found to be about 300 mμ; where concentration was determined, the band was found to be quite weak, with a_M generally between 6 and 12. In all cases, the overlapping absorption edge of the strong second band was observed. In aqueous solutions high concentrations of strongly polarizing cations such as Li^+ and Ca^{++} and of some anions such as Cl^- are especially effective in shifting the first band maximum toward shorter wave lengths and higher molar absorbancy indices, whereas high concentrations of K^+ ions have only a slight effect.

The measurements of Maslakowez[3] indicate that the ratio of the strength of the first band to that of the second is very much smaller for crystalline KNO_3 than for all aqueous solutions. This would indicate a strong perturbation, but whether of the first or the second or both bands remains unknown.

Studies of the electronic absorption spectra of fused nitrates are limited. As early as 1916, Schaefer[8] determined the profile of the ultraviolet spectrum of a KNO_3 melt and found the first band at about 300 mμ, followed by a steeply rising absorption edge at shorter wave lengths. His relative profile is in general agreement with our results for pure fused KNO_3. Keenan[9] has reported the ultraviolet spectrum of fused ammonium nitrate. He found the first nitrate band in the vicinity of 300 mμ with an approximate a_M value of 3 followed, at shorter wave lengths, by a composite band with at least 3 maxima not much stronger than the 300-mμ band. This second band is unlike any nitrate spectrum previously measured. The spectral region for which the weak, multipeak band is reported, 220 to 260 mμ, is in all other instances dominated by a very strong absorption edge. Sakai[10] and Sundheim and Greenberg[11] have measured ultraviolet absorption edges for several fused alkali metal nitrates and ammonium nitrate that were characterized by single wave-length values. The absorption edges for $CsNO_3$ and $RbNO_3$ reported by Sakai are displaced substantially and significantly toward higher energies compared with those for $LiNO_3$ and $NaNO_3$ reported by Sundheim and Greenberg. Furthermore, measurements of Sakai[10] on the absorption edge for NH_4NO_3 cannot be reconciled with the work of Keenan because Sakai reports the strong absorption edge occurring at a wave length where Keenan finds the weak complex band occurring.

The electronic spectrum of the chromate ion in aqueous solutions shows 2 moderately strong maxima with molar absorbancy indices between 3000 and 5000 liters/mole-cm. The lowest-energy band is slightly stronger than the second band and has an absorption edge that extends into the visible and gives chromate crystals and solutions their distinctive yellow color. This spectrum is well known for aqueous solutions and has been recommended as an absorbance standard.[12] Schaumann[6] reports the first band maximum for crystalline K_2CrO_4 to lie at 365 mμ at room temperature. This is only slightly different from the aqueous solution value of 366 mμ. In recent research as yet undescribed in print R. A. Osteryoung* of Rensselaer Polytechnic Institute, Troy, N.Y., measured the first band of the chromate ion dissolved in the $LiNO_3$-KNO_3 eutectic and obtained a spectral profile that was very similar to ours.

The electronic spectrum of the nitrite ion in aqueous KNO_2 consists of a weak broad asymmetric band at about 360 mμ skewed toward short wave lengths and a very strong peak between 200 and 220 mμ with a shoulder due to a weaker band at slightly longer wave lengths.[3,4] In crystalline $NaNO_2$ at liquid nitrogen temperatures, it has been shown that there is a very weak band at about 300 mμ that is overlapped at higher temperatures by the 360-mμ band so that a single, skewed band results.[13] This very weak band must account also for the skewing of the first band for aqueous nitrites. The spectrum of crystalline KNO_2 at room temperature gives some indication of a similar very weak band between 260 and 290 mμ, and also indicates that the ratio of the strength of the 360-mμ band so that of the strong, 200-mμ band is much smaller than that for aqueous solutions.[3]

Experimental

The nomenclature and symbolism used in this paper are similar to those of Gibson.[12] However, in order to assign numerical absorption values to the spectrum of pure $LiNO_3$, the term molar absorbancy index, which Gibson carefully restricts to solutions, has been used. The molar absorbancy index of pure $LiNO_3$ was obtained by measuring log $1/T$ (T = transmittance) and subtracting corrections for light losses due to interfacial reflections and absorption by the cell and insert. A detailed description of these corrections will be published later.

---

* We acknowledge Osteryoung's generosity in allowing us to examine his results prior to publication.

The high-temperature spectrophotometer and the general procedure for measuring spectra have been described.[14] In the measurements given here, stoppered cells with flowing inert atmospheres rather than sealed cells were used. The path lengths used in this work were from 0.006 to 0.02 cm., depending on the absorbance of the fused salt, so as to keep the measurements within the limits set by stray light in the spectrophotometer.

The LiCl-KCl eutectic was prepared as previously described.[14] Pure LiCl was prepared by a similar procedure, except that a fused-silica apparatus replaced the Pyrex apparatus because of the high melting point of LiCl. The remaining pure components, KNO_2, KNO_3, $LiClO_4$, and K_2CrO_4, were recrystallized reagent-grade material and oven-dried prior to use.

Pure $LiNO_3$ and the $LiNO_3$-$LiClO_4$ and $LiNO_3$-LiCl mixtures were weighed and loaded into the optical cells in a dry box; the cells remained stoppered after removal from the dry box. Some water remained in the $LiClO_4$ after oven drying; this was removed by bubbling argon through the $LiNO_3$-$LiClO_4$ melt in the stoppered cell. The weight change accompanying this dehydration was determined by weighing the stoppered cell and its contents before and after dehydration. The remaining mixtures were prepared by weighing the solvent salt, KNO_3 or LiCl-KCl eutectic, and loading it into the cell in a dry box. Later, weighed samples of the solute, KNO_2 or K_2CrO_4, were added to the molten solvent by momentarily opening the cell while a strong flow of argon was passed as previously described.[14]

Each of three of the reference substances for the mixtures $LiClO_4$, KNO_3, and the LiCl-KCl eutectic was measured at the same temperatures as the mixtures. The fourth reference substance, LiCl, melts much above the temperature at which the nitrate ion in $LiNO_3$-LiCl mixtures decomposes. Consequently, the LiCl-KCl eutectic was used as an artificial reference. Over the wave-length range covered the LiCl-KCl eutectic should not differ much from the spectrum of LiCl plus cell. The first band of the chloride ion is sufficiently far in the ultraviolet so that its low-energy edge in the presence of lithium ions or mixed lithium and potassium ions makes a relatively small contribution in the neighborhood of the first band of the nitrate ion. Measurements on $LiNO_3$ in $LiClO_4$, $LiNO_3$ in LiCl, and KNO_2 in KNO_3 were made at moderate to large concentrations of $LiNO_3$ and KNO_2. Furthermore, in the case of the KNO_2-KNO_3 mixture the solvent, KNO_3, absorbs significantly throughout the range studied. Consequently, the KNO_3 reference curve for KNO_2-KNO_3 was corrected for dilution of the solvent nitrate ions by nitrite ions. The method for doing this was to scale down the part of the pure KNO_3 plus the cell-and-insert curve due to KNO_3 absorption by an amount proportional to the decrease in KNO_3 concentration. The chromate spectrum was measured at concentrations so low that the reference curves consisting of solvent plus cell and insert were not corrected for dilution effects.

Density values for the various fused-salt mixtures were required for assigning concentrations. For LiCl-KCl mixtures the density values of Van Artsdalen and Yaffee[15] were used. All other density values were taken from the measurements of G. P. Smith, G. F. Petersen, and W. M. Ewing (to be published). The concentrations of K_2CrO_4 in KNO_3 and in the LiCl-KCl eutectic were considered to be sufficiently small so that the density of the solvents was taken as the density of the solutions.

For the spectra reported here absorbancy values were reproducible to within 2 per cent, while the total of all errors associated with path length and concentration may be as great as 20 per cent except for $LiNO_3$. The spectrum for $LiNO_3$ is based on repeated measurements of all quantities that enter into the spectral computations and is assigned an error in molar absorbancy index of less than 5 per cent.

Results and Discussion

Three nitrate spectra are shown in FIGURE 1. They are pure $LiNO_3$ at 367° C., $LiClO_4$-70.1 mole per cent $LiNO_3$ at 325° C., and LiCl-71.5 mole per cent $LiNO_3$ at 366° C. All three spectra have the characteristic nitrate profile with a weak lowest-energy band and the steeply rising absorption edge of the second band. The coordinates of the first band maxima for these spectra are 288 mμ and 16.7 liters/mole-cm. for pure $LiNO_3$, 285 mμ and 18.2 liters/mole-cm. for the $LiClO_4$-$LiNO_3$ mixture, and 288 mμ and 19.9 liters/mole-cm. for the LiCl-$LiNO_3$ mixture. These values are to be compared with the following for nonfused-salt solutions: 292 mμ and approximately 8 liters/mole-cm. for 11.8 *N* aqueous $LiNO_3$,[4] approximately 288 mμ and approximately 11.2 liters/mole-cm. for dilute, aqueous KNO_3 plus 13.9 *N* LiCl,[4] approximately 295 mμ and 8.5 liters/mole-cm. for $LiNO_3$ in *t*-butyl alcohol,[7] and 295 mμ for crystalline $LiNO_3$ (powder reflection spectrum).[5] The displacements of these maxima from that for the nitrate ion in dilute, aqueous solutions (302 mμ and 6.4 liters/mole-cm.) are all in the same direction.

In addition to the nitrate spectra illustrated in FIGURE 1, measurements were made of the spectrum of the nitrate ion in sodium, potassium, rubidium, and cesium nitrates, in a number of binary mixtures of alkali nitrates, and of alkaline earth and alkali nitrates, in the reciprocal system $LiNO_3$-KCl, for which a composition on the $LiNO_3$-LiCl binary is shown in FIGURE 1, and in the binary system $LiNO_3$-$LiClO_4$, for which a composition is shown in FIGURE 1. These measurements were made at temperatures ranging from the melting points of the mixtures up to temperatures at which decomposition was just appreciable. Space does not permit a presentation of these data or an assessment of their significance. This is deferred to subsequent publications. However, a few comments will be made to indicate the substantial evidence that bears on the general subject of this report.

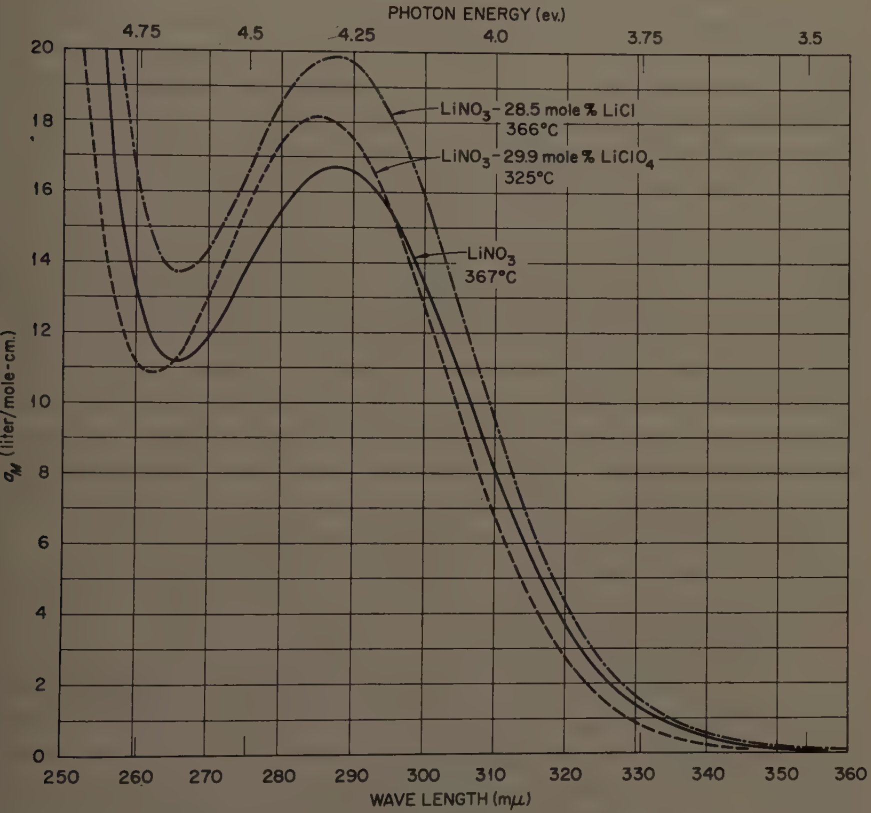

FIGURE 1. Spectrum of the nitrate ion in fused lithium nitrate and in two binary fused-salt mixtures.

The profile of the nitrate spectrum in these fused-salt mixtures consists of the weak, lowest-energy band and the absorption edge of the second band as illustrated by FIGURE 1. The latter absorption edge was followed up to values much greater than the lowest-energy band maximum for potassium, rubidium, and cesium nitrates. No evidence was found for the kind of weak bands at high energies that Keenan[9] reports for fused NH_4NO_3.

The absorption edges reported by Sundheim and Greenberg[11] for $LiNO_3$ and $NaNO_3$ melts may be accounted for in terms of our $LiNO_3$ and $NaNO_3$ spectra as lying near the foot of the low-energy edge of the first band. The numerical values and the failure to observe structural details at wave lengths shorter than the absorption edge are completely in line with the fact that a much longer optical path was used by these investigators than in the work reported here. Likewise, the absorption edges reported by Sakai[10] for $RbNO_3$ and $CsNO_3$, when compared with our measurements on these compounds, are explained readily as lying on the edge of the second nitrate band.

The amplitude, mean energy, and width of the lowest-energy band are shifted by changes in fused-salt composition to a greater extent than has been found for aqueous solutions, but these shifts are not such as to destroy in any way the identity of the characteristic nitrate spectrum. This conclusion is backed by detailed, quantitative analyses of the nitrate spectral profile as a function of photon energy for the alkali nitrates to be reported later.

There are small profile shifts induced by temperature changes, but the shift in mean energy is relatively small, and changes in the integrated molar absorbancy index per 100° C. are virtually nil.

The shifts in spectral parameters induced by changes in fused-salt composition correlate in a quantitative way with atomic parameters of neighbor ions in the melt. We illustrate this by a single example. The characteristic "blue shift" in the mean energy of a $n \rightarrow \pi^*$ transition in an organic compound dissolved in solvents of increasing polarity has a striking counterpart in fused alkali and alkaline earth nitrates for which the mean transition energy is found to decrease linearly with decreasing cationic potential.

It is concluded that the spectral profile of fused nitrates in the neighborhood of the first band is that which is characteristic of nitrate solutions in nonfused-salt media subject to mild perturbations.

It is mentioned in passing that studies also have been made of the effect that the cations Ag(I), Cd(II), Tl(I) and Pb(II) have on the nitrate profile. This effect cannot be described as a small perturbation, so that the interaction between these ions and NO_3^- involves a stronger coupling than is the case with the rare-gas configuration cations. This result is in agreement with recent Raman spectral studies of fused $AgNO_3$.

The spectrum of 2.48 M KNO_2 in fused KNO_3 at 342° C. is shown in FIGURE 2. In this spectrum are found the expected weak first band and the absorption edge of a second band at shorter wave lengths. The first maximum occurs at a wave length of 359 mμ with a molar absorbancy index of 30.6. These values are to be compared with those for dilute aqueous solutions of 366 mμ and 21.9 liters/mole-cm., respectively,[16] and with a maximum at about 360 mμ for crystalline[3] KNO_2. The existence of the very weak band at about 300 mμ is uncertain. Its presence may account for the flattening of the minimum in that wave-length region. Inasmuch as the nitrate solvent absorbs strongly near 300 mμ and the nitrite solute only weakly, this portion of the spectrum is the least accurately known.

Further measurements will be made at higher nitrite concentrations in order to determine more exactly the profile of the spectrum at about 300 mμ.

It is concluded that the lowest-energy band of the characteristic nitrite spectrum is found for the above KNO_2-KNO_3 mixture. The band maximum occurs at a wave length very close to that for crystalline KNO_2 at room temperature. The band strength, compared with that for aqueous solutions, is significantly increased.

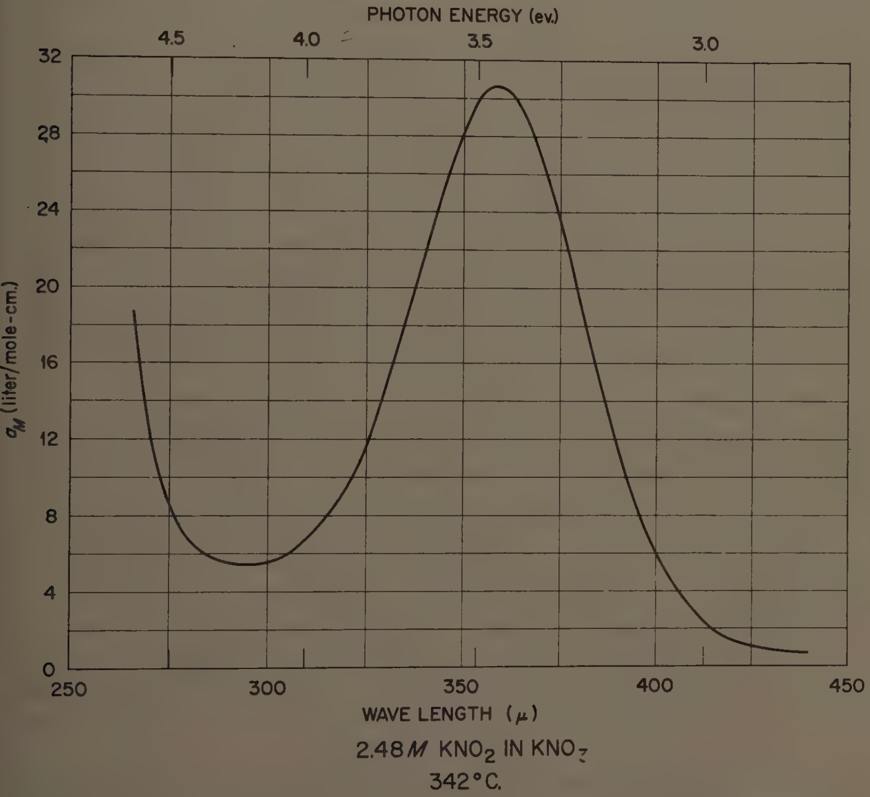

FIGURE 2. Spectrum of the nitrite ion in a fused mixture of KNO_2 and KNO_3.

Chromate spectra are shown in FIGURE 3. They are for 0.0287 M K_2CrO_4 in KNO_3 at 362° C., for 0.0189 M K_2CrO_4 in the LiCl-KCl eutectic at 370° C., and for a dilute, alkaline, aqueous solution plotted from the data of Haupt reported by Gibson.[12] The two principal bands of the characteristic near-ultraviolet spectrum are observed for the LiCl-KCl solvent. These have maxima at 371 mμ and 3080 liters/mole-cm., and 269 mμ and 2850 liters/mole-cm., respectively. Only the first band and a part of the second could be measured for the KNO_3 solvent because of the strong nitrate absorption at shorter wave lengths. The first band for the KNO_3 solvent occurred at 371 mμ and 3380 liters/mole-cm. These values are to be compared with those for dilute, alkaline, aqueous solutions for which the coordinates of the maxima are 372 mμ and 4820 liters/mole-cm. and 275 mμ and 3700 liters/mole-cm., respectively.

Measurements also have been made on dilute solutions of the chromate ion in the fused nitrates of lithium and cesium at several temperatures and concentrations. The spectral profiles in these cases closely follow those for the fused-salt solutions shown in FIGURE 3. In general, the first band occurs with only small shifts due to changes in solvent composition. These shifts are small enough and expected differences in refractive indices of the solvent media are large enough so that it cannot be said to what extent, if any, these shifts reflect corresponding changes in transition probability. Auxiliary measurements and computations are now in progress to determine this.

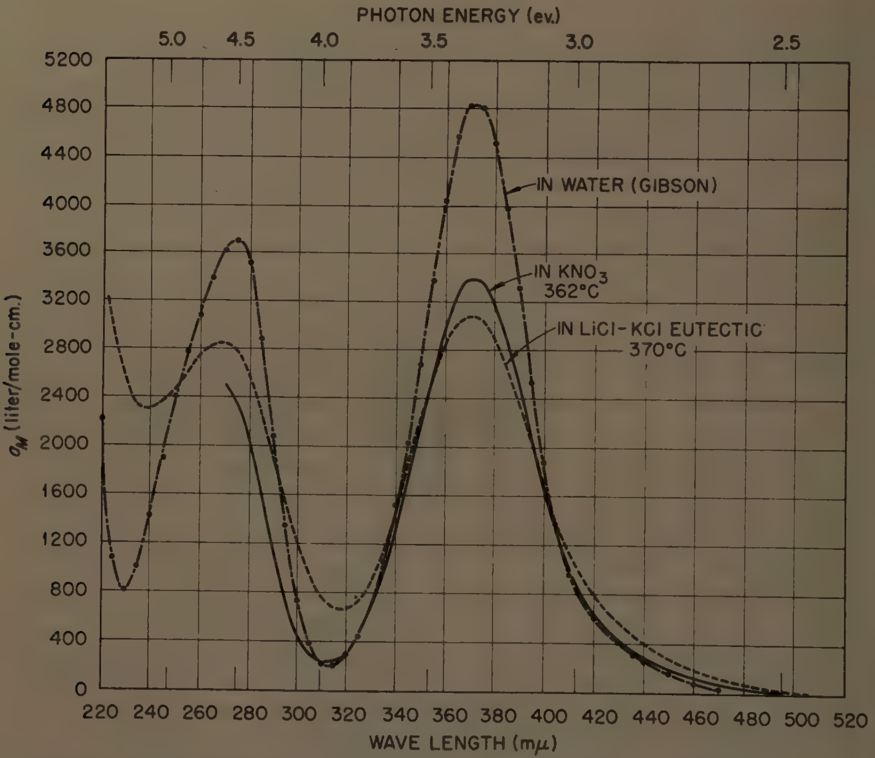

FIGURE 3. Spectrum of the chromate ion in dilute solutions of K_2CrO_4 in alkaline water, fused KNO_3, and the fused LiCl-KCl eutectic. The aqueous spectrum is plotted from data given by Gibson.[12]

The bands that were found for fused-salt solutions are undoubtedly those observed for aqueous solutions; the wave lengths agree very closely and the band strengths are of the same order of magnitude. Nevertheless, the fused salts have the effect of significantly diminishing the band maxima as compared with aqueous solutions.

One purpose of this report has been to outline some recent measurements of optical transitions in a special class of fused salts, namely, those with cations of rare-gas electronic configurations and complex oxy-anions. Such melts should be the fluid counterpart of the classic ionic crystal. In addition, some of the anions were a special variety of light absorber. They were shown to display in the melts their characteristic internal absorption spectra mildly disturbed by neighboring ions. These mild disturbances or shifts indicate a degree of relative change in ion polarization for the ground or excited states, but by their mildness ensure that this degree is small. Furthermore, they reflect differences in the ion configurations and strengths about an anion in different melts. This fact permits in principle the use of spectral shifts to relate spectral theory to information concerning ion configurations and the reverse.

Studies of this kind have a close relation to other fields of fused-salt research. The measurement of spectral shifts should permit a determination of the relative extent to which an anion of given size and charge prefers to surround itself with one type of cation rather than another in a reciprocal mixture. We refer here not to the strong and specific ion associations which yield complex ions, but to statistical associations. This phenomenon is of importance in understanding equilibrium behavior. In addition, certain electronic transitions should be quite sensitive to the statistical prevalence of particularly asymmetric configurations of ion neighbors. These asymmetric configurations are related intimately to kinetic processes in a melt.

References

1a. Nadungadi, T. M. K. 1938. Proc. Indian Acad. Sci. **8A:** 397; 1941. *Ibid.* **14A:** 242.
1b. Moses, P. A. 1939. *Ibid.* **10A:** 71.
1c. Rao, B. S. R. 1939. *Ibid.* **10A:** 167.
1d. Gross, E. F. & V. A. Kolesova. 1952. Akad. Nauk. S. S. S. R., Pamyati S. I. Vavilova. : 231.
2. Scheibe, G. 1926. Ber. deut. chem. Ges. **59:** 1321.
3. Maslakowez, I. 1928. Z. Physik. **51:** 696.
4. van Halban, H. 1928. Z. Elektrochem. **34:** 489.
5. Berton, A. 1941. Compt. rend. **213:** 653.
6. Schaumann, H. 1932. Z. Physik. **76:** 106.
7. Katzin, L. I. & E. Gebert. 1950. J. Am. Chem. Soc. **72:** 5455. These authors give the spectrum of $LiNO_3$ in *t*-butyl alcohol.
8. Schaefer, K. 1916. Z. anorg. u. allgem. Chem. **97:** 285.
9. Keenan, A. G. 1957. Kinetics and Mechanisms in Ionic Melts: Final Report, Sept. 1954–Sept. 1957; Air Force Office Sci. Res., Project No. Chem. 40–18, Contract No. AF 18(600)-1148; Ill. Inst. Tech. Chicago, Ill.
10. Sakai, K. 1957. J. Phys. Chem. **61:** 1131.
11. Sundheim, B. R. & J. Greenberg. 1958. J. Chem. Phys. **28:** 439.
12. Gibson, K. S. 1949. Natl. Bur. Standards Circular. **484.**

13. Trawick, W. G. & W. H. Eberhardt. 1954. J. Chem. Phys. **22:** 1462.
14. Boston, C. R. & G. P. Smith. 1958. J. Phys. Chem. **62:** 409.
15. Van Artsdalen, E. R. & I. S. Yaffee. 1955. J. Phys. Chem. **59:** 118.
16. Scheibe, G. & W. Frömel. 1937. Molekülspektren von Lösungen and Flüssigkeiten. Sec. IV. **9:** 162. *In* Hand- und Jahrbuch der Chemischen Physik. A. Eucken and K. L. Wolf, Eds. Akademische Verlagsgesellschaft. Leipzig, Germany.

OXIDATION STATES OF THE ELEMENTS AND THEIR POTENTIALS IN FUSED-SALT SOLUTIONS: THE ACTINIDE ELEMENTS*

Dieter M. Gruen, R. L. McBeth, J. Kooi,† W. T. Carnall
Argonne National Laboratory, Lemont, Ill.

Fused salts, the largest class of nonaqueous inorganic solvents, are extremely versatile media in which to carry out chemical reactions. The large number of technological applications involving fused salts attests this versatility.

Until recently, however, very little information was available concerning the oxidation states of the elements and their potentials in fused-salt solutions. This situation is gradually being remedied. Increasingly, aqueous-solution techniques are being adapted, with encouraging results, to studies of fused-salt systems. It is to be hoped that these investigations will bring about a much better understanding of fused-salt-solution chemistry in the not-too-distant future.

This paper summarizes current knowledge concerning the oxidation states and potentials of the actinide elements in fused nitrates and chlorides. In particular, recent spectrophotometric studies of plutonium and americium solutions in fused chlorides are discussed. All potentials are expressed relative to the Ag(I)-Ag(O) potential (on the mole fraction scale) at 450° C. in chloride melts. No information on potentials of the actinides in nitrate melts is presently available.

Actinium. No measurements have been reported on actinium in fused salts. It is to be presumed that the +3 oxidation will be exhibited exclusively. The Ac(III)-Ac(O) potential would be expected to be more negative than the U(III)-U(O) potential, which is −1.61 v. in LiCl-KCl eutectic.

Thorium. Inman *et al.* have measured the Th(IV)-Th(O) potential in LiCl-KCl eutectic. The measurements are discussed in detail in their paper, elsewhere in these pages. These workers found no evidence for the formation of Th(II) in chloride melts, contrary to a claim recently made by Smirnov and Ivanovskii.[1] In an effort to obtain evidence for Th(II), we dissolved 1 gm. $ThCl_4$ in 10 gm. of LiCl-KCl eutectic contained in a single-crystal sapphire crucible and placed a piece of Th metal in contact with the melt at 500° C. for 4 hours. There was no change in the weight of the Th metal nor any visual change in the color of the melt, as would have been expected had the reaction $Th + ThCl_4 = 2ThCl_2$ occurred. The

---

* The work reported in this paper was performed under the auspices of the United States Atomic Energy Commission, Washington, D.C. It is the first of a series of papers on the oxidation states of the elements and their potentials in fused-salt solutions.

† On leave from Reactor Centrum Nederland, Amsterdam, Netherlands.

results described by Inman *et al.* in their presentation, as well as the results obtained at our laboratory, indicate that Th(II) at low concentrations is not stable in chloride melts at temperatures below 500° C.

In other experiments, we treated $ThCl_4$ with $LiNO_3$-KNO_3 eutectic at 160° C. A precipitate formed, and NO_2 fumes were evolved. We have observed similar behavior with $CeCl_4$ and $PuCl_3$.[2] It has long been known that $Ce(NO_3)_4$ is less stable thermally than the nitrates of the other rare earths,[3,4] and the behavior of $ThCl_4$ and $PuCl_3$ in nitrate melts indicates that $Th(NO_3)_4$ and $Pu(NO_3)_4$ are also unstable. ($PuCl_3$ is presumed to undergo oxidation to the IV state prior to the formation of the precipitate.) The Th and Pu precipitates which are formed are probably oxides.

Protactinium. No measurements have as yet been reported on protactinium solutions in fused salts. The tendency for Pa to hydrolyze makes for great difficulties in studying its aqueous-solution chemistry. It is likely that these difficulties can be largely overcome in fused-salt solutions. Such media may therefore become useful for chemical studies of this element. In water, the IV and the V oxidation states are known, the V state being the more stable. It has been suggested[5] that the PaO_2^+ ion is the prototype of the oxygenated pentavalent ions of U, Np, Pu, and Am.

In chloride melts both the IV and V states of Pa should be stable. Although $PaCl_5$ has been prepared in the dry state,[6] it is likely that only an oxygenated species of Pa(V) will be found in chloride melts. Unoxygenated species of U(V) and Np(V) have not been observed in chloride melts, presumably because at the melt temperatures dissociation to U(IV) [or Np(IV)] and Cl_2 occurs. Probably, Pa(V) will exist in the form of oxygenated ions of the type PaO_2^+, while ions of the type $PaCl_6^=$ will be found for the IV state. Such behavior would be analogous with the behavior of U, Np, and Pu in chloride melts. The Pa(III) state should be looked for in chloride melts.

In oxygen containing melts (for example, nitrates, sulfates, perchlorates) the Pa(V) state would be expected to be the only stable oxidation state.

Uranium. The III, IV, and VI oxidation states of uranium are stable in LiCl-KCl eutectic and have been identified spectrophotometrically.[7] The U(V) state is probably unstable in melts. In connection with this earlier work it was found that Al as well as U metal reduces U(IV) to U(III), while Mg metal reduces U(III) to U(O) in LiCl-KCl eutectic.[7] On the basis of these experiments and using the Al(III)-Al(O) and Mg(II)-Mg(O) potentials of Laitinen and Liu,[8] the U(III)-U(O) potential was predicted to lie between −1.16 v. and −1.92 v., while the U(IV)-U(III) potential was expected to be more positive than −1.16 v. In their presentation Gruen and Osteryoung show the U(III)-U(O) potential as −1.61 v. in LiCl-KCl eutectic. Preliminary measurements by Hill and Osteryoung have yielded the value −0.56 v. for the U(IV)-U(III) potential in the same melt.[9]

From available thermodynamic data on the free energies of formation of pure UCl_3 and UCl_4 Hill and Osteryoung calculate the U(IV)-U(III) redox potential to be −0.2 v.[9] The difference of 0.36 v. between the calculated and observed values may be in part due to stabilization of the U(IV) state through formation of $UCl_6^=$ complex ions in the melt.[7]

No information is as yet available concerning the U(VI)-U(IV) potential. Uranium in the VI state is present in chloride melts as the ion UO_2(II).[7] This being the case, reduction to the IV state should lead to formation of UO_2. It should be possible then to establish a reversible potential at an electrode composed of UO_2. Similar situations should be obtained with chloride or nitrate melts containing oxygenated ions of the other actinide elements.

In nitrate melts only the VI state of uranium has been observed, the lower oxidation states being oxidized rapidly to it.[7]

Neptunium. The III, IV, and V oxidation states of neptunium have been identified in LiCl-KCl eutectic by means of spectrophotometric techniques.[10] Neptunium (IV) is present as the ion $NpCl_6^=$. The absorption spectrum of Np(V) in the melt is characteristic of the ion NpO_2^+. An unoxygenated species of Np(V) in chloride has not yet been produced, nor has the VI state been observed as yet.

Neither the Np(IV)-Np(III) nor the Np(III)-Np(O) potential has been measured. The Np(III)-Np(O) potential would be expected to be more negative by about 0.1 v. than the U(III)-U(O) potential, while the Np(IV)-Np(III) potential should be somewhat more positive than the corresponding uranium couple. These predictions are based on the trends of the analogous potentials in aqueous solutions.[11]

In $LiNO_3$-KNO_3 eutectic, the Np(V) state has been observed spectrophotometrically.[2,10] Lower oxidation states of Np are oxidized to the V state in the nitrate melt. Again, it is the NpO_2^+ ion that is present.

Plutonium. The techniques employed for obtaining absorption spectra of plutonium solutions in LiCl-KCl eutectic were similar to those described for uranium[7] and neptunium[10] solutions. As a precautionary measure in working with Pu, a ducted glove box of special design was fitted to the top of the furnace compartment (see FIGURE 1 of Gruen and McBeth[7]) which houses the optical cells during a run. The samples were prepared as in previous work,[7] except that all manipulations were carried out in a vacuum-frame hood.

Pu(IV). Solutions of PuF_4 or of the double salt Cs_2PuCl_6 in LiCl-KCl eutectic are brown in color. Absorption spectra of these solutions taken at 400° C. are reproduced in FIGURE 1*B* and *C*. In FIGURE 1*A*, the spectrum of Cs_2PuCl_6 dissolved in 6 *M* HCl is given for comparison. It will be seen that there is a correspondence in gross features between the aqueous and the melt spectra. The bands in the melt tend to be somewhat broader, more lacking in detail, and of lower intensity compared to the aqueous-solution spectrum. Two features deserve mention: one is the absorption valley in the 900 to 1000 mμ region that occurs both in the water and in the melt spectra; the other feature to be observed is the strong absorption band that has its origin at about 640 mμ in the melt, and at about 580 mμ in concentrated HCl solution. This strong absorption is responsible for the brown color of Pu(IV) solutions and is presumably due to a charge-transfer process. The qualitative correlation of the long wave length edges of these bands in U, Np, and Pu solutions with the U(IV)-U(III) potentials will be discussed at the conclusion of this paper.

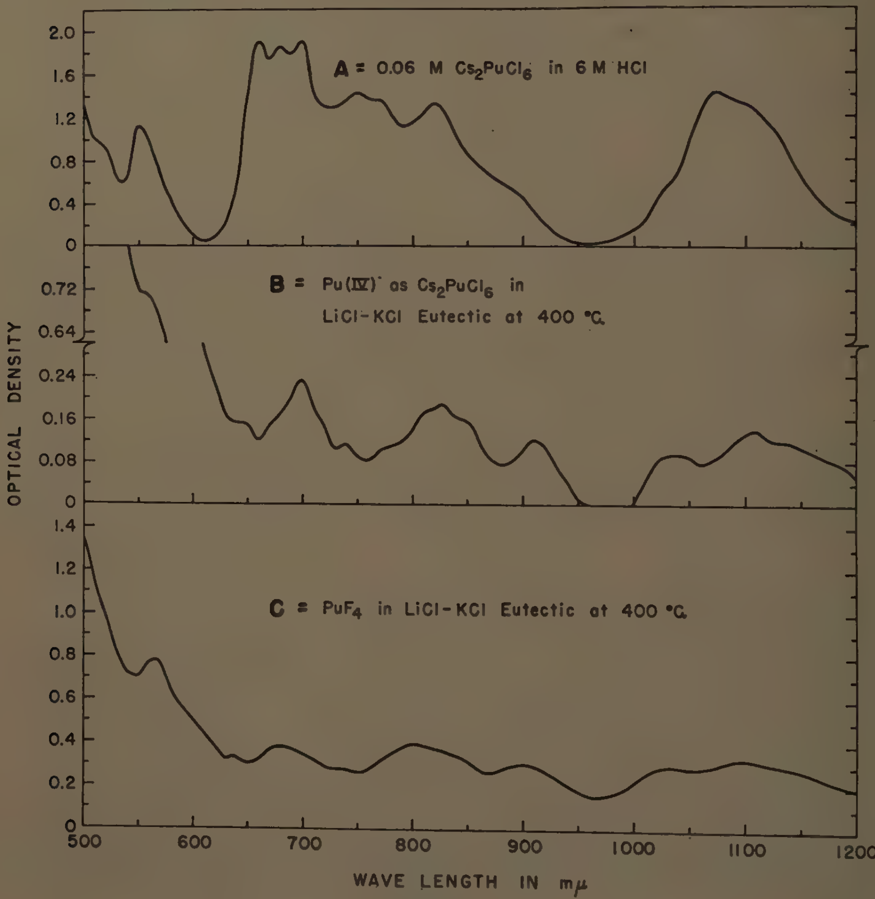

FIGURE 1.

In order to be certain that the Pu solutions contained only Pu(IV) and not a mixture of Pu(IV) and Pu(III), Cl_2 gas was bubbled through the melt for 10 min.; the spectrum was remeasured with results the same as those given in FIGURES 1*B* and *C*.

In other experiments it was found that Pu(IV) decomposes thermally to Pu(III) in the melt when the temperature is increased. The easiest way to demonstrate this is to heat a solution of Pu(IV) at 700° C. in a vacuum. The dark brown color gradually becomes lighter. The first change observable in the absorption spectrum during the decomposition is a marked decrease in the intensity of the charge transfer band that manifests itself as a shift of the band toward shorter wave lengths.

A preliminary study of the decomposition was made under 1 atmosphere of N_2 pressure, while the Pu(IV) solution was situated in the spectrophotometer furnace block. Spectra were taken in the temperature range 400 to 750° C. at 100° intervals, with the cell maintained at a fixed temperature for one half hour prior to taking a measurement. When a melt was employed that had not previously been saturated with Cl_2, decomposition began at 650° C. as evidenced by a shift to shorter wavelengths of the charge-transfer band. These shifts continued as long as the temperature was increased. When the temperature was lowered, the spectral changes retraced their path. The interpretation of these results is that Pu(IV) decomposes reversibly to Pu(III) and Cl_2. The chlorine produced during the decomposition remains dissolved in the melt and reacts with Pu(III) at lower temperatures to re-form Pu(IV).

The existence of Pu(IV) in chloride melts at temperatures up to 650° C. is evidence for the stabilization achieved through the formation of $PuCl_6^=$ complex ions. This finding is particularly interesting in view of the nonexistence of solid $PuCl_4$.

Pu(III). Solutions of Pu(III) were prepared by reducing Pu(IV) solutions with Al at 500° C. Solutions of Pu(III) in LiCl-KCl eutectic are blue just as are aqueous Pu(III) solutions. The spectrum of a Pu(III) solution in the melt is reproduced in FIGURE 2*C*. A solution of Pu(III) in concentrated HCl is shown for comparison in FIGURE 2*A*. The two spectra are extremely similar both in the position of the absorption maxima as well as in the half widths of the individual bands. The spectrum of a LiCl-KCl eutectic solution of PuF_3 is reproduced in FIGURE 2*B*.* This spectrum is very similar to that shown in FIGURE 2*C* at wave lengths longer than 550 mμ. At wave lengths shorter than 550 mμ, however, the absorption is much more intense than in the pure Pu(III) solution (FIGURE 2*C*), which is indicative of the presence of a small amount of Pu(IV). The spectrum thus shows that this particular sample of PuF_3 contained a small amount of PuF_4.

The Pu(III)-Pu(O) potential has recently been measured by Benz.[12] Extrapolation to 450° C. of these measurements which were carried out in KCl melts in the range 600° to 800° C. lead to an $E°$ value of -1.72 v. The Pu(IV)-Pu(III) potential has not yet been measured, but it should be more positive than either the U(IV)-U(III) or the Np(IV)-Np(III) potentials.

* The PuF_3 was kindly supplied by John Malm, Argonne National Laboratory.

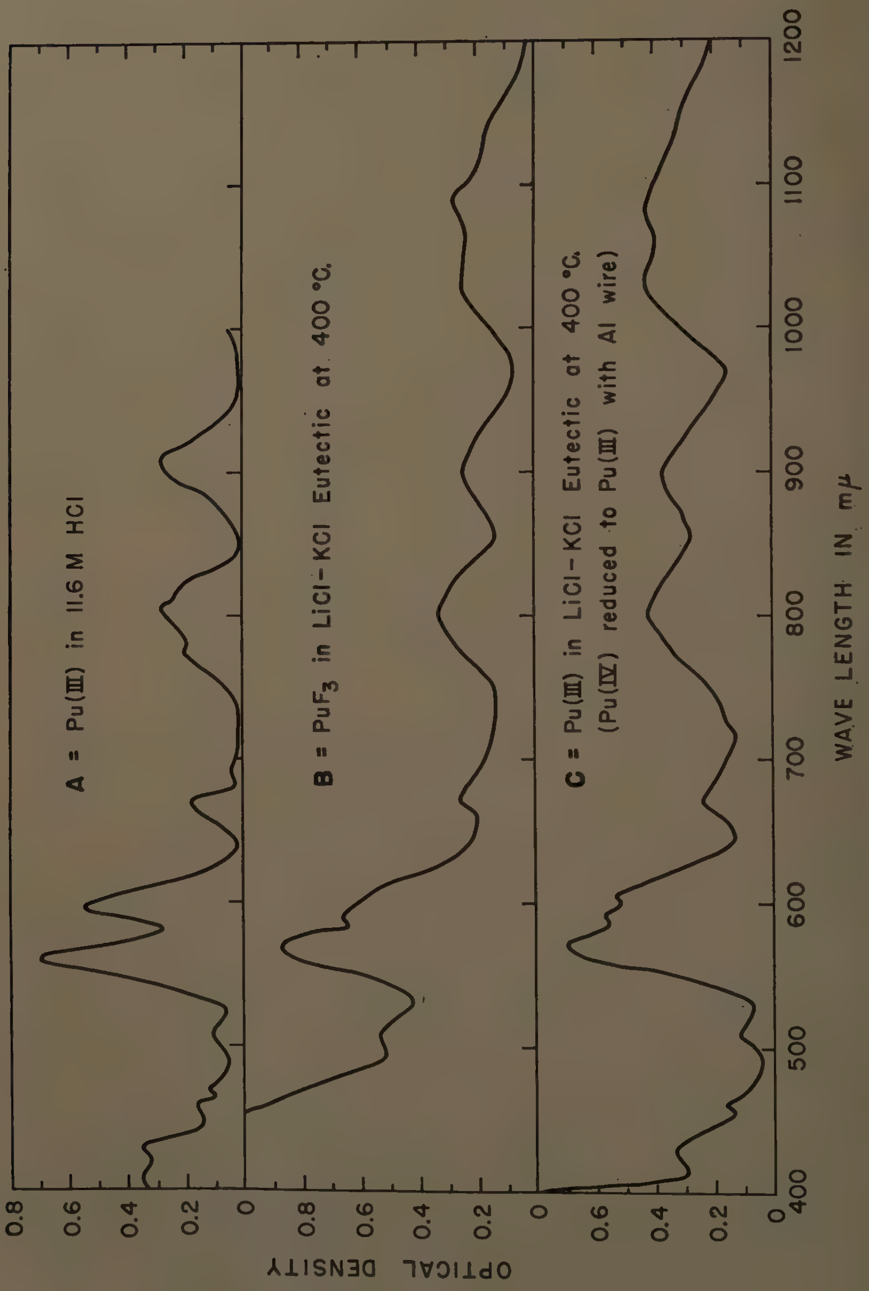
A = Pu(III) in 11.6 M HCl
B = PuF$_3$ in LiCl-KCl Eutectic at 400 °C.
C = Pu(III) in LiCl-KCl Eutectic at 400 °C.
(Pu(IV) reduced to Pu(III) with Al wire)
OPTICAL DENSITY
0.8
0.6
0.4
0.2
0
0.8
0.6
0.4
0.2
0
0.6
0.4
0.2
0
WAVE LENGTH IN mμ
400
500
600
700
800
900
1000
1100
1200

FIGURE 2.

Pu(VI). The Pu(VI) state has not yet been observed in chloride melts; however, it has been observed in nitrate melts.[2,10]

Americium. The III state of americium had previously been identified in nitrate melts,[2,10] but no studies had been made of americium solutions in chloride melts. About 5 mg. of $^{241}AmCl_3$ was dissolved in LiCl-KCl eutectic. The spectrum of this solution taken at 450° C. on a Cary Model 12 Spectrophotometer is reproduced in FIGURE 3*B*. An absorption spectrum of Am(III) in concentrated HCl is shown for comparison in FIGURE 3*A*. The similarity in the two spectra makes it clear that the melt spectrum contains Am in the III state. It was of interest to see if a lower oxidation state of Am could be produced in this melt analogous to the dipositive oxidation state of Eu. Pure Mg ribbon was introduced into a solution containing Am(III). In the course of about 15 min. and while maintaining the melt temperature at 450° C., the surface of the Mg ribbon turned black. Examination of the solution spectrum showed that the intensity of all the peaks had decreased by about 25 per cent. No other spectral changes were observed. It was tentatively concluded that the blackening of the Mg ribbon surface was due to partial reduction of Am(III) to Am metal and that the Am(II) state is not stable in the melt. The extrapolated potential of −1.72 v. for the Pu(III)-Pu(O) couple and the partial reduction of Am(III) to Am metal by Mg metal indicate that the Am(III)-Am(O) potential lies close to the Mg(II)-Mg(O) potential of −1.92 v.

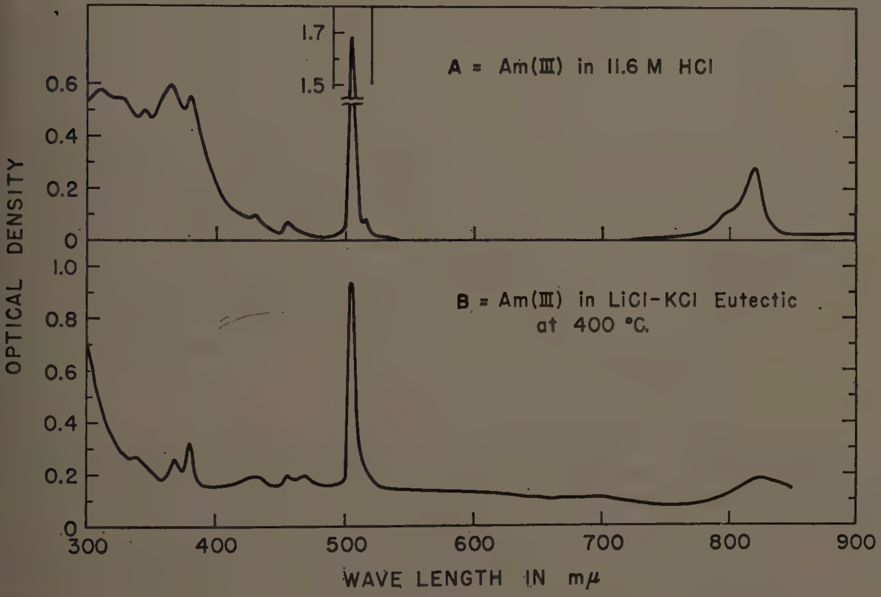

FIGURE 3.

In other experiments, Cl_2 gas was bubbled through the Am(III) solution in attempts to produce Am(IV). No change in the spectrum was observed after 30-min. treatment with Cl_2 gas, although this treatment is sufficient to oxidize Pu(III) to Pu(IV). It was concluded that the Am(IV) state is probably unstable in the chloride melt at 400° C. with respect to the formation of Am(III) and Cl_2. This is not unexpected, since the Am(IV) state is unstable in aqueous solutions as well.

Attempts to prepare higher oxidation states of Am (oxygenated ions) in chloride melts are being made.

Curium and the transcurides. The studies that have been carried out thus far and have been discussed in this paper have made it clear that the fused salt-solution chemistry of the actinides resembles in its chief features the aqueous-solution chemistry of these elements. With curium, the "actinide" character of the elements is very firmly established, and it would be surprising indeed if the trends observed thus far should not become increasingly pronounced. The M(III)-M(O) potentials should become increasingly more negative with each succeeding element. Curium and the rest of the actinides should exhibit only the tripositive oxidation state in melts with the exception of berkelium, where it is likely that the tetrapositive state ($BkCl_6^{=}$) will be observed in chloride melts.

The resistance to radiation damage of alkali-halide melts make them attractive solvents in which to study macroscopic amounts of the extremely radioactive transcuride elements.

Concluding Remarks

The absorption spectra of U(IV), Np(IV), and Pu(IV) solutions in LiCl-KCl eutectic reveal a progressive shift of the edge of the continuous absorption band toward longer wave lengths with increasing atomic number. Thus, the band in U(IV) solutions begins at 417 mμ, in Np(IV) solutions at 605 mμ, and in Pu(IV) solutions at 650 mμ. It is reasonable to associate the continuous absorption band with a charge transfer process which may be formally written as

$$M^{+4} + Cl^{-} \xrightleftharpoons{h\nu} M^{+3} + Cl^{\circ} \qquad (1)$$

Qualitatively, there should be a correlation between the potentials of the M(IV)-M(III) couples and the energy ($h\nu$) required for the process represented by EQUATION 1. On this basis, one would predict that the potentials measured in chloride melts should become more positive with increasing atomic number. Such a trend is observed in aqueous solutions,[11] and the spectral data are consistent with the existence of a similar trend in the chloride melts. No quantitative calculations of potentials can be made, of course, on the basis of the spectral observations.

The absorption spectral of trivalent actinide ions in LiCl-KCl eutectic, on the other hand, have intense absorption bands that occur at progressively shorter wave lengths with increasing atomic number.

Thus, the U(III) band edge occurs at 710 mμ, the Np(III) band at 546 mμ, the Pu(III) band at 410 mμ, and the Am(III) band at 329 mμ in LiCl-KCl eutectic. Stewart[13] observed similar bands in aqueous solutions of the trivalent actinides and suggested that they arise from allowed *f-d* transitions. The intense bands observed in the melt may be thought of similarly as due to *f-d* transitions. (In a particular melt, however, these bands occur at somewhat lower energies than in aqueous solutions. Complexing, which would be more pronounced in a chloride melt, for example, could well be responsible for lowering the energy of the *f-d* transition.) For a particular solvent, the shift toward higher energies of the *f-d* transitions with increasing atomic number is undoubtedly associated with the stabilization of the *f* electrons.

Summary

Information of the oxidation states and potentials of the actinide elements in fused nitrates and chlorides and chlorides is summarized.

Recent work on the absorption spectra of Pu and Am in LiCl-KCl eutectic is presented. These experiments have resulted in the identification of the III and IV states of Pu and of the III state of Am in molten LiCl-KCl eutectic.

Acknowledgments

We thank D. L. Hill and R. A. Osteryoung of Rensselaer Polytechnic Institute, Troy, N.Y. for making available to us their report on "Chemical Behavior of U and Th in Fused Salts"[9] prior to its publication.

References

1. Smirnov, M. V. & L. E. Ivanovskii. 1957. Zhur. Fiz. Khim. **31:** 801.
2. Gruen, D. M., P. Graf & S. Fried. 1957. Spectrophotometric and chromatographic studies of actinide ions in fused salts. Proc. 7th ICPAC. Paris, France.
3. Dennis, L. M. & W. H. Magee. 1894. Z. Anorg. Chem. **7:** 240.
4. Johnson, R. W. & E. H. Olson. AEC Research Report No. ISC-1069.
5. Welch, G. A. 1953. Nature. **172:** 458.
6. Elson, R. E. 1954. The chemistry of protactinium. Chap. 5. p. 103. *In* The Actinide Elements. G. T. Seaborg and J. J. Katz, Eds. Natl. Nuclear Energy Ser. Div. **IV:** 14A.
7. Gruen, D. M. & R. L. McBeth. 1959. J. Inorg. Nuclear Chem. **9:** 290.
8. Laitinen, H. A. & C. H. Liu. 1958. J. Am. Chem. Soc. **80:** 1015.
9. Hill, D. L. & R. A. Osteryoung. 1959. Report No. 6, Prime Contract No. AT 30-2-GEB-16, Subcontract No. S-348.
10. Gruen, D. M., S. Fried, P. Graf & R. L. McBeth. 1959. The Chemistry of Fused Salts, Paper # 940. Proc. 2nd United Nations Intern. Conf. on the Peaceful Uses of Atomic Energy, Basic Chemistry in Atomic Energy. In press.
11. Latimer, W. M. 1952. The Oxidation States of the Elements and Their Potentials in Aqueous Solutions. 2nd ed. Prentice-Hall. New York, N.Y.
12. Benz, R. 1958. Doctoral Dissertation. Univ. N. Mex. Albuquerque, N. Mex.
13. Stewart, D. C. 1952. **ANL-4812**. Argonne Natl. Lab.

ABSORPTION SPECTRA IN MOLTEN SALTS*

George Harrington† and Benson R. Sundheim
Department of Chemistry, New York University, New York, N.Y.

The concept of complex ions is not always clear for solutions in molten salts, since any given ion is always closely surrounded by other ions in a more or less definite packing arrangement. Several criteria might be adopted for distinguishing a complex ionic entity from a group of ions that happen to be in close proximity. The radial distribution function as determined by X-ray methods, the occurrence or nonoccurrence of vibrations that could be attributed to bonds as detected by infrared or Raman spectra, and unusual features of activity versus concentration curves or of phase diagrams have been discussed in this connection. The existence of a set of discrete energy levels, which might be detected spectrophotometrically, would seem to be an especially sound basis for considering that a new ionic species had been formed. It might be expected that the continual perturbations caused by fluctuations in the ionic atmosphere of an ion would broaden any energy-level pattern to the point where no definite transitions could be discerned in the optical absorption spectrum. When a well-defined structure is found in the spectrum of a molten salt solution, it is proper to treat it as presumptive evidence of the existence of one or more clear-cut species in the melt. In certain cases this evidence can be consolidated by identifying the spectrum as corresponding to that of species known in the crystal (where the configuration may be known from X-ray studies) or by rationalizing the spectrum on the basis of theoretical considerations as described below.

The metal ions of the first transition series are particularly well suited to this type of study. Not only do they frequently form stable complex ionic species, but they also possess internal energy levels that are now well known to be highly responsive to the arrangement and spacing of surrounding groups.

In this publication we report on the electronic absorption spectra of ions of the first transition series dissolved in the molten LiCl-KCl eutectic and, in some cases, in the molten LiBr-KBr eutectic or in molten KSCN.

A more or less definite identification of complex ionic species is possible for most of these ions. In this paper we survey the spectra and establish the framework of the method by which the species can be identified.

---

* The work reported in this paper was abstracted in part from a dissertation submitted by George Harrington to the Graduate Faculty of Arts and Sciences, New York University, in partial fulfillment of the requirements for the degree of Doctor of Philosophy.

† Present address: Temple University, Philadelphia, Pa.

EXPERIMENTAL METHODS

The spectrophotometer consisted of the light source and monochromator of a Beckman Model DU spectrophotometer, a thermostated furnace carrying the absorption cells, and a photomultiplier detector. The details of construction and operation have been described previously.[1] The furnace has been modified further by fitting a micrometer screw and dial to the horizontal traverse system used to place the sample and reference cells alternatively in the light beam. In this way the cells can be positioned smoothly and accurately.

The salts were analytical grade reagents that had been dried rigorously before use. The eutectic mixtures were prepared by careful predrying followed by washing the molten mixture with the appropriate anhydrous hydrogen halide gas and purging with nitrogen. The molten salt was forced through a sintered glass filter, allowed to freeze, and stored until needed. The salts were weighed out and loaded into the cells in a dry box. The cells were evacuated for several hours, sealed off, and inserted in the furnace. At the same time a reference cell of pure solvent was prepared in the same way. Quartz cells with 2-mm. or 1-cm. light paths were used according to the absorbance of the solution.

EXPERIMENTAL RESULTS

Molten KSCN as Solvent

During the course of molten salt investigations, it was observed that pure potassium thiocyanate, when melted and maintained a few degrees above its melting point, gave a water-white melt that did not undergo noticeable decomposition for several hours.[2] Electric conductivity measurements showed that the specific conductivity of the melt remained constant for several hours when heated just above the melting point of 173° C.

Addition of transition metal halides to this solvent gave brightly colored solutions in some cases. These halides were cobalt (II), nickel (II), and chromium (III); their solutions were blue, yellow, and green, respectively. Copper (II) chloride and manganese (II) chloride did not dissolve. Iron (III) chloride reacted; analysis showed that all of the Fe(III) had been reduced to Fe(II), which did not appear to dissolve in the melt.

Cobalt (II). The spectrum of $CoCl_2$ dissolved in KSCN is shown in FIGURE 1. An absorption edge began at about 400 $m\mu$, complete absorption taking place below this wave length. The maximum of the band in the visible region occurred at 625 $m\mu$. This band was not quite symmetrical, displaying a shoulder between 570 and 580 $m\mu$. KCl was added to this solution in an attempt to form a chloro complex, but no change in the spectrum was detected. In fact, the KCl was not noticeably soluble, suggesting that KCl precipitated from KSCN when $CoCl_2$ was added. The spectrum of pure $Co(SCN)_2$ was found to be identical with that shown in

FIGURE 1. The peak maximum occurred at 625 mμ, and the absorbancy index had the value 86 at this point.

Graphs of the optical density versus mole per cent of Co(II) were prepared for five different wave lengths. Data from thiocyanate, chloride, and bromide salts were used. It was found that an excellent straight line was obtained. This conformity with the Beer-Lambert-Bougert law was taken as evidence of the nonoccurrence of halide complex ions in this melt. Addition of KCN to the KSCN melt containing Co(II) resulted in the formation of a black precipitate.

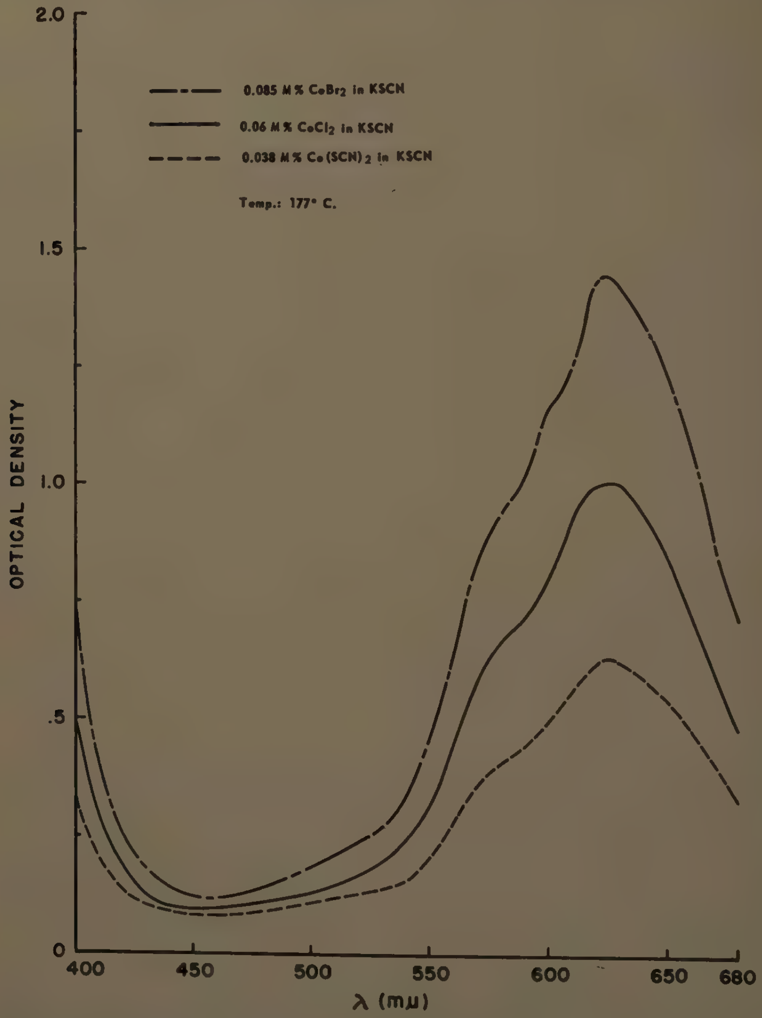

FIGURE 1. Absorption spectra of solutions of $CoCl_2$, $CoBr_2$, and $Co(SCN)_2$ in molten KSCN.

Nickel (II). Behavior analogous to that of the cobalt system was found for Ni(II) solutions in molten KSCN. $NiCl_2$ and $NiBr_2$ gave identical spectra in this solvent. The absorption spectrum is shown in FIGURE 2. An absorption edge started at approximately 400 mμ, complete absorption occurring below this wave length. The broad band in the near infrared region had its maximum at approximately 715 mμ. In this region, the maximum value of the absorbancy index was only 4.6. Beer's law graphs of data collected on solutions to which chloride and bromide ions had been added showed that no halide complexes formed. Addition of KCN led to formation of a black precipitate. KSCN containing $NiCl_2$ or $NiBr_2$ was a pale yellow when solid and a clear light gree when molten.

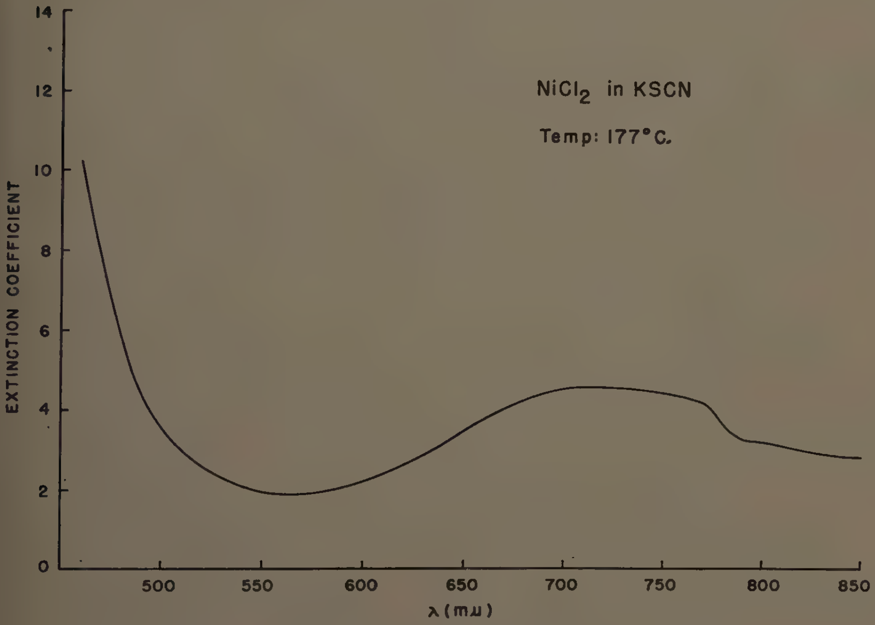

FIGURE 2. Absorption spectrum of nickel (II) in KSCN.

Chromium (III). Solutions of $CrCl_3$ in KSCN were green. The spectrum, FIGURE 3, showed an absorption edge below 400 mμ and a band in the visible range with a maximum at 600 mμ. The absorbancy index at this point was 15. Upon freezing, the green solution first gave a green solid but, upon further cooling, abruptly became violet, the color of anhydrous $CrCl_3$.

Additions of KCl led to no change in the absorption spectrum. On the other hand, progressive additions of KCN gradually converted the green solution into a red one. The spectra of solutions containing various ratios of Cr:CN are shown in FIGURE 3. The band maximum shifted continuously toward shorter wave lengths as the ratio was lowered.

It would be interesting to study this system in detail, since it is possible that a variety of mixed complex ions can form here.

Molten LiCl-KCl Eutectic as Solvent

Scandium (III). This solution was colorless and showed a spectrum consisting of a simple absorption edge beginning at approximately 250 mμ at

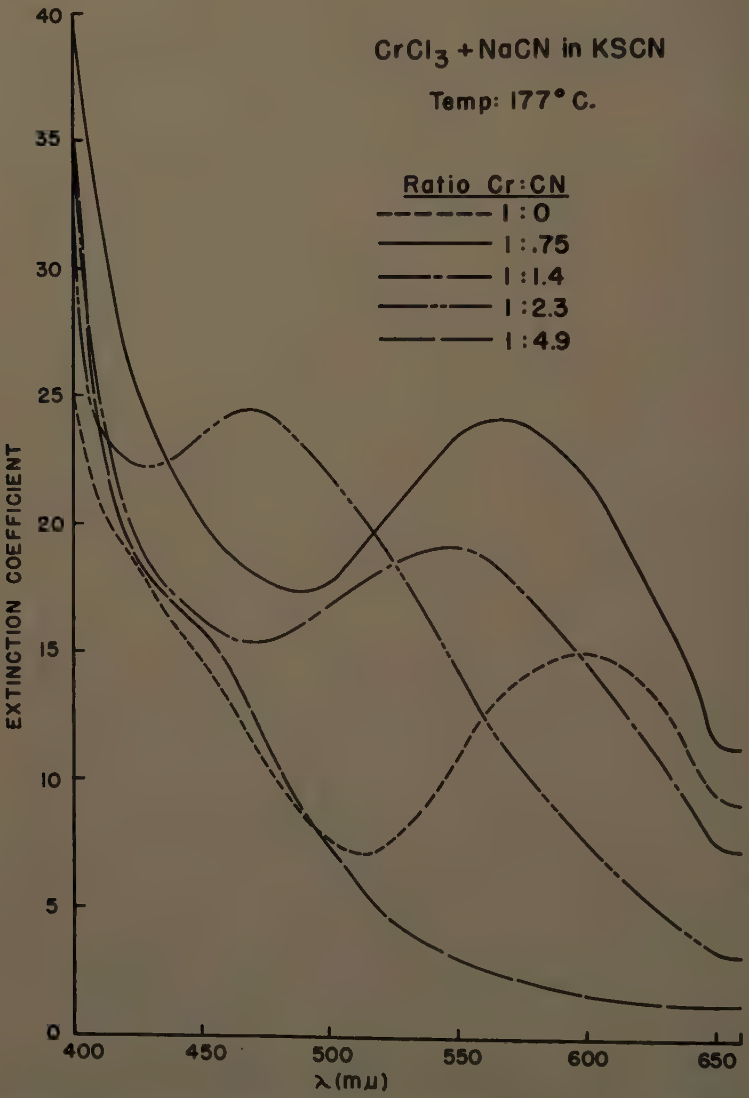

FIGURE 3. Absorption spectra of solutions of chromium (III) in KSCN, with addition of NaCN.

371° C. and moving slightly toward the red with increasing temperature. The spectrum is given in FIGURE 4.

Titanium (IV). This solution was a light yellow and showed a spectrum consisting of an absorption edge beginning at about 460 mμ. The spectrum is given in FIGURE 5.

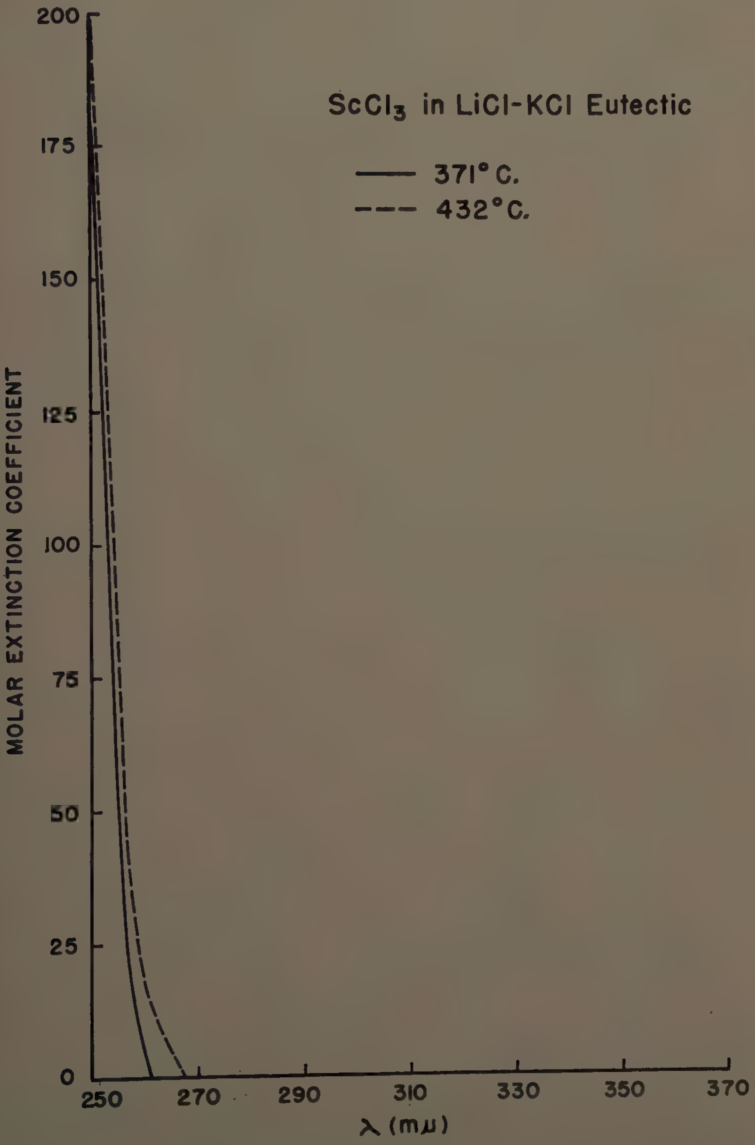

FIGURE 4. Absorption spectrum of scandium (III) in LiCl-KCl eutectic.

Vanadium (III). VCl_3 formed a dark green solution in this solvent with an absorption edge at about 400 mμ and a band with a maximum at 545 mμ (absorbancy index 35 at 372° C.). Toward the longer wave lengths this band, shown in FIGURE 6, was skewed into a long tail.

Chromium (III). The spectrum of this green solution (FIGURE 7) had an absorption edge at about 400 mμ and two peaks in the visible and near

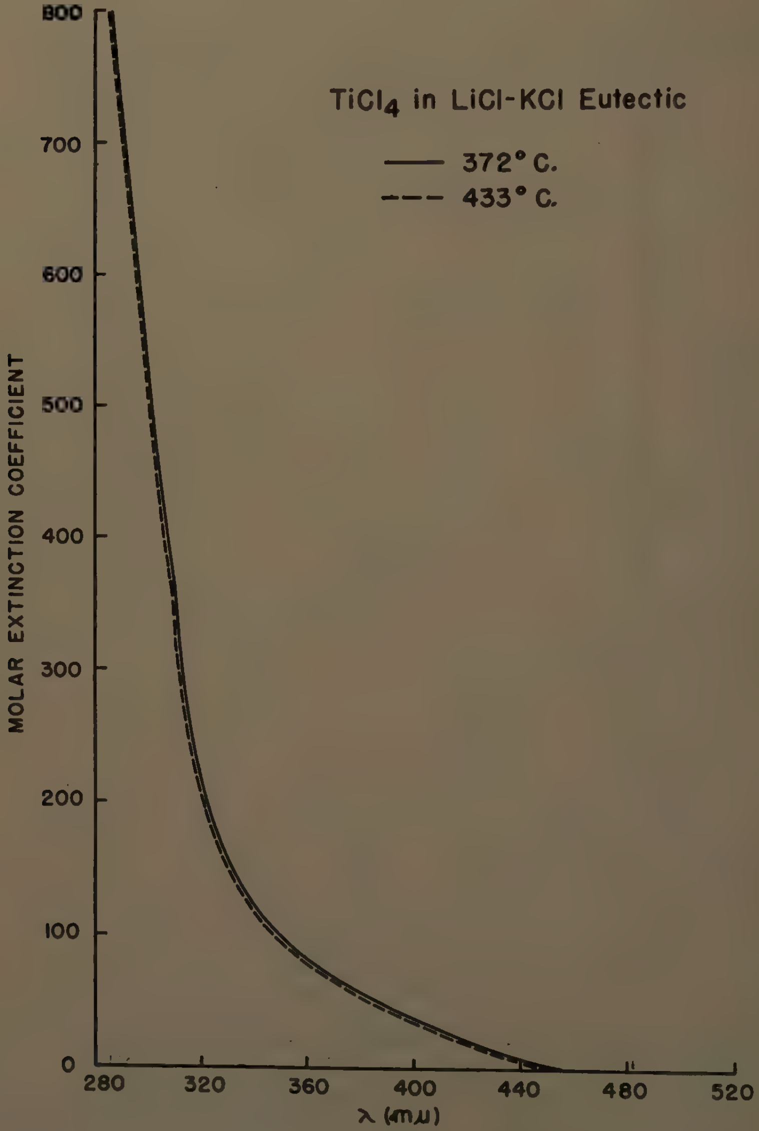

FIGURE 5. Absorption spectrum of titanium (IV) solution in LiCl-KCl eutectic.

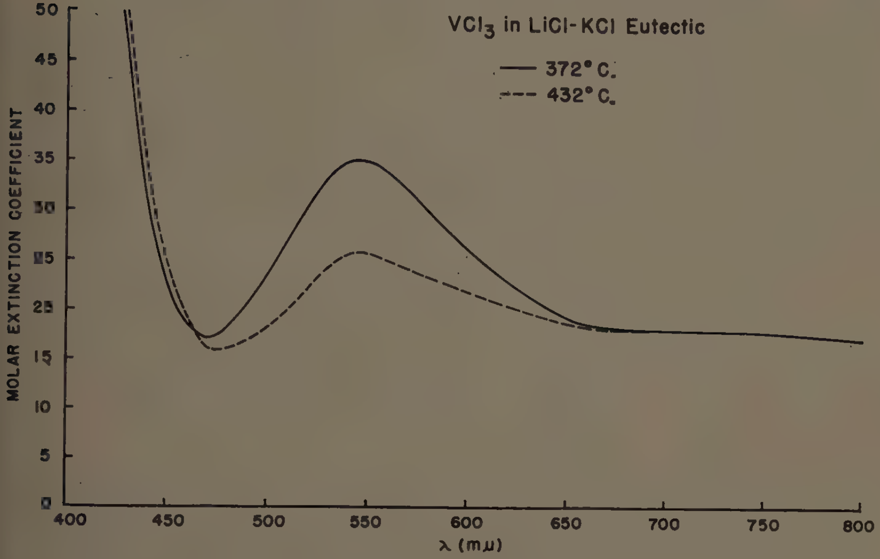

FIGURE 6. Absorption spectrum of vanadium (III) in LiCl-KCl eutectic.

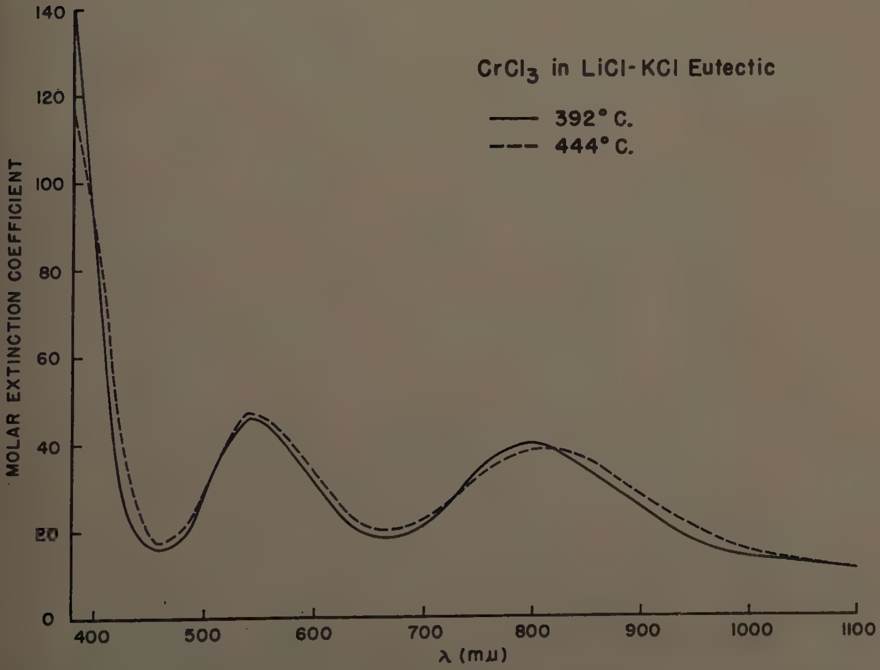

FIGURE 7. Absorption spectrum of solution of chromium (III) in LiCl-KCl eutectic.

infrared. The band in the visible had a maximum at 545 mμ (absorptivity index 46), whereas the maximum of the broader infrared band occurred at 795 mμ (absorptivity index 40 at 392° C.). Increasing the temperature affected each of these bands differently. The visible peak increased its absorptivity with increasing temperature, whereas the infrared peak decreased, broadened, and shifted slightly to longer wave lengths.

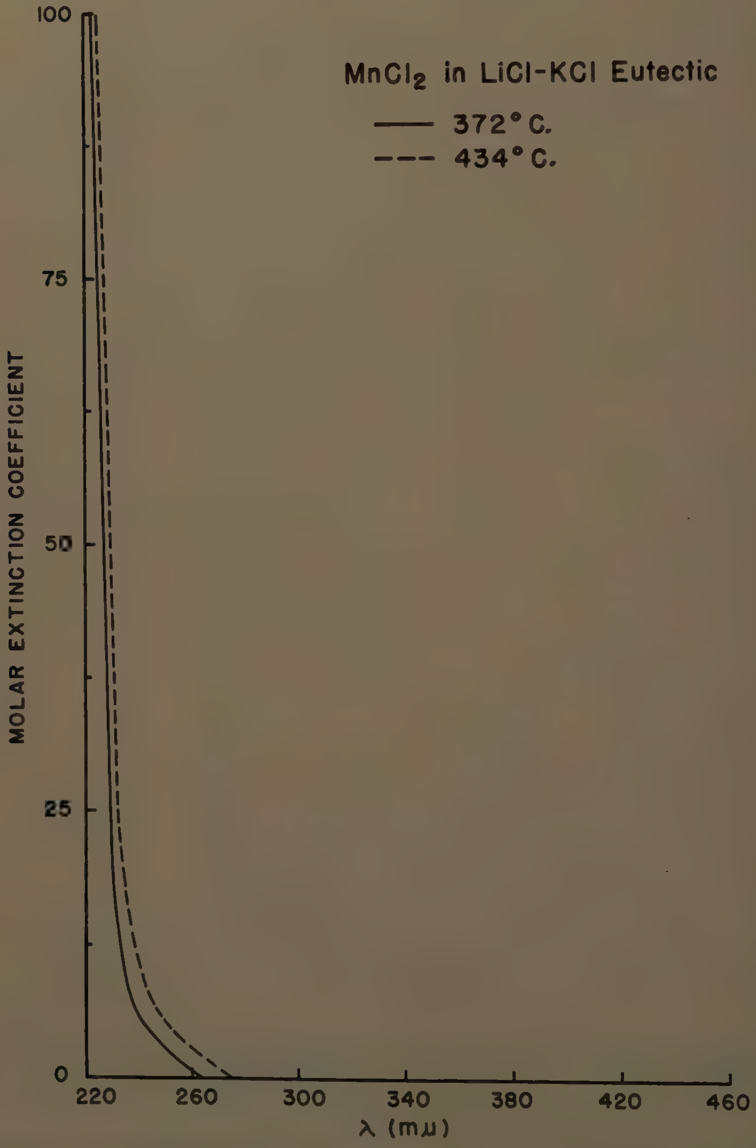

Figure 8. Absorption spectrum of manganese (II) solution in LiCl-KCl eutectic.

Manganese (II). The absorption spectrum of this colorless solution is shown in FIGURE 8. It displayed only an absorption edge beginning at approximately 265 mμ at 372° C. and shifting slightly to the red with increasing temperature.

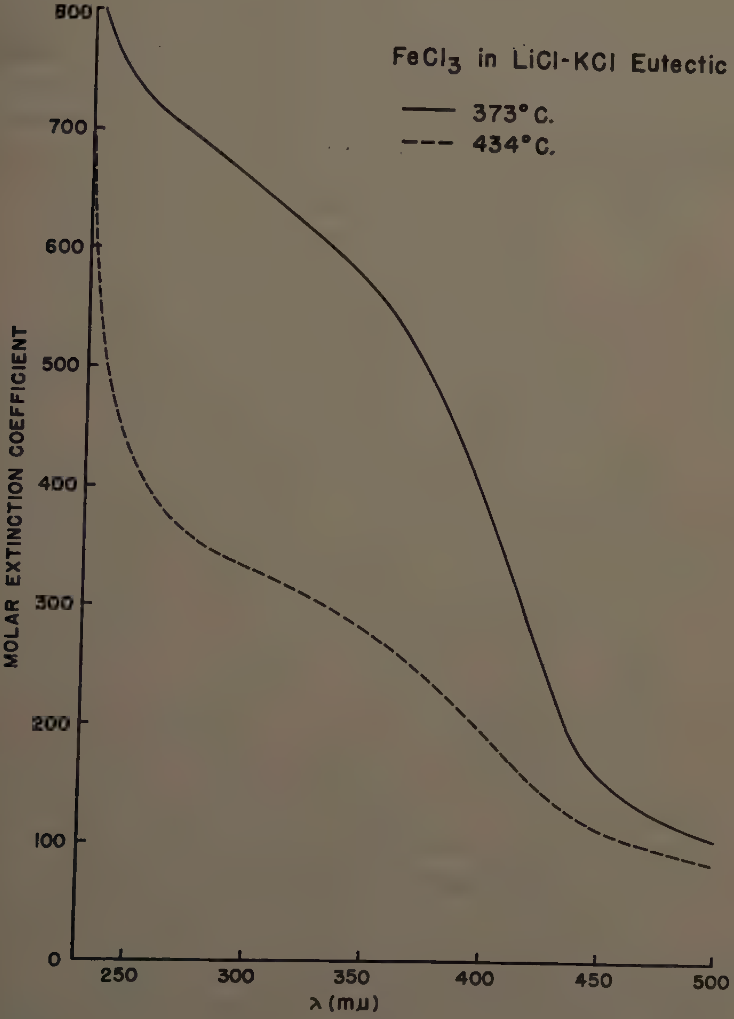

FIGURE 9. Absorption spectrum of iron (III) in LiCl-KCl eutectic.

Iron (III). These solutions were yellow. The spectrum, which is shown in FIGURE 9, consisted of a broad band merging into an absorption edge. Increasing the temperature caused the entire band to fall, the effect being most pronounced near 300 mμ.

Cobalt (II). The spectrum of this blue-green solution is shown in FIGURE

10. In the ultraviolet region there was a broad band with a maximum at approximately 255 mμ. Its absorptivity coefficient at the maximum was about 130 at 394° C. The band was broader and less intense at higher temperatures. The visible and infrared contained two peaks, one at 610 mμ (absorptivity index 120) and a broader one at 680 mμ (absorptivity index 175 at 394° C.). Raising the temperature caused each of these bands to decrease in intensity and to broaden, but in slightly different proportions.

Nickel (*II*). The spectrum of $NiCl_2$ in this solvent is shown in FIGURES 11 and 12. This was a violet solution whose spectrum was characterized by peaks in the near ultraviolet and visible regions. In the ultraviolet, the peak occurred at 260 mμ (absorptivity index 3500 at 393° C.). This peak shifted toward the red and decreased slightly with increasing temperature. At 446° C. the maximum had shifted to 265 mμ (absorptivity index 3300).

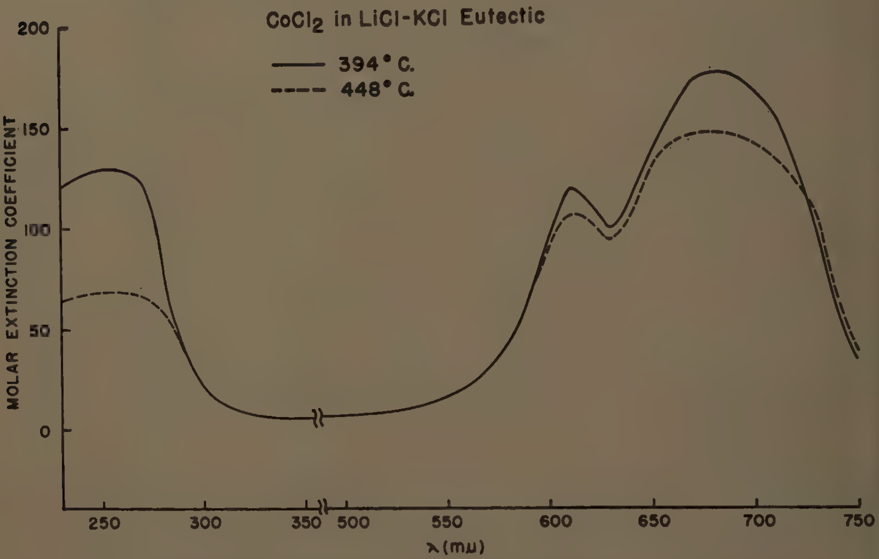

FIGURE 10. Absorption spectrum of cobalt (II) solution in LiCl-KCl eutectic.

The visible spectrum displayed peaks at 510, 590, 628, and 698 mμ (398° C.). The absorptivity indices at these maxima were 56, 59, 61.7, and 48, respectively. Increasing the temperature affected each of these peaks differently. The band at 510 mμ practically disappeared. The one at 590 mμ increased and broadened into a hump with an absorptivity of 63 at the center. The band at 628 mμ increased its absorptivity index to 66. The 695-mμ band increased and broadened to a band with an absorptivity index of 52.5 at the maximum.

These results are in excellent agreement with those reported by Boston and Smith[3] and by Gruen and McBeth.[4]

Copper (*II*). This solution was yellow when dilute, golden when concentrated. The spectrum, shown in FIGURE 13, displayed maxima at 260 mμ (absorptivity index 1520) and 370 mμ (absorptivity index 680 at 367° C.). As the temperature was increased, the highest peak, that at 260 mμ, merely decreased intensity. At the same time the smaller one decreased, broadened, and shifted slightly toward the blue. At 464° C. its absorptivity index had decreased to 430.

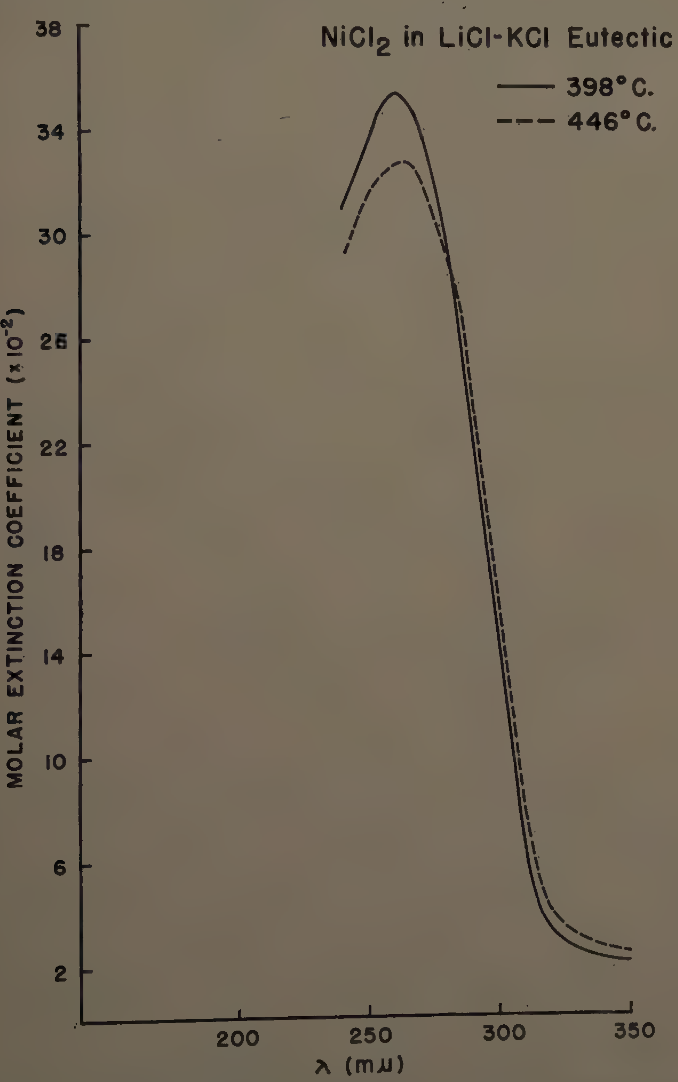

FIGURE 11. Ultraviolet absorption spectrum of nickel (II) solution in LiCl-KCl eutectic.

DISCUSSION

Scandium (III) and titanium (IV). These are d^0 configurations, and consequently do not display *d-d* spectra. Solutions of Ti(IV) in 12 *M* HCl have been studied,[5] but not fully interpreted. The spectrum consisted of a very broad band in the near UV extending from 230 to 320 mμ with no distinct structure. The spectrum of Ti(IV) in molten chlorides is similar (FIGURE 5) in that it consists of a broad band extending from 260 to 450 mμ.

Vanadium (III). The spectra of $V(H_2O)_6^{+++}$ in concentrated perchloric acid solutions show[6] absorption bands at 400 and at 580 mμ. In a sequence of alcohols the main band at 580 mμ was observed to shift to the red as the size of the alcohol increased.[7] The spectra were interpreted as arising from alcoholates with coordination numbers of six. Liehr and Ballhausen[8] commented that these were trigonally distorted. Low[9] obtained the spectrum of V(III) octahedrally surrounded by oxygen atoms by embedding the ion in the Al_2O_3 host lattice. The principal bands in this spectrum occurred at 572, 397 and 290 mμ. These bands were fitted readily to the energy-level diagram computed by Liehr and Ballhausen,[8] using a value of Dq = 1860 cm.$^{-1}$

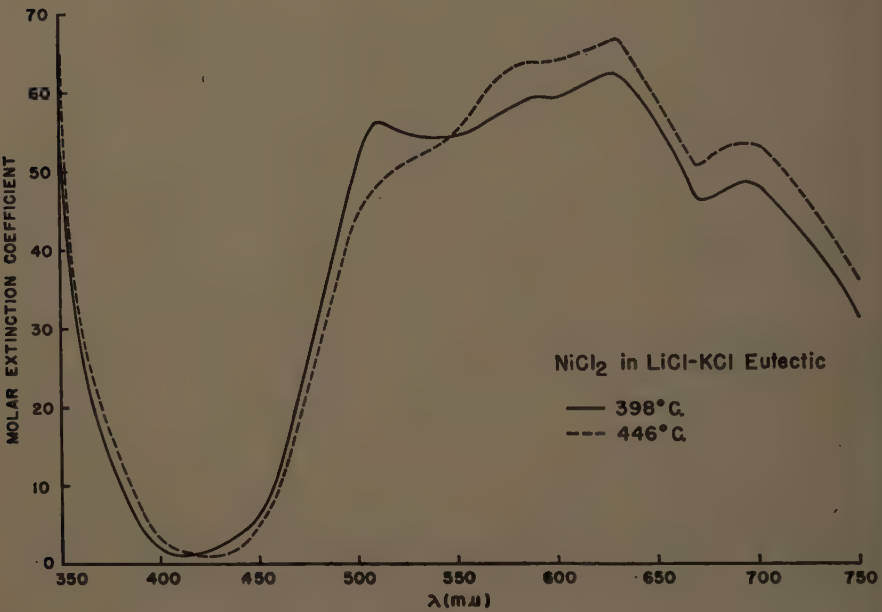

FIGURE 12. Visible absorption spectrum of nickel (II) solution in LiCl-KCl eutectic.

The data from the molten salt solution may be fitted to this diagram by selecting Dq as 800 cm.$^{-1}$ (FIGURE 14). The main band at 545 mμ would correspond to a $^3T_{1g}$-$^3T_{1g}$ transition. A lower energy transition (to a $^3T_{2g}$ state) is predicted at about 1000 mμ. This may be identified by the long tail extending through the near infrared, which was observed. It is not possible to estimate whether the spectrum indicates that significant trigonal distortion has taken place.

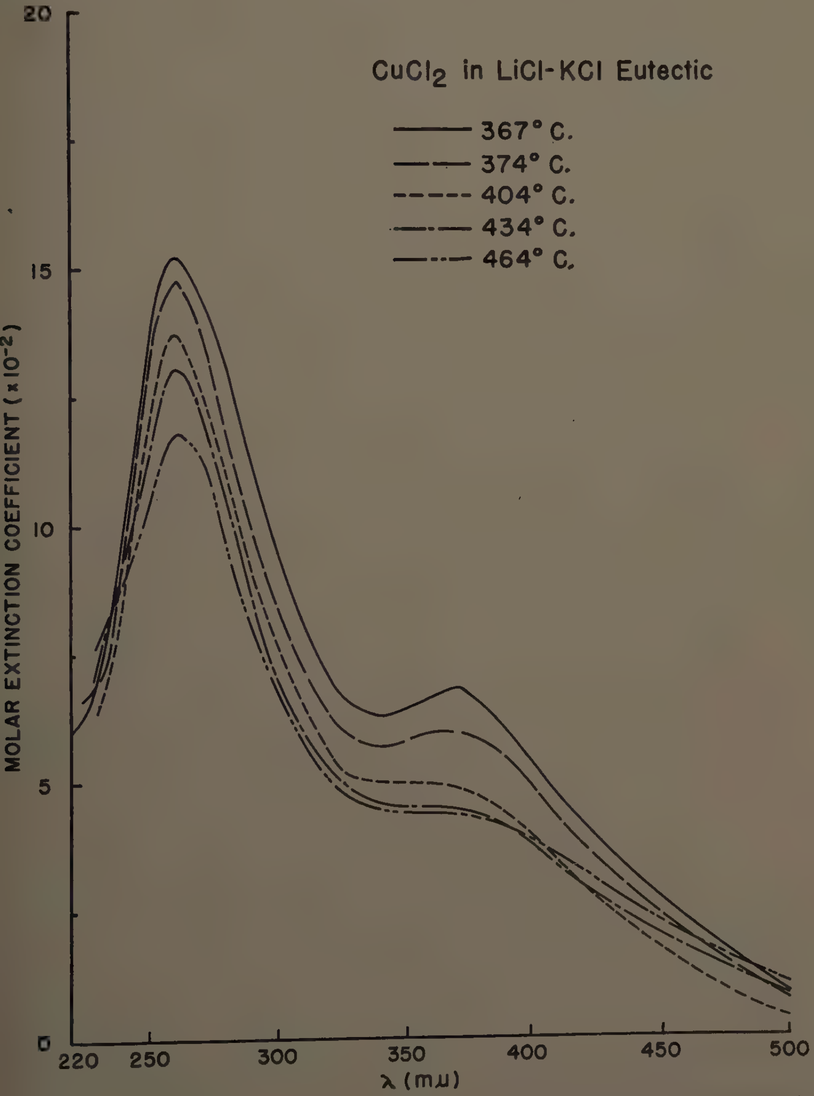

Figure 13. Absorption spectrum of copper (II) solution in LiCl-KCl eutectic.

Chromium (III). The spectra of aqueous solutions of Cr(III) containing excess of thiocyanate ions consist of two bands[10a,b] occurring at 410 and 570 mμ. Analysis of these has shown that the absorbing species are $Cr(H_2O)_6^{+++}$, $Cr(H_2O)_5(SCN)_2^{++}$, and $Cr(H_2O)_4(SCN)_2^{+}$. No evidence has been found for the sixfold complex $Cr(SCN)_6^{---}$, although its existence has been predicted[11] on a purely theoretical basis. The molten salt spectrum has a peak at 600 mμ and an edge at 400 mμ, the latter probably being due to the solvent which effectively cuts off at this wave length. The 600-mμ band could be attributed to the species $Cr(SCN)_6^{---}$, but not with certainty, since there is nothing comparable in aqueous solutions. A lower coordination is unlikely, since chromium (III) does not change coordination number readily, as does iron (III).[10b] The coordination number 6 is well established for chromium in both solutions and crystals.[12a,b] In 12 *M* HCl two rather broad bands occur with maxima at approximately 650 to 660 mμ and 465 to 475 mμ.[13] Gradual addition of Cl^- caused a continuous shift toward longer wave lengths. It has been shown that the lower chloro-aquo complexes, such as $Cr(H_2O)_4(Cl)_2^+$ are very stable, so that it is not perfectly clear that the principal absorbing species in 12 *M* HCl is $CrCl_6^{---}$.

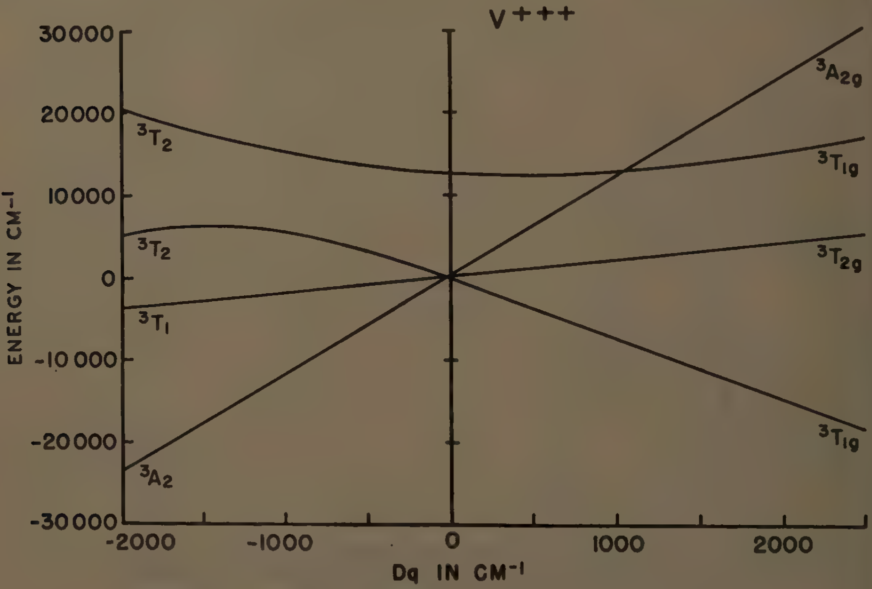

FIGURE 14. Energy level diagram for vanadium (III) ion.

The energy level diagram for octahedrally coordinated Cr(III)[14] may be used to obtain a systematic interpretation of the molten salt spectra. Selecting $Dq = 1000$ cm.$^{-1}$, which is close to the value predicted by Orgel for this ion, the observed transitions are identified as $^4A_{2g} \rightarrow {}^4T_{2g}, {}^4T_{1g}$. The selection rules forbid these transitions, but a slight distortion of the octahedron, for example by extending two opposite ligands so as to give D_{4h} symmetry, removes the restriction. In an atmosphere of Li^+ and K^+ some distortion seems inevitable.

The effect of temperature on this system is somewhat unusual. The short wave-length band rises slightly with temperature, whereas the long wave-length band broadens and decreases slightly. Neither of these effects is very large, suggesting that both are due to small thermal perturbations. The longer wave-length band moves slightly toward the red. This could be due to the change in field strength. The tetragonal distortion mentioned above not only relieves the selection rules, but also splits the two ^4T states into two sets containing two levels apiece. It may be that the shift of one band with respect to the other represents a curvature in the graphs of these energy levels as a function of field strength.

The spectrum of Cr(III) in molten KSCN readily fits the energy level diagram when a value of 1625 $cm.^{-1}$ is taken for Dq.

The addition of CN^- causes the main bands to shift steadily toward the blue. The set of maxima of the sequence of spectra obtained may be fit to the energy-level diagram by employing successively larger values of Dq. Eventually the highest transition is obscured by the solvent absorption below 400 $m\mu$.

The usual order of field strengths for ligands[15] is $CN^- > SCN^- > Cl^-$, which is the sequence observed here. The change in contour of the absorption spectrum of the thiocyanate solution as cyanide is added suggested that mixed complexes $Cr(SCN)_m(CN)_{6-m}^{---}$ might have been formed.

Manganese (II). No absorption was detected for dilute solutions of $MnCl_2$ in the visible and near ultraviolet. The edge beginning near 265 $m\mu$ may well be associated with a charge-transfer band. Transitions are possible in the d^5 Mn(II) case only between states of different spin multiplicity; they are expected to be of very low intensity.[16]

Iron (III). The spectra of Fe(III) ions have been investigated thoroughly in both aqueous and nonaqueous solutions.[5,17-19] In solutions that are dilute with respect to chloride ions, three peaks appear at 240, 320, 365 $m\mu$, respectively. As the chloride ion concentration is raised, all three of these bands decrease in intensity and eventually become a broad band with ripples at approximately 320 $m\mu$ and 365 $m\mu$.

Analysis of these spectra has tended to suggest that, in the presence of excess chloride ion, the absorbing species is $FeCl_4^-$ and not $FeCl_6^{---}$. Further evidence of the tetrachloro structure is found in the spectra of solutions in organic solvents in which the principal species was identified[19] as $HFeCl_4$. These spectra are identical with the ones in concentrated chloride solutions and strongly resemble the spectra in the LiCl-KCl eutectic. The temperature broadening in the molten salt solutions apparently washes out the small undulations observed in the room temperature solutions.

The spectrum of the salt $KFeCl_4$ is the same as those of the aqueous and molten salt solutions. Although the configuration of the tetrachloroferrate ion has not been determined directly by X-ray or electron diffraction studies, it has been deduced from magnetic susceptibility studies.[19] These measurements have shown that there are five unpaired electrons, presumably the five 3*d* electrons. The bonding is then interpreted as sp^3 so that the configuration is tetrahedral. However, Brady[20] has obtained evidence from X-ray scattering in concentrated aqueous solution that the predominant species is $FeCl_6^{---}$. The final identification of the configuration in the molten salt system may have to await the determination of the structure of the aqueous solutions.

Cobalt (II). A solution of cobalt (II) chloride in 12 *N* HCl shows a spectrum consisting of a broad band at 580 to 720 mμ. The maximum of this band occurs at approximately 660 to 680 mμ, with a small shoulder at 610 mμ. Analysis of this spectrum as a function of concentration[14] showed the absorbing species to be $CoCl_4^{--}$. A more recent study[21] has resolved one of the bands of this spectrum into two peaks of equal intensities at 561 and 690 mμ. Smaller peaks were found at 623 and 510 mμ. The most complete study[22] was carried out in acetone. In the presence of excess chloride ion two peaks of equal intensity appear at 670 and 700 mμ, respectively. On the blue side of this band a smaller peak appears at 620 mμ and a still smaller one at 615 mμ. Application of the method of continuous variations to this system showed the absorbing species to be $CoCl_4^{--}$. The general red-blue phenomena of cobalt (II) solutions was shown to be a consequence of changes in coordination number; blue solutions are 4-coordinated and red ones are 6-coordinated.

A recent work of Gruen[23] affords another significant comparison. The spectrum of $Co(NO_3)_2$ in $LiNO_3$-KNO_3 eutectic was studied as a function of added chloride ion. As the chloride ion concentrations increased, the spectrum shifted steadily toward the red. In the presence of a large excess of chloride ion two peaks of almost equal intensity appeared at 670 mμ and 690 mμ, respectively, a smaller peak appearing as a shoulder at approximately 620 mμ. The absorbing species was again interpreted as $CoCl_4^{--}$.

By comparison with these various spectra, it seems clear that the spectrum of $CoCl_2$ in the LiCl-KCl eutectic is due to the $CoCl_4^{--}$ species.

X-ray and electron diffraction studies of the solid Cs_2CoCl_4 have shown that the complex species is a slightly distorted tetrahedron.[24,25] The absorption spectrum of this crystal contains a small peak at 532 mμ and a broad band[26] at from 560 to 700 mμ. The center of this band occurs at approximately 660 mμ. This spectrum is not identical with that of the molten salt solution, but it is quite similar. The broadening of the main band probably is due to temperature broadening with perhaps a further distortion of the tetrahedron. The absence of the small peak at 532 mμ is probably a consequence of the temperature broadening.

The studies of the spectra of Co(II) solutions containing thiocyanate ions are extensive. The similarity between the molten salt spectra (FIGURE 1) and aqueous solution spectra is quite striking. In the room temperature solutions the maximum occurs at 625 mμ, with a shoulder at 570 mμ and a high peak[27-31] at 310 mμ. In the molten salt, the edge begins at 400 mμ due to absorption by the solvent; this precludes examination of the spectrum in the near ultraviolet.

These investigators all concluded that the highest complex was the 4-coordinated one, on the basis of continuous variations studies. Recently some doubt has been cast on the conclusion,[32,33] opening at least the possibility that a 6-coordinated complex might occur. Without further evidence it would seem reasonable to identify the absorbing species in the molten case with the 4-coordinated species. Although the spectrum has not been measured, the structure of the crystal $K_2Co(SCN)_4$ has been determined by X-ray diffraction[34] and has been shown to contain tetrahedral $Co(SCN)_4^{--}$.

Nickel (*II*). The spectrum of tetrahedrally coordinated $NiCl_4^{--}$ incorporated in a host lattice of Cs_2ZnCl_4 has been obtained by Gruen and McBeth.[35] This ion displays peaks in its absorption spectrum near 590, 625, and 695 mμ, as well as a large charge transfer peak near 260 mμ. These authors also showed that the spectrum of $NiCl_2$ in molten CsCl is essentially the same. On the other hand, their spectra in molten LiCl have an additional peak near 510 mμ. They interpret this result as indicating that "the shift of the absorption spectrum to longer wave lengths which already makes itself felt in fused CsCl and is extremely pronounced in fused LiCl could be due to progressive distortions of the $NiCl_4^{--}$ ion from tetrahedral symmetry."

In the LiCl-KCl eutectic the three bands at 590, 625, and 695 mμ are present, together with the one at 510 mμ. With increasing temperature the first three broaden and become more intense, whereas the last (at 510 mμ) shrinks. The variation in temperature also reveals the fact that the shoulder of the charge-transfer band, which shrinks with increasing temperature, conceals another small band that increases with temperature (this band has not been pointed out previously, although it is easily seen). Boston and Smith[36] interpreted these data as showing that "these absorption bands were caused by at least two light absorbing species derived from $NiCl_2$." Jørgensen[37] similarly concluded that the peaks at 590, 625, and 695 mμ were due to tetrahedrally coordinated Ni(II) and that the peak at 510 mμ was due to octahedrally coordinated Ni(II). Sundheim and Harrington[38] demonstrated that the spectrum could be interpreted as arising from tetrahedrally coordinated Ni(II). The temperature dependence of the peak at 510 mμ may be taken as revealing the relaxation of a selection rule as the tetrahedral structure is distorted.

The peak in question cannot arise from a gradual distortion of an existing structure, the amount of distortion increasing, on the average, with increasing temperature. This would lead to a gradual separation of the peak into two peaks, or at least to distinct broadening. The change in intensity, without accompanying change in frequency, indicates that the transition probability or the concentration of a species is being affected by the perturbation without any pronounced change in its energy-level structure.

Gruen and McBeth have shown that the 510 mμ peak is not associated with the tetrahedral structure.

The contention that the 510 mμ peak is due to octahedrally coordinated Ni(II) cannot be supported. It has been shown[39] that the intensities of *d-d* bands for octahedral divalent transitions are only about one one hundredth of those of the corresponding bands for the tetrahedral case. Furthermore, the energy-level diagram for the octahedral case, which strongly resembles that of the tetrahedral case, indicates that a set of lines is to be expected, rather than a single one. Examination of the absorption spectrum of the hexaquo Ni(II) species[40] confirms this prediction.

Finally, a computation of the energy level diagram of Ni(II) in fields of tetrahedral and octahedral symmetry has been published by Liehr and Ballhausen.[41] With its aid we have identified the transitions occurring in the spectrum. By selecting a value of $Dq = 500$ cm.$^{-1}$, a reasonably good fit is obtained (FIGURE 15). On testing the selection rules[42,*] it is seen that the transitions are all permitted by electric dipole radiation except for the one from the ground ${}^3T_{1g}$ state to the ${}^3A_{1g}$ state. (This corresponds in energy to the 510 mμ peak.) Distortion of the tetrahedral T_d field to, say, C_{3v} symmetry, as could be accomplished by slightly moving one of the four ligands nearer to or further from the central ion, causes a splitting in which the former ground state (${}^3T_{1g}$) separates into a ${}^3E_g$ and a ${}^3A_{1g}$ state. One or the other of these becomes the new ground state. Examination of the new set of selection rules shows that the previously forbidden transition to the ${}^3A_{1g}$ state is not allowed from the new ground state. Distortion to the C_{3v} symmetry leads to similar conclusions.

Thus, it appears that the *d-d* peaks can be correlated easily with the tetrahedral Ni(II) energy level diagram and that the peak at 510 mμ is due to the relaxation of a selection rule brought about by a slight tetragonal or other distortion of the tetrahedral structure.

Copper (*II*). Cu(II) in 12 *M* HCl by the method of continuous variations[43-45] has shown that the highest chlorocomplex occurring is $CuCl_4^{--}$. The absorption spectra of these solutions is similar to the spectra obtained for the molten salt solutions.

In 12 *M* HCl, peaks are found at 250 to 260 mμ and at 360 mμ.[43] Another investigator located these peaks at 263 and 384 mμ.[46] At 364° C. peaks are found at 260 and 370 mμ.

The configuration and spectrum of the solid double salt Cs_2CuCl_4 have been determined and show the ion to be a flattened tetrahedron having absorption bands of almost equal intensity at 332 mμ and at 415 mμ.[46,47] The

[*] The *g-g* rule may be ignored in discussion of these weak *d-d* transitions.

profile of the crystal spectrum resembles that of the molten salt, but is displaced distinctly with respect to it. The gradual disappearance of one peak in the molten solution as the temperature is raised suggests that there may be a progressive change in configuration, as in the case of Ni(II), probably from tetragonally distorted to more nearly regular tetrahedral.

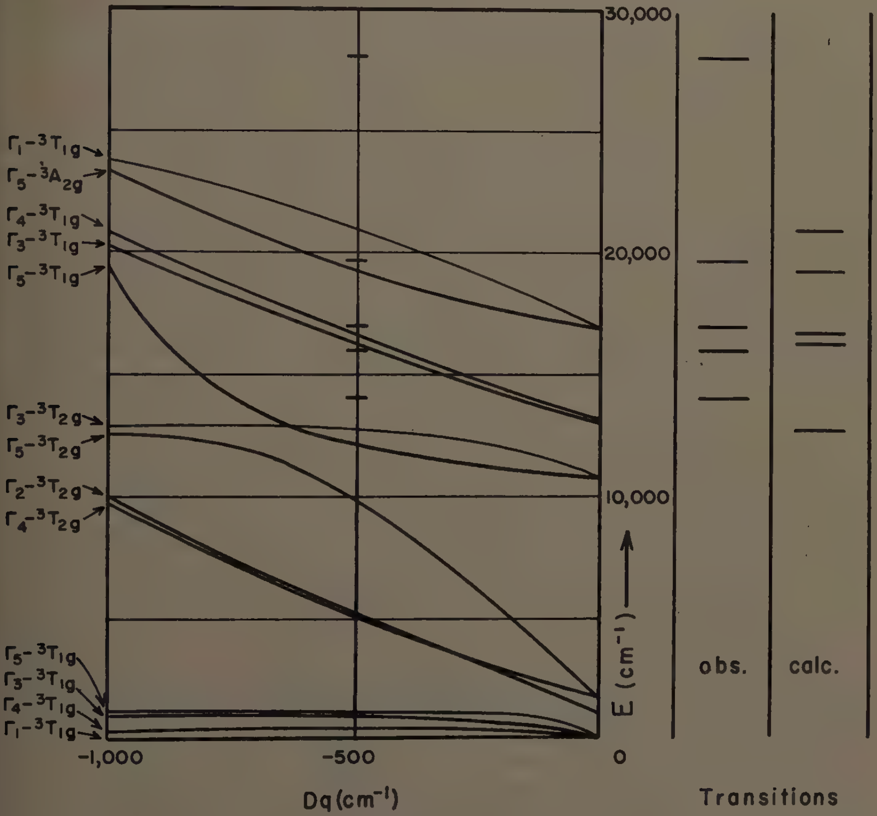

FIGURE 15. Energy level diagram for nickel (II) ion.

The ligand field theory predicts the occurrence of a single transition: $^2T_2$ - ^2E for a tetrahedral configuration; energy of this transition[45,48] is below 13,000 cm.$^{-1}$ Consequently, the peaks described above correspond to charge-transfer rather than *d-d* transitions. Until an analysis of the near-infrared absorption spectra of Cu(II) solutions is performed, ligand field theory cannot contribute to the theory of the configuration of this ion.

SUMMARY

The absorption spectra of metal ions of the first transition series dissolved in molten LiCl-KCl eutectic are given, together with the spectra of some

of the ions dissolved in molten KSCN. It is shown that the stoichiometry and geometry of complex ions occurring in these melts can be determined, in most cases, by comparing the spectra with those of crystals or solutions where the configuration of the ion is known and by utilizing the ligand field theory.

References

1. Sundheim, B. R. & J. Greenberg. 1956. Rev. Sci. Inst. **27:** 703.
2. Greenberg, J. & B. R. Sundheim. 1958. J. Chem. Phys. **23:** 461.
3. Boston, C. R. & G. P. Smith. 1958. J. Phys. Chem. **62:** 409.
4. Gruen, D. M. & R. L. McBeth. 1959. J. Phys. Chem. In press.
5. Kanzelmeyer, J. & H. Freund. 1953. Anal. Chem. **25:** 1807.
6. Furman, S. & C. Garnn. 1950. J. Am. Chem. Soc. **72:** 1785.
7. Hartman, H. & H. Schlafer. 1951. Z. Naturforsch. **6A:** 754, 760, 781.
8. Liehr, A. & C. J. Ballhausen. 1957. Ann. Phys. **1:** 221.
9. Low, W. 1957. Z. physik. Chem. (Frankfurt). **13:** 107.

10a. King, E. & E. Dismukes. 1952. J. Am. Chem. Soc. **74:** 1674.
10b. Gates, H. & E. King. 1958. J. Am. Chem. Soc. **80:** 5011.
11. Bjerrum, N. 1921. Z. anorg. u. allgem. Chem. **119:** 179.
12a. Wooster, N. 1930. Z. Krist. **74:** 363.
12b. Handy, E. & N. Gregory. 1952. J. Am. Chem. Soc. **74:** 891.
13. Datta, S. & M. Deb. 1935. Phil. Mag. **20:** 1121.
14. Orgel, L. 1955. J. Chem. Phys. **23:** 1004.
15. Basolo, F. & R. Pearson. 1958. Mechanism of Inorganic Reactions. Wiley. New York, N.Y.
16. Jørgensen, C. K. 1954. Acta Chem. Scand. **8:** 1502.
17. Metzler, D. & R. Myers. 1950. J. Am. Chem. Soc. **72:** 3776.
18. Gamlen, G. & D. Jordan. 1953. J. Chem. Soc. : 1453.
19. Friedman, J. 1952. J. Am. Chem. Soc. **74:** 5.
20. Brady, G. W. 1958. J. Chem. Phys. **29:** 1371.
21. Katzin, L. 1954. J. Am. Chem. Soc. **76:** 3099.
22. Katzin, L. & E. Gebert. 1950. J. Am. Chem. Soc. **72:** 5464.
23. Gruen, D. 1954. J. Inorg. & Nuclear Chem. **4:** 74.
24. Tishchenko, G. & Z. Pinska. 1955. Doklady Akad. Nauk. S.S.S.R. : 100.
25. Porai-Koshitz, M. 1954. Trudy Inst. Krist. Akad. Nauk. S.S.S.R. **10:** 117.
26. Katzin, L. & E. Gebert. 1953. J. Am. Chem. Soc. **75:** 2830.
27. Kiss, A. & P. Csokan. 1940. Z. Physik. Chem. **186:** 239.
28. Howell, O. & A. Jackson. 1937. J. Chem. Soc. : 621.
29. Babko, A. & O. Drako. 1949. J. Gen. Chem. SSSR. **19:** 1809.
30. Selyem, J. 1950. Magyer Kem. Folyiral. **56:** 170.
31. West, D. & C. DeVries. 1951. Anal. Chem. **23:** 334.
32. Katzin, L. & E. Gebert. 1950. J. Am. Chem. Soc. **72:** 5659.
33. Brubaker, C. & C. Johnson. 1958. J. Am. Chem. Soc. **80:** 5037.
34. Zhadanov, G. & Z. Zvonkona. 1951. Izvest. Sektora Platiny i Drug. Blagorod. Metal. Inst. Obshchi i Neorg. Khim. Akad. Nauk. S.S.S.R. **No. 26:** 235.
35. Gruen, D. M. & R. L. McBeth. 1959. J. Phys. Chem. **63:** 393.
36. Boston, C. R. & G. P. Smith. 1958. J. Phys. Chem. **62:** 409.
37. Jørgensen, C. K. 1958. J. Mol. Phys. **1:** 410.
38. Sundheim, B. & G. Harrington. 1959. J. Chem. Phys. **31:** 700.
39. Ballhausen, C. J. & A. D. Liehr. 1958. Mol. Spect. **2:** 342.
40. Holmes, O. G. & D. D. McClure. 1957. J. Chem. Phys. **26:** 1687.
41. Liehr, A. D. & C. J. Ballhausen. 1959. Ann. Phys. In press.
42. E.g., Margenau, H. & G. M. Murphy. 1957. Mathematics of Physics and Chemistry. : 564. Van Nostrand. New York, N.Y.
43. McConnell, H. & N. Davidson. 1950. J. Am. Chem. Soc. **72:** 3164.
44. Kanzelmeyer, J. & H. Freund. 1953. Anal. Chem. **25:** 1807.
45. Helmholtz, L. & R. Kruh. 1952. J. Am. Chem. Soc. **74:** 1176.
46. Moeller, T. 1944. J. Phys. Chem. **48:** 111.
47. Tishchenko, G. & Z. Pinska. 1955. Doklady Akad. Nauk. S.S.S.R. **100:** 913.
48. Ballhausen, C. J. 1954. Kgl. Danske Videnskab. Selskab, Mat.-fys. Medd. **29**(4).

ISOTHERMAL AND ISOPIESTIC DECOMPOSITION OF POTASSIUM PERCHLORATE AND POTASSIUM CHLORATE*

Aubrey E. Harvey, Carl J. Wassink,† Tommy A. Rodgers,†
Kurt H. Stern
Department of Chemistry, University of Arkansas, Fayetteville, Ark.

Introduction

By far the largest part of the work done on fused salts in recent years has been concerned with their physical properties, that is, with behavior that does not change the chemical composition of the salt during measurement. Among these one may mention density, conductance, transference, and surface tension.

In surveying the actual substances used in such studies, the predominance of the halides is striking but not surprising; their thermal stability qualifies them for the purpose.

On the other hand, our knowledge of the behavior of salts with oxygen-containing anions at high temperatures is relatively slight. Of the twenty-odd common ions of this type in which a nonmetal is combined with oxygen, the majority decompose below the boiling point, and several do so in the solid state (one may think of the anions combined with an alkali metal cation in order to visualize the actual compound). There seems to be no simple rule that will predict which anions will be thermally stable. In general, if the electronegativity of the element combined with oxygen differs greatly from that of the latter, the ion is more probably stable. Thus oxyanions of silicon, boron, arsenic, and phosphorus are generally stable (the differences in electronegativity ranging from 1.4 to 1.7), those of carbon, bromine, iodine, chlorine, and nitrogen are generally unstable (0.5 to 1.1); sulfur and selenium (1.0 and 1.1, respectively) occupy a middle ground; sulfate is stable, but sulfite is not.

The decomposition products of the oxyanions are generally fairly well known, but the mechanism of the decomposition and other kinetic data generally are not.

Because of its practical importance, the thermal decomposition of potassium perchlorate has been studied more than that of other salts but, despite a number of studies, the mechanism of the reaction is not yet entirely clear. The present work is intended to shed more light on this mechanism.

---

* The work reported in this paper was supported in part by a grant from the Office of Ordnance Research, United States Army, Washington, D.C.

† This paper is based in part upon the Master of Science theses of C. J. Wassink and T. A. Rodgers.

Historical Background

The action of heat on potassium perchlorate has been studied by various workers for a number of years. Only in comparatively recent years has the kinetic approach been applied to studies of the thermal decomposition of potassium perchlorate.

Glasner and Simchen[1-4] and Glasner and Weidenfeld[5] studied the thermal decomposition of potassium perchlorate *in vacuo* and at atmospheric pressure. In both cases it was concluded that the reaction is independent of the physical state of the system and that the decomposition is of the type

$$\text{Solid } A \rightarrow \text{Solid } B + \text{gas}$$

even after melting occurs. A modified form of the rate equation formulated by Prout and Tompkins[6] for the decomposition of solids was applied to the data. The authors were able to account for the phenomena observed in both the liquid and solid phases with this rate expression and concluded that the molten phase is quasicrystalline.

Bircumshaw and Phillips[7] described the thermal decomposition of potassium perchlorate *in vacuo* as follows:

(1) A solid-phase decomposition occurs initially with the formation of potassium chloride and potassium chlorate. The chloride formed accelerates the reaction and, due to the accumulation of potassium chlorate, melting occurs.

(2) A liquid-phase decomposition begins at the end of the transition to the liquid phase.

(3) The melt solidifies due to the accumulation of potassium chloride, and gas evolution becomes slower.

It was concluded that the decomposition cannot be represented by a single equation and is probably the net result of several simultaneous reactions.

Harvey *et al.*[8] studied the thermal decomposition of potassium perchlorate under pressure of evolved oxygen in a constant-volume system and observed that the rate of decomposition of potassium perchlorate under these conditions is dependent upon the concentration of perchlorate and upon the physical state of the reacting material. It was further found that the decomposition, before the appearance of a second solid phase, proceeds by two first-order reactions: a solid-phase decomposition followed by a liquid-phase decomposition. During the transition from the solid to the liquid phases, both reactions occur simultaneously. It was postulated that the decomposition is step-wise with the reaction

$$KClO_4 \rightarrow KClO_3 + [O]$$

as the rate-determining step. Rate constants for the liquid and solid phase reactions were measured at various constant temperatures. The activation energies, Arrhenius-frequency factors, and activation entropies were calculated from these measurements.

Previous investigations of the thermal decomposition of potassium chlorate have been concerned chiefly with the examination of decomposition products in an effort to determine the identity and relative quantities of the substances formed in decomposition.[9-14]

The thermal decomposition of potassium chlorate and chlorate-chloride mixtures has been studied kinetically by Glasner and Weidenfeld.[11] On the basis of their experimental studies these authors proposed that the thermal decomposition of potassium chlorate involves two consecutive reactions in which potassium chlorate decomposes to potassium chloride and oxygen, followed by the absorption of atomic oxygen by potassium chloride to form potassium perchlorate.

This mechanism was examined by Bosch and Aten,[15] who decomposed mixtures of $NaClO_3$ and $NaCl$, the latter containing Cl^{34} and Cl^{38}. The decomposition products were isolated and measured for specific activity. The very low ratio of labeled chlorine in the perchlorate to that in the chloride led these investigators to conclude that the formation of perchlorate from chloride does not occur to an appreciable extent in the decomposition of potassium chlorate.

Experimental Procedure

Preparation of samples. Reagent-grade potassium perchlorate was recrystallized twice from distilled water, dried in an oven at 110° C., and stored in a desiccator. Tests for chlorate and chloride were negative. Portions of the prepared stock were taken as needed and crushed into fine particles with a mortar and pestle.

Potassium chlorate, radiochemically tagged with Cl^{36} in tracer amounts, was prepared by an electrolytic process,[16] using Cl^{36} in the form of hydrochloric acid. A solution of KCl, $K_2Cr_2O_7$, and HCl^{36} was electrolyzed on platinum electrodes for 20 hours. The product was recrystallized several times until the dichromate color was removed from the crystals of the residue. These crystals gave negative tests for perchlorate and chloride. The activity of the $KClO_3$ was found to be 136 disintegrations/min./mg., as measured in a beta-proportional counter.

Reagent-grade potassium chlorate was recrystallized twice from distilled water and dried at 110° C. for 3 days. The purified material was stored in a desiccator, and samples for experiments were taken from this stock. The samples were crushed into fine particles prior to use.

Apparatus. The apparatus used in the isothermal decomposition of potassium perchlorate at constant pressure is represented diagrammatically in FIGURE 1. The apparatus consists of a Pyrex glass reaction tube heated by an electric furnace and connected by a three-way stopcock to a duplicate gas-volume measurement system.

The two gas-volume measurement systems are mirror images of each other and are connected to the reaction tube by a three-way stopcock so that the tube may be opened to either or both sections at any time. The volume of oxygen evolved during decomposition is measured in a standard gas burette that is initially filled with mercury. The displacement of mercury from the gas burette is regulated by a solenoid valve. The valve is activated by an electronic relay controlled by a differential mercury manostat. The manostat is connected on one side to the gas burette and, on the other, to a compensator tube that is maintained at the operating pressure. During the course of a kinetic run the two sections of the volume measurement system are used alternately; one side is used while the other is readjusted.

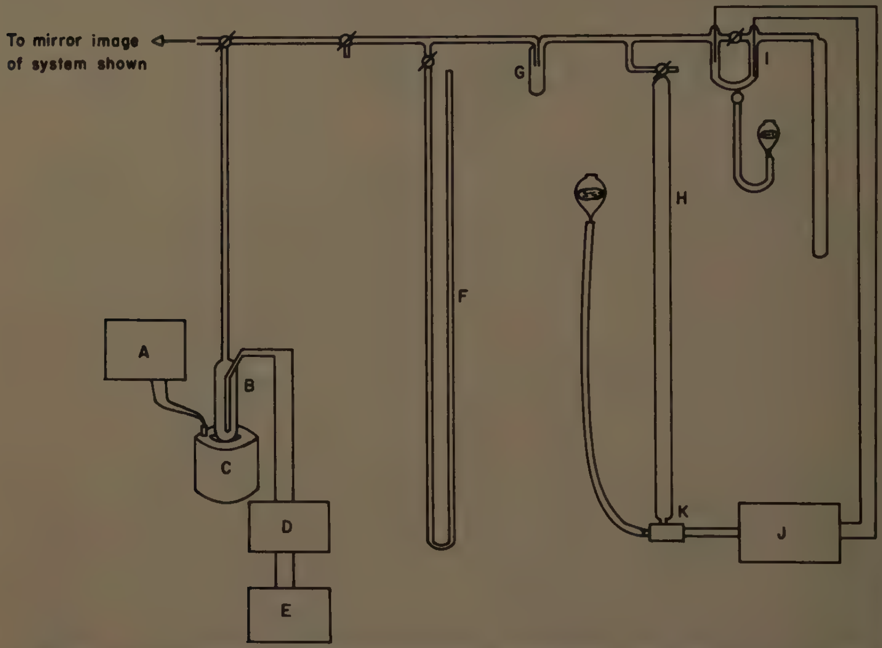

FIGURE 1. Apparatus for the measurement of oxygen volume during the isopiestic thermal decomposition of potassium perchlorate. Keys: A, micromax temperature controller; B, reaction tube; C, electric furnace; D, microvolt amplifier; E, recording potentiometer; F, mercury manometer; G, mercury; H, gas burette; I, mercury differential; J, electronic relay; and K, solenoid valve.

In the original apparatus the reaction tube consisted of a cylindrical tube with one arm of a Pt-Pt (90 per cent), Rh (10 per cent) thermocouple so placed in the tube that it was covered by the sample being decomposed. The junction of the external arm is immersed in an ice bath. The sample temperature was determined by measuring the potential of the thermocouple circuit with a K2 potentiometer. The reaction tube was heated in an electric furnace, the temperature of which was controlled with a Leeds and Northrup Micromax controller.

In later stages of the work two improvements were made on the original apparatus:

(1) A new reaction tube with a magnetically operated sample feeder was constructed. The sample feeder is in the form of a small glass dish with a piece of iron sealed into its bottom. The feeder is placed on 2 pivot rests inside the reaction tube at the top. The sample is dumped into the bottom of the tube by manipulating an external magnet perpendicular to the pivot axis of the feeder. In order to make this modification, it was necessary to seal the thermocouple junction into the bottom of the reaction tube so that the leads are external to the tube.

(2) The output of the thermocouple is fed into a DC amplifier and then to a Brown recording potentiometer. This assembly provides an instantaneous and continuous record of sample temperature. A mercury cell that gives a constant voltage over a considerable period of time is used as the reference potential for this automatic recording device. This arrangement permits adjustment to give a desired deflection of the recorder pen for a given change in sample temperature at the temperature level chosen for the isothermal decomposition. The electric circuit is so constructed that a K2 potentiometer can be connected at any time to make calibration points.

With these additional features it is possible to bring the reaction tube to the proper temperature before introducing the sample and to control the temperature more closely than is possible with manual measurements.

Differential thermal analysis(DTA) studies and isothermal decompositions of potassium chlorate at constant volume were carried out using the apparatus already described by Harvey *et al.*[8] A 2-compartment reaction tube with Pt-Pt (90 per cent), Rh (10 per cent) thermocouple circuitry was used in the DTA studies. Sample temperature was recorded versus differential temperature on a Leeds and Northrup X/Y recorder.

Analysis of residues. In certain experiments the decomposition residues were analyzed for chloride, chlorate, and perchlorate content. These residues were recovered, weighed, and dissolved in distilled water for analysis. Aliquot portions of these solutions were analyzed for chloride by the Mohr method. Total chlorate and chloride were determined by reducing the chlorate with sulfurous acid and then analyzing the resulting solution for chloride by the Mohr method. Perchlorate was calculated by difference. Representative data are shown in TABLE 1.

In the tracer studies, perchlorate in the residues was recovered and isolated for counting by precipitating as tetraphenylarsonium perchlorate.[17] All activites of samples and residue fractions were measured with a beta proportional counter. Data are shown in TABLE 2.

It was observed that, after considerable use of the decomposition apparatus, the platinum leads in the pressure controlling device became slightly corroded. The gas evolved during an isothermal decomposition of potassium perchlorate was investigated for the presence of chlorine or an oxychloro compound. Using *o*-toluidine in a colorimetric method, very small amounts of Cl_2 or ClO_2 were detected. The concentration of the substance appeared to be less than 0.01 ppm.

TABLE 1

KINETIC DATA ON THE SOLID-PHASE THERMAL DECOMPOSITION OF POTASSIUM PERCHLORATE AT 561 ± 2° C.

Time (min.)*	Mole per cent		
	$KClO_4$	$KClO_3$	KCl
25	96.3	2.0	1.7
30	96.2	2.1	1.7
30	96.1	2.0	1.9
34	95.4	2.4	2.2
37	94.6	2.3	3.1
42	94.8	2.7	2.5

* Each line represents a separate run carried out for the length of time indicated

TABLE 2

DATA FROM ISOTHERMAL DECOMPOSITIONS UNDER PRESSURE OF 1 ATMOSPHERE OF OXYGEN OF POTASSIUM PERCHLORATE CONTAINING TAGGED POTASSIUM CHLORATE

Sample number*		I	II	III	IV	V
Decomposition temp. (°C.)		562 ± 1	575 ± 1	575 ± 1	561 ± 1	560 ± 1
Vol. of O_2 liberated, ml.		12.5	51	46.7	50	72
Mole % perchlorate remaining (calc.)		86	70	68	55	38
Time of decomposition, min.		33	17	20	52	75
Initial activity of sample, cpm		2355	4710	4710	2360	2360
Perchlorate activity after decomposition, cpm	A	732	3230	3050	1042	635
	B	717	3300	2750	1047	589
	C	—	—	3000	—	—
Per cent of initial activity found in $KClO_4$ residue	A	34	69	65	44	27
	B	33	70	59	44	25
	C	—	—	64	—	—

* Sample weights: I, IV and V contained 0.3289 gm. of $KClO_4$ and 0.0153 gm. of $KClO_3$; II and III contained 0.6579 gm. of $KClO_4$ and 0.0306 gm. of $KClO_3$.

Isothermal decomposition of potassium perchlorate. Samples of purified potassium perchlorate were decomposed in the apparatus described above at various constant pressures of air or oxygen and at various constant temperatures from 555° C. to 590° C. Sample temperatures were measured with a K2 potentiometer in earlier experiments and were recorded continuously after the recording potentiometer was incorporated into the apparatus.

The experimental procedure used in obtaining the kinetic data was as follows. For the decompositions carried out under constant pressure of air, the system was adjusted initially to atmospheric pressure (725 to 730 mm. Hg), and the pressure was held constant within 1 mm. during the experiment. A sample of pure potassium perchlorate weighing 0.500 gm. was used in each run, except that 2.000-gm. samples were used in 3 experiments designed to study the solid-phase decomposition only. Sample temperature was recorded at 3-min. intervals when manual measurements were made. The volume of oxygen evolved was measured at intervals of 2 to 5 min., depending upon the length of the run.

When decompositions were carried out under constant pressures of oxygen, the entire system was isolated from the atmosphere and evacuated, and then oxygen was introduced into the apparatus. This process of evacuating and filling with oxygen was repeated 3 times to ensure a pure atmosphere. The entire system was adjusted to the desired pressure as measured by the open-arm manometers. The stopcocks to the compensator tubes then were closed, establishing the constant pressure for the decomposition.

Initial volume measurements corresponding to zero were taken when the temperature of the sample reached 550° C. This temperature was reached within a minute after the sample was introduced into the heated zone of the sample tube, and the maximum temperature in every case was reached within 3 min. No appreciable decomposition occurred below 550° C., and the thermal expansion above 550° C. of the oxygen initially present was negligible.

The temperature assigned to an experiment was determined by studying the graph of time versus sample temperature given by the Brown potentiometer. The curve fluctuates as a result of control cycling, and the average temperature of the decomposition is given by that isothermal line so drawn that areas enclosed by the curve above and below the line are nearly equal. Sample temperature was controlled to the nearest ±2° C., and the root mean-square temperature of a decomposition was determined to the nearest ±0.2° C.

Volume measurements were taken at suitable intervals, ranging from every 30 sec. for a rapid decomposition at high temperature to every 5 min. for low-temperature decompositions. During the decomposition in the solid phase, volume readings were taken immediately after the solenoid valve had closed, since the gas was evolved so slowly that often 2 to 3 min. elapsed between successive increments in volume. When one burette was filled, the stopcock above the reaction tube was turned to connect the other half of the system. The first burette then was isolated from the system, opened to the air, and refilled with mercury.

Sample size was regulated by, and directly proportional to, the pressure at which the decomposition took place. No more than 4 burettes (400 ml.) of gas were collected for a single decomposition; therefore, at a pressure of one fourth atmosphere of oxygen, a 0.250-gm. sample was used. For decompositions at a constant pressure of 1¼ atmosphere, 1.000-gm. samples were used. Several decompositions in the solid phase alone were undertaken with a 2.000-gm. sample size.

The relative amounts of potassium chlorate and potassium chloride formed at each stage of decomposition must be known in order to calculate the fraction of residual potassium perchlorate from the volume of oxygen evolved. The molar ratio $KClO_3/KCl$ as a function of mole percentage $KClO_4$ was reported by Harvey *et al.*[8] for the decomposition of potassium perchlorate under pressure of evolved oxygen. In order to use this graph in the present work it was necessary to establish the fact that the $KClO_3/KCl$ ratio varies in the same way under conditions of constant pressure. Three duplicate runs were made in which potassium perchlorate was decomposed at different temperatures and the residues were recovered and analyzed for chlorate and chloride. The results of these experiments, superimposed upon the original data,[8] are given in FIGURE 2. The data from these experiments (triangular points on plot) establish the fact that the graph is valid for decomposition at constant pressure.

Differential thermal analysis of potassium chlorate. A number of differential thermal analyses of potassium chlorate were made in which the runs were stopped at various temperatures ranging from 330° C. (below the melting point) to about 600° C. The purpose of these studies was twofold: (1) to establish a record of the thermal behavior of potassium chlorate throughout the range from room temperature to 600° C.; and (2) to determine the relative amounts of products formed at various stages of decomposition. In addition, isothermal decompositions of potassium chlorate were made at 400° and 500° C. in an effort to establish the temperature range in which this material begins to decompose. In all experiments the decomposition residues were recovered, weighed, and analyzed for chloride and chlorate content. Perchlorate was calculated by difference.

In the differential thermal analyses, 0.8000-gm. samples of potassium chlorate and 1.0 gm. of potassium chloride as reference material were placed into the appropriate compartments of the reaction tube. The tube was sealed into the rest of the apparatus, and the entire system was evacuated with an oil-vacuum pump. The mercury manometer was read with a cathetometer, and heating was begun. The rate of heating was maintained at about 7° C./min. with a variable voltage transformer (Variac). Measurements of change in pressure and of sample temperature were made alternately at 3-min. intervals. In a few cases the sample was observed visually throughout the run to note the occurrence of phase changes. At the end of a run the decomposition residue was recovered by dissolving the remaining material in distilled water and evaporating this solution to dryness. The resulting residue was weighed and dissolved in distilled water for analysis.

FIGURE 3 shows the corresponding heating-rate curve and pressure-time curve for the same sample.

From FIGURE 3 it may be seen that potassium chlorate undergoes no changes in crystal structure or other phase changes in the range from room temperature up to the melting point. Melting starts at 350° ± 0.9° C. and is complete at 359° ± 0.9° C. under DTA conditions. It was observed visually that a large dip in the DTA curve is produced at the transition from solid phase to liquid phase. As the temperature rises the liquid potassium chlorate begins to decompose, evolving oxygen. At temperatures above 500° C. decomposition is rapid. After melting occurs the sample remains in the liquid phase during differential thermal analysis up to 600° C., the highest temperature of any experiment.

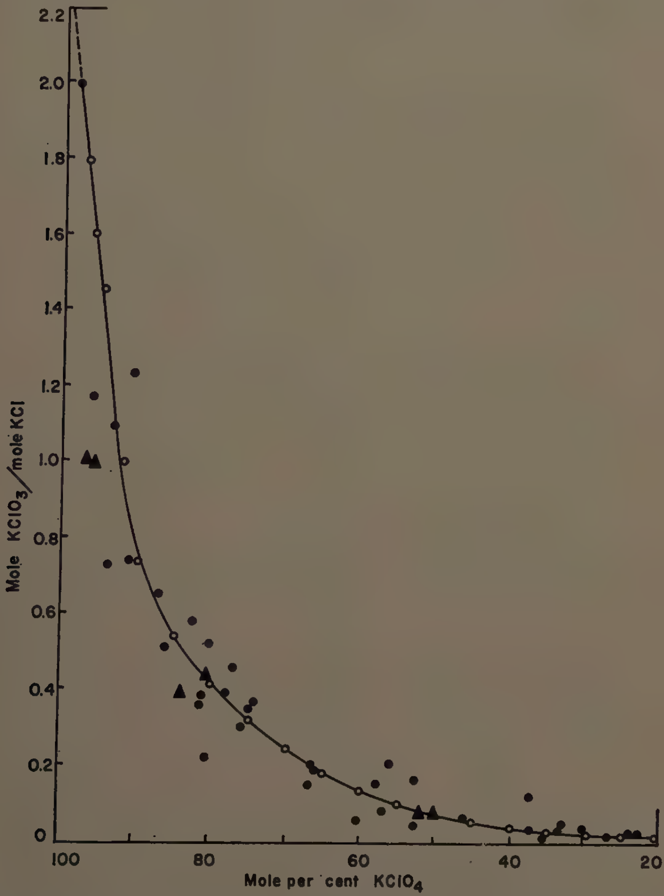

FIGURE 2. Chlorate/chloride ratio during thermal decomposition of potassium perchlorate. Symbols: solid circle, experimental points from decompositions, under pressure, of evolved gas; open circles, calculated by method of least squares (graphical); triangles, experimental check points at atmospheric pressure.

The results of the chemical analyses of the DTA decomposition residues are presented in TABLE 3.

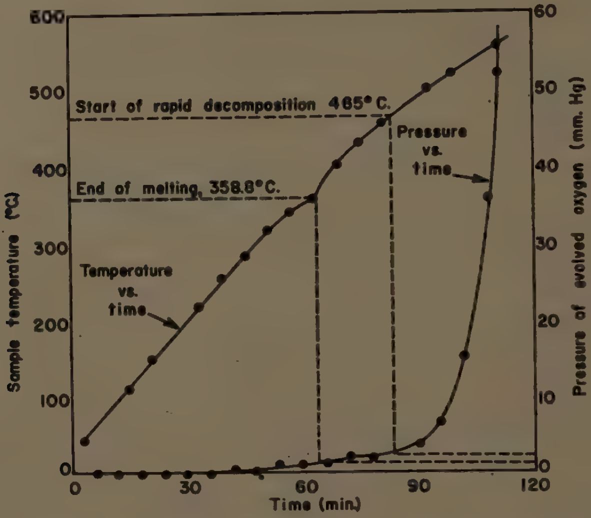

FIGURE 3. Decomposition and heating rates of 0.8000-gm. sample of potassium chlorate.

TABLE 3

DECOMPOSITION OF POTASSIUM CHLORATE AT VARIOUS STAGES OF DIFFERENTIAL THERMAL ANALYSIS

Sample number	Temperature at end of run (°C.)	$KClO_3$ decomposed (mole %)	Ratio* (mole/mole)	$KClO_4/KCl$ in residue (mole/mole)
A-5	478	0.0	—	—
A-6	498	0.0	—	—
A-10	504	8.9	†	2.7
A-9	509	11.2	7.8	2.5
A-8	555	83.7	5.8	2.0
A-7	556	83.7	6.1	1.9

* Ratio of moles of $KClO_3$ decomposing by $KClO_3 = \frac{3}{4}KClO_4 + KCl$ to moles of $KClO_3$ decomposing by $KClO_3 = KCl + \frac{3}{2}O_2$.

† Slight leak in system prevented calculation of this value.

Results

Representative kinetic curves for the isothermal decomposition of potassium perchlorate are presented in FIGURE 4. These curves show that the reaction occurs by two first-order reactions: a solid-phase decomposition followed by a liquid-phase decomposition. During the phase transition, both reactions occur simultaneously, as indicated by the nonlinear portions of the curves. Toward the end of decomposition a solid phase reappears, and the reaction rate decreases.

Initial experiments were carried out under an atmosphere of air; pressures were held constant at prevailing atmospheric pressure (725 to 730 mm. Hg). The rate constants for the decomposition under these conditions are presented in TABLE 4.

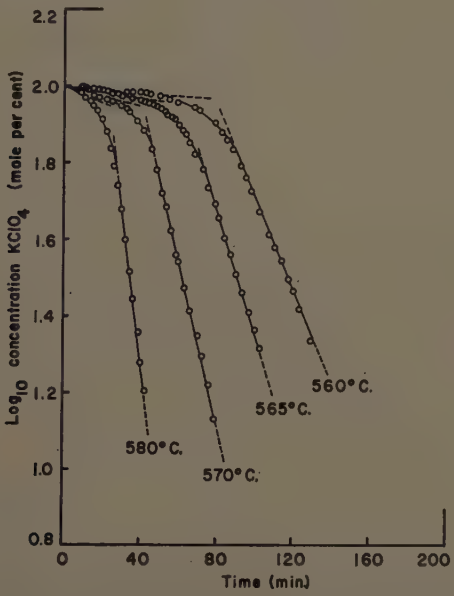

FIGURE 4. Isothermal decomposition of potassium perchlorate at various temperatures.

TABLE 4

RATE CONSTANTS FOR THE ISOTHERMAL DECOMPOSITION OF POTASSIUM PERCHLORATE UNDER ATMOSPHERIC PRESSURE

Temp. (°K)	Solid-phase reaction $k_s \times 10^5$ (sec.$^{-1}$)	Liquid-phase reaction $k_l \times 10^4$ (sec.$^{-1}$)
828.0	2.01	3.61
832.0	2.48	—
832.5	2.54	—
833.5	—	4.58
833.5	—	4.32
834.0	3.84	—
837.5	2.58	—
838.5	5.91	—
839.0	5.41	6.18
840.0	4.53	—
843.0	7.60	8.00
843.5	—	9.08
844.0	4.80	9.54
845.0	7.29	—
846.0	5.07	—
846.5	5.22	—
848.0	8.75	10.7
849.5	8.98	9.61
852.5	9.60	15.7
854.0	—	14.8

In subsequent experiments the system was evacuated and then filled with oxygen so that a constant pressure of oxygen was maintained throughout the runs. In this series of experiments various constant pressures from one quarter to one and one quarter atmospheres of oxygen were used. Rate constants for the solid and liquid phase decompositions are presented in TABLES 5 and 6, respectively.

TABLE 5
RATE CONSTANT FOR THE SOLID-PHASE ISOTHERMAL DECOMPOSITION OF POTASSIUM PERCHLORATE UNDER VARIOUS CONSTANT PRESSURES OF OXYGEN

Pressure (mm. Hg)									
190		380		570		728 ± 4		950	
Temp. (°K)	$k_s \times 10^5$ (sec.$^{-1}$)	Temp. (°K)	$k_s \times 10^5$ (sec.$^{-1}$)	Temp. (°K)	$k_s \times 10^5$ (sec.$^{-1}$)	Temp. (°K)	$k_s \times 10^5$ (sec.$^{-1}$)	Temp. (°K)	$k_s \times 10^5$ (sec.$^{-1}$)
833.8	3.84	832.2	2.89	833.9	2.35	833.0	3.46	831.7	2.40
838.3	4.35	835.2	3.27	844.0	3.79	836.0	2.56	838.6	2.71
838.7	4.21	837.5	3.05	844.2	4.23	842.5	4.22	841.9	3.77
839.6	3.50	839.2	3.70	849.1	5.50	843.0	4.83	843.3	3.68
845.1	5.84	839.8	4.31	857.7	6.76	845.5	5.42	844.0	4.31
847.4	6.53	844.6	5.32	853.3	7.02	847.0	7.98	850.7	5.56
851.0	7.04	845.7	8.42			847.5	10.9	853.0	5.72
854.4	8.40	847.9	6.72						
		848.4	6.88						
		848.6	5.22						
		848.7	7.34						
		848.9	7.86						
		848.9	8.78						

TABLE 6
RATE CONSTANTS FOR THE LIQUID-PHASE ISOTHERMAL DECOMPOSITION OF POTASSIUM PERCHLORATE UNDER VARIOUS CONSTANT PRESSURES OF OXYGEN

Pressure (mm. Hg)									
190		380		570		728 ± 4		950	
Temp. (°K)	$k_1 \times 10^4$ (sec.$^{-1}$)	Temp. (°K)	$k_1 \times 10^4$ (sec.$^{-1}$)	Temp. (°K)	$k_1 \times 10^4$ (sec.$^{-1}$)	Temp. (°K)	$k_1 \times 10^4$ (sec.$^{-1}$)	Temp. (°K)	$k_1 \times 10^4$ (sec.$^{-1}$)
834.8	9.91	836.0	7.92	844.1	7.41	834.0	5.68	838.2	8.08
840.1	11.2	837.1	8.08	852.7	10.7	839.0	7.69	838.2	8.24
843.3	12.3	837.2	8.93	852.5	11.2	842.0	8.14	844.9	10.9
847.5	14.0	841.3	9.74	854.3	13.1	842.5	9.78	844.9	11.2
850.1	15.5	848.6	13.8	861.2	18.6	847.5	11.5	848.0	12.8
851.7	17.7	850.1	15.3			848.0	13.9	848.3	14.1
856.4	20.3	851.4	16.5			848.5	15.6	854.0	18.1
		851.9	17.0					855.3	18.5
		852.8	19.8					857.1	21.1
		855.3	21.2					857.8	20.8
		856.1	22.0						

A representative plot of log k versus $(1/T)$ from which the activational enthalpies and frequency factors are obtained is given in FIGURE 5. Activational entropies were calculated from the Eyring equation, using the above-mentioned activational enthalpies. These entropies are average values for the range of temperatures in which the studies were made. Activational enthalpies and activational entropies for solid- and liquid-phase reactions at various constant pressures are presented in TABLES 7 and 8, respectively.

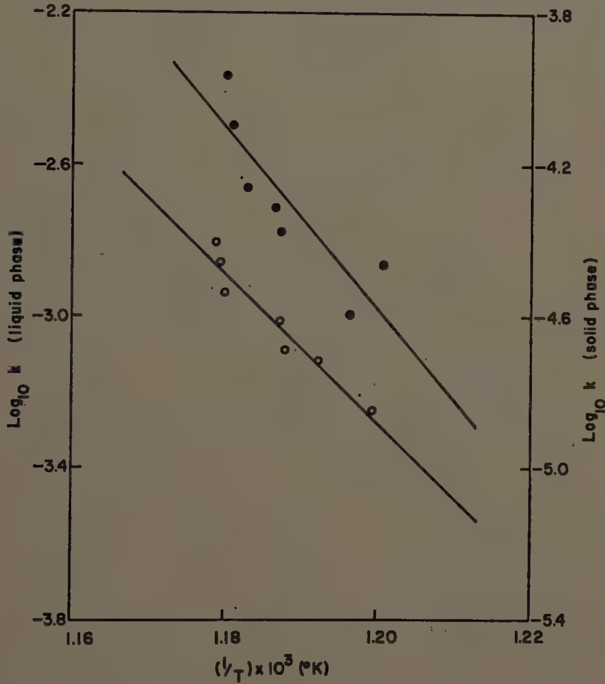

FIGURE 5. Typical data for determination of activational enthalpy for thermal decomposition of potassium perchlorate at an oxygen pressure of 1 atmosphere. Symbols: solid circles, solid phase; open circles, liquid phase.

Discussion

Any mechanism proposed for the thermal decompostion of $KClO_4$ must take account of the four following observations:

(1) The rate of the decomposition, as well as the activational energy, is essentially independent of oxygen pressure, as far as our data show. The rather poor precision does allow for some slight pressure dependence.

(2) When $KClO_4$ is heated at temperatures above 550° C. the amount of $KClO_3$ does not exceed a few mole per cent. The radio tracer experiment shows that $KClO_3$ re-forms $KClO_4$ under these conditions.

(3) If $KClO_4$ is heated long enough above 550° C., the final products are only KCl and O_2.

(4) If $KClO_3$ is decomposed at 500° C., $KClO_4$ builds up in the melt. Under these conditions the rate of disappearance of potassium chlorate, as well as the rates of appearance of potassium perchlorate, potassium chloride, and oxygen, are apparently zero order with respect to mole fraction of the component in each case.

TABLE 7

KINETIC QUANTITIES FOR THE SOLID-PHASE ISOTHERMAL DECOMPOSITION OF POTASSIUM PERCHLORATE UNDER VARIOUS CONSTANT PRESSURES OF OXYGEN

Quantity	190 mm.	380 mm.	570 mm.	728 ± 4 mm.	950 mm.	Decomposition at constant volume (ΔE)
Activational enthalpy, (ΔH kcal./mole)	65.7 ± 8.4	77.1 ± 13.5	69.7 ±3.2	72.5 ± 5.7	72.0 ± 13.7	70.5 ± 4.6
Activational entropy, (ΔS cal./mole-degree)	−2.4 ± 10.0	11.2 ± 13.4	1.4 ± 2.3	3.6 ± 0.5	4.5 ± 9.1	0.6 ± 2.7

TABLE 8

KINETIC QUANTITIES FOR THE LIQUID-PHASE ISOTHERMAL DECOMPOSITION OF POTASSIUM PERCHLORATE UNDER VARIOUS CONSTANT PRESSURES OF OXYGEN

Quantity	190 mm.	380 mm.	570 mm.	728 ± 4 mm.	950 mm.	Decomposition at constant volume (ΔE)
Activational enthalpy, (ΔH kcal./mole)	67.2 ± 5.2	71.6 ± 3.1	73.1 ± 3.6	70.1 ± 10.6	70.6 ± 2.0	70.5 ± 3.2
Activational entropy, (ΔS cal./mole-degree)	−1.7 ± 3.1	10.9 ± 3.7	4.6 ± 3.2	3.1 ± 2.0	9.5 ± 1.8	8.6 ± 4.6

The above observations are consistent with the following reaction sequence for the decomposition of $KClO_4$ above 550° C.:

$$KClO_4 \xrightarrow{k_1} KClO_3 + \tfrac{1}{2}O_2 \qquad (1)$$

$$KClO_3 \xrightarrow{k_2} KCl + \tfrac{3}{2}O_2 \qquad (2)$$

$$KClO_3 \xrightarrow{k_3} \tfrac{3}{4}KClO_4 + \tfrac{1}{4}KCl \qquad (3)$$

Since a plot of log $[KClO_4]$* versus time is linear and since $[KClO_3]$ never builds up above a few mole per cent, REACTION 1 is first-order and rate-determining. The tracer studies provide evidence for REACTION 3.

---

* Brackets [ ] are used in this paper to denote mole fractions.

The differential equations for the appearance of each reaction component are:

$$d\,\frac{[\mathrm{KClO_4}]}{dt} = -k_1[\mathrm{KClO_4}] + \frac{3}{4}\,k_3[\mathrm{KClO_3}] \qquad (A)$$

$$d\,\frac{[\mathrm{KClO_3}]}{dt} = k_1[\mathrm{KClO_4}] - k_2[\mathrm{KClO_3}] - k_3[\mathrm{KClO_3}] \qquad (B)$$

$$d\,\frac{[\mathrm{KCl}]}{dt} = k_2[\mathrm{KClO_3}] + \frac{1}{4}\,k_3[\mathrm{KClO_3}] \qquad (C)$$

$$d\,\frac{[\mathrm{O_2}]}{dt} = \frac{1}{2}\,k_1[\mathrm{KClO_4}] + \frac{3}{2}\,k_2[\mathrm{KClO_3}] \qquad (D)$$

Consider the case in which one begins with 1 mole $\mathrm{KClO_4}$. Then the boundary conditions are:

$$[\mathrm{KClO_4}] + [\mathrm{KClO_3}] + [\mathrm{KCl}] = 1$$

At $t = 0$

$$[\mathrm{KClO_4}] = 1, \qquad [\mathrm{KClO_3}] = [\mathrm{KCl}] = [\mathrm{O_2}] = 0$$

At $t = \infty$

$$[\mathrm{KClO_4}] = [\mathrm{KClO_3}] = 0, \qquad [\mathrm{KCl}] = 1, \qquad [\mathrm{O_2}] = 2$$

Since $[\mathrm{KClO_3}]$ always remains small, a solution of EQUATION A that conforms to observations is A', $[\mathrm{KClO_4}] = e^{-k_1 t}$. Subsequent substitution of this into EQUATION B, C and D yields for the solutions of these equations:

$$[\mathrm{KClO_3}] = \frac{k_1}{k_2 + k_3 - k_1}\,[e^{-k_1 t} - e^{-(k_2+k_3)t}] \qquad (B')$$

$$[\mathrm{KCl}] = 1 - e^{-k_1 t} - \frac{k_1}{k_2 + k_3 - k_1}\,[e^{-k_1 t} - e^{-(k_2+k_3)t}] \qquad (C')$$

$$[\mathrm{O_2}] = -\frac{(\frac{1}{2}k_1 + a)e^{-k_1 t}}{k_1} + \frac{a}{k_2 + k_3}\,e^{-(k_2+k_3)t} + \frac{1}{2}\frac{(k_1 + a)}{K_k} - \frac{a}{k_2 + k_3} \qquad (D')$$

where

$$a = \frac{3}{2}\,\frac{k_1 k_2}{k_2 + k_3 - k_1}$$

It is not unreasonable to suppose that $k_2 > k_1$ (this accounts for the low $\mathrm{KClO_3}$ concentration throughout the course of the reaction) and that, since an appreciable amount of the $\mathrm{KClO_3}$ produced re-forms $\mathrm{KClO_4}$, $k_3 > k_2$ and k_1. Tentatively, then, the order of rate constants is $k_3 > k_2 > k_1$. Analysis of melts at various periods of time for $\mathrm{KClO_3}$ shows that EQUATION (B') accounts well for the experimental observations, but $[\mathrm{KClO_3}]$ is fairly independent of postulated k_2/k_1 ratios. The ratio lies between 2 and 100. If the above arguments are valid, the following simplifications can be effected in EQUATIONS B' and C':

$$[\mathrm{KClO_3}] = \frac{k_1}{k_2 + k_3} e^{-k_1 t} \qquad (B'')$$

$$[\mathrm{KCl}] = 1 - e^{-k_1 t} - \frac{k_1}{k_2 + k_3} e^{-k_1 t} = 1 - e^{-k_1 t}\left(1 + \frac{k_1}{k_2 + k_3}\right) \qquad (C'')$$

From a consideration of these equations one can argue that $k_1/(k_2 + k_3)$ cannot be negligibly small, for otherwise no $KClO_3$ would appear. The value $(k_2 + k_3)$ can be estimated using the data of TABLE 1. Thus, for the solid-phase decomposition of $KClO_4$ at 561° C. $k_1 \simeq 3 \times 10^{-5}$ sec.$^{-1}$ (*see* TABLE 5). We then calculate $(k_2 + k_3)$ from EQUATION (B'') and experimental values of $[\mathrm{KClO_3}]$. Unfortunately, $[\mathrm{KClO_3}]$ and $[\mathrm{KCl}]$ are not particularly time-sensitive in the initial stages of the reaction when the equations would be expected to apply best. For the various values in TABLE 1 $(k_2 + k_3)$ varies from 0.0010 to 0.0014 sec.$^{-1}$ If these values are then used to calculate [KCl] from EQUATION (C''), the calculated values agree fairly well with the experimental ones. The above range of values for $(k_2 + k_3)$ is also consistent with the hypothesis that REACTION 1 is rate-determining.

An accurate determination of k_2 and k_3 individually is not possible from our data. However, at 400° C., where $KClO_3$ is solid, the ratio of $KClO_3$ decomposed by REACTION 3 to REACTION 2 is 3.4. If this ratio holds at 560° C. for the solid phase decomposition of $KClO_4$, k_2 and k_3 can be estimated as 0.0003 and 0.0007 sec.$^{-1}$ respectively. This also agrees with the statement (made previously) that $k_3 > k_2 > k_1$.

The problem of determining k_2 and k_3 for the liquid-phase decomposition of $KClO_4$ is more involved because it is not possible to start with pure liquid $KClO_4$. One can well argue from the data, however, that the reactions in the liquid are essentially the same as in the solid: (1) the disappearance of $KClO_4$ follows a first-order law, but k_1 is about 20 times as great as for the solid-phase reaction; (2) $KClO_3$ and KCl are also formed; and (3) activational energies, enthalpies, and entropies are about the same. It may be, however, that the relative magnitudes of k_2 and k_3 are different. For example, in the decomposition of $KClO_3$ at 500° C. it was found that the ratio of $KClO_3$ disappearing by REACTION 3 compared to REACTION 2 had changed from 3.4 (at 400° C.) to 8.2, which suggests that k_3 is larger relative to k_2 in the liquid decomposition. However, insufficient data are available to establish this with more certainty.

We consider next the activational energies. Unfortunately, their precision is rather poor. The relative constancy of $\Delta H^{\neq}$ at various oxygen pressures suggests that the gas is not involved in any equilibrium reaction.

Tracer studies with O^{18} above the reaction mixture would be useful to establish this point. If REACTION 1 is rate-determining, $\Delta H^{\neq}$ and $\Delta S^{\neq}$ are the activational quantities for that reaction. The standard enthalpies of formation of $KClO_4$ and $KClO_3$ at 25° C. are −103.6 and −93.5 kcal./mole respectively and, since their heat capacities do not differ greatly, ΔH^0 for the reaction $KClO_4 \rightarrow KClO_3 + \frac{1}{2}O_2$ at 560° C. should be close to that at 25° C. The above values yield only 10.1 kcal. for ΔH^0, whereas $\Delta H^{\neq}$ is 70 kcal. The reaction essentially involves the breaking of a Cl—O bond. However, if atomic oxygen is formed in the reaction ($\Delta H_f{}^0 = 59.2$ kcal./mole) we get for ΔH^0 69.3 kcal., in excellent agreement with the experimental $\Delta H^{\neq}$. The small values of $\Delta S^{\neq}$ suggest that the activated complex is not ordered differently from the reactants; that is, bond distances in $ClO_4{}^-$ ion do not change perceptibly prior to decomposition.

References

1. Glasner, A. & A. E. Simchen. 1951. Bull. soc. Chim. France. **18**(5): 233.
2. Simchen, A. E. & A. Glasner. 1952. Bull. soc. Chim. France. **19**: 963.
3. Simchen, A. E. & A. Glasner. 1953. Bull. soc. Chim. France. **20**: 127.
4. Simchen, A. E., A. Glasner & B. Fraenkel. 1952. Bull. Research Council Israel. **2**(1): 70.
5. Glasner, A. & L. Weidenfeld. 1952. J. Am. Chem. Soc. **74**: 2467.
6. Prout, E. G. & F. C. Tompkins. 1944. Trans. Faraday. Soc. **40**: 488.
7. Bircumshaw, L. L. & T. A. Phillips. 1952. J. Chem. Soc. **142**: 703.
8. Harvey, A. E., M. T. Edmison, E. D. Jones, R. A. Seybert & K. A. Catto. 1954. J. Am. Chem. Soc. **76**: 3270.
9. Farmer, W. & J. B. Firth. 1924. J. Chem. Soc. **125**(I): 82.
10. Franklin, P. F. & J. Dingwall. 1887. J. Chem. Soc. **51**: 274.
11. Glasner, A. & L. Weidenfeld. 1952. J. Am. Chem. Soc. **74**: 2464.
12. Serullas, M. 1831. Ann. Chim. **46**: 323.
13. Sodeau, W. H. 1900. J. Chem. Soc. **77**: 137.
14. Teed, F. L. 1887. J. Chem. Soc. **51**: 283.
15. Bosch, A. V. & A. H. W. Aten. 1953. J. Am. Chem. Soc. **75**: 3853.
16. Palmer, W. G. 1954. Experimental Inorganic Chemistry. : 465–466. Cambridge Univ. Press. Cambridge, England.
17. Willard, H. H. & G. M. Smith. 1939. Ind. Eng. Chem. Anal. Ed. **11**: 305.

ISOTOPE ENRICHMENT BY ELECTROMIGRATION IN A MIXTURE OF MOLTEN $RbNO_3$ AND $LiNO_3$*

Arnold Lundén

Department of Physics, Chalmers Institute of Technology, Gothenburg, Sweden

The discovery that chemical elements can consist of several isotopes led to attempts to find methods by which the isotopes of an element could be separated from each other. Lindemann[1] suggested in 1921 that this could be done by electromigration if the mobility of an ion depended on its mass. At that time Kendall and his co-workers[2-4] had already begun attempts to enrich chlorine isotopes by ionic migration in solutions enclosed in agar gels in order to suppress mixing by convection. However, neither they nor other investigators[5] could produce any detectable shifts in isotopic composition, and it was concluded[6,7] that if there existed any difference in mobility for a pair of isotopes, it was too small to be detected. The interest shifted to more promising methods for isotope separation, but during World War II the electromigration method was studied again. The first successful experiments in aqueous solutions were performed at the National Bureau of Standards, Washington, D.C., by Brewer *et al.*,[8,9] who enriched both light and heavy isotopes of potassium. Since then few electromigration experiments have been carried out in aqueous solutions.[10-18]

From the early unsuccessful work with aqueous solutions Klemm concluded that it would be easier to detect isotope effects if the electromigration were carried out in a medium in which solvation did not decrease the relative difference between the masses of the migrating units. Hence, he studied electromigration in a solid salt with good conductivity,[19,20] α-AgI_0 and was able to show that the heavy isotope of silver was enriched toward the anode, as was to be expected if the mobility of the silver ions was mass-dependent. Later Klemm began to study electromigration in molten salts and, thus far, isotopes of about ten elements have been enriched by this method,[21,22] mainly in halides, but also in lithium and potassium nitrate. Chemla[23] has used a slightly different method when measuring isotope effects for electromigration in molten nitrates.

The primary aim of the present investigation was to measure the isotope effect for rubidium ions in $RbNO_3$. I chose to work with the salt chain cathode-$LiNO_3$-$RbNO_3$-anode with which it should be possible to obtain a sharp boundary between the two nitrates, due to the difference in conductivity.[24,25] The apparatus of Supremax glass used (FIGURE 1) was somewhat similar to the cells used previously for $LiNO_3$[26] and KNO_3;[27] where, however, only one salt was used in the cell. The two electrode compart-

---

* The work reported in this paper was supported in part by grants from the Atomkommittén, Stockholm, Sweden and by the Chalmerska Forskningsfonden, Gothenburg, Sweden.

ments were separated by a U-bent separation column (length, 24 cm.; inner diameter, 4.2 mm.), packed with glass powder (grain size, 0.15 to 0.20 mm.), held in place by fritted glass disks. The salts used were of C.P. grade. The anode compartment (at the left of FIGURE 1) was filled with 17.96 gm. $RbNO_3$, which was melted under a vacuum, during which procedure the melt penetrated into the separation column and nearly filled the column to the top on the cathode side of the bend. Lumps of $LiNO_3$ (12.84 gm.), previously remelted under a vacuum, were placed in the cath-

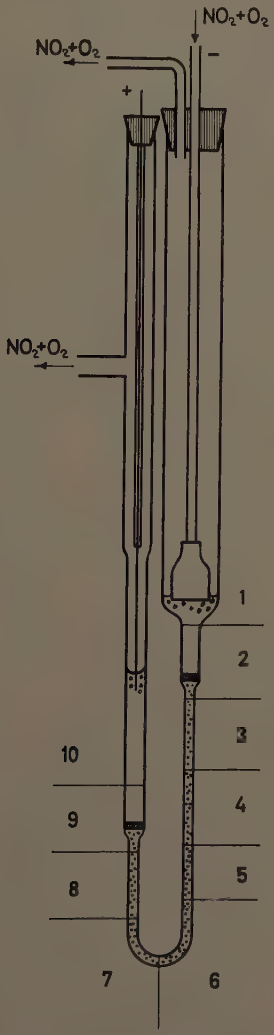

FIGURE 1. The electromigration cell. After the run the cell was divided into ten samples.

ode compartment; after a final evacuation for more than 1 hour hardly any gas evolved from the melt. The electrodes were inserted and the electrolysis started. The anode was a platinum wire, while the cathode of stainless steel was bell-shaped and hollow, with the opening covered by a steel net, through which a mixture of nitrogen dioxide and oxygen bubbled into the melt, thus regenerating $LiNO_3$ at the cathode.[26] I had calculated the amount of salts so that the boundary between the 2 nitrates should be in the upper part of the separation column (somewhere near the boundary between sample 3 and 4 in FIGURE 1), but there was no way of detecting the position of the boundary. The only check I had was made by following the height of the salt in the anode compartment with a cathetometer. The transported charge was measured with a copper coulometer and, at frequent intervals, I took readings of the current and voltage across the cell. The cell resistance showed rapid fluctuations in which an increase in resistance often was connected with gas evolving from the separation column. I tried to counteract these disturbances by altering the input current. The run was shut down after 106.8 hours, when the transported charge was 79,500 coulombs, corresponding to a mean current of 207 mAmp. and a current density in the column of 3.5 amp./cm.^{2}

After the cell had cooled, it was divided into 10 samples (FIGURE 1). The samples were weighed and the salt soaked out in boiling water. By weighing the remaining glass the total amount of salt was determined. The perchlorate-alcohol method[28] was used to separate the rubidium and lithium salts. Of other alkali metals present as impurities, potassium and cesium followed the first fraction, and sodium, the second. The chemical analysis (TABLE 1) showed that there had not been a sharp boundary between the two components in the separation column (nor was this the case in other runs not quoted here). An indication that the salts had mixed actually appeared when the cell was quenched, since the salt in the anode compartment solidified at a much lower temperature than expected for pure $RbNO_3$ (compare these results with the phase diagram[29] for $LiNO_3$-$RbNO_3$). The fact that I did not obtain a sharp boundary between the two salts could be due to the occurrence of mixing when gas bubbles were evolved and moved through the separation column, but such bulk movements of salt in the column should have counteracted the isotope-enrichment effect considerably, which does not seem to have been the case. That gas evolution in the column caused more trouble in the present experiment than in previous work with $LiNO_3$[26] and KNO_3[27] is due both to the higher temperature in the column this time (in the previous experiments the separation column was surrounded by the lower part of the big cathode compartment, thus providing more efficient cooling) and to the fact that decomposition begins at lower temperatures for a mixture of nitrates than for pure salts.[30] The temperature in the oven was 350° C. (measured on a level with the bottom of the cell); it could be estimated to be about 450° C. in the separation column.[31]

The perchlorates were converted to nitrates for the determination of the isotopic abundance ratios. The mass spectrometer was equipped with a three-filament thermal ion source[32,33] suitable for measuring alkali metals as nitrates. The procedure used in my measurements is described elsewhere.[33] In the analysis of the samples, not only the isotopic abundance ratio in question, but also the amounts of chemical impurities in the different samples were measured. This was done by comparing the heights of the peaks for Li^7, Na, K^{39}, Rb^{85}, and Cs, both in the samples and in standard samples of known composition. The peak heights themselves are very sensitive to changes in the filament current (and thus in the temperature) in the ion source, but the ratios are fairly stable. At the present stage of development, this simple mass spectrometer arrangement cannot be expected to give accurate results concerning the chemical composition,[34] but the method surely can be improved. The measured mass and abundance ratios are given in TABLE 1. After some corrections, for example, estimation of the amount of measured potassium due to "memory" in the mass spectrometer, I calculated the corrected chemical composition (TABLE 2).

TABLE 1

GRAVIMETRICAL AND MASS SPECTROMETRICAL ANALYSES OF SAMPLES

Sample No.	Fraction		Rb^{85}/Rb^{87}	Li^7/Li^6	K^{39}/K^{41}	$(K/Rb)\cdot 10^3$	$(Cs/Rb)\cdot 10^3$	$(Na/Li)\cdot 10^3$
	$RbNO_3$ (mg.)	$LiNO_3$ (mg.)						
1	258.4	4050.5	2.89	11.45	14.3	509	2.8	6
2	75.8	3783.3	2.97	11.59	14.2	103	0.2	190
3	132.1	395.7	3.21	12.24	—	240*	0.2	9
4	447.5	189.2	3.00	13.95	—	19	1.0	70
5	325.0	115.6	2.77	13.92	—	13	0.2	—
6	332.2	120.7	2.69	14.09	—	11	—	190
7	372.4	129.9	2.65	14.32	—	26	3.9	106
8	520.6	136.2	2.62	14.66	—	16	5.9	170
9	2980.7	586.8	2.62	15.24	—	4	12.5	76
10	12581.6	1838.5	2.62	14.97	—	6	7.9	73

* High contents of K partly due to memory effects in mass spectrometer.

For K/Rb, Cs/Rb, and Na/Li the ratios of the mass spectrometer readings were multiplied by 0.57, 0.33, and 6.2, respectively, to give weight ratios. These correction factors were determined by measuring standard samples of known chemical composition. The correction factor for Na/Li is the least accurate one.

The normal K^{39}/K^{41} abundance ratio is 14.0.

As expected, it is found that the light isotopes of rubidium, potassium, and lithium are enriched toward the cathode and the heavy isotope of lithium toward the anode. Measured relative to $RbNO_3$ the potassium salt is enriched toward the cathode and the cesium toward the anode. Sodium shows no pronounced displacement relative to lithium in either direction. Klemm and Monse[35] have discussed different methods to determine in a mixture the mobility b_{ik} of the component i relative to another component k. The present experiment corresponds to the simple case of enclosing a melt in a convection-free tube AC, the wall A of which is impermeable to the two components i and k. A charge Q is transported by a direct current through the melt. When the current is shut off, there still remains, at some distance from A, a region with the original composition. All the material between a point B in this region and the wall A is analyzed and is found to contain N_i and N_k moles of the components i and k. In the original composition the melt had the specific conductivity κ and the mole concentrations c_i and c_k. The mobility b_{ik} can now be calculated:

TABLE 2

CALCULATED AMOUNTS OF NITRATES (EXCEPT $NaNO_3$)

Sample No.	$RbNO_3$ (mg.)	KNO_3 (mg.)	$CsNO_3$ (mg.)	$LiNO_3$ (mg.)
1	165	88	0.5	3605
2	68	7	0.01	3367
3	119	13	0.01	352
4	434	9	0.4	168
5	315	7	0.06	103
6	322	7	—	107
7	361	7	1.4	116
8	505	8	3.0	121
9	2891	30	37	522
10	12204	75	96	1636

According to the mass spectrometer analysis there were minor impurities of $RbNO_3$ and KNO_3 in the $LiNO_3$ fraction and of $LiNO_3$ in the $RbNO_3$ fraction, but these quantities are ignored here.

$$b_{ik} = \frac{\kappa}{Q}\left(\frac{N_i}{c_i} - \frac{N_k}{c_k}\right)$$

This equation is derived by considering N_k moles of component k. Before the current transport N_k moles of component k were mixed with $(c_i/c_k)N_k$ moles of component i. While the charge Q was transported, a total amount Qc_ib_{ik}/κ of moles of component i migrated in the direction CA into the region containing N_k moles of k. In this region the final amount of component i is

$$N_i = \frac{c_i}{c_k} N_k + \frac{Q}{\kappa} c_i b_{ik}$$

which expression is equivalent to the equation given above. The two components i and k can correspond either to two isotopes of the same element or to two different elements (or polyatomic ions). I shall use the subscript n for an anion (always nitrate), p, q, . . . for cations, and a and b for two isotopes.

Consider first b_{pq}, the mobility of one cation relative to another. As $b_{pq} = b_{pn} - b_{qn}$, the expected b_{pq} can be estimated from the individual b_{pn}, which are calculated from the conductivities[24,25] and densities[36] of pure nitrates. Thus is obtained for $b_{pn} \cdot 10^4$ at 450° C. $LiNO_3$, 8.57; $NaNO_3$, 7.53; KNO_3, 5.72; $RbNO_3$, 4.69; and $CsNO_3$, 4.37 $cm.^2 V^{-1} sec.^{-1}$ For calculating b_{pq} from the present experiment certain assumptions concerning c_i, c_k and κ must be made, since the original composition of the melt in the part of the cell that is of interest for the individual calculation is not known definitely. Starting with the displacement of K relative to Rb, it is found that a pronounced enrichment of K has taken place in samples 1 to 3, while the concentration is fairly constant in the other samples. If it is estimated that $c_K = 1.3 \cdot 10^{-5}$ and $c_{Rb} = 61.8 \cdot 10^{-5}$ moles/cm.^{3}, a mobility $b_{K,Rb}$ of the order of $19 \cdot 10^{-4}$ $cm.^2 V^{-1} sec.^{-1}$, is obtained instead of about $1.0 \cdot 10^{-4}$ as expected. In this special case $N_K/c_K \gg N_{Rb}/c_{Rb}$, and the calculation is very sensitive to the assumed value of c_K. The total amount of K (and still more of Na) is higher than expected from the manufacturer's information on the chemicals used; the probable explanation is that some of the impurities are due to reactions between the melt and the glass. If this increase in the amount of KNO_3 had occurred with the same rate throughout the whole cell, a correction for this would give a still higher value for $b_{K,Rb}$, but an investigation of the glass of the cell and separation column showed clearly that the glass had been attacked primarily in samples 1 to 3, in which there was a high concentration of $LiNO_3$, which is much more corrosive than $RbNO_3$; hence the strong enrichment of K in these samples is due not only to electromigration.

If the enrichment of Cs relative to Rb, is considered, a very pronounced enrichment of Cs in samples 7 to 10 is found. However, these samples contain about 90 per cent of the bulk of Rb; therefore accuracy with the equation under these circumstances can not be expected. Moreover, a rapid estimation shows that there does not seem to be any sample remaining that has the original concentration, and that the enrichment might have reached a steady state. Thus, a calculation should give too low values for b_{pq}; this is the case if a calculation is carried out under reasonable assumptions.

The light rubidium isotope is enriched in samples 1 to 7. For calculating the mobility $b_{85,87}$, it may be assumed that in the beginning of the experiment the salt at the boundary between samples 7 and 8 held at least 98 per cent $RbNO_3$, the main impurities being KNO_3 and $CsNO_3$. It is found then that $b_{85,87} = 5.3 \cdot 10^{-7}$ $cm.^2 V^{-1} sec.^{-1}$ at 450° C. For isotope enrichment experiments, however, the quantity of interest usually is the separation coefficient (or elementary process separation factor), which in this case is the relative difference in mobility of the two isotopes $b_{ab}/b_{pn} = \Delta b/b$. For the rubidium isotopes $\Delta b/b = 0.0011$. If, instead, it is assumed that there was already a certain concentration of $LiNO_3$ in sample 7 at the beginning of the run, a corresponding increase in $b_{85,87}$ and $\Delta b/b$ is obtained.

The abundance ratio for the lithium isotopes varies throughout the entire cell; there is no sufficient length of the separation column in which the original abundance ratio is preserved. An average over the composition of all 10 samples gives an initial abundance ratio of about 12.31, which is in good agreement with normal samples measured in other experiments with lithium salts.[33] Thus, in the present experiment the light isotope is enriched in samples 1 to 3 and the heavy one in samples 4 to 10. The run was too long to allow a determination of b_{ab} or $\Delta b/b$ for the lithium isotopes; if, in spite of this, the formal calculations are carried out, the apparent value for the mobility $b_{7,6}$ is expected to be smaller than the true mobility. Moreover, a considerable amount of $LiNO_3$ containing a certain enrichment of Li^6 was lost by sublimation from the cathode compartment (sample 1). If $b_{7,6}$ is estimated under the simplified assumption that in the beginning of the run there was pure $LiNO_3$ at the boundary between samples 3 and 4, it is found that $b_{6,7} = 7 \cdot 10^{-6}$ cm.^{2} V^{-1} sec.$^{-1}$ and $\Delta b/b = 0.0084$. No calculations were carried out on the enrichment of potassium isotopes.

For a comparison with isotope effects in other nitrates it is convenient to calculate the mass effect μ, that is, the relative difference in mobility divided by the relative difference in mass, $\mu = (\Delta b/b/\Delta m/m)$. I found that $\mu = -0.05$ for $RbNO_3$ and $\mu = -0.06$ for $LiNO_3$. The latter figure cannot be given much significance, but it supports recent measurements (Lundén, unpublished work) indicating that the mass effect for Li in $LiNO_3$ might be somewhat higher than -0.050, the value that was first reported.[26,37] It is surprising at first sight that the mass effect is higher for $RbNO_3$ than for KNO_3,[27] where $\mu = -0.035$, but the latter value was determined in a pure salt, while in the present work the $RbNO_3$ was mixed with $LiNO_3$. It is not unlikely that the mass effect is higher in this mixture than in the pure salt, an observation similar to that found by Klemm and Monse for LiCl in $PbCl_2$.[35] Mangalo *et al.*[28] have studied the electromigration at 350° C. of Rb ions in a strip of asbestos impregnated with $NaNO_3$. They reported a relative difference in mobility of 0.0012 (and a mass effect of 0.05) where, however, the reference frame is the asbestos and not the anions as in the present experiment; if the latter reference frame were to be chosen, the recalculated entities would be slightly smaller.[39] The agreement between the present experiment and the measurement on asbestos is about as good as could be expected with the experimental accuracy, considering that the experiments were carried out at different temperatures, that the rubidium ions migrated in different media, and that their concentration was not the same.

Summary

Applying Klemm's method[21] for studying electromigration, the molten salt chain cathode-$LiNO_3$-$RbNO_3$-anode was electrolyzed for 107 hours at

450° C. with a current density in the separation column of 3.5 amp./cm^2. The boundary between the two nitrates was not sharp; after the run both main compounds were present in all samples, together with various amounts of the impurities $NaNO_3$, KNO_3, and $CsNO_3$. The experiment was designed for studying the enrichment of Rb^{85} relative to Rb^{87}; the abundance ratio Rb^{85}/Rb^{87} was increased from 2.62 to 3.21. The elementary process separation factor, which is equal to the relative difference in mobility for the two ions, was 0.0011. The result is compared with isotope effects found in other mixtures and in pure salts. In addition, the isotope abundance ratios Li^7/Li^6 and K^{39}/K^{41} and the concentration ratios K/Rb, Cs/Rb, and Na/Li were measured, and their significance for mobility measurements are discussed.

Acknowledgment

I appreciate the mass spectrometer analyses performed by A. Lodding and the assistance of B. Stenemur and M. Lövenby in the chemical work with the samples.

References

1. Lindemann, F. A. 1921. Proc. Roy. Soc. London. **99A:** 102.
2. Kendall, J. & E. D. Crittenden. 1923. Proc. Natl. Acad. Sci. U. S. **9:** 75.
3. Kendall, J. 1923. Phys. Rev. **21:** 389.
4. Kendall, J. & J. F. White. 1924. Proc. Natl. Acad. Sci. U. S. **10:** 458.
5. Pilley, J. E. G. 1925. Phil. Mag. **49**(6): 889.
6. Jette, E. R. 1927. *Ibid.* **3**(7): 258.
7. Kendall, J. 1942. Nature. **150:** 136.
8. Brewer, A. K., S. L. Madorsky & J. W. Westhaver. 1946. Science. **104:** 156.
9. Brewer, A. K., S. L. Madorsky et al. 1947. J. Research Natl. Bur. Standards. **38:** 137.
10. Madorsky, S. L. & S. Straus. 1947. *Ibid.* **38:** 185.
11. Madorsky, S. L. & S. Straus. 1948. *Ibid.* **41:** 41.
12. Ramirez, E. R. 1954. J. Am. Chem. Soc. **76:** 6237.
13. Ramirez, E. R. 1958. J. Phys. Chem. **62:** 760.
14. Bonnin, A., M. Chemla & P. Sue. 1955. Compt. rend. **241:** 40.
15. Bonnin, A. & M. Chemla. 1956. *Ibid.* **243:** 1112.
16. Bonnin, A. & M. Chemla. 1958. *Ibid.* **246:** 1189.
17. Bonnin, A. 1957. *Ibid.* **244:** 2708.
18. Martin, H. & E. Harmsen. 1958. Z. Electrochem. **62:** 152.
19. Klemm, A. 1944. Naturwiss. **32:** 69.
20. Klemm, A. 1947. Z. Naturforsch. **2a:** 9.
21. Klemm, A. 1958. Proc. Intern. Symp. Isotope Sep., Amsterdam, 1957. : 275. J. Kistemaker, Ed. North Holland, Amsterdam.
22. Lundén, A. 1958. *Ibid.* : 283.
23. Chemla, M. 1958. J. Chromatography. **1:** 2.
24. Sakai, K. 1954. J. Chem. Soc. Japan, Pure Chem. Sect. **75:** 182.
25. Jaeger, F. M. & B. Kapma. 1920. Z. anorg. Chem. **113:** 51.
26. Lundén, A., E. U. Monse & N. G. Sjöberg. 1956. Z. Naturforsch. **11a:** 75.
27. Lundén, A., C. Reuterswärd & N. G. Sjöberg. 1955. *Ibid.* **10a:** 279.
28. Treadwell, F. P. & W. T. Hall. 1942. Analytical Chemistry. **2:** 273. 9th ed. Wiley. New York, N.Y.
29. Puschin, N. A. & M. Radoičič. 1937. Z. anorg. Chem. **233:** 44.
30. Centnerszwer, M. 1930. J. chim. phys. **27:** 9.
31. Herzog, W. & A. Klemm. 1958. Z. Naturforsch. **13a:** 7.
32. Palmer, G. H. 1956. Proc. 1955 Harwell Isotope Conf. Chap. 19. M. L. Smith, Ed. Butterworth. London, England.
33. Lundén, A., S. Christofferson & A. Lodding. 1958. Z. Naturforsch. **13a:** 1034.

34. Voshage, H. 1957. Dissertation. Mainz, Germany.
35. Klemm, A. & E. U. Monse. 1957. Z. Naturforsch. **12a:** 319.
36. Jaeger, F. M. 1917. Z. anorg. Chem. **101:** 1.
37. Vallet, Kepes, Beaufils & Belilowsky. 1958. International Conference for the Peaceful Uses of Atomic Energy. A/Conf. 15/P/1270. Geneva, Switzerland.
38. Mangalo, C., H. J. Arnikar & M. Chemla. 1957. Compt. rend. **244:** 2796.
39. Lundén, A. 1959. Z. Naturforsch. **14A:** 801.

INTERIONIC FRICTION COEFFICIENTS IN MOLTEN SALTS

Richard W. Laity
Frick Chemical Laboratory, Princeton University, Princeton, N.J.

The general formulation for the description of electric and mass-transport phenomena that I have described recently[1] permits the recasting of conductivity, diffusion, and transference data for electrolytic systems into a formalism in which a single type of rate constant suffices to characterize the results of all such experiments. This quantity has been called a friction coefficient. It is defined for a system composed of N distinct ionic and/or neutral species by the relations

$$K_i = -(\nabla\mu_i \pm z_i F \nabla\phi) = \sum_{k=1}^{N} r_{ik} X_k (v_i - v_k) \quad (i = 1, 2, \ldots, N-1) \qquad (1)$$

$$r_{ik} = r_{ki} \qquad (i, k = 1, 2, \ldots, N) \qquad (2)$$

Here the negative gradient of the electrochemical potential of the ith species $-\nabla(\mu_i \pm z_i F\phi)$, which may be called the thermodynamic force K_i on component i, is equated to a sum of terms that are linear in the velocity $(v_i - v_k)$ of i relative to each of the other species k. This sum may be called the frictional force on species i. It is characterized by the set of friction coefficients r_{ik}, the dimensions and magnitudes of which are partially determined by the choice of units for the concentrations X_k. In the present work friction coefficients for various types of molten-salt systems will be calculated from available transport data by considering the melts to be composed only of simple ionic species and expressing the X_k as mole fractions of these ions. The principal objective in examining the results of these computations will be to determine the extent to which a knowledge of the interionic friction coefficients provides useful insight into the nature of transport processes in molten-salt systems.

Before choosing the units in which to express an interionic friction coefficient it may be instructive to consider the physical significance of this quantity in a conceptually simple situation. Suppose that the forces (diffusional and electric) in a system composed of N different ionic species are chosen in such a way that, within a region sufficiently small that each species k may be assigned a concentration X_k, all of the $(N - 1)$ species $k \neq j$ have the same velocity $(v_k - v_j)$ relative to the particular species j. Let i be a particular member of the group, so that $v_i - v_k = 0$ for $k \neq j$. From EQUATION 1 it is seen that the friction coefficient r_{ij} is equal to the total force per unit concentration of j that must be exerted on each mole of species i (within the region under consideration) in order to maintain unit velocity of i relative to j. The reciprocal relation (EQUATION 2) shows that this is identical in magnitude to the force per unit concentration of i

that must be exerted on each mole of j when the roles of i and j are reversed. These quantities are, of course, all macroscopic and thus represent only the net motions of the species under consideration rather than the detailed molecular and ionic movements. To the extent that the species chosen as components correspond to the microscopic entities of transport, however, it may be useful to think of the quantity $1/r_{ij}$ as a measure of the mobility that ion i would have in a "solvent" of pure j in which the j ions offered the same hydrodynamic resistance to transport of i ions as in the system under consideration.

The conductivity data used in calculating the r_{ij} for electrolytes are normally expressed in electric units, yielding friction coefficients with the dimensions ohm coulomb^2 cm.$^{-2}$ mole^{-1}, which are equivalent to joule sec. cm.$^{-2}$ mole^{-1}. The latter units also arise naturally in the calculation of friction coefficients from diffusion coefficients when the gas constant is expressed in joules deg.$^{-1}$ mole^{-1}. For convenience in relating them to the more familiar rate constants, therefore, the r_{ij} will be expressed in these units here. In C.G.S. units the friction coefficients would have the dimensions gram sec.$^{-1}$ mole^{-1}, the conversion factor being 1.0×10^7.

Pure Salts

The equations relating the interionic friction coefficients in pure binary molten salts to measured transport quantities can be shown to be:[1]

$$r_{+-} = \frac{(z_+ + z_-)F^2}{\Lambda} \tag{3}$$

$$r_{++} = \frac{1}{z_-}\left[\frac{(z_+ + z_-)RT}{D_{++}} - z_+ r_{+-}\right] \tag{4}$$

and

$$r_{--} = \frac{1}{z_+}\left[\frac{(z_+ + z_-)RT}{D_{--}} - z_- r_{+-}\right] \tag{5}$$

In these equations the subscripts + and − refer to the cationic and anionic species, respectively, the z_i being the absolute values of their charges. The equivalent conductance Λ is that computed from the measured specific conductance on the assumption of complete ionization, that is, $\Lambda = \kappa E/d$, where E is the equivalent weight and d the density of the molten salt. The self-diffusion coefficients D_{ii} are taken to be equivalent to the appropriate tracer-diffusion coefficients in cases where isotope effects can be neglected. The quantities R, T, and F have their usual significance.

The interionic friction coefficients calculated from these equations for a number of pure molten salts are presented in TABLE 1, together with the transport data used in the calculations. All the salts for which both conductance and self-diffusion data are available have been included,* as well as a number of representative examples for which only the former type of data have been reported. The value of r_{+-} could have been added for many more salts, since a wealth of information on conductivity and bensity is to be found in the literature. Convenient sources of such material, in addition to those figures most recently reported in the periodical literature, are the compilations in Conway's *Electrochemical Data*[2] (1952) and, for the older literature, a review by Biltz and Klemm[3] (1926). The salts for which only r_{+-} has been tabulated here were selected on the basis of relevance to the discussion that follows. Transport data on pure water are included for the same reason.

The reliability of the conductivity and density data generally warrants recording at least as many significant figures as are shown for the equivalent conductances, standard techniques having been carefully employed in most cases. The one questionable figure is that quoted for the conductance of zinc bromide. Although many of the conductivity values reported by Graetz[4] in 1890 subsequently have been shown to be in error, no other results seem to have been reported for this salt. From the fact that Graetz' values for zinc chloride, a salt with similar physical properties, were much too large, we may speculate that the conductance of zinc bromide listed here is more likely to be too large than too small† (Graetz also reported high values for lead chloride, but his figures for cadmium chloride were too small and those for potassium nitrate about right, so that his errors were not systematic). The accuracy of Λ in each case determines the accuracy of the figure listed for r_{+-}.

All the self-diffusion coefficients listed were obtained in isotope-diffusion experiments employing the open-end capillary technique[5] (with the probable exception of D_{++} in lead chloride, for which the method was not stated in the literature source used here[6]). This method is subject to a possible error due to convectional mixing of the solutions, especially when a high stirring rate is employed, that gives high results for D. While it is not possible to estimate the magnitude of this error, if present, in each of the cases cited here, it has been shown to amount to as much as 4 per cent in some of the self-diffusion measurements in aqueous sodium chloride.[7,8] An error of this magnitude would be comparable to the random fluctuations encountered in some of the molten-salt work. The effect of these random errors has been minimized here by interpolating or extrapolating from conventional log D versus $1/T$ plots, using the best straight line through experimental points. Uncertainties remain, however, which are particularly important in the cation self-diffusion coefficients in NaCl, $PbCl_2$, and TlCl, as well as the anion self-diffusion coefficient for the latter. Here the reliably significant figures are lost in the subtractions in EQUATIONS 4 and 5, so that errors in the calculated like-ion friction coefficients r_{++} and r_{--} may amount to more than 100 per cent in these cases. By contrast, a 4 per cent (too high) error in the value of D_{++} for sodium nitrate would give only a 19 per cent error in the value of r_{++}. Thus, it is seen that, in general, the figures for the like-ion friction coefficients listed in TABLE 1 are much less reliable than those for the r_{+-}.

---

* Following the presentation of this paper Max A. Bredig revealed that the self-diffusion coefficients of all of the alkali metal ions in their pure molten nitrates have been determined at the Oak Ridge National Laboratory, Oak Ridge, Tenn., the sodium nitrate data listed here being the only results thus far reported in the literature. (Added since the conference at which this paper was presented.)

† At the conference on which this monograph is based, E. H. Crook disclosed that he had recently redetermined the conductivity of molten zinc bromide in J. O'M. Bockris' laboratory at the University of Pennsylvania, Philadelphia, Pa. The value of Λ calculated from Crook's result at 460° C. is 1.7, confirming the fact that the figure reported in TABLE 1 is too high. The value of r_{+-} based on the new result is 170×10^8, while the corresponding figure for r_{++} is -190×10^8.

TABLE 1

SOME INTERIONIC FRICTION COEFFICIENTS IN PURE MOLTEN SALTS

Salt	Temp. (°C.)	Λ (mho cm.² equiv.⁻¹)	$10^5 D_{++}$	$10^5 D_{--}$	$10^{-8} r_{+-}$	$10^{-8} r_{++}$	$10^{-8} r_{--}$	$R\frac{d \ln r_{+-}}{d(1/T)}$	$R\frac{d \ln r_{++}}{d(1/T)}$	$R\frac{d \ln r_{--}}{d(1/T)}$	Reference
			(cm.² sec.⁻¹)		(joule sec. cm.⁻² mole⁻¹)			(kcal. mole⁻¹)			
LiCl	800	198			0.94			2.0			9
NaCl	800	135	12.3	5.5	1.38	0.1	1.9	2.8	(<0)	9.4	9, 10
KCl	800	110			1.69			3.5			9
KI	800	108			1.72			3.5			9
$MgCl_2$	800	35			8.0			4.0			12, 24, 25
$CaCl_2$	800	57			4.9			4.7			12, 24, 25
YCl_3	800	16			24			8.6			3
TlCl	550	68	4.6	5.3	2.7	0.2	−0.1	3.3	(<0)		3, 26, 27
$PbCl_2$	575	53	2.0		5.3	0.0		4.2			3, 28
$ZnCl_2$	460	1.4			200			18			3
$ZnBr_2$	460	3*	0.13		80*	−30*		11†			4, 25, 29
$AlBr_3$	200	4×10^{-6}			1×10^8			9			3
$NaNO_3$	330	48	2.03	1.29	3.9	1.1	3.9	3.2	4.9	4.6	16, 17
$AgNO_3$	330	52			3.6			2.7			16
H_2O	25	5×10^{-7}	2.6	2.6	6×10^8	-3×10^8	-12×10^8	9.5			30, 31

* See footnote to page 999.
† See footnote to page 1004.

Each of the interionic friction coefficients listed in the table applies only to the particular salt at the temperature indicated and a pressure of about 1 atmosphere. Before further consideration of the significance of these figures is undertaken, therefore, the effects of experimental variables must be examined.

Size of the thermodynamic force. This effect has already been discussed briefly.[1] It was pointed out that the application of an unusually large force such as an electric potential gradient would probably cause a breakdown of the linear relations between forces and fluxes. Such an observation has long been known in the case of aqueous electrolytes (Wien effect), but analogous experiments have not, to my knowledge, been reported for molten salts. A qualitative estimate of the relative importance of such effects at high temperatures may be obtained from the equations applied by Eyring and his co-workers[11] to a simple model for ionic migration. The treatment assumes that the random thermal motion of a given ion may be broken down into a sequence of jumps over the energy barriers between successive positions of minimum potential energy. Application of an electric field $\nabla\phi$ reduces the energy of successive minima in the direction of the field by the amount $\lambda z\epsilon\nabla\phi$, where $z\epsilon$ is the charge on the ion and λ the distance between minima. Letting α equal the fraction of this distance, an ion moving with the field must travel to reach the top of the energy barrier, I_f the ion flux in this (forward) direction, and I_b the ion flux in the opposite direction (against the field), the net ion flux is shown to be

$$I_{\text{net}} = I_f - I_b = N\lambda cKe^{\alpha W/kT}(1 - e^{-w/kT}) \tag{6}$$

Here $w = \lambda z\epsilon\nabla\phi$, c is the concentration of the ion, K the specific rate in the absence of the field, and N, k, and T have their usual significance. The series expansions of the two exponential terms show that if w is small compared with kT, EQUATION 6 becomes

$$I_{\text{net}} = N\lambda cK\left(\frac{w}{kT}\right) = \frac{NcK\lambda^2 z\epsilon\nabla\phi}{kT} \tag{7}$$

Thus, if λ is assumed to be independent of $\nabla\phi$, a linear equation of the type

$$I_i = C_i\nabla\phi \tag{8}$$

can be written for each ion in a system of fixed composition and temperature. Although this oversimplified treatment fails to take account of the interference between moving species (the derivation thus leading eventually to the Nernst-Einstein relation[1]), it provides a basis for consideration of the effect of temperature on the validity of the linear laws. It was seen that the necessary assumption in the derivation of EQUATION 7 from EQUATION 6 was that w (and hence αw) is small compared with kT. For a univalent ion in a potential gradient of 1 volt cm.$^{-1}$ at 300° K. the value of w/kT is about 10^{-6}, taking λ to be of the order of molecular dimensions. While the assumption would clearly be justified in this case, the linear dependence of w on the size $\nabla\phi$ shows why the approximation gradually becomes less valid as the field strength is increased.

From the preceding discussion it is seen that an increase in T favors the assumption upon which the linearity of the relations between forces and fluxes depends. The high temperatures of molten salts thus improve the likelihood that friction coefficients (which are the proportionality "constants") will be independent of applied forces of normal magnitudes in these systems. In physical terms we may say that the linear relations depend upon the assumption that such forces superimpose only a small disturbance or "drift" on the random thermal motion of the ion, so that increasing its thermal motion favors the applicability of the assumption. Although extensive experimental tests of these relations have not been carried out in molten salts, the measurement of conductance itself implies the validity of Ohm's law, which is the sum of the relations (EQUATION 8) for the ions in the system. Constancy of the individual rate "constants" in systems of more than two ions could be checked by varying the field strength at which transference experiments are carried out. There is little reason to believe an effect would be observed, however, since the energy changes over the distance λ due to interference between moving ions are also small compared with kT.

Temperature. It has been found that in many cases the temperature dependence of Λ in molten salts can be described by a relation of the type[12]

$$\Lambda = Ae^{-E^*/RT} \tag{9}$$

where the quantities A and E^* are nearly independent of temperature. An equation of this form for the conductance of each ion has been justified both experimentally and theoretically for the case of ionic crystals. It follows directly from the Eyring approach described above, when the specific rate constant is broken up into the product

$$K = (kT/h)e^{-\Delta F^*/RT} \tag{10}$$

where the "free energy of activation" ΔF^* is related to the experimental "activation energy" E^* by

$$\Delta F^* = \Delta H^* - T\Delta S^* \approx E^* - T\Delta S^* \tag{11}$$

Here E^* represents the height of the potential energy barrier that an ion must traverse in passing between positions of relative stability. If the barrier heights are not too different for different ions in the same system, EQUATION 9 may still hold approximately, the value of E^* depending on both the E^*_i and the A_i for each ion when their mobilities are of comparable magnitude.[13]

An important feature of such microscopic theories is the inclusion in the system of a reference entity that might be called the "medium" relative to which the ionic motions are described. In the case of ionic crystals the medium is the crystal lattice that is defined by the large number of ions occupying fixed lattice sites at any instant. The structures of liquid salts are less well defined, but the view that even here relatively few of the ions at a given instant have the necessary activation energy for translational motion gives content to the notion of a "medium" consisting of those ions whose motions may be described as entirely vibrational. In the paper setting forth the approach upon which the present work is based,[1] I pointed out that the macroscopic treatment of a pure binary salt could be made to conform to either a Type I or a Type II model. Type I refers to a system composed only of 2 ionic species, while the Type II system contains also a third "component" that would be identified here with the medium. In the limiting case where the ions having translational motion constitute an extremely dilute "solution" in this medium, it was shown that the friction coefficients of the ions against the medium could be determined by means of self-diffusion experiments. By comparison with the density of current carriers in pure water, for which the "solution" *is* sufficiently dilute, the "solution" of mobile ions in solid crystals was seen to be susceptible to this treatment, a conclusion that the applicability of the Nernst-Einstein relation has supported experimentally. The treatment of a pure salt in which the carrier density is too large to ignore interference between the moving ions, for example, a molten salt (presumably), was not, however, elaborated for the Type II model. In the following paragraph I show why such an extension cannot be carried out profitably, the usefulness of this model for pure substances being limited to cases where only the ion-medium friction coefficients are important in determining transport properties.

Three independent friction coefficients are needed to characterize the transport properties of a Type II electrolyte, corresponding to the interactions of each of the ions with the medium and with each other. However, only one experiment can be performed, the measurement of conductance (not counting self-diffusion measurements, each of which involves a new friction coefficient—that of the ion against its own kind—and thus does not contribute a solution to the problem). Clearly, it would be necessary to define two additional independent transport experiments to permit a determination of all 3 friction coefficients. In an aqueous solution of a binary salt, where the medium is a chemically different entity (water), the required experiments are the measurements of transference numbers relative to the medium, and of salt-medium interdiffusion coefficients. Molten-salt "transference-number" experiments in which a porous plug serves as reference[14] thus represent an attempt to obtain some of the necessary data. Some workers have questioned the ability of such experiments to yield the desired information.[1,15] Whether or not the motion of the porous plug may be identified validly with that of the medium, however, it is clear that at least one more experiment is needed to obtain the necessary parameters for the Type II treatment. No analogue of the interdiffusion experiment is possible in a pure substance.

The Type II model for a pure molten salt appears admirably suited to treatment by the Eyring rate theory. We have seen, however, that the necessary parameters for such a treatment, while conceptually unambiguous, have not yet been operationally defined. Rather than pursue this model further, therefore, I have chosen in the present work to concentrate on the well-defined rate constants obtained in the Type I treatment in the hope that the results may suggest alternative microscopic approaches. My viewpoint will thus be largely empirical.

Since r_{+-} is inversely proportional to Λ (EQUATION 3) it follows that the temperature dependence of r_{+-} is also described by a simple exponential relationship in most fused salts. The slope of $R \ln r_{+-}$ versus $1/T$ for any salt is seen to be identical in magnitude but opposite in sign to that of the plot from which the "activation energy" for Λ is usually determined. The positive values of this slope in kcal./mole have been included for each of the salts listed in TABLE 1.*

In view of the simple empirical relation between r_{+-} and temperature in pure molten salts, it is of interest to test whether similar relations hold for the like-ion coefficients r_{++} and r_{--} in these melts. From EQUATIONS 4 and 5 it appears that temperature dependences of this form would not be obvious consequences of the exponential relations for Λ and the D_{ii} in the (usual) case where the two terms on the right are of comparable magnitude in each equation.

Those data which are sufficiently reliable to be used in this test, however, indicate that relations of the type

$$r = Be^{C/RT} \tag{12}$$

may prove to be generally adequate to describe the temperature dependence of all interionic friction coefficients in pure salts. This includes, in addition to the wealth of r_{+-} data already noted, the results for r_{--} in molten NaCl and in $NaNO_3$, as well as those for r_{++} in the latter melt. FIGURE 1 shows semilogarithmic plots of r versus $1/T$ based on experimental data[16,17] for each of the three friction coefficients in sodium nitrate. Values of the empirical constant C in EQUATION 12 based on the slopes of these straight lines are reported in TABLE 1, together with similarly obtained results for the other salts. The extreme uncertainty of the values for r_{++} in sodium and thallium chlorides makes a plot of this type relatively meaningless. Nevertheless, I have recorded the qualitative result that the slopes in each of these cases seem to be negative. No figure is reported for the slope of r_{++} or r_{--} in water, nor for r_{++} in zinc bromide, since the logarithm of a negative number is undefined. The data employed in the calculation of r_{++} in $PbCl_2$ and of r_{--} in TlCl were each available only for the one temperature listed.

Pressure. This factor has been included in the discussion only because it is an experimental variable. No data have been reported, however, with which to calculate its effect on the friction coefficients. Qualitatively, we may say that small pressure variations have a relatively insignificant effect, since otherwise the transport data in which this factor has not been controlled would exhibit greater fluctuations. It would nevertheless be surprising if marked increases in the values of the friction coefficients were not observed under conditions of extremely high pressure.

---

* A plot of the more recent data for $ZnBr_2$ (see second footnote to page 999) shows considerable curvature, the slope at 460° C. being 16 kcal./mole and becoming smaller with increasing temperature. (Added since the conference at which this paper was presented.)

Having completed a review of the effect of external conditions on interionic friction coefficients in pure molten salts, we may consider the possible correlations of the experimental values listed in TABLE 1 with known properties of the constituent ions of these melts, such as charge and size. Such a comparison can be meaningful, however, only if the simple ions for which the friction coefficients have been calculated move as discrete entities in the elementary steps of the processes under consideration. When transport of associated aggregates occurs such as the diffusion of H_2O molecules during self-diffusion of the ions in pure water, friction coefficients calculated on the assumption of complete ionization are of little value except as indicators of this fact. In examining the tabulated data, therefore, we should first consider whether they provide evidence of incomplete dissociation in any of the pure salts listed.

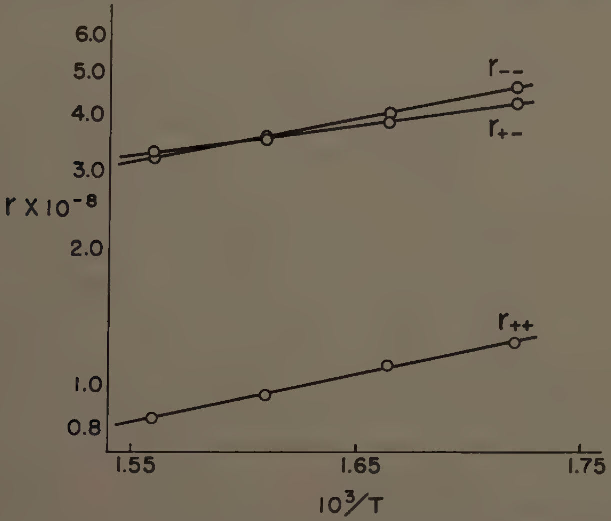

FIGURE 1. Interionic friction coefficients in molten sodium nitrate.

Extent of association. Although positive (for example, spectrographic) evidence for the existence of associated complexes in certain molten salt mixtures has been reported, the concept of ionic association in pure binary salts, where each ion is closely surrounded by the only species present of the opposite charge, remains poorly defined. The cohesive forces that must be present in the liquid provide an indisputable basis for the statement that all the ions in a molten salt are associated with their neighbors in the same sense that they are associated in ionic crystals. In the study of transport processes, however, we are concerned only with those ions undergoing translational motion relative to their environment, and whether they move singly or in groups of two or more. A criterion for the presence of association of this type between the oppositely charged ions in a pure liquid has been proposed from a simple consideration of the interionic friction coefficients.[1] It is the occurrence of negative values for the like-ion coefficients, illustrated in TABLE 1 for the case of pure water treated in the calculations as a purely ionic substance.

It will be seen that only one of the fused salts for which like-ion friction coefficients are listed in the table gives definite evidence of association (the negative value of r_{--} in TlCl is within the experimental error of being zero or positive). The associated salt is zinc bromide for which, as indicated earlier, the conductivity data are least reliable. It was pointed out, however, that the value reported for the conductance, if in error, was more likely to be high than low, which seems consistent with the fact that, as it stands, it is twice as great as the corresponding (correct) figure for zinc chloride at the same temperature. If the true conductance of zinc bromide is actually lower than the value used in the present calculations, this will serve only to make the calculated value of r_{++} more negative. It should be noted also that the change in r_{++} with temperature, which is not indicated in the table, was found to be such that this friction coefficient becomes even more negative as the temperature is increased, which is contrary to the behavior of r_{++} in water.* It is worthwhile at this point to consider the effect of temperature in associated systems.

When transport data for a highly associated system such as pure water are inserted into EQUATION 4, the value of r_{+-} is so large that the first term on the right is negligible by comparison with the second, which gives $r_{++} = -(z_+/z_-)r_{+-}$. The temperature dependence of r_{++} is thus proportional to the negative of that for r_{+-}. I have already shown how the Eyring approach relates the temperature dependence of r_{+-} in completely dissociated systems to the "activation energy for ionic migration." In associated substances the enhanced concentration of ions due to increase of dissociation with increasing temperature is also an important factor. The plot of $R \ln \Lambda$ versus $1/T$ will nevertheless exhibit the usual linear behavior, since the temperature dependence of the dissociation constant is of the same functional form (van't Hoff equation). From the fact that conductance depends on the product of concentration times mobility, it is clear that the slope of such a graph may be considered to represent the sum of two terms: one for the heat of dissociation into ions and one for their activation energy. When the principal dissociation is that of a neutral molecule into two ions, it is easy to show that the former term is actually equal to one half the value of ΔH for the dissociation reaction in weakly ionized liquids. Thus, in the case of pure water, each of the two energies may be evaluated separately from known data. The heat of dissociation is, of course, 13.6 kcal., while the "activation energy" is found to be 2.7 kcal., so that more than two thirds of the value for the slope of $R \ln r_{+-}$ versus $1/T$ listed in TABLE 1 is due to dissociation (or "ionization") of water molecules. In the case of zinc bromide the two terms in EQUATION 4 are found to be of comparable magnitudes, so that the temperature dependence of the first term also becomes important. This term decreases even faster than that containing r_{+-}, giving rise to the decrease in their difference as the temperature is raised. In view of our criterion, this increase in the negative value of r_{++} may appear to represent an anomolous increase in the degree of association with increasing temperature, an effect that might be interpreted as proof of the inaccuracy of the data. Since a result of this type may be given a reasonable physical interpretation in terms of rate theory, however, it is worthy of further consideration.*

---

* When the new conductance figures for $ZnBr_2$ (see second footnote to page 999) are used to calculate r_{++} this result is reversed; that is, its value becomes less negative with increasing temperature. It nevertheless remains negative all the way to the boiling point of the salt. (Added since the conference at which this paper was presented.)

The view that association occurs in molten zinc halides is not new, being indicated qualitatively by their high viscosities and low conductivities, as well as by the strong temperature dependence of these quantities. Thus, the fulfillment of our criterion for association in $ZnBr_2$ is not unexpected, although it would be more gratifying if the data were more reliable. By comparison of r_{+-} in this salt with the corresponding figure for an extremely associated salt like $AlBr_3$, however, it is apparent that the concentration of ions in the former must be very much greater. The ionic concentrations in $ZnBr_2$ may still be small, however, in comparison with that of the molecules (or whatever the larger aggregates may be). Transport of both ions and molecules may thus be important in self-diffusion experiments, even though diffusion of the latter would presumably require a much larger activation energy due to their greater size. An increase in temperature would thus favor transport by molecules, an effect that would outweigh that due to increased dissociation, provided the activation energy for transport of molecules was greater than the sum of their heat of dissociation and the activation energy for ionic transport. Such an effect would account for the observed temperature dependence of r_{++} noted above. We see that the increasing negative value with temperature can be interpreted as signifying greater applicability of our criterion for association as the extent of transport by the associated entities increases.

The "association" of positive and negative ions in molten salts has been discussed here in terms of stoichiometric entities, such as molecules and complex ions. In a broader sense, however, the term association applies to any type of coupling between the fluxes of oppositely charged species which would be reflected in a negative like-ion friction coefficient. The possibility that zinc bromide exhibits simply an extreme manifestation of a phenomenon present to some extent in all molten salts cannot be ruled out by the data. A better-defined criterion than the negative friction coefficient will be necessary to establish transport by stoichiometric aggregates. A discussion of the zinc bromide friction coefficients in terms of the properties of Zn^{+2} and Br^-, on the other hand, does not seem to be warranted by our limited data.

---

* Although the more "normal" dependence of r_{++} upon temperature found using Crook's conductivity data for $ZnBr_2$ (see footnote to page 1006) makes the rationalization of "anomalous" behavior unnecessary for this salt, the discussion shows why observations of such behavior in any salt need not be considered self-contradictory. (Added since the conference at which this paper was presented.)

In view of the stability of the nitrate ion, it is reasonable to include nitrates on our list of binary salts. The values of the friction coefficients found when sodium nitrate is considered in this way give no indication of additional association in this melt, that is, association of sodium ion with nitrate. Although self-diffusion data for silver nitrate are not available, it appears likely, by comparison of r_{+-} with the corresponding figure for sodium nitrate, that silver and nitrate ions alone are responsible for transport in this salt.

The like-ion friction coefficients reported in TABLE 1 are similarly consistent with the view that only simple ions are the moving entities in sodium, thallium, and lead chlorides. Again using the magnitude of r_{+-} as a qualitative indicator of association in cases where self-diffusion data are unavailable, it seems reasonable to discuss the transport properties of the following halides in terms of simple ions only: LiCl, NaCl, KCl, KI, TlCl, $MgCl_2$, $CaCl_2$, and $PbCl_2$. The case of YCl_3 is ambiguous. By comparison with $ZnBr_2$, however, moderate association of some sort is definitely indicated for $ZnCl_2$, while the ions of molten $AlBr_3$ appear to be almost completely associated. These classifications of the salts in TABLE 1 provide a basis for subsequent discussion of the possible correlations of their interionic friction coefficients with known properties of the constituent ions.

Ionic charge. From EQUATION 3 it will be noted that a comparison of the values of r_{+-} for 2 salts of the same charge type is equivalent to a comparison of their conductances. When salts of different charge type are compared, however, this statement is true only if the sum $(z_+ + z_-)$ is the same for both salts. By inclusion of this charge-dependent term, the friction coefficient r_{+-} affords a better basis for comparison of salts than the equivalent conductance. This is because the latter rate constant fails to take account of the fact that the electric force on an ion depends on its own charge, as well as on the strength of the applied field. Comparing the mobilities of two differently charged ions under the same potential gradient is thus different from comparing their velocities under the same applied force. This factor has been recognized in the definition of the friction coefficients (EQUATION 1), with a resulting effect on their magnitudes, which may be seen by comparing the figures for Λ in TABLE 1 with the corresponding figures for r_{+-}. Comparing alkali and alkaline earth chlorides at the same temperature, for example, the qualitative generalization that increasing the charge of the cation is accompanied by a decrease in the relative mobilities of cation and anion is found to be strengthened by taking account of the charge factor in calculating the friction coefficient.

The increase in r_{+-} with increasing ionic charge seems to be a general rule, even when ionic association is not involved. Since unusually small conductances have not been found for the molten halides of any univalent cations (including Ag^+ and Cu^+, which are not tabulated), the figures for $ZnBr_2$ and $AlBr_3$ show that increasing cationic charge also increases the likelihood of association.

The preceding facts about r_{+-} are well known in terms of conductivity results, since the inclusion of the specific charge factor noted above alters the quantitative results but not the qualitative conclusions. It would therefore be of greater interest in the present work to consider the effect of charge on the like-ion friction coefficients. The case of r_{++} in $ZnBr_2$ has already been discussed in terms of its implication of association. The more "normal" value of r_{++} in $PbCl_2$ demonstrates that the former result was not solely a consequence of the double charge on the cation. As for the effect of magnitude of charge on r_{++} in unassociated salts, however, it is impossible to draw any quantitative conclusions for the molten halides since, in all cases listed, the size of this coefficient is so small as to be almost undetectable in self-diffusion experiments.

We can, of course, consider the effect of the sign of the charge by comparing the friction coefficients for different pairs of ions (of like or opposite charge) in the same melt. This will be done in the following section.

Ionic size and shape. In considering the effect of ionic size and shape on the values of r_{+-}, we are again dealing with comparisons that have been discussed already many times in terms of equivalent conductances. Thus, it would be overly repetitious to give more than a brief resume of the observations. For the completely dissociated salts the following facts stand out:

(1) In melts consisting of spherically symmetrical alkali and halide ions, increasing the size of the former increases the value of r_{+-}, while a corresponding increase in the latter has a relatively smaller effect on this friction coefficient. This is usually explained by asserting that conductivity in these melts must be largely cationic. The rule regarding cation size does not hold for the alkaline earth halides, where the higher charge density on this ion might be expected to bind it more tightly to its immediate environment.

(2) Salts with spherically symmetrical cations whose electronic structures are more easily distorted (polarizable) than alkali metal ions of the

same size (or even considerably smaller) exhibit smaller values of r_{+-} than the corresponding alkali metal salts. This is illustrated in TABLE 1 for the case of silver nitrate versus sodium nitrate, sodium ion having a smaller crystal radius than the more polarizable silver ion.

(3) Changing the shape of the anion from its spherical symmetry in the halides to the relatively flatter and broader nitrate ion does not produce a very marked effect on r_{+-} in alkali metal salts. This may be seen qualitatively from the figures for NaCl and $NaNO_3$ in TABLE 1, even though they are reported for very different temperatures. Note particularly the similarity in the temperature dependence of r_{+-}.

We may now compare the results found for the like-ion coefficients with the corresponding cation-anion coefficients. The following observations appear significant:

(1) The value of r_{++} in every case is markedly smaller than r_{+-} for the same salt. In some halides this value is so small that its magnitude cannot be detected in the self-diffusion experiment. In such cases the combined form of EQUATIONS (3) and (4), which may be written*

$$\frac{z_+ D_{++}}{RT} = \frac{\Lambda}{F^2}\left(1 + \frac{z_- r_{++}}{z_+ r_{+-}}\right)^{-1} \tag{13}$$

reduces to an expression identical with the Nernst-Einstein relation, except that here D_{++} is related to the total equivalent conductance of the salt, rather than to a hypothetical single-ion conductance. No such relation holds for D_{++} in sodium nitrate, however, since r_{++} and r_{+-} are of comparable magnitude.

(2) The value of r_{--} in molten TlCl is so small compared to r_{+-} that Nernst-Einstein-type relations are approximated by both the ions in this salt.

(3) Those like-ion coefficients whose magnitudes are large enough to be measurably significant compared with the values of r_{+-} in the same salts invariably become less important relative to the latter coefficient as temperature is increased. This may be seen for sodium nitrate in FIGURE 1, and follows from the temperature dependences in TABLE 1 for r_{--} in NaCl.

It is worthwhile to consider the physical significance of these facts in the light of the results found for like-ion friction coefficients in crystalline salts. The Nernst-Einstein relation normally applies only to one of the ions (the smaller) in a binary solid salt, the like-ion coefficient for the other species being orders of magnitude larger than r_{+-}. This result merely reflects the fact that passage of the smaller ion between successive potential energy minima along the lattice is relatively uninfluenced by the more distant ions of its own kind. The larger ions, on the other hand, play a more important role in defining the lattice structure, and thus find motion relative to one another more difficult.

---

* The exponent (−1) was inadvertently omitted from this equation in the introductory paper,[1] as well as from the corresponding equation for D_{--}. These were Equations (24*a* and 24*b*) in that publication.

It is apparent from the molten salt results just listed that the process of fusion produces major changes in the nature of ionic transport. These changes presumably reflect the fundamental differences between the solid and liquid states, which include both the absence of long-range order and the greatly increased population of highly energetic ions undergoing translational motion in the liquid as compared with the solid. The observations we have just listed for molten salt friction coefficients may be reexamined in the light of these differences:

(1) Although the like-ion coefficients for the smaller cations are smaller than the corresponding r_{+-}, thus giving a superficial resemblance to crystals by approximate adherence to the Nernst-Einstein relation, it is of greater significance that these two types of friction coefficient are of much more nearly the same magnitude in the liquids, as is demonstrated especially by r_{++} in sodium nitrate. This is consistent with the existence of a much higher density of moving ions in the liquid, which must involve greatly increased interference between their motions.

(2) The motions of the larger anions, on the other hand, are relatively less restricted by neighboring anions in the liquid, since the latter are second-nearest neighbors and thus already at a distance where the entire array has begun to loose the highly ordered structure of a crystal lattice.

(3) As the temperature is raised the liquid structure becomes still more random. Even the hindrance to motion of a cation by ions of its own kind becomes less important in comparison with that due to anions, since the latter constitute its immediate coordination sphere.

Ionic mass. The use of isotopes permits the effect of ionic mass to be isolated for study more satisfactorily than other ionic properties. Since the masses of both cation and anion can be varied separately, the effect of 2 types of variations on each of the 3 friction coefficients in a binary salt can be studied. In order to measure these effects one could in principle determine the effect of each change in isotopic mass on each of the 3 rate constants from which the friction coefficients are calculated. Such effects are so small, however, that they would be almost impossible to detect by means of a direct measurement. In fact, the tracer technique for measuring self-diffusion coefficients relies on these effects being negligibly small. The only practicable method, therefore, is to carry out experiments in which the 2 isotopes of interest are present simultaneously, so that their velocity difference under the same applied force can be measured. Since tracers are normally used in self-diffusion measurements in any case, at least 3 different isotopes of each ion are necessary to employ this technique in determining the 6 mass effects of interest.

Of the two types of differential-velocity (or isotope-enrichment) experiments just mentioned, electromigration experiments are the only kind for which results have been reported in the literature. These have been carried out principally by Klemm, Lundén, and their co-workers,[6] who have found for many salts that electrolysis of melts provides a considerably more efficient method of isotope separation than the same experiment in aqueous solutions. This result is attributed to the fact that the elementary unit of migration is the simple ion rather than a solvated or complexed species, so that the percentage of difference in mass between two such units involving different isotopes is maximized. These workers have reported their results in terms of the mass effect μ, defined by

$$\mu = (\Delta v/v)(m/\Delta m) \approx d \ln v/d \ln m \tag{14}$$

where v is the velocity of the ion of interest relative to the oppositely charged ion and m is the mass of the former ion. In order to find the effect of mass on the friction coefficient, therefore, we must first derive the relation of the latter to μ. To do this we follow the approach of Klemm[18] in writing the phenomenological EQUATIONS 1 and 2 for a system composed of 3 ionic species (Type III electrolyte) in which the two cations differ only in isotopic mass. Equating the applied forces K_i on the 2 cations and taking the limit as the difference in their velocities approaches zero leads to

$$\frac{d \ln r_{+-}}{d \ln m_+} = -\frac{d \ln (v_+ - v_-)}{d \ln m_+}\left(1 + \frac{z_- r_{++}}{z_+ r_{+-}}\right) = -\mu_+\left(1 + \frac{z_- r_{++}}{z_+ r_{+-}}\right) \tag{15}$$

This relation shows that the effect of mass of the cation on the friction coefficient r_{+-} can be ascertained only when the value of the like-ion coefficient r_{++} is known. The corresponding relation for the effect of anionic mass on r_{+-} is obtained by reversing the signs of all subscripts in EQUATION 15, so that r_{--} must also be known to determine this mass effect.

The values of μ_+ and μ_- in molten salts have been found to range from about -0.02 to -0.3.[6] Since the factors $(1 + (z_j r_{ii}/z_i r_{ij}))$ such as that on the right of EQUATION 15 will not, if consistent with available data (TABLE 1), change the order of magnitude of their product with μ_i, it follows that a 1 per cent increase in the mass of either ion increases the value of r_{+-} by 0.02 to 0.3 per cent. Mass effects on interionic friction coefficients are thus seen to be relatively small in comparison with the effects discussed in previous sections.

Before leaving this topic it is of interest to mention an empirical correlation which Klemm[19] and others[6] have observed among a large number of the mass effects they have determined. This correlation is based on the atomic weights m_+ and m_- of both ionic constituents of the salt. It may be expressed by the equation:

$$\mu_+ = -0.15\left(1 + \frac{m_+}{2.1 m_-}\right)^{-1} \tag{16}$$

The applicability of this equation appears to be generally valid for the cations in molten halides, as well as for Ag^+ in solid α-AgI. No such correlation was found possible in molten halides for the effect of changes in anionic mass, however, nor was EQUATION 16 applicable to the cation mass effects in the 2 molten nitrates studied. These are $LiNO_3$ and KNO_3, for which the calculated values are found to be much too small. Although the physical basis for this empirical relation is not yet understood, a study of the like-ion friction coefficients in TABLE 1 suggests a possible source of its failure in the cases indicated. With the exception of the questionable zinc bromide data, it is seen that r_{++} in all the molten halides for which it is known has a value very small compared to r_{+-}. Thus, from EQUATION 15 it is seen that a relation identical in form to EQUATION 16 must hold for the effect of mass on r_{+-} in these cases. If we assume that the small values of r_{++} are a general property of molten halides, then it would be equally valid to express the empirical relation in terms of either $(v_+ - v_-)$ or r_{+-}. This is not true for the anions of the halides, however, since r_{--} in NaCl is large. Nor would such an identity apply to the cations of molten nitrates, as we may see from the significant r_{++} in $NaNO_3$. These observations indicate, therefore, that the importance of like-ion interactions may be responsible for the failure of EQUATION 15 in all those cases where it has been shown not to hold. They suggest further that a more general correlation might be based on the mass effects of r_{+-} rather than of $(v_+ - v_-)$.

Molten Salt Mixtures

The study of melts consisting of more than two ions provides an opportunity to extend our understanding of interionic friction coefficients immensely. In addition to those quantities already discussed, coefficients descriptive of the interference between ions of different species with charges of the same sign can be determined; the effects of changing the third ion on the friction coefficient for the remaining pair can be observed; and it becomes possible to compare the coefficients for different pairs of oppositely charged ions in the same melt rather than to compare pure salts with each other. Finally, the important effect of changing concentration upon all the coefficients can be studied.

It will be recalled that there are 6 independent friction coefficients in a 3-ion melt (Type III electrolyte),[1] corresponding to the interactions of each ion with each other ion and with itself. The 6 independent transport experiments by which these coefficients may be determined are well defined, including 3 measurements of self-diffusion, 1 of interdiffusion (along with the determination of required thermodynamic information), one of transference numbers relative to an arbitrary reference, and 1 of equivalent conductance. It is necessary to perform all of the latter 3 measurements before any of the 6 coefficients can be calculated. In a paper developing the necessary relations,[1] I pointed out that there was no molten salt mixture for which the results of all 3 required experiments had been published at that time. Particularly conspicuous by their complete absence from the literature were the interdiffusion data for any system. The same situation exists at the time of the present writing, although steps are being taken in this laboratory to rectify it. In spite of the deficiency, however, it is possible to base a semiquantitative discussion of the concentration dependence of some interionic friction coefficients upon the partial experimental data available for certain 3-ion systems.

A particularly fortunate result found in the transference number data for the silver nitrate-sodium nitrate system makes 2 of the friction coefficients very nearly assessable from available conductivity data. In the transference experiment a parameter P is measured that is equal to $1 - t_1 - X_{13}t_3$, where the subscripts refer to the ions, X_{13} being the equivalent fraction of, say, silver nitrate, and t_1 and t_3 the transport numbers of Ag^+ and NO_3^- relative to an arbitrary reference, for example, Na^+ (P is independent of the reference chosen).[20] For a system composed of univalent ions P is related to the friction coefficients by[1]

$$P = \frac{X_{23}(r_{12} + r_{13})}{r_{12} + X_{13}r_{23} + X_{23}r_{13}} \tag{17}$$

the subscript 2 referring here to the sodium ion. The important experimental observation is that P/X_{23} is equal to unity over the entire concentration range, at least to within the accuracy of the measurements.[20,21] Substitution of this figure into EQUATION 17 yields the result that $r_{13} = r_{23}$, regardless of the value of r_{12}. Now the equation relating the friction coefficients to the equivalent conductance for a system of 3 univalent ions is[1]

$$\frac{\Lambda}{F^2} = \frac{2(r_{12} + X_{13}r_{23} + X_{23}r_{13})}{X_{13}r_{12}r_{13} + X_{23}r_{12}r_{23} + r_{13}r_{23}} \tag{18}$$

For the case $r_{13} = r_{23}$, however, EQUATION 18 reduces to

$$\frac{\Lambda}{F^2} = \frac{2}{r_{13}} = \frac{2}{r_{23}} \tag{19}$$

so that these 2 friction coefficients can be calculated from equivalent conductance data alone at any concentration for which $r_{13} = r_{23}$. The physical reason for this simplification is the following. The transference result $P/X_{23} = 1$ reveals that the 2 cations move with the same velocity in an applied field.[20,21] Thus, they have no velocity relative to one another, so that the friction coefficient for their relative motion is immaterial. By comparison with EQUATION 4, EQUATIONS 19 are seen to be identical to those for a 2-ion melt, since the transport properties of Ag^+ and Na^+ cannot be distinguished in this experiment. By finding the values of these 2 coefficients exactly from just 2 experiments, we must sacrifice, of course, any knowledge whatever of the value of r_{12} from these experiments, its value being determined completely by the interdiffusion coefficient.

The experimental accuracy of the data for P in the silver nitrate-sodium nitrate system varies with the concentration at which it is determined, the error being no greater than 5 per cent at any of the concentrations studied. Thus, we are not warranted in setting P/X_{23} exactly equal to unity, but can reasonably define limits from the data. On the basis of these limits, combined with conductivity and density data for the system as reported by Wetmore and his co-workers,[16] the friction coefficients r_{13} and r_{23} at 330° C. have been plotted in FIGURE 2 for the entire range of composition. The actual points shown in the figure refer to the value calculated on the assumption $r_{13} = r_{23}$ exactly, their accuracy depending on the reliability of the conductance data. The upper limits are those prescribed by the accuracy of the transport data for the maximum value of r_{23}, while the lower limits give corresponding minimum figures for r_{13}. It was necessary, of course, in establishing these limits to choose an approximate value for r_{12}, since this quantity enters into any calculations for which r_{13} does not exactly equal r_{23}. The estimation employed here was based on the value for r_{++} in pure sodium nitrate given in TABLE 1, since this is a like-ion coefficient for cations in the same system, and the transport properties of the 2 cations in this system have been seen to be very similar. It may be mentioned that, to the extent that such an estimation is reliable, it is possible to predict the interdiffusion coefficients that will be found for this system.

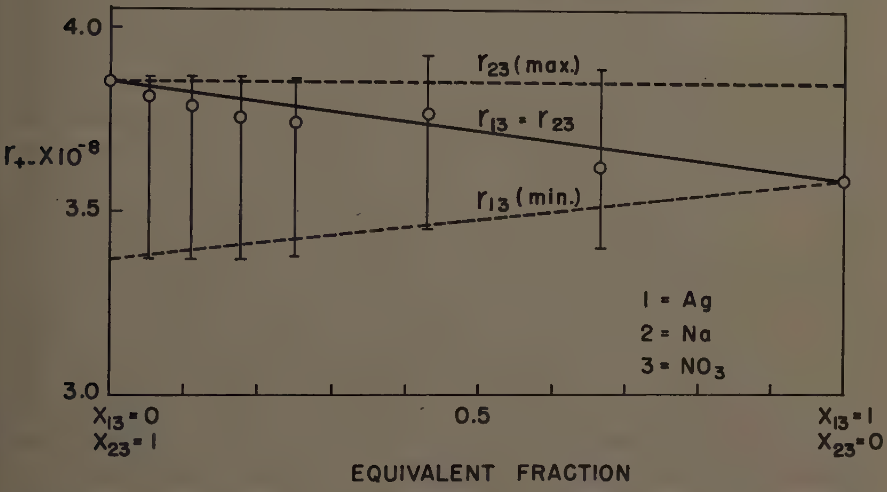

FIGURE 2. Cation-anion friction coefficients in the system silver nitrate-sodium nitrate.

A glance at FIGURE 2 shows that the concentration dependence of these friction coefficients is so small that their behavior might be characterized as ideal. Two types of ideality suggest themselves: (1) the values of r_{13} and r_{23} are equal at all concentrations and vary linearly with composition of the melt, as illustrated by the solid line in FIGURE 2; and (2) the two coefficients have slightly different values, but each remains constant (and hence equal to the pure salt value) throughout the composition range. A third and slightly less restricted type of ideality is suggested by the dashed lines defined roughly by the limiting values in FIGURE 2. Until the interdiffusion experiments in progress on this system are completed, however, it is impossible to say with certainty whether the friction coefficients conform exactly to any of these ideals.

In discussing silver nitrate-sodium nitrate melts we have been considering a system made up from 2 salts of very similar properties. Not only are their conductivities nearly equal, but their molar or equivalent volumes are identical within experimental error and equal to the partial molar volumes in all intermediate mixtures. It seems reasonable to infer that the structures of these melts vary only slightly with concentration. From the known behavior of pure sodium nitrate (TABLE 1) it would thus follow that association of oppositely charged ions does not occur during transport in these mixtures. Let us now consider another system that resembles this one only in the fact that the 2 pure salts from which it is formed, namely, lithium chloride and potassium chloride, are also completely dissociated. The latter salts have molar volumes differing by a factor of more than 1.5 (although the partial molar volumes are nearly constant), and equivalent conductances differing by almost a factor of 2.

The variation of equivalent conductance with composition in the lithium-chloride-potassium chloride system at 800° C. is illustrated by the solid line in FIGURE 3.[9] The strong negative deviation from linearity shown has been found characteristic of systems made up from completely dissociated pure salts whose conductivities differ markedly. In previous discussion of molten salt systems[1] I have noted that the effect of increasing values of the r_{12} term in EQUATION 18 is to reduce the intermediate values of Λ below the straight line (dashed line in FIGURE 3) that would be found according to EQUATION 18 for a mixture with constant (pure salt) values of r_{13} and r_{23}, with $r_{12} = 0$. The question of whether a large positive value of r_{12} could account for the experimental deviations can be settled quickly by calculating the limiting value of Λ as r_{12} goes to infinity in EQUATION 18. The resulting relation is

$$\frac{\Lambda}{F^2} = \frac{2}{X_{13}r_{13} + X_{23}r_{23}} \tag{20}$$

Now if r_{13} and r_{23} retained their limiting values in the intermediate mixtures, the limiting (minimum) conductance that would be calculated from EQUATION 20 is illustrated by the dotted line in FIGURE 3. It falls far short of accounting for the negative experimental deviations, so that we can rule out this type of ideal behavior for the lithium chloride-potassium chloride system.

The other type of ideal behavior suggested for the silver nitrate-sodium nitrate system was a linear variation of r_{13} and r_{23} such that they remain equal at all concentrations. EQUATION 19 was shown to be applicable to this case but, when the assumed linear dependence of r_{13} is taken into account, this becomes identical in form to EQUATION 20, so that the dotted line in FIGURE 3 represents this situation also. Ideal behavior of any sort seems unlikely to account for the experimental curve.

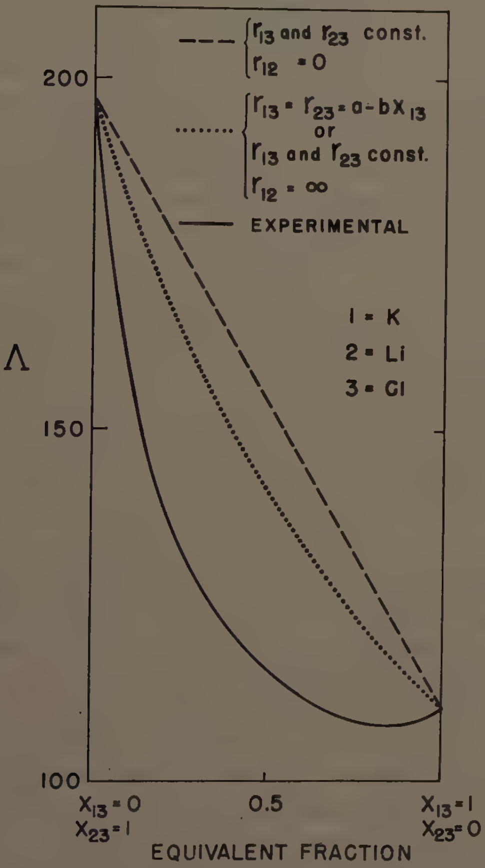

FIGURE 3. Conductivity isotherms in the system lithium chloride-potassium chloride (experimental curve based on data of Van Artsdalen and Yaffe[9]).

We have noted that one major difference between the properties of the LiCl-KCl system and those of the $AgNO_3$-$NaNO_3$ system is the strong dependence of the molar volume on composition in the former. By expressing in units of mole fraction the concentrations X_k in EQUATIONS 1 and 2 which define the friction coefficients r_{ik}, the formal dependence on volume has been removed from the coefficients R_{ik} originally defined by Onsager's "dissipation function."[32] In an earlier paper[33] I pointed out that the R_{ik}, which are related to the present coefficients by $R_{ik} = -\bar{V}r_{ik}$, where $\bar{V}$ is the molar volume of the solution, might be expected to exhibit a smaller dependence on volume. This is because the molecules or ions are crowded closer together as the molar volume decreases, so that a corresponding increase in the friction coefficients r_{ik} is plausible. In view of the failure of the LiCl-KCl conductivity isotherm to be consistent with any sort of ideal behavior of these coefficients, it is of some interest to test whether alternatively defined friction coefficients might furnish ideals capable of correctly describing the experimental curve. Of particular value, of course, would be coefficients independent of concentration in completely dissociated systems. It is possible to test whether the Onsager coefficients R_{ik} could fulfill this condition in the LiCl-KCl system by again calculating the limiting (minimum) value for Λ, this time as R_{12} approaches infinity. The result at $X_{13} = 0.2$ is $\Lambda_{\text{min.}} = 160$, and at $X_{13} = 0.8$, $\Lambda_{\text{min.}} = 117$, the experimental values at these concentrations being 143 and 108, respectively. While these results represent an improvement over the corresponding minima calculated from the r_{ik} (171 and 121), they show that the LiCl-KCl system could not be considered ideal in terms of the R_{ik} either. This is not surprising, since it is presumably true that more complex considerations than that of volume alone are involved in the concentration dependence of any friction coefficients.

It may be noted that constant (pure salt) values of the cation-anion friction coefficients (using either of the above definitions) combined with suitably chosen negative values of r_{12} could account mathematically for the form of the experimental isotherm. Since the latter condition implies association, however, this would be inconsistent with the concept of ideal behavior.

Some transport data for the LiCl-KCl system reported by Klemm and his co-workers[23] may help to establish what sort of variation in the friction coefficients is connected with the observed conductivity isotherm. In the process of carrying out an isotope-enrichment experiment, they performed the equivalent of a Hittorf transference-number determination that permits calculation of the transport parameter P in EQUATION 17. The equivalent fraction X_{13} of KCl in this experiment was 0.0224, a region where the negative deviation of Λ per unit concentration of KCl is seen in FIGURE 3 to be very large. The value of P calculated from their data is 0.9805. Substitution of this value into EQUATION 17 gives the result that $r_{12} = 6.5\ r_{13} - 7.5\ r_{23}$ at this concentration. The friction coefficient for the pair of like-charged ions will therefore have a positive value at this concentration if r_{13} exceeds r_{23} by 15 per cent or more. This seems likely in view of the fact that r_{+-} in pure KCl exceeds that in pure LiCl by 80 per cent. (Although the latter figure is quoted for a temperature of 800° C., while

Klemm's experiment was carried out at 630° C., the qualitative comparison is clearly valid.) The data are thus consistent with the view that dissociation is complete in LiCl-KCl mixtures, the strong decrease in conductance apparently being associated with a corresponding increase in both the cation-anion friction coefficients as either salt is diluted by the other. We may note that if the coefficients r_{12} for the interference between positive ions in mixed halides turn out to be small compared with cation-anion friction coefficients in the same systems, as was found to be the case in pure molten chlorides, it will in general be possible to predict the interdiffusion coefficients in such systems from results of conductivity and transference measurements, provided the thermodynamic data are known.

The transport data of Isbekow[34] for a solution of potassium bromide in aluminum bromide may be used to demonstrate the application of the negative friction coefficient criterion for association in molten salt mixtures. When this system is treated as a Type III electrolyte the value of P calculated from Isbekow's data is 1.1 at $X_{23} = 0.074$, where the subscript 2 refers to K^+. Now if ion 3, the bromide ion, is taken as reference for the velocities of the cations, $P = 1 - t_1$ is the transport number of the potassium ion. Association is already demonstrated, then, by the fact that the transport number of Al^{+3} relative to Br^- must be negative. The definition of the friction coefficients shows that such a result must imply negative values. This is borne out by substitution of Isbekow's figures into the analogue of EQUATION 17 for a system of this charge type.[1] The result is $r_{12} = -0.01\, r_{13} - 3\, r_{23}$, showing that at least 1 coefficient must be negative. On the basis of r_{+-} for pure $AlBr_3$ (TABLE 1), it would clearly be more realistic to treat this liquid as a neutral solvent, just as Isbekow himself did in calculating transference numbers.

I conclude with an interesting case for which the question of association has not yet been settled unambiguously. The system is $PbCl_2$-KCl, for which we designate the ions as follows: $1 = Pb^{+2}$, $2 = K^+$, $3 = Cl^-$. Transport data on this system were first gathered by Lorenz and his coworkers,[35,36] who found that at $X_{23} = 0.7$ the lead ion migrated out of the cathode compartment defined by a porous "clay" partition between the electrodes. Since the significance of "transference numbers" measured by this method is not entirely clear, it is perhaps of greater relevance that the values of P at 800° C. based on their data for 2 runs in this concentration region are found to be 2.4 and 2.7. As in the bromide system just described, association is clearly indicated by these results.

A somewhat different experimental approach led Bloom and Heymann[12] to conclude that complex ions must be present in the $PbCl_2$-KCl system at concentrations around $X_{23} = 0.67$. Their reasoning was based on the results of careful determinations of the conductivity isotherms at a variety of temperatures, which showed that the "activation energy for ionic migration" (E^*) apparently passes through a maximum at about this concentration. Subsequent determination of the corresponding viscosity isotherms, however, yielded data that were puzzling to Harrap and Heymann[37] in the light of the conductivity results. For the "activation energies for viscous flow" calculated from the slope of $R \ln 1/\eta$ versus $1/T$ showed a continuous uniform variation with composition, no anomalous behavior being observable in the neighborhood of $X_{23} = 0.67$. These workers attributed their result to the operation of a different mechanism for the flow process that is less sensitive to association of the ions into small complexes.

Finally, "transport number" determinations similar to those first carried out by Lorenz and Fausti[35] were repeated about 55 years later by Duke and Fleming[38] with very different results. None of the transport numbers relative to the latter workers' partition was found to be either greater than unity or less than zero at any concentration, the value of P at 850° C. for $X_{23} = 0.68$ being 0.79.

In principle, determinations of P required no partition or "membrane" to separate the electrode compartments, provided the distance from cathode to anode is sufficiently great (and convection currents sufficiently small) for an appreciable region between the electrodes to retain its initial composition throughout the experiment. While the use of porous membranes prevents mixing by convection between the 2 compartments, it is possible for such mixing to occur within one compartment followed by flow through the membrane, which would produce, of course, the same sort of error. Another possible source of error connected with the use of such membranes is the phenomenon of electro-osmosis, which may result when a particular species is adsorbed preferentially onto the pore surfaces within the membrane, giving rise to an appreciable ζ potential. For a membrane with sufficiently small pores, a potential of this sort could exert a considerable influence on the relative mobilities of the ions.

It is unlikely that either of the sources of error that I have mentioned was an important factor in the results of Duke and Fleming.[38] Previous work on pure lead chloride using the same membranes,[22] as well as some very different ones, had shown the mobilities of cation and anion relative to the membrane to be almost independent of membrane material and porosity, provided the pores were sufficiently small to prevent flow between compartments. Determinations of P in the $AgNO_3$-$NaNO_3$ system employing cells both with and without such membranes had been shown to give self-consistent results.[21] Furthermore, Duke and Fleming altered the type of membrane used in their experiments on the $PbCl_2$-KCl mixtures and found no effect on their results.[38] It thus appears likely that the data of Lorenz and his co-workers[35,36] were subject systematically to 1 of the 2 sources of error mentioned above. (Discrepancies from the results of Duke and Fleming[38] are also found in the data of Lorenz and Ruckstuhl[36] at $X_{23} = 0.33$, even though the latter determinations showed good reproducibility.) If the electro-osmotic effect is involved, this would indicate that considerable care should be exercised in the selection of such membranes. The powdered quartz packing used by Klemm and his co-workers[23] to prevent convection in the experiments on the LiCl-KCl system is similarly suspect, although, as I have indicated, the results they reported were quite reasonable.

Assuming the data of Duke and Fleming to be correct, we may substitute their results into the equation relating P to the friction coefficients in a system of this charge type.[1] The result is $r_{12} = 1.33\ r_{13} - 4.66\ r_{23}$, from which it follows that, in order for r_{12} to have a positive value, r_{13} must exceed r_{23} by at least a factor of 3.5. The corresponding ratio of the cation-anion friction coefficients for the pure salts at the same temperature is less than one half this figure, but, of course, the concentration dependence of these quantities remains unknown. Thus, the question of the existence of association in the $PbCl_2$-KCl system cannot be given a clear-cut answer until the necessary diffusion data become available.

Summary

Interionic friction coefficients for a number of pure molten salts have been calculated from available data and are summarized in tabular form. The list includes all of those salts for which results of self-diffusion experiments have been reported, as well as a number of examples for which only conductivity and density have been measured.

The effects of 3 experimentally variable conditions on the magnitudes of the friction coefficients are discussed separately; that is, size of the thermodynamic force, temperature, and pressure. A simple exponential relation is shown to describe the temperature dependence of both cation-anion and like-ion coefficients.

A criterion for association between the oppositely charged species in pure binary salts, based on the occurrence of negative like-ion friction coefficients, is shown to give evidence for the existence of such association in molten $ZnBr_2$.

The interionic friction coefficients for completely dissociated salts are discussed with regard to their possible correlations with the microscopic properties of the ions; that is, charge, size, shape, and mass.

A semi-quantitative discussion of the friction coefficients in molten salt mixtures is based on the incomplete transport data currently available for a number of systems. Cation-anion friction coefficients are shown to approximate ideal concentration dependence in the $AgNO_3$-$NaNO_3$ system, while such behavior is ruled out by the data for the system LiCl-KCl. Association between ions in the KBr-$AlBr_3$ system is demonstrated by the occurrence of negative coefficients, while the case of KCl-$PbCl_2$ is seen to remain ambiguous in the absence of complete transport data.

References

1. Laity, R. W. 1959. J. Chem. Phys. **30:** 682.
2. Conway, B. E. 1952. Electrochemical Data. Elsevier. London, England.
3. Biltz, W. & W. Klemm. 1926. Z. anorg. u. allgem. Chem. **152:** 267.
4. Graetz, L. 1890. Wied. Ann. **40:** 26.
5. Anderson, J. S. & K. Saddington. 1949. J. Chem. Soc. London. 381.
6. Lundén, A. 1956. Ph.D. Thesis. Gothenburg, Sweden.
7. Mills, R. & A. W. Adamson. 1955. J. Am. Chem. Soc. **77:** 3454.
8. Mills, R. 1955. J. Am. Chem. Soc. **77:** 6116.
9. Van Artsdalen, E. R. & I. S. Yaffe. 1955. J. Phys. Chem. **59:** 118.
10. Borucka, A. S., J. O'M. Bockris & J. A. Kitchener. 1957. Proc. Roy. Soc. London. **A241:** 554.
11. Glasstone, S., K. J. Laidler & H. Eyring. 1941. The Theory of Rate Processes. : 552. McGraw-Hill. New York, N.Y.
12. Bloom, H. & E. Heymann. 1947. Proc. Roy. Soc. London. **A188:** 392.
13. Laity, R. W. & F. R. Duke. 1955. AEC Rept. No. ISC-**654:** 30.
14. Duke, F. R. & R. Laity. 1954. J. Am. Chem. Soc. **76:** 4046.
15. Sundheim, B. R. 1956. J. Phys. Chem. **60:** 1381.
16. Byrne, J., H. Fleming & F. E. W. Wetmore. 1952. Can. J. Chem. **30:** 922.
17. Van Artsdalen, E. R., D. Brown, A. S. Dworkin & F. J. Miller. 1956. J. Am. Chem. Soc. **78:** 1772.
18. Klemm, A. 1953. Z. Naturforsch. **8a:** 397.
19. Klemm, A. 1951. Z. Naturforsch. **6a:** 487.
20. Laity, R. W. 1957. J. Am. Chem. Soc. **79:** 1849.
21. Duke, F. R., R. W. Laity & B. Owens. 1957. J. Electrochem. Soc. **104:** 299.
22. Duke, F. R. & R. W. Laity. 1955. J. Phys. Chem. **59:** 549.
23. Klemm, A., H. Hintenberger & P. Hoernes. 1947. Z. Naturforsch. **2a:** 245.
24. Lee, E. K. & E. P. Pearson. 1945. Trans. Electrochem. Soc. **88:** 171.
25. Drossbach, P. 1938. Die Elektrochemie Geschmolzener Salze. Springer. Berlin, Germany.
26. Klemm, A. 1953. Z. Naturforsch. **8a:** 400.
27. Herr, W. & A. Klemm. Private communication to A. Lundén.[6]
28. Hevesy, G. v. 1916. Jahrb. Radioakt. u. Elektronik. **13:** 171.[6]
29. Wallin, L.-E. & A. Lundén. Z. Naturforsch. (In press.)
30. Adamson, A. W. & R. Irani. 1957. J. Am. Chem. Soc. **79:** 2967.
31. International Critical Tables. 1929. **VI:** 152, 230. E. W. Washburn, Ed. McGraw-Hill. New York, N.Y.
32. Onsager, L. 1945. Ann. N.Y. Acad. Sci. **46**(5): 241.
33. Laity, R. W. 1959. J. Phys. Chem. **63:** 80.
34. Isbekow, W. 1926. Z. anorg. u. allgem. Chem. **158:** 87.
35. Lorenz, R. & G. Fausti. 1904. Z. Elektrochem. **10:** 630.
36. Lorenz, R. & W. Ruckstuhl. 1907. Z. anorg. Chem. **52:** 41.
37. Harrap, B. S. & E. Heymann. 1955. Trans. Faraday Soc. **51:** 268.
38. Duke, F. R. & R. A. Fleming. 1959. J. Electrochem. Soc. **106:** 130.

ION MOBILITIES IN PURE FUSED SILVER CHLORIDE*

F. R. Duke, A. L. Bowman, E. Wolf, H. Garfinkel
Institute for Atomic Research and Department of Chemistry,
Iowa State University, Ames, Iowa

Ion mobilities in a number of pure fused salts and salt mixtures have been determined, using radiotracers to follow the progress of ions through porous membranes.[1-3] This work has now been extended to include pure AgCl.

Experimental

Small quartz or Pyrex cells of the type previously described were used;[2] the U-shaped cells were fitted with a porous membrane of either ultrafine Pyrex or fine-porosity quartz treated successively with ethyl orthosilicate and hydrochloric acid to make the pores even finer. Each side of the U tube was filled with molten AgCl, the cathode compartment also containing radiochloride. Silver electrodes were used.

The cells were kept at the desired temperature in a Marshall furnace, and the temperature was controlled by means of a Brown electronic controller. Shunts between taps on the furnace were adjusted to insure that the temperature remained constant over several centimeters' more length than the cell occupied.

The total equivalents of charge passed through the cell were measured by timing a current. After passage of the current, the cell was allowed to cool and the anode and cathode compartments broken apart. The AgCl was dissolved in concentrated NH_4OH, and a portion of the AgCl was precipitated for counting by the slow addition of $AgNO_3$. A 1.0-gm. sample was counted on a 2-cm.-diameter filter paper, and the corrections for self-absorption were made.

The ratio of radiochloride found in the anode compartment to the total radioactivity multiplied by the equivalents of AgCl originally present in the catholyte yields the equivalents of Cl^- passing from cathode to anode.

Results and Discussion

It has been shown[2] that $(C_A N_{oc}/C_T Z) = t\mathrm{Cl}^-$, where C_A is the radioactive count in the anolyte at the end of the run, C_T is total radioactive counts originally present in the catholyte, N_{oc} is the number of equivalents of AgCl originally present in the catholyte, tCl is the transport number of the chloride ion, and Z is the number of equivalents of charge passed through the cell. The transport number of the chloride ion is given at the various temperatures in TABLE 1.

---

* The work reported in this paper was performed in the Ames Laboratory (Ames, Iowa) of the United States Atomic Energy Commission, Washington, D.C.

The ionic equivalent conductances and total conductance of AgCl are listed in TABLE 2.

The first point of interest is the zero transport number of chloride ion in those cases in which Pyrex disks were used. Either electroendosmosis or conduction by sodium ions in the Pyrex disk must be responsible for this result, since no break of any type is noted in the total conductivity of AgCl in this temperature range. Lorenz and Janz[4] have shown that AgCl does not wet Pyrex, making the latter postulate appear tenable. In any case, it is apparent that Pyrex should be viewed with suspicion as a membrane material in transport studies.

TABLE 1
TRANSPORT NUMBERS OF FUSED AgCl AT VARIOUS TEMPERATURES

T (°C.)	Membrane	t_{Cl^-}
550	Pyrex	0
600	Pyrex	0
650	Silica	0.15 ± .03
750	Silica	0.16 ± .03
850	Silica	0.17 ± .03
925	Silica	0.19 ± .03

TABLE 2
IONIC EQUIVALENT CONDUCTANCES IN FUSED AgCl
AT VARIOUS TEMPERATURES

T (°C.)	λ[5,6]	λAg^+	λCl^-
650	135	115	20
750	145	122	23
850	153	127	26
925	159	129	30

A second point of interest is the relatively high mobility of the silver ion compared with the chloride ion. The radius ratio calculation[1] and the mass ratio equation[7] are both very much in error as applied to silver chloride. No obvious explanation of the magnitude of these transport numbers is apparent.

References

1. DUKE, F. R. & B. OWENS. 1958. J. Electrochem. Soc. **105:** 548.
2. DUKE, F. R. & R. A. FLEMING. 1959. J. Electrochem. Soc. **106:** 130.
3. DUKE, F. R., R. LAITY & B. OWENS. 1957. J. Electrochem. Soc. **104:** 299.
4. LORENZ, M. R. & G. J. JANZ. 1959. J. Phys. Chem. **61:** 1683.
5. SPOONER, R. C. & F. E. W. WETMORE. 1951. Can. J. Chem. **29:** 777.
6. SAKAI, K. 1954. J. Chem. Soc. Japan. **75:** 182.
7. SUNDHEIM, B. R. 1956. J. Phys. Chem. **60:** 1381.

REFERENCE ELECTRODES AND OVERVOLTAGE MEASUREMENTS IN MOLTEN SALTS

R. Piontelli
Laboratory of Electrochemistry, Chemical Physics and Metallurgy, Politecnico di Milano, Milan, Italy

GLOSSARY OF SYMBOLS

$\equiv$ = equal by definition
PC = polarization cell
RE = reference electrode
PT = tensiometric cell
TA = tensiometric apparatus (including potentiometer and/or oscilloscope)
I^{MB} = electric current (conventional), circulating in a PC from the terminal M toward the terminal B
V^P = electric potential (macroscopically defined) at the position P
E^{MB} = electric potential difference, measured by a TA, between the metallic terminals M and B of a PC or PT (taken as positive when M is the positive pole of the chain)
t = time
EV = electrode voltage
ρ = electric resistivity of a conducting medium
T = absolute temperature, °K
P = pressure
V = volume
U = internal energy
S = entropy
G = $U + PV - TS$ (Gibbs free energy, or free enthalpy)
$\Delta G \equiv \left(\frac{\partial G}{\partial \xi_r}\right)_{T,P,\xi\neq r}$
$\text{đ}S^*$ = entropy increase in dt
ξ_r = degree of advancement of a reaction r (see *Section* I.3)
z_r = equivalence of a reaction r (in absolute value)
z_J = valence of the ionic species J (in algebraic value)
$\mu_Y{}^P$ = chemical potential of the chemical species Y in the position P
${}^{\rho}a_Y{}^P$ = chemical activity, in the molar fraction scale, of Y at P, with reference to the state ρ.
$\eta_J{}^P$ = electrochemical potential of the ionic species J (the electron θ included) in P (see APPENDIX I)
${}^{\rho}\tilde{a}_J{}^P$ = electrochemical activity of the ionic species J at P with reference to ρ (see APPENDIX I)
q^{MB} = conventional electric charge
ψ_M^{QP} = electrode overvoltage as given by an ideal isoelectrodic RE
Θ^{QP} = dissipative contribution
$E_{I=0}^{PP'}$ = zero-current voltage output of the PT formed by two identical RE connected to the points P and P′ in a given chemical configuration
$\delta_\Omega{}^{PP'}$ = ohmic contribution to the apparent overvoltage as given by an RE connected to a point P′
δ_c = contribution to the EV due to chemical changes at a given position or to the difference in chemical composition between two positions

The field or overvoltage in the electrolysis of molten salts has been somewhat neglected in the past, perhaps owing to the technical difficulties encountered in measurements of this class. Furthermore, with respect to the general position of the problem itself, not a few divergent opinions seem to exist.

In this paper the "phenomenological-operative" point of view will be taken; this viewpoint has as its main goal the statement of the laws of operation of electrolytic cells expressed only in quantities accessible, at least in principle, to experiment, and meaningful in the framework of classical thermodynamics or thermodynamics as extended to cover the theory of irreversible processes. Thus these laws may constitute a consistent starting point for further study of the kinetics and mechanism of the electrolysis processes within the very convenient framework of the thermodynamic method; moreover, they summarize data almost indispensable to the matter and energy balances in an electrowinning or electrorefining process, or in a fuel cell.

PART I

Section I.1

Consider[1-9] a polarization cell (PC), formed by two metal or graphite electronic conductors. These electrodes, $\mathfrak{M}$ and $\mathfrak{B}$, are plunged into an electrolytic conductor β, the bath* (FIGURE 1). Consider PC as a thermodynamic system outlined by a given contour surface and including two terminals, or poles M and B (two electronic conductors connected to, or part of, $\mathfrak{M}$ and $\mathfrak{B}$, respectively) by means of which PC can exchange electric currents with foreign conductors.

The energetic exchanges between PC and the foreign bodies may consist of (1) mechanical work due to volume changes under the surrounding pressure P; (2) electromagnetic work corresponding to the circulation, through PC, of unidirectional currents under steady, or quasisteady conditions†; and (3) heat.

The working conditions of PC, at any given time, are thus defined by (1) the temperature T (°K.) and pressure P of PC, both of which we shall assume to be uniform in the system and constant in time; (2) the chemical configuration of the electrodes $\mathfrak{M}$ and $\mathfrak{B}$ and of the bath β‡; (3) the intensity I^{MB} (amp.) of the electric current[*]; and (4) the voltage E^{MB} (volts), given by a tensiometric apparatus (TA), connected to the terminals M and B of PC.[†]

---

* From the geometric point of view, PC will be assumed to be "simply connected."

† The magnetic (inductive) effects and those corresponding to electric capacity of the conductors constituting the cell, in respect to surrounding conductors (side capacity effects), are both neglected here.

‡ Each electrode, plus a conventionally outlined region in β adjacent to the electrode itself, and the reservoir phases (that is, the phases in contact with the electrodes and not traversed by current, although taking part in the chemical changes by matter exchanges with the electrode or β) constitute what we shall call an electrodic system.

$E^{MB}I^{MB}\,dt$ is thus the electric work done on the cell in the time dt, being positive when the signs of E^{MB} and I^{MB} are the same. By considering PC as a system that is closed, on the whole, to matter exchanges,[‡] and by neglecting any kinetic contribution to its macroscopic energy, we may write[§]:

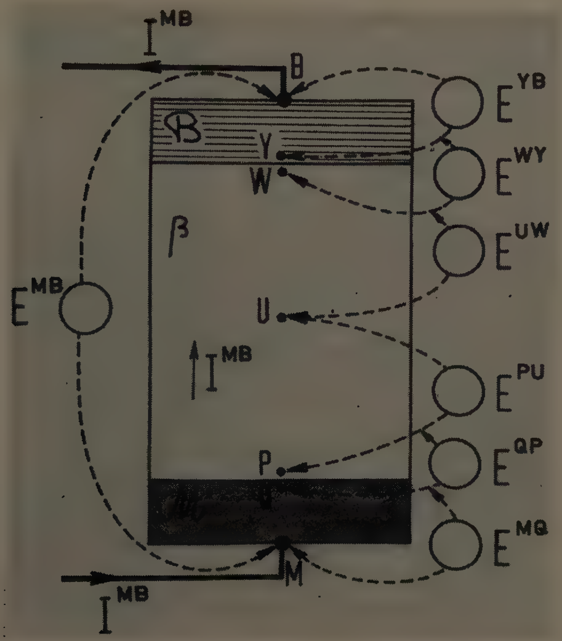

Figure 1. Schematized PC, with PT and TA to obtain a complete voltage balance.

---

[*] We shall consider conventional current as that supposed to be carried by only positive carriers. The sign of I^{MB} will be taken positive when this conventional current circulates in the cell from M toward B.

[†] TA (potentiometer, oscilloscope, electrometer) is connected to PC by means of two identical conductors m and b, and the measured voltage E^{MB} expresses the difference $V^M - V^B$ of the electrostatic potentials of these conductors when connected to the poles of PC. By conventional choice (indicated by the order of the indices in E^{MB}), E^{MB} is taken positive when $V^M > V^B$, and therefore M is the positive pole in PC (see Appendix II for further information on E^{MB}).

[‡] Also, the electron exchanges at the two (electronic conductor) terminals of PC are mutually compensating (side-capacitive currents being neglected).

[§] The meaning of the symbols above is (with reference to PC): U = internal energy; S = entropy; $G \equiv U + PV - TS$ (Gibbs free energy, or free enthalpy); and $\text{đ}S^*$ is the entropy creation in the cell by irreversible processes during dt. We assume that in every one of the configurations in which the macroscopic properties of

$$E^{MB} I^{MB}\, dt - P\, dV + \text{đ}Q = dU$$

$$\text{đ}Q = T\, dS - T\, \text{đ}S^{*} \qquad \text{(I.1:1)}$$

By putting $I^{MB}\, dt \equiv dq^{MB}$ (that is, the conventional charge carried by the current from M toward B in the time dt), we may write:

$$E^{MB}\, dq^{MB} = d_{T,P}\, G + T\, \text{đ}S^{*} \qquad \text{(I.1:2)}$$

The equation above gives the thermodynamic balance of the cell in its general form.

I.2 *Reference Electrodes*[7-9]

Into the polarization cell PC is now introduced some supplementary electrode systems called reference electrodes (RE). Assume, at first, for these RE the following idealized properties:*

(1) The chemical changes due to the current circulation in RE are well defined and reproducible.

(2) These processes fulfill the requirements of thermodynamic reversibility when the RE carries the very small currents involved in measurements.

(3) Any ohmic voltage drop (and thus joule dissipation) in the metallic parts of RE due to these currents may be neglected. No appreciable dissipation or entropy creation occurs, therefore, in RE.

(4) The presence of RE does not involve any disturbance of the field of current in β or on the electrode surfaces.

(5) RE may be assumed to be connected with a given point position of β.

(6) The eventual interliquid junction between β and the electrolyte of RE also fulfills the thermodynamic conditions of equilibrium.

(7) If RE includes one or more reservoir phases, the matter-transfer processes between the electrode, the electrolyte, and these phases are reversible.

By coupling through a TA (1) an RE with $\mathfrak{M}/\beta$, or $\mathfrak{B}/\beta$, or (2) two RE together a tensiometric cell (PT) is obtained. By introducing RE, PC becomes a multipole.

The following problems are now considered: (1) the meaning of the "voltage answers" of PT to the power impressed on PC, through its ter-

---

the system are assumed to be definable, not only U, but S and thus G also are definable and possess a well-determined value (affected by conventional choice of zero). We shall consider all of these quantities to be expressed in joules. A symbolic distinction is adopted here between the complete (or exact) differentials, dU, dV, dS, and the other elementary quantities $\text{đ}Q$ and $\text{đ}S^{*}$.

* The divergences of the real from the idealized properties are possible sources of systematic errors, which will be discussed later (*Section* II.6).

minals M and B*; and (2) the theoretical and practical requirements for a correspondence as near as possible to the idealized properties attributed to RE.

I.3 *Detailed Voltage Balance in PC*

During current circulation, PC is the seat of chemical processes, a part of which may be considered to be a direct consequence of (1) the migration of the carriers of electric charge in each conductor, and (2) the transfer of the carriers themselves from one conductor to another.

Consider, first, an idealized condition in which:

(1) The chemical configuration is completely uniform along both of the electrode surfaces.

(2) The chemical composition of β may be assumed to be uniform.

(3) The resulting chemical modifications in PC, occurring only during the current circulation, may be expressed by a reaction equation of the form

$$l_1L_1 + l_2L_2 + \cdots = b_1B_1 + b_2B_2 + \cdots$$

or, in synthetic form,†

$$\textstyle\sum_i \nu_i Y_i = 0 \tag{I.3:1}$$

The degree of advancement, ξ_q^{MB}, of this reaction is defined by:

$$d\xi_q^{MB} = \frac{dn_{B_1}}{b_1} = \frac{dn_{B_2}}{b_2} = \cdots = -\frac{dn_{L_1}}{l_1} = -\frac{dn_{L_2}}{l_2} = -\frac{dn_{Y_i}}{\nu_i} \tag{I.3:2}$$

dn_{Y_i} being the change occurring in dt in the number of moles n_{Y_i} of the substance Y_i, for which ν_i is the stoichiometric coefficient (taken in algebraic value).

We define the (positive) number z, called the equivalence of the cell reaction, as follows:

$$dq^{MB} \equiv z\mathfrak{F}\, d\xi_q^{MB} \tag{I.3:3}$$

where $\mathfrak{F} = 96{,}500$ coulomb gm.-equiv.

---

* The superscripts in the symbols, as in E^{MB} refer to the terminals of the galvanic chain (PC or PT). Whenever there is no ambiguity, these terminals are indicated by the letter denoting the phase to which the terminal belongs. For example, M indicates the terminal belonging to the phase $\mathfrak{M}$. The use of the double superscripts for the point positions (for example, $E^{PP'}$) makes the algebra of the partial voltages immediately apparent. For example:

$$E^{PP'} + E^{P'U} = E^{PP'} - E^{UP'} = E^{PU}$$

† For example,[1-9]

$$PbCl_{2\,(\beta)} = Pb_{(l)} + Cl_{2\,(g)}$$

We define:

$$\mathfrak{E}^{MB} \equiv -\frac{1}{z\mathfrak{F}}\left(\frac{\partial G}{\partial \xi_q^{MB}}\right)_{T,P} \equiv -\frac{\Delta G_q^{MB}}{z\mathfrak{F}} \tag{I.3:4}$$

Then:

$$E^{MB} + \mathfrak{E}^{MB} = e^{M*B} \tag{I.3:5}$$

which is the voltage balance equation. $\mathfrak{E}^{MB}$ is the (intrinsic) electromotive force (emf) of the system in the condition under consideration. The sum in the left member is the resulting emf (or electrochemical affinity) acting as the driving force for the circulation of the unit of (conventional) charge, in the cell from M toward B. When this sum is zero, the cell condition is one of thermodynamic equilibrium. The voltage dissipated in PC is e^{M*B}.

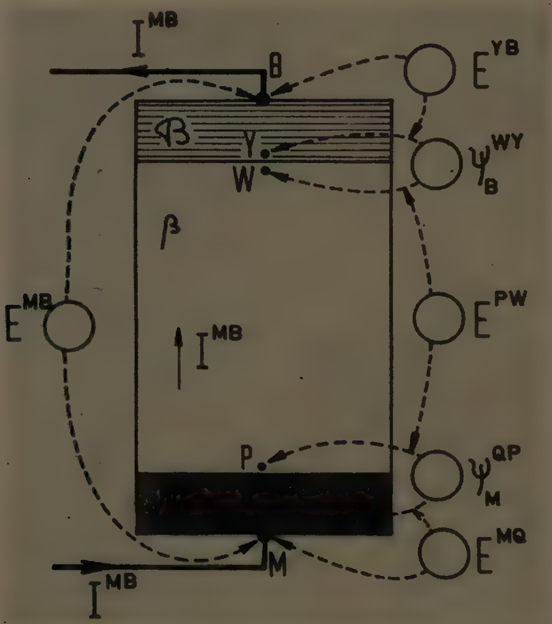

FIGURE 2. PC with RE of the isoelectrodic class (idealized condition: uniformity in β).

Now consider, for the idealized condition above, two ideal RE introduced as follows (FIGURE 2).

(1) An RE $\mathfrak{M}'/\beta$ whose electrode reaction is assumed to be exactly the same as that occurring on the $\mathfrak{M}/\beta$ surface (that is, it is isoelectrodic with respect to $\mathfrak{M}/\beta$), and whose metallic part is directly in contact with a point P in β situated at very small distance from a position Q on the $\mathfrak{M}$ surface. A TA is inserted between Q and the metallic terminal of RE.

The properties of $\mathfrak{M}'/\beta$ and $\mathfrak{M}/\beta$, may be different before, during, and after the current circulation in PC. The voltage output ψ_M^{QP} of the PT* $\mathfrak{M}_Q/\beta_P/\mathfrak{M}'$ will be called the electrode overvoltage for $\mathfrak{M}'/\beta$ in the position QP.

(2) An RE $\mathfrak{B}'/\beta_W$ having analogous properties and position W in respect to the electrode system $\mathfrak{B}_Y/\beta_W$ forms, with the latter, a second PT whose voltage output will be called ψ_B^{YW}.†

By connecting through a TA the two RE $\mathfrak{M}'/\beta_P$ and $\mathfrak{B}'/\beta_W$, we obtain a third PT whose voltage output is called E^{PW}. In the idealized condition here considered (involving, in particular, the uniformity of β), E^{PW} does not change when, in the absence of current ($I^{MB} = 0$), the junction points of RE with β are displaced from P to P′, or from W to W′, respectively. On the contrary, when $I^{MB} \neq 0$, E^{PW} depends on the position of these junction points.‡

Along surfaces parallel to the electrode surfaces (assumed to be perpendicular at any point to the current density vector), the displacement of the junction point does not affect the voltage output.

Considering the junction points of RE with β, again situated in P and W, we may then write:

$$\begin{aligned} E^{PW} &= E^{PW}_{I=0} + R^{PW} I^{MB} \\ &= E^{PW}_{dec.} + I^{MB} \rho_\beta \int_P^W \frac{dl}{A} = \frac{\Delta G_q^{PW}}{z\mathfrak{F}} + I^{MB} \rho_\beta \Gamma_\beta \end{aligned} \tag{I.3:6}$$

$$E^{PW}_{I=0} = E^{PW}_{dec.} = \frac{\Delta G_q^{PW}}{z\mathfrak{F}} \tag{I.3:7}$$

is the decomposition voltage corresponding to the chain reaction occurring in $\mathfrak{M}'/\beta_P//\beta_W/\mathfrak{B}'$ when the (conventional) current circulates from P toward W.

$$R^{PW} \equiv \rho_\beta \int_P^W \frac{dl}{A} = \rho_\beta \Gamma_\beta \tag{I.3:8}$$

---

* The terminals are supposed to be identical from the chemicophysical point of view (the electric status excluded), in a way to allow the meaning of the electric potential difference $V^M - V^{M'}$ to be attributed to ψ_M^{QP}, the sign convention being adopted according to which ψ_M^{QP} is positive when the positive pole of PT is on the $\mathfrak{M}$ side.

The ohmic contributions to ψ_M^{QP} also are supposed to be negligible insofar as $\mathfrak{M}$ is concerned. Therefore, only the eventual covering layers at the $\mathfrak{M}/\beta$ surface could make ohmic contributions to ψ_M^{QP} (*Section* III.2).

† Its sign being conventionally assumed positive when the positive pole of PT is on the $\mathfrak{B}$ side.

‡ By conventional choice (again correlated with the order of the indices P and W), E^{PW} is positive when the positive pole of PT is on the $\mathfrak{M}'$ side.

is the ohmic resistance of the bath, of which ρ_β is the resistivity* and Γ_β the resistance capacity.

E^{MB} then is given by

$$\begin{aligned} E^{MB} &= R^{MQ} I^{MB} + \psi_M^{QP} + E^{PW} - \psi_B^{YW} + R^{YW} I^{MB} \\ &= E_{dec.}^{PW} + (\psi_M^{QP} - \psi_B^{YW}) + R^{PW} I^{MB} + R_m I^{MB} \end{aligned} \qquad \text{(I.3:9)}$$

where R_m is the cumulative ohmic resistance of the metallic conductors. By I.3:5,

$$E^{MB} = -\mathfrak{E}^{MB} + e^{M*B} = \frac{\Delta G_q^{MB}}{z\mathfrak{F}} + e^{M*B} = E_{dec.}^{MB} + e^{M*B}$$

or

$$e^{M*B} = (R^{PW} + R_m) I^{MB} + (E_{dec.}^{PW} - E_{dec.}^{MB}) + (\psi_M^{QP} - \psi_B^{YW}) \qquad \text{(I.3:10)}$$

In the idealized condition shown above, e^{M*B} includes the ohmic potential drop in β and in the metallic conductors, and

$$(E_{dec.}^{PW} - E_{dec.}^{MB}) + (\psi_M^{QP} - \psi_B^{YW}) \equiv \Theta_M^{QP} + \Theta_B^{WY} \qquad \text{(I.3:11)}$$

that is, the sum of the dissipative overvoltages Θ_M^{QP} and Θ_B^{WY} corresponding respectively to the processes at the contact surfaces $\mathfrak{M}/\beta$ and $\mathfrak{B}/\beta$.

The meaning of these quantities deserves some comment. Assuming the configuration of each electrode system $\mathfrak{M}/\beta$ or $\mathfrak{B}/\beta$ respectively to be coincident (for all of the phases involved) with that of the corresponding RE ($\mathfrak{M}'/\beta$ or $\mathfrak{B}'/\beta$, respectively), we obtain $E_{dec.}^{PW} = E_{dec.}^{MB}$ and thus

$$\psi_M^{QP} - \psi_B^{WY} = \Theta_M^{QP} + \Theta_B^{YW}$$

In the case in which the processes at the $\mathfrak{M}/\beta$ and $\mathfrak{B}/\beta$ surfaces are reversible and $I^{MB} \neq 0$,

$$\psi_M^{QP} = 0 = \Theta_M^{QP} \quad \text{and} \quad \psi_B^{WY} = 0 = \Theta_B^{WY}$$

In the general case (but always for a condition idealized as indicated), the following may be written:

$$\begin{aligned} \psi_M^{QP} &= \frac{\Delta G_q^{MM'}}{z\mathfrak{F}} + \Theta_M^{QP} = E_{dec.}^{MM'} + \Theta_M^{QP} \\ \psi_B^{YW} &= \frac{\Delta G_q^{BB'}}{z\mathfrak{F}} + \Theta_B^{YW} = E_{dec.}^{BB'} + \Theta_B^{YW} \end{aligned} \qquad \text{(I.3:12)}$$

---

* We assume ρ_β to be a scalar quantity also when the chemical configuration depends on the position in β. Thus the continuous change in the chemical properties of β and hence the existence of a vectorial field of generalized forces is assumed not to affect the β isotropy.

so that

$$\frac{\Delta G_q^{MM'} - \Delta G_q^{BB'}}{z\mathfrak{F}} = E_{dec.}^{MM'} - E_{dec.}^{BB'} = E_{dec.}^{PW} - E_{dec.}^{MB}$$

$\Delta G_q^{MM'}$ and $\Delta G_q^{BB'}$ represent the free enthalpy increments (per unit change in their respective ξ_q, or due to circulation of a charge $z\mathfrak{F}$*) involved in the processes occurring in the PT $\mathfrak{M}/\beta/\mathfrak{M}'$ or $\mathfrak{B}/\beta/\mathfrak{B}'$, respectively, as a consequence of the differences of chemical configuration between $\mathfrak{M}/\beta$ or $\mathfrak{B}/\beta$ and the RE coupled with them in their respective PT.

Section I.4

In order to exemplify this point, let us assume the electrochemical reaction at the $\mathfrak{M}/\beta$ surface to be represented by the equation:

$$M^{z_M+}_{(\mathfrak{M})} \underset{\text{cat.}}{\overset{\text{an.}}{\rightleftarrows}} M^{z_M+}_{(\beta)}$$

that is, it corresponds to an ion-exchange process, for example:

$$\text{Pb}^{2+}_{(\mathfrak{M})} \rightleftarrows \text{Pb}^{2+}_{(\beta)}$$

Let us now consider the electrode $\mathfrak{M}/\beta$ to be coupled with RE $\mathfrak{M}'/\beta$, on whose surface the same reaction occurs. To the voltage output $E^{MM'} = V^M - V^{M'}$ of PT (the electric potential difference being taken in the region of identical chemical and physical properties), may be attributed the form:

$$E^{MM'} = (\eta_\theta^{M'} - \eta_\theta^{M})/\mathfrak{F} = \frac{RT}{\mathfrak{F}} \ln \frac{{}^{\delta}\tilde{a}_\theta^{M'}}{{}^{\delta}\tilde{a}_\theta^{M}} \tag{I.4:1}$$

η_θ is the electrochemical potential (joules/mole) of the electrons in the position denoted by the superscript M' or M, and ${}^{\delta}\tilde{a}_\theta$ is their electrochemical activity† referred to a reference state δ for the electrons. The circulation of current in $\mathfrak{M}/\beta/\mathfrak{M}'$ involves the chain reaction

$$M^{z_M+}_{(\mathfrak{M})} \rightleftarrows M^{z_M+}_{(\mathfrak{M}')}$$

superimposed (in the form of a very small disturbance) on that produced by I^{MB} on $\mathfrak{M}/\beta$.

By the hypothesis of electrochemical equilibrium at the $\mathfrak{M}'/\beta$ surface, we may write:

$$\overset{\mathfrak{M}'}{\eta}_{M^{z_M+}} = \overset{P}{\eta}_{M^{z_M+}}$$

Assume also the existence in both the phases $\mathfrak{M}$ and $\mathfrak{M}'$ of ionic dissociation equilibrium* and that the value of η_θ in each phase is uniform.† Then

---

* Here these reactions are assumed to be written in such a way as to make their equivalences have a common value z.

† See Appendix I.

$$\overset{Q}{\mu}_M = \overset{\sigma}{\mu}_M + RT \ln {}^{\sigma}\overset{Q}{a}_M = \overset{Q}{\eta}_{M^{z_M+}} + z_M \overset{Q}{\eta_\theta}$$
$$\overset{M'}{\mu}_M = \overset{\sigma}{\mu}_M + RT \ln {}^{\sigma}\overset{M'}{a}_M = \overset{M'}{\eta}_{M^{z_M+}} + z_M \overset{M'}{\eta_\theta} = \overset{P}{\eta}_{M^{z_M+}} + z_M \overset{M'}{\eta_\theta}$$

Alternatively,

$$\psi_M^{QP} = \frac{\overset{M'}{\eta_\theta} - \overset{Q}{\eta_\theta}}{\mathfrak{F}} = \frac{\overset{M'}{\mu}_M - \overset{Q}{\mu}_M}{z_M \mathfrak{F}} + \frac{\overset{Q}{\eta}_{M^{z_M+}} - \overset{P}{\eta}_{M^{z_M+}}}{z_M \mathfrak{F}}$$
$$= \frac{RT}{z_M \mathfrak{F}} \ln \frac{{}^{\sigma}\overset{M'}{a}_M}{{}^{\sigma}\overset{Q}{a}_M} + \frac{\overset{Q}{\eta}_{M^{z_M+}} - \overset{P}{\eta}_{M^{z_M+}}}{z_M \mathfrak{F}} \qquad \text{(I.4:2)}$$

This expression becomes coincident with I.3:5, if we write:

$$E_{dec.}^{MM'} \equiv \frac{RT}{z_M \mathfrak{F}} \ln \frac{{}^{\sigma}\overset{M'}{a}_M}{{}^{\sigma}\overset{Q}{a}_M}; \qquad \Theta_M^{QP} \equiv \frac{\overset{Q}{\eta}_{M^{z_M+}} - \overset{P}{\eta}_{M^{z_M+}}}{z_M \mathfrak{F}} \qquad \text{(I.4:3)}$$

In fact, the first quantity is expressive of the chemical work involved in the current circulation in PT (corresponding to the chain reaction $M_{(\mathfrak{M})} \rightleftarrows M_{(\mathfrak{M}')}$), due to the assumed difference in the properties of $\mathfrak{M}$ and $\mathfrak{M}'$, involving a difference in thermodynamic level for the M atom. In the case of pure molten metals such a difference does not exist, as a rule, while it may appear both for differences in chemical composition of $\mathfrak{M}$ and $\mathfrak{M}'$, and for differences in structure, in the case of solid phases. The quantity Θ_M^{QP} represents the work dissipated in the exchange of ions between the phases $\mathfrak{M}$ and β. By the assumption that P is very near Q, this quantity does not include any significant ohmic drop contribution; it may be considered, therefore, as the dissipative part of the electrode overvoltage. This treatment may be extended to any other kind of electrode process, and hence to $\mathfrak{B}/\beta/\mathfrak{B}'$.

I.5 *More General Conditions*

The following restrictions corresponding to the idealized condition now will be relinquished: (1) the uniformity of the chemical configuration of β,

---

* This assumption is supported by strong indirect evidence; for example, a well-realized intermetallic contact is practically nonpolarizable, even when carrying very high current densities.

† In the material that follows, the ohmic voltage drops in the metallic conductors will be neglected, as a rule, so that the electrochemical electron potential η_θ becomes uniform; the conductors themselves will be considered as homogeneous from the physicochemical point of view. The electrochemical or chemical potentials, or activities, of the different chemical species are considered to be uniform within the phases. However, when these phases are solid and the electrode reaction involves processes of crystal growth or demolition, the ions and atoms at the electrode interface of the metal may be considered to exist in adsorption states before entering or leaving the lattice. The equations I.4:2 and I.4:3 also may be applied in this case, when the considered values of η and μ are those inherent to the normal condition in the lattice.

(2) the uniqueness of the electrode reaction, and (3) the absence of spontaneous* processes.

To simplify the task, assume that the chemical configuration (that is to say, the local values of the molar fractions of the constituents) remains unchanged in the intermediate region of PC (around the cross-section including the point U of PC); this configuration can be adopted as the relative reference chemical composition for β.

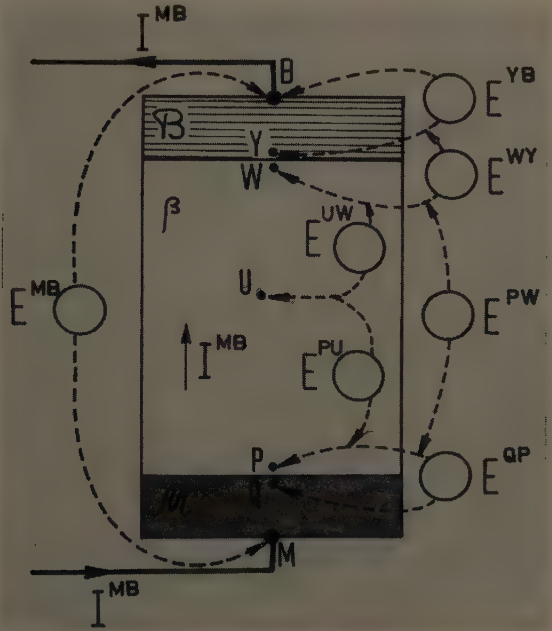

FIGURE 3. PC with RE of the isolectrodic class (more general condition).

Consider two RE, $\mathfrak{M}''/\beta_U$ and $\mathfrak{B}''/\beta_U$, again isoelectrodic with respect to $\mathfrak{M}/\beta_P$ or $\mathfrak{B}/\beta_W$ respectively, and both connected at the point U in β.

By the above hypothesis, the voltage output $E^{U}_{dec.}$ of the PT formed by these RE is constant and independent of the current circulation in PC.

The voltage balance of PC (FIGURE 3) now becomes:

$$\begin{aligned} E^{MB} &= E^{MQ} + E^{QP} + E^{PU} + E^{U}_{dec.} + E^{UW} + E^{WY} + E^{YB} \\ &= E^{MQ} + \psi_M^{QP} + E^{PU} + E^{U}_{dec.} + E^{UW} + \psi_B^{WY} + E^{YB} \end{aligned} \qquad (I.5:1)$$

---

* Here I call a process spontaneous that can occur also in the absence of the current circulation. The uniformity of β is then a necessary condition (unsufficient, as a rule) for the absence of spontaneous processes. When β is nonuniform, diffusion, at least, occurs.

where

$$\begin{aligned} E^{PU} &= E^{PU}_{I=0} + R^{PU} I^{MB} \\ E^{UW} &= E^{UW}_{I=0} + R^{UW} I^{MB} \end{aligned} \qquad (I.5{:}2)$$

The ohmic voltage drops in the metallic conductors are again:

$$E^{MQ} = R^{MQ} I^{MB} \quad \text{and} \quad E^{YB} = R^{YB} I^{MB}$$

The sum

$$E^{PU}_{I=0} + E^{UW}_{I=0} \equiv E_c \qquad (I.5{:}3)$$

of the voltage outputs of the couples

$$\mathfrak{M}'/\beta_P\,{/}'\,\beta_U/\mathfrak{M}'' \quad \text{and} \quad \mathfrak{B}''/\beta_U\,{/}'\,\beta_W/\mathfrak{B}'$$

(in the absence of current, but in the actual chemical configuration of the region included between P and U) may be considered as the operative definition of the concentration polarization in PC, as a consequence of the changes in chemical configuration produced by current.

This definition of E_c is affected by the choice of (1) the chemical composition in U, as the reference composition; and (2) the RE (here assumed to be isoelectrodic in respect to $\mathfrak{M}/\beta$ and $\mathfrak{B}/\beta$).

$E_c + E^U_{dec.}$ is the voltage output (again for $I = 0$, but in the actual chemical configuration) of the PT

$$\mathfrak{M}'/\beta_P\,{/}'\,\beta_W/\mathfrak{B}'$$

Therefore E_c represents the electric work, in excess of $E^U_{dec.}$, required by the charge circulation in this PT due to the configuration changes produced in β by the current circulation. The above choices appear, therefore, to be almost natural.

Two points deserve further consideration: (1) the possibility of correlating the values of $E^{PU}_{I=0}$ and $E^{UW}_{I=0}$ with the chemical configuration (assumed to be known in any detail) in the corresponding regions of β (*Section* II) and of evaluating them, in particular by thermodynamics; and (2) the consequences of the utilization, in usual practice, of heteroelectrodic RE.

The first point seems to correspond, at first glance, to the classic problem of the thermodynamic evaluation of a liquid junction potential difference by which the difficulty is met concerning the individual values of the chemical potential (or chemical activity) of charged chemical species (ions).* In fact, the quantities considered here represent the voltage outputs of galvanic chains (complete, in this case); their physical meaning cannot be questioned, but only the possibility of their correct evaluation on the basis of the knowledge of the chemical configuration.

---

* The possibility of defining this potential difference (a galvanic potential difference in common terminology) between regions differing in physicochemical properties has been questioned from Gibbs to recent times (see APPENDIX III).

The occurrence of the spontaneous diffusion processes contributes, of course, to the chemical configuration changes in PC and thus also to the free enthalpy balance, while its influence on the instantaneous voltage balance remains only an indirect one. I shall return to this point when considering the spontaneous processes at the electrode surface.

The meaning and the value of $E_{I=0}^{PU}$ depend, however, on the choice of the RE, and when the latter are taken as heteroelectrodic, instead of isoelectrodic, the problem must be reconsidered. One of the questions arising from this new condition is the second point above. The evaluation by a quasi-thermodynamic method may be considered as an adequate approximation, whose theoretical foundations are justified in the thermodynamics of irreversible processes (throughout the range in which the linear laws are valid).

It is perhaps worth remembering that the so-called experimental control of the quasi-thermodynamic evaluations of the contributions of the liquid-liquid junctions, in ultimate analysis always concern the emf of a complete chain. Thus, these experimental results may be considered rather as a confirmation of the possibility of a satisfactory evaluation, by the quasi-thermodynamic method, of the operative quantities considered here.

The possibility of realizing, in the case of molten salts, electrolytic short circuits to reduce the liquid junction contributions to a minimum, will not be considered here. This corresponds to reducing as much as possible the chemical work involved in the charge circulation through the junction. According to the operative definition adopted here of the contributions of $E_{I=0}^{PP'}$ to a voltage balance due to nonuniform regions of electrolyte, the introduction of an electrolytic short circuit does not eliminate such a contribution, but reduces it to that appropriate to the difference in thermodynamic levels of the ionic species whose exchange is assumed to constitute the electrode reaction.

I.6 *Simultaneous and Spontaneous Processes*

Consider that at the $\mathfrak{M}/\beta$ surface during the charge circulation (both in PC, in the form of I^{MB}, and in PT) a group of simultaneous electrode processes occurs, the pth process consuming a fraction ϵ_p (current efficiency) of the exchanged charge dq, thus:

$$dq_p \equiv \epsilon_p \, dq$$

Let $\sum_i \nu_{i,p} V_i = 0$ be the reaction equation of the process; ξ_p and z_p its degree of advancement from an arbitrary zero and its equivalence, respectively. Then

$$dq_p \equiv z_p \mathfrak{F} \, d\xi_p$$

At the RE surface the electrode reaction is again unique by hypothesis and is reversible. By the reasoning followed in *Section* I.3, which is unaffected by the new conditions at the $\mathfrak{M}/\beta$ surface,

$$E^{QP} = \frac{\Delta G_M^{MM'}}{z_M \mathfrak{F}} + \Theta_M^{QP} \tag{I.6:1}$$

The symbols have the same meaning, and thus

$$\Delta G_M^{MM'} = \left(\frac{\partial G}{\partial \xi_M^{MM'}} \right)_{T,P,\xi \neq M}$$

corresponds again to the occurrence of the same reaction, though under different conditions, at both the RE and $\mathfrak{M}/\beta$ surfaces.

The simultaneous occurrence of other processes at the $\mathfrak{M}/\beta$ surface has the following main consequences: (1) a change in the chemical configuration at the electrode surface and thus in $\Delta G_M^{MM'}$; and (2) the fact that now only the fraction ϵ_M of the circulating charge is spent for the reaction being considered. Considering all of the concurrent processes, the following may be written:

$$E^{QP} = \sum_p \epsilon_p \left(\frac{\Delta G_p^{MM'}}{z_p \mathfrak{F}} + \Theta_p^{QP} \right) \tag{I.6:2}$$

where

$$\Delta G_p^{MM'} \equiv \left(\frac{\partial G}{\partial \xi_p^{MM'}} \right)_{T,P,\xi \neq p}$$

corresponds to the chain reaction in PT resulting from the electrode reaction at RE and the p reaction at $\mathfrak{M}/\beta_P$.

EQUATIONS I.6:1 and I.6:2 are, in fact, coincident since

$$\frac{\Delta G_p^{MM'}}{z_p \mathfrak{F}} + \Theta_p^{QP}$$

has a common value for all of the concurrent processes p, and $\sum_p \epsilon_p = 1$. In fact, E^{QP} represents the electric work involved in the circulation of the unit of (conventional) charge in PT, and thus it is the same for all of the simultaneously occurring processes whose individual nature, however, is decisive for the distribution of this electric work between the nondissipative contribution* $\Delta G_p^{MM'}/z_p\mathfrak{F}$ and the dissipative one Θ_p^{QP}. We must note however that the individual value of Θ_p for each of the concurrent processes depends on (1) its own rate (and thus, for given current density, on its current efficiency); (2) the rate of all of the others; and (3) the rate of the eventual, simultaneous occurring, spontaneous processes. Thus apart from any mutual interference through chemical configuration and eventual coupling effects (through the generalized forces), the concurrent electrochemical processes can interfere, as a rule, by their mutual kinetic influence.

---

* It may be worthwhile to note that when $\Delta G_p^{MM'}/z_p\mathfrak{F}$ is being considered as a non-dissipative contribution, only the direct, or primary, effects of the charge circulation are being taken into account; these then may be followed by spontaneous processes, in which a part or the whole of $\Delta G_p^{MM'}$ may act as the driving force (chemical affinity), being thus dissipated.

The above analysis is still incomplete because the occurrence of spontaneous processes, superimposed on and inseparable from those accompanying the charge circulation, also must be considered.

The problems inherent in the occurrence of these spontaneous processes are those of their eventual contribution to the balances of voltages, free enthalpy changes, and to dissipation.

The situation of the spontaneous processes whose coupling with the current exchange at the electrode surface is excluded by the symmetry properties of the conjugate generalized forces* may be considered sufficiently clear-cut. In fact, the free enthalpy balance for these processes (*sp*) is simply

$$-\left(\frac{\partial G}{\partial \xi_{sp}}\right)_{T,P,\xi\neq sp} d\xi_{sp} = T\,\text{đ}S^{*}_{sp}$$

and thus the contribution of the latter disappears from the voltage balance equation I.3:5 for PC as a whole or for PT only.

This conclusion holds true for all spontaneous processes having the character of local chemical processes, that is, not involving ionic species and not influenced by the electric field. Among the classes of spontaneous processes that may occur at an electrode surface in molten salts, two possible exceptions deserve consideration: (1) the eventual displacement reaction by which an elementary constituent of the metallic phase displaces another element, contained in β in any form; and (2) reactions involving species adsorbed at the $\mathfrak{M}/\beta$ interface. With the former class, a form of mutual interference through the chemical configuration at the electrode interface is inevitable. As regards the probable electrochemical mechanism of these reactions, despite their local and spontaneous character, the possibility of coupling with the processes directly produced by current seems to exist.†

Any uncertainty in this respect may introduce indecision in relation to the values and the meaning of the different individual contributions to the balances of free enthalpy, dissipation, and voltages. The utilization of

* The generalized forces whose conjugate fluxes are the charge transfer at the electrode surface possess a vectorial character (gradient of η). Their coupling then is excluded in processes whose generalized forces are, on the contrary (as in chemical affinity), scalar.

† Especially in relation to the mechanism of dissipation, either as a direct consequence of the current circulation or by the simultaneous occurrence of spontaneous processes eventually coupled to the fluxes involving charge transfer at the electrode surface.

phenomenological laws to interpret the mechanism of the electrode processes becomes questionable.

The lack of information on these points, however, does not affect the global balances themselves in their formal and phenomenological aspects considered here. A more detailed analysis of this interesting problem would exceed the scope of this paper.

I.7 *Heteroelectrodic RE*

The practical impossibility of obtaining an isoelectrodic RE closely corresponding to the ideal conditions* for any of the electrode processes to be investigated makes necessary the systematic utilization of heteroelectrodic RE. The change thus introduced may be appreciated easily when two heteroelectrodic RE, $\mathfrak{N}/\beta$ for $\mathfrak{M}/\beta$ and $\mathfrak{F}/\beta$ for $\mathfrak{B}/\beta$, are assumed to be introduced in PC, together with the isoelectrodic RE $\mathfrak{M}'/\beta_P$ and $\mathfrak{B}'/\beta_W$ previously considered, and to be connected with the same points P and W respectively in β. Therefore

$$\begin{aligned} E^{MN} &= E^{MM'} + E^{M'N} = \psi_M^{QP} + E^{M'N} \\ E^{BF} &= E^{BB'} + E^{B'F} = \psi_B^{YW} + E^{B'F} \end{aligned} \qquad \text{(I.7:1)}$$

All of the RE are assumed to be connected to the same point in β in such a way as not to include in their voltage any appreciable contribution by ohmic drop. Assuming idealized properties, and

$$\begin{aligned} E^{M'N} &= \Delta G_q^{M'N}/z\mathfrak{F} \\ E^{B'F} &= \Delta G_q^{B'F}/z\mathfrak{F} \end{aligned}$$

or,

$$\begin{aligned} E^{MN} &= (\Delta G_q^{MM'} + \Delta G_q^{M'N})/z\mathfrak{F} + \Theta_M^{QP} = \frac{\Delta G_q^{MN}}{z\mathfrak{F}} + \Theta_M^{QP} \\ E^{BF} &= (\Delta G_q^{BB''} + \Delta G_q^{B''F})/z\mathfrak{F} - \Theta_B^{WY} = (\Delta G_q^{BF}/z\mathfrak{F}) - \Theta_B^{WY} \end{aligned} \qquad \text{(I.7:2)}$$

Thus the voltage outputs of the PT again result from two contributions, the dissipative one again being Θ. The other, thermodynamic part now corresponds to the electrode reaction as this occurs on $\mathfrak{M}/\beta$ or $\mathfrak{B}/\beta$, under the actual conditions of $\mathfrak{M}$ or $\mathfrak{B}$, respectively.

Let the heteroelectrodic RE be an electrode system whose electrode reaction is

$$N_{(s)} + r_N X_{(\beta)_p}^{z_X^-} = NX_{r_N}$$

---

* The ionic valences z_M, z_N, z_X are algebraic values unlike the reaction equivalence z_r

$$r_N \equiv \frac{z_N}{|z_X|}; \qquad r_M \equiv \frac{z_M}{|z_X|}; \qquad \text{while} \qquad z = \frac{z_M}{z_N} = \frac{r_M}{r_N}$$

(for example, $Ag_{(s)} + Cl^{-}_{(\beta)} = AgCl_{(s)} + \theta_{(Ag)}$, that is, a second-class electrode*). In the PT $\mathfrak{M}/\beta_P/\mathfrak{N}'$ the chain reaction is

$$M_{(\mathfrak{M})} + zNX_{r_{N}(s)} = r_M X^{zX-}_{(\beta)_p} + zN_{(\mathfrak{N})} + M^{zM+}_{(\beta)_p}$$

By assuming the RE to correspond to the ideality conditions, the electrochemical equilibrium condition at the $\mathfrak{N}/\beta_P$ surface may be written

$$\mu_N^{N'} + r_N \eta^{P}_{X^{z}X-} = \mu^{s}_{NX_r} + z_N \eta_\theta^{N'}$$

Since:

$$E^{MN'} = (\eta_\theta^{N'} - \eta_\theta^{M})/\mathfrak{F} \quad \text{and} \quad \eta_\theta^{M} = (\mu_M^{Q} - \eta^{Q}_{M^{z}M+})/z_M$$

therefore:

$$E^{MN'} = \frac{-\mu_M^{Q} + \eta^{Q}_{M^{z}M+}}{z_M\mathfrak{F}} + \frac{\mu_N^{N'} + r_N\eta^{P}_{X^{z}X-} - \mu^{s}_{NX_{r_N}}}{z_M\mathfrak{F}} \qquad \text{(I.7:3)}$$

In a reference configuration for β (indicated by *in*), assume

$${}^{in}\eta^{P}_{M^{z}M+} + r_M\, {}^{in}\eta^{P}_{X^{z}X-} = {}^{in}\mu^{P}_{MX_{r_M}}$$

$$E^{MN} = \frac{{}^{in}\mu_M - \mu_M^{Q}}{z_M\mathfrak{F}} + \frac{\eta^{Q}_{M^{z}M+} - \eta^{P}_{M^{z}M+}}{z_M\mathfrak{F}} + \frac{\eta^{P}_{M^{z}M+} + r_M\eta^{P}_{X^{z}X-} - \mu^{P}_{MX_{r_M}}}{z_M\mathfrak{F}}$$
$$+ \frac{\mu^{P}_{MX_{r_M}} - {}^{in}\mu_{MX_{r_M}}}{z_M\mathfrak{F}} + \frac{\mu_N^{N'} - \mu^{s}_{NX_{r_N}}}{z_N\mathfrak{F}} - \frac{{}^{in}\mu_M - {}^{in}\mu_{MX_{r_M}}}{z_M\mathfrak{F}}$$

By keeping†

$${}^{in}\mu_M = \mu_M^{\sigma} + RT \ln {}^{\sigma}a_M{}^{in} = \mu_M^{M'} = \mu_M^{\sigma} + RT \ln {}^{\sigma}a_M^{M'}$$

the following is obtained:

$$E^{MN} = \psi_M^{QP} + \frac{\Delta G_{in}^{M'N'}}{z\mathfrak{F}} + \frac{\eta^{P}_{M^{z}M+} + r_M\eta^{P}_{X^{z}x-} - \mu^{P}_{MX_{r_M}}}{z_M\mathfrak{F}}$$
$$+ \frac{\mu^{P}_{MX_{r_M}} - {}^{in}\mu_{MX_{r_M}}}{z_M\mathfrak{F}} \qquad \text{(I.7:4)}$$

$$= \psi_M^{QP} + E_{g,in}^{M'N'} + \delta^{P}_{c,r,om} + \delta^{P}_{c,in}$$

By the change in the nature of RE in the voltage output of PT, the following contributions now appear, in addition to ψ_M^{QP}:

$$E_{g,in}^{M'N'} = \frac{\Delta G_{in}^{M'N'}}{z\mathfrak{F}} \qquad \text{(I.7:5)}$$

---

* $AgCl_{(s)}$ assumes here the character of a reservoir phase.

† $\mu_M^{M'}$ is the chemical potential and ${}^{\sigma}a_M^{M'}$ the activity of the M atom under the conditions considered to be realized at the surface of the isoelectrodic RE $\mathfrak{M}'/\beta$ (see APPENDIX I).

that is, the chemical work involved by the charge circulation in a PT $\mathfrak{M}'/\beta_P/\mathfrak{N}$, taken in its reference configuration (*in*); the term

$$\delta^P_{c,r,om} = \frac{\overset{P}{\eta}_{M^{z_M+}} + r_M \overset{P}{\eta}_{X^{z_X-}} - \overset{P}{\mu}_{MX_{r_M}}}{z_M \mathfrak{F}} \qquad (I.7{:}6)$$

expressing the overvoltage corresponding to the eventual deviations of the chemical configuration in P from that corresponding to the equilibrium condition for the dissociation reaction of MX_{r_M}; and the term:

$$\delta^P_{c,in} = (\mu_{MX_{r_M}} - {}^{in}\mu_{MX_{r_M}})/z_M \mathfrak{F} \qquad (I.7{:}7)$$

expressing the influence of the changes in chemical composition in P, on the thermodynamic level of MX_{r_M}.

Also,

$$E^{MN}_P = \left(\frac{\Delta G^{MM'}_M}{z_M \mathfrak{F}} + \frac{\Delta G^{MN}_{in}}{z \mathfrak{F}} + \delta^P_{c,r,om} + \delta^P_{c,in} \right) + \Theta^{QP}_M$$

expresses E^{MN}_P again as the sum of two contributions, one of which (Θ^{QP}_M) gives the work directly dissipated in the electrode reaction on $\mathfrak{M}/\beta_P$.

The sum $\delta_{c,r,om} + \overset{P}{\delta}_{c,in}$ may be considered as the expression of the overvoltage due to composition change, in the given position P in β, with reference to: (1) the given electrode reaction r; (2) a reference composition for β; (3) the RE being considered.*

I.8 *Voltage Balance of PC Using Heteroelectrodic RE*

In practice, the most usual condition is that heteroelectrodic RE of a single class are utilized and connected with β at the point positions P and W (see FIGURE 1). Assume the RE to be of the $\mathfrak{N}/\beta$ class (reversible in respect to X^{z_x-} exchanges and directly coupled with β_P).

The equation expressive of the voltage balance in PC is now:

$$E^{MB} = E^{MN}_P + E^{PW}_{I=0} + R^{PW} I^{MB} + E^{NB}_W + (R^{MQ} + R^{YB}) I^{MB} \qquad (I.8{:}1)$$

$$E^{MN} = \psi^{QP}_M + E^{M'N}_{g,in} + \delta^P_{c,r,om} + \delta^{P,in}_c \qquad (I.8{:}2)$$

$$E^{NB}_W = \psi^{WY}_B + E^{NB'}_{g,in} + \delta^W_{c,r,om} + \delta^{W,in}_c; \; E^{PW}_{I=0} = \frac{\overset{W}{\eta}_{X^{z_x-}} - \overset{P}{\eta}_{X^{z_x-}}}{|z_x| \mathfrak{F}} \qquad (I.8{:}3)$$

When the reference configuration is assumed to be the same everywhere in β,

$$E^{M'N}_{g,in} + E^{NB'}_{g,in} = E^{M'B'}_{g,in} \equiv E^{M'B'}_{dec.,in} = \frac{\Delta G^{M'B'}}{z \mathfrak{F}} \qquad (I.8{:}4)$$

---

* This overvoltage is defined as follows. Consider a PT formed by coupling the RE with an electrodic system directly connected with β at P, and being in permanent equilibrium in respect to r. The difference between the voltage outputs of this PT, when the β_P composition is the present one or the reference one, respectively, gives the overvoltage by composition change in β_P relative to r, to the reference composition of β, and to the adopted RE.

leading to

$$E^{M'N'}_{g,in} + E^{NB'}_{g,in} + \delta^{P}_{c,r,om} + \delta^{P}_{c,in} + \delta^{W}_{c,r,om} + \delta^{W}_{c,in} + \delta^{PW}_{c} = E^{PU}_{I=0} + E^{UW}_{I=0} + E^{U}_{dec.} \tag{I.8:5}$$

(the implicit assumption being that the constant composition in β corresponds to the in reference composition in the first member). The change in the nature of RE, although obviously not affecting the sum total, changes the proportions of the individual contributions (or partial voltages and overvoltages).

Section I.9

In the most common arrangement in laboratory experiments, the overvoltage phenomena are investigated separately at each of the electrodes of PC. Consider (FIGURE 4) the electrode $\mathfrak{M}/\beta$ on whose surface the current distribution and properties of both phases are assumed to be uniform. The voltage output $E^{MP'}$, which is obtained by utilizing an isoelectrodic RE, then may be considered as resulting from the contributions

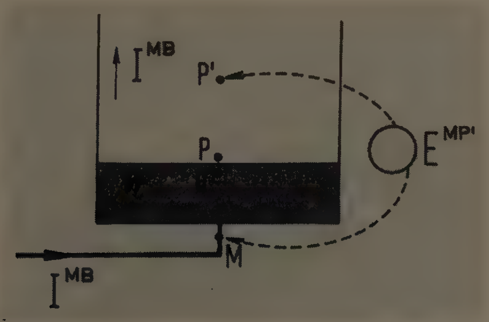

FIGURE 4. Arrangement for studying overvoltages at a single electrode $\mathfrak{M}/\beta$.

$$\begin{aligned} E^{MP'} &= \psi^{QP}_{M} + E^{PP'} = \psi^{QP}_{M} + \frac{\overset{P}{\eta}_{M^{z_M+}} - \overset{P'}{\eta}_{M^{z_M+}}}{z_M\mathfrak{F}} \\ &= \psi^{QP}_{M} + R^{PP'}I^{MB} + E^{PP'}_{I=0} = \psi^{QP}_{M} + \delta^{PP'}_{\Omega} + \delta^{PP'}_{c,M} \end{aligned} \tag{I.9:1}$$

This and any other condition measurable but different from ψ^{QP}_{M} is referred to as apparent (electrode) overvoltage.

The spurious contributions $\delta^{PP'}_{\Omega}$ (by ohmic voltage drop) and $\delta^{PP'}_{c,M}$ (by concentration polarization*) may be considered as sources of systematic errors, to be avoided or corrected as accurately as possible. When, instead of an isoelectrodic RE, a heteroelectrodic $\mathfrak{N}/\gamma$ RE is utilized, assumed to be connected at a point position P', $E^{MP'}$ may be considered as resulting from the different contributions

---

* With reference to the electrode reaction $M^{z_M+}_{(\mathfrak{M})} \rightleftarrows M^{z_M+}_{(\beta)}$ and isoelectrodic RE (see *Section* II.6).

$$\psi_M^{QP}, \qquad E_{g,in}^{MN}, \qquad \delta_{c,r,om}^{P}, \qquad \delta_{c,N}^{PP'}, \qquad \delta_{\Omega}^{PP'}$$

the meaning of terms being that previously given. $\delta_{c,N}^{PP'}$ is now different, in the general case, from $\delta_{c,M}^{PP'}$, the electrodes of the PT whose voltage output this quantity represents, being of the type $\mathfrak{N}/\gamma$ instead of $\mathfrak{M}/\beta$.*

Consider now the case in which the RE $\mathfrak{D}/\gamma_{P'}$ is heteroelectrodic and not in direct contact with $\beta_{P'}$ while, moreover, its electrode reaction having the oxidation-reduction form

$$\text{Ox.}_{(\gamma)} + z_D\theta_{(D)} \rightarrow \text{Red.}_{(\gamma)}$$

does not involve X^{z_x-}.

A general expression of E^{MD} is obtained in the form

$$E^{MD} = E^{MM'} + E^{M'D} = \psi_M^{QP} + E^{M'D} \tag{I.9:2}$$

that is, as the sum of the voltage outputs of the PT

$$\mathfrak{M}/\beta_P/\mathfrak{M}' \quad \text{and} \quad \mathfrak{M}'/\beta_P/\!/\gamma_{P'}/\mathfrak{D}$$

Thus, the following may be written:

$$\mu_M^{M'} = \mu_M^{\sigma} = z_M\eta_\theta^{M'} + \eta_{M^zM+}^{M'} = z_\theta\eta_\theta^{M'} + \eta_{M^zM+}^{P}$$

$$\eta_{\text{Ox.}}^{P'} + z_D\eta_\theta^{D} = \eta_{\text{Red.}}^{P'}$$

and thus:

$$E_{PP'}^{M'D} = \frac{\eta_\theta^{D} - \eta_\theta^{M'}}{\mathfrak{F}} = \frac{\eta_{\text{Red.}}^{P'} - \eta_{\text{Ox.}}^{P'}}{z_D\mathfrak{F}} - \frac{\mu_M^{\sigma} - \eta_{M^zM+}^{P}}{z_M\mathfrak{F}} \tag{I.9:3}$$

FIGURE 5 represents in schematic form the arrangement of a PC with only one RE placed in an accessible position U. This compromise may become a necessary one in practice. The results above require only trivial adaptations to cover this condition.

I.10 *More Complex Electrode Reactions*

The considerations above may be applied easily to more complicated electrode reactions, for example, oxidation-reduction processes, or reactions involving complexes. I shall consider only the case of the anodic reactions in an aluminum reduction cell for both its intrinsic interest and its relatively general character. At the anode $\mathfrak{B}/\beta$ (see FIGURE 10) of an

---

* For RE reversible in respect to X^{z_x-}:

$$\delta_{c,N}^{PP'} = (\eta_{x^{z_x-}}^{P'} - \eta_{x^{z_x-}}^{P})/|z_X|\mathfrak{F}$$

aluminum reduction cell, in a quasisteady condition* the matter balance† assumes the form‡

$$\tfrac{3}{2}D_{O\,(\beta)} + yC_{(\mathfrak{B})} \rightarrow \tfrac{3}{2}R_{(\beta)} + (\tfrac{3}{2} - y)CO_{2\,(g)} + (2y - \tfrac{3}{2})CO_{(g)}$$

D_O is the oxygen donor in β (for example, Al_2O_3, AlO_2^-, or another, not necessarily unique) and R_β is the residue left by D_O after giving up oxygen.§

For given physical conditions (T, P), the value of y depends upon (1) the physicochemical properties of $\mathfrak{B}$ (carbon, graphite of the various types); (2) the chemical composition of the bath at the anode surface (β_W); and (3) the value $i = z\mathfrak{F}d\xi/dt$ of the anodic current density.‖ Let us now consider a PT:

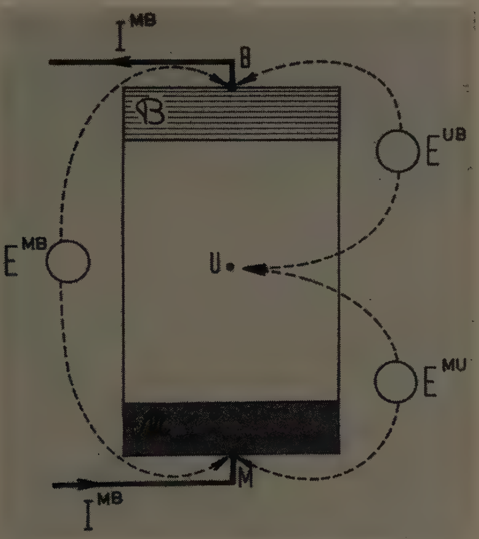

FIGURE 5. PC with a single RE.

$$\mathfrak{B}/\beta_W /\!/ \beta'/\mathfrak{A}$$

(FIGURE 6) $\mathfrak{A}/\beta'$ being an RE of the class $Al_{(l)}$/cryolite + Al_2O_3 (sat.).[18-22] Consider a second PT to be introduced, formed by an RE $\mathfrak{B}'/\beta_W$ (isoelec-

---

* Far enough from the condition in which anode effect occurs and in which, therefore, the parts taken by fluorine and oxygen production may be neglected finally.

† Referred to the unit of apparent electrode surface.

‡ Taking into account oxygen as a possible final product, the equation would be:

$$\tfrac{3}{2}D_{O\,(\beta)} + yC_{(\mathfrak{B})} \rightarrow \tfrac{3}{2}R_{(\beta)} + {}_mO_{2\,(g)} + (\tfrac{3}{2} - 2m - y)\,CO_{2\,(g)} + (2y + 2m - \tfrac{3}{2})\,CO_{(g)}$$

$m \simeq 0$ as a rule.

§ Each D_O is assumed, here, to give up an oxygen atom.

‖ Also referred to the unit of apparent electrode surface.

trodic in respect to $\mathfrak{B}/\beta_W$ and placed in contact with β_W); and an RE $\mathfrak{B}''/\beta'$ (again isoelectrodic in respect to $\mathfrak{B}/\beta$, but placed in contact with β'). The voltage output E^{BA} of this PT then may be written as the sum of three different contributions (all of which have an unambiguous operative meaning):

$$E^{BA} = E^{BB'} + E^{B'B''} + E^{B''A}$$

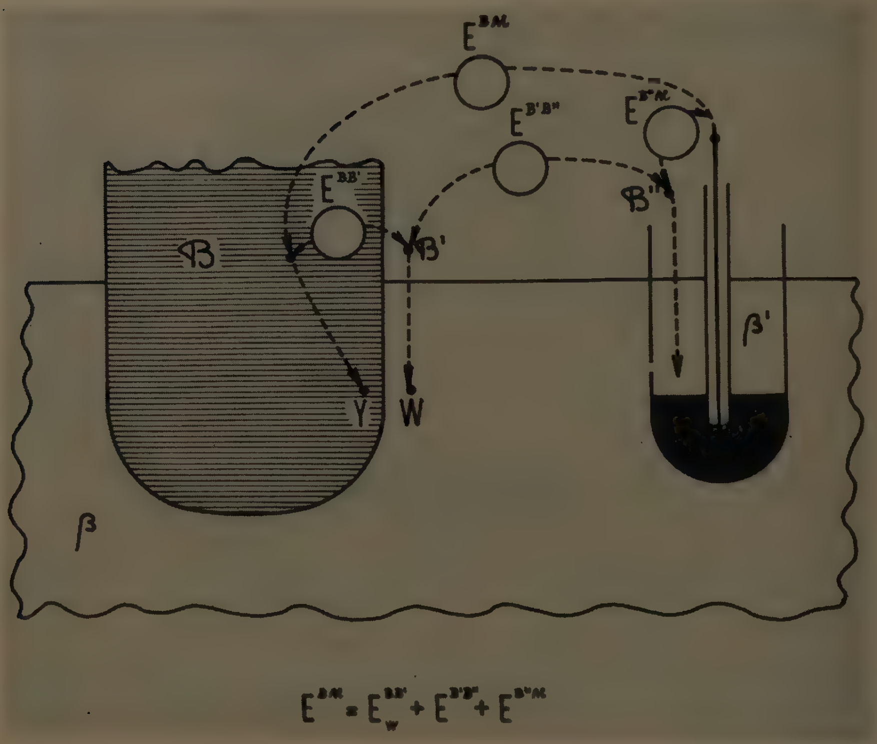

FIGURE 6. Scheme corresponding to the arrangement for studying overvoltage phenomena at the anode of a PC for the Al production.

where

$$E^{BB'} = \frac{(\eta_\theta^{B'} - \eta_\theta^{B})}{\mathfrak{F}} \text{ is the voltage of PT } \mathfrak{B}/\beta_W/\mathfrak{B}'$$

$$E^{B'B''} = \frac{\eta_\theta^{B''} - \eta_\theta^{B'}}{\mathfrak{F}} \text{ is that of the PT } \mathfrak{B}'/\beta_W/\beta'/\mathfrak{B}''$$

$$E^{B''A} = \frac{\eta_\theta^{A} - \eta_\theta^{B''}}{\mathfrak{F}} \text{ is that of the PT } \mathfrak{B}''/\beta'/\mathfrak{A}$$

Assume $\mathfrak{B}'$ and $\mathfrak{B}''$ to be made of carbon, taken in a reference state (in which it is assumed that $\mu_C^{B''} = \mu_C^{B'}$ and $a_C^{B''} = a_C^{B'}$, as the values of its chemical potential and activity, respectively). The gaseous atmosphere surrounding both $\mathfrak{B}'$ and $\mathfrak{B}''$ is assumed to be at equilibrium, that is, containing CO_2, CO, O_2 at partial pressures (or more generally fugacities) corresponding to the equilibria

$$C_{(B')} + \tfrac{1}{2}O_{2\,(g)} = CO_{(g)}$$

$$CO_{(g)} + \tfrac{1}{2}O_{2\,(g)} = CO_{2\,(g)}$$

and thus also to:

$$C_{(B')} + O_{2\,(g)} = CO_{2\,(g)}$$

$$CO_{2\,(g)} + C_{(B')} = 2\,CO_{(g)}$$

for the given physical conditions.

By the ideality condition, the charge circulation (in the amounts involved in overvoltage measurements) does not affect this composition. Assume the donors D_{Al} of Al, and D_O of O, to be in permanent equilibrium in β' with the source of both, that is, the Al_2O_3 saturating β'. Evaluate the different contributions $E^{BB'}$, $E^{B'B''}$, $E^{B''A}$ on all of the three carbon electrodes ($\mathfrak{B}$, $\mathfrak{B}'$, $\mathfrak{B}''$). The electrode reaction may be considered to be divided into effective steps (or steps equivalent, on the whole, to the effective ones):

$$D_O \rightleftarrows O^{=}_{(\mathrm{bath})} + R_O \qquad \text{(Step I)}$$

$$O^{=}_{(\mathrm{bath})} \rightarrow O^{=}_{(\mathrm{electrode})} \qquad \text{(Step II)}$$

$$O^{=}_{(\mathrm{electrode})} \rightarrow O_{(\mathrm{electrode})} + 2\theta_{(\mathrm{electrode})} \qquad \text{(Step III)}$$

By the ideality conditions, these steps are assumed to correspond to electrochemical equilibrium on $\mathfrak{B}'/\beta_W$ and $\mathfrak{B}''/\beta''$, and thus:

$$\eta_{O^{=}}^{B'} = \eta_{O^{=}}^{W}; \qquad 2\eta_{\theta}^{B'} = \eta_{O^{=}}^{B'} - \mu_O^{B'} \doteq \eta_{O^{=}}^{W} - \mu_O^{B'}$$

$$\eta_{O^{=}}^{B''} = \eta_{O^{=}}^{B'}; \qquad 2\eta_{\theta}^{B''} = \eta_{O^{=}}^{B''} - \mu_O^{B''} = \eta_{O^{=}}^{B''} - \mu_O^{B''}$$

By the ideality condition a further step occurs at the $\mathfrak{B}'$ and $\mathfrak{B}''$ surfaces:

$$\tfrac{3}{2}O + eC_{(s)} = (\tfrac{3}{2} - e)CO_{2\,(g)} + (2e - \tfrac{3}{2})CO_{(g)}$$

Where the ratio $(\tfrac{3}{2} - e)/(2e - \tfrac{3}{2})$ must correspond to the ratio $(P_{CO_2}/P_{CO})_{eq.}$ in an equilibrium atmosphere with the carbon and in the physical conditions attributed to both $\mathfrak{B}'$ and $\mathfrak{B}''$. The chain reaction in $\mathfrak{B}''/\beta'/\mathfrak{A}$ (when current circulates from $\mathfrak{B}''$ to $\mathfrak{A}$), may be then written

$$\tfrac{1}{2}Al_2O_{3\,(s)} + eC_{(s)} = Al_{(l)} + (\tfrac{3}{2} - e)CO_{2\,(g)} + (2e - \tfrac{3}{2})CO_{(g)}$$

Therefore

$$E^{B''A} = \frac{\Delta G^{B''A}}{3\mathfrak{F}}$$

$$= \frac{\mu^{A}_{\mathrm{Al}} + (3/2 - e)\mu^{B'}_{\mathrm{CO_2}} + (2e - 3/2)\mu^{B'}_{\mathrm{CO_2}} - 1/2\mu^{B'}_{\mathrm{Al_2O_3}} - e\mu^{B'}_{\mathrm{C}}}{3\mathfrak{F}}$$

$E^{B'B''}$ depends on the difference in the chemical configuration of the electrolyte in passing from W to β'.

From the relations above, the following is obtained:

$$E^{B'B''} = \frac{(\eta^{\beta'}_{D_{\mathrm{O}}} - \eta^{W}_{D_{\mathrm{O}}}) + (\eta^{W}_{R_{\mathrm{O}}} - \eta^{\beta'}_{R_{\mathrm{O}}})}{2\mathfrak{F}}$$

With respect to $E^{BB'}$, the reaction at the $\mathfrak{B}/\beta_W$ surface may be broken into the equivalent Steps I, II, and III. These partial reactions will not correspond, however, to the equilibrium conditions; likewise, the subsequent carbon/oxygen reaction will not correspond, as a rule, to equilibrium, and therefore must be written in the modified form:

$$3/2\mathrm{O}_{(\mathfrak{B})} + y\mathrm{C}_{(\mathfrak{B})} \rightarrow (3/2 - y)\mathrm{CO}_{2\,(g)} + (2y - 3/2)\mathrm{CO}_{(g)}$$

(Again, in view of the final matter balance, the oxygen production is neglected.) By setting:

$$-3/2\Delta G^{B}_{\mathrm{Ox.}} \equiv y\mu^{B}_{\mathrm{C}} + 3/2\mu^{B}_{\mathrm{O}} - (3/2 - y)\mu^{B}_{\mathrm{CO_2}} - (2y - 3/2)\mu^{B}_{\mathrm{CO}}$$

and

$$-\Delta G^{B}_{J} = -2\eta^{B}_{\theta} - \mu^{B}_{\mathrm{O}} + \eta^{B}_{\mathrm{O}^{=}}$$

the following is obtained

$$E^{BB'} = \eta^{B'}_{\theta} - \eta^{B}_{\theta} = \frac{\eta^{W}_{\mathrm{O}^{=}} - \eta^{B}_{\mathrm{O}^{=}}}{2\mathfrak{F}} - \frac{\Delta G^{B}_{J}}{2\mathfrak{F}} - \frac{\Delta G^{B}_{\mathrm{Ox.}}}{2\mathfrak{F}} + \frac{e\mu^{B'}_{\mathrm{C}} - y\mu^{B}_{\mathrm{C}}}{3\mathfrak{F}}$$

$$+ \frac{(1 - 4/3e)\mu^{B'}_{\mathrm{CO}} - (1 - 4/3y)\mu^{B}_{\mathrm{CO}} + (2/3e - 1)\mu^{B'}_{\mathrm{CO_2}} - (2/3e - 1)\mu^{B}_{\mathrm{CO_2}}}{2\mathfrak{F}}$$

The first term

$$\frac{\eta^{W}_{\mathrm{O}^{=}} - \eta^{B}_{\mathrm{O}^{=}}}{2\mathfrak{F}}$$

represents the dissipative overvoltage involved in the charge exchange at the $\mathfrak{B}/\beta_W$ surface, assumed to occur in the form of oxygen ions. It includes, therefore, the voltage actually dissipated in overcoming any eventual transfer resistance.

$-(\Delta G_J/2\mathfrak{F})$ is the overvoltage involved in the nonequilibrium oxygen ion–electron reaction at the B surface. $-(\Delta G_{\mathrm{Ox.}}/2\mathfrak{F})$ is the overvoltage involved in the oxygen–carbon reaction.

The term referring to the reaction at the $\mathfrak{B}/\beta_W$ surface,

$$\frac{e\mu_C^{B'} - y\mu_C^{B}}{3\mathfrak{F}}$$

takes into account the influences both of the eventual difference in thermodynamic reactivity of the anode carbon and of the difference in the stoichiometric coefficients of the carbon itself upon e for carbon, in the reaction leading to equilibrium composition. The last term in the preceding equation has an analogous meaning in respect to CO and CO_2.

It may be worth noticing that the considerations above do not involve any detailed hypotheses on the mechanism and the kinetic laws of the electrode processes. We are concerned only with some possible chemical species whose thermodynamic properties may be assumed to be determined from the working conditions of the electrode.

The effective path followed by the electrode reaction could involve the successive formation of oxygen ions in β, their transfer, neutralization, and reaction. Moreover, many different paths may be in operation simultaneously (as parallel paths). If, however, to each of the different steps here considered is correlated a definite species in a definite thermodynamic state, the whole path, from the thermodynamic point of view, can be predicted. The different mechanisms then can result in only different partitions of the total work done between the chemical work and the work directly dissipated. The final balance of both being determined unequivocally, the paths involving a primary work accumulation must be followed by successive dissipation in spontaneous processes, leading to the final effective chemical configuration and to the final balances of free enthalpy, voltage, and dissipation.

Any statement in these macroscopically and operatively defined terms would correspond to technical possibilities, subject to our skill in improving the energetic and qualitative characteristics of the processes studied. Finally, kinetic and microscopic analysis may find in results of this class the surest starting point for any further development. The entire problem is discussed in detail on the basis of new experimental evidence in a paper in preparation; some examples are shown in FIGURES 17 to 19.

PART II

II.1 *Some General Principles in Experimental Technique*

The questions now arise: To what extent do the practical measurements conform to the ideal conditions previously considered? What general technical rules will permit reliable overvoltage measurements in molten salts to be made?

To study the overvoltages in a PC* whose chemical configuration is given, problems involving the following classes are met: (1) materials, (2) geometric characteristics of both PC and PT, (3) the nature of the RE, (4) temperature[*] and atmosphere control, and (5) electric supply and voltage outputs record. I shall consider here only the points 2, 3, and 4.

---

* I shall not consider those analytical methods in which measurement of the cell

II.2 *The Geometric Characteristics of PC*

These must be such as to: (1) allow uniformity of current distribution on the electrode surface, and whenever possible in the bath β (where, in any case, this distribution must be regular and known); (2) make the mass transfer processes regular and, whenever possible, well controlled; (3) permit the inclusion of RE without disturbance of the conditions above; and (4) avoid mutually interfering anodic and cathodic reactions, the electrodes being kept far enough and so arranged as to prevent, during measurements, the products of the reaction at one electrode from reaching the surface of the other.

Two class of cells may be especially suited to fit these requirements; these correspond respectively to cylindrical and spherical symmetry (FIGURES 7 and 8). G is a graphite body placed in an insulating support J and internally lined by an insulating wall. The assembly is placed in an electric furnace F. For operating the cell at constant temperature and under controlled atmosphere (N_2, A), a thermocouple T, gas inlet g and outlet g' are provided. $\mathfrak{M}$ is the metal electrode to be investigated and $\mathfrak{B}$ are the counter-electrodes. The metallic part $\mathfrak{M}'$ of RE (supported on graphite) is contained in a cup (C) of insulating material (sintered corundum), being connected by means of a special lead Z (platinum or tungsten) to TA (oscilloscope, potentiometer), to which the investigated electrode also is connected (see FIGURE 9). $\mathfrak{M}$ is connected through a similar lead. The symmetrical arrangement avoids thermoelectric effects.

II.3 *The Geometrical Characteristics of the RE*

These characteristics for overvoltage measurements depend, in practice, on those of PC. Realizable, cylindrically symmetric forms suitable for RE to be utilized in PC (the RE being isoelectrodic or reversible in respect to

---

(or electrode) voltage is used investigating the nature of the electrode reaction, or reactions, or to determine the thermodynamic properties of the reactants (and thus, eventually, their molality) in order to throw light on the chemical composition of the bath. Of course, the determination of the slope of the voltage/current characteristic, in the cases in which the dissipated work may be neglected, may assist greatly the investigations of the class here considered.

[*] The measurements of overvoltages, although more delicate, in principle, than those of equilibrium emf, require constancy of temperature and of its distribution, rather than the exact uniformity required by the equilibrium emf determinations. The eventual thermoelectric effects that thus may be introduced may leave the overvoltages unaffected. Of course, due to temperature differences, convection flow in the bath, as well as other inconveniences, are likely to occur.

some constituent of β) are shown in FIGURE 9. The insulating sheet C, covering all but a small slit providing the liquid junction, makes the current distribution uniform in the part of β involved in the processes at the electrode and on the electrode itself. The presence of RE does not involve any perturbation in the working conditions of the electrode, nor in the mass-transfer processes.

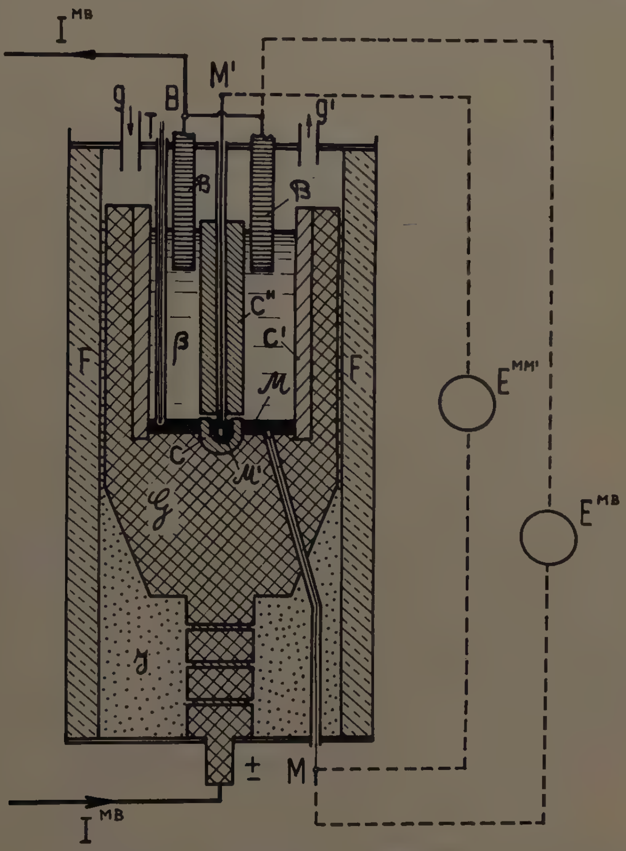

FIGURE 7. PC (symmetrical in respect to the vertical axis) for the study of the overvoltage at the $\mathfrak{M}/\beta$ surface. Key: $\mathfrak{M}'/\beta$, RE; F, furnace; T, thermocouple; g, g', gas inlet and outlet; G, graphite body; C, C', C'', insulating walls (corundum).

In relation to the electrodic system which forms the RE, I shall briefly consider only those systems whose reliability has been established in my experiments. Several metals (either in the molten or solid state), when put in contact with their molten chlorides (for a short account see *Section* III.2) show the practical absence of any ψ_M contribution even when they are carrying high current densities, in both anodic and cathodic senses. The electrodic systems of this class are thus very suitable for use in preparing ER for overvoltage measurements, either in the form of isoelectrodic or in heteroelectrodic RE.

An isoelectrodic RE directly connected with the bath, the use of which makes the overvoltage values especially significant, does not represent, however, a fixed reference zero for the various electrode processes. This disadvantage and the fact that not all of the electrode processes allow a reversible isoelectrodic RE makes the introduction of standard RE necessary. The literature on the RE of the Ag/AgCl class is abundant.*

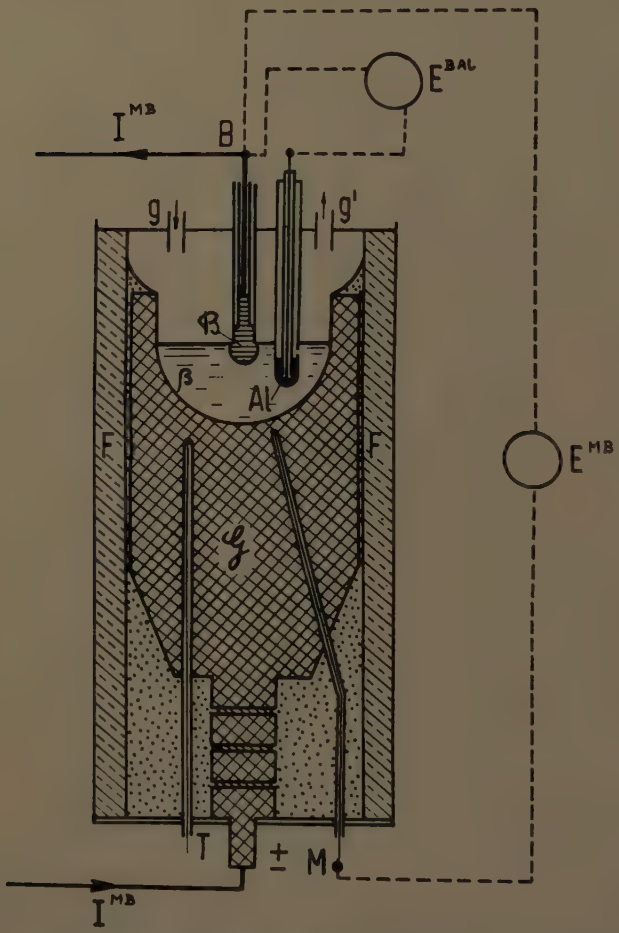

Figure 8. RE suitable for the PC shown in figure 5: (*a*) isoelectrodic RE (*z*, lead; *C*, *C′*, *C″*, insulating walls; *L*, side channel for the interliquid junction); (*b*) heteroelectrodic RE. The traces of the equipotential surfaces (full horizontal lines) and the current lines (vertical with arrows) also are indicated.

---

* For an excellent review see the Ph.D. thesis of Pankey.[20]

It is necessary to remember only, in the cases of chlorine containing baths that are not too aggressive in respect to metallic silver, that by simply exposing an Ag tip to a bath position, where the change in composition may be neglected, a satisfactory RE, suitable for overvoltage measurements* may be obtained. Finding a suitable standard RE for overvoltage measurements in fluoride baths, in which only graphite may be kept in permanent contact with the baths is a difficult problem. The graphite-oxygen RE preferred by authors in the Unions of Soviet Socialist Republics[21-25] requires, in practice, care to obtain adequate control of the atmosphere, and also involves some material problems.

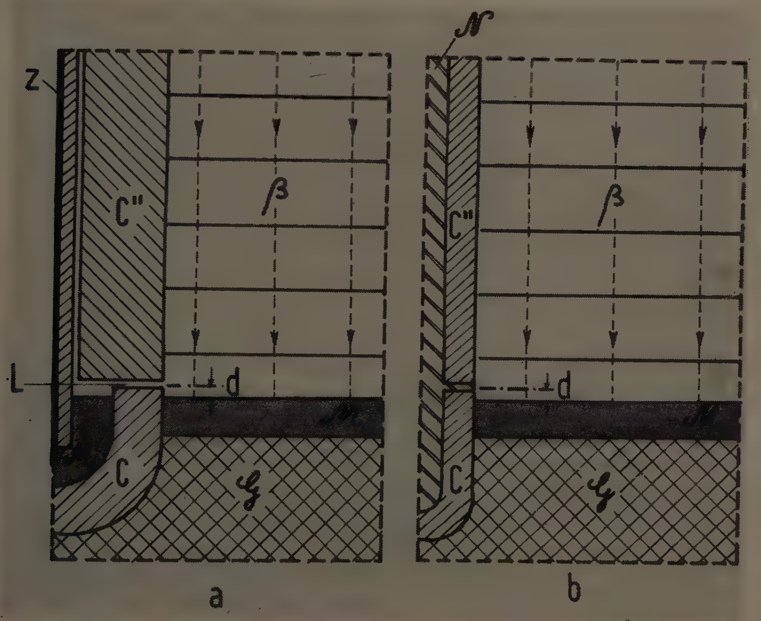

FIGURE 9. PC (hemispherical symmetry) for overvoltage measurements on the $\mathfrak{B}/\beta$ surface.

---

* This RE may act as an isoelectrodic RE for electrodes whose reaction involves Cl^-. In the general case, the contribution of this RE to the thermodynamic effects of the chain reaction depends on the value of the individual activity of the chlorine ions in the region with which the RE exchanges Cl^-. It is, however, easy to check it with a standard RE (in particular again RE such as $Ag/AgCl/\gamma$ provided that in γ the thermodynamic level of the chlorine ion is well defined and that the junction between the two RE is realized with a suitable policy). For the Ag/AgCl, NaCl electrode, a peculiar arrangement is utilized by Coriou *et al.*[27] in which a silica tube containing Ag and molten AgCl is separated by means of an asbestos and ZrO_2 plug from a NaCl melt, in a graphite container. The liquid junction is obtained through a graphite screw. This arrangement is suggested as a possible solution of the problem of RE in fluoride baths.

A satisfactory solution was attained recently[26] by which my previously adopted RE Al/cryolite in a sintered corundum container, definitely has been improved by the following changes (FIGURE 10):

(1) The electrolyte β' is oversaturated with alumina, thus ensuring stability and reproducibility and moreover hindering attack on the internal walls of the corundum container.

(2) The external walls of this corundum container are protected by means of a graphite lining.*

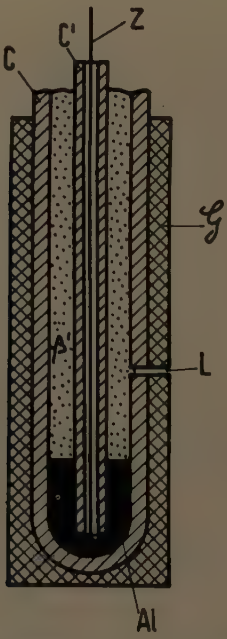

FIGURE 10. RE for fluoride baths. Key: Al, molten aluminum; *G*, graphite lining; *C* and *C'*, corundum tubes; *z*, tungsten lead; β', cryolite with excess Al_2O_3 ; *L*, interliquid junction (provided with a graphite stopper not indicated).

(3) The triple graphite-Al-bath contact, which now appears to be a main source of instability for the Al RE, has been eliminated. In the new form, Al is in contact only with the bath β', with a tungsten lead *z* protected by a corundum tube and not exposed to the bath, and with the corundum wall of the container.

(4) The junction between β' and β is effected through a small channel (1 mm. in diameter or less) in the walls of the corundum container and graphite lining. This channel also may be realized in the form of the small liquid layer allowed by a graphite stopper.†

---

* A graphite container has been used previously by Coriou *et al.*[27] for their RE. It makes use of a graphite screw to obtain the interliquid junction.

† A point that may deserve consideration in measurement practice, when this

By the very nature of the liquid junction, its contribution is small for measurements in cryolite melts and tolerable in the case of many of the fluoride melts already investigated.

II.4 *Electric Supply of PC During Measurements*

The instrument facilities are very satisfactory at present and it is necessary only to choose between the different current sources and voltage-recording apparatus. In view of the chiefly phenomenological goals of my investigations, the preferred measurement policy is that by which, through a PC, current pulses are made to circulate whose form, intensity, duration, and pauses may be varied in each particular case.

By the amperostatic pulses method (belonging to the class of the so-called direct methods), the voltage outputs of a PT are recorded before, during, and after the circulation of rectangular* current pulses in PC (FIGURE 13). When the external source corresponds to the requirements of adequate power availability and absence of any practical lag, the current may be considered as rigorously constant during rectangular pulses, and thus to be the controlled (independently variable) factor; the voltage outputs of the whole PC, and of the various PT in it, thus have the meaning of responses of the system to the imposed current.

In the conditions in which current efficiency approaches or attains the theoretical value, the imposed current also defines the rate of the processes whose study is the main goal. This is a quite suitable policy, as the meaning of the voltage answers of the various utilized PT often may be obvious and sufficiently clear. For the sake of brevity, I shall not consider here the apparatus suited for such a supply form. Detailed information is given elsewhere.[10–16]†

II.5 *Current Efficiency*

The study of the voltage balance in general and of the electrode overvoltages in particular cannot be separated from the knowledge of the matter balance in the cell and at each of the electrodes. The determination of the qualitative nature and the amounts of the products of the electrode reactions is by no means simple, however, in the case of molten salt products entering secondary reactions with the electrode or container materials,

---

involves the circulation in PC of not very small currents, is the fact that too-constrained liquid junctions can engender quite important concentration-polarization effects, the final result being in the opposite sense in respect to that sought. These junctions seldom permit definite and reproducible results. For this reason the use of a good RE when, due to the incompatibility of the electrolytes, very restrictive junctions are necessary, is seldom preferable in the practice of overvoltage measurements to use of a simpler RE, which may be not as reliable in itself.

* The triangular pulse form also has been utilized to give interesting results, especially in relation to concentration polarization.

† The only point to be recalled is the need of a very regular pulse form which will allow a simple and correct interpretation of the voltage responses.

the bath, or the atmosphere; the products of these complementary reactions may hinder any accurate determinations on the primary products. Therefore the experimental results here quoted concern, as a rule, conditions in which the current efficiency may be considered close to unity, at least in sufficiently short experiments and when the experimental technique is such as to bring the rate of the secondary processes to a minimum.

II.6 *Systematic Errors*

In the class of the systematic errors involved in overvoltage measurements are included all of the contributions arising from deviations from the ideality conditions and all of the contributions that cannot be evaluated or measured.

The lack of ideality may concern the defective reproducibility and stability of the electrode reaction, anomalies inherent to liquid junctions, and the fact that the connection with β concerns positions neither sufficiently close to the electrode surface, nor comparable to point positions. These defects involve the introduction of such spurious contributions as ohmic voltage drops and concentration overvoltages (*Section* I.9); the possibility that the RE, when its metallic part is directly exposed to β or surrounded by a conducting envelope (for example, graphite), becomes a bipolar electrode; and the disturbance of the working conditions at the electrode surface for both the current distribution and the mass-transfer processes.

Some of these sources of error, although difficult to avoid in practice, may permit an acceptable correction. Others must be avoided carefully in any precision measurement, as the quantitative importance and sometimes the qualitative nature of their consequences is very difficult to forsee and change in a given PC, when the work conditions vary. Regarding the intrinsic characteristics of the RE, reproducibility and stability obviously are indispensable, and any deficiency in them corresponds to unavoidable measurement errors. With reference to reversibility, it is sufficient, in practice, that a true equilibrium condition be attained and remain unaffected by the very small currents involved in the measurements with any modern TA.

To eliminate the ohmic drop contributions δ_Ω, from the apparent overvoltages, the following criteria may be applied:

(1) In the oscillographic recording of the overvoltages, these contributions must appear (when the current flows), and disappear (when current is turned off), within a time of the order of 10^{-6} sec., or less.

(2) The contributions must be proportional both to the current intensity and the resistivity ρ (provided the current density is uniform), and also to the effective distance d from the electrode surface to the RE connection with β.

(3) When the current is inverted, δ_Ω must follow the same dependence law, although of opposite sign. In other words, by plotting δ_Ω as a function

of I^{MB}, one must obtain linear characteristics, passing through the origin, and thus symmetrical in respect to the origin itself when the sign of I^{MB} changes. Of course, some of these criteria may appear and be redundant but, only when the whole of them is granted, may the δ_Ω correction be considered to be effected surely without loss of any other contribution to the true overvoltages.

The control of the current distribution on the electrode surface (whose usefulness, in view of the correction of the ohmic drop contributions, is made evident by the previous considerations) becomes an essential requirement for correct measurements of the overvoltages. Any disturbance of this distribution, apart from the mass-transfer anomalies thus introduced, makes the average current density (which may be assumed as the variable to be introduced in the phenomenological laws governing overvoltages) a compromise that may prove to be deceptive.

The liquid junction contributions to the apparent overvoltages deserve special consideration. This class may include: (1) changes in time of the contribution of liquid junction to the voltage output of PT, independent of the configuration changes in the part of β which is included in PT; and (2) the consequences of the changes themselves, the concentration polarization (*Section* I.7). Of course, while the first-named effect is a spurious one and is to be avoided whenever possible, the second one appears as one of the goals of any investigation concerning the whole of the contributions to the voltage balance of PC. The problem has been studied already (*Section* I.7). The unfavorable aspect of this intervention of the concentration polarization in electrode overvoltage measurements is the difficulty of superimposing it on the overvoltage inherent in the electrode reaction.

II.7 *Bipolar Electrodes*

A point that may deserve special consideration in the overvoltage measurements in molten salts is the possibility that either the RE surface or its conductive lining may function as a bipolar electrode when the voltage drops in the bath are large enough, due to the high current intensity often imposed and to the bath resistivity.

The eventuality to be considered first is that of an RE whose metallic surface is exposed directly to β in order to avoid any liquid junction. The situation is illustrated in FIGURE 11, taken from the results of model experiments (see APPENDIX IV for details). The alternative path offered by RE to the current, although eventually corresponding to a lower ohmic resistance, involves the creation at the surface of RE of a cathodic area through which current enters RE, and an anodic area where current leaves RE.

Due to the ohmic drop and the influence of the differences in composition in the bath region between these points, a driving force larger than that required by the bipolar working of RE may become available. Consider, first, the case of an isoelectrodic RE $\mathfrak{M}'/\beta$ whose electrode reaction is the exchange of the ions M^{z_M+} contained into the solution. H' and H'' are the β positions and K' and K'' the corresponding points on the RE surface where the possibility of formation of a cathodic or anodic area respectively is to be investigated.

The driving force per unit of charge for the cathodic exchange of M^{z_M+}, that is, from H' to K', may be taken as

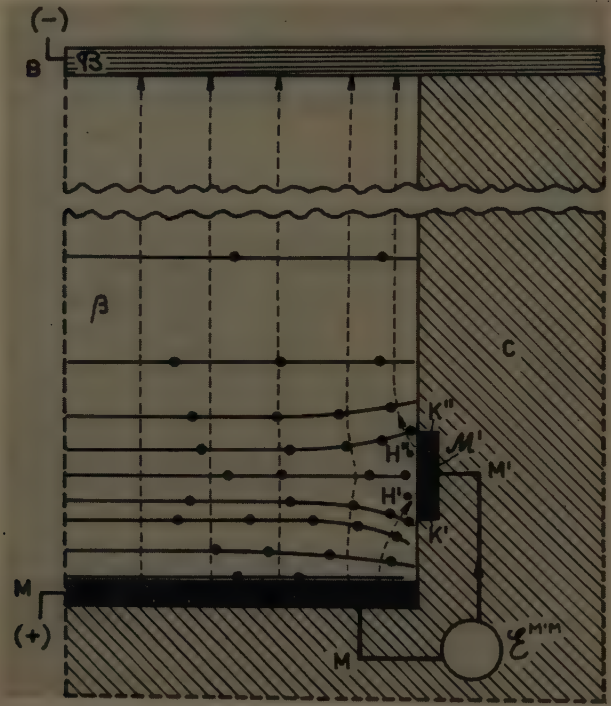

FIGURE 11. Model experiments on bipolar electrodes. Full horizontal lines represent equipotential lines; vertical lines with arrows, current lines. 𝔐 and 𝔅 are the electrodes of PC; 𝔐'/β, RE functioning as a bipolar electrode; $H'K'$, cathodic area; $K''H''$, anodic area.

$$(\overset{H'}{\eta}_{M^{z_M+}} - \overset{K'}{\eta}_{M^{z_M+}})/z_M\mathfrak{F}$$

The driving force for the anodic exchange from K'' to H'' is

$$(\overset{K''}{\eta}_{M^{z_M+}} - \overset{H''}{}_{M^{z_M+}})/z_M\mathfrak{F}$$

By neglecting the ohmic drop in 𝔐' (at least, when the exchanged current is very small), and by assuming 𝔐' to be uniform,

$$\overset{K'}{\eta}_{M^{z_M+}} = \overset{K''}{\eta}_{M^{z_M+}}$$

and the total driving force may then be expressed in the form

$$(\overset{H'}{\eta}_{M^{z_M+}} - \overset{H''}{\eta}_{M^{z_M+}})/z_M\mathfrak{F}$$

Let $\lim\limits_{I\to 0} (\Theta_M^{H'K'} + \Theta_M^{K''H''})$ be the value of the work dissipated in the assumed bipolar operation of RE as the intensity of the exchanged current I_M is reduced to zero.

For $\mathfrak{M}$ to work as a bipolar electrode, the following condition must be realized:*

$$(\eta_{M^zM+}^{H'} - \eta_{M^zM+}^{H''})/z_M\mathfrak{F} \geqq \lim_{I\to 0} (\Theta_M^{H'K'} + \Theta_M^{K''H''})$$

If the bath composition is uniform between H' and H'', the resulting driving force is simply:

$$V^{H'} - V^{H''} = \rho i d^{H'H''}$$

(ρ being the resistivity of the melt, i the current density and $d^{H'H''}$ the distance of H' from H''). Since the utilization of $\mathfrak{M}'/\beta$ as an RE requires, however, Θ to be less than a certain value, the condition above corresponds in practice, to the requirement that $\rho i d^{H'H''}$ be constant.

In cases in which the anodic process is not the inverse of the cathodic one, a bipolar electrode $\mathfrak{U}$ requires, in addition to the dissipated work, the chemical work corresponding to the chain reaction ending in $E_{dec.}$. Let the reaction

$$\mathrm{Ox.}_{(H')}^{\mathrm{I}} + z\theta_{(K')} \rightarrow \mathrm{Red.}_{(H')}^{\mathrm{I}}$$

occur at the cathode, and

$$\mathrm{Red.}_{(H'')}^{\mathrm{II}} \rightarrow \mathrm{Ox.}_{(H'')}^{\mathrm{II}} + z\theta_{(K'')}$$

occur at the anode, written in such a way as to make the reaction equivalence assume a common value z for both. The driving force for the former is then

$$\eta_{\mathrm{Ox.I}}^{H'} + z\eta_\theta^{K'} - \eta_{\mathrm{Red.I}}^{H'}$$

and that for the latter,

$$\eta_{\mathrm{Red.I}}^{H''} - (z\eta_\theta^{K''} + \eta_{\mathrm{Ox.II}}^{H''})$$

The total driving force (again neglecting the ohmic drop in the metallic conductor) is then

$$\frac{(\eta_{\mathrm{Ox.I}}^{H'} - \eta_{\mathrm{Red.I}}^{H'}) + (\eta_{\mathrm{Red.II}}^{H''} - \eta_{\mathrm{Ox.II}}^{H''})}{z\mathfrak{F}}$$

Let ΔG_f be the free enthalpy increment in the chain reaction, and

$$\lim_{I_f\to 0} (\Theta_f^{H'K'} + \Theta_f^{H''K''})$$

---

* An analogous conclusion may be reached in the case in which the RE exchanges anions with β.

be the limit value of the work dissipated. The condition for bipolar operation* is then

$$\frac{(\eta^{H'}_{\mathrm{Ox.I}} - \eta^{H'}_{\mathrm{Red.I}}) + (\eta^{H''}_{\mathrm{Red.II}} - \eta^{H''}_{\mathrm{Ox.II}})}{z\mathfrak{F}} > \left[\frac{\Delta G_f}{z\mathfrak{F}} + \lim_{I_f \to 0} (\theta_f^{H'K'} + \theta_f^{H''K''})\right]$$

An analogous situation in which the RE is protected by a conductive container may occur. This condition is met in fluoride baths in which graphite is, in practice, the only material resistant to permanent contact with the bath. For this reason, in some of the most recent types of RE a graphite protection has been adopted (see *Section* II.3).

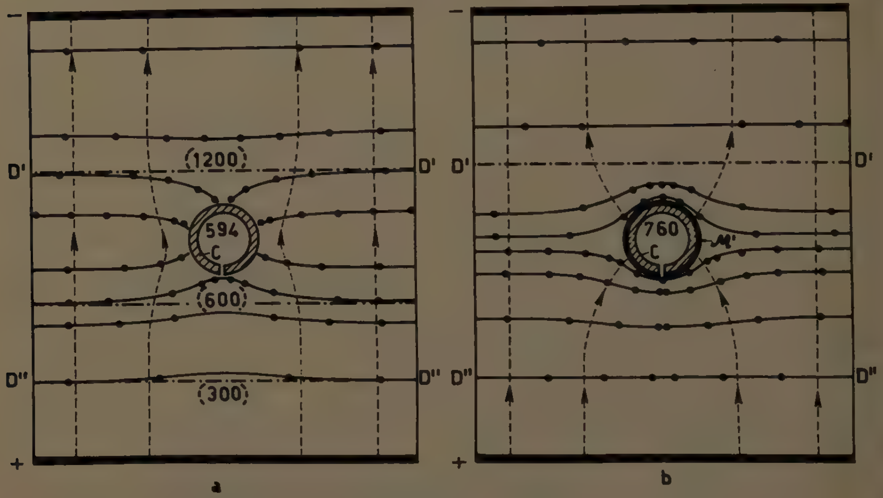

FIGURE 12. Model experiments on bipolar electrodes. Key: *C*, insulating obstacle with a channel; full horizontal lines, equipotential lines; dotted lines with arrows, current lines; black circles, experimental points. The horizontal lines *D'D'* and *D''D''* correspond to the condition in the absence of *C*. The corresponding measured *EV* are given in brackets. (*a*) Represents the condition for the presence of *C* only or also the presence of a conductive lining unable to act as a bipolar electrode. The conductive lining $\mathfrak{M}'$ in *b*) can act as a bipolar electrode. The resulting *EV* in the center of *C* (where RE is located) are indicated in both *a* and *b*.

While the inner part of the RE thus may be protected effectively against attack, the possibility arises that this envelope operates as a bipolar electrode. This situation is reflected in the experiments on models (see APPENDIX IV for some technical details), as shown in FIGURE 12.

Assume an RE enclosed in a first insulating container (sintered alumina, in the case of my RE for fluoride baths), surrounded by a conductive lining, and communicating with β through a narrow channel in the walls. The introduction of RE in β, when β carries current, disturbs the current field there, and (in the absence of any difference in composition between β' and the external bath*) the voltage output of PT does not correspond to that which would be obtained in the absence of container and envelope. This circumstance requires consideration in itself, because it involves a change in the effective distance d to be considered, for example, in evaluating the ohmic contribution to the apparent overvoltages. When the conductive envelope does not work as a bipolar electrode (the available voltage in the bath region in contact with it being insufficient), the external surface of the envelope may be considered to be an equipotential surface that does not interfere with the measured voltage output (provided RE is isolated from the envelope).

---

* If many processes are possible a priori, the condition above must be checked for the one requiring the minimum of driving force.

When, on the contrary, this envelope acts as a bipolar electrode, a disturbance of the current field due to RE in β arises that changes with the working conditions, and follows complicated laws. This disturbance must, therefore, be avoided whenever possible.

Part III

III.1 *Experimental Results*

I shall review some typical results obtained in my systematic investigations of the overvoltages in molten salts. In the simplest case, provided the concentration polarization is kept negligible (see below) the voltage response of PT may be rectangular (FIGURE 13). When the form above meets the checking tests stated in *Section* II.5 the purely ohmic character of this apparent δ_Ω overvoltage (due to the inclusion in PT of a layer of bath carrying current), and thus of the electrode overvoltage ψ_M^{QP} may be concluded to be zero.† This is a very common form for the class of electrode processes whose reaction equation may be written

$$M^{z_M+}_{(\mathfrak{M})} \underset{\text{cat.}}{\overset{\text{an.}}{\rightleftarrows}} M^{z_M+}_{(\beta)}$$

that is, as a cation-exchange reaction. If preferred the reaction may be written

$$M_{(\mathfrak{M})} \underset{\text{cat.}}{\overset{\text{an.}}{\rightleftarrows}} M^{z_M+}_{(\beta)} + z_M\theta_{(\mathfrak{M})}$$

The cations may be present in β in some form or bond condition other than that which would be considered free.

A second, relatively common form of voltage response, for PT not corresponding to ideality in relation to the position of the junction with β, is the response corresponding to superposition on the apparent overvoltage of an ohmic and a concentration polarization contribution.

---

* In the model experiments, whose results are summarized by FIGURES 11 and 12, the composition of the bath was everywhere the same.

† This means that both of the possible contributions to ψ_M^{QP} are individually zero (a mutual compensation being excluded).

When the intensity and duration of pulses and time intervals between successive pulses are changed, the form of the voltage responses changes progressively, the details, however, depend on such factors as (1) initial concentrations and transference numbers of the ions exchanged at the electrode and of the other ion species carrying current simultaneously, and (2) conditions controlling the matter-transfer processes by diffusion and convection.

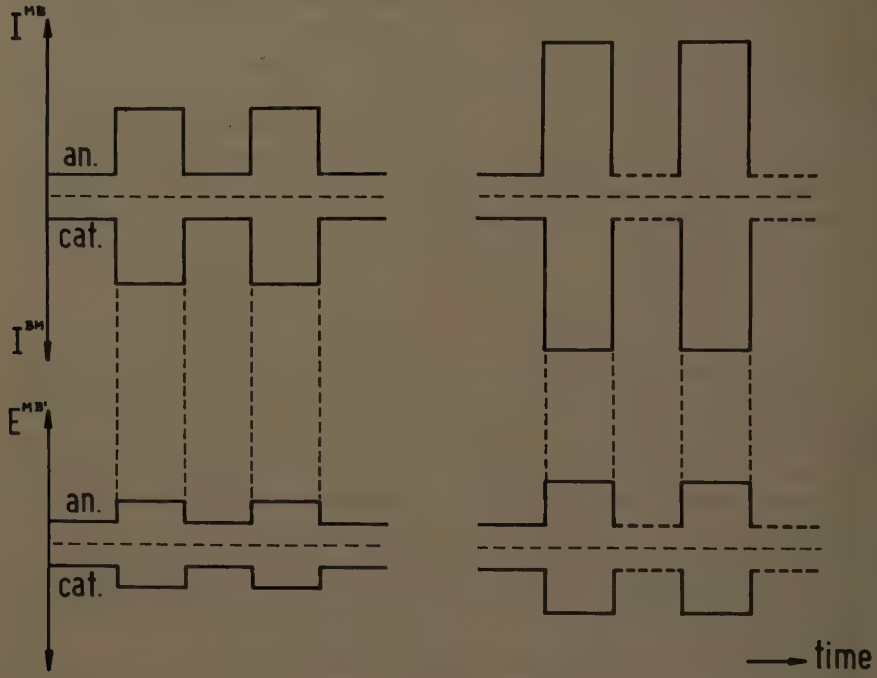

FIGURE 13. Current pulses I^{MB} (circulating in PC, in an anodic or a cathodic sense) and corresponding apparent overvoltages in the case in which these result only from an ohmic voltage drop contribution (δ_Ω).

By an adequate reduction of the pulse duration (in respect to the corresponding density values and the concentration of the reacting species), the rectangular form of the voltage outputs may be restored. A clear-cut distinction between the contribution by concentration polarization and the eventual slow contributions to the overvoltages involved in electrode processes can no longer be made by the methods described above, especially at the highest current densities. Rotating electrodes and stirred baths (by suitable electromagnetic devices) may, however, be utilized. Some subsidiary information also may be obtained by arranging concentration cells. In these, the bath composition is varied* at the two electrode surfaces in a manner that may be seen to be a consequence of the current circulation in PC.

The values of the voltages of the cell and of the PT formed by coupling each electrode separately with an isoelectrodic RE connected with an intermediate region (of reference composition) measured as a function of time (in the absence of current—that required by measurement being negligible) may give very interesting information on the laws of relaxation (by diffusion) of the uneven configuration in the cell, and thus may confirm the inferences concerning the concentration polarization contributions to the apparent electrode overvoltages. The modern techniques available for studying electrode processes[28-30] may prove to be a decisive help. Consideration of these techniques, however, would surpass the limits of this paper.

III.2 *Examples*

The absence of electrode overvoltages, within the approximation permitted by measurement, has been found for the following electrode systems, among others:

(1) $Pb_{(l)}/PbCl_{2\,(l)}$ at 530° C. up to 200 amp./dm.^{2}
In this bath, formed by a single constituent, no changes in composition are encountered and, therefore, no concentration polarization effects occur. Troubles due to metallic fog formation do occur, however, especially at higher temperatures.

(2) $Pb_{(l)}/PbCl_2 + KCl$ (various amounts and temperatures, in the range 560° to 670° C.)
(3) $Cd_{(l)}/CdCl_2 + KCl$ (various amounts, 590° C.) (FIGURE 14)
(4) $Sn_{(l)}/SnCl_2 + KCl$ (various amounts, 350° C.) (FIGURE 15)
(5) $Zn_{(l)}/ZnCl_2 + KCl$ (various amounts, 490° C.)
(6) $Mg/MgCl_2$ (35 per cent by weight) + KCl (47 per cent) + NaCl (18 per cent) (550° C.)
(7) $Al_{(s)}/AlCl_3$ (70 per cent) + NaCl (30 per cent) (220° C.)
$Ni_{(s)}/NiCl_2$ (10 to 20 per cent by weight) + KCl (740° C.)
(8) $Cu_{(s)}/CuCl_2$ (10 per cent) + KCl (740° C.)
(9) $C_{(graphite)}/Cl_{2\,(a\ 1\ atm.)}/NaCl + MgCl_2$ ($\chi_{MgCl_2} = 0.35$, 700° C.)
(10) $C_{graphite}/KCl + PbCl_2$ ($\chi_{PbCl_2} = 0.35$, 700° C.

---

* The conclusion often arrived at in the case of the metal ion exchange reactions—that ψ_M is negligible over a relatively large current density range, although generally sufficient for purposes of application—does not settle the kinetic problem of the equilibrium rates that may be attributed to the ionic exchanges on the electrodes themselves. These rates must be considered not only finite but, moreover, different for various metals under different conditions of T and bath composition. The problem can be solved, not by the methods considered here, but by the methods appropriate to ultrarapid processes. The Berzins and Delahay method appears to be especially promising from this point of view.[29-30]

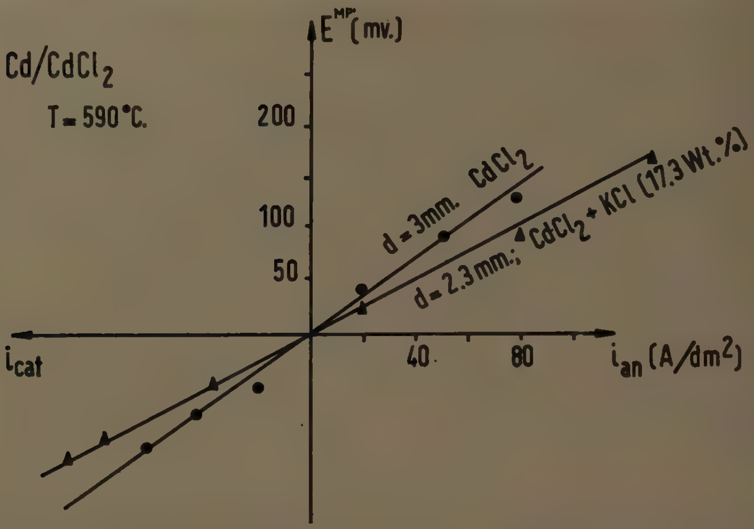

FIGURE 14. Experimental results for apparent overvoltages $E^{MP'}$ as a function of the current density for the system Cd/$CdCl_2$ + KCl (cell as in FIGURE 7).

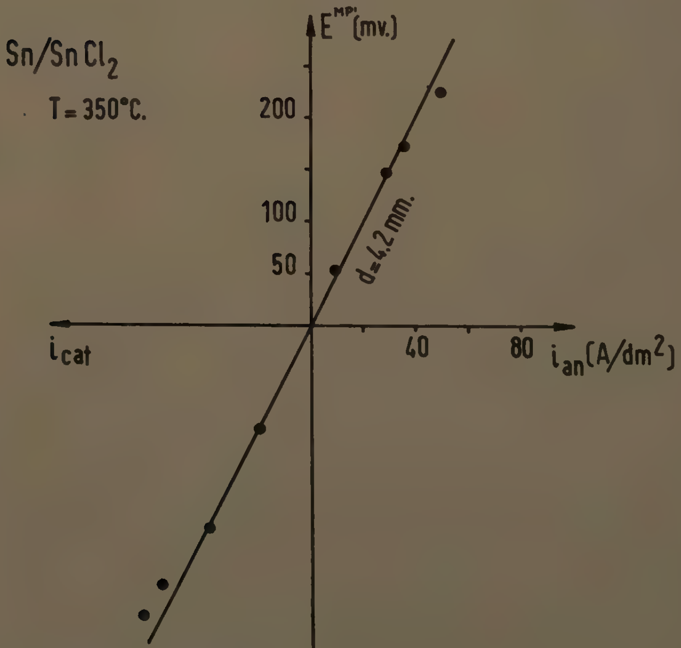

FIGURE 15. Data similar to those shown in FIGURE 14, for the system Sn/$SnCl_2$.

The practical vanishing of electrode overvoltages in chloride melts and for metal-ion exchanges appears to be a property that is shared at sufficiently high temperatures by those metals whose overvoltages are very small in aqueous solutions at ordinary temperatures and by such metals as Ni, which are characterized by high overvoltages. However, the experiments referred to give clear evidence of anodic passivity phenomena occurring with melted electrolytes, as a consequence of the presence or formation of covering layers on the electrode surface. These layers may consist of: (1) oxides or oxychlorides formed by spontaneous reaction or by anodic process, when the baths are not purified carefully of the last traces of water; (2) oxides formed on the metal surface prior to the introduction of the metals in the cells; and (3) the chloride of the electrode metal, when an oversaturation condition in respect to this salt in a multicomponent bath has been attained at the electrode surface.

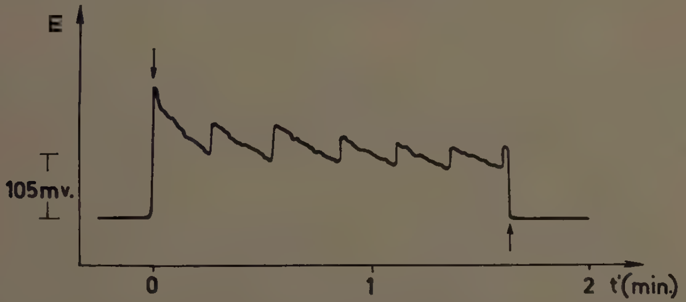

FIGURE 16. Passivation oscillatory phenomena at a solid, oxidized Mg anode (β: $MgCl_2$, $\chi = 0.35$; KCl, $\chi = 0.47$; NaCl, $\chi = 0.18$) at 9 amp./dm.^{2}; 550° C.

The analogy between these and more well-known phenomena observed with aqueous solutions is made clearer by the intervening instability and oscillatory conditions. This is true also for melted salts (FIGURE 16). The passivity of Mg electrodes disappears upon heating to the melting point of Mg. Passivity phenomena in molten electrolytes have been studied especially with solid Ni electrodes immersed in baths suitable to oxidize these electrodes in the absence of current.[31]

When Ni electrodes are plunged into melts of the type $NaNO_3 + KNO_3$ (50 per cent by weight) in the temperature range from the melting point to 360° C., spontaneous formation of compact and uniform yellow layers of cubic NiO having the normal lattice parameter occurs, as is confirmed by electron diffraction. The rate of oxide film formation increases with T (at 360° C). Ten or 15 min. are required to give the EV its final value, which is stable at 400 to 550 mv. greater than the initial EV. When current circulates in the cell, gas is evolved at the Ni anode, but it corresponds to only a small fraction of the current, the main part corresponding to attack on the metal.

The current efficiency, calculated in terms of formation of divalent nickel, is of the order of 80 to 90 per cent. The black layer found adhering to the electrode contains active oxygen, as confirmed iodometrically after dissolution. Therefore, it corresponds to a formula $NiO_{(1+n)}$. The anode attack also occurs, however, by dissolution of the nickel in ionic form and is successively precipitated in the bath as black flaky nickel oxide.

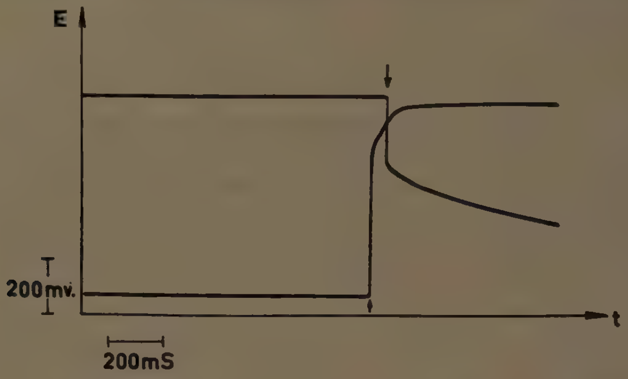

FIGURE 17. Oscillographic recording of the overvoltage at a graphite anode in cryolite + 0.02 wt. per cent Al_2O_3 (1050° C.; cell as in FIGURE 9). Graphite RE, 8.85 amp./dm.^{2} ↑, start of the rectangular current pulse; ↓, end of the pulse.

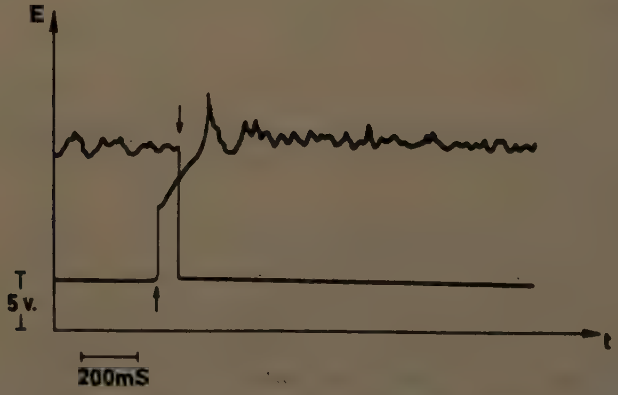

FIGURE 18. Oscillographic recording of the anode effect (graphite anode in a mixed chloride-carbonate bath; 720° C.; 660 amp./dm.^{2}; cell as in FIGURE 9).

In all of these conditions, the formation of the oxide layers does not involve complete passivity, and a fairly uniform attack may continue, either by ionic migration through the layer formed or because of discontinuities in the layer itself. Actually, the initial discharge of oxygen, captured by the oxide layer, lowers its equivalent resistance, while the layer itself undergoes disintegration. At very high current density ($\geq$ 10,000 amp./m.^{2}), the *EV* falls, after current interruption, to values lower than those corresponding to the oxidized electrodes at rest. The surface from which the oxide films has been eliminated in this way suffers quick spontaneous reoxidation, in the absence of current. The *EV* after current interruption thus are characterized by the occurrence of minima. By adding NaCl to the bath, the current efficiency is increased and at high chloride content (more than 25 per cent by weight) spontaneous attack accompanied by strong gas evolution suddenly begins. In pure chloride baths at 720° C., no appreciable exchange overvoltages are encountered on Ni electrodes in the absence of covering layers, as mentioned previously.

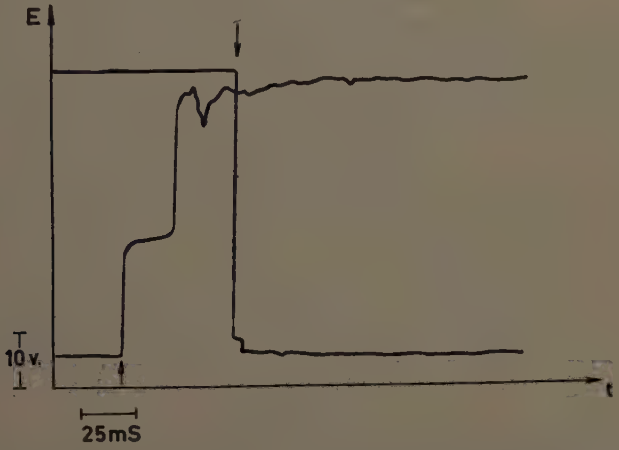

FIGURE 19. Same conditions as for FIGURE 18 but for a graphite anode in a cryolite + 4 per cent Al_2O_3 bath (1100° C.); 1200 amp./dm.^{2}

Examples of overvoltage oscillographic recordings in the cases of gas development are given in FIGURES 17 through 19. The last two figures show that the oscillations caused by the anodic effect occur when the electrode surface becomes effectively isolated from the bath by a layer of gaseous products.

APPENDIX I

Consider a system[1,2] in which T is assumed to be uniform and which includes all of the electric changes involved in any way in processes considered. Let $d_{T,V}F$ be the change in $F = U - TS$, when a very small number $dn_J^{\alpha\beta}$ of moles of a charged (or ionic) chemical species J (electron included) is transferred from a region α to another region β, the volumes of both α and β being taken as constant (and surface effects being considered as negligible). Then

$$d_{T,V}F/dn_J^{\alpha\beta} \equiv \eta_J^{\beta} - \eta_J^{\alpha}$$

is, by definition, the difference between the values assumed in β and α respectively. The quantity η_J (thus defined only as to the relative value), is termed the electrochemical potential of J. When the physical conditions may be considered as defined in both α and β by the values of T (identical in α and β), and the scalar pressures P^α and P^β, the following may be stated:

$$d_{T,P}G/dn_J^{\alpha\beta} \equiv \eta_J^\beta - \eta_J^\alpha$$

When macroscopic electric potentials V^α and V^β in α and β are assumed to be definable (and uniform in the region considered),

$$\eta_J^\beta - \eta_J^\alpha \equiv (V^\beta - V^\alpha)z_J\mathfrak{F} + \mu_J^\beta - \mu_J^\alpha$$

z_J being the electric valency (in algebraic value) and μ_J, the chemical potential of J.

Choosing a reference condition ρ for J at the T and P existing in α, we shall set

$$\eta_J^\alpha - \eta_J^\rho \equiv RT \ln {}^\rho\tilde{a}_J^\alpha$$

${}^\rho\tilde{a}_J^\alpha$ being, by definition, the electrochemical activity of J in α with reference to ρ.

By the same assumptions:

$$\eta_J^\alpha - \eta_J^\rho \equiv (V^\epsilon - V^\rho)z_J\mathfrak{F} + RT \ln {}^\rho a_J^\alpha$$

where ${}^\rho a_J^\alpha$ is the activity of J in α relative to the reference condition ρ.

APPENDIX II

Equilibrium conditions for voltage measurements by means of a TA for a PC $\mathfrak{M}/\beta/\mathfrak{B}$ at the $\mathfrak{M}/m$ and $b/\mathfrak{B}$ contacts are as follows:[1]

$$\eta_\theta^M = \eta_\theta^M = -\mathfrak{F}V^M + \mu_\theta^M$$

$$\eta_\theta^b = \eta_\theta^B = -\mathfrak{F}V^B + \mu_\theta^B$$

Therefore:

$$E^{MB} = \frac{\eta_\theta^b - \eta_\theta^m}{\mathfrak{F}} = E^{mb} = \frac{\eta_\theta^B - \eta_\theta^M}{\mathfrak{F}}$$

$$= V^M - V^B + \frac{\mu_\theta^B - \mu_\theta^M}{\mathfrak{F}}$$

When PC is made a complete chain by soldering to $\mathfrak{M}$ a metallic conductor $\mathfrak{B}'$ of identical chemical and physical properties in respect to $\mathfrak{B}$, then $\eta_\theta^{B'} = \eta_\theta^M$ (equilibrium condition for the electron exchanges at the intermetallic contact $\mathfrak{M}/\mathfrak{B}'$).

$$E^{mb} = V^m - V^b = \frac{\eta_\theta^B - \eta_\theta^{B'}}{\mathfrak{F}} = V^{B'} - V^B = E^{B'B}$$

$$= V^M - V^B + \frac{\mu_\theta^B - \mu_\theta^M}{\mathfrak{F}} = E^{MB}$$

The measurable voltage is thus identical to that for the incomplete chain, but it now signifies the electric potential difference between the terminals B' and B of PC. The identity above tends to deny any contribution of the intermetallic contacts in the galvanic chains to the voltage balance of the chains. In fact, the term $(\overset{B}{\mu}_\theta - \overset{M}{\mu}_\theta)/\mathfrak{F}$, which may be considered to represent the chemical contribution of the intermetallic contact to the emf of the chain (being expressive of the work involved in the change in chemical environment of the electrons), applies in the same manner to both the complete and the incomplete chains. The equality of the quantities measured by the potentiometer does not signify that the contribution (as defined) of the intermetallic contact is negligible.

The changes in chemical environment encountered by electrons directly at the intermetallic contact or intermediately in an open chain are parts of the chain reaction, as is the exchange in the ions at the metal/solution interfaces. The corresponding chemical work contributions must be taken into account together in the energetic balance of the system.

The above conclusions concern the equilibrium emf (and thus the "nobility" of the electrode processes). The intermetallic contacts are nonpolarizable, in practice, and hence do not contribute to the overvoltages or play a decisive role in the kinetic behavior of electrodes. The latter, therefore, depends only on the dissipative and storage phenomena at the metal/electrolyte interface.

Appendix III

To clarify the problem, consider[1-9] again the example in which the electrode reactions at $\mathfrak{M}/\beta$ and at the corresponding (isoelectrodic) RE $\mathfrak{M}'/\beta_P$ and $\mathfrak{M}''/\beta_U$ are represented by the equation

$$M^{z_M+}_{(\mathfrak{M})} \rightleftarrows M^{z_M+}_{(\beta)}$$

From analogous considerations and the assumption that $\overset{M''}{\mu}_M = \overset{M'}{\mu}_M$ or $\overset{M''}{a}_M = \overset{M'}{a}_M$, the following results:

$$\begin{aligned} E^{PU}_{I=0} &= \frac{\overset{M''}{\eta}_\theta - \overset{M'}{\eta}_\theta}{\mathfrak{F}} = \frac{\overset{M''}{\mu}_M - \overset{M'}{\mu}_M}{z_M\mathfrak{F}} + \frac{\overset{M'}{\eta}_{M^{z_M+}} - \overset{M''}{\eta}_{M^{z_M+}}}{z_M\mathfrak{F}} \\ &= \frac{\overset{P}{\eta}_{M^{z_M+}} - \overset{U}{\eta}_{M^{z_M+}}}{z_M\mathfrak{F}} = \frac{RT}{z_M\mathfrak{F}} \ln \left({}^\lambda\overset{P}{\tilde{a}}_{M^{z_M+}}/{}^\lambda\overset{U}{\tilde{a}}_{M^{z_M+}}\right) \end{aligned} \qquad \text{(AIII.1)}$$

By the partition:

$$\overset{P}{\eta}_{M^{z_M+}}\ z_M\mathfrak{F}V^P + \overset{P}{\mu}_{M^{z_M+}}; \qquad \overset{U}{\eta}_{M^{z_M+}} = z_M\mathfrak{F}V^U + \overset{U}{\mu}_{M^{z_M+}}$$

Equation AIII.1 becomes

$$\begin{aligned} E^{PU}_{I=0} &= V^P - V^U + \frac{\overset{P}{\mu}_{M^{z_M+}} - \overset{U}{\mu}_{M^{z_M+}}}{z_M\mathfrak{F}} \\ &= V^P - V^U + \frac{RT}{z_M\mathfrak{F}} \ln \left({}^\lambda\overset{P}{a}_{M^{z_M+}}/{}^\lambda\overset{U}{a}_{M^{z_M+}}\right) \end{aligned} \qquad \text{(AIII.2)}$$

The first term $\varphi_L^{PU} = V^P - V^U$ gives the liquid junction potential difference, in the usual sense.* It also contains a contribution of individual ionic activities. In $E_{I=0}^{PU}$ this indeterminateness disappears, however.†

$E_{I=0}^{PU}$ is expressed in EQUATION AIII.1 by means of thermodynamic quantities only (as are the electrochemical activities). This result may appear irreconcilable with the fact that in PT the irreversible diffusion processes are linked inseparably with the charge circulation during the measurement of $E_{I=0}^{PU}$ as the voltage output of PT when $I^{MB} = 0$. The diffusive fluxes of matter involve a gradual spontaneous change in time of the chemical configuration, and thus of E^{PU}, even when $I^{MB} = 0$, a circumstance that makes only the instantaneous values of E^{PU} significant.

The inertia of TA is in practice negligible compared to the relaxation times of the chemical configuration by spontaneous diffusive flow.‡ A difficulty arises, however, out of the possibility of coupling (in the sense used in thermodynamics of irreversible processes§) between the diffusive and electric fluxes, both depending on generalized vector forces—the gradient of the chemical potential of the diffusing molecular species, or respectively that of the electrochemical potential of the migrating ionic species. It is perhaps worth recalling that this difficulty, too, concerns only the possibility of a quasithermodynamic evaluation of $E_{I=0}^{PU}$, not its operative meaning nor the possibility of expressing it in the form of EQUATION AIII.1. For the charge circulation in PT, the simultaneous occurrence of spontaneous diffusive processes and their eventual contribution to the effective driving force involves only changes in the ratio ${}^{\lambda}\tilde{a}_{M^{z}M+}^{P}/{}^{\lambda}\tilde{a}_{M^{z}M+}^{U}$. Thus $E_{I=0}^{UP}$ may still be expressed by use of EQUATION AIII.1.

Appendix IV: Experiments on Models[33-38]

The experiments on electrochemical models, of which FIGURES 11 and 12 give examples, are effected in PC containing a $Pb(NH_2SO_3)_2$, 0.5 M bath (of uniform composition) and utilizing Pb electrodes.

By the practical absence of electrode polarization, the voltages measured between a Pb RE (plunged in a capillary glass probe displaced in the bath along a horizontal plane) and one or the other of the electrodes of PC, during the circulation of continuous current in PC, give the distribution of the traces on the explored plane of the equipotential surfaces (that is, the surfaces on which the measured voltages are uniform); the orthogonal paths to the latter are the current lines, as defined by the geometrical conditions.

---

* This one may be calculated by the original Helmholtz equation or by those of Nernst, Planck, Henderson, Taylor, and others.

† This same condition is verified finally in the so-called experimental control of the above equations.

‡ Statements to the contrary found in the literature seem to be due to a misinterpretation.

§ The coupling with directional fluxes is excluded by reasons of symmetry, in the case of the spontaneous homogeneous chemical reactions driven by generalized scalar forces.

In the experiments illustrated in FIGURE 12, the presence of an insulating obstacle C (a Plexiglas cylinder) in the bath deforms the current field there. The identical distribution is encountered when a thin metallic sheet is wound around the insulating cylinder, this sheet being incapable of functioning as a bipolar electrode. (In my experiment I used a Ni sheet which was practically passive.) When, on the contrary, the metallic sheet may work as a bipolar electrode (this is the case when the sheet is made of Pb), the current field is disturbed more, and this disturbance is by no means a merely geometric one, depending also on the work conditions in PC.

Summary

Some definitions are given, and the general concepts involved in the overvoltage measurements in molten salts are summarized.

The problem of the reference electrodes, in view of the overvoltage measurements, is discussed. Some practical solutions are presented. Examples of measurement results are given and discussed briefly.

References

1. Piontelli, R. 1955. Gazz. chim. ital. **85:** 665.
2. Piontelli, R. 1951. CITCE 2nd Meeting. : 334. Tamburini. Milan, Italy.
3. Piontelli, R. 1952. CITCE 3rd Meeting. : 275. Manfredi. Milan, Italy.
4. Piontelli, R. 1953. Rend. ist. lombardo sci. **86:** 803.
5. Piontelli, R. 1956. Colloque Intern. Electrolyse. ECNRS. Paris, France.
6. Piontelli, R. 1958. Rend. ist. lombardo sci. **92:** 367.
7. Piontelli, R. 1953. Gazz. chim. ital. **83:** 357, 370.
8. Piontelli, R. 1955. Z. Elektrochemie. **59:** 778.
9. Piontelli, R. 1955. Rend. ist. lombardo sci. **88:** 51.
10. Piontelli, R., B. Rivolta & G. Montanelli. 1955. Z. Elektrochem. **59:** 64.
11. Piontelli, R. & G. Montanelli. 1954. J. Chem. Phys. **22:** 178.
12. Piontelli, R. & G. Montanelli. 1956. Alluminio. **25:** 79.
13. Piontelli, R. & G. Sternheim. 1955. J. Chem. Phys. **23:** 1358.
14. Piontelli, R., G. Sternheim & M. Francini. 1956. J. Chem. Phys. **24:** 1113.
15. Piontelli, R., G. Sternheim & M. Francini. 1956. Rev. mét. **53:** 248.
16. Piontelli, R., G Sternheim & M. Francini. 1955. Compt. rend. acad. sci. **242:** 1301.
17. Piontelli, R., G. Sternheim, M. Francini & R. Manocha. 1956. Rend. ist. lombardo sci. **90:** 34.
18. Piontelli, R. 1953. Rend. ist. lombardo sci. **86:** 803.
19. Piontelli, R., G. Sternheim & F. Fumagalli. 1958. Ricerca sci. **28:** 160.
20. Pankey, J. W. 1958. Ph.D. Thesis. Univ. Ill. Urbana, Ill.
21. Rempel, S. I. & L. P. Khodak. 1953. Zhur. Priklad. Khim. **26:** 857.
22. Antipin, K. 1955. Compt. rend. acad. U.R.S.S. **100:** 95.
23. Rempel, S. I. 1950. *Ibid.* **76:** 411.
24. Rempel, S. I & L. P. Khodak. 1950. *Ibid.* **75:** 833.
25. Rempel, A. & L. P. Khodak. 1954. DAN. **97:** 859.
26. Piontelli, R. 1959. Rend. accad. naz. Lincei (A). **26**(8): 18.
27. Coriou, H., J. Dirian & J. Hure. 1955. J. Chim. Phys. **52:** 479.
28. Delahay, P. 1954. New Instrumental Methods in Electrochemistry. Interscience. New York, N.Y.
29. Berzins, T. & P. Delahay. 1955. J. Am. Chem. Soc. **77:** 6448.
30. Vielstich, W. & P. Delahay. 1957. *Ibid.* **79:** 1874.
31. Piontelli, R., U. Bertocci & G. Sternheim. 1958. Z. Elektrochem. **62:** 772.

32. Piontelli, R. & G. Bianchi. 1949. Gazz. chim. ital. **79:** 867, 877.
33. Piontelli, R. & G. Bianchi. 1950. Gazz. chim. ital. **80:** 581.
34. Piontelli, R., G. Bianchi & R. Aletti. 1952. Z. Elektrochem. **56:** 863.
35. Piontelli, R., G. Bianchi, U. Bertocci & B. Rivolta. 1956. Ricerca sci. **26:** 838.
36. Aletti, R., U. Bertocci, G. Bianchi, C. Guerci, R. Piontelli, G. Poli & G. Serravalle. 1951. CITCE 3rd Meeting : 30. Manfredi. Milan, Italy.
37. Piontelli, R., G. Bianchi, U. Bertocci, C. Guerci & B. Rivolta. 1954. Z. Elektrochem. **58:** 54.
38. Piontelli, R., U. Bertocci, G. Bianchi, C. Guerci & G. Poli. 1954. Z. Elektrochem. **58:** 86.

COMPOSITION OF VAPORS IN EQUILIBRIUM WITH SALTS AT HIGH TEMPERATURES

Joseph Berkowitz and William A. Chupka
Argonne National Laboratory, Lemont, Ill.

Introduction

Of the various methods employed to determine the activity of the components of a molten salt, one of the most direct is the determination of the partial pressures composing the vapor in equilibrium with the melt. The purpose of this article is to indicate several techniques by which mass spectrometric analysis can yield data concerning these activities, as well as information regarding the extent of polymer and compound formation and the binding energies of the molecular bonds involved.

The specific experimental details have been described elsewhere;[1,2] the following is a cursory representation of the current development of the apparatus.

The salt under study is placed in a crucible so chosen as to minimize reaction between salt and container (in some experiments a smaller crucible containing a calibrating material was located concentrically within the larger crucible). The cylindrical crucible is heated by radiation from 2 surrounding filaments, and heat loss minimized by a set of concentric shields surrounding the oven assembly. Salt vapor effuses from a 1-mm. orifice in the top of the crucible. It is collimated by a slit plate that may be manipulated from outside the vacuum system. This arrangement permits the operator to discern that portion of a particular ion peak attributable to the salt vapor. The slit plate effectively isolates the oven assembly from the adjacent ionization chamber when in the closed position and, in normal operation, provides a differential pumping factor of about 10 in addition to keeping the ionization chamber relatively free of vaporized material. The molecular beam entering the ionization chamber is traversed perpendicularly by a controlled electron beam emanating from an oxide-coated iridium filament, and the resulting ions are drawn off, focused, and accelerated by a series of slit plates. The ionization chamber communicates with the analyzer only by a narrow beam-defining plate (0.006″ slit width), permitting another factor of about 30 in differential pumping. This entire assembly is shown in FIGURE 1.

The ion beam is mass-analyzed in a 60°-sector magnetic field. Two detectors now present themselves to the beam: (1) A wire grid, having 50 per cent transmission and located in front of the final detector slit; and (2) A 12-stage electron multiplier located beyond the final detector slit. Both outputs are amplified by vibrating-reed electrometers and simultaneously recorded. This procedure eliminates the correction due to secondary electron emission, which previously had been based upon an empirical correlation. In the present arrangement the relative secondary electron efficiency of the various ions can be determined at high intensity when the wire grid has sufficient signal and the result employed over the much larger operating range provided by the electron multiplier.

The lone important correction remaining is the determination of the comparative efficiency of ionization. When necessary, this has been estimated

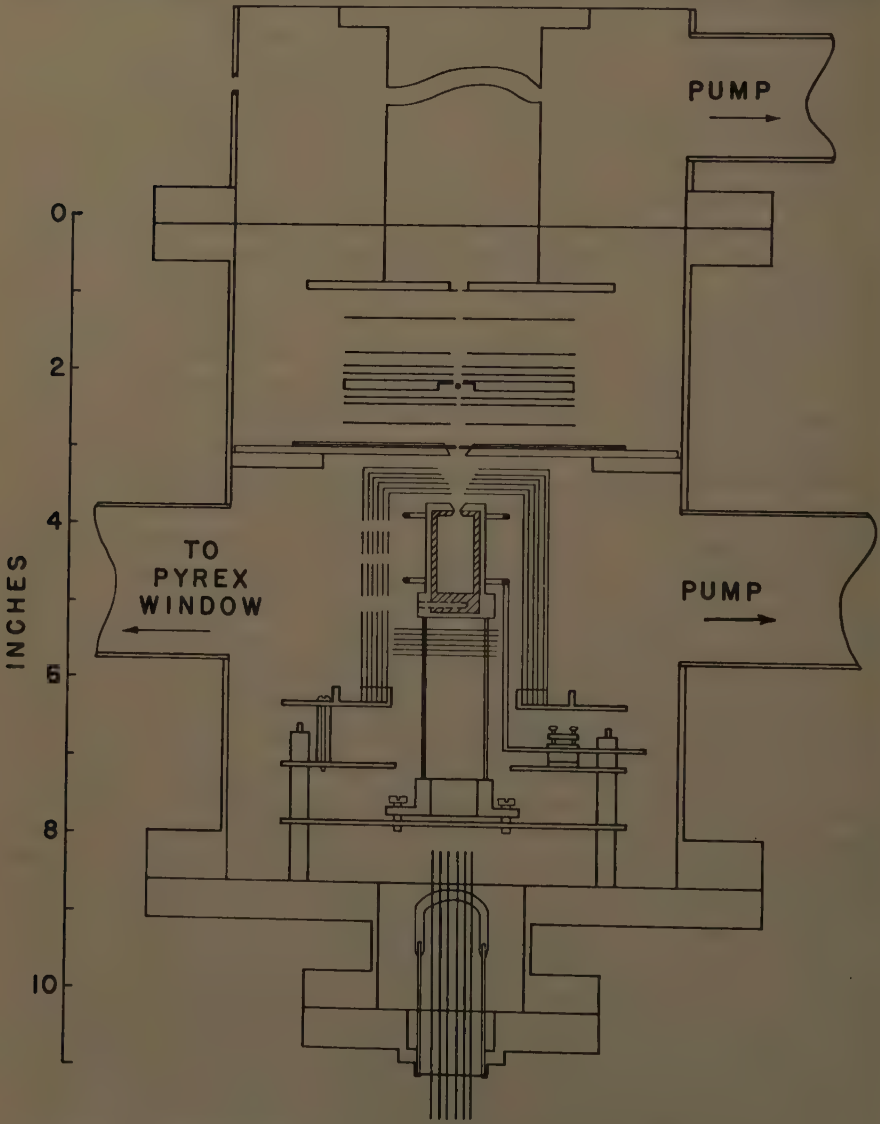

FIGURE 1. Arrangement of crucible and ion source for mass spectrometer.

from Otvos and Stevenson's[3] table of calculated cross sections. However, the activities of components can be determined in at least two ways without recourse to cross section calculations.

Employment of Monomer:Dimer Ratios

When both monomer and dimer exist in a particular salt vapor (and this seems to occur in an astonishing number of cases[4]), the following analysis applies:

$$K_{\text{equil.}} = \left[\frac{(P_{MX})^2}{P_{M_2X_2}}\right]_{\text{Pure salt}} = \left[\frac{(P_{MX})^2}{P_{M_2X_2}}\right]_{\text{Mixed salt}} \qquad (1)$$

$$\left(\frac{P_{MX}}{P_{M_2X_2}}\right)_{\text{Pure}} (P_{MX})_{\text{Pure}} = \left(\frac{P_{MX}}{P_{M_2X_2}}\right)_{\text{Mixed}} (P_{MX})_{\text{Mixed}}$$

$$\text{Activity} = \frac{(P_{MX})_{\text{Mixed}}}{(P_{MX})_{\text{Pure}}} = \frac{(P_{MX}/P_{M_2X_2})_{\text{Pure}}}{(P_{MX}/P_{M_2X_2})_{\text{Mixed}}} \qquad (2)$$

$$\text{Activity} = \frac{(I^+_{MX}/I^+_{M_2X_2})_{\text{Pure}}}{(I^+_{MX}/I^+_{M_2X_2})_{\text{Mixed}}}, \qquad (3)$$

where I^+_{MX} is an ion intensity resulting solely from an MX molecule, and hence proportional to P_{MX}.

P_{MX} is the partial pressure of molecular species MX; $P_{M_2X_2}$ is the partial pressure of molecular species M_2X_2; I^+_{MX} is the ion intensity resulting solely from an MX molecule, and hence is proportional to P_{MX}; and $I^+_{M_2X_2}$ is the ion intensity resulting solely from an M_2X_2 molecule, and hence is proportional to $P_{M_2X_2}$.

As long as the same temperature exists in both instances EQUATION 3 is exact and does not depend upon any corrections.

Employment of a Calibrating Material

Bismuth metal has a vapor pressure comparable with those of many fused salts. If it is present in the crubicle at unit activity, it serves as a constant measure of the over-all sensitivity of the apparatus. It also provides a convenient comparison substance for the determination of relative heats of vaporization or reaction. For the determination of activities one need only compare the salt monomer:bismuth ion ratio for mixed salt and pure salt at the same temperature. The resulting ratio provides an independent measurement of activity.

When applicable, the first method intrinsically yields higher accuracy. Since the sensitivity of mass spectrometric analysis permits the detection of species present in approximately 1 part in 10^6, and the vast majority of substances examined to date appear to have at least that fraction of dimer, this method will probably become the more popular one.

Because of its sensitivity, the mass spectrometer can show the presence of a minute quantity of compound in a mixed salt and hence yield some quantitative measure of the energetics of the interaction between the salts involved.

EXPERIMENTAL RESULTS

Pure Alkali Halides

Interest in these salts stems partially from a conflict arising among several groups of workers,[5-7] employing different techniques regarding the fraction of polymer forms present in the equilibrium vapor. TABLE 1 is reproduced from a previously published article to give some idea of the complexity of these vapors as well as the sensitivity of the method. These ion intensities have been corrected for secondary electron efficiency of all major peaks by applying the wire-grid detector.

TABLE 1*

ION INTENSITIES† OF ALKALI HALIDE VAPORS IN ARBITRARY UNITS

	M^+	MX^+	M_2X^+	$M_3X_2^+$	$M_4X_3^+$
LiF	410	90.8	793	57.3	0.133
LiCl	405	486.5	2230	95.4	3.2
LiBr	988	1000	4540	~175	5.1
NaF	2080	54	620	12	0.12
NaCl	595	351.5	424	3.5	—
NaBr	375	265	243	3.8	—
NaI	385	450	240	1.5	—
KF	1050	1.9	184	1.3	—
KCl	1110	186	238	0.64	—
KBr	840	240	187	0.72	—
KI	705	392.5	118	0.285	—
RbCl	1170	82.3	159	0.0717	—
CsCl	445	5.15	31.8	<0.03	—

* Reproduced with permission from *The Journal of Chemical Physics*.[4]

† Total pressures in all instances are about 10^{-2} mm. Hg, using 75-ev ionizing electron energies.

By a combination of classic vapor-pressure measurements[8] it is often possible to determine the average molecular weight of a pure salt vapor, as well as its vapor pressure. When only two molecular forms exist, this procedure uniquely predicts their ratio. When more than two species are present in comparable intensities, such an analysis is inadequate. This situation applies particularly to the lithium halides.

Pure BeF_2 and $FeCl_2$

Preliminary experimental results yield a vapor composition above these pure salts shown in TABLE 2.

It is interesting to note that, whereas the major alkali halide ion peaks were deficient in 1 halogen atom, neither BeF_2 nor $FeCl_2$ shows this property (however, Be_2F_4 appears to fragment chiefly to $Be_2F_3^+$).

Mixed Salts

LiF-BeF₂. An equimolar mixture has been analyzed in the same temperature range as pure BeF_2. Mass peaks corresponding to the ions Li^+, LiF^+, Li_2F^+, $BeF_2{}^+$, BeF^+, $Be_2F_3{}^+$, and $LiBeF_2{}^+$ were observed. Their relative intensities at approximately 900° K are shown in TABLE 3. Employing EQUATION 3 one obtains the following activities:

TABLE 2

RELATIVE ION INTENSITIES OBSERVED ABOVE PURE BeF_2 AND $FeCl_2$

BeF_2		$FeCl_2$	
Mass 47 ($BeF_2{}^+$):	386	Mass 126 ($FeCl_2{}^+$):	77.5
94 ($Be_2F_4{}^+$):	<0.35	254 ($Fe_2Cl_4{}^+$):	1
75 ($Be_2F_3{}^+$):	1		

TABLE 3

RELATIVE ION INTENSITIES OBSERVED ABOVE AN EQUIMOLAR MELT OF LiF AND BeF_2

Mass 7 (Li^+):	61.6
33 (Li_2F^+):	2.94
47 ($BeF_2{}^+$):	917
94 ($Be_2F_4{}^+$):	<0.022
75 ($Be_2F_3{}^+$):	1
54 ($LiBeF_2{}^+$):	20.9

TABLE 4

RELATIVE ION INTENSITIES OBSERVED ABOVE AN EQUIMOLAR MELT OF LiCl AND $FeCl_2$

Mass 7 (Li^+):	104.3
49 (Li_2Cl^+):	6.0
126 ($FeCl_2{}^+$):	181.8
254 ($Fe_2Cl_4{}^+$):	1.
133 ($FeLiCl_2{}^+$):	14.1

$$a_{\mathrm{LiF}} = 0.0246$$

and

$$a_{\mathrm{BeF_2}} = 0.443$$

In this experiment bismuth metal was also present, and its vapor pressure (as evidenced by its ion intensity) served as a measure of the temperature. However, some doubt was cast upon the prevailing opinion regarding the vapor pressure of bismuth by our observation that the $\mathrm{Bi_{2/Bi}}$ ratio was an order of magnitude larger than reported.[9] A crude evaluation of the change of the equilibrium constant

$$K = \frac{(\mathrm{LiF\cdot BeF_2})}{(\mathrm{LiF})(\mathrm{BeF_2})}$$

with temperature yielded 53 kcal./mole for the binding energy of LiF to BeF_2 at about 900° K.

$LiCl$-$FeCl_2$. Examination of the equimolar melt revealed the ion intensities shown in TABLE 4. Application of EQUATION 3 yields $A_{LiCl} = 0.0105$ and $A_{FeCl_2} = 0.426$.

The $LiCl$-$FeCl_2$ bond energy, as determined by the variation of the equilibrium constant

$$K = \frac{(LiCl \cdot FeCl_2)}{(LiCl)(FeCl_2)}$$

with temperature according to the equation

$$\frac{d \ln K}{dT} = \frac{\Delta H}{RT^2}$$

yielded 43 kcal./mole at about 750° K.

Discussion and Conclusions

It has been shown that methods are available for obviating the corrections heretofore applied in mass spectrometric analysis of high-temperature vapors, particularly when monomeric and dimeric forms coexist and information regarding the activity of individual components of a melt is desired. Improved temperature-measuring devices are required, as well as more complete experimental studies over the entire composition range of binary melts, before the accuracy of the method is fully evaluated.

In view of the unusual ionic breakdown patterns encountered among the halides, it will be necessary in some instances to determine the ionic fragments resulting from each molecular species. This can be done by independently varying temperature and pressure, using double-oven techniques. With this further information the activities may be determined unambiguously.

When sufficient data are available it will be of interest to determine internal consistency of activity measurements with the aid of the Gibbs-Dubem equation. A comparison with other methods of measurement is also desirable and should shortly be forthcoming.

References

1. Chupka, W. A. & M. G. Inghram. 1955. J. Phys. Chem. **59:** 100.
2. Chupka, W. A., J. Berkowitz & C. F. Giese. 1959. J. Chem. Phys. **30:** 827.
3. Otvos, J. W. & D. P. Stevenson. 1956. J. Am. Chem. Soc. **78:** 546.
4. Berkowitz, J. & W. A. Chupka. 1958. J. Chem. Phys. **29:** 653.
5. Friedman, L. 1955. J. Chem. Phys. **23:** 477.
6. Miller, R. C. & P. Kusch. 1956. J. Chem. Phys. **25:** 860.
7. Klemperer, W. & S. A. Rice. 1957. J. Chem. Phys. **26:** 618.
8. Beusman, C. 1957. Oak Ridge Natl. Lab. Rept. ORNL-2323. Oak Ridge, Tenn.
9. Stull, D. R. & G. C. Sinke. 1956. Thermodynamic Properties of the Elements. Am. Chem. Soc. Washington, D.C.

SOLUBILITIES OF SALTS IN METALS*

S. J. Yosim and E. B. Luchsinger
Atomics International Division, North American Aviation, Inc., Canoga Park, Calif.

Introduction

Relatively little work has been carried out on solutions of salts dissolved in metals. Solubility studies of such systems have been confined mainly to solutions of alkali,[1-3] alkaline earth,[4,5] and bismuth[6,7] halides dissolved in their metals. One purpose of the work described in this paper was to extend solubility studies to other systems of halides and their metals in order to see if any correlation of the extent of solubility with properties of the system could be made.

It was also of interest to learn whether nonspecificity of solubility exists at high temperatures; that is, to determine if solubilities exist between salts and foreign metals (for example, NaCl in bismuth) at high temperatures. The results of cryoscopic experiments of NaCl, NaBr, $ZnCl_2$, $SnCl_2$, UCl_3, and $ThCl_4$ in bismuth[8] indicated that the solubility of these salts in the metal at its freezing point was less than 0.02 mole per cent. However, since the solubilities of most salts in their metals at the freezing point of the latter are low, these studies were extended to higher temperatures where complete miscibility of salts and their metals sometimes occurs.[1-4,7]

Experimental

Material. All materials used in this work were reagent-grade. NaCl, $PbCl_2$, AgCl, Cu_2Cl_2, and InCl were dried over P_2O_5 *in vacuo* for 60 hours before use, and the remaining salts were fused under a current of HCl gas. Bismuth and stannous chloride were purified further by distillation after dehydration. The hygroscopic salts were handled at all times in a dry box flushed with argon. The metals were purified by maintaining them at just above the melting point *in vacuo* for 10 min. and tapping the container gently in order to liberate dissolved gases. The molten metal was then filtered under argon through glass wool.

Apparatus and procedure. It was desirable to measure the solubility at equilibration temperature rather than to quench the sample. The solubility was therefore determined by a visual method. The mixture of salt and metal was placed in a heavy-walled quartz tube and sealed under vacuum. The free volume above the mixture was such that the volatilization of the salt phase was negligible. The tube was then fastened to a nickel rod and suspended in a Marshall furnace equipped with 2 sight windows opposite one another. The tube was illuminated from the rear and from a

---

* The work reported in this paper was supported in part by the United States Atomic Energy Commission, Washington, D.C.

third window at one side. A Chromel-Alumel thermocouple fastened to the tube was employed for measurement of temperature. The furnace was mounted on a metal base provided with a rocking mechanism. In this way the entire system could be inverted frequently to insure adequate surface contact of the 2 phases. The sample was heated until the salt phase disappeared or to a maximum temperature of 1000° C. (1200° C. in the case of AgCl and Cu_2Cl_2). The solution process was found in all cases to be reversible with temperature.

TABLE 1
SOLUBILITY OF CHLORIDES IN THEIR METALS

Salt	Metal	Temperature (°C.)	Solubility (mole %)
$BiCl_3$	Bi	374	2.0
		387	2.2
		427	2.9
		462	3.8
		498	5.3
		597	10.5
Hg_2Cl_2	Hg	322	0.53
		350	0.97
		365	1.22
		396	2.05
		431	3.07
		477	4.23
		506	6.29
$PbCl_2$	Pb	753	0.30
		848	0.52
		916	0.70
		1009	1.02
$CdCl_2$	Cd	1000	<0.05*
$ZnCl_2$	Zn	1000	<0.05*
$SnCl_2$	Sn	1000	<0.08*
InCl	In	1000	<0.08*
AgCl	Ag	1200	<0.3*
Cu_2Cl_2	Cu	1200	<0.15*

* Salt phase persisted.

Results and Discussion

The solubilities of salts in their metals are shown in TABLE 1. Those that were determined as a function of temperature are shown in FIGURE 1, together with the NaCl-Na[1] and KCl-K[1] systems.

The low solubilities at 1000° C. of $PbCl_2$ in Pb (1 per cent) and the low maximum solubilities of $CdCl_2$, $ZnCl_2$, InCl, AgCl, and Cu_2Cl_2 in their metals are in marked contrast to the very high solubilities of the alkali halides, $BaCl_2$ and $BiCl_3$ in their metals and the appreciable solubility of Hg_2Cl_2 in mercury. There appears to be no single criterion for predicting even qualitatively the solubility of salts in their metals. That is, no generalization comes to mind that explains why $BiCl_3$, Hg_2Cl_2, $BaCl_2$, and the alkali halides are so soluble in their metals while the rest of the systems discussed above are so very much less soluble. Three possible generalizations that were discarded because of the exceptions found during the course of this work. They are:

(1) Salts that possess a stable +1 oxidation state should be quite soluble. Some exceptions are AgCl, Cu_2Cl_2 and, most important, InCl, since it has such a low melting point (225° C.).

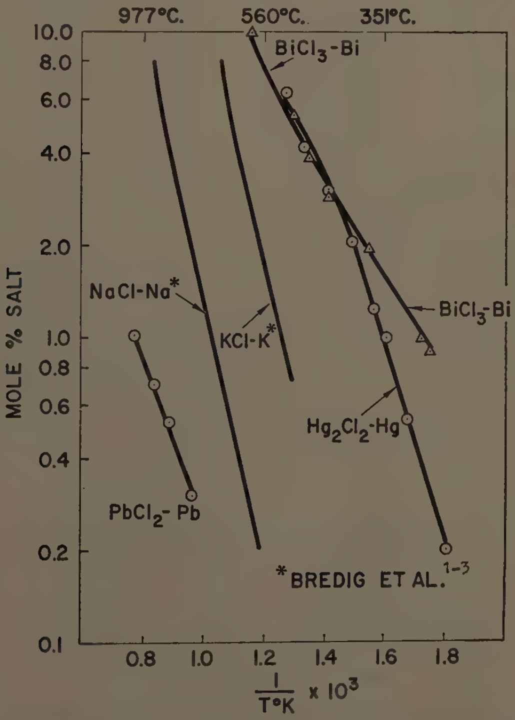

FIGURE 1. Solubilities of chlorides in their metals.

(2) Metals with low melting points should dissolve their salts. Some exceptions are Sn (232° C.), In (157° C.), and Cd (303° C.).

(3) Systems in which salts dissolve their metals will exhibit solubilities of salts in their metals. An exception is the Cd-$CdCl_2$ system in which Cd is soluble in $CdCl_2$ to the extent of 12.5 mole per cent at 530° C.,[9] but in which the solubility of $CdCl_2$ in Cd is less than 0.05 per cent at 1000° C.

It thus appears that solubility is complex, presumably involving a number of factors.

The solubilities of foreign salts in metals are shown in TABLE 2. The solubilities of salts in bismuth measured as a function of temperature are shown in FIGURE 2, where they are compared with the solubility of $BiCl_3$ in Bi. It may be seen that the solubilities of foreign salts in Bi are considerably less than that of $BiCl_3$ in Bi, and that in no case does the solubility in a metal exceed that of its own salt. However, the converse is not true; that is, a salt can dissolve to a higher degree in a foreign metal than in its own metal (for example, solubility of $PbCl_2$ and $CdCl_2$ in Bi versus the lower solubilities of these salts in their own metals).

TABLE 2
SOLUBILITY OF FOREIGN SALTS IN METALS

Metal	Salt	Temperature (°C.)	Solubility (mole %)
Bi	$PbCl_2$	622	0.39
		756	0.98
		824	1.47
		907	1.81
		942	1.94
Bi	$CdCl_2$	805	0.42
		862	0.60
		944	0.90
Bi	$SnCl_2$	620	0.40
		676	0.50
		822	0.89
Bi	$ZnCl_2$	784	0.08
		848	0.13
		936	0.20
Bi	NaCl	1000	<0.02*
Pb	$ZnCl_2$	770	0.07
Pb	$SnCl_2$	636	0.04
Sn	$PbCl_2$	1000	<0.10*
Sn	$ZnCl_2$	1000	<0.07*
Zn	$PbCl_2$	1000	<0.05*

* Salt phase persisted.

It has thus been shown that at these elevated temperatures, at least in the cases of bismuth and lead, metals dissolve salts other than their own halides.

One possible mechanism of solution of a foreign salt in a metal is an oxidation-reduction reaction of the metal with the foreign salt to produce a soluble salt of the metal. If this is true, then, for a given metal, the less stable the foreign salt, the greater would be the solubility of that salt in the metal. This is found to be the case, at least for bismuth. TABLE 3 shows the solubility of salts in bismuth at 900° C. and the stabilities* of the molten salts with respect to their elements at this temperature. It may be seen that, as the salt becomes more stable, the solubility of the salt in Bi decreases. Therefore, from these experiments one might conclude that the less stable the foreign salt the greater will be the solubility of that salt in a metal until the solubility approaches that of the salt of the metal. However, in the case of solution of foreign salts in the nobler metals such as bismuth, the standard free energy of reaction of Bi and the salt to form

---

* The free energy of formation of solid $BiCl_3$ is in error due to the incorrect heat of fusion of $BiCl_3$.[10] Therefore, the value given by Darnell and Yosim[10] for solid $BiCl_3$ has been used, and the ΔF^0_{form} of liquid $BiCl_3$ has been obtained with these values.

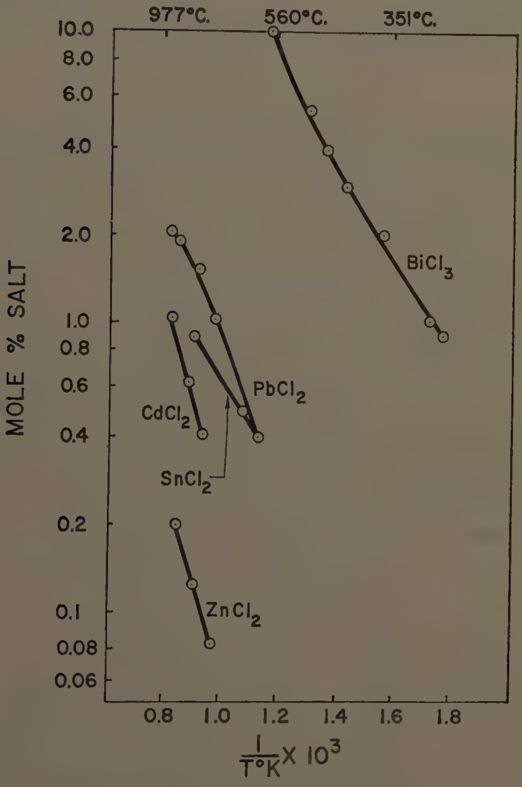

Figure 2. Solubilities of chlorides in bismuth.

Table 3
Solubility of Salts in Bismuth at 900° C.

Salt	Solubility (mole %)	$\Delta F^0_{form/Cl}$ of molten salt-kcal.
$BiCl_3$	Completely miscible	−10.9
$PbCl_2$	1.80	−23.7
$SnCl_2$	1.12	−24.0
$CdCl_2$	0.75	−27.7
$ZnCl_2$	0.19	−31.4
NaCl	<0.01	−72.5

$BiCl_3$ and the reduced metal can be quite positive. For example, the standard free energy for the reaction $3PbCl_2 + 2Bi \rightarrow 2BiCl_3 + 3Pb$ at 1000° K. (the standard states being the pure liquids) is +12.3 kcal. per gram atom of Cl. Consequently, it is of interest to see if such a mechanism can account for the observed solubility. For purposes of illustration, the $PbCl_2$-Bi case will be discussed. Here three equilibrium reactions are involved:

$$2\mathrm{Bi}(m) + 3\mathrm{PbCl}_2(s) \rightleftharpoons 2\mathrm{BiCl}_3(m) + 3\mathrm{Pb}(m) \tag{1}$$

$$\mathrm{BiCl}_3(m) \rightleftharpoons \mathrm{BiCl}_3(s) \tag{2}$$

$$\mathrm{BiCl}_3(m) \rightleftharpoons \mathrm{BiCl}_3(g) \tag{3}$$

where m, s, and g refer to the metal, salt, and gas phases, respectively. If the activity of $PbCl_2$ can be considered to be unity, the equilibrium constant, K_1,* for REACTION 1 is

$$K_1 = 0.44\, N^{0\,5}_{\mathrm{PbCl}_2} \gamma^2_{\mathrm{BiCl}_3(m)} \gamma^3_{\mathrm{Pb}(m)} \tag{4}$$

where $N^0_{\mathrm{PbCl}_2}$ is the apparent solubility of $PbCl_2$ and γ is the activity coefficient, the standard state being the pure liquid.

Values of $\gamma_{\mathrm{BiCl}_3(m)}$ were obtained from EQUATION 4 by substituting values of $N^0_{\mathrm{PbCl}_2}$ and K_1, which can be obtained from tables of free energy of formation data[12] and from the corrected thermodynamic values of $BiCl_3$.[10] The activity coefficients of lead in bismuth at the desired temperatures were calculated from existing data.[13] Activity coefficients obtained in this manner for $BiCl_3$ formed from reaction of $PbCl_2$, $CdCl_2$, and $SnCl_2$ with

---

* A more rigorous derivation leads to the following expression for K_1:

$$K_1 = \frac{0.44\, N^{0\,5}_{\mathrm{PbCl}_2} \dfrac{\gamma^2_{\mathrm{BiCl}_3(m)} \gamma^3_{\mathrm{Pb}(m)}}{\gamma^3_{\mathrm{PbCl}_2(s)}} \left(1 + \dfrac{P^0_{\mathrm{BiCl}_3}}{bRT} V \gamma_{\mathrm{BiCl}_3(m)}\right)}{\left[\dfrac{P^0_{\mathrm{BiCl}_3}}{bRT} V \gamma_{\mathrm{BiCl}_3(m)} - 0.67 \dfrac{N^0_{\mathrm{PbCl}_2} \gamma_{\mathrm{BiCl}_3(m)}}{\gamma_{\mathrm{BiCl}_3(s)}}\right]^3}$$

where $P^0_{\mathrm{BiCl}_3}$ is the vapor pressure of pure $BiCl_3$, V is the free volume above the liquid, RT has its usual significance, and b is the number of moles of Bi. To illustrate the magnitude of the terms in the above equation, the values for the case where the solubility of $PbCl_2$ in Bi at 756° C. was 0.98 mole per cent are substituted. ($P^0_{\mathrm{BiCl}_3} =$ 32.3 atm., $V = 0.30$ cc., $b = 0.0479$ moles and $T = 1029°$ K.) The activity coefficients of $PbCl_2(s)$ and $BiCl_3(s)$ are assumed to be unity, although in the $BiCl_3$-$PbCl_2$ system there is a compound that melts incongruently at 320° C.[11] The value of K_1 is then

$$K_1 = \frac{0.44\, N^{0\,5}_{\mathrm{PbCl}_2}(1 + 0.00245\, \gamma_{\mathrm{BiCl}_3(m)}) \gamma^2_{\mathrm{BiCl}_3(m)} \gamma^3_{\mathrm{Pb}(m)}}{[1 + 0.00180\, \gamma_{\mathrm{BiCl}_3(m)}]^3}$$

If $\gamma_{\mathrm{BiCl}_3(m)}$ is less than 100, the ratio

$$\frac{(1 + 0.00245\, \gamma_{\mathrm{BiCl}_3(m)})}{(1 + 0.00180\, \gamma_{\mathrm{BiCl}_3(m)})^3}$$

is essentially unity, and EQUATION 4 is obtained.

Bi are given in the fifth column of TABLE 4 (the same treatment was not applied to the $ZnCl_2$-Bi system since both the Zn-Bi[14] and the $ZnCl_2$-$BiCl_3$[11] systems have miscibility gaps).

The very small values for $\gamma_{BiCl_3(m)}$ would indicate that considerable negative deviation from Raoult's law exists between $BiCl_3$ and Bi in the metal phase. This is contrary to what might be expected in a binary system with a miscibility gap.

An alternate oxidation-reduction reaction that may be considered as a possible mechanism of solution in Bi of the salts discussed above is the formation of BiCl, which is, in turn, soluble in bismuth. Illustrating again with $PbCl_2$, and writing the reaction with the same number of chlorines as REACTION 1, we have

TABLE 4

CALCULATED ACTIVITY COEFFICIENTS OF $BiCl_3$ AND BiCl

Bi-$PbCl_2$ System

Temp. (°C.)	$N^0_{PbCl_2}$	K	$\gamma_{Pb(m)}$	$\gamma_{BiCl_3(m)}$	$\gamma_{BiCl(m)}$
622	0.0039	$10^{-18.34}$	0.46	3.5×10^{-3}	2.7
756	0.0098	$10^{-16.12}$	0.53	3.6×10^{-3}	1.5
824	0.0147	$10^{-15.20}$	0.55	3.7×10^{-3}	1.1
907	0.0181	$10^{-14.20}$	0.56	5.1×10^{-3}	1.1
942	0.0194	$10^{-13.84}$	0.57	8.1×10^{-3}	1.2

Bi-$CdCl_2$ System

Temp. (°C.)	$N^0_{CdCl_2}$	K	$\gamma_{Cd(m)}$	$\gamma_{BiCl_3(m)}$	$\gamma_{BiCl(m)}$
805	0.0042	$10^{-20.30}$	0.584	2.1×10^{-4}	1.02
862	0.0060	$10^{-19.37}$	0.644	2.1×10^{-4}	0.80
944	0.0095	$10^{-18.12}$	0.672	2.9×10^{-4}	0.63

Bi-$SnCl_2$ System

Temp. (°C.)	$N^0_{SnCl_2}$	K	$\gamma_{Sn(m)}$	$\gamma_{BiCl_3(m)}$	$\gamma_{BiCl(m)}$
628	0.0040	$10^{-18.25}$	1.07	1.0×10^{-3}	1.7
676	0.0050	$10^{-17.45}$	1.18	1.3×10^{-3}	1.6
822	0.0089	$10^{-15.45}$	1.16	3.0×10^{-3}	1.5

$$3PbCl_2(s) + 6Bi(m) \rightleftharpoons 6BiCl(m) + 3Pb(m) \qquad (5)$$

If again the activity of $PbCl_2$ is assumed to be unity, then

$$K = 64\, N^{0\,9}_{PbCl_2} \gamma^{6}_{BiCl(m)} \gamma^{3}_{Pb(m)} \qquad (6)$$

The value of K for REACTION 5 is not known, since the stability of molten BiCl is not known. However, it has been shown that the free energy of formation, per gram atom of chlorine, of solid BiCl is essentially equal to that of solid $BiCl_3$.[10] Therefore, it is assumed for these calculations that the stabilities of liquid BiCl and $BiCl_3$ are equal, and that therefore, for a given temperature, the Ks of EQUATIONS 6 and 4 are equal.

Activity coefficients for BiCl formed from $PbCl_2$ and $CdCl_2$ are given in the sixth column of TABLE 4. In this case the activity coefficients are much greater than those obtained when $BiCl_3$ was considered. While $\gamma_{BiCl(m)}$ is still not as large as one would expect, in view of the many assumptions made this mechanism seems a more feasible one.

Thus, at least in the case of bismuth, it has been shown that the apparent nonspecificity of solution can be explained in terms of an oxidation-reduction reaction resulting in the formation of a salt of the metal that dissolves in the metal. Therefore, it appears that specificity is one principle that must be satisfied by any theory explaining the behavior of these systems.

Summary

A series of experiments to determine the solubilities of metal chlorides in their metals was carried out, using a visual technique. The systems studied were: Bi, Hg, Pb, Cd, Zn, Sn, In, Ag, and Cu, with their chlorides. The results show that $BiCl_3$ and Hg_2Cl_2 are most soluble, the former being completely miscible with Bi at 778° C., while the latter is soluble to the extent of 7 mole per cent at 600° C. $PbCl_2$ is slightly soluble (1 mole per cent at 1000° C.), while the remaining salts are considered insoluble in their metals. There appears to be no single criterion for predicting the solubility of salts in their metals.

Experiments were also carried out to see if nonspecificity of solubility exists at high temperatures, that is, to determine if metals dissolve salts other than their own halides. It was found that solubility does occur. It was also found that the less stable the salt, the greater is the solubility of the salt in a given metal, until the solubility approaches that of the salt of the metal. Thermodynamic calculations indicate that the solubility of a foreign salt in a metal can be explained in terms of oxidation-reduction reactions to form the halide of the metal, which in turn dissolves in the metal. These calculations suggest that $BiCl_3$ dissolves in bismuth metal as BiCl.

References

1. Bredig, M. A., J. W. Johnson & W. T. Smith. 1955. J. Am. Chem. Soc. **77:** 307.
2. Bredig, M. A., H. R. Bronstein & W. T. Smith. 1955. *Ibid.* **77:** 1454.
3. Johnson, J. W. & M. A. Bredig. 1958. J. Phys. Chem. **62:** 604.
4. Schafer, H. & A. Niklas. 1952. Angew. Chem. **64:** 611.
5. Cubicciotti, D. D. & C. D. Thurmond. 1949. J. Am. Chem. Soc. **71:** 2149.
6. Eggink, B. G. 1908. Z. Phys. Chem. **64:** 449.
7. Yosim, S. J., A. J. Darnell, W. G. Gehman & S. W. Mayer. 1959. J. Phys. Chem. **63:** 230.
8. Mayer, S. W., S. J. Yosim & A. J. Darnell. 1957. Abstract of Papers. : 285. ACS Meeting. New York, N.Y.
9. Hedger, R. & H. Terrey. 1936. Trans. Faraday Soc. **32:** 1614.
10. Darnell, A. J. & S. J. Yosim. J. Phys. Chem. In press.

11. Herrmann, G. 1911. Z. anorg. Chem. **71:** 257.
12. Brewer, L. 1950. The Chemistry and Metallurgy of Miscellaneous Materials—Thermodynamics. L. L. Quill, Ed. NNES IV-19B. McGraw-Hill. New York, N.Y.
13. Kubaschewski, O. & J. Catterall. 1956. Thermochemical Data of Alloys. Pergamon Press. New York, N.Y.
14. Hansen, M. 1958. Constitution of Binary Alloys. McGraw-Hill. New York, N.Y.

ELECTROLYSIS OF LIQUID BISMUTH-BISMUTH CHLORIDE MIXTURES*

Daniel Cubicciotti
Stanford Research Institute, Menlo Park, Calif.

Norman L. Lofgren
Chico State College, Chico, Calif.

Introduction

The properties of bismuth in molten bismuth chloride have been studied more extensively than other liquid metal-salt systems, probably because of the relative ease in handling these materials. The general nature of the phase diagram has been known for some time.[1-5] A recent version of the phase diagram given by Yosim *et al.*[1] is shown in FIGURE 1. The high solubility of metal in the salt phase has stimulated the curiosity of investigators concerning the nature of such solutions and the species that constitute them. Measurements have been made of electrical conductivity,[7] viscosity,[7] density,[7,8] and activity of $BiCl_3$.[9,10]

Graphs of the electric conductivity determined by Aten[7] are shown in FIGURE 2. Although specific conductance as a function of composition shows pronounced maxima at the higher temperatures, the maxima barely appear in the molar conductance curves (molar conductance is defined as the product of the specific conductance and the volume of a mole of mixture). A transformation of the data into the conductance of that amount of solution containing 1 mole of bismuth chloride is given in FIGURE 2*c*. This conductance, which is equal to the molar conductance divided by the mole fraction $BiCl_3$ in the solution, remains almost constant with composition. As the bismuth concentration increases there is an increase of this conductance to a maximum and then a decrease at all temperatures except the lowest. This behavior may indicate that the addition of bismuth to bismuth chloride produces additional conducting species, but the concurrent increase in viscosity acts to reduce the conductance, thus producing the maximum. If this is the case, then the additional conducting species is more readily produced at higher temperatures since the maximum is greater at higher temperatures, while the viscosity increase with composition is approximately the same at all temperatures (*see* FIGURE 2*d*).

The activity of the bismuth chloride in the solutions, both from vapor pressures and from freezing-point lowerings, has been used to postulate the species present. Unfortunately, more than one set of species can be postulated from the same data because of the spread in the experimental points (particularly in the vapor pressures). We believe that the activity data

---

* The work reported in this paper was supported in part by the Research Division of the United States Atomic Energy Commission, Washington, D.C.

are in accord with the postulate of a solution of monatomically dispersed bismuth dissolved in the salt and the positive deviations of the activity of $BiCl_3$ arising primarily from a heat of solution. Corbett[11] has suggested that species such as Bi_nCl_n should be postulated, particularly Bi_4Cl_4 (but he interpreted the freezing point data with an incorrect heat of fusion for bismuth chloride). Topol and Mayer[10] have indicated that the cryoscopic number of particles formed per bismuth atom dissolved (equal to 0.75) is in accord with the formation of Bi_2Cl_2, Bi plus Bi_2, or Bi with deviations from ideal solution behavior.

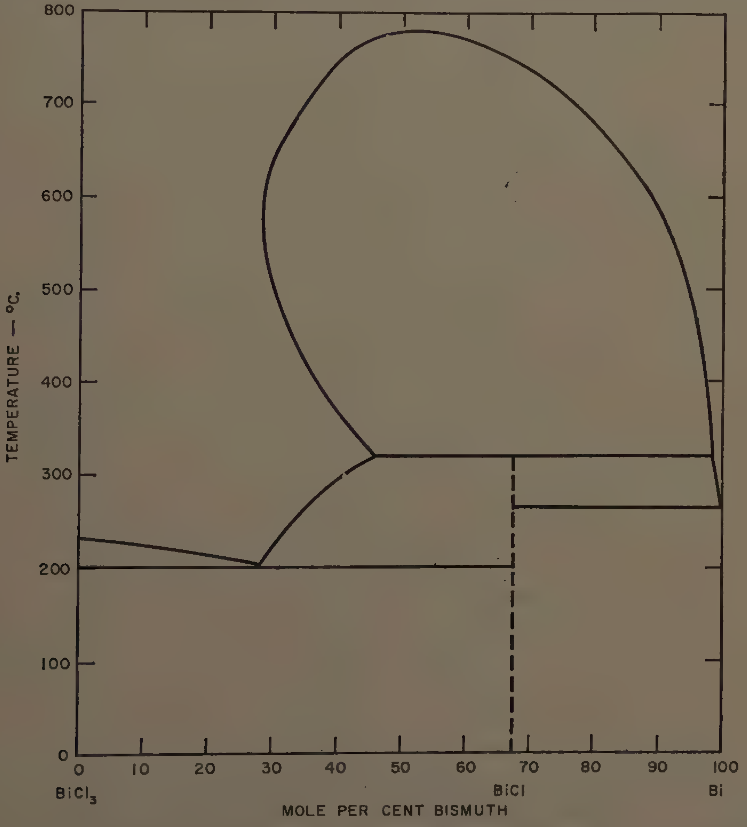

FIGURE 1. Bismuth-bismuth chloride diagram as reported by Yosim *et al.*[1]

As we believed that some insight concerning the nature of the solution might be obtained from electrolytic measurements, we undertook the present study. Our hope was to determine the current-carrying species in the salt and, possibly, to detect some electronic conduction.

Method

Principle. Measurements were designed to determine the ratio of electric current passed to the mass current of bismuth through the salt phase of a cell in which the only chemical process was the transfer of bismuth from anode to cathode. TABLE 1 is a schematic representation of the processes that might be expected to occur in such a cell. As the cell was designed with 2 bismuth electrodes, there was no net transport of chloride

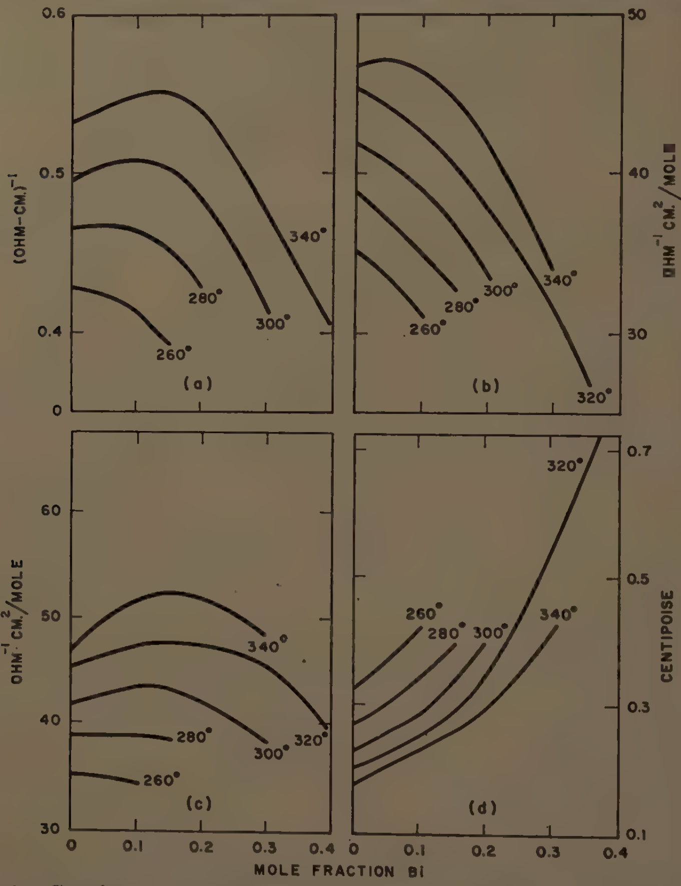

FIGURE 2. Graphs of electric conductivity: (*a*) specific conductance of $BiCl_3$;[7] (*b*) conductance per mole of Bi-$BiCl_3$ mixture (calculated from the specific conductance data of Aten[7] and the density data of Keneshea and Cubicciotti[8]); (*c*) conductance of solutions containing 1 mole $BiCl_3$; (*d*) viscosity of Bi-$BiCl_3$ solutions from data of Aten.[7]

TABLE 1
SCHEMATIC REPRESENTATION OF ELECTROLYSIS

Bi (Saturated with salt)	$BiCl_3$ (Saturated with metal)	Bi (Saturated with salt)
← e^-	→ + Bi ions ←e^- ? Cl^- stationary	← e^-
Bi → Bi ions + e^-		Bi ions → Bi + e^-

ion, and the only current carriers were the various possible bismuth species and/or electrons. It was expected that the ratio (R) of electric current to bismuth current would be greater than 3 if appreciable electronic conduction occurred, and less than 3 if lower-valent bismuth species carried the current.

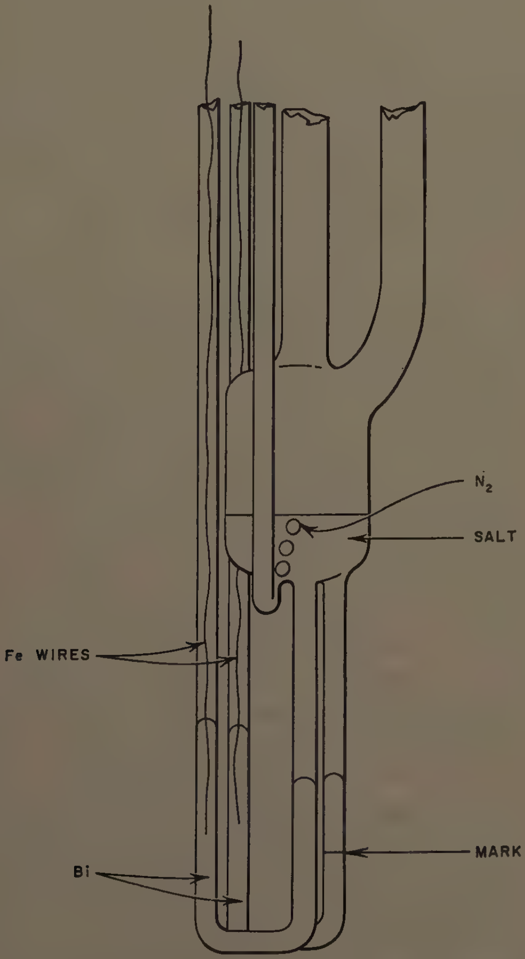

FIGURE 3. Schematic diagram of electrolysis cell.

Apparatus. The cell used for the purpose is shown schematically in FIGURE 3. As the electrolysis progressed, the amount of bismuth in each U-tube electrode could be determined by measuring, with a traveling telescope, the height of the liquid bismuth relative to a fiducial mark. The amount of current passed was determined by measuring the area under the curve of a recording coulometer that was calibrated with an aqueous silver coulometer. The source of direct current was a full-wave AC rectifier equipped with a choke to reduce ripple.

The furnace was constructed of "clamshell" heaters fixed around a vertical Pyrex tube with a three-quarter-inch slit for sighting. Temperature was controlled with a Chromel-Alumel thermocouple and potentiometer controller.

Materials. Reagent-grade $BiCl_3$ was dehydrated in a stream of HCl and distilled in a stream of dry N_2 into tubes that were then sealed until used. LiCl-KCl eutectic was prepared by weighing "dry" salts in the ratio 9.0 to 11.0 into a Pyrex tube, heating them in a stream of dry N_2, and keeping them at 400° C. for 1 hour with N_2 bubbling through them. The melt was drawn up into predried, calibrated pipettes that were subsequently sealed until used. Reagent-grade lump bismuth metal was filtered through Pyrex fritted disks and cast into long glass tubes under an N_2 atmosphere.

Operation. The tubes of the cell were all closed with ground joints outside the furnace. N_2 inlets and outlets were provided in the caps. The electric leads were Fe wires sealed through the proper caps. The cell was heated to operating temperature and cooled under a stream of dry N_2. The proper amount of Bi was then introduced into the 2 legs under a stream of N_2. A measured length of $BiCl_3$-filled glass tube was broken off and dropped into the cell. A special flexible plastic container was devised so that the $BiCl_3$ was always in a stream of dry N_2. With a rapid flow of N_2 through the cell, a pipette of LiCl-KCl was lowered into it. After the salt had melted it was blown out of the pipette, and a stream of N_2 bubbling through the salt phase stirred the melt and mixed it with a droplet of Bi to saturate the salt before the electrolysis began.

A current of about 250 mAmp. was impressed on the cell, and the heights of the Bi in the 2 legs were measured relative to the fiducial mark about every 20 min. Each electrolysis lasted about 2 hours and resulted in changes of about 0.5 cm. in the heights of the Bi columns. The electrode-salt interface showed a tendency to stick at the position maintained during electrolysis. To obtain a reproducible position for the Bi-salt interfaces, they were maintained elevated during electrolysis by a slight N_2 pressure on the electrodes, and then allowed to drop, by releasing that pressure, for measurement.

Upon the completion of an electrolysis either the composition of the salt melt was altered by the addition of $BiCl_3$ or LiCl-KCl or the temperature of the cell was altered, and another electrolysis was performed. Usually 3 or 4 runs were made before the cell was dismantled and reassembled for a new series.

To see if the electrode reactions were current-dependent, an electrolysis at 330° C. was run at 20 mAmp. instead of the usual 240 mAmp. The results agreed with a 240-mAmp. electrolysis; therefore, it was assumed that in this study the character of the electrode reactions did not change with current density.

Calculation. To analyze the results, the heights of bismuth in the 2 electrodes were plotted as a function of time. Straight lines were drawn through the points for each electrode, and the mass current of bismuth was calculated from the average of the 2 slopes, the diameters of the bismuth columns, and the densities[8] of metal and salt phases. The electric current was essentially constant during each run. The R of the electric current to bismuth current was then calculated.

Figure 4 shows an example of the data. It was observed that the heights of both electrode columns increased slowly during the time before and after electrolysis. During electrolysis the increase continued at the same rate; the cathode increase was greater than the anode decrease by the amount expected for a constant rate. In our opinion, the increase in the amount of electrode material was due to the dissolution and slow diffusion of $BiCl_3$ in the bismuth. In substantiation of this opinion, it was noted after long periods of operation that the Fe electrodes were corroded, and that a saltlike substance appeared on the open surface of the bismuth.

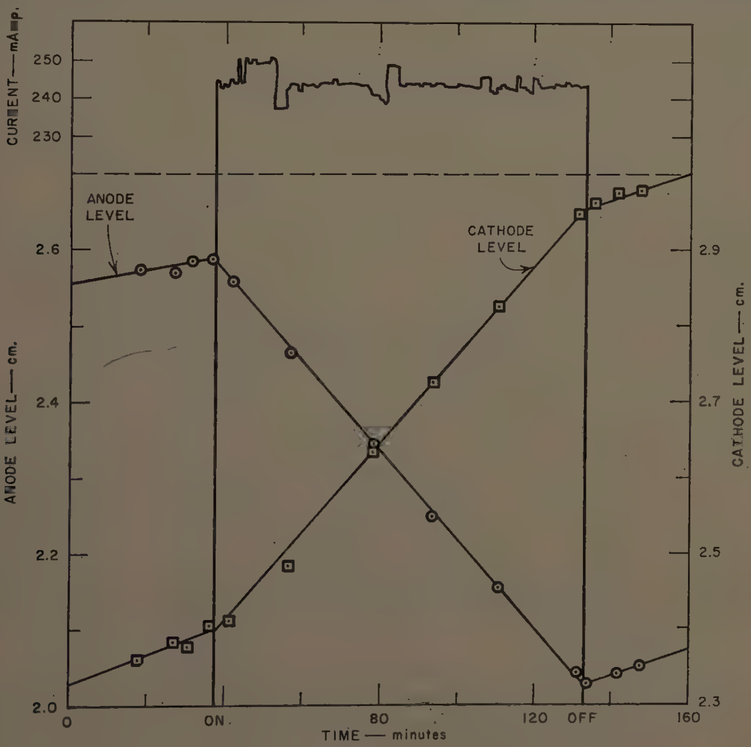

Figure 4. Type of data obtained in electrolysis (370° C.).

Results and Discussion

Electrolysis of Bi-$BiCl_3$ mixtures. Electrolysis of a series of Bi-$BiCl_3$ mixtures in equilibrium with bismuth was performed over the temperature range 330° to 425° C. The results obtained are shown in FIGURE 5, where R is plotted against temperature. The points are experimental values and range from 1.5 to 2.0. Our first reaction was that this was evidence for univalent bismuth (in order to obtain transport ratios under 2.0, it seemed necessary that there be some univalent bismuth in the melt).

However, when the average oxidation numbers of bismuth were calculated from the compositions of the salt melts in the 2-phase liquid region,[1] they gave the shaded line shown in FIGURE 5. Thus, the oxidation numbers calculated from equilibrium compositions were essentially the same as the ratios of number of electrons to the number of bismuth atoms transferred through the salt by electrolysis. As the coincidence of the results seemed more than fortuitous, we sought an explanation.

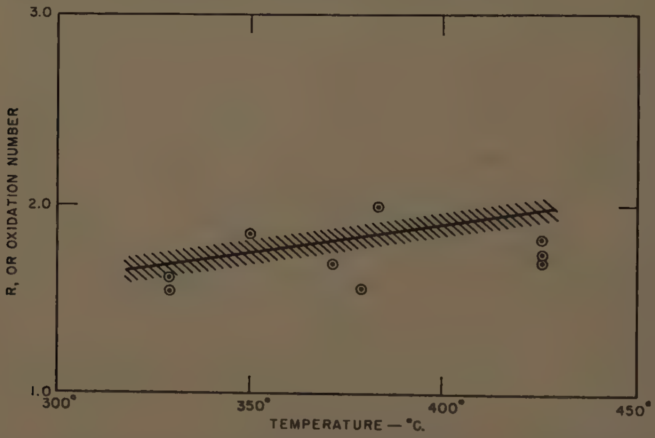

FIGURE 5. Ratio (R) of electric current to bismuth current in the electrolysis of Bi-BiCl$_3$ mixtures at several temperatures. Symbols: dotted circles are values of R: line represents average oxidation numbers for Bi in equilibrium mixtures (data from Yosim *et al.*[1]).

Electrode processes. Detailed consideration of the processes occurring at the electrodes led us to the following explanation of the coincidence. In fact, we were forced to conclude that, in the absence of electronic conduction, the two should have been predicted to be equal, and thus no information concerning the species in the melt could have been forthcoming.

FIGURE 6 gives a schematic representation of the electrode processes. The interface between the metal and the salt phase in the absence of electrolytic current is shown in the first panel. The metal phase consists of bismuth ions in some geometrical array and a complement of metallic electrons that may be considered mobile (plus an equilibrium concentration of chloride ions). The salt phase consists of an array of chloride ions, probably in contact with each other, with the normal Bi^{+3} ions and dissolved bismuth probably quite regularly arranged in the interstices among the chlorides.

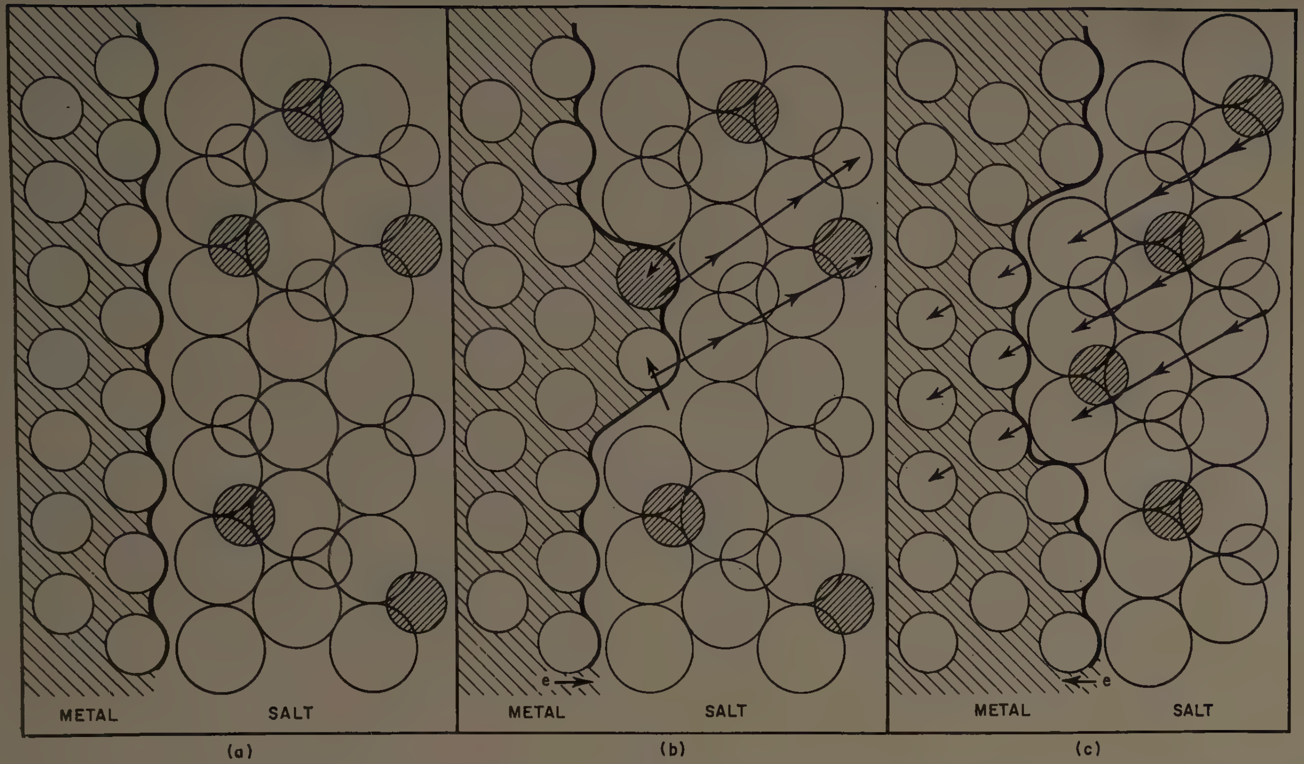

FIGURE 6. Schematic representation of electrode processes: (*a*) metal-salt interface with no current flowing; (*b*) cathode interface during electrolysis; (*c*) anode interface during electrolysis. Symbols: large circles are Cl; small circles are Bi; shaded circles are dissolved Bi.

The electrode process at the cathode may be visualized (second panel of FIGURE 6) as an extension of the electron cloud of the metal phase to encompass a nearby Bi^{+3} and a simultaneous repulsion of the associated chlorides. As a result, the local volume of salt becomes supersaturated with dissolved bismuth, and some of it is transferred into the metal phase to re-establish equilibrium. In this process the ratio of dissolved Bi to Bi^{+3} that is transferred from the salt to the metal is exactly the equilibrium ratio of the two in the salt phase.

At the anode (*see* FIGURE 6*c*) the reverse process occurs. Passage of current causes the metallic electron cloud to retreat and leave a Bi^{+3}, which becomes enveloped in advancing chloride ions. As a local volume of salt that is undersaturated with dissolved bismuth is formed, some bismuth dissolves; again, the equilibrium ratio of Bi to Bi^{+3} is transferred from metal to salt.

The net result of the 2-electrode processes is the transport of Bi and Bi^{+3} in the ratio determined by the equilibrium salt composition. Thus, the ratio of electric current to bismuth current observed in electrolysis is predictable from the composition of the salt phase. A comparable analysis of the electrolysis can be made for any proposed set of bismuth species in the salt. Such an analysis depends on rapid attainment of the solution equilibrium between the metal and salt relative to the ionic transport through the salt.

Electrolysis of Bi-$BiCl_3$-LiCl-KCl mixtures. The addition of other chlorides reduces the solubility[12] of bismuth in bismuth chloride. It is thus possible to obtain salt phases with different concentrations of dissolved bismuth in contact with bismuth metal. We chose to add LiCl-KCl eutectic because of its low melting point. The results of electrolysis with LiCl-KCl added to $BiCl_3$ are shown in FIGURE 7, in which R is plotted against the composition of salt not including dissolved bismuth.

R was essentially constant from 0 to 0.2 in mole fractions of added LiCl-KCl. The ratio of dissolved bismuth to bismuth chloride in the salt was essentially constant in that range, as determined by the analyses shown in FIGURE 7; that is, both concentrations decreased proportionately. Thus, in that range, the average oxidation number of bismuth was again essentially equal to R.

Beyond 0.2, R increased until it reached the value 3 at about 0.6 in LiCl-KCl mole fraction and remained at 3 for greater mole fractions. It may be thus inferred that the concentration of dissolved bismuth was much smaller than that of bismuth chloride in melts greater than about 0.6 in LiCl-KCl mole fraction, because only plus-3 bismuth was transported. This result is in accord with measurements of the solubility of bismuth in the $BiCl_3$-NaCl system.[12]

Laitinen *et al.*[13] have found that in the polarographic reduction of dilute $BiCl_3$ (mole fraction $\sim 10^{-4}$) in LiCl-KCl there is a single polarographic wave the concentration dependence of which indicates an oxidation number change of 3.

Density and composition measurements of Bi-$BiCl_3$-LiCl-KCl. Determinations were made of the concentration of bismuth dissolved in various compositions of $BiCl_3$-LiCl-KCl equilibrated with bismuth so that the average oxidation number could be calculated. At the same time density measurements were made for use in the calculations. The method was very simple. A melt of the desired $BiCl_3$-LiCl-KCl composition was prepared and equilibrated with bismuth. A J-shaped calibrated pipette, its short leg made of small-bore tubing, was filled with melt by submerging the short leg. The weight and volume of the sample gave the density.

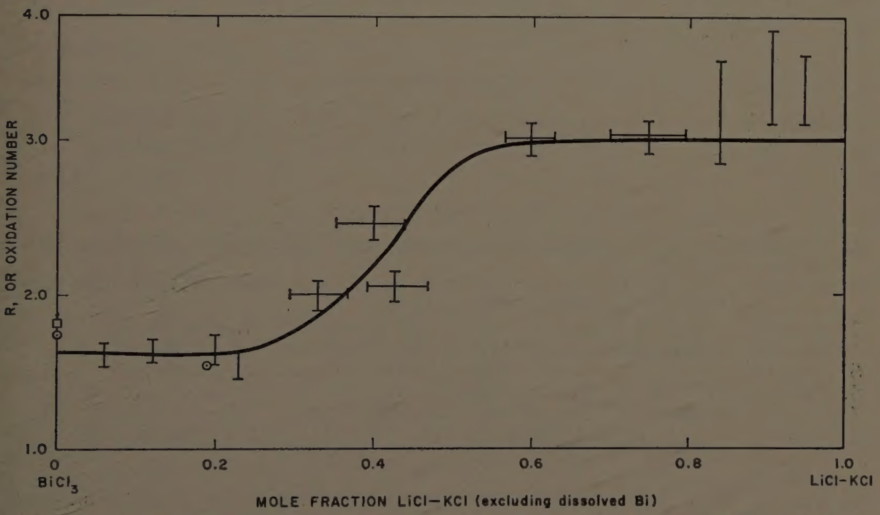

FIGURE 7. Variation of R with LiCl-KCl added to $BiCl_3$ at 370° C. Symbols: fine lines represent experimental values of R; circles are average oxidation numbers by chemical analysis; square is the value from the phase diagram of Yosim *et al.*[1]

Determination of the reducing power of the sample to ferric chloride solution and subsequent titration with ceric sulfate solution established the bismuth content.

In these measurements we observed that a solid, which floated on the melt, was formed from compositions greater than about 0.3 in LiCl-KCl mole fraction. This phenomenon made composition and density measurements beyond 0.3 untrustworthy, and meant that the compositions of the melts were indefinite beyond 0.3. Therefore, no oxidation numbers derived from compositions are given beyond 0.3 in FIGURE 7. The Rs from electrolysis are acceptable, even though the compositions of the melts were not well known.

The densities observed in the range 0 to 0.3 in LiCl-KCl mole fraction were linear with the salt composition and coincided with the line drawn between the density of saturated Bi-$BiCl_3$ and pure LiCl-KCl eutectic. The determinations of concentration of bismuth that were reliable are plotted in FIGURE 7.

Summary

Electrolytic experiments were performed on bismuth-bismuth chloride melts, saturated with metal, between liquid bismuth electrodes. The R of the quantity of electric current passed to the quantity of bismuth transported through the melt during electrolysis was determined. This R was found to be the same as the average oxidation number for bismuth in the salt phase as calculated from the composition. A consideration of the electrode processes led to an explanation of the equality between the current R and the average oxidation number.

Acknowledgment

We are indebted to our colleague C. M. Kelley for many fruitful discussions.

References

1. Yosim, S. J., A. J. Darnell, W. G. Gehman & S. W. Mayer. 1959. J. Phys. Chem. **63:** 230.
2. Sokolova, M. A., G. G. Urazov & V. G. Kuznetsov. 1954. Akad. Nauk. S. S. S. R. Inst. Gen. Inorg. Chem. **1:** 102.
3. Marino, L. & R. Becarelli. 1915. Atti accad. nazl. Lincei. **24:** 625.
4. Marino, L. & R. Becarelli. 1916. Atti accad. nazl. Lincei. **25:** 221.
5. Marino, L. & R. Becarelli. 1916. Atti accad. nazl. Lincei. **25:** 326.
6. Egginк, B. 1908. Z. physik. Chem. **64:** 449.
7. Aten, A. H. W. 1909. Z. physik. Chem. **66:** 41.
8. Keneshea, F. J., Jr. & D. Cubicciotti. 1958. J. Phys. Chem. **62:** 843.
9. Cubicciotti, D., F. J. Keneshea, Jr. & C. M. Kelley. 1958. J. Phys. Chem. **62:** 463.
10. Topol, L. E. & S. W. Mayer. 1958. 134th Ann. Meeting Am. Chem. Soc. Abstr. No. **29:** 145.
11. Corbett, J. D. 1958. J. Phys. Chem. **62:** 1149.
12. Cleary, G. & D. Cubicciotti. 1952. J. Am. Chem. Soc. **74:** 557.
13. Laitinen, H. A., C. H. Liu & W. S. Ferguson. 1958. Anal. Chem. **30:** 1266.

Printed in the United States of America

MONOGRAPHIC PUBLICATIONS
OF
THE NEW YORK ACADEMY OF SCIENCES

(Lyceum of Natural History, 1817–1876)

(1) The Annals (octavo series), established in 1823, contain the scientific contributions and reports of researches, together with the records of meetings of the Academy. The articles that comprise each volume are printed separately, each in its own cover, and are distributed immediately upon publication. The prices of the separate articles depend upon their length and the number of illustrations, and may be ascertained upon application to the Executive Director of the Academy.

Current numbers of the Annals are sent free to all Members of the Academy desiring them.

(2) The Special Publications, established in 1939, are issued at irregular intervals as clothbound volumes. The price of each volume will be advertised at time of issue.

(3) The Memoirs (quarto series), established in 1895, are issued at irregular intervals. It is intended that each volume shall be devoted to monographs relating to some particular department of science. Volume I, Part 1 is devoted to Astronomical Memoirs, Volume II to Zoological Memoirs. No more parts of the Memoirs have been published to date. The price is one dollar per part.

(4) The Scientific Survey of Porto Rico and the Virgin Islands (octavo series), established in 1919, gives the detailed reports of the anthropological, botanical, geological, paleontological, zoological, and meteorological surveys of these islands.

Subscriptions and inquiries concerning current and back numbers of any of the publications of the Academy should be addressed to

EXECUTIVE DIRECTOR
The New York Academy of Sciences
2 East Sixty-third Street
New York 21, N. Y.

DATE DUE

GAYLORD			PRINTED IN U.S.A.